THE
PHYSICAL REVIEW

A journal of experimental and theoretical physics established by E. L. Nichols in 1893

SECOND SERIES, VOL. 80, NO. 6 DECEMBER 15, 1950

The Conservation of Energy and Momentum in Compton Scattering*

WILLIAM G. CROSS† AND NORMAN F. RAMSEY
Harvard University, Cambridge, Massachusetts
(Received July 18, 1950)

An experiment similar to that of Bothe and Maier-Leibnitz and others has been carried out to verify that in Compton scattering of 2.62-Mev quanta the scattered quantum and recoil electron are emitted without delay and in the relative directions demanded by the conservation laws. Better angular resolution and statistics and fewer experimental uncertainties than in the previous experiments were obtained. The results are in agreement with simultaneity and the conservation of energy and momentum.

I. INTRODUCTION

IN 1936 an attempt was made by Shankland[1] to verify that energy and momentum are conserved in Compton scattering. The negative result he at first obtained stimulated a number of repetitions of this experiment[2] as well as considerable theoretical speculation,[3] particularly over a possible revival of the statistical theory of Bohr, Kramers, and Slater.[4] In these experiments it was hoped to show that when a beam of gamma-quanta is scattered, coincidences between the counters detecting the scattered photon and recoil electron could be obtained only when the counters were in the relative directions from the scattering foil required by the conservation laws.

Although these experiments were carried out with relatively poor angular resolution and statistics, and with a number of uncertainties, difficult to estimate quantitatively, there is no reason to doubt their unanimous conclusion that contrary to Shankland's original result the conservation laws are indeed satisfied.[5] Neither do we know of any further evidence suggesting that energy and momentum are not conserved in this process. Nevertheless it was felt that the technical advances made since 1936, which permitted a considerable reduction in the large experimental uncertainties, justified the repetition of an experiment on so fundamental a point.

II. GENERAL ARRANGEMENT

The general arrangement of this experiment, shown in Fig. 1, is similar to that used by Bothe and Maier-Leibnitz and others. A filtered, collimated beam of gamma-rays from RaTh strikes a Be foil. The recoil electron and scattered photon are detected by two counters whose output pulses are put in coincidence. According to the photon theory and the conservation laws, coincidences should be obtained when and only when the two counters and the beam are coplanar, and when the angles θ and ϕ of the gamma- and electron counters satisfy

$$\cot\phi=(1+\gamma)\tan\tfrac{1}{2}\theta, \qquad (1)$$

where γ is the energy of the incident quantum in units of the rest energy of the electron.

The primary difficulty of the experiment lies in the

* This work was assisted by the joint program of the ONR and AEC. It is taken from a Ph.D. thesis submitted to Harvard University by one of the authors (WGC).

† Whiting Fellow, 1948–49. Present address: Chalk River Laboratory, National Research Council of Canada, Chalk River, Ontario.

[1] R. S. Shankland, Phys. Rev. **49**, 8 (1936).

[2] R. S. Shankland, Phys. Rev. **50**, 571 (1936); **52**, 414 (1937). J. C. Jacobsen, Nature **138**, 25 (1936); W. Bothe and H. Maier-Leibnitz, Zeits. f. Physik **102**, 143 (1936); Phys. Rev. **50**, 187 (1936); G. Bernardini and S. Franchetti, see Bretscher, *"Kernphysik"* (Verlag. Julius Springer, Berlin, 1936).

[3] P. A. M. Dirac, Nature **137**, 298 (1936); R. Peierls, Nature **137**, 904 (1936); E. J. Williams, Nature **137**, 614 (1936); N. Bohr, Nature **138**, 25 (1936); F. Cernuschi, Comptes Rendus **203**, 777 (1936).

[4] Bohr, Kramers, and Slater, Phil. Mag. **47**, 785 (1924); Zeits. f. Physik **24**, 69 (1924).

[5] The conservation laws were also supported by the cloud-chamber experiments of A. H. Compton and A. W. Simon, Phys. Rev. **26**, 289 (1925) and of Crane, Gaerttner, and Turin, Phys. Rev. **50**, 302 (1936). Simultaneity, although not the conservation laws, was verified by the experiments of W. Bothe and H. Geiger, Zeits. f. Physik **26**, 44 (1924), Naturwiss. **13**, 440 (1925); W. E. Burcham and W. B. Lewis, Proc. Camb. Phil. Soc. **32**, 637 (1936); A. Picard and S. Stahel, J. de phys. et rad. **7**, 326 (1936); and R. Hofstadter and J. A. McIntyre, Phys. Rev. **78**, 24 (1950).

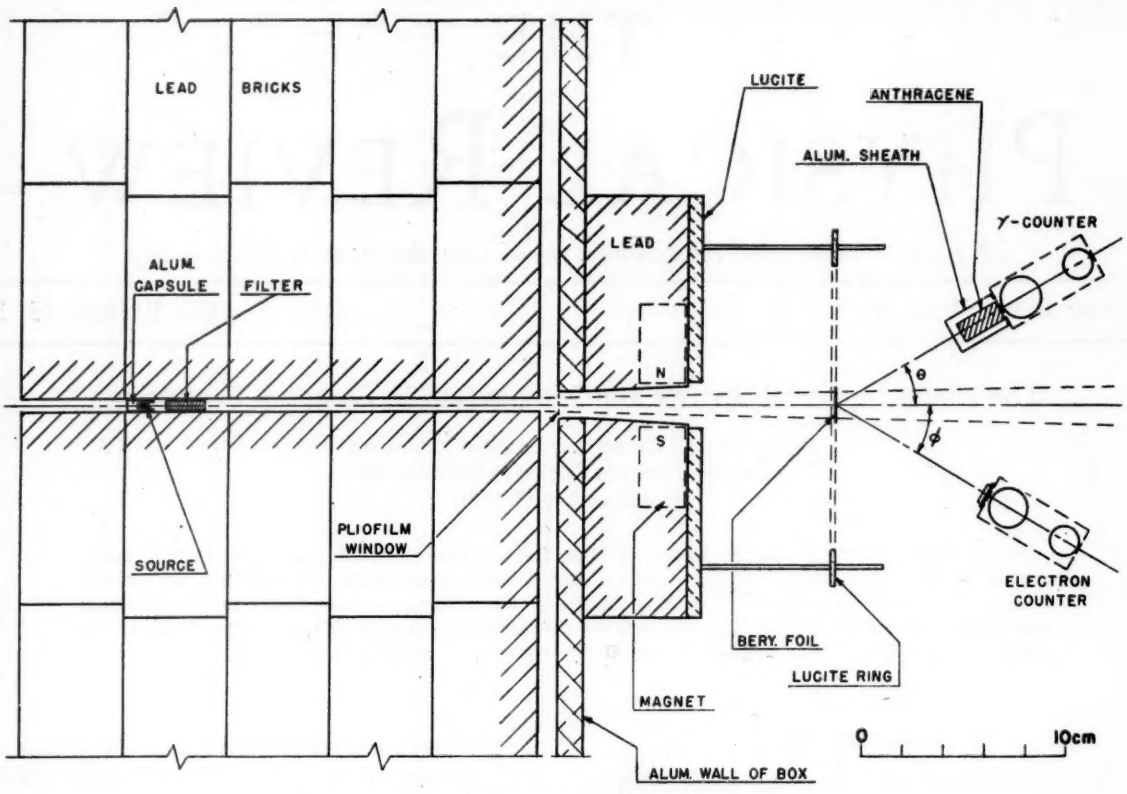

FIG. 1. General arrangement of apparatus.

low coincidence rate. To achieve a rate considerably larger than the background rate without the scattering foil, it is necessary to make the foil thick enough so that further scattering of the recoil electrons in it is appreciable. To minimize this scattering the electrons, and hence also the incident quanta, should have as high an energy as possible. Since there exists no long-lived source of sufficiently high energy monochromatic gamma-rays, corrections must be made for components of other energies in the beam.

It is the aim of the present experiment to show that for a given angle θ of the gamma-counter, the greatest number of coincidences is obtained for that angle ϕ which satisfies Eq. (1), and further that the distribution of coincidences about this angle is accounted for quantitatively by scattering of the recoil electrons in the foil, inhomogeneity of the gamma-radiation, and other reasons to be discussed. Most of the improvements in the present experiment are due to the use of a scintillation counter (instead of a Geiger counter) for detecting the scattered gamma-rays. The higher efficiency and long-term stability of the former, and the use of a stronger source of RaTh than was available to the previous investigators, have permitted us to improve the angular resolution, to reduce the thickness of the foil (and hence the effect of electron scattering in it), and to increase the filtering of the gamma-rays, and at the same time to obtain many more coincidences for each angular position.

The gamma-counter was set at a scattering angle of 30° to which, for the 2.62-Mev quanta of ThC'',[6] corresponds a recoil angle of 31.3°. Some advantages of this almost symmetrical arrangement are discussed by Bothe and Maier-Lebnitz.[2] Rather than keep the angle of one counter fixed and vary that of the other about the "correct" direction, we chose, as Bothe and Maier-Leibnitz did, to fix the positions of both counters and move the foil further from or closer to the source than that "correct" position for which the counters were in corresponding directions from the foil. This had the advantage that the background rate without the foil, which depends on the positions of the counters, remained constant, thereby reducing the long counting time.

III. APPARATUS

Gamma-rays from a 195-mg Ra equivalent of RaTh were filtered through 2 cm of lead and collimated in a 3.2-mm diameter hole through a lead shield. The flaring at the end of the collimator was designed to minimize the number of gamma-rays and electrons scattered from the collimator walls which reach the counters. A magnet at the end of the collimator deflected these electrons and reduced the background in the electron counter by

[6] C. D. Ellis, Proc. Roy. Soc. A138, 318 (1934). Recent measurements of Hornyak, Lauritsen, and Rasmussen, Phys. Rev. 76, 731 (1949) and of J. L. Wolfson, Phys. Rev. 78, 176 (1950) give values from 2.613 to 2.618 Mev.

40 percent. The beryllium scattering foil, 16 mm square and 13.8 mg/cm² thick was supported on a strip of Pliofilm 1 mg/cm² thick whose ends were fastened to a light ring of Lucite. Ring and foil could be moved parallel to the beam.

To reduce scattering of the gamma-rays and recoil electrons from the air, the scattering foil and counters were enclosed in a large box, with 0.5-mm thick metal walls, filled with helium. The box walls did not contribute appreciably to the background, while replacing the air with helium reduced the gas scattering by a factor of seven.

The gamma-ray detector was a rectangular parallelopiped of anthracene, 10×18 mm in area and 24 mm thick, in front of a 1*P*21 photo-multiplier. The crystal was covered with an Al foil reflector, while tube and crystal were wrapped with black tape to keep out light. A 3.2-mm thick Al sheath over the crystal kept out scattered electrons. A thicker sheath made no further measurable change in the coincidence rate.

The electron detector was a plate of anthracene, 13×17 mm in area and 2 mm thick, covered by a thin Al window. Between the crystal and 1*P*21 photo-multiplier was a 3-mm thick Lucite plate to give the crystal mechanical support. For the electrons which it is required to count (about 1 Mev) the efficiency of this counter was essentially 100 percent. The detectors were mounted on light Al frames, and could be rotated about a vertical axis through the center of the scatterer.

The pulses were amplified in Jordan-Bell-type linear amplifiers,[7] passed through a discriminator and fed into a crystal diode coincidence circuit. The resolving time was set at 0.3 μsec. so that no coincidences would be lost due to the rise times of the linear amplifiers (about 0.17 μsec.).

To determine the absolute number of coincidences to be expected it is essential to know the absolute efficiency of the gamma-detector for quanta of different energies. From the weight and thickness of the anthracene crystal and the Klein-Nishina cross section, the number of recoil electrons produced in the crystal by gamma-rays of any energy can be calculated readily. While there is little doubt that this value is accurate to within about one percent, the uncertainty in the efficiency arises from the fact that only a fraction of these electrons is detected (the "detection efficiency").

For the gamma-counter used, and for gamma-rays from a Co^{60} source calibrated by the Bureau of Standards, it was determined that projecting the integral pulse-height curve back to zero pulse height gave rates which agreed with the calculated ones to within five percent. Some precautions to be observed in such absolute gamma-counting have been given previously.[8] From the pulse-height curve the fraction of recoil electrons detected at various other discriminator biases can therefore be determined, and amounted to 0.92 ±0.03 under the conditions used in the experiment. For these same conditions the absolute efficiency for annihilation radiation from Cu^{64} was measured by gamma-gamma-coincidence counting at 180°, and from the thickness of the crystal the detection efficiency was thereby calculated to be 0.70±0.03. This was in agreement with the value obtained from the integral pulse height curve for this energy, on the assumption that projecting the curve to zero pulse height gives 100 percent detection efficiency. Since this assumption was satisfied for these two energies, the detection efficiencies for other energies were calculated from their integral pulse-height curves.

Corrections were made for the Al sheath over the crystal. For the different positions of the foil the energy of the 2.62-Mev quanta after scattering into the gamma-counter varied from 1.2 to 1.8 Mev, and the detection efficiency from 0.92 to 0.95, while the absolute efficiency varied from 15.4 to 13 percent. In no part of the experiments did the results depend appreciably on the measurement of quanta with energies below that of annihilation radiation, for which the detection efficiencies were known only roughly.

IV. EXPERIMENTAL PROCEDURE

Measurement of the Background

The background coincidence rate without the foil in position is due to purely accidental coincidences, true coincidences due to cosmic rays and room background, and true coincidences from scattered quanta and recoil electrons produced at the mouth of the collimator or in the gas. The contributions of these different sources were determined and are given in Table I.

While it was not essential to the experiment to separate the background into its components, this was done with the purpose of deciding whether any further reduction in the background rate were possible. Attempts to reduce the contribution due to scattering from the collimator by reshaping the end of the hole and lining it with aluminum were unsuccessful.

Angular Distribution of Coincidences

The first experiment consisted in measuring the coincidence rate with the foil at various distances from the end of the collimator. For each foil position the coincidence rate was measured over a total period of 24 hr. or more to obtain between 1000 and 3000 coincidences. The constancy of the rates in the separate

TABLE I. Sources of background coincidences.

Source	Coincidences/hr.
Accidentals	0.5
Cosmic rays and room background	3.8
Scattering in helium	2.5
Scattering from collimator	7.5
Total	14.3

[7] W. H. Jordan and P. R. Bell, Rev. Sci. Inst. **18**, 703 (1947).
[8] W. G. Cross, Phys. Rev. **78**, 185 (1950).

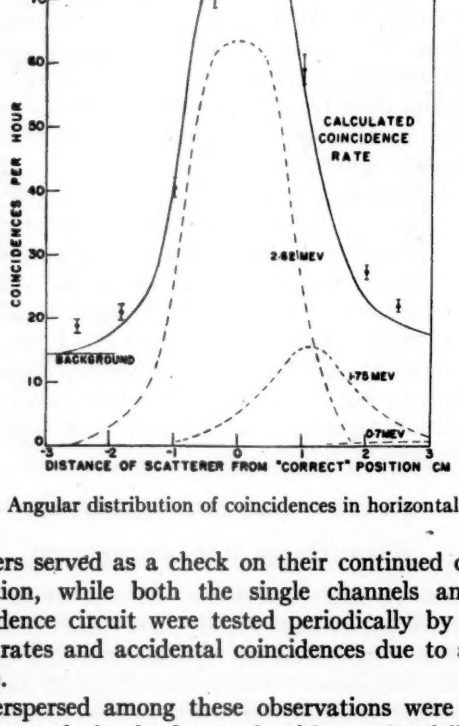

FIG. 2. Angular distribution of coincidences in horizontal plane.

counters served as a check on their continued correct operation, while both the single channels and the coincidence circuit were tested periodically by measuring rates and accidental coincidences due to a Co^{60} source.

Interspersed among these observations were measurements of the background without the foil. The resulting coincidence rates with their statistical errors are shown in Fig. 2. The full curve is the rate calculated as described later.

Coplanarity

To verify that the incident beam and scattered quantum and recoil electron directions lie in a plane, the foil was left in its correct position and the coincidence rate compared for the electron counter in its usual position and with its center raised 2.5 cm above the horizontal plane. Because about half of the background coincidences are due to scattering at the mouth of the collimator, the electrons so produced, and which correspond to quanta passing through the gamma-counter, would be expected to be concentrated in the horizontal plane. Raising the counter was consequently found to reduce the background by a factor of two. The rates obtained are given in Table II.

More Accurate Determination of the Recoil Angle

A third experiment was carried out to locate more accurately the peak of the coincidence distribution curve. For this purpose the method of leaving the counters fixed and moving the foil is not so suitable, since uncertainties in corrections which have to be made when this method is used might shift the peak of the curve by a small amount. Further, the effect of lower energy components in shifting the peak, is less when one of the counters is moved.

Accordingly the foil was left fixed and the electron counter rotated through about 2° on each side of the correct position. As expected, no appreciable variation in the background rate was found over this range. The coincidence rates (including background) with the foil in position and their statistical errors are given in Fig. 3. The individual angular settings may be in error by 0.4°.

The curve drawn in Fig. 3 is the calculated distribution with its maximum at 31.3°. Within the experimental error the measured maximum is in agreement with this value, and almost certainly cannot differ from it by more than 1°.

Simultaneity

In the previous experiments and in the discussion which follows it is shown that the expected number of electrons appear in the direction predicted by the conservation laws, simultaneous (within 0.3 μsec.) with the scattered photons. A fourth experiment was carried out to reduce the uncertainty in the simultaneity. This experiment was similar in principle to those of Bothe and Geiger and others[5] in that simultaneity alone was determined, and not the relative angles of the recoil electron and scattered photon. While simultaneity alone discriminates against the theory of Bohr, Kramers, and Slater, it does not by itself prove that energy and momentum are conserved.

For this experiment, Co^{60} gamma-quanta, collimated in a narrow beam were scattered from one anthracene counter crystal, which detected the recoil electrons, into a second anthracene counter whose output was set in coincidence with that of the first. The second crystal was covered with a plastic shield to make it insensitive to scattered electrons. The 1*P*21 photo-multiplier voltages were increased to 190 volts per stage so that no external amplification was necessary. Output pulses were limited in amplitude, shortened to 8×10^{-9} sec. with a delay-line clipper and fed into a crystal diode coincidence circuit. A delay of 1.5×10^{-8} sec. or more introduced into either channel (by adding lengths of coaxial cable) reduced the coincidence rate by a factor of fifty, the remaining coincidences being attributable to accidentals. Adding this delay in both channels decreased the coincidence rate by less than ten percent. The accidental rate was determined both by adding

TABLE II. Variation of coincidence rate with counter position.

Position of electron counter	Coincidences/hr.		
	No foil	Foil in position	Rate due to foil
In plane	14.3±0.6	83.0±1.4	68.7
2.5 cm above plane	7.3±0.5	23.7±1.0	16.4

long delays in one channel and by shielding the second counter from gamma-rays scattered by the first and restoring the original rate in the second counter by means of an additional small source. The experiment was carried out with the second counter at mean scattering angles of 45° and 70°.

The result, in agreement with the recent measurement of Hofstadter and McIntyre,[5] indicates that the recoil electrons produced in two separate, successive Compton scattering events are simultaneous within 1.5×10^{-8} sec. A consideration of the various possibilities shows that this requires that there be no delay (greater than 0.015 μsec.) between the arrival of the incident quantum and the emission of the scattered quantum. Further, except for the extremely unlikely possibility that the recoil electron is delayed by a fixed amount in *all* such events, the electrons must have been emitted simultaneous with the arrival of the incident quanta.

A similar but more accurate measurement of simultaneity has recently been made by Bell and Graham[9] of the Chalk River Laboratory, National Research Council of Canada. Using coincidence methods described previously[10] they have verified that for scattering of Co^{60} gamma-rays at 90°, the successive Compton recoil electrons are simultaneous to within less than 5×10^{-10} sec.

Determination of the Strength of the Beam

To calculate the coincidence rates to be expected in the first experiment it was necessary to know the number of 2.62 Mev quanta which struck the scattering foil per second. The strength of the gamma-beam was determined both by direct measurement and by calculation from the known strength of the source and the geometry of the collimator.

Direct measurement was made with a scintillation counter at the position of the foil. For a measured rate of 8420 counts/sec. corrections were necessary for counting losses in the scaler and for a pile-up effect which tended to increase the rate. The net magnitude of these effects was determined by comparing the rate due to two sources together with the sum of their separate rates. It was necessary to repeat this a number of times, the source strengths being progressively increased (so that at each stage the effect in the rate for a single source was known) until the total rate equaled that from the collimator. A further one percent of the measured rate may have been due to electrons from the collimator.

Of the remaining rate, the part due to 2.62-Mev quanta must be separated from that due to lower energy quanta in the beam. The gamma-ray spectrum[10a]

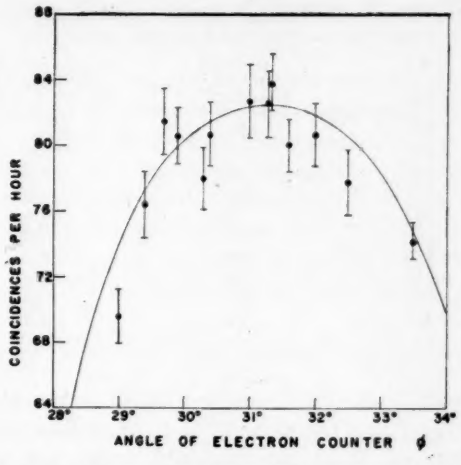

FIG. 3. More accurate determination of recoil angle.

of RaTh has been determined[11] both by direct measurements and by indirect information from alpha- and beta-spectra. While there is no general agreement on the relative intensities of the lines, and even some doubt as to whether some of the lines reported belong to the spectrum of Th*C* and its decay products, the intensities are probably known with sufficient accuracy for our purposes. From the available data we have selected the intensities given in Table III. Lines of energies lower than 0.510 Mev will be removed by the filtering. In addition, there may be a weak 3.2-Mev line, whose intensity is probably much less than one percent of the 2.62-Mev line.[12]

From the intensities given and the known efficiencies of the gamma-counter for the different energies, the fraction of the measured rate which was due to 2.62-Mev quanta was calculated to be 60 percent, and the beam strength to be 78,000 quanta per second of 2.62 Mev.

The strength of the source was determined (in April, 1949) by the Radiochemical Centre, Amersham, Bucks., to be 195 mg Ra equivalent when measured through 5 mm Pb. From the measurements of Shenstone and Schlund[13] and of Gurney[14] and using the branching ratio

[9] Private communication.

[10] R. E. Bell and H. E. Petch, Phys. Rev. **76**, 1409 (1949); R. E. Bell and R. L. Graham, Phys. Rev. **78**, 490 (1950); T. D. Newton, Phys. Rev. **78**, 490 (1950).

[10a] It is actually the spectrum of the active deposit from thoron which was measured in the experiments quoted. The transitions from RaTh to Th*B* are not believed to give rise to any gamma-rays with energies above 0.5 Mev.

[11] C. D. Ellis, Proc. Roy. Soc. **A138**, 318 (1932), **A143**, 350 (1933); D. V. Skobelzyn, Comptes Rendus **194**, 1486 (1932); F. Oppenheimer, Proc. Camb. Phil. Soc. **32**, 328 (1936); R. Arnoult, Ann. de physique **12**, 241 (1939); A. Flammersfeld, Zeits. f. Physik **114**, 227 (1939); Curran, Dee, and Strothers, Proc. Roy. Soc. **A174**, 546 (1940); J. Itoh and Y. Watase, Proc. Phys. Math. Soc. Japan **23**, 142 (1941); G. D. Latyshev and L. A. Kulchitsky, J. Phys. USSR **4**, 515 (1941); A. I. Alichanov and V. P. Dzelepov, Doklady **20**, 113 (1938); G. D. Latyshev, Rev. Mod. Phys. **19**, 132 (1947); A. Johansson, Arkiv. f. Mat. Ast. o. Fys. **34A**, No. 9 (1947); D. G. E. Martin and H. O. W. Richardson, Proc. Roy. Soc. **195A**, 287 (1948); Martin, Richardson, and Hsü, Proc. Phys. Soc. London **60**, 466 (1948); H. O. W. Richardson, Nature **161**, 516 (1948); D. G. E. Martin and H. O. W. Richardson, Proc. Phys. Soc. London **63**, 223 (1950).

[12] R. E. Bell and L. G. Elliott, Can. J. Research **26A**, 379 (1948).

[13] A. G. Shenstone and H. Schlund, Phil. Mag. **43**, 1038 (1922).

[14] R. W. Gurney, Proc. Roy. Soc. **A112**, 380 (1926).

TABLE III. Intensities in incident gamma-beam.

Energy	Assumed initial intensity	Relative intensity after filtration through 2 cm Pb
2.62	100	100
2.20	5	4.8
1.80	6	5.3
1.62	10	8.0
1.50	3.5	2.6
1.35	4	2.8
0.859	18	5.2
0.726	16	3.6
0.582	100	12.8
0.510	20	1.7

66:34 for[15] ThC′:ThC″, and 3.60×10^7 as the number of disintegrations per second[16] of 1 mg of Ra, 1 mg Ra equivalent of RaTh so measured emits per second 1.38×10^7 quanta of 2.62 Mev. This value is in close agreement with the calculations of Bouchez[17] based on measurements of the heating effect[18] and total ionization[19] of the alpha-particles from the active deposit of thoron.

The strength of the source was hence estimated to be (in September, 1949) 2.32×10^9 quanta per second of 2.62 Mev, and the strength of the beam 65,000 quanta per second of 2.62 Mev. Scattering in the collimator probably increased this value. In view of the uncertainties involved in the calculations of both these methods, we do not consider these to be in disagreement, and believe that the value which will be used—73,000 quanta per second of 2.62 Mev—can be relied upon only to within ten percent.

V. DISCUSSION

In these experiments it has been shown clearly that there are many more coincidences in the direction predicted by the conservation laws than for other directions. There remains to be explained quantitatively the observed width of the angular distribution of coincidences, and the absolute coincidence rate for the correct position. Contributing factors to this width will be scattering of the electrons in the foil and gas, coincidences produced by other energy components in the gamma-spectrum of RaTh, and to a small extent, the finite width of the initial gamma-beam.

For each position of the foil the absolute rate in the gamma-counter due to 2.62-Mev quanta scattered from the foil is

$$R_\gamma = N\sigma(\theta)t\Omega\epsilon_\theta, \qquad (2)$$

where N is the strength of the incident gamma-beam in 2.62-Mev quanta per second, $\sigma(\theta)$ the Compton scattering coefficient per unit solid angle (at angle θ) per cm of Be, t the thickness of the Be foil in cm, Ω the solid angle subtended by the counter at the foil, and ϵ_θ the absolute efficiency of the gamma-counter for the gamma-energy corresponding to scattering of 2.62-Mev quanta through an angle θ. A similar expression gives the contribution of the Pliofilm support.

To these quanta corresponds a cone of electrons. For an "ideal" experiment the electron counter in the correct direction would just intercept all of this cone and the coincidence rate would equal R_γ. When the electron counter is at other angles the coincidence rate would be multiplied by the fraction of the cone intercepted by the counter. Because of electron scattering, lower energy gamma-rays and geometrical factors the rate will be altered.

In the Appendix is calculated an expression for the fraction $f_h f_v$ of this electron cone which, due to scattering of the electrons, actually enters the electron counter when the latter is at an angle η from the "correct" angle. $R_\gamma f_h f_v$ then gives the theoretical rate for a particular foil position and for the 2.62-Mev quanta. For each foil position used in the experiment, this calculation should in principle be repeated for each energy component present in the initial gamma-beam, the result multiplied by the component's intensity, and summed over all components. Because of the length of these calculations we have replaced the numerous lower energy components (given in Table III) with two fictitious "equivalent" lines at 1.75 and 0.70 Mev and with respective intensities 24 and 23 percent of the main line, and for each foil position have summed the rates due to these three components. The resulting curve is given in Fig. 2 where are also plotted the separate contributions of the three components.

In these calculations we have neglected the effect of the finite size and divergence of the incident gamma-beam. The resultant calculated distribution is therefore slightly too narrow. However, for the correct position of the foil the effect of beam size has been included. [The value of f_h is now given by putting $\eta=0$ in Eq. (I-4) of the Appendix.] For our conditions these equations lead to a value of $f_h f_v$ which is four percent lower than was obtained when the size of the incident beam was neglected. For this position about 38 percent of the true coincidences are lost due to electron scattering.

Finally, we must consider the loss of coincidences due to the fact that the cone of electrons which corresponds to quanta passing through the gamma-counter does not have a rectangular cross section (as the electron counter does) but is distorted. For the correct position of the foil this distortion was calculated to result in a four percent loss. In Fig. 4 is shown the shape of this distorted area. To show the deformation more clearly a gamma-area almost twice the width of our gamma-counter has been drawn. The distribution in the experiment will differ from a rectangle by a smaller amount than is shown. For other positions of the foil this

[15] L. Meitner and K. Freitag, Zeits. f. Physik **37**, 481 (1926); R. Gregoire, Ann. de physique **2**, 161 (1934); A. F. Kovarick and N. I. Adams, Jr., Phys. Rev. **54**, 413 (1938).
[16] T. P. Kohman *et al.*, MDDC 852 (unpublished).
[17] R. Bouchez, J. de phys. et rad. **10**, 415 (1949).
[18] L. Winand, J. de phys. et rad. **10**, 361 (1939).
[19] A. Ricoux, J. de phys. et rad. **8**, 388 (1937).

distortion will be somewhat increased, resulting in the loss of more coincidences and making the actual coincidence distribution slightly narrower than the calculated one.

Comparison between Calculated and Measured Coincidence Rates

The calculated value for the absolute coincidence rate, for the electron counter in the correct position, was 74.5 coincidences per hour: the observed rate was 68.7 ± 1.5. The most important uncertainties in the calculated absolute rate lie in the determination of the beam strength (ten percent), in the efficiency of the gamma-counter (five percent), and in the correction for scattering of the electrons (three to four percent). While it is difficult to assign a probable error to some of these calculations we believe that the estimated value would not be in error by more than 15 percent. Within this error, therefore, the expected number of recoil electrons was emitted at the angle predicted by the conservation laws. The uncertainty provides an upper limit on the fraction of the electrons which could be emitted in other directions.

Turning now to the angular distribution of coincident electrons, in Fig. 2 we have not shown the absolute calculated values but have multiplied these by 68.7/74.5 in order to make the curve agree with the experimental value for the correct position of the foil. This was done so that the shape of the experimental and theoretical distributions could be compared, irrespective of the errors in the absolute value of the latter. In the calculation of electron scattering in the foil, the neglect of the finite width of the gamma-beam and the use of a mean foil thickness rather than averaging the expressions obtained over the thickness of the foil (see Appendix) both make the calculated distribution too narrow at larger angles of scattering. A wider distribution would also have resulted had we used Molière's theory of multiple scattering[20] (which for angles greater than the mean scattering angle is probably more correct than that of Williams) rather than Williams' theory[20] as a basis for the calculations of electron scattering. On the other hand, neglecting the distortion of the electron cone from a rectangular cross section will tend to make our calculated curve wider than it should be. In all the calculations the gamma-counter crystal has been treated as being concentrated all at the same distance from the foil. Actually some quanta whose directions do not pass through this cross section of the counter can be counted in the front half of the crystal. This will further broaden the lower part of the experimental distribution.

[20] W. Bothe, *Handbuch der Physik* (1933), Bd. XXII/2, p. 17; Bethe, Rose, and Smith, Proc. Am. Phil. Soc. **78**, 573 (1938); E. J. Williams, Proc. Roy. Soc. **169A**, 531 (1939), Phys. Rev. **58**, 292 (1940); S. Goudsmidt and J. L. Saunderson, Phys. Rev. **57**, 24 (1940), **58**, 36 (1940); B. Rossi and K. Greisen, Rev. Mod. Phys. **13**, 240 (1941); A. F. Kompaneetz, J. Phys. USSR. **9**, 17 (1944); G. Molière, Zeits. f. Naturforschung **3a**, 78 (1948); W. T. Scott, Phys. Rev. **76**, 212 (1949); H. S. Snyder and W. T. Scott, Phys. Rev. **76**, 220 (1949).

Considering these errors, as well as the uncertainties in the theory of scattering of electrons and in the energy spectrum of RaTh gamma-rays, the agreement between the calculated and experimental distributions is better than we probably have a right to expect, and is certainly well within the errors of calculation. By choosing intensities for the lower energy lines of RaTh and its decay products other than are given in Table III but still consistent with values given in the literature, the agreement can be made slightly better or worse than is shown in Fig. 2.

When in the second experiment the electron counter was moved out of the plane, the coincidence rate dropped to less than one quarter of what it had been for the counter in the plane. This rate, however, is still twice as large as was calculated. We do not know the cause of this discrepancy: unfortunately it was not discovered until after it was impossible to repeat the experiment. Since close to the calculated number of coincidences was observed in the correct position, this indicates an inconsistency between the second experiment and the others rather than a definite disagreement with the conservation laws.

VI. CONCLUSIONS

The experiments described have shown that in Compton scattering: (1) the peak of the angular distribution of electrons coincident with quanta scattered in a given direction is in the direction required by the conservation laws within $\pm1°$; (2) the observed width of the angular distribution about the predicted direction (about 14° total at half-maximum) can be accounted for quantitatively by the scattering of the electrons in the foil, by the components of other energies in the incident gamma-beam, and by small geometrical factors; (3) the scattered quantum and recoil electron are both emitted within 1.5×10^{-8} sec. of the time the incident quantum arrives at the scattering center.

The results therefore indicate that certainly in most Compton encounters simultaneity and the conservation laws are satisfied within the limits indicated above.

We are grateful to Drs. R. W. Birge, D. Bodansky and L. S. Lavatelli for suggestions and assistance.

APPENDIX: SCATTERING OF ELECTRONS IN THE GAS AND SCATTERING FOIL

Expressions for the angular distribution of a collimated beam of monoenergetic electrons after multiple scattering have been

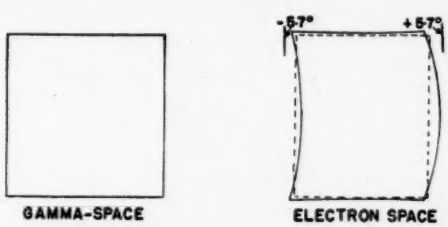

FIG. 4. Corresponding areas in gamma- and electron space.

given by a number of authors.[20] For angles less than the mean scattering angle the distribution is essentially Gaussian and its width can be conveniently characterized by the "half-width" Δ, that angle at which the intensity is down to $1/e$ of its maximum. For the conditions of our experiment—electrons of about 1 Mev and a Be scatterer of effective thickness about 17 mg/cm², the values of Δ given by nearly all these theories agree to within about ten percent and are also within ten percent of the measured values.[21] We shall use a Gaussian distribution with Δ as given by Williams,[20] according to which the probability of the projection of the scattering angle in the horizontal plane lying between ϕ and $\phi+d\phi$ after multiple scattering is

$$P(\phi)d\phi=(2/\Delta\pi^{\frac{1}{2}})\exp[-(\phi/\Delta)^2]d\phi, \quad \text{(I-1)}$$

where Δ depends on the atomic number and thickness of the foil and on the energy of the electrons. It can be shown that for our conditions the effect of scattering of the electrons in the helium is equivalent to increasing the half-width Δ of the scattering foil by about one percent.

Consider first only the horizontal components of the directions of electrons. Neglecting, temporarily, the finite width of the initial gamma-beam, the number of the recoil electrons which correspond to quanta which pass through the gamma-counter, and which are scattered by the foil into $d\alpha$ at angle α, is

$$F(\alpha)d\alpha=[erf((\alpha+\omega)/\Delta)-erf((\alpha-\omega)/\Delta)]d\alpha/4\omega, \quad \text{(I-2)}$$

where

$$erfx\equiv 2/\pi^{\frac{1}{2}}\int_0^x \exp(-t^2)dt,$$

and ω is the horizontal semi-angle in electron space which corresponds [according to Eq. (1)] to the boundaries of the gamma-counter. This gives the angular distribution of the electron beam about its mean direction. If now the center line of the electron counter is not on the center line of the beam but off by a distance which at the foil subtends an angle η (the "error angle"), the fraction f_h of the electron directions whose horizontal components lie within the boundaries $\eta\pm\omega_\beta$ of the electron counter is given by integrating $F(\alpha)$;

$$f_h=\frac{\Delta}{8\omega}\left\{ierf\left(\frac{\eta+\omega+\omega_\beta}{\Delta}\right)+ierf\left(\frac{\eta-\omega-\omega_\beta}{\Delta}\right)-ierf\left(\frac{\eta+\omega-\omega_\beta}{\Delta}\right)-ierf\left(\frac{\eta-\omega+\omega_\beta}{\Delta}\right)\right\}, \quad \text{(I-3)}$$

where we define

$$ierf(x)=\int_0^x erf(t)dt=xerf(x)+\frac{\exp(-x^2)-1}{\pi^{\frac{1}{2}}}.$$

The fraction of the electrons whose vertical direction components lie within the boundaries of the electron counter is given by a similar expression, but with η, ω, and ω_β referring to vertical angles. The relation between vertical angles in electron and gamma-space is not given by Eq. (1), as is the relation for horizontal angles. For θ and ϕ almost equal (as they are) the approximation that a 1° vertical angle in gamma space corresponds to a 1° vertical angle in electron space is not greatly in error and has been used.

To take account of the fact that electrons are produced at different depths in the foil, Eq. (I-3) must be averaged over the thickness of the foil. Taking Δ_x, the half-width for electrons produced at depth x to be proportional to $x^{\frac{1}{2}}$, leads to an expression in the second integral of the error function. We have evaluated this expression and find that the result differs by only a few percent from that obtained by using in Eq. (I-3) a half-width corresponding to a mean foil thickness $4d/9$, where d is the actual thickness.

In now taking into account the finite size of the scattering foil and the angular divergence of the incident beam we have assumed, to simplify the calculations, that the beam has a square, rather than circular, cross section. The intensity distribution of the electron beam in the horizontal plane (before scattering) corresponding to quanta entering the gamma-counter can then be shown to be approximately

$$\begin{cases} d\phi/2\omega & \text{for } \phi<y \\ (d\phi/2\omega)(z-\phi)/(z-y) & \text{for } y<\phi<z \\ 0 & \text{for } \phi>z, \end{cases}$$

where y and z are constant angles, determined by the width and divergence of the incident beam, by the angles subtended by the gamma-counter at the foil and by the cross section of the beam at the gamma-counter, and by the mean angles of the electron and gamma-counter.

The fraction f_h of the electron directions whose horizontal components lie within the boundaries of the electron counter then becomes

$$f_h=\frac{\Delta}{y^2-z^2}\left\{iierf\left(\frac{z+\eta+\omega_\beta}{\Delta}\right)-iierf\left(\frac{z+\eta-\omega_\beta}{\Delta}\right)-iierf\left(\frac{z-\eta-\omega_\beta}{\Delta}\right)+iierf\left(\frac{z-\eta+\omega_\beta}{\Delta}\right)-iierf\left(\frac{y+\eta+\omega_\beta}{\Delta}\right)+iierf\left(\frac{y+\eta-\omega_\beta}{\Delta}\right)+iierf\left(\frac{y-\eta-\omega_\beta}{\Delta}\right)-iierf\left(\frac{y-\eta+\omega_\beta}{\Delta}\right)\right\}, \quad \text{(I-4)}$$

where

$$iierfx\equiv\int_0^x ierf(t)dt,$$

which for our geometry gives a result two percent lower than does Eq. (I-3). Because of the length of the calculation and the fact that the difference is small, these expressions were not averaged over the depth of the foil, but a mean thickness $4d/9$ was used in calculating Δ.

[21] C. W. Sheppard and W. A. Fowler, Phys. Rev. **57**, 273 (1940); M. M. Slawsky and H. R. Crane, Phys. Rev. **56**, 1203 (1939); Oleson, Chao, and Crane, Phys. Rev. **60**, 378 (1941); L. A. Kulchitsky and G. D. Latyshev, J. Phys. USSR **5**, 249 (1941); Andrievsky, Kulchitsky, and Latyshev, J. Phys. USSR **6**, 278 (1942).

Auger Effect in Astatine*

LAWRENCE S. GERMAIN†
Radiation Laboratory, Department of Physics, University of California, Berkeley, California
(Received July 28, 1950)

The K-capture decay of At^{211} has been studied using photographic emulsions. The number of Auger electrons per K shell vacated, defined as the Auger coefficient, has been found to be 0.106. This value is somewhat higher than that calculated from theory. Bi^{207}, which arises from the alpha-decay of At^{211}, was observed to decay by K-capture.

I. INTRODUCTION

THE Auger effect associated with orbital electron capture can be described briefly as follows. An orbital electron capture process is followed by x-rays which arise from the filling of the K shell and to a lesser extent L, M, etc. shell vacancies. However, some of these x-rays are not observed but are internally converted, producing a photo-electron within the atom which emitted the x-ray (Auger electron).

For brevity, let us define the number of Auger electrons per K shell vacated as the Auger coefficient. This quantity, which is one minus the fluorescence yield, has been found for many K-capture decays. Both experimental and theoretical results show a high Auger coefficient for elements of low atomic number, falling off with increasing atomic number.[1] However, no experimental results are quoted for $Z>60$. It is, therefore, of interest to measure the Auger coefficient for some element in this region.

It was suggested by Segrè that a study of the decay of At^{211} by impregnating photographic plates with At^{211} would offer a good opportunity for finding the Auger coefficient of its daughter Po^{211}. The decay scheme[2] at At^{211} is shown in Fig. 1. Since the alpha-decay of $Po^{211}(AcC')$ occurs with a half-life of a few milliseconds, any At^{211} orbital electron capture is followed immediately by an alpha-emission of Po^{211}. At the starting point of this alpha-particle we know that a K or L shell of Po has been vacated. It is true that the alpha-particles of the dual decay of At^{211} will also be present and at their origin no K shell has been vacated. However, these two alpha-particles have considerably different ranges, and one can identify each alpha-particle by measuring its range. For example, in a photographic emulsion, the range of a Po^{211} alpha-particle is 37 microns while the range of an At^{211} alpha-particle is 27 microns. Thus, to measure the Auger coefficient one need only count the number of Po^{211} alpha-tracks and the number of such tracks which have at their starting point an electron track of the proper energy to have come from a K x-ray conversion. Most of the conversion electrons would be knocked out of the L shell. Therefore, they should have a kinetic energy equal to the K x-ray energy less the binding energy of the L electron. For Po this kinetic energy is 59 kev.

II. PROCEDURE

Eastman NTB-3 electron-sensitive plates were chosen for this experiment since the conversion electrons were certain to be visible in these plates. Since these plates are sensitive to particles of all energies, all particles entering the plate after the emulsion has been placed on the plate will be recorded. Thus, the plates soon acquire a considerable number of background tracks. It is desirable to remove all old background tracks before using the plates. Following a procedure recommended by the Eastman-Kodak Company,[3] the plates were placed in a high humidity atmosphere at 35°C for 20 hr. before use. About 80 percent of the old tracks were removed by this process.

At^{211} was made by bombarding Bi with 30-Mev alpha-particles from the 184-inch cyclotron. At 30 Mev, the excitation function for the formation of At^{211} by an $(\alpha,2n)$ reaction is at a maximum, while the threshold for the formation of At^{210} by an $(\alpha,3n)$ reaction[4] is also

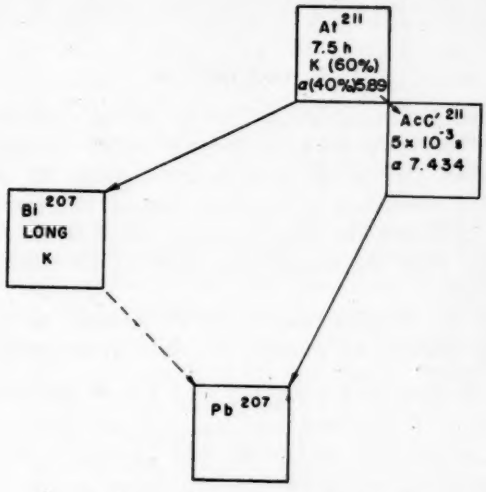

FIG. 1. Decay scheme of At^{211}.

* The work described in this paper was done under the auspices of the AEC.
† Now at Reed College, Portland, Oregon.
[1] H. S. W. Massey and E. H. S. Burhop, Proc. Roy. Soc. A153, 661 (1936).
[2] Corson, MacKenzie, and Segrè, Phys. Rev. 58, 672 (1940).
[3] Private communication.
[4] E. L. Kelly and E. Segrè, Phys. Rev. 75, 999 (1949).

30 Mev. The At was separated chemically upon the conclusion of the bombardment. The At, in a water solution, was placed on the surface of several plates which were then dried within an hour. It is necessary that nearly all of the decays occur in a dry plate. In the first place, wet plates suffer from a loss of sensitivity. Furthermore, it was found that it was impossible to distinguish Po^{211} alpha-particles from At^{211} alpha-particles if many of the decays occurred when the emulsion was wet. Wet plates are considerably swollen, and the range of the decay particle is longer than it would be in a dry emulsion. Since the experiment depended upon being able to distinguish these alpha-particles, the plates had to be dry before an appreciable number of decays occurred. Measurement of the ranges of the alpha-particles found in the plates showed two well-defined groups of particles with ranges of the Po^{211} and the At^{211} alpha-particles. The absence of particles of greater ranges showed that the drying had been accomplished in a sufficiently short time. The plates were allowed to rest eight hours before being developed.

III. RESULTS

In the process of scanning the At loaded plates, fields of view were selected at random and each alpha-track which was completely in the field of view was examined and counted provided that another alpha-track did not obscure one of the ends of the alpha-track. A total of 1849 Po^{211} alpha-tracks were examined and 171 of these were found to have Auger electrons at one end. This would lead one to a value of $171/1849=0.0925$ for the Auger coefficient. However, Rose and Jackson[5] have calculated that for an element in this region of the periodic table the ratio of L-capture to K-capture is 0.15. Correcting for the cases of L-capture one obtains a value of 0.106 ± 0.005 for the Auger coefficient, and the fluorescence yield is 0.894 ± 0.005. The error stated is the probable error based on the number of counts taken.

IV. DISCUSSION

Theoretical calculations[1] predict about 0.06 for the Auger coefficient for an element of atomic number 84. However, the calculations do not consider all of the possible transitions in an exact manner, and are made with hydrogen-like eigenfunctions; a deviation of 50 percent from the theoretical results is not out of the question.

Let us consider the activities present in an At loaded plate to see whether any of them can cause any confusion in the measurement of the Auger coefficient. The chemical separation should rule out all activities other than those of astatine. At^{210}, At^{211}, and At^{212} may be formed during the bombardment. However, At^{212} decays with a 0.25-sec. half-life and would all decay in the short time between the bombardment and the separation. A small amount of At^{210} was present because of a spread in the cyclotron beam energy giving some alpha-particles with an energy greater than 30 Mev, the threshold for the formation of At^{210}. At^{210} decays by K-capture with an 8.3-hr. half-life giving Po^{210}, a 140-day alpha-emitter. The Po^{210} alpha-particles can be easily distinguished from the Po^{211} alpha-particles because of their different ranges, and any Auger electron background which may be present will cause little trouble since, in order to be counted, the end of the Auger electron must coincide with the end of a Po^{211} alpha-particle track. The probability for such an event to occur by chance is negligible. Bi^{207} is also produced in the plate by the alpha-decay at At^{211}. While the activity of Bi^{207} has not been reported it is expected that it decays by K-capture and has a long half-life. None of these activities interfere with observations of the Auger effect in the decay at At^{211}.

V. ACTIVITY OF Bi^{207}

Since the activity of Bi^{207} has not been reported, it was considered worth while to attempt to detect the activity with photographic plates. NTB-3 emulsions loaded with the At solution 10 days after the bombardment and chemical separation showed many Auger electrons. After 10 days, the activities of At^{210} and At^{211} would be only 10^{-10} of the original activities. Thus, these Auger electrons must have come from a daughter activity. The possible daughters are Pb^{207}, Po^{210}, and Bi^{207}. It is known that Pb^{207} is stable and Po^{210} is an alpha-emitter. Therefore, these Auger electrons in all probability have come from the K-capture decay of Bi^{207}. Furthermore, the only alpha-particles found on the plate were those of Po^{210} (these coming from the decay of At^{210}). Therefore, one can conclude that Bi^{207} decays by K-capture and its half-life is very long, probably several years. This follows not only from the fact that past experiments failed to detect its activity but also from the fact that the activity was allowed to decay in the plate for a week before a workable number of tracks grew in the plate.

The author is indebted to Professor Segrè, Dr. Eugene Gardner, and Dr. Hugh Bradner for many helpful discussions. The chemical separation of the At was done by Dr. R. F. Leininger.

[5] M. E. Rose and J. L. Jackson, Phys. Rev. **76**, 1540 (1949).

An Experimental Verification of the Theory of Compound Nucleus*

S. N. GHOSHAL†
Radiation Laboratory, Department of Physics, University of California, Berkeley, California
(Received July 28, 1950)

The compound nucleus Zn^{64} was formed by bombarding Ni^{60} with α-particles and Cu^{63} with protons. The ratios of the cross sections $\sigma(\alpha,n):\sigma(\alpha,2n):\sigma(\alpha,pn)$ for Ni^{60} were found to agree with the ratios $\sigma(p,n):\sigma(p,2n):\sigma(p,pn)$ for Cu^{63}, giving a direct verification of the theory of compound nucleus. The observed cross sections for the (p,n), $(p,2n)$, and (p,pn) reactions on Cu^{63} and (α,n), $(\alpha,2n)$, and (α,pn) reactions on Ni^{60} have been compared with the theoretical cross sections calculated on the basis of the statistical model. The observed anomalous behavior of the (p,pn) and (α,pn) cross sections with respect to the $(p,2n)$ and $(\alpha,2n)$ cross sections respectively are discussed.

I. INTRODUCTION

THE present theories of nuclear reactions, for not too high an excitation ($<\sim$100 Mev), are based on the famous compound nucleus assumption of Bohr.[1] According to this assumption a nuclear reaction proceeds in two stages: first, the formation of a quasi-stable compound nucleus through the absorption of the incident particle by the target nucleus; second, the disintegration of the compound nucleus by the emission of either the original incident particle (scattering) or the emission of another particle or a photon. For fairly heavy nuclei ($Z>30$), the intermediate compound state has a mean life which is long compared with the time a nucleon takes to cross the nucleus ($\sim 10^{-21}$ to 10^{-22} sec.). As a result of the comparatively long mean life of the compound state, the second process is independent of the first. This permits us to express the cross section of a reaction of the type $A+a\rightarrow C^*\rightarrow B+b$ in the following manner:[2]

$$\sigma(a,b)=\sigma_a(\epsilon)\eta_b(E), \qquad (1)$$

where $\sigma_a(\epsilon)$ is the cross section for the absorption of the particle a of kinetic energy ϵ by the target nucleus A to form the compound state C^*. $\eta_b(E)$ is the probability of disintegration of C^* into the final state $B+b$. $E=\epsilon+B_a$ is the excitation energy of the compound state C^*, B_a being the binding energy of the particle a to the target nucleus A.

If the compound nucleus C^* is now formed in the same state of excitation by another process $A'+a'$, the cross section for disintegration into the same final state, $B+b$, will be given by

$$\sigma(a',b)=\sigma_{a'}(\epsilon')\eta_b(E),$$

where ϵ' is the kinetic energy of the incident particle a'. Because of the differences in the binding energies between the two cases, ϵ' will be different from the kinetic energy ϵ of a of the previous case. $\eta_b(E)$ will be the same in the two cases, because of the basic assumption that the mode of decay of the compound nucleus C^* is independent of the mode of its formation.

If C^* decays into a different final state, $D+d$, the corresponding cross sections will be given by $\sigma(a,d)=\sigma_a(\epsilon)\eta_d(E)$, $\sigma(a',d)=\sigma_{a'}(\epsilon')\eta_d(E)$. Hence we have

$$\sigma(a,b)/\sigma(a,d)=\eta_b(E)/\eta_d(E)=\sigma(a',b)/\sigma(a',d). \qquad (2)$$

An experimental verification of the relationship (2) constitutes a direct test for the validity of Bohr's compound nucleus assumption.

II. EXPERIMENTAL METHOD

In the present experiment the compound nucleus Zn^{64} was formed by alpha-bombardment of Ni^{60} and proton bombardment of Cu^{63}. The following reactions were studied:

$$\left.\begin{matrix}Ni^{60}(\alpha,n)\\ Cu^{63}(p,n)\end{matrix}\right\}Zn^{63};\quad \left.\begin{matrix}Ni^{60}(\alpha,2n)\\ Cu^{63}(p,2n)\end{matrix}\right\}Zn^{62};\quad \left.\begin{matrix}Ni^{60}(\alpha,pn)\\ Cu^{63}(p,pn)\end{matrix}\right\}Cu^{62}.$$

The excitation curves were determined by the usual stacked foil method. The alpha excitation curves were obtained by the same procedure as was followed by Kelly and Segrè,[3] using the 40 Mev alpha-beam from the 60-inch cyclotron. The proton excitation curves were determined by using the 32-Mev proton beam from the Berkeley linear accelerator. The method used in this case was essentially the same as in the determination of the alpha excitation curves, differing only in slight details.

In the case of the nickel experiment, thin foils of enriched Ni^{60} were prepared by electroplating the nickel on to copper; the copper was then dissolved by $AgNO_3$ solution. The abundance of Ni^{60} in the enriched sample was more than 85 percent. Since the exact value of this abundance was not known, this value was used in deriving the cross sections. No activity ascribable to other nickel isotopes outside of Ni^{60} was observed. Ni^{61} would produce the isotopes studied, but only at higher excitation energies. In view of its low abundance, its effect in the present experiment will be small, and therefore has been neglected.

* This work was sponsored by the AEC.
† Present address: Institute of Nuclear Physics, Science College, Calcutta, India.
[1] N. Bohr, Nature **137**, 344 (1936).
[2] Lecture Series in Nuclear Physics, U. S. Government Printing Office (MDDC-1175), (1947).
[3] E. L. Kelly and E. Segrè, Phys. Rev. **75**, 999 (1949).

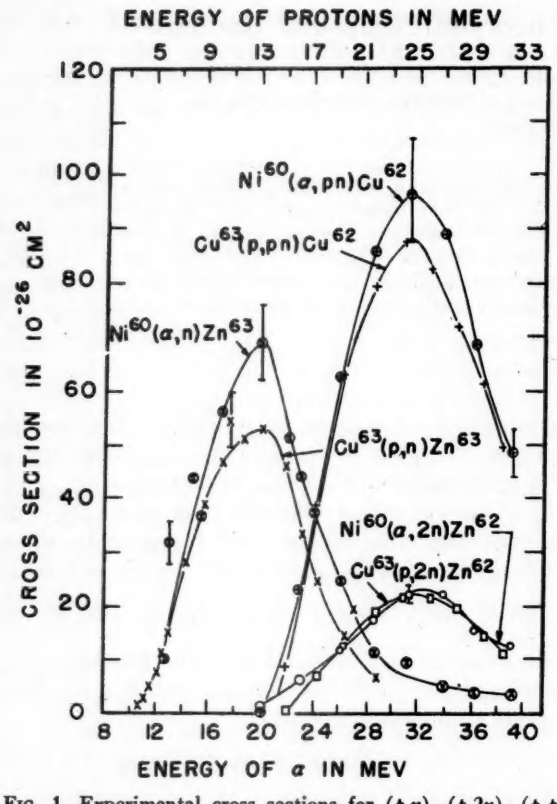

FIG. 1. Experimental cross sections for (p,n), $(p,2n)$, (p,pn) reactions on Cu^{63} and for (α,n), $(\alpha,2n)$, (α,pn) reactions on Ni^{60} plotted against ϵ_p and ϵ_α respectively. The scale of ϵ_p has been shifted by 7 Mev with respect to the scale of ϵ_α.

In the case of the Cu+H[1] experiment, ordinary copper, consisting of Cu^{63} (69.1 percent) and Cu^{65} (30.9 percent) was used. Cu^{65} produces the 250-day Zn^{65} and the 12.8 hr. Cu^{64} activities by proton bombardment. The activity due to the former is negligible. The Cu^{64} activity, however, interferes with the measurement of the 9.5-hr. activity of Zn^{62}. This difficulty was eliminated in the present experiment by the use of a 300 mg/cm^2 aluminum absorber in front of the counter. The radiations from Cu^{64} were stopped completely by this absorber; but the radiations from the isotopes studied were only reduced by factors of 2 or 3.

The activities of the various isotopes studied in the present experiment were determined on an absolute scale by means of a counter with a known geometry. This was possible because of the fact that all the activities studied consisted of relatively high energy positrons. Approximately 85 percent of the time Zn^{63} decays with the half-life of 38 min. by the emission of a positron of 2.3-Mev end point. It has two softer positrons (1.5 Mev, 7 percent; 0.5 Mev, 1 percent) and also decays by K-capture 7 percent of the time.[4] Cu^{62} decays with a half-life[5] of 10.5 min. with the emission of a positron[6] of end point 2.92-Mev. Zn^{62} decays with a half-life of 9.5 hr. into Cu^{62}, predominantly by K-capture (>90 percent). It decays by a softer positron emission (0.65 Mev) the rest of the time.[6] Assuming a very small efficiency for the detection of the x-rays following the K-capture, as compared with the positrons, the observed activity of Zn^{62} will consist primarily of the 3-Mev positrons from its daughter, Cu^{62}. Since the absorption and scattering of these positrons of high energy in a thin window counter is small and can be accounted for, it is possible to determine their absolute number by means of a counter with a known geometry. The counter used had a 2.3 mg/cm^2 mica window and was placed at a distance of 10 inches from the source, the intervening space being evacuated. Four carbon baffles with openings of increasing diameter between the source and the counter prevented scattered positrons from reaching the counter.

The excitation curves of all three isotopes studied were determined simultaneously. As mentioned previously, a 300 mg/cm^2 aluminum absorber was used to absorb the radiations from Cu^{64}. The Zn^{62} and Cu^{62} excitation curves could thus be directly compared, since they are measured through the same radiation. The Zn^{63} excitation curve was obtained on a scale relative to the other two by counting the chemically separated zinc fraction and comparing the Zn^{62} and Zn^{63} activities. The similarity of the radiations of Zn^{62} and Zn^{63} makes this comparison possible. Finally a thin Ni^{60} foil irradiated with α-particles of one specific energy was used to determine the absolute activity of Zn^{62} by the method described above. This was done several hours after the bombardment, so that only the 9.5-hr. Zn^{62} activity was present.

III. EXPERIMENTAL RESULTS AND DISCUSSION

The experimental results are shown in Fig. 1, where the observed cross sections for (α,n), $(\alpha,2n)$, (α,pn) reactions on Ni^{60} and (p,n), $(p,2n)$, (p,pn) reactions on Cu^{63} are plotted as functions of the kinetic energy of the α-particles and protons respectively. The proton energy scale has been shifted by 7 Mev with respect to the alpha-energy scale in order to bring the peaks of the proton curves into approximate correspondence with those of the alpha-curves. It is clear from this figure that the ratios $\sigma(\alpha,n):\sigma(\alpha,2n):\sigma(\alpha,pn)$ for Ni^{60} agree, within the limits of experimental errors, with the ratios $\sigma(p,n):\sigma(p,2n):\sigma(p,pn)$ for Cu^{63}. This agreement, according to relationship (2), provides a direct test for the validity of the compound nucleus assumption.

The kinetic energy ϵ_p of the proton required to produce a given excitation E of the compound nucleus Zn^{64} will be different from the kinetic energy ϵ_α of the α-particle to produce the same excitation in Zn^{64}. This difference is due to the difference in the masses of $Cu^{63}+H^1$ and $Ni^{60}+He^4$. From Fig. 1, we find that its

[4] Huber, Medicus, Preiswerk, and Steffen, Helv. Phys. Acta 20, 495 (1947).
[5] F. A. Heyn, Physica 4, 1224 (1937).
[6] R. Hayward, Phys. Rev. 79, 541 (1950).

value is about 7±1 Mev. Mass-spectrographic measurements by Duckworth *et al.* give a value of 5.74±0.5 Mev for this difference.[7] The two values agree within limits of experimental errors.

If the three reactions studied were the only ones which take place when Cu^{63} is bombarded with protons then the sum of the observed cross sections should give $\sigma_p(\epsilon_p)$, the cross section for the absorption of a proton by the Cu^{63} nucleus to form Zn^{64}. The sum of the observed alpha-cross sections should similarly give $\sigma_\alpha(\epsilon_\alpha)$. The sum of the observed proton and alpha-cross sections are plotted in Figs. 2 and 3 respectively, and are compared with the theoretical values calculated by Weisskopf.[2] It is seen from Fig. 2 that the experimental curve for the total proton cross section shows a point of inflection at a proton energy of about 14 Mev. A similar inflection is shown by the total alpha-cross-section curve in Fig. 3. It is clear from the inflections in the experimental curves that some reactions have not been observed at low energies. When the cross sections for these reactions are added to the experimental curves in Figs. 2 and 3 they should give smoothly increasing curves as required by the theory. It seems reasonable to ascribe the unobserved reactions to a process involving the emission of a proton, which should be prominent in this energy region. In Fig. 2, the unobserved reaction is the inelastic (p,p) scattering while in Fig. 3, it is the (α,p) reaction. The cross sections $\sigma(p,n)$ and $\sigma_{\text{inel}}(p,p)$ have been calculated on the basis of the statistical model,[2] and are compared with the experimental $\sigma(p,n)$ curve for the $Cu^{63}(p,n)Zn^{63}$ process in Fig. 4. The cross sections have been calculated for two values of the nuclear radius, $r=r_0A^{\frac{1}{3}}$ cm, with $r_0=1.3\times10^{-13}$ and $r_0=1.5\times10^{-13}$ respectively. Neither of the values agree well with the experimental results, which lie in between the two.[8] This is also the case with total cross sections as seen from Figs. 2 and 3.

At higher alpha- and proton energies reactions involving the emission of two or more particles become more and more probable and processes involving one particle emission go down. This is seen in Fig. 1. One

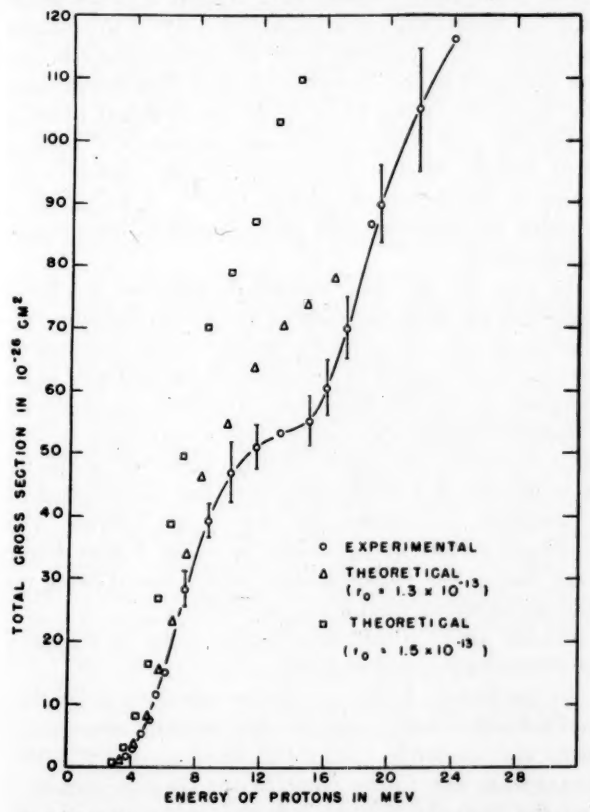

FIG. 2. Total cross section which is the sum of (p,n), $(p,2n)$ and (p,pn) cross sections on Cu^{63} as determined experimentally is compared with theoretical σ_p which is the cross section for the absorption of a proton by Cu^{63} nucleus.

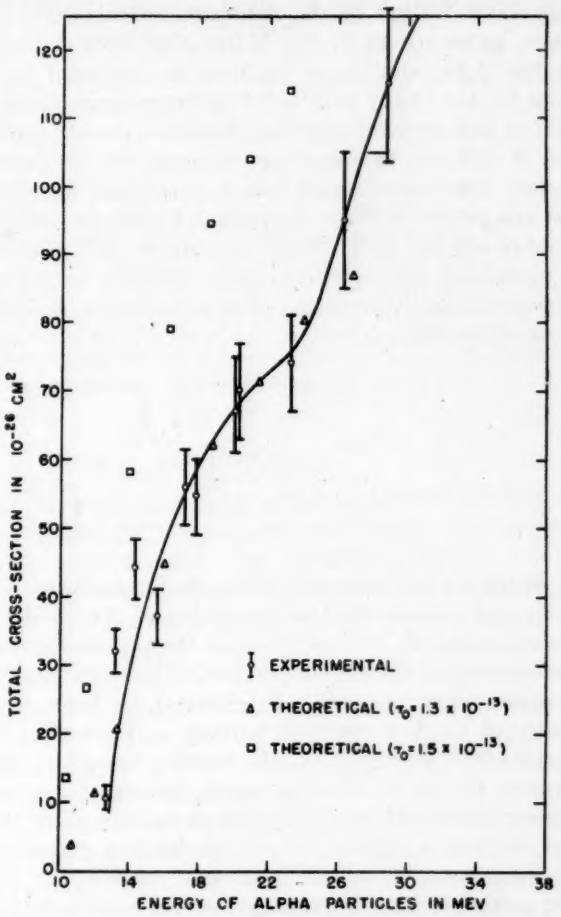
TOTAL CROSS-SECTION IN 10^{-26} CM^2
ENERGY OF ALPHA PARTICLES IN MEV
EXPERIMENTAL
THEORETICAL (r_0 = 1.3 x 10^{-13})
THEORETICAL (r_0 = 1.5 x 10^{-13})

FIG. 3. Total cross section which is the sum of (α,n), $(\alpha,2n)$, (α,pn) cross sections on Ni^{60} as determined experimentally is compared with theoretical $\sigma\phi_\alpha$ which is the cross section for the absorption of an α-particle by Ni^{60} nucleus.

[7] I am indebted to Dr. Duckworth for kindly communicating to me the values of the masses of Cu^{63} and Ni^{60} as measured by the Wesleyan group.

[8] It should be noted that the calculated values of $\sigma(p,n)$ are quite sensitive to the exact value of the threshold of the (p,n) process. In the present experiment this threshold could not be determined too accurately, because of the straggling effect. We used a value of 4.0 Mev for this threshold in the present calculations, which was derived from the energy release in the $Zn^{63}\rightarrow Cu^{63}$ transformation.

remarkable feature of the two particle emission processes, as seen from Fig. 1, is the large cross sections for the (p,pn) and (α,pn) reactions as compared with those for the $(p,2n)$ and $(\alpha,2n)$ processes respectively. This, at first, appears surprising, because a proton would find it difficult to come out through the Coulomb barrier. The experimental values of $\sigma(p,pn)$ for Cu^{63} and $\sigma(\alpha,pn)$ for Ni^{60} are each about 4 times as high as those of $\sigma(p,2n)$ for Cu^{63} and $\sigma(\alpha,2n)$ for Ni^{60}. This is in agreement with a similar ratio between the cross sections of the (γ,pn) and $(\gamma,2n)$ processes on Zn^{64} as observed by Strauch.[9]

The theoretical cross sections for these processes can be calculated on the basis of the statistical model.[2] In a process like (p,pn), either a neutron or a proton can be the first particle to be emitted following the formation of the compound nucleus. A second particle will follow the first particle. Let $I_n(\epsilon)d\epsilon$ denote the distribution in energy of the first emitted neutron and $I_p(\epsilon)d\epsilon$ that for the first emitted proton. Then the cross section of a process in which a neutron is emitted as the first particle after the formation of the compound nucleus and is then followed by the emission of a second particle b, will be given by

$$\sigma(p,nb)=\sigma_p\frac{\int_0^{\epsilon_p+B_p-B_{n_1}-B_b} I_n(\epsilon)\eta_b(\epsilon_p+B_b-B_{n_1}-B_b-\epsilon)d\epsilon}{\int_0^{\epsilon_p+B_p-B_{n_1}} I_n(\epsilon)d\epsilon+\int_0^{\epsilon_p} I_p(\epsilon')d\epsilon'}$$

σ_p represents the cross section for the formation of the compound nucleus by the absorption of the incident proton. $\eta_b(\epsilon_p+B_p-B_{n_1}-B_b-\epsilon)$ is the probability for the emission of the second particle with the maximum possible energy $(\epsilon_p+B_p-B_{n_1}-B_b-\epsilon)$, ϵ being the energy of the first emitted neutron, ϵ_p the energy of the incident proton. B_p is the binding energy of the incident proton to the compound nucleus. B_b is the binding energy of b to the residual nucleus after the first neutron is emitted. B_{n_1} is the binding energy of the first neutron to the compound nucleus. If the first particle emitted is a proton, then the cross section is

$$\sigma(p,pb)=\sigma_p\frac{\int_0^{\epsilon_p-B_b} I_p(\epsilon')\eta_b(\epsilon_p-B_b-\epsilon')d\epsilon'}{\int_0^{\epsilon_p+B_p-B_{n_1}} I_n(\epsilon)d\epsilon+\int_0^{\epsilon_p} I_p(\epsilon')d\epsilon'},$$

where ϵ' is the energy of the first emitted proton. The values of the various quantities involved can be estimated.

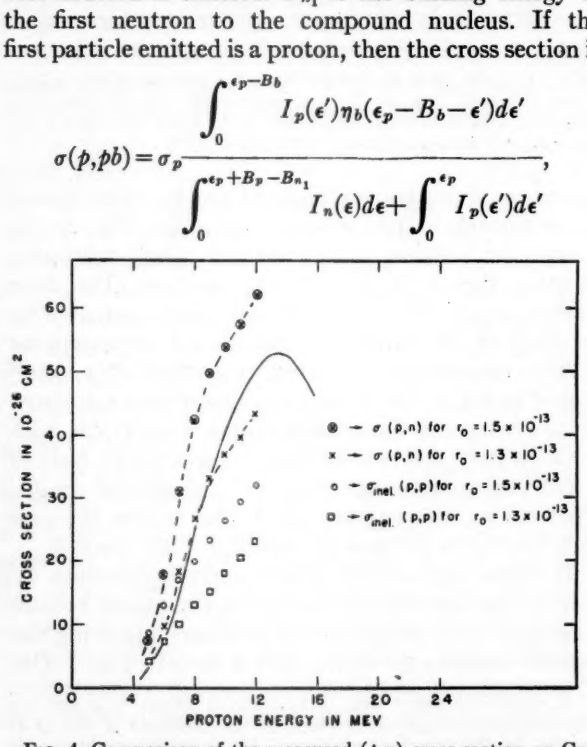

FIG. 4. Comparison of the measured (p,n) cross section on Cu^{63} with theoretical values, calculated on the basis of statistical theory. The solid line is the experimental cross-section curve.

The cross sections obtained on the basis of the above considerations show that $\sigma(p,pn)$ is of the same order of magnitude as $\sigma(p,2n)$ for Cu^{63}. Two factors favor the (p,pn) process over the $(p,2n)$ process: (a) the threshold of the former is about 3 Mev lower than the threshold of the latter;[10] (b) the residual nucleus in the first case being an odd-odd nucleus (Cu^{62}) has a level density greater than that in the second case which is an even-even nucleus (Zn^{62}). A factor of 4 between the level densities was assumed in the present calculations.[2]

In view of the very meager information available regarding the level densities of nuclei, no definite conclusion can be reached with respect to the validity of the statistical model in this part of the isotope chart. Whether or not the factor of 4 between the observed values of $\sigma(p,pn)$ and $\sigma(p,2n)$ can be explained on this basis cannot be decided at present. However, it should be noted that if a mechanism involving the emission of a deuteron is assumed in the (p,pn) process, the threshold of the process would be about 5 Mev lower than that of the $(p,2n)$ process, which would bring up the calculated values for $\sigma(p,pn)$ further.

All the above considerations also apply to the ratio between $\sigma(\alpha,pn)$ and $\sigma(\alpha,2n)$.

In conclusion, I wish to express my deep obligation to Professor Emilio Segrè for his constant encouragement and guidance during the progress of the work. Thanks are due to the crews of the 60-inch cyclotron and the Berkeley linear accelerator for their valuable cooperation in making the bombardments.

[9] K. Strauch, Phys. Rev. 79, 241 (1950).

[10] The exact value of this difference, as in the case of the (p,n) threshold, is quite important in these calculations. The present value of 3 Mev was deduced from the energies of the radiations emitted in the $Zn^{62}\rightarrow Cu^{62}$ transformation. It may be off by as much as 1 Mev.

Abundance of Lithium, Beryllium, Boron, and Other Light Nuclei in the Primary Cosmic Radiation and the Problem of Cosmic-Ray Origin*

H. L. BRADT† AND B. PETERS
University of Rochester, Rochester, New York

(Received July 28, 1950)

A combination of sensitive and insensitive photographic emulsions is used to improve the accuracy of measurement of the specific energy loss of relativistic nuclei. The method is applied to the determination of the charge spectrum of the primary cosmic radiation at geomagnetic latitude $\lambda=30°$ and results in nearly complete resolution between neighboring elements up to $Z\sim14$. It is shown that lithium, beryllium, and boron nuclei are almost or entirely absent in the primary cosmic ray beam. Since nuclear disintegrations of energetic heavy ions frequently lead to fragments of $3\leqslant Z\leqslant 5$ it is concluded that most heavy primary nuclei do not suffer nuclear collisions between the time of acceleration and arrival and that this time must be less than $10^6/\rho$ years, where ρ is the density of atoms along the trajectory.

This result seems to be in disagreement with several recent theories on the origin of cosmic rays and raises some general difficulties for theories assuming galactic origin.

I. INTRODUCTION

IN recent years various new theories of the origin, of cosmic rays have been proposed.[1–6] These theories may be classified according to the proposed mechanism for acceleration of the nuclei of the primary cosmic radiation (electromagnetic acceleration, radiation pressure, etc.) or according to the assumptions made concerning the source region. The question of whether cosmic rays are of solar, galactic, or extragalactic origin may ultimately find a conclusive answer on the basis of observations on the dependence of cosmic-ray intensity on sidereal or solar time.[7–9] Another classification, which is independent of the assumed specific mechanism of acceleration and not necessarily uniquely correlated with the problem of the source region may be based on the answer to the following question: What happens to the nuclei of the cosmic radiation after they have been accelerated but before they hit the earth's atmosphere? In particular, have the cosmic-ray nuclei, on their voyage through space, traversed an amount of interstellar matter sufficient to establish equilibrium with their collision products? A theory based on the assumption of magnetic fields sufficiently strong to retain the particles in a closed region (containing the source and the earth) until they collide with interstellar matter, in gaseous or dust form, would imply a positive answer. A negative answer would, for instance, result from a theory which assumes that the majority of the primary nuclei, after being accelerated in a given region, either escape from that region, or are adiabatically decelerated or collide with bodies sufficiently large to absorb both the primaries and their break-up products and that these processes take place in a time short compared with the time between collisions with atoms in interstellar space. A negative answer would also result from a non-equilibrium theory like that proposed by Lemaître.[10] It is the purpose of this paper to show how an empirical answer to the question formulated above can be obtained and to present the results of an investigation which provides a partial answer.

The absence in the incident radiation of the lighter particles (mesons, electrons, and photons), which must be produced in collisions of cosmic ray nuclei with matter gives us no obvious clue as to the importance of collisions in interstellar space, since the mesons decay spontaneously, the photons would not be retained by assumed magnetic fields and electrons will in general be emitted with momenta much lower than that of heavier collision fragments and may in addition lose their energy by absorption processes which are much less effective for protons and heavier nuclei.[11]

If a nucleus with relativistic energy per nucleon ϵ collides with a proton and produces a radioactive fragment the decay electron will on the average obtain an energy $\epsilon'=\epsilon(\epsilon_0/Mc^2)$, where ϵ_0 is the total energy of the electron in the rest system of the nucleus and M is the nucleon mass.

If the electron is produced by the decay of a charged meson it will still receive a relatively low energy. Assuming that the mesons in the center of mass system are on the average created with a kinetic energy comparable to their rest energy and that the average energy of a decay electron is 40 Mev we get

$$\epsilon'\approx\epsilon/10.$$

Thus the magnetic rigidity of electrons produced in interstellar collisions is greatly reduced as compared with that of the primary nucleonic component and the large majority of such electrons would be excluded by the earth's magnetic field. Electrons produced by γ-rays resulting from neutral meson decay do not have to be considered since the γ-rays will not have a chance to be converted in traversing the solar system or the galaxy.

* This work was assisted by the joint program of the ONR and AEC.

† On May 24, 1950 Helmut L. Bradt died unexpectedly, as this work, to which he devoted the last months of his life, was nearing completion.

[1] E. Fermi, Phys. Rev. **75**, 1169 (1949).
[2] R. D. Richtmyer and E. Teller, Phys. Rev. **75**, 1729 (1949).
[3] H. Alfvén, Phys. Rev. **75**, 1732 (1949); **77**, 375 (1950).
[4] L. Spitzer, Jr., Phys. Rev. **583** (1949).
[5] A. Unsöld, Zeits. f. Astrophys. **26**, 176 (1949).
[6] E. McMillan, Phys. Rev. **79**, 498 (1950).
[7] A. H. Compton and I. A. Getting, Phys. Rev. **47**, 817 (1935).
[8] M. S. Vallarta, Rev. Mod. Phys. **21**, 356 (1949).
[9] Auger, Daudin, Denisse, and Daudin, Comptes Rendus **228**, 1116 (1949).
[10] G. Lemaître, Rev. Mod. Phys. **21**, 366 (1949).
[11] E. Feenberg and H. Primakoff, Phys. Rev. **73**, 449 (1948).

In order to study the importance of collisions with interstellar matter we may then turn our attention to the relative abundance of the various elements that are found to be present in the incident radiation. The most abundant elements in the primary cosmic radiation are hydrogen, helium, carbon, oxygen, nitrogen, magnesium, silicon, etc.,[12] which are also the most abundant elements in the known universe.[13] The elements between helium and carbon in the periodic system, lithium, beryllium, and boron, are elements of very low abundance, as compared with the neighboring elements. In meteorites (Goldschmidt) and in the solar atmosphere (Russell) their abundance is some 100,000 times smaller than the abundance of oxygen.[13] In interstellar space, according to Spitzer[13] the abundance of Li is at least 10^{-1} and the abundance of Be $\sim 10^{-4}$ times smaller than the abundance of Na, the cosmic abundance of which is 500 times smaller than that of oxygen. If the parallelism between the abundances in the primary cosmic radiation and the cosmic abundances still holds even approximately for these light elements, we may expect Li, Be, and B to be practically absent from the primary cosmic radiation *near their source region*. But this will no longer be true for the *incident* radiation, if nuclear collisions are important. As is known from recent emulsion work,[14] Li, Be, and B are quite frequently produced as "splinters" in collisions of fast nucleons with heavy nuclei, such as Ag and Br. High energy collisions between protons and the more abundant heavy cosmic-ray nuclei such as carbon and oxygen are also expected to result frequently not in complete dissociation of these nuclei into nucleons and alpha-particles, but to leave behind a residual fragment of charge $Z=3$, 4, or 5. We shall show below that on the assumption of equilibrium between the acceleration of cosmic ray nuclei of charge $Z \geqslant 6$ and their destruction in collisions with interstellar hydrogen we must expect that Li, Be, and B nuclei, produced in these collisions as fragments, must have an abundance comparable to that of all the heavier nuclei together.

If the abundances of Li, Be, and B nuclei in the incident radiation should turn out to be much greater than the lower limit given by the production of these nuclei in interstellar collisions, one would have to conclude that these nuclei are abundant in the source region and thus constitute an important fraction of the true primary radiation. On the other hand, the absence of Li, Be, and B among the incident nuclei would be incompatible with the assumption of an equilibrium between the production of the heavy nuclei of the primary cosmic radiation and their destruction in collisions with interstellar atoms.

[12] H. L. Bradt and B. Peters, Phys. Rev. 77, 54 (1950).
[13] H. Brown, Rev. Mod. Phys. 21, 625 (1949).
[14] D. H. Perkins, Intern. Cosmic Ray Conf. Como, Italy, 1949. We are indebted to Dr. Perkins for communicating to us details of his results before publication.

II. THE CHARGE SPECTRUM OF NUCLEI WITH $2<Z\leq 14$ at $\lambda_{geom}=30°$ BELOW 20 G/CM² OF AIR

(1) Charge Determination

In a previous paper[12] we have shown that at least up to charge $Z=14$ primary nuclei are completely stripped of electrons before they enter the earth's magnetic field and therefore arrive at a geomagnetic latitude $\lambda=30°$ with a kinetic energy of at least 3.5 Bev/nucleon. The energy loss which these particles suffer by ionization in the first 20 g/cm² of atmosphere is only a small fraction of this minimum energy. They will therefore enter a stack of photographic plates exposed at $\sim$90,000 ft. with relativistic velocities. Neglecting the relativistic increase of ionization, their specific energy loss in the photographic emulsions is therefore a function of their charge only and is proportional to Z^2.

The specific energy loss in emulsions is measured in this work by the grain density along the track. By comparing the grain density along tracks of electron-positron pairs produced with widely differing angular divergence it has been shown that the relativistic increase of grain density for electrons in the energy range between 10 mc^2 and 10^4 mc^2 is less than seven percent. A study of the relativistic increase of grain density for multiply charged particles has not yet been completed. There is an indication for such an effect but its magnitude is less than 20 percent.

Heretofore charge determinations were mostly carried out using the method of δ-ray counting. The accuracy of this method has been discussed[12] previously and permits the determination of charges $Z \geqslant 6$ with an error of approximately 10 percent. For particles lighter than carbon the number of δ-rays approaches the random background of slow electrons, and charge determination by this method becomes very inaccurate except for tracks of exceptional length.

For the purposes of this investigation we must not only extend the charge determination to the lighter elements, but must also improve the accuracy to the point where one element can be distinguished from its immediate neighbors in the periodic system.

The method of counting the number of developed silver grains along the track of a particle gives more accurate values for the specific energy loss, but in an emulsion of given sensitivity discrimination between tracks is feasible only if their specific ionization does not differ by more than a factor of about 15. If a given particle makes a track which can just be perceived against the random background, another particle of 15 times this ionizing power will leave a track so dense that clogging of grains makes grain counting difficult. In order to extend the range of applicability of the grain counting method we have exposed a closely packed stack of plates in which highly sensitive emulsions alternate with emulsions of very low sensitivity. The ionization loss of a particle which traverses the stack can therefore be studied in both types of emulsion.

The sensitive plates consisted of Eastman *NTB*3 emulsions developed by the standard temperature method first suggested by Dilworth and Occhialini and

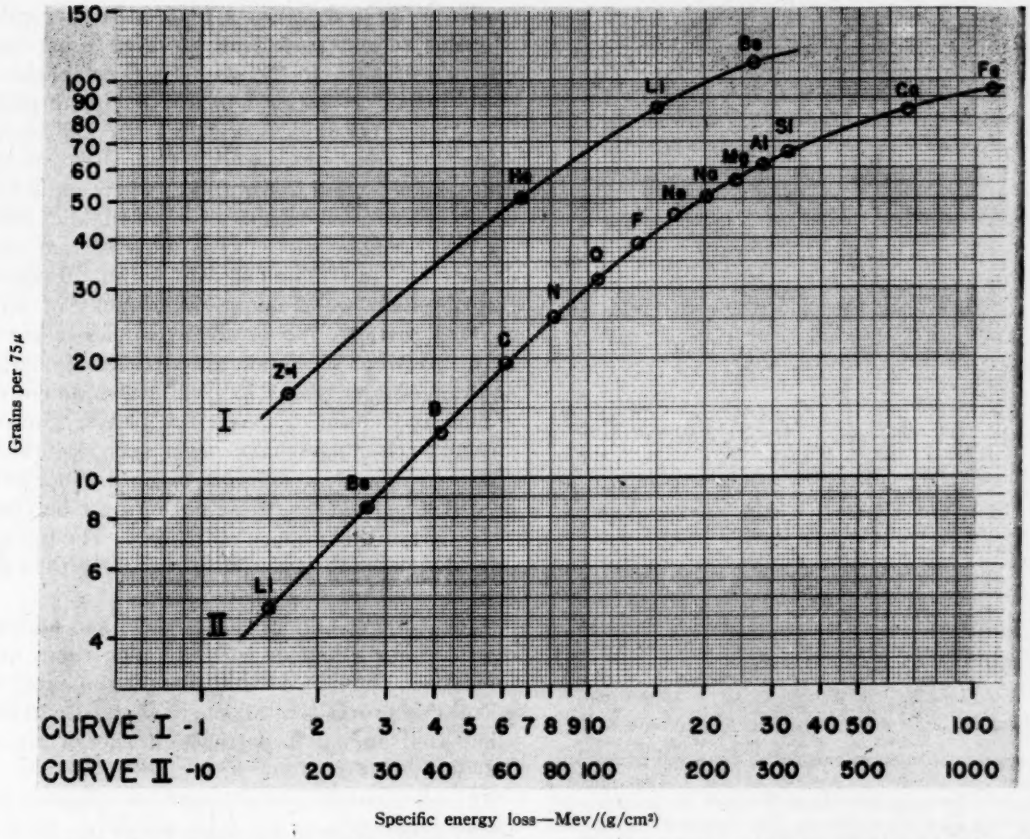

FIG. 1. Grain density *versus* specific energy loss. Curve I refers to NTB3 emulsion. Curve II refers to strongly underdeveloped *NTA* emulsions. The expected grain density of tracks due to various relativistic nuclei is indicated on the diagram.

Payne.[15] The insensitive plates consisted of Eastman *NTA* emulsions developed by the same method but using 20 parts of water to one part of *D*-19 developer. This development procedure was chosen such as to make the heaviest countable tracks in the *NTB*3 emulsions just barely detectable in the *NTA* emulsion.[16] In Fig. 1 the grain density for both emulsions is plotted against the specific energy loss of the particle.

Curve I refers to the electron sensitive emulsion. Shower particles and high energy electron-positron pairs created by γ-rays in the emulsion were used to establish the grain density corresponding to a relativistic singly charged particle. This point is marked $Z=1$ on the curve. The points marked He, Li, Be giving the grain density corresponding to 4, 9, and 16 times minimum ionization were determined from the particle tracks shown in Fig. 2. Here a nitrogen nucleus after traversing several plates in the stack breaks up into a nucleus of lithium and a nucleus of beryllium, the latter in turn breaks up, after traversing several additional plates, into two α-particles. The small angle between the collision fragments and in particular the small divergence between the two α-particles from the disintegration of beryllium makes it certain that all the particles have relativistic energies. The grain density curve obtained in this way was checked by grain counting other relativistic α-particles and singly charged particles of long range.

Curve II refers to the emulsions which were strongly underdeveloped. Here the point marked Be was calibrated by using the relativistic beryllium nucleus previously identified and several other such nuclei found in the course of this investigation. The points marked O and Mg were fixed by grain counting tracks which in the neighboring sensitive emulsion were identified by δ-ray count as due to relativistic oxygen and magnesium nuclei. The calibration curve was then drawn through these three points and the grain density corresponding to relativistic nuclei of other charges was obtained from this curve by assuming a specific energy loss proportional to Z^2. A relativistic carbon nucleus is then expected to give a grain count of 20 grains/75μ. Since previous work has established the existence of a strong carbon peak in the primary radiation, the appearance of such a peak in the charge spectrum (Fig. 3) at the predicted value of grain density establishes the correctness of the calibration curve used for the underdeveloped emulsions. The uniformity of development

[15] Dilworth, Occhialini, and Payne, Nature **162**, 102 (1948).
[16] We are indebted to Mr. T. Putnam for carrying out the necessary development tests.

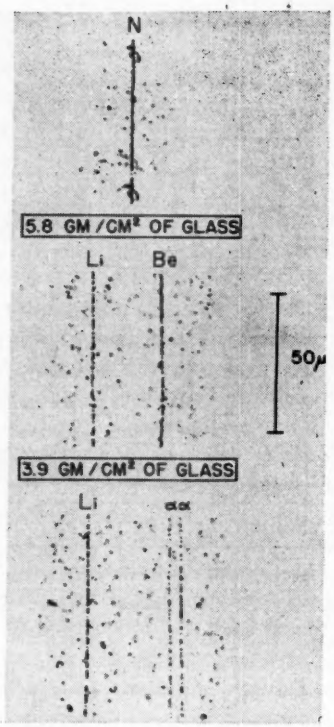

FIG. 2. A relativistic nitrogen nucleus is destroyed in two successive collisions as it traverses a stack of plates. The collisions occur in the glass between emulsions. Sections of the track are shown before and after the collisions. The nitrogen nucleus first disintegrates into a nucleus of lithium and a nucleus of beryllium, the latter then disintegrates into two α-particles.

of successive *NTA* plates may be judged from the grain densities in several plates of five long tracks listed in Table I. The over-all resolution is not as good as is suggested by these examples, since most of the tracks have shorter paths in the stack. Figure 4 shows the appearance of tracks of different particles in both types of emulsion.

(2) The Survey for Tracks of Primary Particles of Charge $Z>2$

The stack was arranged in such a way that successive sensitive plates (separated by insensitive plates) were exactly 3 mm apart. The thickness of the emulsions was $d=80\mu$. From the position, length, and inclination of a track observed in one sensitive plate one could determine its position accurately in the next sensitive plate provided the particle penetrated the intervening glass without appreciable scattering. A sensitive plate was surveyed for all tracks traversing the emulsion, having a projected track length $l>300\mu$ and a grain density larger than that corresponding to five times the ionization of a relativistic singly charged particle. Most of the tracks so selected were of course not due to relativistic particles of charge $Z>2$ but to singly charged particles with velocity $v/c<0.37$ or doubly charged particles with velocity $v/c<0.78$. The positions of all tracks in the next sensitive plate were then calculated and this second plate was surveyed using the same criteria as before. In this way it was established which of the particles observed in the first plate penetrated $0.3l/d>1.12$ cm of glass or 2.75 g/cm² and reached the second plate without changing their direction by more than about 5°. For those tracks where grain counting was possible (grain density less than 16 times minimum) the additional restriction was imposed that the grain density had to remain constant within 10 percent. By this selection we eliminate the tracks of all singly charged particles and of all α-particles of energy less than 260 Mev. We retain all particles of charge $Z>2$ and range larger than 2.75 g/cm² which do not undergo a nuclear collision between the plates. (Since heavy ions of such ranges have never been observed to be produced in nuclear collisions except by incident nuclei of still larger charge, these nuclei must be considered to be part of the primary radiation.[12]) The tracks which appeared in both sensitive plates were then followed through all the plates of the stack.

It was found that (a) all of them had an ionization density larger than or equal to nine times minimum ionization. Combined with a minimum range of 2.75 g/cm² this proves that all singly charged particles were eliminated and all α-particles of energy higher than 700 Mev.

(b) all particle tracks could be followed into the upper hemisphere to the point where the track entered the stack indicating that none of these particles were produced in the stack by other than heavily ionizing particles.

(c) the minimum range of any of these tracks to the point of exit or to the point where the particle suffered a nuclear collision was 5.8 g/cm². Combining this fact with the absence of an appreciable increase of ionization

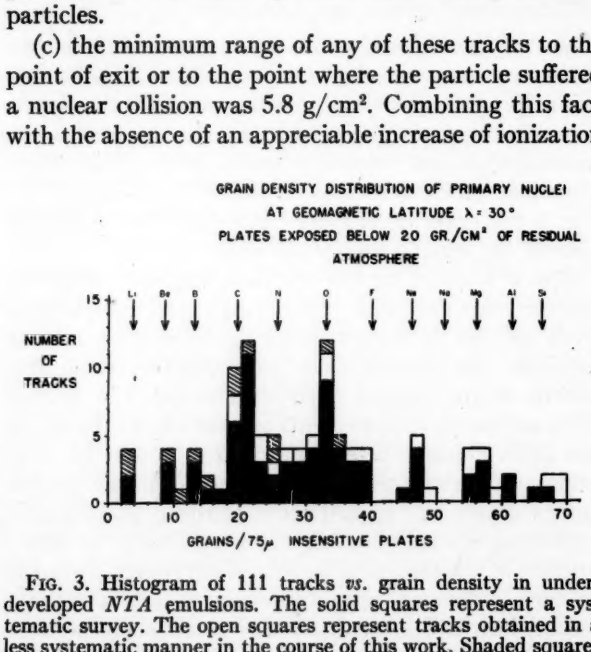

FIG. 3. Histogram of 111 tracks *vs.* grain density in underdeveloped *NTA* emulsions. The solid squares represent a systematic survey. The open squares represent tracks obtained in a less systematic manner in the course of this work. Shaded squares represent relativistic fragments produced by heavier primary nuclei in collisions in the stack. The expected grain densities from different nuclei obtained from Fig. 1 are indicated by arrows. Lithium tracks as explained in the text are included in the diagram although they were identified in neighboring emulsions of higher sensitivity.

within this distance all α-particles are also excluded whatever their energy.

The tracks have therefore to be ascribed to fast particles of charge $Z>2$ entering from the outside. On the basis of arguments previously presented[12] we conclude that they are primary cosmic-ray particles. The only primaries of $Z>2$ which could have been missed in such a survey are those which suffered nuclear collisions in the glass between the two plates which were surveyed. This correction is small and it is negligible as far as the ratio of particles of different charges are concerned.

In order to make sure that no particles were missed by this method the results were checked by surveying in two adjacent sensitive plates for all tracks longer than 400μ and a grain density corresponding to more than *three* times minimum ionization. The tracks in both plates were then matched and followed through the rest of the stack. The results were identical with those obtained by the first method.

(3) The Charge Spectrum of Primary Nuclei at $\lambda=30°$

The tracks obtained in the surveys were grain counted in the underdeveloped (*NTA*) emulsions. Four tracks which in the sensitive emulsion indicated an ionization loss equal to 9 times minimum ionization and are therefore ascribed to Lithium nuclei did not leave a visible track in the *NTA* plates. For completeness sake they have been included, however, in the histogram Fig. 3 at their calculated (but unobservable) grain density of 4.8 grains/75μ. The grain density of all other tracks as determined in the *NTA* plates is shown in Fig. 3. The charge values corresponding to these grain densities were obtained from Curve II, Fig. 1 as explained above.

The solid squares in the histogram of Fig. 3 refer to tracks obtained in a systematic survey. The open squares represent additional tracks obtained in a less systematic manner. The shaded squares represent relativistic fragments of heavier nuclei which suffered collisions in the glass.

Figure 3 confirms our previous result that among the nuclei with charge $Z>2$ carbon and oxygen are the most abundant. They are responsible for the two most prominent peaks of about equal intensities. Though nitrogen nuclei have been identified (Table I), their number seems to be at least three times smaller than the number of either C or O nuclei and the nitrogen peak disappears in the high grain density "tail" of carbon. The "tail" of the oxygen peak makes it difficult to judge whether or not there is a significant number of fluorine nuclei. Between $Z=8$ and $Z=12$ we have a group corresponding to the charge $Z=10$ (neon). Next comes the Mg, Al, Si-group: these three elements are only poorly resolved, since the grain-density *vs.* energy-loss curve (Fig. 1) flattens already considerably in this region.

TABLE I. Grain counts for successive 1000-micron intervals for five tracks traced through several insensitive plates.

Track no. Element	B 403 Carbon	568 Nitrogen	B 12 Oxygen	B 416 Neon	408 Magnesium
	265	391	403	555	726
	266	359	390	553	722
	283	307	394	572	737
	251	353	465		
	257	347	385		
	275	348	393		
		350	394		
		351			
Average grains/1000μ	266	351	404	560	728

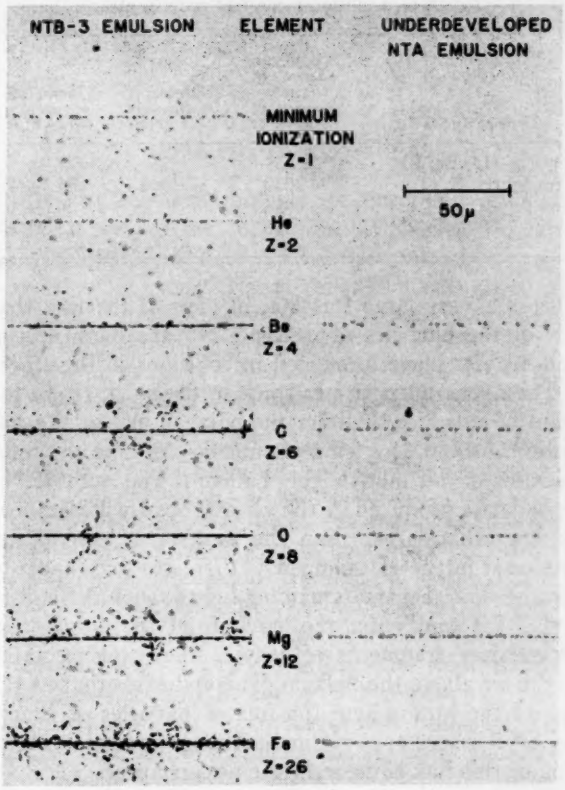

FIG. 4. Tracks of relativistic nuclei of different charge as they appear in electron sensitive *NTB* emulsions and in underdeveloped *NTA* emulsions.

Although the resolution by grain counting is not very good for particles of charge $Z>14$, insensitive plates will permit better charge determination than the sensitive plates for these particles also. While δ-ray tracks are not visible in the insensitive plates there are many background grains in the immediate neighborhood of heavy particle tracks which are apparently due to δ-rays ending in the emulsion. Their number is proportional to Z^2 and it is much easier to count these background grains than it is to count δ-rays on heavy tracks in electron sensitive emulsions. Charge determination by this method will be described elsewhere.

Among the 93 tracks resulting from a systematic survey shown in Fig. 3, 16 tracks belong to the Li, Be, B group. Six of those particles are fragments produced by heavier nuclei making collisions in the stack of plates.

TABLE II. Collision mean free path in glass.

Type of nuclei	Aggregate length of track observed (g/cm²)	Number of collisions observed	Mean free path (g/cm²)
A nuclei (Li, Be, B)	237	5	(47.4)
B nuclei (C, N, O)	2030	59	34.5±4
C nuclei ($10\leqslant Z\leqslant 18$)	954	36	26.5±4
($19\leqslant Z\leqslant 26$)	256	11	23.3±7

This is a very large fraction, in view of the fact that few of the particles of charge $Z>5$ are fragments of still heavier nuclei produced in collisions in the stack.

The average length per track in the stack (from the point of entrance to either the point of exit or the collision) is about 15 g/cm², about two-thirds of the total amount of air above the balloon. The number of secondaries produced in the air overhead will therefore be somewhat larger than the number of secondaries produced in the glass and it is therefore reasonable to assume that also the remaining light nuclei (3 Be, 5 B, and 2 Li) that enter the stack from the outside are secondaries, fragments of heavier nuclei disintegrated in the air above the balloon. This indicates that at the top of the atmosphere the flux of particles of charge $3\leqslant Z\leqslant 5$ is zero or very small. A more accurate evaluation of this flux is made in the next chapter.

The flux of nuclei with $6\leqslant Z\leqslant 10$, extrapolated to the top of the atmosphere had been determined previously:[12] $I=(3.5\pm 0.6)\cdot 10^{-4}$ nuclei/cm²-sec.-sterad. for a geomagnetic latitude of 30°. The data of this flight, which was carried out near the same geomagnetic latitude, yield a flux value of $(3.3\pm 0.7)\times 10^{-4}$ in good agreement with the previously determined value.

Excluding fragments produced in the glass we find in a systematic survey below 20 g/cm² of residual atmosphere:

	Li	Be	B	$6\leqslant Z\leqslant 8$	$Z>8$
No. of nuclei	2	3	5	51	19

At this altitude then the flux of Li, Be, and B nuclei constitutes approximately 20 percent of the flux of CNO nuclei.

III. THE PRODUCTION OF Li, Be AND B FRAGMENTS IN ENERGETIC COLLISIONS BETWEEN NUCLEI

Let us assume that Li, Be, and B nuclei are not found with any appreciable abundance among the true primaries; that is, among the nuclei originally accelerated at the source of the cosmic radiation. Li, Be, and B nuclei, observed at a certain depth h below the top of the atmosphere, may then be fragments produced in collisions of heavier cosmic-ray nuclei: (1) with air nuclei at the top of the atmosphere or (2) with interstellar matter (mostly hydrogen).

In order to estimate the contribution from these two sources we have to know the probability $p_A(Z)$ and $p_H(Z)$ that a stable fragment of Li, Be, or B will be produced in a high energy collision of a nucleus of charge Z with an air nucleus or a hydrogen nucleus respectively. For the purpose of this discussion we shall divide the heavy cosmic-ray nuclei into 3 groups:

A nuclei $(3\leqslant Z\leqslant 5)$,
B nuclei $(6\leqslant Z\leqslant 9)$,
C nuclei $(10\leqslant Z)$.

TABLE III. Stable relativistic nuclei of charges $Z>2$ resulting from collisions.

Type of primary nuclei	Fragments							Number of collisions	Number of A-nuclei produced per collision
	Li	Be	B	C	N	O	Z>8		
B nuclei	6	6	3	6	3	—	—	65	0.23
C nuclei	5	4	—	8	3	3	9	38	0.24
	11	10	3	14	6	3	9	103	0.23

Below $h=20$ g/cm² of residual atmosphere the relative number of these three components is approximately $N(A):N(B):N(C)=1:6:2$.

(1) Collisions in Air

(a) *The probability $p_A(Z)$ of producing an A nucleus in a collision of B or C nuclei with nuclei of the atmosphere*

The mean free path for collisions of B and C nuclei with nitrogen and oxygen nuclei of the atmosphere and the type of fragmentation occurring in such collisions may be inferred from the observed collision of such nuclei in the glass of photographic plates.

Table II gives the collision mean free path in glass for A, B, and C nuclei. The values obtained for B and C nuclei are in agreement with those reported earlier.[12] The mean free path for A nuclei (λ_A) is based on an as yet insufficient number of collisions and is only given as an indication that, as expected, it is longer than λ_B or λ_C.

Table III above shows the number of stable relativistic nuclei of charge $Z>2$ observed to result from 103 collisions of B and C nuclei in glass. Thus we get 0.23 A type nuclei (Li, Be, or B) produced per collisions of B or C type nuclei in glass. We may assume that the fragmentation of these nuclei in glass (mostly SiO_2) is very nearly identical to that occurring in air:

$$p_A(B)=p_A(C)=0.23$$

and that their collision mean free paths in air are about 10 percent less than the corresponding paths in glass.

(b) *Relativistic Li, Be, and B fragments produced in the air above the balloon*

We can now calculate the number of A nuclei which should be observed under 20 g/cm² of air. This number

if given by:

$$N_A(\theta)=\lambda_A p_A\left\{\frac{N_B(\theta)}{\lambda_A-\lambda_B}\left[\exp\left(\frac{x}{\lambda_B}-\frac{x}{\lambda_A}\right)-1\right]+\frac{N_C(\theta)}{\lambda_A-\lambda_C}\left[\exp\left(\frac{x}{\lambda_C}-\frac{x}{\lambda_A}\right)-1\right]\right\}+RN_B(\theta)\exp\left(\frac{x}{\lambda_B}-\frac{x}{\lambda_A}\right).$$

Here $N_{A,B,C}(\theta)$ is the number of nuclei of a given type incident under an angle,

θ with the zenith direction below h g/cm² of residual atmosphere,

$x=h/\cos\theta$ is the path traversed in the atmosphere,

$\lambda_{A,B,C}$ is the collision mean free paths in air (about 10 percent less than the mean free paths measured for collisions in glass),

p_A is the probability that a collision of a B or C nucleus in air will lead to the production of a relativistic A nucleus and,

R is the flux ratio of A and B nuclei at the top of the atmosphere.

We can integrate the formula over θ, since $N_B(\theta)$ and $N_C(\theta)$ are known experimentally. Using the values: $\lambda_B=31$ g/cm²; $\lambda_C=24.5$ g/cm² and $p_A=0.23$ we obtain below 20 g/cm² of atmosphere

$$N_A=(0.28+R)N_B \text{ for } \lambda_A=31 \text{ g/cm}^2,$$
$$N_A=(0.31+1.2R)N_B \text{ for } \lambda_A=40 \text{ g/cm}^2.$$

We should therefore expect that even if no A nuclei were incident at the top of the atmosphere the number of A nuclei entering the stack of plates below 20 g/cm² of air should equal about 30 percent of the number of B nuclei.

Furthermore since the average track traverses about $L=15$ g/cm² of glass before it either leaves the stack or undergoes a collision we should expect an additional number of A nuclei to be produced in the stack given by $N_A'=p_A[N_B(1-\exp(-L/\lambda_B))+N_C(1-\exp(-L/\lambda_C))]$ leading to

$$N_A'/N_B=0.14.$$

A systematic survey of 173 cm² of emulsion yielded 51 tracks of B nuclei entering the stack from the air. Of these about 10 must be due to collisions of C nuclei in the air above the balloons. Thus 41 of the B nuclei incident at the top of the atmosphere reached the plates below 20 g/cm² of air. On the basis of our calculation we should expect in the same survey about 12 A nuclei to enter the stack from the air and 6 to be produced in the glass. We actually observed 10 A nuclei entering from the air and 6 produced in the glass. It seems therefore that we can easily account for all A nuclei observed to enter the stack by assuming that they result from disintegrations of B and C nuclei in the air above the balloons. The probability of observing 10 or less A nuclei entering the stack from the outside is

17.6 percent for $R=0$
2.5 percent for $R=0.1$
0.24 percent for $R=0.2$.

Our results therefore indicate for the flux ratios of A and B nuclei at the top of the atmosphere a value $0\leq R<0.1$.

We conclude that lithium beryllium, and boron are rare elements in the region where cosmic-ray particles are accelerated.

(2) Collisions with Interstellar Hydrogen

(a) *The probability $p_H(B)$ and $p_H(C)$ of producing A nuclei in collision between B or C nuclei and protons.*

Consider a C, N, or O nucleus at rest being struck by an incoming particle. If the incident particle is a heavy ion (say oxygen or silicon) the nuclear material of the target will disintegrate in a certain way and the probability of obtaining *from the target material* a fragment of charge $3\leqslant Z\leqslant 5$ is $p_A(B)=0.23$, the same number which was obtained in the previous sections by observing collisions in which target and projectile were interchanged. If the stationary C, N, or O nucleus is not struck by a heavy ion but by a relativistic nucleon we would obtain a star with fewer prongs (less complete disintegration) and therefore a higher probability for a fragment of charge $3\leqslant Z\leqslant 5$. This probability is the quantity $p_H(B)$ defined previously. A lower limit for $p_H(B)$ is therefore given by

$$p_H(B)>p_A(B)=0.23.$$

The same argument will apply for collisions of C nuclei ($Z\geqslant 10$) although we would expect that the probabilities depend less strongly on the weight of the nucleus with which the C nuclei collide. Therefore we have also

$$p_H(C)\geqslant p_A(C)=0.23.$$

A more accurate estimate of these probabilities can be made in the following way.

D. H. Perkins[14] has studied the production of heavy nuclear "splinters" in Ag and Br stars in nuclear emulsions exposed both at mountain altitude and in the stratosphere. He finds in all those collisions where at least half of the nuclear matter is disintegrated (number of prongs >12) about 22 percent lead to the emission of a stable Li, Be, or B nucleus of more than 30μ-range. The frequency of such fragments is found to be independent of the number of shower particles produced in the collision and therefore independent of energy at sufficiently high energies. From his data one obtains therefore $p_H(Z)\sim 0.22$ (for $Z\sim 40$).

No direct measurements of $p_H(Z)$ are available for smaller values of Z, but for $Z=6$ to 8 an estimate of this probability can be made from an analysis of stars

produced in the gelatine of nuclear emulsions. Harding[17] has made such an analysis using thin gelatine layers imbedded in nuclear emulsions. (The emulsions used were not electron sensitive.)

He found (α) that the size frequency distribution of stars made in the gelatine (C, N, O nuclei) is essentially the same as that for stars of less than 6 prongs made in ordinary emulsions.

(β) That stars of more than 5 prongs are absent or very rare.

(γ) That $\sim$36 percent of stars in ordinary emulsions must be due to the disintegration of C, N, or O nuclei.

(δ) That charge conservation requires that the number of fragments of charge $Z>2$ from light nuclei is on the average about 0.7 per star.

In order to check whether the probability of producing a fragment of charge $Z>2$ in a collision between a light nucleus and a nucleon is as high as indicated by Harding's data, even if one confines one self to high energy primaries, we have made an analysis in an ordinary electron sensitive emulsion exposed at balloon altitudes of stars with less than 6 prongs produced by a singly charged relativistic primary particle. According to Salant *et al.*,[18] almost all such events represent disintegration of C, N, O nuclei contained in the gelatine of the emulsion.

Counting as prongs all tracks including recoils but excluding the incident primary we have examined 33 stars with a total of 131 prongs.

The nuclear fragments of an average star produced by a singly charged particle in the light nuclei of the emulsion must carry 7.95 units of charge, assuming a contribution from carbon, nitrogen and oxygen nuclei proportional to their geometric cross sections (water content corresponding to 50 percent humidity included). The 33 stars with a total of 131 prongs found in the survey will then emit a total of $33\times7.95=263$ units of charge. Of the 131 prongs, 37 could be identified as due to singly charged particles, leaving 226 charges to be divided among the remaining 94 prongs. Assuming, as is indicated by the data of Perkins,[14] that stable nuclear fragments of charge 3, 4, and 5 occur with approximately equal probabilities, and making the extreme assumption that none of the unidentified prongs were due to singly charged particles, at least 19 prongs must be due to fragments of charge $Z>2$ ($Z_{Ne}=4$) and the total charge is accounted for by

37 prongs caused by particles of $Z=1$	37 charges
75 prongs caused by particles of $Z=2$	150 charges
19 prongs caused by particles of $Z_{Ne}=4$	76 charges
131 prongs	263

Thus at least 0.6 A nuclei are produced in an energetic collision between a proton and a B nucleus, in agreement with Harding's result. It would be desirable to measure this quantity directly by studying stars produced by single charged relativistic primaries in gelatine layers imbedded in electron sensitive emulsions. In the absence of such measurements we shall use as lower limit

$$p_H(B)=p_H(C)=0.23,$$

although present evidence indicates that this limit is considerably lower than the true value.

(b) *Production of Relativistic Li, Be, and B Nuclei as Collision Fragments in Interstellar Space*

(α) *Effect of Radioactive Transmutations on the Expected Abundance Ratios.*—We have estimated the frequency of occurrence of Li, Be, and B fragments in collisions of heavier nuclei with hydrogen or other targets from the available data on cosmic-ray stars. Some of these fragments are certainly unstable and radioactive decay has to be considered in a discussion of the expected abundance ratios. We may, for instance, expect that some of the observed Be fragments are Be^{10} nuclei which will transform into B^{10} with a half-life of 2.5×10^6 years. Hence Be^9 and Be^7 (which is stable in the absence of an electronic shell) fragments and part of the Be^{10} fragments will contribute to the equilibrium abundance of beryllium, whereas another part of Be^{10} fragments may contribute to the equilibrium abundance of boron. This transmutation, of course, does not affect the lumped abundance of the Li—Be—B group with respect to the heavier elements. The only beta-activities that reduce this lumped abundance are those of Li^8 (beta-decay to Be^8, which dissociates into two alphas) and of B^{12} (which transforms into C^{12}); on the other hand, the lumped abundance is increased by the He^6 beta-decay into Li^6 and the decay of C^{10} and C^{11} into B^{10} and B^{11} respectively. If these processes are taken into account, only a comparatively small correction of the estimated abundance of the group may be expected. Actually, since He^6 fragments are probably more frequent than Li^8 and B^{12} fragments together, neglecting the effect of radioactive decay altogether may underestimate rather than overestimate the equilibrium abundance of Li, Be, and B nuclei.

It is not necessary to consider isotopes like Be^8 or B^9 which dissociate into fragments immediately. Their lifetimes are so short that only the dissociation fragments appear in the photographic stars; hence they are not included in the estimate number of Li, Be, and B fragments. For instance, a N^{14} nucleus disintegrating into a B^9 fragment, an alpha particle and a neutron, does not give rise to a 2-prong star but to a 4-pronged star, which is considered to correspond to complete dissociation into alphas and protons.

(β) *Comparison of the Energy Spectra of Primaries and Fragments.*—In order to correlate the expected frequency of the production of A nuclei in interstellar collisions with the corresponding abundance of these

[17] J. B. Harding, Nature **163**, 440 (1949).
[18] Salant, Hornbostel, Fisk, and Smith, Phys. Rev. **79**, 184 (1950).

nuclei in the incident radiation at a given geomagnetic latitude, we have also to consider the energy relations.

According to Perkins,[14] the velocity of the "splinters" in the rest system of the Ag or Br target nucleus rarely exceeds the value $\beta_0=v_0/c=0.1$. The velocity of the Li, Be, and B fragments in two- or three-pronged stars produced by fast protons in the gelatine also in general cannot exceed this value, since otherwise these fragments would give rise to easily identifiable prongs. A relativistic B or C nucleus with total energy per nucleon (ϵ) will give rise to an A nucleus with total energy per nucleon (ϵ') where ϵ'/ϵ lies within the range of values given by $(1\pm\beta\beta_0)/(1-\beta_0^2)$ and β is the velocity of the B or C nucleus. Since at geomagnetic latitude 30° $\beta\approx 1$ and since $\beta_0\lesssim 0.1$ we have $|\epsilon-\epsilon'|/\epsilon\lesssim 10$ percent. Thus at relativistic energies A nuclei produced in collisions in interstellar space will essentially have the same velocity spectrum as the B and C nuclei from which they derive.

(c) *The Relation between the Flux of A Nuclei and Nuclear Collisions in Interstellar Space*

Let us assume that B and C nuclei after being accelerated at the source of cosmic radiation are retained by magnetic fields in some region surrounding the source until they are destroyed by collision with interstellar hydrogen gas. On these assumptions the radiation will contain a certain fraction of A nuclei produced in collisions even if no A nuclei were originally accelerated at the source.

The relative number of A and B nuclei which we would expect to be incident at the top of the atmosphere is then

$$R=p_H(B)(\sigma_B/\sigma_A)+p_H(C)(\sigma_C/\sigma_A)(N_C/N_B).$$

Here $p_H(B)$ and $p_H(C)$ are the probabilities that the collision between a B or C nucleus with hydrogen will lead to the formation of an A nucleus. $\sigma_{A,B,C}$ are the cross sections for the disintegration of A, B, or C nuclei in collision with hydrogen and $N_C/N_B=\frac{1}{3}$ is the relative intensity of the C and B component. Assuming the cross sections to be proportional to the geometric areas of the nuclei we obtain

$$R\gtrsim 0.5 \text{ if we use } p_H(B)=p_H(C)\gtrsim 0.23.$$

If we use the more reasonable values discussed in Section IIa:

$$p_H(B)>0.6, \quad p_H(C)>0.23 \text{ we obtain } R>1.0.$$

Thus collision equilibrium of primary particles in hydrogen gas should lead to a composition in which the number of A nuclei is at least half as great as that of B nuclei and probably considerably larger.

The ratio $R=0.5$ is also obtained if we make the (less plausible) assumption that most of the interstellar collisions occur not with hydrogen nuclei but with dust particles (with an assumed average composition comparable to SiO_2).

Since the measurements discussed in Section III(1), give a value for R less than 0.1 we conclude that only a small fraction of the observed primary cosmic-ray particles suffer nuclear collisions between the time they are accelerated and their arrival at the top of the atmosphere.

IV. ON THE RELATION BETWEEN THE CHEMICAL COMPOSITION OF PRIMARY RADIATION AND THEORIES ON THE ORIGIN OF COSMIC RAYS

In a previous paper[12] we have shown that if the primary cosmic radiation were in equilibrium with its collision products most of its proton and helium would have to be ascribed to collision fragments from heavier nuclei. In that case in order to account for the observed chemical composition of the radiation we would have to assume that the amount of hydrogen and helium accelerated at the source is at most equal in *weight* to the amount of heavier nuclei. Therefore

(α) either the source region where cosmic-ray particles are accelerated contains a very much smaller fraction of hydrogen and helium than those regions of the universe which are accessible to spectral analysis, or

(β) the acceleration of heavy particles ($Z>2$) is greatly favored by the accelerating mechanism compared to the acceleration of light particles ($Z\leqslant 2$). Since an electromagnetic acceleration process requires that the atom is initially ionized one might expect that elements with low ionization potential are more frequently accelerated than those with high ionization potential. Such a selective action in the accelerating process does not seem to exist. For instance Brown[13] gives the relative abundance of the elements oxygen (ioniz. pot. 13.55 ev), neon (ioniz. pot. 21.47 ev), magnesium (ioniz. pot. 7.6 ev) as 5:1:2. A comparison of these ratios with the histogram of Fig. 3 (observed ratio 22:5:5) shows that the ratios of these elements in the primary cosmic radiation do not differ significantly from the universal abundance ratios in spite of the large differences in ionization potentials. In view of this it seems difficult to think of an electromagnetic accelerating mechanism which strongly favors the acceleration of heavy elements.

These difficulties are removed if, based on the measurements described in the previous sections, we conclude that most of the cosmic-ray particles have *not* undergone nuclear collisions between their acceleration and their arrival. The chemical composition of primary particles will then reflect the composition of elements at the source; the relative number of protons and α-particles in the primary beam will not be increased compared to heavier elements by their longer mean free path for nuclear collisions or by the addition of collision fragments.

The absence or scarcity of lithium, beryllium, and boron nuclei in the primary radiation indicates therefore that as far as the distribution between light and heavy elements is concerned the chemical composition at the

source is similar to the average chemical composition of the universe.

If we assume an electromagnetic accelerating process the chemical composition *within* the heavy component indicates that the source region differs from stellar atmospheres; in the source even the noble gas atoms are predominantly in an ionized state and therefore the relative abundance of ions in the source region parallels the relative abundance of elements.

The results derived in the previous sections can be expressed by the statement that for most of the primary particles of charge $Z>2$ and kinetic energy per nucleon $\epsilon>3.5$ Bev, the time τ between their acceleration and their entry into the earth's atmosphere must be such that $\tau\leq 10^6/\rho$ years, where ρ is the number of atoms per cc along their trajectory. This condition could be satisfied

(α) If the particles came from outside the galaxy (where $\rho<10^{-3}$) as part of primordial matter. They do not, however, show the large deficiency in protons predicted by Lemaître.[10]

(β) If they were of galactic, but relatively recent, origin and did not have time to establish equilibrium with their collision products.

This possibility cannot as yet be disregarded, but recent work by Arnold and Libby[19] on the C^{14} content of historical relics seems to prove that the intensity of cosmic radiation has undergone no appreciable change at least during the last 20,000 years.

(γ) If they were produced in the galaxy but leak out at an appreciable rate.

(δ) If they were produced in the galaxy (in the neighborhood of stars) but adiabatically decelerated in interstellar space in a time short compared to τ.

This deceleration must be much more effective than the deceleration caused by ionization losses, since the ionization loss in hydrogen in a distance corresponding to a mean free path for nuclear collision is small for all particles whatever their charge. If K is the specific ionization loss per g/cm² of a relativistic singly charged particle, the energy loss per nucleon for a heavy particle (charge Z, atomic number A) is Z^2K/A. If we assume that the mean free path for heavy nuclei is inversely proportional to their geometrical area and therefore proportional to $A^{-\frac{1}{3}}$, the specific energy loss per nucleon per mean free path increases only as $A^{\frac{1}{3}}$. Using Fermi's[1] value for the ionization loss of relativistic protons in the interstellar matter $K=4.6$ Mev/(g/cm²) we find that even for nuclei as heavy as iron the energy loss per nucleon by ionization amounts only to some 87 Mev over a distance corresponding to a mean free path for nuclear collisions in hydrogen.

(ϵ) If cosmic-ray particles were absorbed by bodies larger than bricks (such that the particle is absorbed together with its fragments) and that the mean free path for collision with these larger objects is shorter than that for collision with nuclei.

Assuming the most frequently quoted value for the average number of atoms in interstellar space ($\rho=1$), the last three conditions when applied to our galaxy have one feature in common: In order to account for the observed energy density of cosmic radiation an accelerating mechanism must be devised efficient enough to permit the transformation of approximately one percent of the entire stellar energy production into cosmic radiation. The difficulty of conceiving a high efficiency accelerating process which was pointed out by Richtmyer and Teller[2] has been increased by a substantial factor.

Apart from raising this serious difficulty about galactic origin, the apparent absence of nuclear collisions in the life history of primary particles seems to lead to difficulties with the specific theories proposed by Spitzer[4] and by Fermi.[1]

In Spitzer's theory the particles are originally accelerated as dust grains by radiation pressure in the vicinity of a supernova. Since noble gases could not be present in the dust grains in any appreciable amount, their presence in the primary cosmic ray beam and particularly the large primary helium flux[12] requires that these nuclei are fragments produced in nuclear collisions of the heavier nuclei present in dust grains. We have shown previously that the large helium flux requires complete equilibrium between heavy primary nuclei and their collision products. In view of the absence of other expected collision products in the primary beam such an explanation is no longer possible.

In the theory proposed by Fermi[1] particles are accelerated by collisions in our galaxy with inhomogeneous moving magnetic fields. Fermi points out that while protons can be accelerated and regenerated by such a process, heavy nuclei will have to be injected continuously with energies above 1 Bev per nucleon before they can gain energy by these collisions and therefore require an additional accelerating mechanism.

If one now assumes that heavy cosmic ray nuclei either leak out of the galaxy or are adiabatically decelerated or absorbed in large bodies in a time shorter than $10^6/\rho$ years one must assume similar effects for the proton component. By depriving the protons of their ability to make nuclear collisions with interstellar hydrogen one would deprive Fermi's theory of its regenerative mechanism. By reducing the lifetime of fast particles to approximately one million years as compared to the 60 million years assumed in Fermi's theory it may be more difficult to obtain agreement with the observed energy spectrum.

It seems perhaps most promising to consider the absence of nuclear collision products in the cosmic ray beam as an argument in favor of solar origin or at least in favor of a source region sufficiently close such that the chemical composition of the radiation still reflects the abundance ratios at the source.

In the theory of solar origin proposed by Richtmyer and Teller[2] and by Alfvén[3] a magnetic field is assumed to exist in the planetary system, weak enough to escape detection by direct measurements at the earth, yet strong enough to obtain isotropy and time independence especially for particles of very high energy. In its

[19] J. R. Arnold and W. F. Libby, Science **110**, 678 (1949).

present form, however, this theory allocates to the cosmic radiation a volume (radius $\sim 10^{17}$ cm) which seems to be too large to avoid nuclear collisions of primary nuclei with intraplanetary matter unless condition (ϵ) is satisfied and an appreciable fraction of the radiation is absorbed in meteoric material.

We wish to express our gratitude to Dr. John Spence of Eastman Kodak Company for preparing special plates, to Miss K. Haile and Mr. R. Richard who carried out most of the scanning, to Mr. T. Putnam for the careful development tests and the microphotographs.

PHYSICAL REVIEW VOLUME 80, NUMBER 6 DECEMBER 15, 1950

Double Transmission and Depolarization of Neutrons

M. Burgy, D. J. Hughes,* J. R. Wallace, R. B. Heller,† and W. E. Woolf
Argonne National Laboratory, Chicago, Illinois
(Received August 2, 1950)

Slow neutrons from the chain reacting pile, polarized by passage through highly magnetized iron, have been analyzed by transmission through additional iron (the "double transmission" effect). The large double transmission effects expected from the polarization cross section of iron were obtained only when the magnetic field between polarizer and analyzer was adjusted carefully to obtain non-adiabatic transitions of the neutrons relative to the field. The general methods developed have been used to measure the change in polarization of a neutron beam with passage through unmagnetized iron. The rate of depolarization is a measure of the domain size in the iron and domain sizes have been measured in this way for a number of Armco iron samples of different metallurgical treatment.

I. INTRODUCTION

NUMEROUS investigations[1–13] of the polarization of slow neutrons have been made since Bloch[14] first pointed out the possibility of producing such polarization. This phenomenon arises from the presence of an appreciable magnetic interaction between a slow neutron and a paramagnetic atom and in addition the presence of interference between the nuclear and magnetically scattered neutron waves in the case of a ferromagnetic scatterer. The scattering cross section, σ, per atom in a ferromagnet can be written in the form

$$\sigma=\sigma_0\pm p, \tag{1}$$

where p is the term arising from interference and σ_0 is the sum of the cross sections due to the nuclear interaction alone and the magnetic interaction alone. The double sign of the interference term refers to the two cases of neutron spin parallel and antiparallel to the atomic spins in the ferromagnet. In the case of transmission through a nearly saturated ferromagnet, these two neutron spin states are attenuated to a different extent, corresponding to the difference in the scattering cross sections for these states. Thus an initially unpolarized beam is changed to a polarized one in which there is an excess of neutrons with one sign of spin component, along the field direction in the ferromagnet, over those with spin component of opposite sign. If the ferromagnet is far from saturation, strong depolarizing effects are present also, which nullify the polarizing effects in the magnetic domains.

The first studies of neutron polarization used a polarizer-analyzer arrangement[1–4] in which the intensity of the beam transmitted by two magnetized blocks of iron was measured before and after reversing one of the fields and these intensities compared with the intensity with the blocks unmagnetized. The dependence of the transmission of the analyzer block on its state of magnetization is empirically a measure of the polarization of the incident beam and this effect furnishes a direct way of studying neutron polarization. The intensity differences to be expected from the postulated nature of the magnetic interaction can be understood as follows. With I_+ and I_- as the intensities of neutrons in the two spin states relative to the field, the intensity I transmitted by a saturated iron slab of thickness d is given by

$$\begin{aligned} I\equiv I_+ + I_- &= \tfrac{1}{2}I_0\exp[-Nd(\sigma_t-p)] \\ &\quad +\tfrac{1}{2}I_0\exp[-Nd(\sigma_t+p)] \\ &= I_0\exp(-N\sigma_t d)\cdot\cosh(Npd), \end{aligned} \tag{2}$$

* Now at Brookhaven National Laboratory, Upton, Long Island, New York.
† Now at St. Louis University, St. Louis, Missouri.
[1] Hoffmann, Livingston, and Bethe, Phys. Rev. **51**, 214 (1937).
[2] Dunning, Powers, and Beyer, Phys. Rev. **51**, 382 (1937).
[3] Powers, Beyer, and Dunning, Phys. Rev. **51**, 371 (1937).
[4] Frisch, von Halban, and Koch, Nature **139**, 756, 1021 (1937); Nature **140**, 360 (1937); Phys. Rev. **53**, 719 (1938).
[5] Powers, Carroll, and Dunning, Phys. Rev. **51**, 1112 (1937).
[6] Powers, Carroll, Beyer, and Dunning, Phys. Rev. **52**, 38 (1937).
[7] Beyer, Carrol, Witcher, and Dunning, Phys. Rev. **53**, 947 (1938).
[8] P. N. Powers, Phys. Rev. **54**, 827 (1938).
[9] Bloch, Hamermesh, and Staub, Phys. Rev. **64**, 47 (1943).
[10] E. M. Fryer, Phys. Rev. **70**, 235 (1946).
[11] Bloch, Condit, and Staub, Phys. Rev. **70**, 972 (1946).
[12] Hughes, Wallace, and Holtzman, Phys. Rev. **73**, 1277 (1948).
[13] Fleeman, Nicodemus, and Staub, Phys. Rev. **76**, 1774 (1949).
[14] F. Bloch, Phys. Rev. **50**, 259 (1936); **51**, 994 (1937).

where N is the atomic density of iron, σ_t the total cross section for unmagnetized iron, and I_0 the incident (unpolarized) intensity. The transmitted intensity, I, is greater than $I_0 \exp(-N\sigma_t d)$, the intensity transmitted in the unmagnetized case. In the real case of near-saturation compared with zero magnetization, the difference is smaller because of depolarizing effects. With two blocks magnetized parallel, the second augments the difference between the magnetized and unmagnetized intensity. When the two blocks are magnetized antiparallel, the neutrons in the spin state for which the cross section is σ_t+p in the polarizer are attenuated with cross section σ_t-p in the analyzer, and conversely. Thus the second block counteracts the changes in polarization and intensity produced by the first and results in an intensity nearer to that for zero magnetization than with parallel fields.

In the early experiments[1-4] polarization effects were obtained by this method but they were small, and when zero field measurements were included they were inconsistent; i.e., the antiparallel intensities were uniformly higher than those calculated from the parallel and zero field intensities. It was recognized that depolarization within the blocks and between them was the likely explanation of the inconsistency, but the lack of a developed theory of depolarization within the blocks and the poor geometry required by the low intensity sources prevented the solution of the difficulties. Other early methods involving transmission-scattering combination suffered from the same difficulties with the intensity problem accentuated. Emphasis was placed increasingly upon measurements of the intensity change, due to magnetization, in a single iron slab or a series of slabs which would be magnetized only parallel.[3,5,7,8] Subsequently, Halpern and Holstein[15] developed the theory of neutron polarization including the depolarization within the material and the "single transmission effect," E_1, defined as the fractional increase[16] in transmitted intensity produced by magnetizing a ferromagnetic material, has since been the basis of all measurements of the polarization cross section, p.[9-13]

The high intensity thermal neutron beams available from present chain reacting piles provide the resource necessary for a fresh examination of neutron polarization by the polarizer-analyzer method or "double transmission effect." In addition to the intrinsic desirability of a direct and quantitatively satisfactory detection of neutron polarization, this effect provides an independent measurement of the polarization cross section, p. At the time we began this investigation, there was a large discrepancy between the value of p measured experimentally at this Laboratory[12] and the smaller values calculated theoretically,[17,18] and, to a lesser extent with the recent measurements of other investigators.[9-11] It was felt to be important to show by a direct measurement of polarization that the high degree of polarization predicted by the high p value could be produced. Since the present work was begun, however, Steinberger and Wick[19] have obtained a theoretical value of p in agreement with that of reference 12, and the difference in experimental values has been accounted for as due to differences in the neutron spectra used.[13]

In addition to the study of the double transmission effect, we have applied the techniques developed for double transmission studies to the measurement of magnetic domain sizes in unmagnetized specimens of iron. The depolarization which occurs in a ferromagnet which is not saturated is related theoretically[15] to the linear dimensions of the magnetic domains in the specimen. The fields of the domains deviate in direction from the average so that many irregular precessions of the neutron spin are produced by the components of the domain fields normal to the spin or moment. In the unmagnetized state a ferromagnet has no polarizing effect, the depolarizing effect is isolated, and a measurement of the change in polarization it produces can be related directly to the average linear dimension of the domains of the specimen. We have made such measurements to get information on the range of domain sizes that occur from several treatments of the specimens.

II. THEORY OF DOUBLE TRANSMISSION AND DEPOLARIZATION

For the quantitative description of the double transmission effect we have used the formulas derived by Halpern and Holstein.[15]

$$I=\exp[-(N\sigma_t+\tfrac{1}{2}q)d]\cdot\{I_0[\cosh(d/D)+\tfrac{1}{2}qD\sinh(d/D)]+S_0wD\sinh(d/D)\}, \quad (3)$$

$$S=\exp[-(N\sigma_t+\tfrac{1}{2}q)d]\cdot\{S_0[\cosh(d/D)-\tfrac{1}{2}qD\sinh(d/D)]+I_0wD\sinh(d/D)\}, \quad (4)$$

where I_0, I, N, σ_t, and d have been previously defined, $w=Np$ is the polarization coefficient, q is the depolarization coefficient, and $D=(w^2+\frac{1}{4}q^2)^{-\frac{1}{2}}$. $S=IP=I_+-I_-$, where P is the polarization and $I_\pm$, are the intensities of neutrons with the two orientations relative to the field, and S_0 is the initial value of S.

Equation (3), with the initial polarization zero ($S_0=0$), gives the single transmission effect $E_1(d)$,

$$E_1(d)=[I-I_0\exp(-N\sigma_t d)]/I_0\exp(-N\sigma_t d). \quad (5)$$

The intensities for the parallel and antiparallel cases in a double transmission measurement are obtained by

[15] O. Halpern and T. Holstein, Phys. Rev. **59**, 960 (1941).

[16] The theory of magnetic scattering predicts the existence of a small negative transmission effect, due to purely magnetic scattering, superposed upon the positive effect from interference of nuclear and magnetic scattering. Estimates of its magnitude indicate that its effect on our measurements is negligible. See: F. Bloch and M. Hamermesh, Phys. Rev. **61**, 203 (1942); M. Hamermesh, Argonne National Laboratory Report, ANL-4208, (1948, unpublished); O. Halpern, Phys. Rev. **76**, 1130 (1949).

[17] Halpern, Hamermesh, and Johnson, Phys. Rev. **59**, 981 (1941).

[18] M. Hamermesh, Phys. Rev. **61**, 17 (1942).

[19] J. Steinberger and G. C. Wick, Phys. Rev. **76**, 994 (1949).

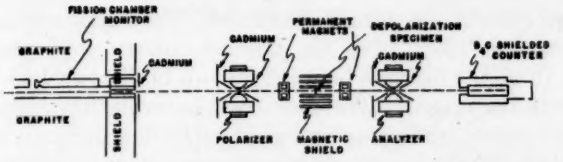

FIG. 1. Apparatus for measurement of double transmission effect and of depolarization of neutrons in magnetic materials.

successive application of Eqs. (3) and (4) for the two blocks. The I and S obtained for the first block from (3) and (4) with $S_0=0$ serves as I_0 and S_0 in (3) for the intensity after the second block, with the sign of S_0 being reversed for the antiparallel case. When w has the same value in polarizer and analyzer, and q likewise, these intensities may be simply expressed in terms of the single transmission effect, E_1, for these values of w and q.

$$I_{\text{par}}=I_0\exp[-N\sigma_t(d_1+d_2)]\cdot[1+E_1(d_1+d_2)],$$
$$I_{\text{anti}}=I_0\exp[-N\sigma_t(d_1+d_2)]\cdot[2(1+E_1(d_1))\times(1+E_1(d_2))-(1+E_1(d_1+d_2))]. \quad (6)$$

It is evident that I_{par} and I_{anti} are symmetric with respect to the value

$$I_0\exp[-N\sigma_t(d_1+d_2)]\cdot[1+E_1(d_1)][1+E_1(d_2)], \quad (7)$$

which corresponds to the final intensity when complete depolarization without loss of intensity occurs between polarizer and analyzer, and also, of course, to the average of the two intensities, I_{par} and I_{anti}. The differences of I_{par} and I_{anti} from (7) represent the effects of the polarization of the beam upon the transmission of the analyzer.

As the measure of the double transmission effect, E_2, we have taken the ratio of the difference of the intensities, measured with fields parallel and antiparallel, to their average,

$$E_2(d_1, d_2)\equiv 2(I_{\text{par}}-I_{\text{anti}})/(I_{\text{par}}+I_{\text{anti}}), \quad (8)$$

so that, from (6) and (7),

$$E_2(d_1, d_2)=2[(1+E_1(d_1+d_2))-(1+E_1(d_1))\times(1+E_1(d_2))]/[1+E_1(d_1)][1+E_1(d_2)]. \quad (9)$$

Previously,[15] the double transmission effect has been defined as the ratio of the difference of intensities with fields parallel and antiparallel to the intensity with both fields zero. While this definition gives a simpler formula, the last member of (9) reducing to the numerator, the inclusion of the zero field measurements brings in the complications of magnetic small angle scattering,[20] especially so when beams of small cross section are used. The effect of this extraneous process can be eliminated only by taking considerable pains. Since other considerations demanded that beams of small cross section be used, it was simpler to use measurements made at high fields, where the small angle scattering is absent, in defining E_2. The formula (9) is convenient for comparison of E_2 measurements with the values to be expected from E_1 measurements on the same material at the same magnetization. Also, it seems to be a simple form for computations when E_2 measurements are being used as an independent measurement of p.

The intensity observed after transmission through a block of magnetized iron depends on both the polarization and the intensity of the incident beam. Thus Eq. (3) has a term proportional to S_0 and one proportional to I_0. In depolarization measurements, the polarization of the beam striking the analyzer is altered by a foil of unmagnetized iron and the corresponding intensity measured. The small additional change produced by scattering and capture in the foil cancels out in the ratios E_p of counts with field to those without. The part associated with the polarization is obtained by subtraction of the ratio obtained with complete depolarization $E_p(\infty)$. The resulting polarization dependent part is studied as a function of depolarizing foil thickness. Formulas relating this dependence to the average linear dimension or size of the magnetic domains in the foil have been given by Halpern and Holstein.[15] These are

$$S=S_0\,\Pi_i[1-\tfrac{1}{3}4\sin^2(gB_i\delta_i/2v)], \quad (10)$$

with the limiting cases

$$S=S_0\exp(-g^2B^2\bar{\delta}d/3v^2), \quad gB_i\delta_i/2v\ll 1, \quad (10a)$$

$$S=S_0\exp[-(\ln 3)d/\bar{\delta}], \quad gB_i\delta_i/2v>1, \quad (10b)$$

where S_0 and S have been defined previously as I_0P_0 and IP, or twice the initial and final spin current densities, g is the gyromagnetic ratio of the neutron, B_i and δ_i the magnetic induction and neutron path length, respectively, in the ith domain along the neutron path, v the neutron velocity, and d the foil thickness.

Equation (10) gives an approximately exponential dependence of S or polarization on thickness for which the half-thickness is given by

$$d_{\frac{1}{2}}=-\frac{0.693\bar{\delta}}{\ln[1-\langle\tfrac{1}{3}4\sin^2(gB_i\delta_i/2v)\rangle_{Av}]}. \quad (11)$$

The limiting forms for $d_{\frac{1}{2}}$ corresponding to (10a) and (10b) are

$$d_{\frac{1}{2}}=2.079v^2/g^2B^2\bar{\delta}, \quad gB_i\delta_i/2v\ll 1, \quad (11a)$$

and

$$d_{\frac{1}{2}}=0.631\bar{\delta}, \quad gB_i\delta_i/2v>1. \quad (11b)$$

The average of $\sin^2(gB_i\delta_i/2v)$ has been taken as the linear average over the interval 0 to $\sqrt{3}(gB\bar{\delta}/2v)$ with $B=4\pi M=21{,}600$ gauss (from the saturation magnetization in iron) and $g=1.83\times10^4$ gauss^{-1} sec.$^{-1}$. We consider this a suitable and consistent evaluation in the intermediate range of domain sizes since Halpern and Holstein[15] state that their formulas give results

[20] Hughes, Burgy, Heller, and Wallace, Phys. Rev. 75, 565 (1949).

correct only as to order of magnitude for values of $\bar{\delta}$, due to uncertainties as to the distribution of domain sizes, demagnetizing fields, and the constancy of the induction B_i within a domain. In view of these uncertainties the effect of "hardening" of the polarization due to the velocity dependence of $d_{\frac{1}{2}}$ has not been included. Instead, the velocity 1500 m/sec. has been used, which corresponds to the average of the exponent in Eq. (10a) over the calculated spectrum for the depolarization work. A plot of $d_{\frac{1}{2}}$ *vs.* $\bar{\delta}$ on these assumptions is given in Fig. 5. The limiting form (11b) is used for $\bar{\delta} > 1.4 \times 10^{-3}$ cm, thus omitting small oscillations given by (11) which are not significant.

III. EXPERIMENTAL ARRANGEMENT AND PROCEDURE

The apparatus used in this work is shown schematically in plan view in Fig. 1. The neutron beam emerges from the thermal column of the Argonne heavy water reactor through a hole in a Cd covered wooden block and passes successively through a steel block between the poles of a polarizing magnet, a magnetic shield, a steel block between the poles of an analyzing magnet, and then passes into a BF_3 proportional counter. The magnets were of identical construction, with 12.7-cm diameter poles of Armco iron coned at 60° to 2.54-cm diameter faces with a 1.27-cm gap. Each magnet was energized by two coils, powered by separate current regulated supplies. Several fans near the magnets provided sufficient cooling for the power absorption of $\frac{1}{4}$ kw per coil. The polarizer and analyzer blocks were of cold-rolled steel, $1.27 \times 1.27 \times d$ cm, cut from the same material that Hughes, Wallace, and Holtzman[12] (hereafter referred to as HWH) used in measurements of the single transmission effect. The blocks were magnetized with a field of 12,000 gauss perpendicular to the beam along the direction of rolling, with the beam direction parallel to the plane of rolling. The field strength was measured at the surfaces of the blocks with a small search coil and a fluxmeter.

The magnetic shield consisted of three coaxial iron cylinders of wall thickness about 1 and 20 cm long, spaced with pieces of brass and Cd, the outer cylinder being an iron pipe with the other two of soft iron. The inner cylinder consisted of two 10-cm lengths so that depolarizing specimens could be mounted at the center of the magnetic shield. The magnetic field at the center of the shield was measured as 0.08 ± 0.08 gauss normal to the shield axis.

The beam was defined by 1-cm square holes in 1-mm Cd diaphragms before and after each steel block, and by a somewhat larger hole at the thermal column which varied in size to obtain the desired neutron intensity, depending upon the block thicknesses. Each magnet was further shielded by a sheet of 1-mm Cd which completely covered the side toward the thermal column, but which had holes sufficiently large and so located that the beam definition by the Cd diaphragms at the steel blocks was not interfered with. The distance of the polarizer block from the thermal column shield was 1.76 m, the distance between the two blocks was 1.65 m with the magnetic shield centered between them, while the center of the counter was 24 cm behind the analyzer block. On the surface of the table supporting the electromagnets and magnetic shield, there were placed two Alnico permanent horseshoe magnets to control the field along the beam outside the magnetic shield.

The counter that we used is the same one that was used by HWH, 20.3 cm in length, 3.74 cm in diameter, filled with 20 cm Hg of B^{10} enriched BF_3 and placed so that the beam traversed the length of the counter. A careful investigation of the effective neutron velocity spectrum with this counter under these conditions by HWH had showed it to be a Maxwell distribution with a most probable velocity of 2250 m/sec. The counter was shielded by a thick surrounding layer of boron carbide. The beam was monitored with a fission chamber inside the thermal column to one side of the beam passing through the double transmission apparatus.

The procedure for measuring the double transmission effect consisted in magnetizing the blocks parallel or antiparallel with predetermined currents, carefully adjusting the permanent magnets so that a compass indicated that the magnetic field at each end of the magnetic shield was accurately perpendicular to the beam and directed the same as the field in the nearer steel block. This resulted also in these field directions in the vicinity of the beam being maintained, approximately, the rest of the way to the respective blocks, and that the field became moderately strong (≈ 50 gauss) a short distance away from the shield and remained strong the rest of the way to the nearer magnetized block. The necessity for these careful adjustments in the attainment of the double transmission effect will be described in Section IV. After taking a counting rate measurement relative to the monitor, the analyzer currents would be reversed, the permanent magnets adjusted for this case and another counting rate measured. Intensities with the magnet currents turned off were taken also, (it was found unnecessary to demagnetize by any special procedure) and frequent background counts were taken. Background measurements, amounting to about three percent of the total counting rate, were taken by placing a 1-mm sheet of Cd over the hole in the Cd shield for the analyzer.

In making depolarization measurements, one or more layers of a certain type of iron would be inserted, normal to the beam, between the two halves of the inner cylinder of the magnetic shield and the transmitted intensity measured as a function of block magnetization as for double transmission measurements. Blocks 2 cm thick were used as polarizer and analyzer. In most cases, only intensities with fields parallel and with no field were measured. This procedure undoubtedly introduces a magnetic small-angle scattering effect through the use of zero current intensity values. How-

TABLE I. Double transmission effect, E_2, and intensity ratios relative to unmagnetized state for parallel (E_{1P}) and antiparallel (E_{1A}) magnetization.

Polarizer thickness (cm)	2.00	2.00	2.00	2.00	1.50	1.00	0.50	1.00
Analyzer thickness (cm)	2.00	1.50	1.00	0.50	1.50	1.50	1.50	1.00
E_2, percent	22.10±0.18	18.30±0.30	13.53±0.59	7.32±0.48	15.01±0.40	10.71±0.53	5.95±0.45	7.49±0.78
E_{1P}, percent	33.99±0.24	27.50±0.32	22.51±1.01	17.66±0.53	20.90±0.89	16.11±0.85	11.15±1.03	11.58±0.81
E_{1A}, percent	7.33±0.23	6.12±0.26	7.00±0.87	9.35±0.46	4.02±0.73	4.31±0.83	4.73±0.88	3.53±0.63

ever, the effect is to introduce a constant factor into the observed ratios E_P, which does not affect the slopes of the curves from which d_i values are obtained.

IV. MEASUREMENTS AND CONCLUSIONS

A. Adiabatic Change of Polarization and the Double Transmission Effect

The observations made on the effect of altering the field between the electromagnets in double transmission were essentially qualitative in nature. No attempt was made to adjust the field to allow quantitative calculations; only the order of magnitude of the field strength was estimated from the oscillation frequency of a compass needle. With 2-cm steel blocks in the polarizer and analyzer magnets, and with the magnetic shield removed, it was found that as long as the field was kept of the order of 100 gauss and slowly varying in direction in the intermediate region, the intensity observed would be independent of reversal of the analyzer field direction, though rotations of the field direction along the beam through 180°, 360°, or more, took place. The intensity in these cases was the same as that observed with the polarizer and analyzer fields parallel and a strong parallel intermediate field. These results are those which one would expect, since for a polarized neutron to change its spin state relative to the field, the field must change direction within a distance small relative to that traveled by the neutron in a Larmor period. For a thermal neutron, this Larmor distance is approximately $80/H$ cm, with H in gauss, so that appreciable changes in the field direction within a distance small compared to 1 cm would be required to effect noticeable depolarization. With the slowly varying field direction that was arranged, the polarized neutrons followed the field direction adiabatically and entered the analyzer with the same orientation relative to the field as in the standard parallel arrangement, whether the analyzer field was parallel to the polarizer field or antiparallel. When the permanent magnets, which were used to control the field in the intermediate region, were removed, the field dropped to a value of the order of one gauss over most of the intermediate region and was irregular in direction. Under these conditions the observed intensity corresponded to complete depolarization, which corresponds to the Larmor precession distance being large relative to the distances over which the field changed direction. It was also found possible, by careful field adjustment, to obtain the full double transmission effect without the use of the magnetic shield. In the parallel fields case the intermediate field was also kept parallel; in the antiparallel case a crossover point was arranged, so that the field as seen by a neutron kept its direction as the neutron left the polarizer but approached zero at a point halfway to the analyzer, then reversed its direction and increased in strength as the analyzer was approached.

These observations bear out the reasons advanced for the failure of previous attempts to obtain double transmission effects of the order expected from measurements of the single transmission effect. With the low intensity sources then available, beams of large cross section and small magnet separations had to be used. Under these conditions the field between the magnets could not be reversed in a manner which prevented most of the neutrons adiabatically reversing their polarization with it.

The measurements of the double transmission effect were made with eight combinations of polarizer and analyzer block thicknesses. The resulting values of E_2 and of the ratios, $E_{1P} \equiv (I_{\text{par}}/I_0)-1$, and $E_{1A} \equiv (I_{\text{anti}}/I_0)-1$, where I_0 is the zero current reading, are given in Table I. The standard deviations listed are the observed root-mean-square deviations of individual measurements and agree well with those calculated from counting statistics. The values of E_2 are also plotted in Fig. 2 as the three functions; (1) $E_2(d, d)$, polarizer and analyzer thicknesses equal; (2) $E_2(2, d)$ polarizer thick-

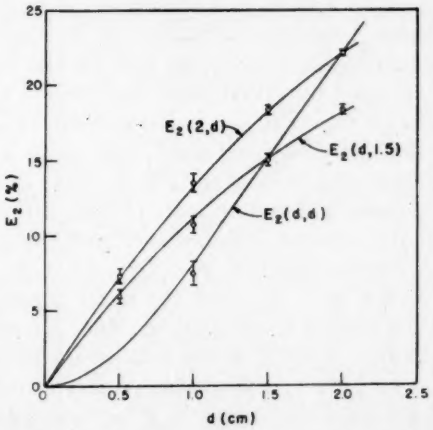

FIG. 2. The double transmission effect as a function of block thickness of polarizer and analyzer. The solid lines are theoretical based on an effective polarization cross section, p, of 2.8 barns and a depolarization coefficient, q, of 0.10 cm^{-1}.

TABLE II. Results of domain size measurements on Armco specimens of different metallurgical treatments.

Specimen	Final treatment	Thickness ($\times 10^3$ cm)	Grain size, Δ ($\times 10^3$ cm)	$d_{\frac{1}{2}}$ ($\times 10^3$ cm)	$\bar{\delta}$ ($\times 10^4$ cm)	$\bar{\delta}/\Delta$
A-1	0% cold reduction after annealing	1.3	0.5	1.9 (2.0)	1.6 (1.5)	
A-2	50% cold reduction after annealing	1.5	0.5	1.8	1.7	
A-3	97% cold reduction after annealing	1.3	1.2	3.9	0.77	
A-4	98.5% cold reduction after annealing	0.4	0.5	11	0.26	
B-1	36% cold reduction after anneal and quench	2.5	2.2	1.6	1.9; 25	
B-2	68% cold reduction after anneal and quench	2.5	1.5	1.7	1.7	
B-3	84% cold reduction after anneal and quench	2.5	1.4	2.0	1.5	
B-4	92% cold reduction after anneal and quench	2.5	1.3	2.4	1.2	
B-5	96% cold reduction after anneal and quench	2.5	1.3	2.8 (0.89)	1.1 (3.3)	
B-6	98% cold reduction after anneal and quench	2.5	0.9	2.5	1.2	
B-7	99% cold reduction after anneal and quench	2.5	1.3	4.0	0.75	
B-8	99.5% cold reduction after anneal and quench	2.5	5.7	3.8	0.80	
B-9	99.75% cold reduction after anneal and quench	1.3	5.7	9.9 (5.8)	0.30 (0.52)	
D-1	Annealed at 700°C before final treatment	2.5	2.5	1.1	2.7; 18	0.11; 0.72
D-2	Annealed at 700°C before final treatment	5.1	3.3	1.5	2.0; 24	0.061; 0.73
D-3	Annealed at 700°C before final treatment	7.6	4.8	2.8	1.1; 44	0.023; 0.92
E-1	Annealed at 750°C after final treatment	2.5	2.4	0.94	3.2; 14	0.13; 0.58
E-2	Annealed at 750°C after final treatment	5.1	4.4	1.5	2.0; 24	0.045; 0.55
E-3	Annealed at 750°C after final treatment	7.6	4.4	2.4	1.2; 39	0.027; 0.89
F-1	Annealed at 800°C before final treatment	2.5	2.5	1.4	2.1; 23	0.084; 0.92
F-2	Annealed at 800°C before final treatment	5.1	4.1	1.3	2.3; 21	0.056; 0.51
F-3	Annealed at 800°C before final treatment	7.6	5.7	2.9	1.0; 46	0.018; 0.81

ness constant and equal to 2 cm; (3) $E(d, 1.5)$, analyzer thickness constant and equal to 1.5 cm.

In order to obtain a value of the polarization cross section from the data, the "hardening" (change in velocity distribution with d) of the beam must be considered. The hardening was calculated from the measurements by HWH of the single transmission effect E_1 and of the total cross section of iron as a function of neutron velocity, with the exception of the values for neutron velocities <980 m/sec. where a value of $E_1=0.2$ percent, derived from more recent measurements,[21] were used. These values of E_1 were averaged over the velocity distribution calculated from the total cross section for a series of d's covering the range of the observations. Assuming the validity of the usual quadratic approximation $E_1=\frac{1}{2}(Npd)^2f(x)$ for the thickness $d=1.32$ cm used by HWH, and their results that the depolarization function $f(x)$ is independent of neutron velocity for the cold-rolled steel used, these averages give numbers proportional to $\langle p^2\rangle_{Av}$ for the corresponding thicknesses. The square roots of their ratios to the value for the incident Maxwell spectrum (p_0) give the desired hardening function, $R=[\langle p^2\rangle_{Av}/\langle p_0^2\rangle_{Av}]^{\frac{1}{2}}$, plotted in Fig. 3. We have not used the usual quadratic approximation further in our analysis, since the condition for its validity, $Npd\ll 1$, is not fulfilled under our conditions, $Np\approx\frac{1}{4}$ cm^{-1}. Expansions of the formulas (3), (5), and (9) show that terms in p^4 become appreciable at our larger thicknesses. However, we have assumed that our root-mean-square averages adequately describe the hardening effect on our measurements. From our values of E_2, we obtain as most probable values, $p_0=2.80\pm0.15$ barns and $q=0.10\pm0.05$ cm^{-1}. The curves in Fig. 2 have been calculated from these values. [For calculating $E_2(d_1, d_2)$ from (9), it should be noted that

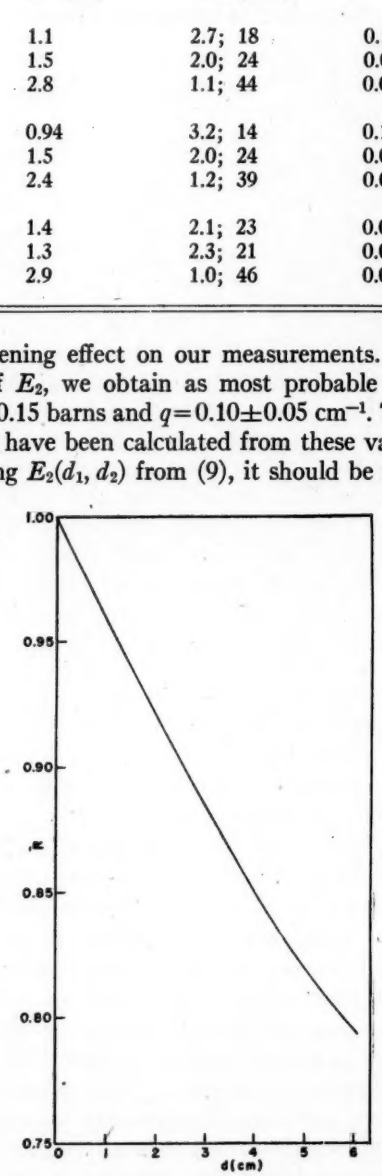

FIG. 3. The theoretical ratio of the r.m.s. value of p to that for a Maxwell distribution. The decrease in p is caused by the hardening of the beam with increasing d.

[21] Burgy, Hughes, and Woolf, Phys. Rev. 76, 188 (1949).

the value of $E_1(d_2)$ must be computed using the hardening correction on p for the thickness d_1+d_2.]

These results are in disagreement with the measurements of HWH with the same neutron spectrum using the single transmission effect. They obtained $p_0=3.15 \pm 0.10$ barns and $q=0.493$ cm^{-1}, that is, a somewhat higher polarization cross section and a much larger depolarization due to incomplete saturation. The most likely systematic error which may have entered into our measurements is incomplete "piping" of the neutrons from the polarizer field into the analyzer field in the antiparallel case. Another possibility of error is that our electromagnets are less likely to provide a uniform field in the steel blocks than did the magnet used by HWH. On the other hand, if our work is correct, the systematic error most likely to have been present in their work is incomplete elimination of small-angle scattering effects. However, in connection with this possibility it should be mentioned that HWH had evidence that these effects had been eliminated and further studies[20] have confirmed the adequacy of their method of elimination. Despite the disagreement, the original purpose of checking that p was about three times the previous theoretical estimates by direct analysis of the polarization, has been fulfilled.

In the depolarization work, in which 2-cm polarizer and analyzer thicknesses were used, the polarization of the beam incident upon the depolarizing foils is 38 percent as calculated from the values of p and q obtained from the double transmission work. The depolarization studies were made on Armco iron after a few preliminary measurements. A wide range of domain sizes was sought by cold-working and annealing the Armco specimens. To obtain small domain sizes, specimens were prepared having cold reduction in thickness ranging from 0 to 99¾ percent. To obtain large domains, growth of large grains was induced by cold-work followed by annealing. Several annealing temperatures

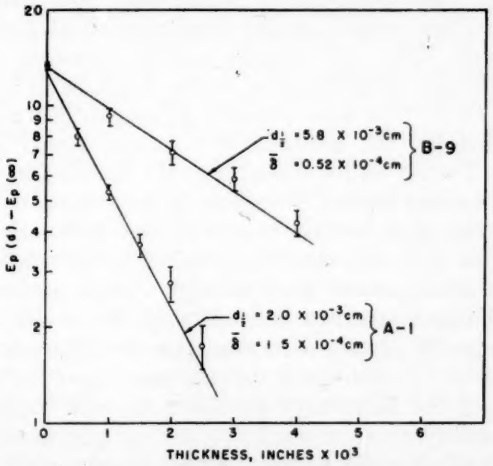

FIG. 4. Decrease of neutron polarization with distance in thin sheets of two Armco samples with different metallurgical treatment (see Table II) and the domain sizes, $\bar{\delta}$, inferred from the rate of depolarization.

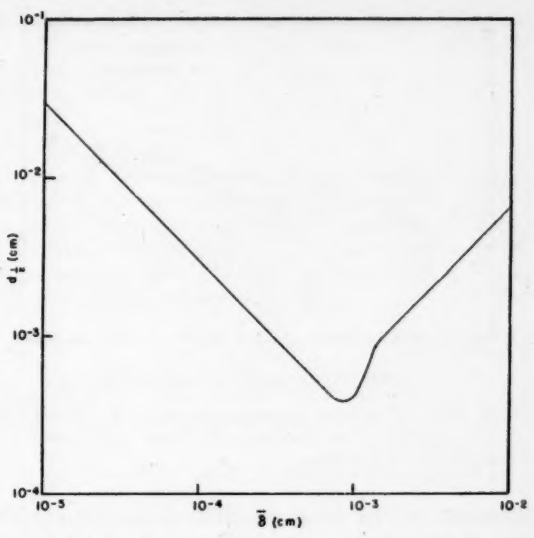

FIG. 5. The theoretical relationship between the half-thickness for depolarization, $d_{\frac{1}{2}}$, and the mean domain size, $\bar{\delta}$.

near the Curie point were used. It was desired to have the specimen thicknesses in the vicinity of 0.025 mm after treatment. Consequently the preparation involved an initial reduction of the Armco stock to a suitable intermediate thickness, followed by annealing to recrystallize the material and free it of strains. The Armco specimens fall into five groups according to their treatment. Those in group A were prepared from 0.0185-in. sheet, and, after the initial reductions in thickness, were annealed at 700°C for 15 min. The final cold reductions are listed in Table II. The specimens in group B were made from 1-in. round stock. Slabs of 0.200-in. thickness were cut from the stock, given an initial cold reduction, annealed at 925°C and water-quenched. The final cold reductions in thickness are listed in Table II. The purpose of the water quench given specimens in group B after annealing was to produce a more uniform grain structure than had been obtained in group A. The average grain sizes in the specimens of groups A and B were measured before giving them the final cold reduction and are listed in Table II. Grain sizes could not be measured after the final reductions. The specimens in groups D, E, and F were rolled from 0.0185 in. to a thickness about 10 percent greater than the planned final thickness, annealed at 710°C, reduced to their final gauge and further annealed 24 hr. The final annealing temperatures were 700°C for group D and 750°C for group E, both below the Curie point, and 800°C for group F, which is above the Curie point. All three annealing temperatures leave the specimens in the alpha-phase. The final thicknesses for groups D, E, and F are given in Table II, together with the grain sizes measured after the final anneal. Standard metallographic techniques were used in all grain size measurements.

To obtain the ratio $E_P(\infty)$ (of count with parallel fields to count without) corresponding to complete de-

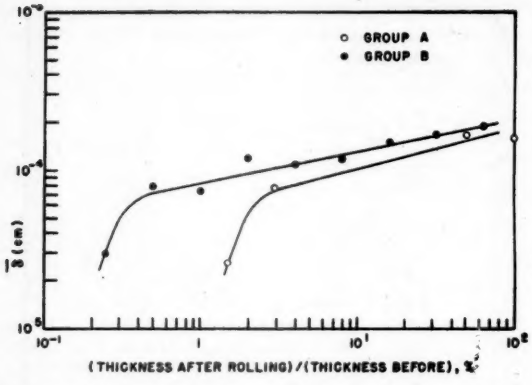

FIG. 6. Relation between domain sizes in groups A and B and the ratio of thickness of specimen after final cold reduction to thickness before, in percent.

polarization of the beam incident upon the analyzer, a foil of steel shim stock, 0.266 mm in thickness was used as the depolarizer. This gave essentially complete depolarization, as checked by the measured half-thickness for depolarization in shim stock and by the double transmission effect with this specimen in place, no difference between parallel and antiparallel intensities being found. Plots of $E_P(d)-E_P(\infty)$ were made for each type of specimen and the half-thickness $d_{\frac{1}{2}}$ for depolarization determined. Curves for two of the specimens are given in Fig. 4.

The $d_{\frac{1}{2}}$ values and corresponding $\bar{\delta}$-values obtained for the specimens are listed in Table II. Figure 5 shows that $\bar{\delta}$ is a two-valued function of $d_{\frac{1}{2}}$, and this results in an ambiguity in the values obtained for $\bar{\delta}$ in ten of the specimens examined. In the remaining twelve a single value is obtained for $\bar{\delta}$, since the larger of the two values given by Fig. 5 is greater than the foil thickness. Where two values of $\bar{\delta}$ are not excluded by this consideration, both are listed in Table II. The values of $d_{\frac{1}{2}}$ and $\bar{\delta}$ given in parentheses are the results of repeat measurements made about six months after the initial studies. An inspection of the results for groups A and B show a considerable decrease in domain size with increase in the severity of cold-working the material. This is shown graphically in Fig. 6 where domain size is plotted against the ratio of sample thickness after the final reduction to thickness before reduction in percent. The cold-working of the iron samples produces strain and breakup of the crystal grains, so that the observed decrease in domain size with increase in cold-work shows that as the size of the crystal grains becomes small, it controls the size of the domains. In groups D, E, and F large-size grains were grown in an effort to obtain large-sized domains, and variations due to difference in the annealing temperature in the vicinity of the Curie point were sought. The measurements show that annealing above the Curie point (group F) gave essentially the same results as annealing below it (groups D, E). The domain sizes of specimens in these three groups are given two values from Fig. 5. Choice of the smaller $\bar{\delta}$-values would give an unlikely inverse relation between domain size and grain size. On the other hand, choice of the larger $\bar{\delta}$-values in these three groups gives an approximate proportionality between domain size and grain size ($\bar{\delta}\approx 75$ percent of grain size). On the assumption of the latter relation the domain sizes of the specimens examined vary in size by a factor of 180, from 0.26×10^{-4} cm (A-4) to 46×10^{-4} cm (F-3). On three of the specimens (A-1, B-5, B-9), the measurements were repeated after a six-month interval (values given in parentheses in Table II). For the two which had had a cold-work treatment the later values of $\bar{\delta}$ were larger than those obtained initially. Thus B-5 and B-9, which had undergone cold reduction of 96 and 99¾ percent, respectively, showed increases in $\bar{\delta}$ by factors of 3 and 1.7, respectively. On the other hand, specimen A-1, which had not undergone cold-working, showed an insignificant change. We interpret the changes in domain size noted in the cold-worked samples as being due to grain growth from recrystallization and release of strain. As part of these later measurements, a test was made to see if extreme cold-rolling had produced preferred orientations of the magnetization of the domains. The specimens in group B had been worked by rolling in a single direction. If this resulted in a clustering of easy axes of magnetization about the rolling direction, the depolarization observed when the neutron polarization was parallel to this direction would be much less than when perpendicular. Measurements were made on the strongly worked sample B-9, and no difference was found between the parallel and perpendicular orientations of the neutron polarization relative to the rolling direction. A further test of the effect of extreme cold-rolling on magnetic domains was made by comparing the depolarization, obtained by sending the neutron beam through a specimen at a 60° angle with the normal to the specimen surface, to the depolarization at normal incidence. With the strongly worked specimen B-9 (99¾ percent reduction) the values $d_{\frac{1}{2}}=4.7\times10^{-3}$ cm, $\bar{\delta}=0.64\times10^{-4}$ cm were obtained at 60° incidence and $d_{\frac{1}{2}}=5.8\times10^{-3}$ cm, $\bar{\delta}=0.52\times10^{-4}$ cm at normal incidence. Thus it would appear that the domains in this specimen have greater dimensions in the plane of rolling than they have normal to this plane. However, this variation of $\bar{\delta}$ with direction relative to the plane of rolling is not present in all strongly worked specimens as a similar comparison with specimen A-3, which had undergone 97 percent reduction, gave no difference.

We wish to acknowledge the extensive help of S. Hugh Paine, of the Metallurgy Division, Argonne National Laboratory, who prepared the Armco specimens for our domain size measurements and made the grain size determinations in them.

Radiations from Mo^{99} and Tc^{99m}

MERLE E. BUNKER AND ROBERT CANADA
Indiana University, Bloomington, Indiana*
(Received July 24, 1950)

The radiations from Mo^{99} (67 hours) and its metastable daughter Tc^{99m} (6 hours) have been measured in a magnetic lens spectrograph. The beta-ray spectrum consists of a group with an end-point energy of 1.23 Mev, one of 0.445 Mev and possibly a third lower energy group. The relative intensities of the 1.23-Mev to 0.445-Mev groups are 4:1. Gamma-rays have been found at 0.040, 0.140, 0.181, 0.367, 0.741, and 0.780 Mev. The gamma-rays at 0.040, 0.140, and 0.181 Mev are internally converted. The spectrum of Tc^{99} consists of one internally converted gamma-ray at 0.140 Mev. A disintegration scheme is proposed.

I. INTRODUCTION

IF molybdenum is bombarded with either deuterons or slow neutrons, a 67-hour activity is produced which has been attributed[1] to Mo^{99}. Furthermore, it has been shown that this isotope is in equilibrium with a 6-hour daughter element,[1,2] an isomer of Tc^{99}. Most of the preliminary measurements that have been made on the radiations from these two activities have been absorption and coincidence measurements, and no thorough spectrometric study has previously been reported. While this work was in progress, a similar study was reported by Medicus, Maeder, and Schneider[3] with results quite similar to those reported here. The present work, however, shows certain additional lines not obtained by them.

Seaborg and Segrè[1] separated the technetium activity from the molybdenum activity by chemical means, and reported the radiations from the technetium fraction to consist of a highly converted gamma-ray of energy 0.136 Mev. The molybdenum fraction was reported to emit beta-rays with an end-point energy of 1.5 Mev and gamma-rays of about 0.4-Mev energy. However, Miller and Curtiss[4] investigated the 67-hour activity with a thin magnetic lens spectrometer and reported gamma-rays of 0.24 and 0.75-Mev energy. More recently, Mandeville and Scherb,[5] using absorption and coincidence techniques, found that Mo^{99} emits two beta-ray groups with end-point energies of about 0.24 Mev and 1.03 Mev. Their coincidence measurements indicated that the low energy beta-ray group is coupled with gamma-rays but that the high energy group is not. The maximum energy of the gamma-rays was found to be 0.71 Mev and a small gamma-gamma-coincidence rate was detected. In addition, they isolated the 6-hour technetium activity by chemical separation and found no particle-gamma or gamma-gamma-coincidences, which would indicate that the metastable state decays with emission of a single partially converted gamma-ray.

II. APPARATUS AND SOURCE PREPARATION

The apparatus used in this investigation was a magnetic lens spectrometer of conventional design. The general details of the instrument have been described elsewhere.[6] During these experiments, the spectrometer was adjusted to give a resolution of about 2.5 percent. An end window Geiger counter with an aperture 7 mm in diameter served as the detector of beta-particles. The Zapon counter window used in examining the data had a low energy cut-off of 11–15 kev, depending on the type of experiment performed.

The Mo^{99} used in the present investigation was obtained by bombarding metallic molybdenum with deuterons in the Indiana University cyclotron. This bombardment also produces a number of radioactive technetium isotopes, whose combined activity is much greater than the activity of the Mo^{99}. Since the half-lives of the technetium activities are of the same order of magnitude as that of Mo^{99}, a great deal of care was taken in the process of chemical purification to remove all the technetium. The method used in the chemical purification was similar to that described by Seaborg and Segrè.[1] In the final stage of the procedure, the molybdenum was precipitated with 8-hydroxyquinoline solution. A small amount of this precipitate was dissolved in nitric acid for use as beta-ray source material. The remainder was dissolved in nitric acid and the molybdenum was precipitated as the sulfide with hydrogen sulfide, centrifuged, and dried for use as the gamma-ray source material.

Before any measurements were made, at least thirty-six hours were allowed to elapse in order to permit the 6-hour metastable state to come to equilibrium with the parent activity.

III. THE BETA-RAY SPECTRUM

The beta-ray source had a surface density of 0.2 mg/cm² and was about 6 mm in diameter. It was mounted on a thin Zapon film of 0.08 mg/cm² surface density.

* This research was assisted by the joint program of the ONR and AEC.

[1] G. T. Seaborg and E. Segrè, Phys. Rev. 55, 808 (1939).
[2] Plutonium Project Report, Rev. Mod. Phys. 18, 513 (1946).
[3] Maeder, Medicus, and Schneider, Helv. Phys. Acta 22, 603 (1949).
[4] L. C. Miller and L. F. Curtiss, Phys. Rev. 70, 983 (1946).
[5] C. E. Mandeville and M. V. Scherb, Phys. Rev. 73, 848 (1948).
[6] Bunker, Canada, and Mitchell, Phys. Rev. 79, 610 (1950).

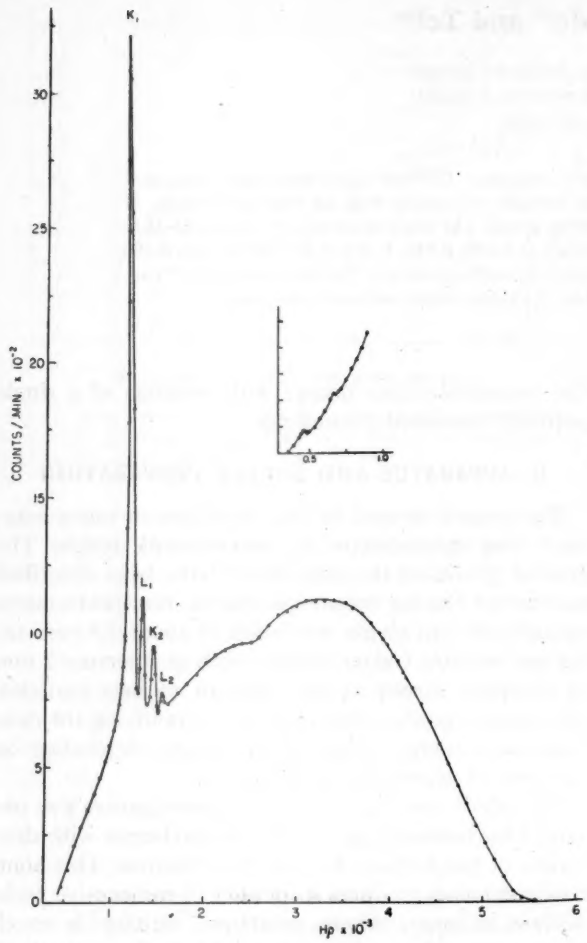

FIG. 1. Beta-ray spectrum of Mo^{99}.

The beta-ray spectrum is shown in Fig. 1. Here the number of counts per minute, corrected for decay, is plotted as ordinate against $H\rho$ (gauss-cm) as abscissa. It can be seen at once that the continuous part of the spectrum is complex. A Fermi analysis has been made of the beta-ray data using the approximation for the Coulomb correction factor, $F(Z, \eta)$, given by Bethe and Bacher.[7] The results are shown in Fig. 2. The end-point energy of the high energy group is 1.23±0.01 Mev and that of the low energy group is 0.445±0.01 Mev. The contribution of these two groups to the low energy portion of the spectrum was calculated by extrapolating the straight lines of the Fermi plot back to zero energy. The ratio of the intensity of the high energy group to that of the low energy group is 4:1. Judging from the appearance of the spectrum below and to the left of the internal conversion lines, it would seem that there is an additional low energy beta-ray group, although it is not possible to say much about its end point energy or intensity due to interference from the group of lines.

Referring to Fig. 1, the peaks at 1228 and 1328 gauss-cm are K and L internal conversion lines corresponding to a gamma-ray energy of 0.140 Mev. Similarly, the peaks at 1457 and 1535 gauss-cm are K and L conversion lines corresponding to a gamma-ray energy of 0.181 Mev. The ratio N_K/N_L was calculated in both cases, although a certain amount of arbitrariness exists in choosing base levels for the lines. For this reason, maximum and minimum values were calculated in the case of the pair of lines of lower energy. The results are shown in Table I.

On the basis of the reports of other investigators, it was assumed that the 0.140-Mev gamma-ray is associated with the 6-hour isomeric state of Tc^{99}. In order to confirm this assumption and to investigate the possibility of the 0.181-Mev gamma-ray also being associated with this (or another) metastable level, the technetium was removed chemically from a portion of the source material, and observation of the internal conversion lines emitted by the molybdenum fraction was begun within three hours after the purification. It was observed that the conversion lines associated with the 0.140-Mev gamma-ray increased in intensity with time at approximately the rate expected from the growth of a 6-hour activity, but that the lines associated with the 0.181-Mev gamma-ray decay with a 67-hour half-life from the beginning of the observations. It is thus concluded that if the 0.181-Mev gamma-ray is associated with a metastable state, this state has a much shorter half-life than 6 hours. Experiments on the Tc^{99} fractions show only the 0.140-Mev gamma-ray (see below).

A later experiment on the beta-ray spectrum of Mo^{99}, in which a thinner window was used, showed two weak internal conversion lines corresponding to K and L lines for a 40-kev gamma-ray. The intensity of the K-line is, no doubt, decreased by window absorption (see inset of Fig. 1).

IV. GAMMA-RAY MEASUREMENTS

The distribution of secondary electrons ejected from a 7 mg/cm² lead radiator by the gamma-radiation of Mo^{99} was examined in the lens, and the result is shown in Figs. 3 and 4. The peaks at 789, 1262, and 1326 denoted by $K_1L_1M_1$, are the K, L, and M photo-electron peaks corresponding to a gamma-ray of 0.140 Mev. The K, L, and M peaks at 1075, 1480 and 1535 gauss-cm, denoted by $K_2L_2M_2$, are due to a gamma-ray of energy 0.181 Mev. Due to the low intensity of the high-energy region of the spectrum the portion of the curve above 1570 gauss-cm is plotted on a larger scale than is used for the rest of the spectrum and is shown in Fig. 4. The K and L peaks which appear at 2014 and 2326 gauss-cm (K_3L_3) are due to a 0.367-Mev gamma-ray and the K and L peaks at 3500 and 3768 gauss-cm (K_4, L_4) correspond to a 0.741-Mev gamma-ray. The peak at 3642 gauss-cm (K_5) is apparently a K line due to a gamma-ray of 0.780-Mev energy. The L line for this gamma-ray should come at 3906 gauss-cm, but it was not resolved and appears only as a bulge on the

[7] H. A. Bethe and R. F. Bacher, Rev. Mod. Phys. 8, 194 (1936).

high energy side of the L line of the 0.741-Mev gamma-ray.

Owing to the numerous weak lines obtained and the uncertainties involved in the chemistry of technetium, the decay of the various lines was followed for a considerable time. All lines appeared to decay with a period of 67 hours. In addition, in some of the earlier runs in which the chemistry was not well carried out, certain strong lines of technetium, produced by the (dn) reaction, were observed. In the present samples these lines were not observed and it is therefore felt that the sample is free of technetium. All lines apparently belong to Mo^{99}.

The relative intensities of the lines of energy greater than 0.300 Mev were calculated with the help of Gray's[8] empirical formula and are shown in Table II.

V. EXPERIMENTS WITH Tc^{99}

In order to investigate the spectrum of Tc^{99} the following procedure was carried out. The Mo^{99} was first separated from technetium. The Tc^{99} was allowed to come into equilibrium with the parent Mo^{99} and was then chemically separated and measured.

The "beta-ray" spectrum, shown in Fig. 5, is seen to consist of K and L internal conversion lines for a gamma-ray of 0.140 Mev. No evidence could be found for an internally converted gamma-ray of 0.181 Mev. In addition, in an incomplete experiment in which a stronger source was used, an Auger line was observed at 14 kev corresponding to the ejection of an L electron by the $K\alpha$ radiation of Tc.

The gamma-rays from Tc^{99} were measured using a lead radiator of 16 mg/cm². As will be seen in Fig. 6, only the K, L, and M photo-lines for the gamma-ray at 0.140 Mev are seen.

VI. DISCUSSION

The beta-ray spectrum of Mo^{99} consists of two beta-ray groups, the energies of whose end points are 1.23 $\pm$0.01 and 0.445$\pm$0.01 Mev. The ratio of the intensity of the high energy group to that lower energy is 4:1. There is some indication of a weaker group of low energy, estimated to have an end point of $\sim$0.08 Mev. The gamma-ray spectrum consists of lines at 0.140 Mev, owing to Tc^{99}, 0.181, 0.367, 0.741, and 0.780 Mev with some evidence for a 0.040-Mev line. The line at 0.741 Mev is about 10 times as strong as the lines at 0.367 and

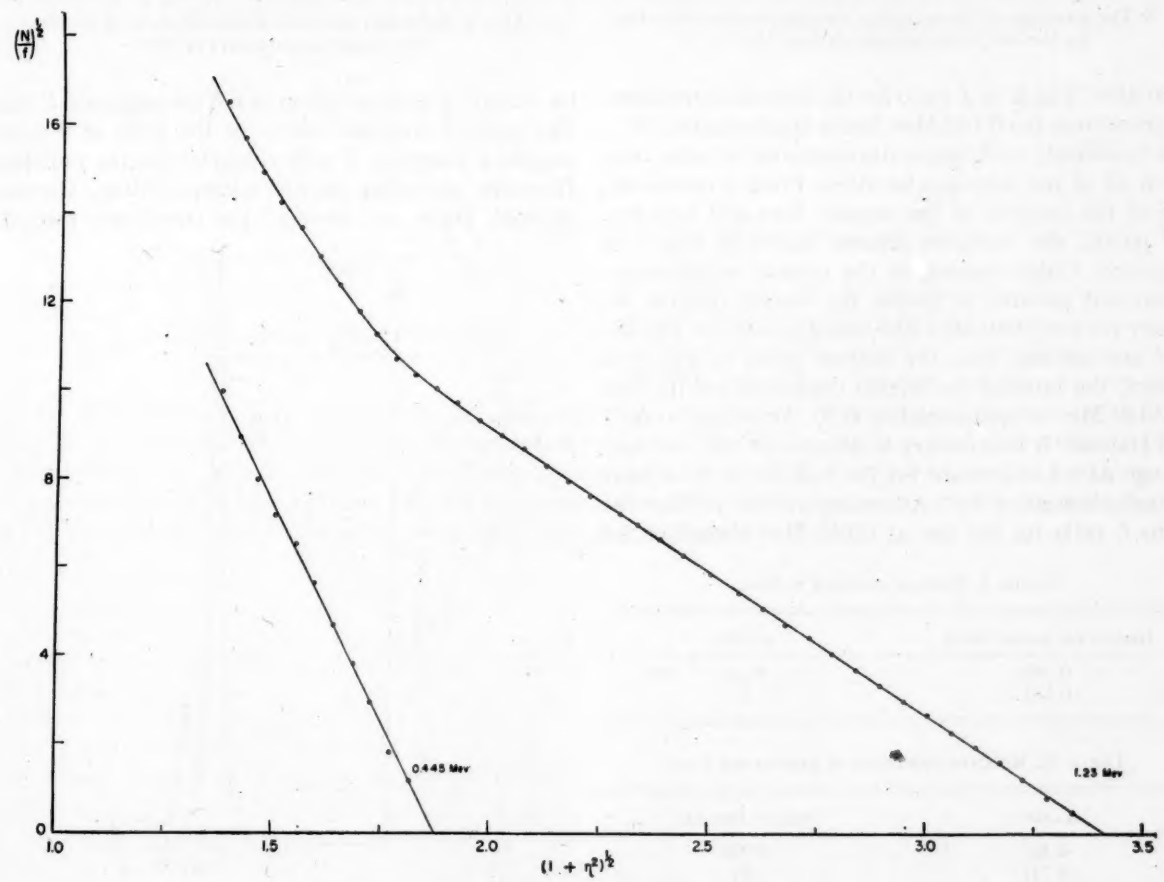

FIG. 2. Fermi plot of beta-ray spectrum of Mo^{99}.

[8] L. H. Gray, Proc. Camb. Phil. Soc. 27, 103 (1931).

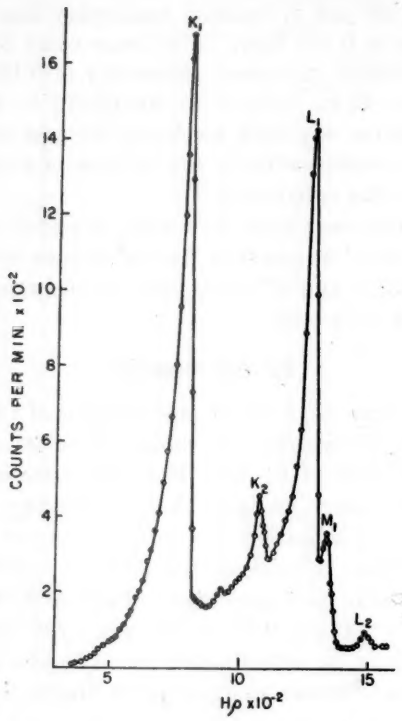

FIG. 3. The spectrum of the secondary electrons ejected from lead by the low energy gamma-rays of Mo^{99}.

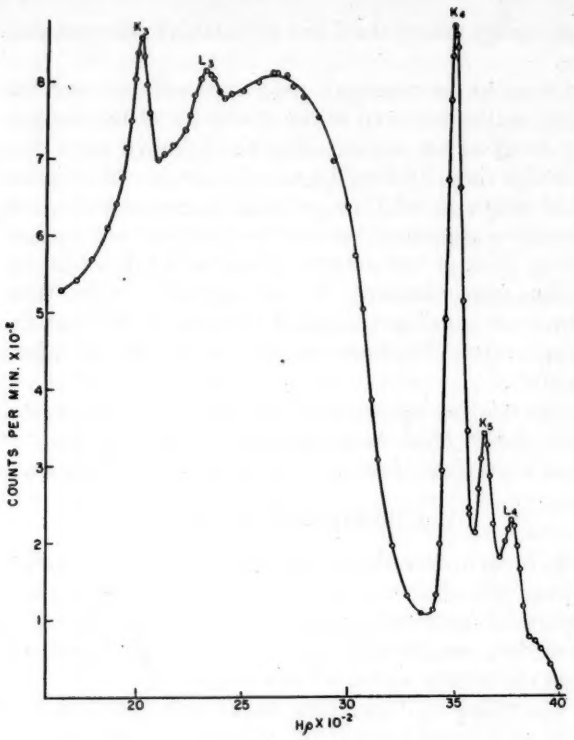

FIG. 4. Secondary electrons ejected from level by the high energy gamma-rays of Mo^{99}.

0.780 Mev. The K to L ratio for the internal conversion electrons from the 0.140-Mev line is approximately 9.

It is difficult to devise a disintegration scheme into which all of the data can be fitted. From a consideration of the energies of the various lines and beta-ray end points, the tentative scheme shown in Fig. 7 is suggested. Unfortunately, in the present experiments, it was not possible to obtain the correct relative intensity for the 0.040-Mev line owing to window cut-off.

If one assumes that the scheme given in Fig. 6 is correct, the internal conversion coefficient for the line at 0.140 Mev is approximately 0.20. According to Axel and Dancoff[9] it is necessary to assume an effective spin change $\Delta I=4$ to account for the half-life of the 6-hour metastable state of Tc^{99}. According to these authors the K to L ratio for the line at 0.140 Mev should be 1.8 for electric 2^4-pole radiation or 6.8 for magnetic 2^3 pole. The present observed value for the ratio of 9 would suggest a magnetic 2^3 pole character for the radiation. However, according to the tables of Rose, Goertzel, Spinrad, Harr, and Strong[10] the conversion ratio, β_3,

TABLE I. Internal conversion data.

Gamma-ray energy (Mev)	N_K/N_L
0.140	9±2
0.181	5

TABLE II. Relative intensities of gamma-ray lines.

E (Mev)	Relative intensity
0.367	0.096
0.741	1.00
0.780	0.144

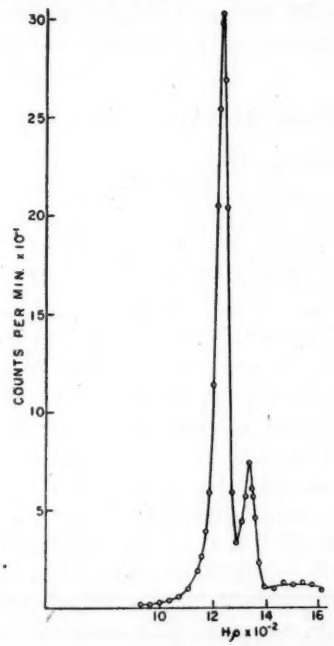

FIG. 5. Internal conversion electron spectrum of Tc^{99m}.

[9] P. Axel and S. M. Dancoff, Phys. Rev. 76, 892 (1949).

[10] Rose, Goertzel, Spinrad, Harr, and Strong, report privately circulated.

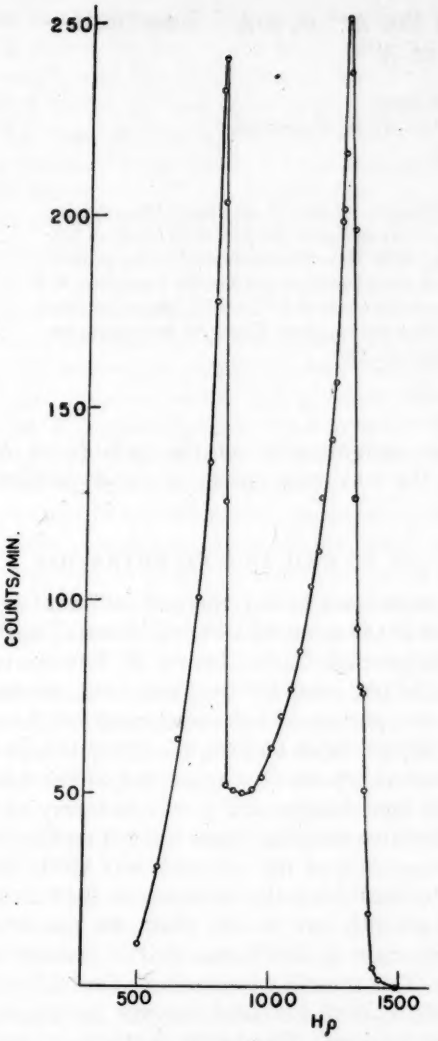

FIG. 6. Secondary electrons ejected from lead by gamma-ray of Tc^{99m}.

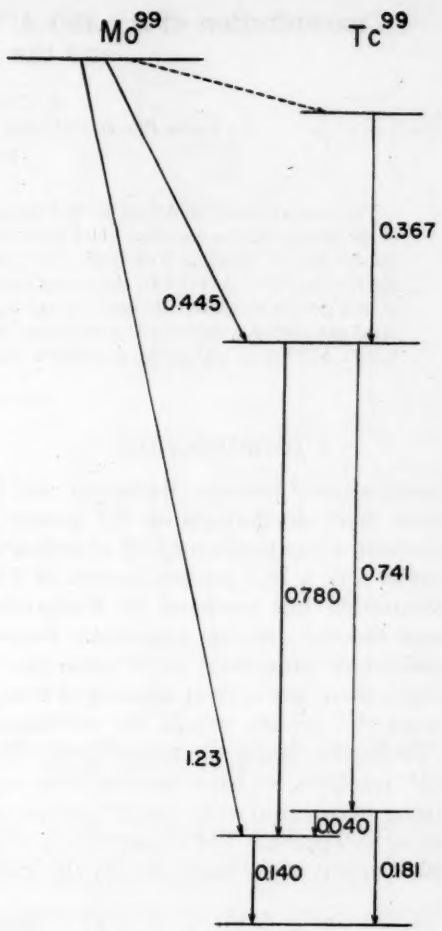

FIG. 7. Suggested energy level diagram for the decay of Mo^{99}.

will be approximately 4, in contrast to the observed value of 0.2. This difficulty appears to have been resolved by Medicus, Maeder, and Schneider,[3] who have evidence for two levels near 140 kev, differing in energy by 1.8 kev. One of these levels is the metastable level responsible for the 6-hour half-life. These two levels are not shown separately in Fig. 7.

The authors are indebted to Professor A. C. G. Mitchell, who suggested this problem, for his advice and many helpful suggestions. They would also like to thank Dr. M. B. Sampson and the members of the cyclotron group who carried out the bombardments and also Miss Elma Lanterman, who did the chemical separations.

Concentration of A^{36} and A^{38} and Study of the $A^{36}(d, p)A^{37}$ Reactions and the Beta-Activity of A^{39}*

A. ZUCKER† AND W. W. WATSON
Sloane Physics Laboratory, Yale University,‡ New Haven, Connecticut

(Received July 21, 1950)

The concentration of A^{36} up to 95.9 percent by the thermal diffusion method is described. Observation of the proton groups resulting from the deuteron bombardment of this gas gives the following Q-values for the $A^{36}(d,p)A^{37}$ reaction: 6.49, 5.05, 3.93, 2.95, 2.09, 1.86, 1.42 and 0.64 Mev. Comparison with the proton distribution from $A^{40}(d,p)A^{41}$ shows the importance of having well-separated isotopes for the resolution of proton groups of nearly the same energy from each isotope. The enrichment of A^{38} to 0.75 percent in this same gas makes measurement possible on the betas from the $A^{38}(d,p)A^{39}$ reaction. These A^{39} beta particles have a half-life of 160±5 seconds and a maximum energy of about 2.1 Mev.

I. INTRODUCTION

IN a recent article,[1] Davison, Buchanan, and Pollard reported their observations on the proton groups from the deuteron bombardment both of ordinary argon and of argon with a 26.2 percent content of A^{36}. This A^{36} concentration was produced by Buchanan[2] in a multi-stage thermal diffusion apparatus. Despite this very considerable enrichment in A^{36} from the normal 0.31 percent, there was evident masking of most of the short range A^{37} proton groups by overlapping A^{41} groups. To display clearly the proton groups from the $A^{36}(d,p)A^{37}$ reactions, we have repeated these measurements, using argon gas in which the A^{36} isotope was concentrated to 95.9 percent. The concentration of the rare A^{38} to 0.75 percent in the same gas has also made possible the determination of the half-life of A^{39} and roughly the maximum energy of the β-particles which it emits.

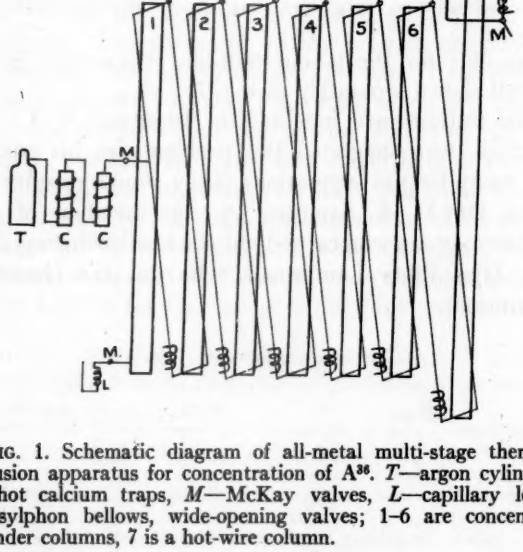

FIG. 1. Schematic diagram of all-metal multi-stage thermal diffusion apparatus for concentration of A^{36}. *T*—argon cylinder, *C*—hot calcium traps, *M*—McKay valves, *L*—capillary leak, *V*—sylphon bellows, wide-opening valves; 1–6 are concentric cylinder columns, 7 is a hot-wire column.

II. A^{36} AND A^{38} CONCENTRATION

The major part of our thermal diffusion apparatus consisted of the same six all-metal columns, each based on a copper-clad Calrod heater of 200 cm effective heating length, used by Buchanan and described recently[3] as a portion of some equipment for the concentration of Ne^{22}. Since for neon the heavy isotope is to be concentrated, whereas for argon one wishes to concentrate the light isotope A^{36}, it was necessary to reverse the convective coupling pipes connecting the columns. The temperature of the hot walls was 450°C, as determined by measuring the extension of the Calrods.

As a seventh unit in this chain, we connected convectively, just as Buchanan did, a 3-meter hot-wire column. This column we constructed entirely of metal, however, so that we could operate the apparatus at elevated pressures. The details of this hot-wire column are similar to those of a column we had operated for some time[4] in a high pressure thermal diffusion apparatus for the concentration of He^3. An innovation was to make the hot wire of 20-mil nichrome which operated successfully for considerable periods of time at 1000°K.

Figure 1 gives the schematic arrangement of this apparatus. It was necessary to remove the nitrogen impurity (about 0.4 percent) in the tank argon, for otherwise the "light" end volume at the top of column 7 would soon become choked with nitrogen. The gas was therefore first purified by passing it through two stainless-steel traps containing calcium metal shavings at about 400°C.

Since our aim was to attain a maximum separation factor, we calculated the gas pressure which would give the desirable value[5] of about two for the ratio K_c/K_d of the two remixing coefficients. This calculation showed that, if $p=1.06$ atmos. this condition would prevail in

* Taken in part from a dissertation submitted by A. Zucker in partial fulfillment of the requirements for the degree of Doctor of Philosophy at Yale University.

† Now at Carbide and Carbon Chemicals Corporation, Oak Ridge, Tennessee.

‡ Assisted by the AEC.

[1] Davison, Buchanan, and Pollard, Phys. Rev. **76**, 890 (1949).

[2] J. O. Buchanan, Phys. Rev. **75**, 1332A (1949).

[3] Watson, Onsager, and Zucker, Rev. Sci. Inst. **20**, 924 (1949).

[4] Schuette, Zucker, and Watson, Rev. Sci. Inst. (to be published).

[5] R. C. Jones and W. H. Furry, Rev. Mod. Phys. **18**, 151 (1946).

columns 5 and 6, with the transport $H=3.48\times10^{-5}$ g sec.$^{-1}$, $K_c=2.59\times10^{-3}$ g cm sec.$^{-1}$, $K_d=1.37\times10^{-3}$ g cm sec.$^{-1}$, and the separation factor $q=33.4$. For columns 1 and 2 at this same pressure $K_c/K_d=10.4$ which is a value well below the critical ratio of ~25 at which turbulence might set in.[6] A preliminary calculation had shown that $\frac{3}{8}''$ i.d. copper pipe was the best available size for the cold wall of the hot-wire column. For this column 7 at this optimum pressure $H=1.69\times10^{-5}$ g sec.$^{-1}$, $K_c=5.72\times10^{-4}$ g cm sec.$^{-1}$, $K_d=2.60\times10^{-4}$ g cm sec.$^{-1}$, and $q=440$.

Column 1 was operated as a scrubber, and the gas was fed into the convective coupler between columns 1 and 2. The argon input was at the rate of about 250 cm^3/hr. At this rate the argon bled into the atmosphere through a capillary leak at the bottom of the scrubber was depleted of about half of its A^{36} content.

The product of the calculated separation factors for the last three columns alone has the impressive value of 14,700, sufficient to give a concentration of 98 percent A^{36} at the top of column 7. In actual performance, however, the A^{36} content in the 200 cm^3 end volume after 200 hours was but 20 percent, while after an additional 200 hours the enrichment had reached only 22.5 percent. In steady operation we found the apparatus capable of producing 200 cm^3 of 20 percent A^{36} every 70 hours. This relatively low experimental separation factor we attribute as usual to a fairly large coefficient of parasitic remixing. The total power consumption of this apparatus was about 7 kw.

To increase the concentration of A^{36} to the desired 90 percent we proceeded to recycle this 20 percent product in a hot-wire column. This was a glass column 3 meters long, with cold wall of 1.018 cm i.d., and with a 20-mil tungsten wire operated at 1500°K. Convective circulation was maintained through an end volume both at the top and the bottom as shown in Fig. 2. The "heavy" end volume had a capacity of 200 cm^3, that at the "light" end 50 cm^3, while the column itself had a volume of 250 cm^3. At 1500°K and 1 atmos. pressure calculation gave for this column $H=1.085\times10^{-5}$ g sec.$^{-1}$, $K_c=3.48\times10^{-4}$ g cm sec.$^{-1}$, $K_d=5.23\times10^{-4}$ g cm sec.$^{-1}$ and $q=42$.

The column was charged with 500 cm^3 of the 20 percent A^{36} gas, operated for 12 hours, and then the lower end volume was isolated and its gas content removed. A fresh 200 cm^3 batch of 20 percent A^{36} was then pumped into this reservoir and connection to the column was re-established for 12 more hours. Then this process was repeated once again. With this 36 hours of operation the separation was completed, the "light" end volume was isolated, and its contents were withdrawn into a breakseal tube.

In order to conserve the concentrated A^{36} material, the increase in concentration was followed by an analysis of the gas in the "heavy" end each time a new batch was about to be added. These mass spectrometer analyses are given in Table I. Knowing the total amount of A^{36} in the column and assuming a uniform concentration gradient up the column, we could then calculate that the light end volume should contain 91.9 percent A^{36}. A mass spectrometer analysis of this product showed its A^{36} content to be 92.6 percent. From another similar set of operations 50 cm^3 of 95.9 percent A^{36} were obtained. The A^{38} content of these samples averaged 0.75 percent.

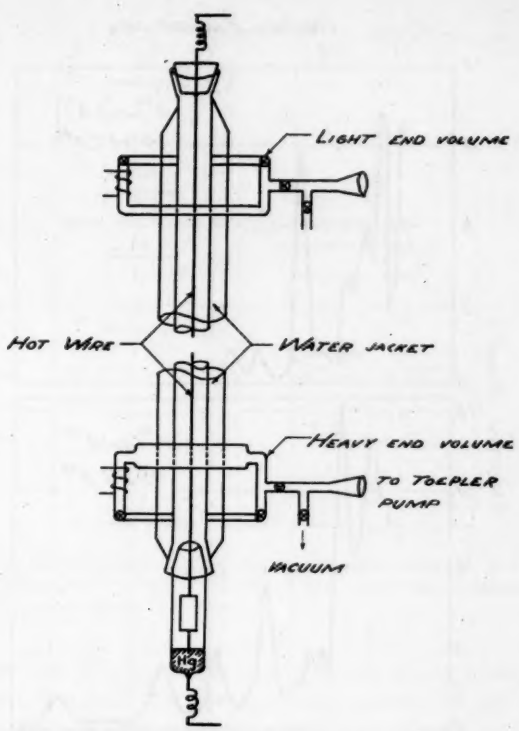

FIG. 2. Details of glass hot-wire column used for recycling the argon partially concentrated in A^{36}.

We conclude that this recycling of the partially concentrated light argon is an effective procedure. The over-all efficiency could be increased by feeding back into the first stage of the all-metal apparatus the product withdrawn from the lower end-volume of the glass hot-wire column before injection of each new batch of 20 percent A^{36} gas. Also it seems obvious that the isotope of intermediate weight, A^{38}, might have its greatest concentration at that point in the glass column where the A^{36}/A^{40} ratio is 50/50, for the thermal diffusion plus thermal syphoning effects would tend to send the A^{38} towards this intermediate point from either end. We

TABLE I. Concentration of A^{36} with time.

Running time (hours)	Concentration A^{36}
0	~20.0 percent
12	3.35
24	5.0
36	7.95

[6] L. Onsager and W. W. Watson, Phys. Rev. **56**, 474 (1939).

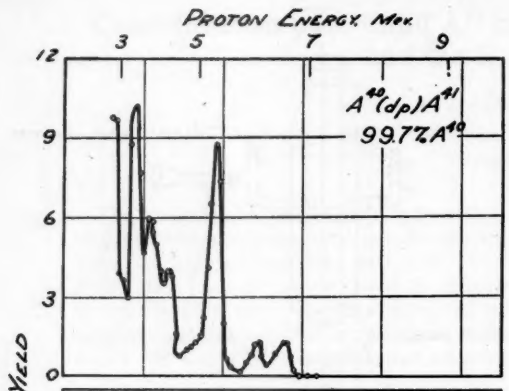

FIG. 3. Yield *vs.* energy plots of the protons from the deuteron bombardment of argon 36 and argon 40.

intend to investigate the distribution of A^{38} along this column both to check this reasoning and to obtain argon with a higher A^{38} content for further research on the β activity of A^{39} (see below).

III. THE $A^{36}(d,p)A^{37}$ REACTIONS

We have investigated the proton groups from the bombardment of this argon highly enriched in A^{36} by 3.9 Mev (extrapolated) deuterons. Before the argon was introduced into the target chamber it was freed of any nitrogen impurity by several passages through a trap containing hot calcium metal. The argon pressure in the chamber was 6.3 cm of Hg. The emitted protons were counted at an angle of 90° with the incident deuteron beam, using a proportional counter so adjusted as to count only those protons whose paths terminated in the counter. The proton energy was measured by interposing varying amounts of absorber between the bombarded gas and the counter.

TABLE II. Proton range and Q-values for the $A^{36}(d,p)A^{37}$ reactions and the energy levels of A^{37}.

Proton range cm	Q Mev	Relative yield	A^{37} energy levels Mev
106.26	6.49±0.08	1.0	ground
78.46	5.05±0.05	2.3	1.44
62.73	3.93±0.05	2.6	2.56
48.51	2.95±0.05	5.0	3.54
37.37	2.09±0.07	2.8	4.40
34.69	1.86±0.07	2.8	4.63
29.62	1.42±0.03	11.5	5.07
21.80	0.64±0.07	10.2	5.85

Figure 3 (lower half) is a plot of the yield of protons against proton energy. For comparison the corresponding measurements for $A^{40}(d,p)A^{41}$ made by Davison, Buchanan, and Pollard[1] are shown in the upper half of the figure. Close inspection of the two plots shows how important it is to have a high degree of isotope separation. The two unambiguous A^{37} proton groups with extrapolated ranges of 106 cm and 78 cm were discovered by Davison, Buchanan, and Pollard. We find no evidence confirming their suspicion that the group at range 78 cm is double. The group at 62-cm range, which is just beyond the longest range A^{41} group, was also accurately measured by Davison *et al.*, but their judgment that this group also is double is not substantiated by our observations. The A^{37} group at 48-cm range was detected and correctly identified by Davison *et al.*, but they could not determine its range accurately because of partial masking by the A^{41} group of 51 cm range.

The sharp dip occurring at 38 cm range in the lower plot in Fig. 3 we believe to come from the 3.5 percent A^{40} present in this enriched gas. The peak for this dip comes just where the prominent peak of the 40-cm-range A^{41} group is observed. We deduce from this that no other A^{37} group shown in our plot could arise from A^{40} contamination. For if the high yield 40-cm-range A^{41} group produces only such a small effect in the A^{37} proton distribution curve, none of the A^{37} peaks higher than the small one extrapolating to 38-cm range could be assigned to A^{41}.

The two A^{37} proton groups at 37-cm and 34-cm range were resolved by means of a range cell which enabled us to vary the proton absorption path by steps of a fraction of a centimeter. The most intense group at 29-cm range is so nearly at the same energy as an A^{41} group that only the argument given above assures us that this is a genuine A^{37} proton group. Finally, there is a proton group at 22 cm air equivalent, partially fused with another group at shorter range.

Table II gives all of these proton ranges and the corresponding Q-values and energy levels of the A^{37} nucleus. The proton groups at ranges 22 cm, 29 cm, 34 cm, and 37 cm are all new, while the group at 48-cm range has been measured more accurately than was possible with argon less well enriched in A^{36}.

The energy levels for A^{37} and A^{41} are plotted in Fig. 4. Most striking is the greater density of excited states in A^{41} as compared to A^{37}. Up to 4 Mev of excitation, the A^{41} nucleus has 9 levels while A^{37} has but 3. Both this difference and the appearance of levels in A^{37} at higher energies are probably related to the lesser stability of A^{41} with its four extra neutrons.

IV. BETA-ACTIVITY OF A^{39}

The A^{39} nucleus should by β-emission change to stable K^{39}. To date the only reference in the literature

to this β-activity is the assignment to A^{39} by Seaborg and Perlman in their table of isotopes[7] of a 4-minute half-life found by Pool, Cork, and Thornton[8] in the neutron bombardment of potassium. The A^{39} might have been produced in their experiment by a $K^{39}(n,p)A^{39}$ reaction. In our deuteron-bombarded argon containing 0.75 percent A^{38}, the A^{39} should be produced in detectable amounts by a (d,p) reaction. We do indeed find a β-activity of half-life 160 ± 5 sec. which from all indications is assignable to A^{39}. There is definitely no 4-min. activity in this enriched gas. Argon 37 decays by K-capture, while A^{41} is a β-emitter of half-life 110 min. The latter is, of course, always present because of the 3.3 percent A^{40} content, but our success in measuring the A^{39} β-activity has been aided as much by the markedly lowered background of A^{41} activity as by the increased percentage of A^{38}.

This A^{38}-enriched argon at a pressure of 15.6 cm of Hg was bombarded for 15 minutes by the deuteron beam in the same target chamber used for the proton-counting experiments. The cyclotron beam was then stopped and the gas was transferred by means of a Toepler pump to a 200 cm^3 counting chamber closed at one end with a 1-mil Al foil and shielded by lead on the side facing the cyclotron. The gas pressure in the counting chamber was 7.9 cm of Hg. Counting of the β's was done with a thin-mica, end-window Geiger counter. The decay curve after correction for background counts, including those from the 110-min. A^{41} β's, clearly indicates just one half-life of 160 ± 5 seconds. Repetition of the experiment using ordinary argon gave an activity of 110 min. within our limits of error, with a slight indication of a short-lived activity at the start of the counting.

To obtain the energy spectrum of these betas with half-life 160 sec., we have done some of this counting with Al absorbers between the counting chamber and the Geiger counter. A Fermi plot made from these data indicates that their maximum energy is about 2.1 Mev. We hope to increase the accuracy and completeness of these energy measurements when argon better enriched in A^{38}, becomes available. It can be taken as definite, however, that the maximum energy of the 160-sec. betas is considerably less than the 3.01 Mev value for Al^{28}, a possible contaminant emitter having about this half-life. The maximum energy of the A^{41} betas is 1.18 Mev.

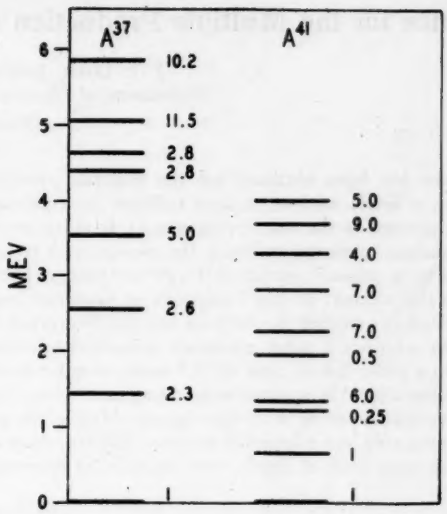

FIG. 4. Energy levels with relative abundances for A^{37} and A^{41}. Note the greater density of levels (3 to 1) for A^{41} as compared to A^{37} in the range up to 4 Mev.

From all the evidence, then, we conclude that these betas of half-life 160 ± 5 sec. and maximum energy roughly 2.1 Mev come from A^{39}.* This energy value should be measured with greater accuracy with a beta-ray spectrometer, using material with a higher concentration of A^{38}.

We wish to thank Professor E. C. Pollard for helpful discussions.

[7] G. T. Seaborg and I. Perlman, Rev. Mod. Phys. **20**, 585 (1948).
[8] Pool, Cork, and Thornton, Phys. Rev. **52**, 239 (1937).

* *Note added in proof:* A beta-activity with half-life longer than 15 years and assigned to A^{39} has recently been reported by by Brosi, Zeldes, and Ketelle (Phys. Rev. **79**, 902 (1950)). They do not have positive isotope assignment, and the time necessary for the processing of their irradiated material probably would preclude the detection of an activity with a period as short as that we observe. We of course would have missed a very long lived activity. Also Haslam, Katz, Moody, and Skarsgard (Phys. Rev. **80**, 318 (1950)) suggest that, since in their study of Cl^{39} no activity that could be attributed to A^{39} was observed, the half-life of A^{39} must be longer than 5 years. Admittedly it is improbable that isomerism exists in so light a nucleus even though it immediately follows the magic number $n=20$. Further research on A^{39} produced by d, p, and n, α reactions in argon better enriched in A^{38} is in progress.

Evidence for the Multiple Production of Mesons in a Single Nucleon-Nucleon Collision*

J. J. Lord, Joseph Fainberg, and Marcel Schein
Department of Physics, University of Chicago, Chicago, Illinois
(Received August 18, 1950)

Evidence has been obtained for the multiple production of mesons in a single nucleon-nucleon collision in a photographic emulsion exposed to the cosmic radiation at an altitude of 95,000 ft. The nuclear encounter in which the mesons were created was produced by a primary proton of 3×10^{13} ev energy. Directly in line with the incident proton 7 particles of minimum ionization were emitted in a central core with an angular divergence of 0.003 radian. In addition 8 other minimum ionization particles were emitted in a wider diffuse cone of 0.13 radian angular divergence. Only one track had the appearance of a fragment which, however, could have been a proton of 10-Mev energy. Most of the particles in the central core had energies in excess of 250 Bev, while those in the diffuse cone were of much lower energies as determined by small angle scattering measurements. A pair of very small angular divergence was produced in the central core 4800 microns from the point of origin of the nuclear interaction. Assuming that the pair were produced by a gamma-ray from the decay of a neutral meson, a lower limit of 2×10^{-15} second was deduced for its mean life. Both the angular and the energy distribution of the emitted particles is in good agreement with the assumption that in the center-of-mass system the mesons are emitted in two distinct cones of angular width of about 30° forward and backward with reference to the direction of the primary proton. The average multiplicity of 15 agrees with the recent calculation by Fermi, and according to his prediction about one-half of the particles could be made up of nucleon-antinucleon pairs.

I. INTRODUCTION

THUS far no clear-cut evidence has been obtained in which a high energy particle has produced more than one meson in a single nucleon-nucleon collision. In several nuclear interactions observed in photographic plates[1–5] on the order of 25 or 30 minimum ionization tracks were produced which have been shown to be predominantly mesons.[6] In all cases, however, the interactions occurred with silver or bromine nuclei, so that the contribution to the production of mesons by the numerous energetic secondaries could not be estimated. In the case of the star observed by the Rochester group,[5] the impinging particle was not a single nucleon but an alpha-particle of very high energy colliding with the nucleus of a heavy atom of the emulsion, as demonstrated by the many heavy tracks present. Numerous mesons were shown to be produced; however, in spite of the strong case for the multiple production of mesons in a single act, many secondary mesons emitted in successive collisions were distributed over such a wide angle cone that they had to be the result of plural production within the same nucleus.[7]

II. DATA

The event shown in Fig. 1 gives an example of the multiple production of mesons in a single act by an extremely high energy proton. This event was observed in an Ilford G-5 type emulsion 200 microns in thickness which was exposed to the cosmic radiation in the stratosphere. A free balloon[8] supported the plates at an elevation above 90,000 ft. for over 16 hours.

The event occurred about midway between the surfaces of the emulsion, and most of the tracks are very nearly parallel to the surface. Track A of minimum ionization extends over 10,000 microns in the emulsion and is taken to be the incident primary proton producing the nuclear interaction. Track B passes into the glass after a short distance and cannot be identified; however, a proton of about 10 Mev would produce a track of similar appearance. Track C is a 200-Mev proton, as determined from its small angle scattering and grain density.

The other 15 tracks, all of minimum ionization, lie in a narrow cone directly opposite the incident track A. In the upper section of Fig. 1, five of the minimum ionization tracks can easily be seen. The other 10 tracks are so closely spaced that they appear as a single heavy black track. The lower section of Fig. 1 shows these 10 tracks at a distance of 4800 microns from the nuclear interaction where they are more widely separated and all but two of them are easily resolved.

The arrow marked γ on the lower section of Fig. 1 is directed toward a point in the region of the core where a pair of charged particles originate and travel parallel to the other tracks in the core. In the region shown in Fig. 1, the angle between the tracks is so small that they appear as a single track.

III. DISCUSSION

The angular distribution of the tracks in the core is shown in Fig. 2. It is to be noticed that the curve in Fig. 2 shows the manner in which 7 minimum ionization particles were emitted in an extremely narrow bundle of 0.003-radian half-width (central core) and the other 8 in a considerably larger cone of 0.13-radian half-width (diffuse cone). Since all of the particles in the central

* Assisted by the joint program of the ONR and AEC.

[1] Brown, Camerini, Fowler, Heitler, King, and Powell, Phil. Mag. 40, 862 (1949).

[2] Schein, Lord, and Elston, Echo Lake Cosmic Ray Symposium, page 66, Office of Naval Research (1949); J. J. Lord and Marcel Schein, Phys. Rev. 77, 19 (1950).

[3] J. Hornbostel and E. O. Salant, Phys. Rev. 76, 859 (1949).

[4] Leprince-Ringuet, Bousser, Hoang, Jauneau, and Morellet, Comptes Rendus 229, 163 (1949).

[5] Kaplon, Peters, and Bradt, Phys. Rev. 76, 1735 (1949).

[6] P. H. Fowler, Phil. Mag. 41, 169 (1950).

[7] W. Heitler and L. Jánossy, Proc. Phys. Soc. London A62, 669 (1949).

[8] The assistance of the Office of Naval Research and the General Mills Company is gratefully acknowledged.

core and some of those in the diffuse cone remain in the emulsion for over 10,000 microns (Table I), it has been possible to measure systematically the relative separation of the tracks, and hence to determine by accurate measurements of the small angle scattering[8] their momentum. Either the measured value or lower limit for the momentum times velocity[9] is given in Table I for each of the tracks. It is to be noted that the energies E, as deduced from the momentum p, of 5 of the tracks in the central core exceed 250 Bev, while the particles of lower energy are found to be in the larger diffuse cone.

The momentum of the two particles forming the pair γ, in Fig. 1, are given in Table I. Assuming that the pair consists of electrons originating from one of the two gamma-rays emitted in the decay of a neutral meson, it is possible to make estimates of the energy of this neutral meson. It can easily be shown that the energy of the neutral meson is given by the following relation:

$$E=Mc^2(1-\beta^2)^{-\frac{1}{2}}=Mc^2[(h\nu'/h\nu)^2-\sin^2\theta]^{\frac{1}{2}}/(\cos\theta-\beta);$$

Mc^2 = rest energy of proton; θ = angle between gamma-ray and the direction of motion of the neutral meson in the laboratory system of coordinates; $h\nu$ = energy of the gamma-ray in the laboratory system of coordinates; $h\nu'$ = energy of the gamma-ray in the reference frame fixed to the neutral meson (equal to one-half of mass energy of neutral meson;[10] about 75 Mev).

TABLE I. Data on the tracks of the event of Fig. 1.

Track numbered from right to left in Fig. 1	Length of track in emulsion of first plate in microns	$p\beta$ in Bev/c
A	11,000	30,000
B	176	0.01
C	2700	0.36
electron Pr_1	3450	3.6
electron Pr_2	4200	3.0
Diffuse cone		
1	605	*
2	1300	
3	10,600	
4	3040	
5	9630	3.91 *
6	2310	2.6 *
7	2360	
8	2620	
Central core		
1′	6990	> 50
2′	9400	>250
3′	10,250	>250
4′	11,700	>250
5′	11,700	>250
6′	10,000	>250
7′	9500	86

* On the remaining 6 tracks in the diffuse cone accurate determinations of momentum are in progress, and will be reported at a later date.

[9] At these very high values of momentum $\beta \backsimeq 1$ and $E \backsimeq pc$.

[10] Bjorkland, Crandall, Moyer, and York, Phys. Rev. 77, 213 (1950).

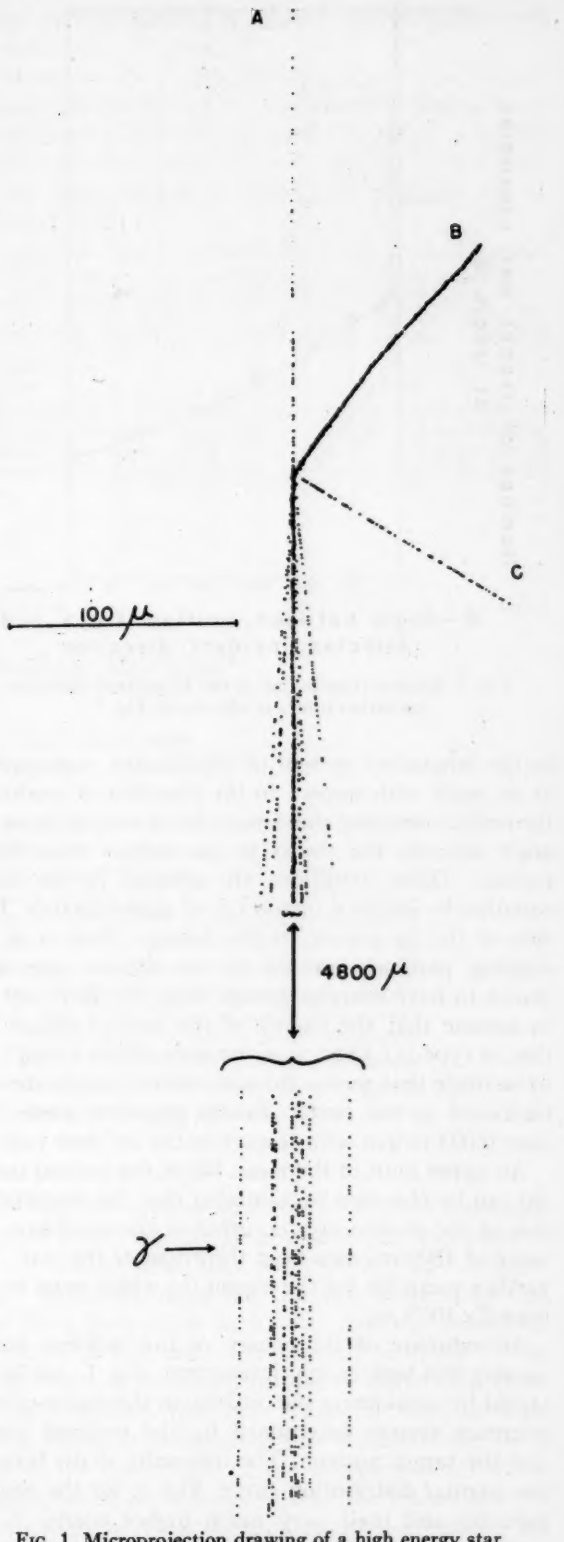

FIG. 1. Microprojection drawing of a high energy star produced by a 3×10^{13}-ev proton.

The pair γ was produced in the central core and the electrons remained in the core over their whole length in the emulsion (4000 microns). Hence the gamma-ray,

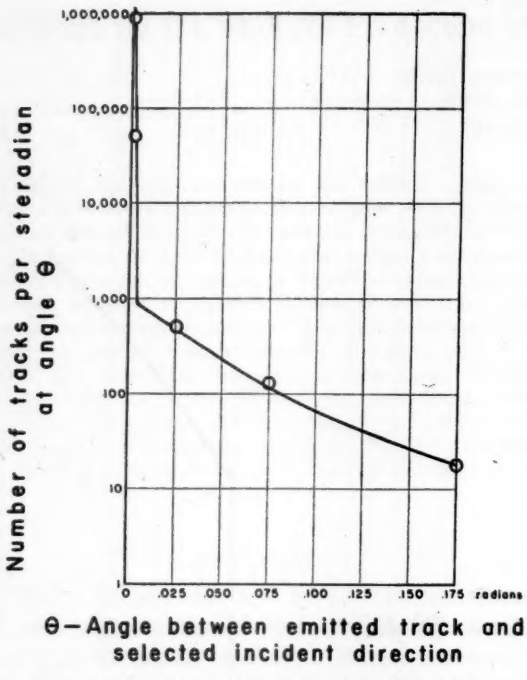

FIG. 2. Angular distribution of the 15 emitted minimum ionization tracks of the star in Fig. 1.

in the laboratory system of coordinates, was emitted at an angle with respect to the direction of motion of the neutral meson of the same order of magnitude as the angle between the tracks in the narrow cone (0.001 radian). These conditions are satisfied in the above equation by either a meson (a) of approximately 1000 Bev or (b) by one of 10-Bev energy. Since 6 of the ionizing particles emitted in the narrow core were shown to have energies greater than 250 Bev, one has to assume that the energy of the neutral meson was that of type (a). Otherwise the assumption would have to be made that meson (b) was emitted almost directly backward in the center-of-mass reference frame (less than 0.003 radian with respect to the incident proton).

An upper limit of the mean life of the neutral meson (b) can be obtained by assuming that the materialization of the gamma-rays occurred at the maximum distance of 4800 microns from the origin of the star. This yields a mean life for the meson (b) which must be less than 2×10^{-15} sec.

An estimate of the energy of the incident proton causing this high energy interaction, Fig. 1, can be obtained by considering the collision in the center-of-mass reference system determined by the incident proton and the target nucleon. The unusually sharp break in the angular distribution curve, Fig. 2, for the emitted particles and their very much higher energy in the central core than in the diffuse cone make it necessary to assume that the 7 tracks in the central core were due to particles emitted in the forward direction (A in Fig. 3) in the center-of-mass system. The 8 tracks of lower energies in the diffuse cone are thus the particles emitted in the backward direction (B in Fig. 3). Accordingly, the energy of the incident proton which is responsible for the production of this star is given by:

$$E=Mc^2\gamma\simeq 2Mc^2\gamma_c^2\simeq 2Mc^2\tan^2\tfrac{1}{2}\theta'/\tan^2\theta,$$

where $\gamma=(1-\beta^2)^{-\frac{1}{2}}$ in the laboratory system; $\gamma_c=(1-\beta_c^2)^{-\frac{1}{2}}$ with β_c the velocity of the center-of-mass reference frame; θ=half-width of the central core in the laboratory system of coordinates (0.003 radian); and θ'=half-width of the central core in the center-of-mass system.

The estimated energy is not strongly dependent upon the value of θ'. However, $\theta'=40°$ as approximately given by Fermi's new formulation of the interaction of high energy particles gives $E=3\times10^{13}$ ev or about 48 ergs. The energy of the primary proton was also calculated from the half-width of the diffuse cone and was found to be in good agreement with the above-mentioned value. This is undoubtedly the highest energy of a single proton which has thus far been directly observed in nature.

The complete lack of slow particles around the central core (Fig. 2) and the fact that only one track could be an ordinary star evaporation nucleon clearly demonstrate that we are dealing here almost entirely with a nucleon-nucleon interaction either in a very light element or possibly in a deuteron or hydrogen nucleus present in the emulsion. It is of particular interest to see that even for energies as high as 3×10^{13} ev the number of charged particles of minimum ionization produced in a single act is as low as 15. The pair of particles produced in the core 4800 microns from the point of interaction is most probably an electron pair formed by a gamma-ray from the decay of a neutral meson. Since this distance represents only about 0.2 radiation units, it seems probable that additional neutral mesons were produced in this very high energy nuclear encounter.

The new calculation by Fermi[11] predicts that in the

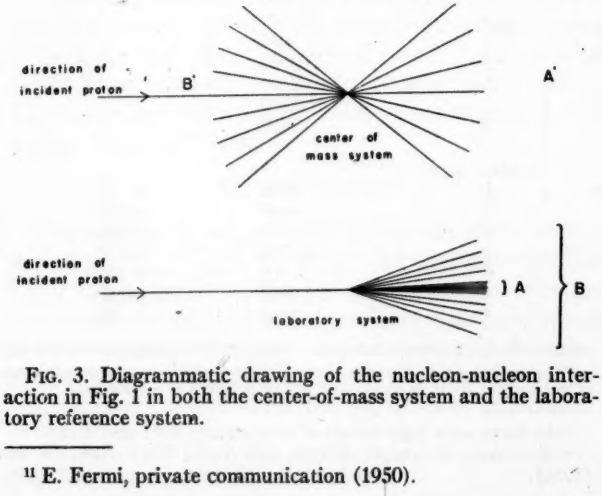

FIG. 3. Diagrammatic drawing of the nucleon-nucleon interaction in Fig. 1 in both the center-of-mass system and the laboratory reference system.

[11] E. Fermi, private communication (1950).

above-described star, there would be about 16 high energy charged particles produced by the 3×10^{13}-ev proton. This is in excellent agreement with the total of 15 sharply collimated minimum ionization tracks which were observed. In addition, Fermi postulates that if nucleon-antinucleon pairs should be produced in addition to mesons, at the extremely high energy of the primary (3×10^{13} ev), the number of emitted particles would then be nearly equally divided between meson and nucleon-antinucleon pairs.

The multiplicity observed here is considerably lower than that calculated by other authors.[12,13] Lewis, Oppenheimer, and Wouthuysen estimate the production of a few hundred mesons by a proton of 3×10^{13}-ev energy and Heisenberg predicts a similar number at this same primary energy.**

This report gives only the results of a preliminary investigation carried out in the emulsion in which the star originates. The emitted tracks pass into a second emulsion in which each of them travels about 20,000 microns. The analysis in the second emulsion will be published later.

We wish to thank Professor Fermi for very illuminating discussions of this nuclear interaction in relation to his new theory, and for his valuable suggestions concerning the small angle scattering of the emitted particles.

[12] Lewis, Oppenheimer, and Wouthuysen, Phys. Rev. **73**, 127 (1948).
[13] W. Heisenberg, Nature **164**, 65 (1949).

** Professor J. R. Oppenheimer pointed out to one of us (Marcel Schein) that his recent calculations in which he assumes a smaller multiplicity of meson production around 10^{10}-ev energy are in agreement with the experimental observations presented in this paper.

PHYSICAL REVIEW VOLUME 80, NUMBER 6 DECEMBER 15, 1950

Scattering of Mesons by Nuclear Particles*

VACHASPATI†
Department of Physics, University of Delhi, Delhi, India
(Received November 9, 1949)

Cross sections for the scattering of mesons by nuclear particles are obtained quantum-mechanically on the basis of the Heitler-Peng version of the perturbation theory. The integral equation taking account of radiation damping in the quantum theory is solved in the classical approximation ($\hbar\to0$). A comparison of these cross sections with those obtained classically reveals certain discrepancies. It is found that though the cross sections calculated classically and those calculated quantum-mechanically in the classical approximation ($\hbar\to0$) broadly agree in most cases, usually one finds that some higher order terms which occur in the purely classical treatment are absent in the quantum-mechanical one. The discrepancy is further accentuated in the case of g_2-scattering where the differential cross sections have generally very different angular dependences and differ from each other in numerical coefficients also. These differences are, in general, such that they cannot be accounted for by postulating quantized orientations of the spin. The correspondence obtained between the classical methods and quantum mechanics by tending $\hbar$ to zero in the results obtained from the latter thus provides a test of the correctness of our theories, and, in the present case it suggests, assuming the classical theory as given by Dirac and Bhabha to be correct, the lines along which a new theory of radiation damping may be developed.

I. INTRODUCTION

WE find in the case of g_1-scattering of neutral mesons that the expressions (1), (7), and (9), on the one hand, and the corresponding expressions (2), (8), and (10), respectively, on the other, differ from each other in the classical values of the cross sections having some more terms than are present in the quantum-mechanical expressions. The same thing happens in the case of charged mesons as a comparison of the cross sections (20) and (21) reveals. Apart from these terms there is a fair agreement in the broad features of the results in the two cases. In case of g_2-scattering, however, the situation is worse. This is at once evident by a glance at the expressions (5) and (6) or (12) and (13). First, one notices again the absence of a number of terms from the quantum-mechanical expressions; second, one remarks that even when these "higher order" terms are neglected the two expressions still differ from each other in having different numerical coefficients of the various terms, not to speak of the angular dependence which in case of differential cross sections is entirely different. While the cross sections without damping being taken into account differ by a factor 3, the coefficients of the damping terms differ by multiples of 2. This shows that the reason for the difference in the cross sections might not entirely lie in the different modes of averaging over the directions of the spin vector in the classical and the quantum theories (Bhabha[1]). In the case of charged mesons, it is

* Revised copy of manuscript received July 24, 1950.
† All India Research Fellow of the University of Delhi. Present address: Institute for Theoretical Physics, Copenhagen, Denmark.

[1] H. J. Bhabha, Proc. Ind. Acad. Sci. A13, 249 (1941).

possible to bring about agreement in the case of g_2-scattering of pseudoscalar mesons by considering quantized orientations of the spin. But the case of vector mesons again presents the same difficulties as are encountered in the case of neutral mesons. These discrepancies show that the neglect of the divergent terms in the Heitler-Peng theory of radiation damping is too drastic. It is probable that these differences can be overcome if one takes a proper account of the contribution from the divergent terms.

II. NOTATION

The calculations are most easily performed in the center-of-mass frame of reference. The initial momenta of the meson and the nucleon are denoted by $\mathbf{p}_0$ and $-\mathbf{p}_0$, while the final momenta are $\mathbf{p}$ and $-\mathbf{p}$. Of course, $|\mathbf{p}|=|\mathbf{p}_0|=p$. By θ we denote the angle of scattering given by $\cos\theta=(\mathbf{p}_0\cdot\mathbf{p})/p^2$. E and E_N are defined by

$$E=(\mu^2C^4+C^2p^2)^{\frac{1}{2}},\quad E_N=(M^2C^4+C^2p^2)^{\frac{1}{2}},$$

μ and M being the masses of the meson and the nucleon, respectively. In passing over to the classical approximation we write

$$E=\hbar\omega,\quad \mathbf{p}_0=\hbar\boldsymbol{\kappa}_0,\quad \mathbf{p}=\hbar\boldsymbol{\kappa},\quad (|\boldsymbol{\kappa}_0|=|\boldsymbol{\kappa}|=\kappa),\quad \mu C=\hbar\chi,$$

and proceed to the limit $\hbar\to0$. A transition from the center-of-mass frame to the coordinate system in which the nucleon is at rest is quite simple in the classical approximation $\hbar\to0$. It can be shown easily that in this approximation the two expressions for the cross sections are completely identical. The constants g_1 and g_2 are used, respectively, to describe the charge and the dipole types of couplings of the meson field with the nucleons. The superscript s refers to the scalar mesons, p to the pseudoscalar mesons and v to vector mesons.

III. NEUTRAL MESONS

A. Scalar Mesons

We consider only the g_1-interaction; the g_2-interaction does not contribute to scattering (compare the corresponding case of charged mesons where it does). We get in the classical approximation the differential cross section

$$[d\phi]_{\substack{\text{quant}\\ \hbar\to0}}=\frac{C^4\kappa^4}{\omega^4}\left(\frac{g_1{}^{s2}}{MC^2}\right)^2\times\cos^2\theta\frac{1}{1+\frac{1}{9}(g_1{}^{s2}/MC^2)^2(C^4\kappa^6/\omega^4)}d\Omega. \quad (1)$$

The corresponding cross section obtained by Harish Chandra[2] in the classical theory is

$$[d\phi]_{\text{class}}=\frac{C^4\kappa^4}{\omega^4}\left(\frac{g_1{}^{s2}}{MC^2}\right)^2\cos^2\theta\frac{d\Omega}{\left[1+\left(\frac{g_1{}^{s2}}{MC^2}\right)\chi-\frac{1}{3}\left(\frac{g_1{}^{s2}}{MC^2}\right)\frac{C^2\chi^3}{\omega^2}\right]^2+\frac{1}{9}\left(\frac{g_1{}^{s2}}{MC^2}\right)^2\frac{C^4\kappa^6}{\omega^4}}. \quad (2)$$

This differs from (1) in having in the square bracket the extra terms

$$(g_1{}^{s2}/MC^2)\chi-\tfrac{1}{3}(g_1{}^{s2}/MC^2)(C^2\chi^3/\omega^2),$$

the first of which can be eliminated by absorbing in the definition of mass M the term proportional to $dv_\mu/d\tau$ occurring in Harish Chandra's equation of motion; i.e., we take the equation of motion to be

$$M\frac{dv_\mu}{d\tau}-\frac{1}{C^2}g_1v_\mu\frac{d}{d\tau}(U'^{\text{mean}})=-g_1U_\mu{}'^{\text{mean}}.$$

The second term is a term of higher order in $C\chi/\omega$ and has been discussed above.

B. Pseudoscalar Mesons

1. g_1 Coupling

One gets in the limit $\hbar\to0$

$$[d\phi]_{\substack{\text{quant}\\ \hbar\to0}}=\left(\frac{g_1{}^{p2}}{MC^2}\right)^2\frac{1}{1+\kappa^2(g^{p2}/MC^2)^2}d\Omega \quad (3)$$

while in the classical theory the scalar and the pseudoscalar cases are not distinguished.

2. g_2 Coupling

The differential cross section is

$$[d\phi]_{\substack{\text{quant}\\ \hbar\to0}}=\left(\frac{g_2{}^{p2}}{IC}\right)^2\frac{C^2\kappa^4}{\omega^2}\times\frac{\sin^2\theta+\frac{4}{9}\left(\frac{g_2{}^{p2}}{IC}\right)^2\cdot\frac{C^2\kappa^6}{\omega^2}\cos^2\theta}{\left[1+\frac{1}{9}\left(\frac{g_2{}^{p2}}{IC}\right)^2\frac{C^2\kappa^6}{\omega^2}\right]\left[1+\frac{4}{9}\left(\frac{g_2{}^{p2}}{IC}\right)^2\frac{C^2\kappa^6}{\omega^2}\right]}d\Omega. \quad (4)$$

We have here replaced $\hbar$ by $2I$ in $g_2{}^{p2}/\hbar C$ which we consider as independent of $\hbar$. Integrating over the solid angle, the total cross section comes out as

$$[\phi]_{\substack{\text{quant}\\ \hbar\to0}}=\frac{8\pi}{3}\left(\frac{g_2{}^{p2}}{IC}\right)^2\frac{C^2\kappa^4}{\omega^2}\times\frac{1+\frac{2}{9}\left(\frac{g_2{}^{p2}}{IC}\right)^2\frac{C^2\kappa^6}{\omega^2}}{\left[1+\frac{1}{9}\left(\frac{g_2{}^{p2}}{IC}\right)^2\frac{C^2\kappa^6}{\omega^2}\right]\left[1+\frac{4}{9}\left(\frac{g_2{}^{p2}}{IC}\right)^2\frac{C^2\kappa^6}{\omega^2}\right]}d\Omega. \quad (5)$$

[2] Harish Chandra, Proc. Ind. Acad. Sci. A21, 135 (1945).

The differential cross section corresponding to (4) in the classical theory is very complicated and the angular distribution bears no simple relation to the direction of the incident field. The total cross section[2] is

$$[\phi]_{\text{class}}=\frac{8\pi}{9}\left(\frac{g_2{}^{v2}}{IC}\right)^2\frac{C^2\kappa^4}{\omega^2}\times\frac{1+\frac{1}{9}\left(\frac{g_2{}^{v2}}{IC}\right)^2\frac{C^2(\kappa^6+\chi^6)}{\omega^2}}{1+\frac{2}{9}\left(\frac{g_2{}^{v2}}{IC}\right)^2\frac{C^2(\kappa^6-\chi^6)}{\omega^2}+\frac{1}{81}\left(\frac{g_2{}^{v2}}{IC}\right)^4\frac{C^4(\kappa^6+\chi^6)^2}{\omega^4}}. \quad (6)$$

If one neglects the χ^6 terms, the denominator can be written as

$$[1+\tfrac{1}{9}(g_2{}^{v2}/IC)^2(C^2\kappa^6/\omega^2)]^2.$$

(b) Initial meson transverse, final meson transverse:

$$[\phi]_{\substack{\text{quant}\\ \hbar\to 0}}=\frac{8\pi}{3}\left(\frac{g_1{}^{v2}}{MC^2}\right)^2\frac{1}{1+4/9(g_1{}^{v2}/MC^2)^2\kappa^2}. \quad (9)$$

The corresponding classical cross section[4] is

$$[\phi]_{\text{class}}=\frac{8\pi}{3}\left(\frac{g_1{}^{v2}}{MC^2}\right)^2\times\frac{1+\frac{1}{2}(C^2\chi^2/\omega^2)}{1+\frac{2}{3}\left(\frac{g_1{}^{v2}}{MC^2}\right)\frac{C^2\chi^3}{\omega^2}+\frac{4}{9}\left(\frac{g_1{}^{v2}}{MC^2}\right)^2\left(\frac{\omega^2}{C^2}-\frac{3}{4}\frac{C^2\chi^4}{\omega^2}\right)}. \quad (10)$$

IV. CHARGED MESONS

It is possible to solve the integral equation giving the effect of radiation damping in case of charged mesons quite generally without making the classical approximation $\hbar\to 0$. Since, however, the results are not of much practical importance, we give here only their classical limits.

C. Vector Mesons

The cross sections in this case have been calculated by Majumdar.[3] The results are as follows.

1. g_1 Coupling

(a) Initial meson longitudinal, final meson longitudinal:

$$[\phi]_{\substack{\text{quant}\\ \hbar\to 0}}=\frac{4\pi}{3}\left(\frac{g_1{}^{v2}}{MC^2}\right)^2\frac{C^4\chi^4}{\omega^4}\frac{1}{1+\frac{1}{9}(g_1{}^{v2}/MC^2)^2\kappa^2}. \quad (7)$$

The corresponding classical cross section[4] is

$$[\phi]_{\text{class}}=\frac{8\pi}{3}\left(\frac{g_1{}^{v2}}{MC^2}\right)^2\frac{C^2\chi^2}{\omega^2}\times\frac{1+\frac{1}{2}(C^2\chi^2/\omega^2)}{1+\frac{2}{3}\frac{g_1{}^{v2}}{MC^2}\frac{C^2\chi^3}{\omega^2}+\frac{4}{9}\left(\frac{g_1{}^{v2}}{MC^2}\right)^2\left[4\frac{C^4\chi^6}{\omega^4}+\frac{\omega^2}{C^2}-\frac{3}{4}\frac{\omega^4}{C^2\chi^2}-\frac{1}{4}\frac{\omega^6}{C^6\chi^4}\right]}. \quad (8)$$

2. g_2 Coupling

(a) Initial meson longitudinal, final meson longitudinal:

$$\phi\to 0. \quad (11)$$

(b) Initial meson transverse, final meson transverse:

$$[\phi]_{\substack{\text{quant}\\ \hbar\to 0}}=\frac{16\pi}{3}\left(\frac{g_2{}^{v2}}{IC}\right)^2\frac{C^2\kappa^4}{\omega^2}\times\frac{1+8/9(g_2{}^{v2}/IC)^2C^2\kappa^6/\omega^2}{\left[1+\frac{4}{9}\left(\frac{g_2{}^{v2}}{IC}\right)^2\frac{C^2\kappa^6}{\omega^2}\right]\left[1+\frac{16}{9}\left(\frac{g_2{}^{v2}}{IC}\right)^2\frac{C^2\kappa^6}{\omega^2}\right]}. \quad (12)$$

It is to be noticed that the cross section (12) is one-half times (5) if we write $g_2{}^v=g_2{}^p/\sqrt{2}$. This is again to be compared with the corresponding classical expression[5]

$$[\phi]_{\text{class}}=\frac{16\pi}{9}\left(\frac{g_2{}^{v2}}{IC}\right)^2\frac{C^2\kappa^4}{\omega^2}\times\frac{1+\frac{4}{9}\left(\frac{g_2{}^{v2}}{IC}\right)^2\frac{C^2(\kappa^6+\chi^6)}{\omega^2}}{1+\frac{8}{9}\left(\frac{g_2{}^{v2}}{IC}\right)^2\frac{C^2(\kappa^6-\chi^6)}{\omega^2}+\frac{16}{81}\left(\frac{g_2{}^{v2}}{IC}\right)^4\frac{C^4(\kappa^6+\chi^6)^2}{\omega^4}}. \quad (13)$$

If the terms involving χ^6 are omitted, the denominator can be written as

$$[1+4/9(g_2{}^{v2}/IC)^2(C^2\kappa^6/\omega^2)]^2.$$

A. Scalar Mesons

1. g_1 Coupling

$$[d\phi]_{\substack{\text{quant}\\ \hbar\to 0}}=4\left(\frac{g_1{}^{s2}}{I\omega}\right)^2\frac{1}{1+4(g_1{}^{s2}/IC)^2(C^2\kappa^2/\omega^2)}d\Omega, \quad (14)$$

where we have replaced $\hbar$ by $\frac{1}{2}I$ in $g_1{}^{s2}/\hbar C$ which we

[3] R. C. Majumdar, Presidential Address at the 32nd Indian Science Congress (1945).
[4] H. J. Bhabha, Proc. Roy. Soc. A172, 384 (1939).
[5] H. J. Bhabha, Proc. Roy. Soc. A178, 314 (1941).

consider to be independent of $\hbar$. This is in agreement with the classical value.

2. g_2 Coupling

In the classical limit we get

$$[d\phi]_{\substack{\text{quant}\\ \hbar\to 0}}=4\left(\frac{g_2{}^{v2}}{IC}\right)^2\frac{\omega^2}{C^2}\frac{1}{1+4(g_2{}^{v2}/IC)^2(\kappa^2\omega^2/C^2)}d\Omega, \quad (15)$$

where again we have replaced $\hbar$ by $\frac{1}{2}I$ in $g_2{}^{v2}/\hbar C$ which we consider to be independent of $\hbar$.

B. Pseudoscalar Mesons

1. g_1 Coupling

The scattering cross section is

$$[d\phi]_{\substack{\text{quant}\\ \hbar\to 0}}=\tfrac{1}{4}(g_1{}^{p2}/MC^2)^2d\Omega \quad (16)$$

which vanishes as M tends to infinity.

2. g_2 Coupling

$$[d\phi]_{\substack{\text{quant}\\ \hbar\to 0}}=4\left(\frac{g_2{}^{p2}}{I\omega}\right)^2\kappa^4\frac{1}{1+4(g_2{}^{p4}\kappa^6/I^2\omega^2)}d\Omega. \quad (17)$$

The corresponding classical expression is

$$[d\phi]_{\text{class}}=2\left(\frac{g_2{}^{p2}}{IC}\right)^2\frac{C^2\kappa^4}{\omega^2}(1-S_z{}^2)\left(1+\frac{(\mathbf{S}\cdot\mathbf{R})^2}{R^2}\right)\times\frac{1}{1+(16/9)(g_2{}^{p2}/IC)^2(C^2\kappa^6/\omega^2)}d\Omega \quad (18a)$$

which becomes on averaging over all directions of the spin vector

$$[d\phi]_{\text{class}}=\frac{4}{15}\left(\frac{g_2{}^{p2}}{IC}\right)^2\frac{C^2\kappa^4}{\omega^2}\times\frac{6+\sin^2\theta}{1+(16/9)(g_2{}^{p2}/IC)^2(C^2\kappa^6/\omega^2)}d\Omega. \quad (18b)$$

It is possible, however, to obtain agreement between (17) and (18) if one considers only quantized orientations of the spin.

C. Vector Mesons

g_1 Coupling

(a) Initial meson is transverse, final meson is also transverse:

$$\phi\to 0. \quad (19)$$

(b) Initial meson is longitudinal, final is also longitudinal:

$$[d\phi]_{\substack{\text{quant}\\ \hbar\to 0}}=4\left(\frac{g_1{}^{v2}}{IC}\right)^2\frac{C^2\kappa^4}{\chi^4\omega^2}\times\frac{1}{1+(g_1{}^{v2}/IC)^2(C^2\kappa^6/\chi^4\omega^2)}d\Omega, \quad (20)$$

which is the same as (17) if we replace $g_2{}^p$ by $g_1{}^v/x$ in the latter. The corresponding classical value is

$$[d\phi]_{\text{class}}=4\left(\frac{g_1{}^{v2}}{IC}\right)^2\frac{C^2\kappa^4}{\chi^4\omega^2}\times\frac{1}{1+4\left(\frac{g_1{}^{v2}}{IC}\right)^2\frac{1}{\chi^4}\left(\frac{C\kappa^3}{\omega}+\frac{3}{2}\chi^2\right)^2}d\Omega. \quad (21)$$

I am grateful to Professor R. C. Majumdar for his suggestion of this investigation, for his constant help throughout the work, and for allowing the use of some of his unpublished calculations. I thank also the authorities of the University of Delhi for the award of an All India Research Fellowship to enable me to carry out this work.

The Natural Radioactivity of In^{115}*

E. A. MARTELL AND W. F. LIBBY
Department of Chemistry and Institute for Nuclear Studies, University of Chicago, Chicago, Illinois
(Received June 19, 1950)

An investigation of the possible natural radioactivities of the Cd^{113}–In^{113} and In^{115}–Sn^{115} pairs of adjacent isobars gave evidence for a natural beta-radioactivity of indium. Four samples of indium differing in geographical origin were subjected to radiochemical purification and then examined in a screen wall counter arranged with anticoincidence counters and steel shielding. Absorption measurements on these samples gave reproducible results indicative of an energetic natural beta-radiation. The energy was measured by comparing the absorption characteristics of the indium radiation with those of Tl^{204} and Co^{60}, whose beta-energies have been measured spectroscopically. Measurement of isotopically enriched samples of indium gave conclusive evidence that the origin of the beta-radiation is the In^{115} isotope. Limits were placed on possible accompanying gamma-radiation. The results indicate that In^{115} emits a natural beta-radiation of 0.63 ± 0.03-Mev energy with a half-life of $6\pm2\times10^{14}$ years.

I. INTRODUCTION

ACCORDING to the rules of nuclear stability, there should exist no pairs of stable isobars differing by one unit in atomic number. Of the known naturally occurring sets of adjacent isobars the expected activities have been found for the cases of $A^{40}K^{40}Ca^{40}$, $Rb^{87}Sr^{87}$, $Y^{176}Lu^{176}Hf^{176}$, and $Re^{187}Os^{187}$. Of the remaining well-established pairs of neighboring isobars, three have been discussed and investigated:[1–7] $Cd^{113}In^{113}$, $In^{115}Sn^{115}$, and $Sb^{123}Te^{123}$. No results were obtained other than the placing of an upper limit to a possible activity of the isobaric species considered.

Eastman[1] predicted the decay of Sn^{115} to In^{115} on the basis of atomic mass considerations and later[2] collected considerable geochemical evidence which appeared to support the possibility of orbital capture decay of Sn^{115} to In^{115}.

Zingg[3] examined the isotopes In^{113}, Sn^{115}, and Te^{123} for orbital capture by looking for the characteristic x-radiation of the product element in each case. His experiments were carried out by placing samples of each element around a cylindrical Geiger-Müller tube counter with copper walls of a thickness that would give an optimum yield of photo-electrons from the K x-rays expected. The results were negative and indicated a minimum half-life of about 1×10^{12} years for K-capture decay of In^{113}, Sn^{115}, and Te^{123}.

A more sensitive technique for x-ray detection was employed by Rusinov and Igelnitsky[4] in the search for K-capture decay of these same isotopes. They used krypton as the counter gas because of the high mass absorption coefficient of krypton for wave-lengths in the region of the K x-ray energies of Cd^{113}, In^{115}, and Sb^{123}. The samples were placed around the outside of aluminum wall counters arranged with sufficient anticoincidence shielding to reduce backgrounds to about 10 percent of normal. The results were negative and placed the minimum half-life for K-capture of In^{113} at 1×10^{14} years, of Sn^{115} at 1×10^{13} years, and of Te^{123} at 2×10^{14} years.

Kohman[6] plotted the known beta-stable nuclides in such a manner as to indicate the charge of maximum stability for odd mass numbers and drew in a curve representing this quantity following considerations based on the liquid drop model. His results indicate that Sn^{115} should decay to In^{115} and Sb^{123} to Te^{123}, while allowing no conclusions to be drawn about Cd^{113} and In^{113}, which lie nearly equidistant from the stability curve.

Considerable geochemical evidence has been presented against the decay of Sn^{115} to In^{115}. Itsikson and Rusanov[5] have pointed out that tin from pegmatite deposits is usually free of any trace of indium. Ahrens[7] indicated that tin from pegmatitic deposits in southeastern Manitoba, Canada, known to be about 2×10^9 years old, was estimated to occur with 75×10^{-6} percent of indium. This corresponds to a lower limit of 5×10^{12} years for the half-life of possible decay of Sn^{115} to In^{115}.

It would appear in these three pairs of neighboring isobars that either the radiations are too soft or that the rates of decay are too slow for detection by the techniques thus far employed. Bethe and Bacher[8] have shown that very long-lived decay, possibly beyond the limits of detection, could be explained on the basis of forbiddenness considerations. In each of the cases of Cd^{113}–In^{113} and In^{115}–Sn^{115}, a nuclear spin change of four is involved which, when considered with possible parity change, would indicate a third- or fourth-order forbidden transition should be expected. Since the lifetime of a beta-radioactive nucleus increases with decreasing energy of the transition as well as with increasing order of forbiddenness, the possible activities for the two cases cited could easily be unobservable unless considerable energy were available for the transition.

* This research was supported in part by the Office of Air Research under contract with the University of Chicago.

[1] E. D. Eastman, Phys. Rev. **46**, 1 (1934).
[2] E. D. Eastman, Phys. Rev. **52**, 1226 (1937).
[3] E. Zingg, Helv. Phys. Acta **13**, 219 (1940).
[4] L. I. Rusinov and J. M. Igelnitsky, C. R. Acad. Sci. U.S.S.R. (Doklady) **49**, 343 (1945).
[5] M. I. Itsikson and A. K. Rusanov, C. R. Acad. Sci. U.S.S.R. **53**, 631 (1946).
[6] T. P. Kohman, Phys. Rev. **73**, 16 (1948).
[7] L. H. Ahrens, Nature **162**, 413 (1948).
[8] H. A. Bethe and R. F. Bacher, Rev. Mod. Phys. **8**, 82 (1936).

In the present investigation the elements tin, indium, and cadmium were examined by more sensitive solid and gas counting techniques, similar to those applied by Naldrett and Libby[9] to the investigation of the Os^{187}–Re^{187} pair of adjacent isobars. Evidence is presented for the natural decay of In^{115} with the emission of an energetic beta-radiation to form Sn^{115}.

II. EXAMINATION OF INDIUM

A. Description of Apparatus

The counting apparatus used for the measurement of solid samples of indium metal and indium hydroxide consisted of a large screen wall counter arranged with anticoincidence shielding counters and steel shielding.

The screen wall counter, described elsewhere,[10–12] introduces the sample directly into the sensitive volume of the counter without an intervening absorber wall by making the sample the counter wall. The counter used consisted essentially of a 3″ diameter brass cylinder 24″ long with a screen-grid counting element suspended concentrically along the middle third of the counter. The sample was placed over 400 cm² area on the inside surface of a 8″ long lead-free brass cylinder. This cylinder was connected by means of a sleeve fitting to an identical cylinder, forming a 16″ unit. Sliding this assembly back and forth inside the counter causes the sample and bare cylinder to be alternately placed in position around the counting element, thus allowing measurement of sample and background counting rates. The counter was operated with the screen-grid grounded and with a negative potential of about 100 volts in the sample cylinder. Application of this "drag-in" voltage makes the effective volume of the counter the entire volume inside the sample cylinder rather than only that inside the screen-grid.

The normal background of the counter described is approximately 450 c.p.m. The employment of a surrounding shield of 8″ to 10″ of hot rolled steel reduced the background rate to about 104 c.p.m. The bulk of this residual count, due principally to the high energy meson component of cosmic radiation, was removed by use of a single completely surrounding layer of counters arranged in anticoincidence. With this combination, samples of 400 cm² area could be measured with backgrounds of about 6 c.p.m.

B. Purification of Indium

Initial measurements on several indium metal samples of high chemical purity gave counting rates of from 50 to 85 c.p.m. above background for 400 cm² sample area and 100 mg/cm² thickness. A rough aluminum absorption curve taken for the lowest activity metal sample indicated that a fairly energetic beta-radiation comprised the bulk of the measured radiation.

Four samples of indium differing widely in geographical origin were submitted to radiochemical purification. The procedure consisted of the dissolution of indium metal in dilute nitric acid, a fluoride precipitation of lanthanum and calcium carriers, a sulfate precipitation of barium carrier, a sulfide precipitation of copper carrier from 0.2*N* acid solution, and finally the precipitation of indium sulfide from acetic acid solution. After washing, the sulfide was converted to pure indium hydroxide, $In(OH)_3$, in which form it was counted.

This purification procedure is believed to remove or at least highly dilute any of the natural radioactive elements that could be present as contamination in the original sample. A single cycle appeared to be sufficient, since a second purification of one of the samples failed to show any detectable change in the measured activity of the sample and all four samples after purification had identical activities and absorption characteristics within an error of twice the standard deviation for the measurements. These data are presented in Table I and plotted as curve A in Fig. 1.

C. Procedure and Results

After purification the four samples were dried to constant weight in the form of indium hydroxide and ground to a fine powder. A 50-g sample of each was mixed with 50 ml of 0.15 percent agar-water solution and deposited evenly over the 400 cm² area on the inside surface of the sample cylinder. The cylinder was placed inside the screen wall counter and the latter sealed and attached to a vacuum line to dry the sample and evacuate the counter. A filling of 0.5-cm ethylene[13] and 9.5-cm argon was used. Because of the insulating characteristics of indium hydroxide, it was necessary to count the hydroxide samples with a thin aluminum foil over the surface.

Aluminum absorption curves were taken for the four purified indium hydroxide samples and for one metal sample found to be quite free of contamination without

TABLE I. Data on purified natural indium samples.

Sample No.	1	2	3	4	5
Origin	Peru	Montana	Pennsylvania	Heterogeneous	Montana
Chem. form.	$In(OH)_3$	$In(OH)_3$	$In(OH)_3$	$In(OH)_3$	In metal
Al. Abs. (mg/cm²)	(c.p.m.)	(c.p.m.)	(c.p.m.)	(c.p.m.)	(c.p.m.)
0					51.1 ±0.4
2.4	30.4 ±0.4	30.1 ±0.4	31.4 ±0.5	28.6 ±0.4	45.5 ±0.4
4.45	27.9 ±0.5				
6.95					38.7 ±0.5
24.0	11.3 ±0.4				
26.4		9.93±0.40	10.94±0.44	10.74±0.42	16.3 ±0.5
48.0	4.47±0.30				
50.4		4.12±0.32	3.62±0.42	3.33±0.26	6.44±0.45
72.0	1.47±0.41				
85.0					2.22±0.21
87.4		0.42±0.27	1.30±0.36	0.85±0.30	
109	0.59±0.23				1.08±0.22

Sample area = 400 cm²
Sample thickness (minimum) = 120 mg/cm²

[9] S. N. Naldrett and W. F. Libby, Phys. Rev. **73**, 487 (1948).
[10] W. F. Libby, Phys. Rev. **46**, 196 (1934).
[11] W. F. Libby and D. D. Lee, Phys. Rev. **55**, 245 (1939).
[12] E. C. Anderson, Doctoral thesis (University of Chicago, 1949).
[13] Morganstern, Cowan, and Hughes, Phys. Rev. **74**, 499 (1948).

purification. The aluminum foils were placed directly against the sample surface. Because the aluminum foils used evidenced a measurable, though uniform, contamination level, identical foils were mounted over both background and sample side of the sample cylinder for each measurement. It should be noted that an initial high counting rate was frequently observed for freshly prepared indium metal and aluminum foil surfaces. This was undoubtedly the effect described by Crane[14,15] as characteristic of certain metal cathode surfaces, of which aluminum is particularly bad.

The results of these absorption measurements are given in Table I. The absorption data for the hydroxide samples are plotted as curve A, Fig. 1, and that for the metal sample as curve B, Fig. 1. The shape of these absorption curves gives evidence that the radiation consists of a single relatively energetic beta-particle. The extrapolated activity of the hydroxide samples at zero absorber is 34.0±0.4 c.p.m. Correction by the direct mass ratio of indium hydroxide to indium metal gives 49.1±0.5 c.p.m. The extra thickness of the indium hydroxide samples as compared with the metal necessitated a small further correction for a decrease in sample area, raising the hydroxide count to 50.7±0.5 c.p.m., in essential agreement with the 51.1±0.4 c.p.m. activity of the bare metal.

III. ENERGY OF THE INDIUM RADIATION

The energy of the indium radiation was calibrated by comparison of its absorption characteristics with those of two beta-radiations whose energies have been measured spectroscopically. A small amount of Tl^{204}, which emits[16] a 0.77-Mev beta-particle with a half-life of about 3 years, was co-precipitated with 60 grams of indium hydroxide. Absorption measurements were taken as before. The data, corrected for the natural indium activity, are given as curve C in Fig. 1.

TABLE II. Energy and half-life of natural $In^{115}\beta^-$.

Isotope used for calibration	$Tl^{204}\beta^-$	$Co^{60}\beta^-$
Energy of radiation	0.77 Mev[a]	0.310 Mev[b]
Range of radiation[c]	284 mg/cm²	80.7 mg/cm²
Absorption half-thickness observed (curves C and D_2, Fig. 1)	20.6 mg/cm²	6.3 mg/cm²
Range $In^{115}\beta^-$ from half-thickness Ratio (H. T. $In^{115}\beta^-$ =16.0 mg/cm²)	220 mg/cm²	205 mg/cm²
Energy[c] $In^{115}\beta^-$	0.64 Mev	0.61 Mev
Half-life $In^{115}\beta^-$	6.2×10^{14} yr.	5.7×10^{14} yr.

Natural $In^{115}\beta^-$

$E(\beta^-)_{max}=0.63\pm0.03$ Mev

$T_{\frac{1}{2}}=(6\pm2)\times10^{14}$ yr.

[a] Reference 16.
[b] Reference 18.
[c] Reference 17.

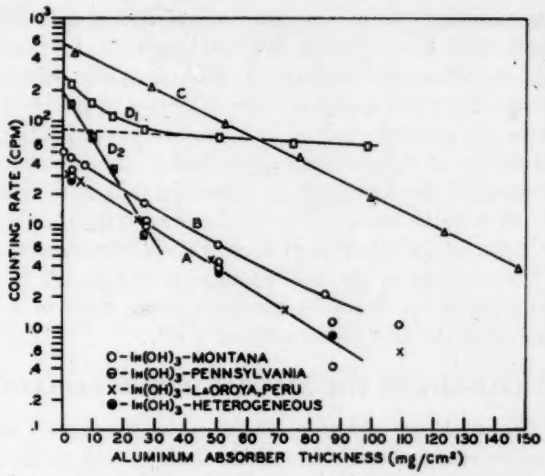

FIG. 1. Absorption curves for natural indium radiation and calibrating Co^{60} and Tl^{204} sources.

It is noted that the absorption curves for both the natural indium activity and the Tl^{204} beta-activity are straight. Therefore, the ratio of the absorption half-thicknesses for the two radiations can be taken as equal to the ratio of their ranges. The range of a 0.77-Mev beta is read from a standard range-energy curve[17] and multiplied by the half-thickness ratio, 16.0/20.6, from curves *A* and *C*. This result, the range of the indium radiation, corresponds to an energy of 0.64 Mev on the standard curve.

In a similar manner a 50-gram sample of indium hydroxide containing a small amount of Co^{60} was prepared and measured. Co^{60} emits a 0.310-Mev beta[18] with a 5.3-year half-life. Curve D_1, Fig. 1, shows the corrected Co^{60} absorption curve including the tail due to gamma-radiation in cascade. Curve D_2, the resolved Co^{60} beta-absorption curve, gives a half-thickness of 6.3 mg/cm² for the cobalt radiation which corresponds to an indium radiation energy of 0.61 Mev. These data are shown in Table II.

Since these two calibrations agree quite well in the resultant energies for the indium radiation, and since the energies of the thallium and cobalt radiations are spectroscopic values, it is believed that the indium radiation has an energy of 0.63±0.03 Mev. This belief, of course, assumes that the shape of the three spectra are similar; but the experimental fact that the absorption curves are linear is perhaps some evidence for this assumption. Moreover, the indium beta is bracketed both in maximum beta-energy and nuclear charge by the Co^{60} and Tl^{204} radiations.

It is of interest to compare this 0.63±0.03 Mev indium beta-energy with that predicted for possible

[14] H. R. Crane, Phys. Rev. **75**, 985 (1949).
[15] M. L. Wiedenbeck and H. R. Crane, Phys. Rev. **75**, 1268 (1949).
[16] Peacock, Jones, and Overman, PPR Mon N-432, 56 (December, 1947), unpublished.
[17] L. E. Glendenin, Nucleonics **2**, No. 1, 25 (1948).
[18] L. C. Miller and L. F. Curtiss, J. Research Nat. Bur. Stand. **38**, 359 (1947).

beta-radiation of In^{115} by the work of Bell *et al.*[19] They found that the 4.4-hour isomeric state of In^{115} gave beta-radiation presumably to Sn^{115} of about 830-kev energy. Since the isomeric state is known to lie 338 kev above the ground state of In^{115}, one might expect that the energy of natural beta-decay of In^{115} to Sn^{115} would be equal to the difference of these two numbers, or 490 kev. It is quite possible either that the discrepancy may be the result of experimental error in the determination of the energies of the beta-radiations or that the beta-transition from the 4.4-hour metastable state of In^{115} may decay to an excited state of Sn^{115}.

IV. HALF-LIFE OF THE NATURAL INDIUM RADIATION

The absolute counting efficiency of the screen wall counter relative to the energetic indium beta-radiation can be estimated from the absorption half-thickness and the energy of the indium radiation which have been experimentally determined above. The mass absorption coefficient, α (in cm^2/mg), is determined from curve A, Fig. 1 to be 0.0436 cm^2/mg.

If a radioactive sample of surface area A and specific activity σ is counted with a physical geometry, g, the measured intensity for a thin element, dl, parallel to the surface is given by,

$$dI = A\sigma g e^{-\alpha l} dl. \quad (1)$$

Then the total measured activity for a sample of thickness l becomes,

$$I = A\sigma g(1-e^{-\alpha l})/\alpha. \quad (2)$$

The intensity for an indium sample of thickness equal to the range l_0 (215 mg/cm^2) is,

$$I_\infty = A\sigma g l_0/9.4. \quad (3)$$

Since g for the screen wall counter used is a little less than 0.5, it appears that the absolute counting efficiency, $g/9.4$, is a little less than 5.3 percent.

In connection with researches on natural radiocarbon[20] the absolute efficiency of the screen wall counter was determined to be 5.46±0.03 percent for a carbon sample of 400 cm^2 area and infinitely thick (20 mg/cm^2) with respect to the 0.15-Mev C^{14} beta-radiation. It appears from the agreement between the estimated efficiency for the indium radiation and the experimental value for C^{14} that the value of 5.46 percent for carbon can be assumed to hold for indium. It is improbable that such an assumption would introduce an error of more than 20 percent in the indium half-life.

It has been shown above that an indium metal sample of 400 cm^2 area and of thickness large with respect to the range of the natural indium radiation gave a counting rate of 51.1±0.4 c.p.m. Using 5.46 percent as the absolute counting efficiency for a sample of thickness equal to the range (215 mg/cm^2), the specific activity σ for indium, by Eq. (3) above, is found to be 10.9 disintegrations per minute per gram. This corresponds to a half-life of $6\pm2\times10^{14}$ years for a beta-radiation from In^{115}. Conclusive evidence that the origin of the indium beta-radiation is the In^{115} will be given in a following section.

TABLE III. Evidence against natural gamma-emission.

Sample	Potassium chloride	Indium metal
Weight	425 g	750 g
Gamma-activity	141.0±2 c.p.m.	0.8±0.6 c.p.m.
Maximum yield for 1.5-Mev γ's		1 per 100 betas
Maximum yield for 0.5-Mev γ's		5 per 100 betas
Maximum yield for 0.1-Mev γ's		84 per 100 betas
Minimum half-life of In^{113} for positron emission		2×10^{15} years

V. EVIDENCE AGAINST NATURAL GAMMA-EMISSION

Because both of the indium isotopes are isobaric with neighboring elements, the beta-radiation from indium could be attributed either to the decay of In^{115} to Sn^{115} with emission of negative betas or to the less probable positron decay of In^{113} to Cd^{113}. A test for the latter possibility was made by looking for the annihilation gamma-radiation that would accompany position decay.

A cylindrical sample of indium metal weighing 750 grams was placed around the outside of a large brass-walled Geiger counter of 670 mg/cm^2 wall thickness. This arrangement, counted with anti-coincidence shielding, yielded an effect of 0.8±0.6 c.p.m. above background. A 425-gram sample of potassium chloride was identically placed and similarly counted with a resultant effect of 141±2 c.p.m. above background. Each of the samples covered a cylindrical area of about 60 square inches around the center half of the counter.

Assuming the energy of the potassium gamma to be 1.5 Mev and taking the half-life of K^{40} as 1.4×10^9 years with a branching ratio of 1:15 for the K-capture decay with which the gamma-radiation appears to be in cascade, the absolute counting efficiency of the brass-walled counter used is determined to be 0.64 percent for 1.5-Mev gammas. Applying this efficiency factor to the measured effect of 0.8±0.6 c.p.m. for the 750-gram indium metal sample, a maximum yield of 1 gamma per 100 betas is obtained. Using the gamma-efficiency data for brass-walled counters given by Maier-Liebnitz[21] and making the necessary self-absorption and wall absorption corrections for the lower gamma-energies, the remainder of the results shown in Table III were calculated. Since the measured rate of natural indium beta-radiation would correspond to a half-life of about 2×10^{13} years, one would expect to get 100 times as many 0.5-Mev gammas from the annihilation of such positions as were obtained in this experiment. Thus the evidence conclusively establishes that no appreciable part of the measured natural indium activity can be attributed to position decay of In^{113}.

[19] Bell, Ketelle, and Cassidy, Phys. Rev. **76**, 574 (1949).
[20] Libby, Anderson, and Arnold, private communication.
[21] von H. Maier-Liebnitz, Zeits. f. Naturforsch. **1**, No. 5 (1946).

The ratios shown in Table III indicate that maximum energy of gamma-radiation that could be in cascade with the 0.63-Mev beta-radiation of indium is certainly less than 0.5 Mev and would appear to be about 100 kev. In all likelihood there is no accompanying gamma-radiation.

VI. ENRICHED SAMPLE MEASUREMENT

To prove the identity of the beta-emitting isotope, two samples of isotopically enriched indium were obtained from the Isotopes Development Division, Oak Ridge, Tennessee. One sample of 400 mg of indium oxide, In_2O_3, was enriched fifteen-fold in In^{113} and the other sample of 22.83 gm of indium oxide was 99.92 percent In^{115}, indicating fifty-threefold dilution of In^{113}.

The enriched In^{113} sample was deposited on a 400 cm^2 area brass foil by evaporation from indium chloride solution and counted. A sample of unenriched indium of similar size was measured for purposes of comparison. The enriched In^{115} sample was counted as indium hydroxide. The results of these measurements appear in Table IV together with predicted values for each sample calculated by Eqs. (2) and (3) above. The initial result for the enriched In^{115} sample indicated radioactive contamination. After purification by the chemical procedure outlined earlier, the enriched In^{115} sample activity showed agreement with the activity expected for natural beta-decay of In^{115}. Purification was not attempted in the case of the smaller sample enriched in In^{113} because of danger of loss and also because the result was quite conclusive despite the contamination. From the data of Table IV it is quite clear that it is indeed In^{115} which is the origin of hard beta-radiation measured in this research.

VII. RESULTS

It has been shown that the In^{115} isotope in its natural state exhibits decay to Sn^{115} by radiation of a beta-particle of 0.63 ± 0.03 Mev energy with a half-life of $6\pm2\times10^{14}$ years. The corresponding specific activity is 11 disintegrations per minute per gram of indium. It was further shown that the maximum energy of accompanying gamma-radiation consistent in a 1:1 ratio with the beta-disintegration rate is of the order of 100 kev. Thus, it appears that the ground state of In^{115} lies between 600 and 760 kev above that of Sn^{115}.

In view of the high energy and long corresponding half-life of the In^{115} radiation, it is of interest to consider the order of forbiddenness of this beta-transition. The spins of these isobars are known, that for In^{115} being 9/2 and that for Sn^{115} being $\frac{1}{2}$. In addition, the orbital assignments[22] are "g" for the ground state of In^{115} and "s" for Sn^{115}, corresponding to no parity change. For a spin change of four and even parity the Gamow-Teller selection rule indicates a fourth-order forbidden transition. The energy and half-life of the In^{115} beta-radiation corresponds to an Ft value of 2×10^{22}. This value is of the order of 10^5 larger than values for known third-order forbidden transitions, lending further support to the argument that the transition from In^{115} to Sn^{115} is fourth forbidden.

[22] M. G. Mayer, Phys. Rev. **75**, 1969 (1949).

TABLE IV. Data on enriched indium samples.

Sample	Natural indium	Enriched in In^{113}	Enriched in In^{115}
Abundance in In^{115}	95.77%	34.6%	99.92%
Abundance in In^{113}	4.23%	65.4%	0.08%
Chemical form	$InCl_3$	$InCl_3$	$In(OH)_3$
$In(OH)_3$ equiv.	0.40 gms	0.48 gms	24.5 gms
Expected rate if activ. is $In^{113}\beta^+$	1.53 c.p.m.	29.0 c.p.m.	0.60 c.p.m.
Expected rate if activ. is $In^{115}\beta^-$	1.53 c.p.m.	0.66	33.0 c.p.m.
Experimental rate without purification	—	2.44 ± 0.5 c.p.m.	44.1 ± 0.5 c.p.m.
Experimental rate after purification	1.64 ± 0.24 c.p.m.	—	33.2 ± 0.4 c.p.m.

Results for the $Cd^{113}-In^{113}$ Pair

In this research several facts relative to the activity limits for each member of the Cd^{113}–In^{113} pair were obtained.

The investigation of possible gamma-radiation from indium indicated that the minimum half-life of In^{113} relative to emission of 0.5-Mev gamma-radiation is 1×10^{15} years, corresponding to a minimum half-life for positron emission of 2×10^{15} years.

The measurement of the enriched In^{113} sample indicated a maximum effect of 2 c.p.m. attributable to the combined effects of contamination, backscattering, and Auger electrons resulting from possible K-orbital capture decay of In^{113}. When it is assumed that 2 c.p.m. are caused by K Augers of about 25-kev energy with 25 percent yield, the corresponding minimum half-life for K-capture decay of In^{113} is determined to be 2×10^{13} years. The investigation of enriched In^{113} as indium trimethyl in large gas counters using proportional counting techniques should provide at least two orders of magnitude greater sensitivity for detection of soft Auger electrons from possible orbital capture activity of In^{113}.

A spectroscopically pure sample of cadmium metal was measured in the screen wall counter with anti-coincidence shielding. This sample, of 500 mg/cm^2 minimum thickness over 400 cm^2 area, gave a net activity of 1.32 ± 0.24 c.p.m. The effect could be at-

TABLE V. Summary of results for $Cd^{1.3}$–In^{113}.

Minimum $T_{\frac{1}{2}}$ of In^{113} for 0.5 Mev γ's	1×10^{15} years
Minimum $T_{\frac{1}{2}}$ of In^{113} for β^+ emission	2×10^{15} years
Minimum $T_{\frac{1}{2}}$ of In^{113} for K-capture	2×10^{13} years
Minimum $T_{\frac{1}{2}}$ of Cd^{113} for β^- emission of energy $\leq$200 kev	$\sim10^{11}[E\ (\text{kev})]^{5/3}$ years
(a) For 20 kev β^-'s	1×10^{13} years
(b) For 200 kev β^-'s	6×10^{14} years

tributed to contamination or to the transition effect. Assuming a 1.5 c.p.m. maximum beta-activity for 400 cm² of cadmium metal counted at 5.46 percent efficiency, the variation of minimum half-life with maximum beta-energy can be determined. Effective sample thickness is taken as the range from standard range-energy curves for beta-radiation. Results for betas up to 200 kev are shown in Table V.

Through the kindness of Dr. J. V. Dunworth, researches conducted in 1947 and described in a Ph.D. thesis by S. G. Cohen on the possible orbital capture activity of In^{113} have recently been made available to us. Their data appear to exhibit evidence of the same activity of natural indium which we have investigated. The authors are indebted to the Isotopes Division of the Oak Ridge National Laboratory for the remarkable isotopically enriched indium samples made available to them.

PHYSICAL REVIEW VOLUME 80, NUMBER 6 DECEMBER 15, 1950

Proton Groups from the Deuteron Bombardment of Boron*

WILLIAM O. BATESON†
Yale University, New Haven, Connecticut‡
(Received July 31, 1950)

Protons emitted when boron enriched to 96 percent B^{10} was bombarded by 3.76-Mev deuterons have been observed at 90° and 0°. Groups corresponding to Q-values of 9.18±0.05, 7.03±0.06, 4.70±0.06, 4.15±0.08, 2.26±0.07, 1.36±0.07, 0.70±0.10, and 0.32±0.10 Mev were found. These have relative intensities at 90° of 1, 0.3, 0.8, 0.6, 16, 13, and 0.8. The intensity of the lowest energy group was not determined, since it was only just distinguishable from the scattered beam. The bombardment of unseparated boron gave no significant results, because of the presence of large amounts of an impurity, probably magnesium as the boride.

I. INTRODUCTION

IT is well known that the study of the particle groups emitted by an element under bombardment gives information concerning the energy levels in the residual nucleus. The reaction $B^{10}(d,p)B^{11}$ is of more than usual interest because of the large energy release, or Q-value, which enables very highly excited levels in the B^{11} nucleus to be observed.

This reaction was first studied by Cockcroft and Walton,[1] and then more carefully by Cockcroft and Lewis,[2] using 550-kev deuterons and unseparated boron isotopes. They observed three proton groups, corresponding to Q-values of 9.14±0.06, 7.00±0.05, and 4.71±0.03 Mev, as corrected by Livingston and Bethe,[3] which they assigned to the $B^{10}(d,p)B^{11}$ reaction. A few years later, a fourth group was found by Pollard, Davidson, and Schultz,[4] having a Q-value of 2.39±0.20 Mev, using 3.1-Mev deuterons from a cyclotron, and again, unseparated isotopes. Although they assigned this group also to the reaction involving B^{10}, its large yield made it seem likely that it was due to $B^{11}(d,p)B^{12}$. Since their resolution was not very good, it was felt that it would be profitable to repeat their work using the separated isotopes now available from Oak Ridge, and the much better resolution possible with our present counting techniques.

II. PROCEDURE

Boron targets having a thickness of about 3 mm of air-equivalent, or 50 kev at our beam energy, were prepared by evaporating the element off a wolfram filament onto a thin (0.04 mil) gold backing in a vacuum of 10^{-5} mm of mercury. It was necessary to replace the filament several times during the evaporation, since the boron reacted with the wolfram to form the rather brittle

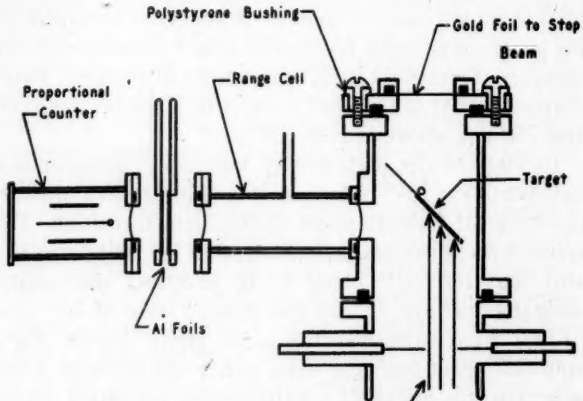

FIG. 1. Schematic diagram of bombardment chamber used. The beam analyzing magnet and slit system have been omitted.

* Part of a dissertation submitted to the Graduate School of Yale University in partial fulfillment of the requirements for the degree of Doctor of Philosophy.
† Now with the Westinghouse Electric Corporation, Atomic Power Division, Pittsburgh, Pennsylvania.
‡ Assisted by the ONR and AEC.
[1] J. D. Cockcroft and E. T. S. Walton, Proc. Roy. Soc. 144, 704 (1934).
[2] J. D. Cockcroft and W. B. Lewis, Proc. Roy. Soc. 154, 246 (1936).
[3] M. S. Livingston and H. A. Bethe, Rev. Mod. Phys. 9, 245 (1937).
[4] Pollard, Davidson, and Schultz, Phys. Rev. 57, 1117 (1940).

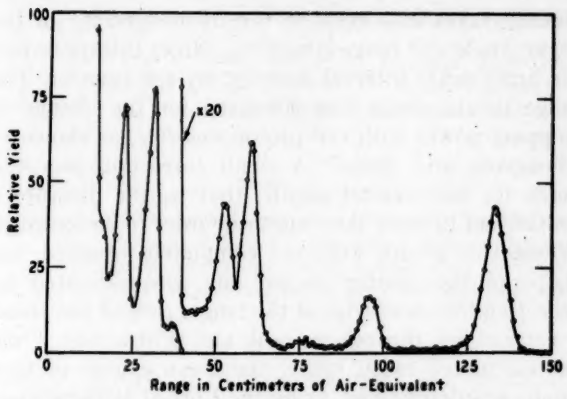

FIG. 2. Protons emitted at 90° when 96 percent B^{10} was bombarded by 3.76-Mev deuterons. The ranges are uncorrected for the change in the stopping power of aluminum with proton energy.

boride. Because of the very high temperature needed to evaporate boron, it was probable that some wolfram was also deposited on the target. There was also the possibility that some of the boron would be oxidized by the residual air in the vacuum chamber where the evaporation was carried out. Since B_2O_3 is much more volatile than boron, it would be deposited very readily on the target, introducing considerable oxygen contamination.

The bombardments were performed in the conventional manner in a chamber built by Martin.[5] The 3.76-Mev deuteron beam emerged from the cyclotron, passed through a slit system and between the pole faces of an analyzing magnet, and impinged on the target, which was held between the arms of a *C*-shaped support. The beam passed through the target and its thin gold backing, between the arms of the *C*, and was stopped in the end plate of the chamber. This was insulated from the rest of the chamber, and was connected to the beam integrating circuit. The protons emitted at 90° to the beam passed out through an exit port covered by a thin aluminum foil, through a range cell, through a set of variable aluminum absorbers, and into a proportional counter. The counting circuits were biased so that only the largest pulses, corresponding to protons at the end of their range, would be recorded. For 0° observation, the target was fastened to the chamber end plate, in front of a window covered with enough gold foil to just stop the beam (about 14 cm of air-equivalent). The bombardment chamber is shown schematically in Fig. 1.

The general procedure was to measure the number of protons as a function of their range emitted from the target. Absorption was added in steps of 1 cm air-equivalent, starting with the minimum amount needed to stop the scattered beam, until a value 10 cm greater than the range of the most energetic proton group was reached. The number of protons emitted with a given range for a constant number of deuterons were thus determined. The run was then repeated in the reverse order, removing the absorbers, and the two results averaged. This method tended to compensate for any slow drifts in the counting level and for the deterioration of the target under bombardment. A total of 18 runs, using 4 different targets were made using the separated B^{10} at 90° observation.[6] A composite of these is shown in Fig. 2. Four runs were also taken with the separated isotope at 0°, and are shown in Fig. 3. Several runs were also taken with commercial unseparated boron, but were of no value because of the large amounts of magnesium present as the boride. In fact, some of the groups due to the impurity were larger than those due to the B^{10}. The contaminant was identified by the presence of a strong 14.8-hour activity in the target, from the $Mg^{26}(d,\alpha)Na^{24}$ reaction.[7]

A total of ten groups can be seen in Fig. 2, some of which are caused by contaminants. The groups with extrapolated ranges of 140, 101, and 65 cm air-equivalent are those reported by Cockcroft and Lewis. The last of these is now seen to be a doublet, which is almost completely resolved. The two at 33 and 25 cm were reported by Pollard, Davidson, and Schultz as one group. The small change in curvature at 18 cm appeared in every run, and so is probably another group. At first it was thought that this small group was due to the energetic alpha-particles from the $B^{10}(d,\alpha)Be^8$ reaction, but further investigation with the counting level set above pulses due to protons of any energy, showed it was due to protons. Finally, another, large yield group can be seen at 16 cm, being just distinguishable from the scattered beam at 14 cm range. The group at 40 cm falls where protons from $C^{12}(d,p)C^{13}$ would be expected, and since its yield varied from run to run by a factor of 50 it is undoubtedly due to this reaction. The very small group at 80 cm is barely twice the neutron background, and is also probably due to an impurity. It has about the right range for the $C^{13}(d,p)C^{14}$ reaction, and its

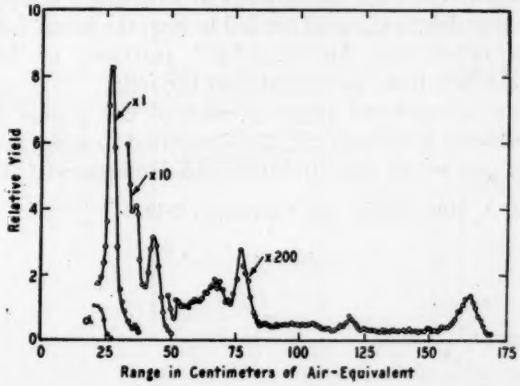

FIG. 3. Protons emitted by the $B^{10}(d,p)B^{11}$ reaction at 0° observation. The ranges are uncorrected for the change in stopping power of gold and aluminum with proton energy. The α-particles from the $B^{10}(d,\alpha)Be^8$ reaction are also shown.

[5] A. B. Martin, Phys. Rev. **71**, 127 (1947).

[6] 96 percent B^{10} was obtained from Oak Ridge.

[7] No analysis of the boron used was available. According to the suppliers, Eimer and Amend, New York, New York, the probable impurities were traces of the alkalies and one or two percent magnesium, as the boride.

TABLE I. Q-values from the reaction $B^{10}(d,p)B^{11}$.

Present work				Buechner and Van Patter
90° (Mev)	90° yield	0° (Mev)	Excitation (Mev)	(Mev)
9.18±0.05	1	9.07±0.15	0	9.232±0.011
7.03±0.06	0.3	6.90±0.15	2.15±0.05	7.091±0.009
4.70±0.06	0.8	4.57±0.15	4.48±0.06	4.775±0.006
4.15±0.08	0.6	4.04±0.20	5.03±0.07	4.199±0.006
2.26±0.07	16	2.30±0.20	6.92±0.07	2.480±0.006
				(2.430±0.007)
1.36±0.07	13	1.50±0.20	7.82±0.07	1.935±0.005
0.70±0.10	0.8	0.81±0.20	8.48±0.10	0.667±0.004
0.32±0.10	large		8.86±0.10	0.311±0.004
				(0.046±0.010)
				(−0.038±0.010)

yield seemed to vary in the same way as that of the 40 cm group, although this is not certain, because of the poor statistics of this group.

Since the two large groups at 25 and 33 cm fall almost exactly where the two from the $O^{16}(d,p)O^{17}$ reaction would appear, it is possible that they are not caused by boron at all. Their very large yield makes it unlikely that they were due to surface contamination, but, as mentioned above, it was possible that the target consisted mostly of the oxide, rather than the elemental boron. To check this possibility, several runs were made at 0°. The energy of the emitted protons depends on the angle relative to the beam at which they are observed, and the change in energy from 90° to 0° observation is fairly dependent on the mass of the target nucleus, especially for light elements. Thus, the groups at 25 and 33 cm at 90° would move out to 34 and 47 cm at 0° if due to boron, but only to 32 and 43 cm if due to oxygen. While the data taken at 0° was not as accurate as that at 90° due to the uncertainty of the range-energy relation in the gold necessary to stop the beam, it is still evident from Fig. 3 that the two groups were due to boron. The high background at long range in the 0° runs was due to the gold needed to stop the beam, being from either the $Au^{197}(d,p)Au^{198}$ reaction, or from $N^{14}(d,p)N^{15}$, from air occluded in the foil.

The extrapolated range of each of the groups was determined from each run and converted to mean range by a procedure due to Motz and Humphreys.[8] This method takes into account the inhomogeneity of the beam, angle and range straggling, target thickness, and the finite range interval detected by the counter. The range in aluminum was corrected for the change in stopping power with the proton velocity, as shown in Livingston and Bethe.[3] A small correction was also made for the counter depth; that is, the distance a proton had to enter the counter in order to be recorded. Where two groups were not completely resolved, the shape of the shorter ranged one was estimated by reflecting the outer edge of the longer ranged one about a vertical line through its peak and subtracting. From the calculated mean range, the mean energy of each group was determined, using the Cornell 1937 relation. From these, and the mean energy of the beam, the Q-value of each group was calculated. They are shown, together with the corresponding levels in the B^{11} nucleus, in Table I. The Q-values obtained from the 0° runs are also given for comparison, although they are not as accurate. The agreement with the results of Cockcroft and Lewis, and Pollard, Davidson, and Schultz is very good, where they can be compared. The levels in B^{11} check within the experimental errors with those found by Fulbright and Bush[9] from the inelastic scattering of protons, who found levels at 2.2±0.3, 4.8±0.4, 6.5±0.3, and 7.8±0.4 Mev. This work can also be compared with the very precise results of Buechner and Van Patter[10] which have been included in Table I. The agreement is good, except for the groups having Q-values of 2.26 and 1.36 Mev. These fall on top of the two oxygen groups, and so may have been distorted somewhat. The three groups in parentheses could not have been detected by our method. That having a Q-value of 2.430 Mev could not have been resolved with our beam width of 250 kev from that at 2.480 Mev. The other two lie within the scattered beam, where we cannot work.

In conclusion, it gives me great pleasure to thank Dr. Ernest C. Pollard for suggesting this problem and for his helpful discussions while directing this research.

[8] H. A. Motz, thesis, Yale University, 1949.

[9] H. W. Fulbright and R. R. Bush, Phys. Rev. **74**, 1323 (1948).

[10] W. W. Buechner and D. M. Van Patter, Phys. Rev. **79**, 240 (1950). I am greatly indebted to Dr. Van Patter for sending me his results prior to publication.

The Neutron Yield from the $C^{13}(p, n)N^{13}$ Reaction*

R. E. Adamson, Jr.,** W. W. Buechner, W. M. Preston,
Clark Goodman, and D. M. Van Patter
Laboratory for Nuclear Science and Engineering, Massachusetts Institute of Technology, Cambridge, Massachusetts

(Received August 23, 1950)

The neutron yield from $C^{13}(p, n)N^{13}$ has been studied up to a proton energy of $E_p = 3.96$ Mev. A resonance is found at $E_p = 3.76$ Mev which corresponds to an excited state in N^{14} at 11.07 Mev and coincides with a previously reported level deduced from the reactions of deuterons on C^{12}. This finding furnishes evidence that the same state of a compound nucleus can be excited by two entirely different processes.

I. INTRODUCTION

THERE is considerable experimental evidence to show that the same energy levels are excited in the residual nucleus from a reaction regardless of its method of formation. Similar evidence regarding the energy levels of compound nuclei, which are formed as an intermediate step in such nuclear reactions, is largely lacking. The energy levels of such compound nuclei are most conveniently studied by observing as a function of the energy of the incident bombarding particle the variations in yield of the decay products. The location and width of any resonances that are observed then provide information regarding the level structure. According to current nuclear theory, it is to be expected that the same levels of a compound nucleus would be excited as a result of different modes of formation; and thus one would expect to observe resonances in the yield of disintegration products corresponding to the same levels in the compound nucleus, regardless of the nature of the target nucleus and the incident particle out of whose interaction it is formed. Usually, however, either the energy relations are such as to make it difficult to reach the same excited state in a compound nucleus by two processes which are not the inverse of each other or only a single appropriate target nucleus is available. The experimental evidence is thus far limited to those excited levels in N^{15} which are excited by the two inverse reactions, $N^{14}(n, p)C^{14}$ and $C^{14}(p, n)N^{14}$. Resonances have been observed in both the proton and neutron yields corresponding to the same levels in N^{15}. There is also evidence that some of these same levels may be involved in the inverse reactions $N^{14}(n, \alpha)B^{11}$ and $B^{11}(\alpha, n)N^{14}$. These processes have been summarized by Hornyak and Lauritsen.[1]

A further test of the theory is possible from a study of the higher levels of N^{14}. An energy-level diagram of N^{14} in this region is shown in Fig. 1. A large number of levels are known from the extensive work of Bonner and his collaborators[2–4] and of Bailey, Freier, and Williams,[5] who have studied the excitation curves for the emission of protons, neutrons, and gamma-rays from C^{12} bombarded with deuterons.

As can be seen from Fig. 1, these same levels in N^{14} can be reached through the bombardment of C^{13} with protons having an energy of the order of 4 Mev. Resonances should then be observed for the neutron production and for the formation of radioactive N^{13} from the reaction $C^{13}(p, n)N^{13}$. This reaction has not been studied in this energy region, although the reaction has been observed and the threshold for neutron production accurately measured by Richards and Smith[6] as 3.236 Mev.

It was the purpose of this experiment to search for resonances in the $C^{13}(p, n)N^{13}$ reaction, and thus to determine whether in this reaction the same energy levels in the compound nucleus N^{14} were excited as are found from the bombardment of C^{12} with deuterons.

II. EXPERIMENTAL PROCEDURE

The Rockefeller electrostatic accelerator at M.I.T. provides a magnetically analyzed proton beam of several microamperes at voltages up to approximately 4

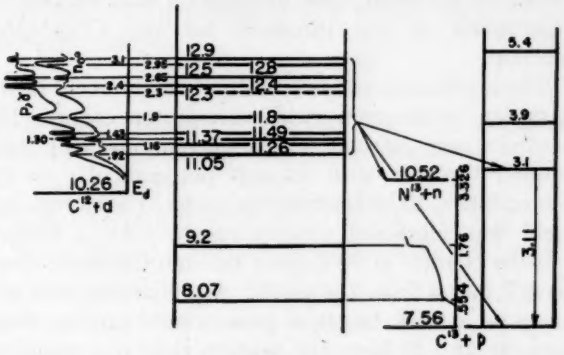

FIG. 1. Virtual energy levels of N^{14}; energies in Mev above the N^{14} ground state.

* This research has been partially supported by the joint program of ONR, AEC, and the Bureau of Ships.

** Lieutenant, U.S.N. Submitted in partial fulfillment of the requirements for the degree of M.S. in physics under the Naval Postgraduate Training Program.

[1] W. F. Hornyak and T. Lauritsen (private communication to be published).

[2] Bennett, Bonner, Hudspeth, Richards, and Watt, Phys. Rev. 59, 781 (1941).

[3] Bonner, Evans, Harris, and Phillips, Phys. Rev. 75, 1401 (1949).

[4] Phillips, Bonner, and Richardson, Phys. Rev. 76, 169 (1949).

[5] Bailey, Freier, and Williams, Phys. Rev. 73, 274 (1948).

[6] H. T. Richards and R. V. Smith, Phys. Rev. 77, 752A (1950).

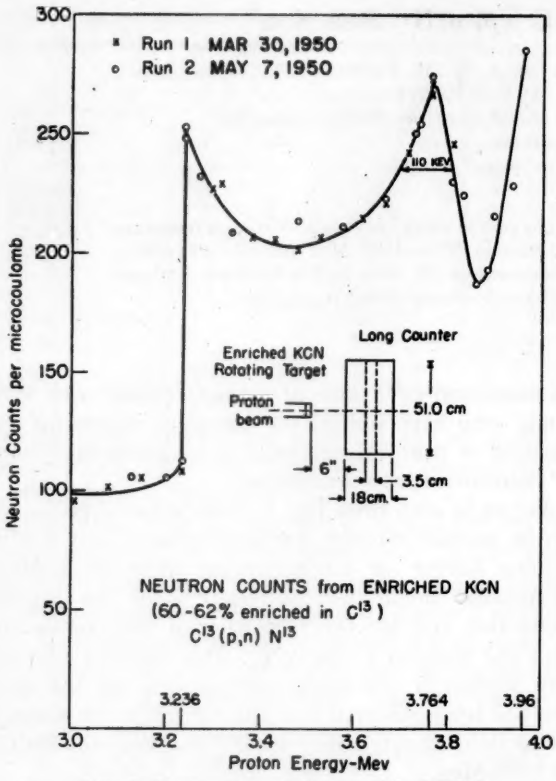

FIG. 2. Neutron counts from enriched KCN.

Mev. The energy resolution is determined by slits placed at the entrance and exit to the analyzing magnet and in these experiments was approximately ±5 kev. The generator voltage in these experiments was measured using a generating voltmeter, the output of which was read on a 0–100 microammeter. Two calibration points were obtained from the $Li^7(p, n)Be^7$ reaction threshold,[7] 1.882 Mev, using successively the proton beam and the mass 2 beam. The scale between was assumed to be linear; this assumption was verified by observation of the threshold for the $C^{13}(p, n)N^{13}$ reaction.

The experiment consisted of the measurement of the variations of neutron yield with proton energy. The neutrons were detected with a conventional BF_3 "long counter"[8] placed with its axis perpendicular to the proton beam, 10 inches from the target. The gamma-ray yield was measured simultaneously with a Geiger-Mueller counter at 90 degrees through the beam direction, 7 inches from the target. A preliminary run was made on a thick target of pure normal carbon. Commencing at 3.26 Mev, the neutron yield rose smoothly from a low background value, and no resonances were observed for proton energies in the range from 3.26 to 3.96 Mev. That the $C^{13}(p, n)N^{13}$ reaction was taking place, however, with the one percent of the C^{13} present in the normal carbon, was determined by plotting the gamma-ray activity in the target as a function of time after shutting off the proton beam. This disclosed an activity of 12±2 min. half-life, which is attributed to N^{13} ($\lambda = 10.1$ min.).

The low yield from the thick carbon target indicated the need for a target enriched in C^{13}. Satisfactory targets were obtained by the evaporation of KCN onto tantalum sheets. The KCN, obtained from Eastman Kodak Company, had the C^{13} content increased to 60 percent. The target with the tantalum backing was mounted in a rotating-target assembly. At first, difficulty was experienced from the disappearance of the KCN during bombardment. This was prevented by the evaporation of a thin layer of gold over the KCN. The final targets thus consisted of a layer of KCN approximately 10 kev thick covered with a layer of gold less than 5 kev in thickness.

III. RESULTS

Figure 2 shows the neutron yield in counts per microcoulomb of protons from the enriched KCN targets as a function of proton energy. The yield increases abruptly by a factor of about 2.5 at a proton energy of 3.24 Mev. Within our meter-reading error of ±10 kev, this value agrees with the threshold value of 3.236 Mev found by Richards and Smith.[6] After an initial drop, the yield again rises and passes through a maximum at a proton energy of 3.76 Mev. After this maximum and the subsequent drop, the yield is again rising at 3.96 Mev, the limiting voltage that could be reached in these experiments. The statistical error in the number of counts represented by each point above the threshold energy in Fig. 2 is about one percent. The close agreement between the results taken at different times indicates that during the course of these experiments there was no appreciable accumulation of contamination on the target surface.

That the observed maximum in the excitation curve was caused by C^{13} was shown by observations made on a target of normal KCN. The neutron yield from this target rose smoothly without a detectable break at the C^{13} threshold and up to a proton energy of 3.7 Mev was small compared with that from the enriched target. The gamma-ray yield from both the enriched and unenriched KCN targets rose smoothly up to about 3.8 Mev with comparable intensities. Maxima in the gamma-ray yield from $C^{13}+p$ are apparently masked by a high background.

IV. CONCLUSIONS

It may be seen in Fig. 1 that the first level of N^{14} excited in the bombardment of C^{12} by deuterons is that corresponding to the 0.92-Mev resonance for the emission of protons, gamma-rays, and neutrons. Using the values of $C^{12}+d^2-N^{14}=10.29$ Mev and $C^{13}+p-N^{14}=7.57$ Mev from the compilation of Tollestrup, Fowler, and Lauritsen[9] and the deuteron-resonance energy[4] $E_d=0.91$ Mev, the corresponding level in N^{14} is calculated to be at 11.07 Mev. If this level is excited in the

[7] Herb, Snowden, and Sala, Phys. Rev. **75**, 246 (1949).
[8] A. O. Hansen and J. L. McKibben, Phys. Rev. **72**, 673 (1947).
[9] Tollestrup, Fowler, and Lauritsen, Phys. Rev. **78**, 372 (1950).

$C^{13}(p, n)N^{13}$ reaction, a resonance for neutron production should be observed at a proton energy of 3.78 Mev. The measured maximum for the resonance shown in Fig. 2 is 3.76 Mev, which is in satisfactory agreement with the predicted value. Similar considerations lead to the expectation of another resonance at a proton energy[10] of 4.01 Mev, a possibility that is not excluded by the data shown in Fig. 2. A rather arbitrary value of the half-width of the observed resonance at 3.76 Mev is 110 kev.

Measured in the same rough fashion, the half-widths of the peaks for the neutron, gamma-ray, and proton yields at $E_d=0.92$ Mev in the $C^{12}+d$ reaction are about 100 kev.[2,3,5] We hope in the near future to be able to extend these measurements to slightly higher voltages in order to reach the next few levels.

[10] There is also the possibility of a resonance at $E_p=3.99$ Mev, corresponding to a resonance in the proton yield from $C^{13}(d, p)C^{13}$ at a deuteron energy of 1.14 Mev, as reported in reference 4.

PHYSICAL REVIEW VOLUME 80, NUMBER 6 DECEMBER 15, 1950

On the Self-Energies of Quantum Field Theory*

GEORGE SNOW AND HARTLAND S. SNYDER
Brookhaven National Laboratory, Upton, Long Island, New York

(Received June 19, 1950)

It is shown that by a means of a canonical transformation in quantum electrodynamics, the photon self-energy and the current associated with a mixture of zero-photon and one-photon states cannot be simultaneously made to vanish to order e^2. This difficulty can be overcome by adding a charged Bose meson field.

THE recent modification of the usual perturbation theory applied to quantum field theory, introduced by one of us,[1] has been applied to the calculation of the photon self-energy. Although the theory has the power to make any single ambiguous divergent integral take on any finite value, including zero, one must be careful that the assignments of ambiguous integrals appearing in the expressions for different physical quantities are consistent one with another. In this note it is shown that to order e^2, both the photon self-energy and the current associated with a mixture of zero-photon and one-photon states cannot be simultaneously set equal to zero.

The Hamiltonian of the coupled Dirac-Maxwell fields may be written:

$$H=H_0+H_1+H_2 \tag{1}$$

with

$$H_0=\int e_{ps}(\alpha_{ps}{}^{+}\alpha_{p's'})\delta(\mathbf{p}-\mathbf{p}')d\mathbf{p}d\mathbf{p}' + \int \kappa a_{\lambda\kappa}{}^{+}a_{\lambda\kappa'}\delta(\kappa-\kappa')d\kappa d\kappa', \tag{2}$$

$$H_1=-\frac{e}{2\pi}\int\frac{d\mathbf{p}d\mathbf{p}'d\kappa}{\kappa^{\frac{1}{2}}}\delta(\mathbf{p}-\mathbf{p}'-\kappa) \times\{(\alpha_{ps}{}^{+}\alpha_{p's'})a_{\lambda\kappa}\langle ps|\alpha_\lambda|p's'\rangle + (\alpha_{p's'}{}^{+}\alpha_{ps})a_{\lambda\kappa}{}^{+}\langle p's'|\alpha_\lambda|ps\rangle\}, \tag{3}$$

$$H_2=\frac{e^2}{2\pi^2}\int\frac{d\mathbf{p}d\mathbf{p}'d\mathbf{p}''d\mathbf{p}'''}{|\mathbf{p}-\mathbf{p}'|^2}\delta(\mathbf{p}-\mathbf{p}'+\mathbf{p}''-\mathbf{p}''') \times(\alpha_{ps}{}^{+}\alpha_{p's'}\alpha_{p''s''}{}^{+}\alpha_{p'''s'''}) \times\langle ps|1|p's'\rangle\langle p''s''|1|p'''s'''\rangle. \tag{4}$$

The notation employed above is the same as in H.S. I. and will not be described here again.

As described in H.S. II, one now transforms the Hamiltonian H by means of a sequence of finite unitary transformations $e^{iS(\epsilon)}$ such that in the limit as the parameter $\epsilon\to\infty$, all the "virtual" terms in H are made to vanish. $S(\epsilon)$ is expanded in a powers series in the electronic charge.

$$S(\epsilon)=S_1(\epsilon)+S_2(\epsilon)+\cdots, \tag{5}$$

where $S_n(\epsilon)$ is of order e^n. One can now write the transformed Hamiltonian H' as a power series in e:

$$H'=e^{-iS(\epsilon)}He^{+iS(\epsilon)},$$
$$H'=H_0+\{H_1-i[S_1(\epsilon), H_0]\}+\{H_2-i[S_1(\epsilon), H_1] -\tfrac{1}{2}[S_1(\epsilon),[S_1(\epsilon), H_0]]-i[S_2(\epsilon), H_0]\}+\cdots. \tag{6}$$

Eliminating the "virtual" terms in H' step by step in powers of e, we first choose $S_1(\epsilon)$ such that

$$\lim_{\epsilon\to\infty}\{H_1-i[S_1(\epsilon), H_0]\}=0. \tag{7}$$

The function $S_1(\epsilon)$ is

$$S_1(\epsilon)=-\frac{ie}{2\pi}\int\frac{d\mathbf{p}d\mathbf{p}'d\kappa\delta(\mathbf{p}-\mathbf{p}'-\kappa)}{\kappa^{\frac{1}{2}}(e_{ps}-e_{p's'}-\kappa)}g(ps|p's'|\epsilon) \times\{(\alpha_{ps}{}^{+}\alpha_{p's'})a_{\lambda\kappa}\langle ps|\alpha_\lambda|p's'\rangle -(\alpha_{p's'}{}^{+}\alpha_{ps})a_{\lambda\kappa}{}^{+}\langle p's'|\alpha_\lambda|ps\rangle\}, \tag{8}$$

* Research carried out under contract with the AEC.

[1] H. Snyder, Phys. Rev. 78, 95 (1950). This article will henceforth be denoted as H.S. I., and the article H. Snyder, Phys. Rev. 79, 520 (1950) will be denoted as H.S. II.

where $g(\mathbf{p}s|\mathbf{p}'s'|\epsilon)$ is a real function invariant under rigid rotations of the vectors $\mathbf{p}$ and $\mathbf{p}'$ and independent of the spins of the particles. It then follows that $S_1(\epsilon)$ is an Hermitian operator that commutes with the angular momentum and linear momentum operators. Furthermore we limit $S_1(\epsilon)$ to be charge symmetrical, which requires that $g(\mathbf{p}s|\mathbf{p}'s'|\epsilon)$ satisfy the relations

$$g(\mathbf{p}s|\mathbf{p}'s'|\epsilon)=g(\mathbf{p}'\bar{s}'|\mathbf{p}\bar{s}|\epsilon), \tag{9}$$

where $\bar{s}$ denotes an energy state of opposite sign to s. In order that $S_1(\epsilon)$ satisfy Eq. (7), one must require only that

$$\lim_{\epsilon\to\infty} g(\mathbf{p}s|\mathbf{p}'s'|\epsilon)=1. \tag{10}$$

$g(\mathbf{p}s|\mathbf{p}'s'|\epsilon)$ may take on positive or negative bounded values subject to the conditions enumerated above. Hence the g function has the property that if it appears in an integrand whose integral exists, the value of that integral is unchanged in the limit $\epsilon\to\infty$, while if it appears in an integrand whose integral is divergent, that integral can be made to take on any limiting value.

Let us now consider the photon self-energy terms that appear in H' to order e^2. These will arise from that part of the operator

$$\{-i[S_1, H_1]-\tfrac{1}{2}[S_1, [S_1, H_0]]\}$$

that contains two photon operators of the form a^+a. It is very important to note that since $[S_1, H_1]$ is linear in g while $[S_1, [S_1, H_0]]$ is quadratic in g, the operator $\{-i[S_1, H_1]-\frac{1}{2}[S_1, [S_1, H_0]]\}$ does not in general reduce to $-\frac{1}{2}i[S_1, H_1]$ as it does in the conventional perturbation theory, which corresponds to the condition that $g(\mathbf{p}s|\mathbf{p}'s'|\epsilon)=1$ or 0.

A simple calculation to order e^2 yields

$$\begin{aligned}(H')_{a^+a}&=\{-i[S_1, H_1]-\tfrac{1}{2}[S_1, [S_1, H_0]]\}_{a^+a}\\&=\frac{e^2}{2\pi^2}\int\frac{d\boldsymbol{\kappa}d\boldsymbol{\kappa}'}{\kappa}\delta(\boldsymbol{\kappa}-\boldsymbol{\kappa}')a_{\lambda'\boldsymbol{\kappa}'}{}^+a_{\lambda\boldsymbol{\kappa}}\\&\quad\times\int d\mathbf{p}Sp(\lambda_{\mathbf{p}}{}^-\alpha_\lambda\lambda_{\mathbf{p}-\boldsymbol{\kappa}}{}^+\alpha_{\lambda'})\\&\quad\times\Bigg[\frac{g(\mathbf{p}_-|\mathbf{p}-\boldsymbol{\kappa},+)-\frac{1}{2}g^2(\mathbf{p}_-|\mathbf{p}-\boldsymbol{\kappa},+)}{-e_{\mathbf{p}}-e_{\mathbf{p}-\boldsymbol{\kappa}}-\kappa}\\&\quad\times\frac{g(\mathbf{p}_+|\mathbf{p}-\boldsymbol{\kappa},-)-\frac{1}{2}g^2(\mathbf{p}_+|\mathbf{p}-\boldsymbol{\kappa},-)}{e_{\mathbf{p}}+e_{\mathbf{p}-\boldsymbol{\kappa}}-\kappa}\Bigg],\end{aligned} \tag{11}$$

where

$$\lambda_{\mathbf{p}}{}^{\pm}=\tfrac{1}{2}\left(1\pm\frac{\boldsymbol{\alpha}\cdot\mathbf{p}+m\beta}{e_p}\right),$$

$\alpha_\lambda=\boldsymbol{\alpha}\cdot\mathbf{e}_\lambda$, $\mathbf{e}_\lambda\perp\boldsymbol{\kappa}$ and the parameter ϵ is understood to be implicit in the g functions.

In Eq. (11) two possibilities arise: (i) $\mathbf{e}_\lambda=\mathbf{e}_{\lambda'}$, (ii) $\mathbf{e}_\lambda\perp\mathbf{e}_{\lambda'}$.

$$\begin{aligned}&\text{(i)}\quad Sp(\lambda_{\mathbf{p}}{}^-\alpha_\lambda\lambda_{\mathbf{p}-\boldsymbol{\kappa}}{}^+\alpha_\lambda)\\&\qquad=[e_pe_{\mathbf{p}-\boldsymbol{\kappa}}+m^2-2(\mathbf{p}\cdot\mathbf{e}_\lambda)^2+\mathbf{p}\cdot(\mathbf{p}-\boldsymbol{\kappa})]/e_pe_{\mathbf{p}-\boldsymbol{\kappa}},\\&\text{(ii)}\quad Sp(\lambda_{\mathbf{p}}{}^-\alpha_\lambda\lambda_{\mathbf{p}-\boldsymbol{\kappa}}{}^+\alpha_{\lambda'})=-2(\mathbf{p}\cdot\mathbf{e}_\lambda)(\mathbf{p}\cdot\mathbf{e}_{\lambda'})/e_pe_{\mathbf{p}-\boldsymbol{\kappa}}.\end{aligned} \tag{12}$$

In both cases (i) and (ii), the redundant integral over $\mathbf{p}$ in $(H')_{a^+a}$ of Eq. (11) is ambiguous with a leading quadratic divergence if $g=1$. However, we can choose the g functions such that $(H')_{a^+a}$ shall vanish. In case (i), $(H')_{a^+a}$ becomes the photon self-energy to order e^2, and the requirement that it vanish yields the following condition on the g functions:

$$\begin{aligned}0=\int\frac{d\mathbf{p}}{e_pe_{\mathbf{p}-\boldsymbol{\kappa}}}&[e_pe_{\mathbf{p}-\boldsymbol{\kappa}}+m^2-2(\mathbf{p}\cdot\mathbf{e}_\lambda)^2+\mathbf{p}\cdot(\mathbf{p}-\boldsymbol{\kappa})]\\&\times\Bigg[\frac{g(\mathbf{p}_-|\mathbf{p}-\boldsymbol{\kappa},+)-\frac{1}{2}g^2(\mathbf{p}_-|\mathbf{p}-\boldsymbol{\kappa},+)}{-e_{\mathbf{p}}-e_{\mathbf{p}-\boldsymbol{\kappa}}-\kappa}\\&\quad-\frac{g(\mathbf{p}_+|\mathbf{p}-\boldsymbol{\kappa},-)-\frac{1}{2}g^2(\mathbf{p}_+|\mathbf{p}-\boldsymbol{\kappa},-)}{e_{\mathbf{p}}+e_{\mathbf{p}-\boldsymbol{\kappa}}-\kappa}\Bigg].\end{aligned} \tag{13}$$

In case (ii), $(H')_{a^+a}$ is a virtual term, and the requirement that it should vanish yields only the condition that the g functions make the redundant $\mathbf{p}$ integral finite in the limit $\epsilon\to\infty$, since it then follows that the azimuthal integral in $\mathbf{p}$ space about the direction $\boldsymbol{\kappa}$ vanishes identically. From the commutability of S_1 with the total angular momentum it follows that $g(\mathbf{p}s|\mathbf{p}-\boldsymbol{\kappa}, s')$ is independent of the azimuthal angle about the direction of $\boldsymbol{\kappa}$. The virtual terms in H' proportional to aa and a^+a^+ of order e^2, which couple the vacuum state to two photon states, can be made to vanish, yielding a condition on the g functions independent of Eq. (13).

Let us now consider how the current density,

$$j_\mu(\mathbf{x})=e\int d\mathbf{p}d\mathbf{p}'(\alpha_{p_s}{}^+\alpha_{p's'})e^{-i(\mathbf{p}-\mathbf{p}')\cdot\mathbf{x}}\langle\mathbf{p}s|\alpha_\mu|\mathbf{p}'s'\rangle, \qquad (\alpha_\mu=\boldsymbol{\alpha}, 1) \tag{14}$$

is transformed by the unitary S transformation. The transformed current density $j_\mu'(\mathbf{x})=e^{-iS}j_\mu(\mathbf{x})e^{+iS}$ will contain the following terms linear in a and a^+, to order e^2:

$$\begin{aligned}[j_\mu'(\mathbf{x})]_{a,a^+}&=-\frac{e^2}{2\pi}\int\frac{d\boldsymbol{\kappa}}{\kappa^{\frac{1}{2}}}[a_{\lambda\boldsymbol{\kappa}}e^{i\boldsymbol{\kappa}\cdot\mathbf{x}}+a_{\lambda\boldsymbol{\kappa}}{}^+e^{-i\boldsymbol{\kappa}\cdot\mathbf{x}}]\\&\quad\times\int d\mathbf{p}Sp(\lambda_{\mathbf{p}}{}^-\alpha_\lambda\lambda_{\mathbf{p}-\boldsymbol{\kappa}}{}^+\alpha_\mu)\\&\quad\times\left[\frac{g(\mathbf{p}_-|\mathbf{p}-\boldsymbol{\kappa},+)}{(-e_{\mathbf{p}}-e_{\mathbf{p}-\boldsymbol{\kappa}}-\kappa)}-(1-2\delta_{\mu 4})\frac{g(\mathbf{p}_+|\mathbf{p}-\boldsymbol{\kappa},-)}{(e_{\mathbf{p}}+e_{\mathbf{p}-\boldsymbol{\kappa}}-\kappa)}\right].\end{aligned} \tag{15}$$

If a state which we label to be a mixture of a zero-photon state and a one-photon state is to have the proper physical behavior, it must not have a current associated with it. Hence it is necessary to make the redundant integral in $[j_\mu'(\mathbf{x})]_{a,a^+}$ vanish, since only then will the expectation value of $j_\mu'(\mathbf{x})$ for a state that is a mixture of zero-photon and a one-photon state vanish. If we consider the component of $[j_\mu'(\mathbf{x})]_{a,a^+}$ in the direction of the electric vector, i.e., $\mathbf{e}_\mu=\mathbf{e}_\lambda$, we obtain the condition

$$0=\int\frac{d\mathbf{p}}{e_\mathbf{p}e_{\mathbf{p}-\boldsymbol{\kappa}}}[e_\mathbf{p}e_{\mathbf{p}-\boldsymbol{\kappa}}+m^2-2(\mathbf{p}\cdot\mathbf{e}_\lambda)^2+\mathbf{p}\cdot(\mathbf{p}-\boldsymbol{\kappa})]\times\left[\frac{g(\mathbf{p}_-|\mathbf{p}-\boldsymbol{\kappa},+)}{-e_\mathbf{p}-e_{\mathbf{p}-\boldsymbol{\kappa}}-\kappa}-\frac{g(\mathbf{p}_+|\mathbf{p}-\boldsymbol{\kappa},-)}{e_\mathbf{p}+e_{\mathbf{p}-\boldsymbol{\kappa}}-\kappa}\right]. \quad (16)$$

For the three other possibilities, $\mathbf{e}_\mu\perp\mathbf{e}_\lambda$ and $\alpha_4=1$, the requirement that the redundant integral with respect to $\mathbf{p}$ in Eq. (15) vanish, implies merely that the g function make each integral finite, since the azimuthal integration about the direction $\boldsymbol{\kappa}$ yields the value zero analogously to case (ii) of $(H')_{a^+a}$. Equations (13) and (16) combine to yield the condition

$$0=\int\frac{d\mathbf{p}}{e_\mathbf{p}e_{\mathbf{p}-\boldsymbol{\kappa}}}[e_\mathbf{p}e_{\mathbf{p}-\boldsymbol{\kappa}}+m^2-2(\mathbf{p}\cdot\mathbf{e}_\lambda)^2+\mathbf{p}\cdot(\mathbf{p}-\boldsymbol{\kappa})]\times\left[-\frac{g^2(\mathbf{p}_-|\mathbf{p}-\boldsymbol{\kappa},+)}{-e_\mathbf{p}-e_{\mathbf{p}-\boldsymbol{\kappa}}-\kappa}+\frac{g^2(\mathbf{p}_+|\mathbf{p}-\boldsymbol{\kappa},-)}{e_\mathbf{p}+e_{\mathbf{p}-\boldsymbol{\kappa}}-\kappa}\right] \quad (17)$$

which cannot be satisfied since the integral is positive definite and quadratically divergent. This contradiction is still present if one allows g to take on complex values, since in that case $g^2(\mathbf{p}_-|\mathbf{p}-\boldsymbol{\kappa},+)$ in (17) is replaced by $|g(\mathbf{p}_-|\mathbf{p}-\boldsymbol{\kappa},+)|^2$. Hence, although the unitary transformation $S_1(\epsilon)$ contains an arbitrary function $g(\mathbf{p}s|\mathbf{p}'s'|\epsilon)$, it is not possible to make the photon self-energy and the current associated with a mixture of zero-photon and one-photon states vanish simultaneously to order e^2. This last result seem to be true for any change of representation in quantum electrodynamics by means of a canonical transformation that still labels states by occupation numbers.

The physical criterion that a one-photon state should actually describe a photon in a relativistically covariant way is not that the photon self-energy must vanish order by order in e^2, but only that the sum over all orders in e^2, higher than the zeroth of the terms in H' proportional to $a_{\lambda\boldsymbol{\kappa}}{}^+a_{\lambda\boldsymbol{\kappa}}$ must vanish. The difficulty that appears in trying to make the photon self-energy and the current present for a mixture of zero-photon and one-photon states vanish simultaneously to order e^2, does not appear at high orders in e^2, since at higher orders the g functions that appear in the infinite redundant integrals of $[j_\mu'(\mathbf{x})]_{a,a^+}$ and of $(H')_{a^+a}$ do not differ by a positive definite combination of g functions. Hence the higher order terms in $[j_\mu'(\mathbf{x})]_{a,a^+}$ and $(H')_{a^+a}$ can be made to take on independent values. However, it is clear that adopting the procedure of imposing a condition on the infinite sum of terms, although possible in principle, would make the theory extremely cumbersome. It would imply that the limiting process that is carried out as $\epsilon\to\infty$ must be a function of the fine structure constant, hence making suspect any order by order calculation in e^2. However a very simple alternative solution to this photon self-energy problem is to introduce into the theory an additional charged Bose field, e.g., a scalar or vector meson field. It has been shown[2] that such charged fields interacting with the quantized electromagnetic field yield quadratically divergent expressions for the photon self-energy of opposite sign to that obtained from the interaction of a photon with the quantized electron field. The photon self-energy and the induced current for a mixture of zero-photon and one-photon states can then simultaneously be set equal to zero to order e^2, and the limiting process as $\epsilon\to\infty$ would then remain independent of the fine structure constant. As has already been pointed out in H.S. I and H.S. II, the electron self-energy to order e^2 can be set equal to zero, in contrast with the photon self-energy, without contradicting any other physical conditions.

[2] D. Feldman, Phys. Rev. **76**, 1369 (1949); H. Umezawa and R. Kawabe, Prog. Theor. Phys. **4**, 443 (1949).

A Precise Determination of the Half-Life and Average Energy of Tritium Decay*†

G. H. JENKS, F. H. SWEETON, AND J. A. GHORMLEY
Chemistry Division, Oak Ridge National Laboratory, Oak Ridge, Tennessee

(Received August 21, 1950)

A precise determination of the half-life of tritium and of the average energy released by the decay has been carried out. The half-life was determined from measurements of the quantity of tritium contained in a sample and the rate at which that quantity gave rise to He^3. The average energy release was determined from additional measurements on the same sample of the rate at which the sample liberated heat. The value found for the half-life was 12.46±0.1 years. That found for the average energy released by decay of neutral tritium to neutral helium was 5.69±0.04 kev.

I. INTRODUCTION

THE half-life of tritium has been reported by several investigators, but considerable variance exists in the results. Thus, early measurements which were made with tracer quantities of the isotope and which involved counting the emitted beta-particles indicated a value of about 30 years.[1] More recent measurements, in which macro-amounts of tritium were employed, showed the half-life to be much shorter. Goldblatt, *et al.*[2] followed the decay with an ionization chamber and found a value of 10.7±2 years. Novick[3] measured the rate at which He^3 was formed by a measured quantity of tritium and reported a value of 12.1±0.5 years.

The average beta-ray energy of tritium has been reported by Nielsen[4] as 6.5 kev and by Alvarez and Cornog[5] as 10 kev. Nielsen's measurements were made by means of a cloud chamber in which the number of ion clusters formed by tritium was compared with the number formed by x-rays of known energy. The value given by Alvarez and Cornog was the result of determining the ratio of the number of active atoms to the number of ion pairs formed in a given volume. More recently, several studies[6,7] of the beta-ray spectrum of tritium have been reported. Approximate average beta-energy values can, of course, be found from the results of these studies although the values as such have not been reported.

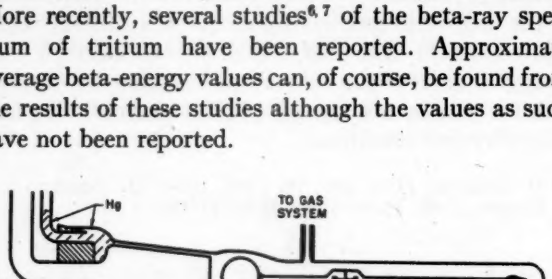

FIG. 1. Gas density balance and case.

II. METHOD

In the presently reported work, the half-life and average energy determinations are based on measurements on the same sample of (1) the quantity of tritium, (2) the rate of evolution of the tritium decay product, He^3, and (3) the rate of evolution of heat. The general method of carrying out these measurements was as follows. A gaseous mixture of tritium and normal hydrogen was purified by passage through palladium and analyzed for the tritium-hydrogen ratio with the aid of a small gas density balance. The volume of the sample was then measured, and the gas transferred to a small Pyrex ampoule, where it was absorbed in palladium foil. Calorimetric measurements of the heat evolved by the sample in this form were then carried out. Following the calorimetric measurement, the hydrogen mixture was driven from the palladium and passed over hot copper oxide, where it was converted to water. The water was collected and sealed in a small silica glass ampoule which was subsequently used in the disintegration rate determination. To check on the completeness of the conversion and transfer, a measurement of the heat evolved by the ampoule was made.

Two different samples of tritium were studied. With one of the samples the above procedure was carried out as described. The other sample was prepared simply by sealing some tritium oxide in a silica glass ampoule and was used to measure only the average energy.

III. PREPARATION OF SAMPLE WITH KNOWN QUANTITY OF TRITIUM

A. Apparatus

The gas density balance which was constructed and used in the analysis of tritium-hydrogen mixture is shown in Fig. 1. In principle and design it was similar to balances which have been described by others.[8] The beam and bulb were constructed of silica glass and had a total weight of 271 mg. The volume of the bulb was about 2 ml. Two tungsten tips, sharpened by being burned in potassium nitrite, were attached to the beam through a graded glass crosspiece and served as a fulcrum. The sensitivity of the balance, adjusted by

* This document is based on work performed for the Atomic Energy Project at Oak Ridge National Laboratory.

† The results of the measurements described here have been published in a Letter to the Editor, Phys. Rev. **75**, 701 (1949).

[1] R. D. O'Neal and M. Goldhaber, Phys. Rev. **58**, 574 (1940).
[2] Goldblatt, Robinson, and Spence, Phys. Rev. **72**, 973 (1947).
[3] A. Novick, Phys. Rev. **72**, 972 (1947).
[4] C. E. Nielsen, Phys. Rev. **60**, 160 (1941).
[5] L. W. Alvarez and R. Cornog, Phys. Rev. **57**, 248 (1940).
[6] Curran, Angus, and Cockcroft, Phil. Mag. **40**, 53 (1949).
[7] G. C. Hanna and B. Pontecorvo, Phys. Rev. **75**, 983 (1949).

[8] A. Farkas and H. W. Melville, *Experimental Methods in Gas Reactions* (Macmillan and Company, London, 1939), pp. 199–201.

bending the beam near the fulcrum, was such that the displacement of the tip caused by a change in buoyancy was 1.2 mm/μg. A buoyant force on the bulb of about 60 μg, equivalent to the buoyance of the bulb in hydrogen at 300 mm pressure, was sufficient to support the balance. The case for the balance was made of Pyrex glass and was shaped to minimize the free space about the balance. A thin glass shelf within the case served as a rest for the balance.

The gas handling system associated with the balance is shown in Fig. 2. This system was constructed of Pyrex. It had provision for introducing the gas to be measured, for controlling and measuring the volume of the final sample, and for transferring the final sample to an ampoule. Mercury valves, designated by *X* on the drawing, were used in place of stopcocks. The minimum volume of the system when the McLeod gauge and manometer were filled with mercury was 25 to 30 ml, sufficiently low to permit determinations on 5 ml (S.T.P.) of gas when operating at reduced pressure.

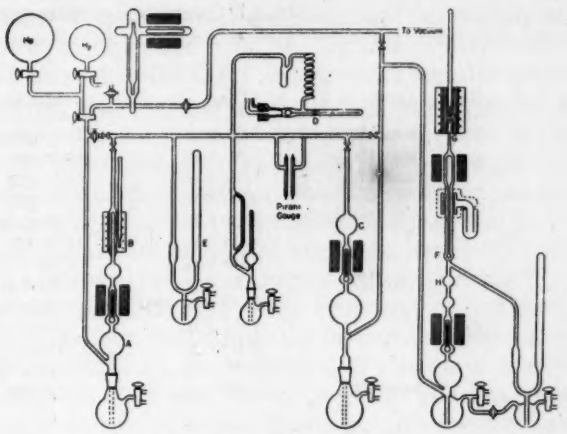

FIG. 2. Gas handling system.

B. Procedure

The determination of tritium abundance in the tritium-hydrogen mixture was made by a comparison of the pressure at which that gas held the balance in a certain position with the pressure of purified tank hydrogen required to hold the balance in the same position. If it is assumed that the characteristics of the balance remained constant as the pressure was varied, the two gases had equal buoyancies and thus equal densities at their balancing pressures. However, the balancing pressures of the two gases were considerably different; and it was possible that the dimensions and thus the buoyancy of the fragile balance bulb were different at the two pressures. To determine whether a change occurred and to establish its magnitude, a comparison of the balancing pressures of tank hydrogen and helium was made. The density found for the hydrogen-tritium mixture was approximately the same as that of helium; and the comparison should, therefore, have given an accurate measure of any necessary correction.

A balancing-pressure determination was made by first adjusting the gas pressure within the balance system until the balance was supported near the desired position. The relative heights of the balance tip and a reference point at the fulcrum were then determined by means of a cathetometer. The difference in heights directly represented the position of the balance and was relatively independent of any error in leveling the cathetometer, which stood five feet away. The gas pressure corresponding to the balance position was read on manometer *E* with a second cathetometer. A thermometer graduated in fifths of degrees was read whenever the pressure was determined.

Seven or more determinations were made in the above manner each time gas was placed in the balance system. Between each determination, the pressure was varied slightly so that the balance was at a new position. However, the total distance through which the position of the tip varied did not exceed 1 mm. The resulting data for balance positions and pressures were plotted graphically, and the pressure corresponding to a standard balance position (chosen as 1.50 mm below the reference point) was found from the graph.

Following the final balancing pressure measurement on the tritium sample, the gas was transferred to the previously calibrated volume in bulb *H* and its pressure and temperature measured. To complete the preparation, valve *F* was opened, and the gas forced into ampoule *G* which contained about 1 g of palladium foil. The palladium rapidly reduced the pressure to about 10 cm of Hg, and at that pressure the ampoule was sealed. Only 0.3 percent of the total sample remained over the mercury after sealing.

C. Results

The data obtained in comparing the balancing pressure of purified tank hydrogen with that of the tritium mixture are shown in Table I. Several separate measurements were made on each gas. Between successive measurements on the tritium sample, the gas was generally repurified by passage through palladium. The reference hydrogen was also repurified from time to time; but this purification consisted of discarding the portion which had been measured and introducing, through the palladium valve, a fresh portion from the tank. A notation indicating whether or not the gas was purified just prior to the measurements is included in Table I in the column listing the gas measured.

Each time the tritium-hydrogen mixture was repurified, a small fraction of the gas was found to remain in the palladium thimble; and, in addition, the gas which passed the palladium was found to exhibit a slight increase in balancing pressure. These effects were apparently the result of removal, by the palladium, of foreign gases which had accumulated in the tritium-hydrogen mixture during the time it was in contact with the glass system. The amount of foreign gases

TABLE I. Comparison of balancing pressures for H_2 and for H_2-T_2 mixture.

Date	Time	Gas measured	Approximate vol. of impurity removed	Balancing pressure (mm. Hg) Hydrogen	Tritium
June 15	7:54 P.M.	Hydrogen (purified)	...	307.33	
June 16	7:56 A.M.	Hydrogen (same)	...	307.03	
June 17	9:19 A.M.	Hydrogen (purified)	...	306.67	
	10:10 A.M.	Hydrogen (same)	...	306.75	
	2:15 P.M.	Tritium (purified)	0.002 ml		154.26
	5:08 P.M.	Hydrogen (purified)	...	307.11	
	6:02 P.M.	Tritium (purified)	0.002 ml		154.87
June 18	3:56 P.M.	Tritium (purified)	0.002 ml		155.17
	6:30 P.M.	Tritium (purified)	0.0006 ml		155.58
	7:34 P.M.	Tritium (same)	...		155.45
	9:03 P.M.	Tritium (purified)	0.0006 ml		155.66
	10:57 P.M.	Tritium (purified)	0.0002 ml		155.71
June 19	2:00 A.M.	Hydrogen (purified)	...	306.78	
			Best values	306.8	155.7

removed, as well as the change observed in balancing pressure, became smaller with successive purifications and reached a negligibly small amount during the final measurements. The approximate volumes of foreign gases removed in each purification are listed in the fourth column of Table I. A fair correlation between these values and observed change in density can be made if it is assumed that the average molecular weight of the foreign gases was about 30.

The data obtained in the comparison of the balancing pressures of hydrogen and helium are shown in Table II. The source of the hydrogen was the same as that described in the previous paragraphs. The helium used was obtained from a tank supply, and its density was determined directly by weighing in a five-liter flask using a second five-liter flask as a tare.

Two separate measurements of the helium density by weighing gave values of 0.1787 g/l and 0.1789 g/l. The best value, 0.1789 g/l, was 0.2 percent greater than the literature value for the density of helium. The density of the helium computed from the data in Table II and from the known density of hydrogen was 0.1771 g/l, 1.0 percent less than the density measured directly by weighing. This observation indicated that the buoyancy of the balance was smaller at 150 mm than at 300 mm by 1 percent. A correction of 1 percent was therefore made in the balancing pressures for the tritium mixture which are listed in Table I before those data were used in computing the tritium-hydrogen ratio in the mixture.

The fraction by volume of tritium in the tritium-hydrogen mixture was computed from the pressure data and found to be 0.4970. This value and the value for the quantity of tritium transferred to the ampoule (5.172_6 ml S.T.P.) were then used to find the quantity of tritium in the ampoule, 2.571 ml S.T.P.

TABLE II. Comparison of balancing pressures for H_0 and for He.

Date	Time	Gas measured	Pressure (mm. Hg) He	H_2
Aug. 12	11:18 A.M.	H_2, freshly purified		299.1
	3:52 P.M.	He, fresh from bulb	152.0	
	4:59 P.M.	Same H_2		300.0_5
	5:58 P.M.	He, fresh from bulb	152.4	
	6:39 P.M.	Same H_2		300.3
	7:45 P.M.	He, fresh from bulb	152.5	
		Best values	152.4	300.3

In estimating the uncertainty of the latter value, the error in determining each of the various physical properties of the sample was considered. For convenient reference the various sources of error and the amount by which each source affected the value for the quantity of tritium are listed in Table III. Combining all errors, the estimated probable error for the quantity of tritium was ±0.5 percent.

IV. CALORIMETRIC MEASUREMENTS

The calorimeter which was used in the thermal study of the various samples was an isothermal type which operated at 77°K. Heat from the source vaporized nitrogen under constant pressure, and the rate of vaporization was used as a measure of the heat input. Details of the design and operation of the calorimeter have been reported previously.[9]

For convenience in discussion, the three tritium samples which were measured are labeled as follows: I—the sample used only in an average beta-energy determination, IIp—the palladium-tritium sample prepared as described in the previous section, IIo—the tritium oxide sample prepared from the tritium in sample IIp.

The calorimetric data for samples I and IIp are given in Tables IV and V, respectively. The heat liberated by the latter sample was great enough to allow both a calibration and a measurement of the sample to be carried out on the same day. In addition, it was possible to make several observations of the rate of nitrogen evolution during each measurement. The rate at which heat was evolved by the smaller sample was so low that it was not feasible to make more than one measurement per day nor to make more than one observation of the rate during a measurement. It should be noted that during the time that the last three measurements were

[9] C. V. Cannon and G. H. Jenks, Rev. Sci. Inst. 21, 236 (1950).

TABLE III. Estimated error in determination of tritium content.

Determination introducing uncertainty	Estimated maximum error in amount of tritium (percentage)
Balancing pressure of hydrogen	±0.2
Balancing pressure of tritium mixture	0.2
Pressure correction for balance:	
Balancing pressure of hydrogen	0.2
Balancing pressure of helium	0.2
Helium density (direct weighing)	0.3
Temperature of gas sample	0.1
Pressure of gas sample	0.1
Volume of bulb *H*	0.1

made on the smaller sample (May 5, 6, 7), the calorimeter showed a smaller background gas evolution than during the earlier measurements, owing to some slight changes which had been made in the calorimeter, and the validity of the results was not affected. The heat liberated by the respective samples was computed from the data and from the calibrated relationship between change of heat input and change in gas evolution rate. This relationship (change of 1 rate unit = change of 1.934×10^{-4} watt) was never found to vary significantly.

In the calorimetric study of sample IIo, it was found that the rate at which the sample evolved heat varied during the measurement. When the normal procedure was followed, the rate at the time of the first observation was several percent lower than that exhibited by sample IIp. However, the rate increased with each successive observation until it levelled off at a value in close agreement with that shown by the palladium sample.

Discussion

The thermal behavior of sample IIo when measured in the normal manner can be satisfactorily explained with the assumption that part of the decay energy was stored in the ice at −196°C and that the amount stored reached a steady-state value. This assumption is substantiated by the observations of Ghormley and Allen.[10] They found that gas, resulting from decomposition of ice, appeared upon melting tritium oxide which had been at −196°C for some time. They also found evidence that the amount of gas evolved approached a limiting value. It is very likely that in the case of the palladium-tritium sample all of the power generated by decay of tritium appeared as heat. Processes such as the trapping of electrons and chemical change, which probably account for storage of energy in ice, should not occur in the palladium-tritium system. Experimentally, no indication that part of the decay energy was being stored was observed during the measurements on sample IIp. Similarly, no indication of storage of energy was observed during measurement of the one-curie sample of tritium oxide. However, this sample was measured about eight months after it was prepared, whereas sample IIo was measured within a few days of the time that it was prepared. Furthermore, the concentration of T_2O in the smaller sample was only about 10 percent compared with 50 percent in the larger sample. Some difference between the two oxide samples would therefore be expected.

Some further observations which were made on the thermal behavior of sample IIo may be of interest in connection with the storage of energy in ice. Several calorimetric measurements were made after the sample had been at −196°C for one to two days and then brought into contact with air at room temperature for a short interval, during which the sample was transferred to the calorimeter. In several of these measurements, the rate of heat evolution was found to start low but to increase with time to a value about 5 percent higher than that obtained with sample IIp. Unfortunately, the measurements were not continued long enough to de-

TABLE IV. Power generated by sample I. Calibration for Set No. 1 carried out at 3.600×10^{-5} watts. Calibration for Set No. 2 carried out at 3.590×10^{-5} watts.

Set number	Date	Rate observed in calibration arbitrary units	Rate observed with T_2O sample arbitrary units
1	April 14	0.212	
	April 15	0.207	
	April 16		0.208
	April 26		0.208
	April 27	0.213	
	April 28		0.205
	April 30		0.204
2	May 5	0.196	
	May 6	0.195	
	May 7		0.190

Power generated by sample—$3.50_3\times10^{-5}$ watt±0.7 percent probable error.

TABLE V. Power generated by sample IIp. Calibration carried out at 2.200×10^{-4} watts.

Date	Rate observed in calibration arbitrary units	Rate observed with T sample arbitrary units
June 28	1.179, 1.185 } 1.182	1.193, 1.189 } 1.191
June 29	1.171, 1.183 } 1.177	1.172, 1.163, 1.172 } 1.169
June 30		1.163, 1.168, 1.174, 1.166 } 1.168
July 1	1.164, 1.164 } 1.164	1.188, 1.193 } 1.191
July 27	1.167, 1.174, 1.169 } 1.170	

Power generated by sample—2.214×10^{-4} watt±0.4 percent probable error.

[10] J. A. Ghormley and A. O. Allen, private communication.

TABLE VI. Disintegration rate of sample I.

Time of measurement t days	Collection period days	Approximate vol. collected ml S.T.P.	Activity at time t	Activity at zero time
28	14	1.62×10^{-3}	1.022	1.026
59	49	5.68×10^{-3}	1.024	1.033
158	49	5.68×10^{-3}	0.993	1.017
206	49	5.68×10^{-3}	0.990	1.021

Average activity at $t_0=1.024\pm0.2$ percent probable error

June 25=0 time

termine the value at which the rate would level off. No explanation of this behavior is known.

V. DISINTEGRATION RATE DETERMINATION

As mentioned previously, the distingegration rates of the tritium samples were determined by measuring the rates at which the decay product, He^3, was created. These measurements were carried out by a method which made use of the passage of helium through silica glass as a means of quantitatively separating pure He^3 from the sample. The sample to be measured was first converted to the oxide so that it could be contained readily in a small volume, and the oxide sealed within a small silica glass ampoule. The rate at which He^3 diffused through the walls was then observed. With this system, it was found that the rate increased with time for a period after preparing the ampoule, but that it finally reached a constant value. It was assumed that the system was then in a steady state in which the rate of diffusion of He^3 was equal to the rate at which it was created within the ampoule.

The steady-state pressures of He^3 for the ampoules at room temperature were estimated to be about 15 cm Hg for sample I and 75 cm Hg for sample IIo. In order to reach these pressures within a reasonable time, the ampoules were placed in liquid nitrogen until the estimated pressures had been formed at the low temperature. The time required for the respective pressures to be formed was less than a month.

Measurements of the rate of diffusion of He^3 were carried out with an apparatus which consisted of a thermostated soft glass bulb connected to a McLeod gauge through a mercury cut-off valve. The gauge was calibrated by standard procedure to measure the volume of gas within the system. When a measurement was carried out, the ampoule was sealed within the soft glass bulb, and the bulb then evacuated and isolated from the rest of the system by the closing of the mercury cut-off. The isolated bulb was subsequently allowed to stand until a measurable quantity of He^3 ($10^{-2}-10^{-3}$ ml) had been collected. The gas was then expanded into the rest of the system and its volume measured with the McLeod gauge. This procedure of collecting and measuring the He^3 emitted by the ampoule was repeated until the rate of collection, after correcting for decay, was constant. Throughout the duration of a disintegration rate determination, the temperature of the bath which surrounded the bulb was maintained constant to ±0.03°C or better. As a check on the composition of the gas collected, some of the portions were brought into contact with hot metallic calcium. No measurable absorption of gas was found, indicating that only helium was present.

TABLE VII. Disintegration rate of sample IIo.

Time of measurement t days	Collection period days	Approximate vol. collected ml S.T.P.	Activity at time t	Activity at zero time
13	10	7.33×10^{-3}	6.468	6.481
32	28	2.05×10^{-2}	6.445	6.476
61	30	2.20×10^{-2}	6.405	6.464
90.5	29	2.13×10^{-2}	6.410	6.498
119	28	2.05×10^{-2}	6.362	6.478
147	28	2.05×10^{-2}	6.357	6.501

Average activity at $t_0=6.483\pm.06$ percent probable error

September 27=0 time

The results obtained in the measurement of the rate of emission of He^3 by samples I and IIo are shown in Tables VI and VII, respectively. The time of measurement listed in the first columns of the tables is the number of days past an arbitrary zero time that the midpoint of the collection period occurred. The fourth and fifth column of the tables list, respectively, the activity at the time of measurement and the activity at the arbitrary zero time calculated on the basis of 12.46-year half-life for the decay. All activities are in units of 3.7×10^{10} dis/sec. The over-all probable error of the disintegration rate results is estimated to be ±0.8 percent for the small sample and ±0.5 percent for the large sample.

VI. HALF-LIFE AND AVERAGE ENERGY OF TRITIUM DECAY

The half-life of tritium was computed from the results of the disintegration rate and quantity of tritium measurements. The average energy was computed from the results of disintegration rate and calorimetric measurements. The data used in the computations, adjusted to a reference time, are listed in Table VIII together with the computed values. A determination of the quantity of tritium was carried out only in the case of sample II so that the half-life was derived entirely from measurements on that sample. Average decay energy values were obtained with both samples I and II.

The estimated probable error associated with the half-life value is ±0.1 years. Probable errors associated

TABLE VIII. Half-life and average decay energy of tritium.

Sample	I	IIp and IIo
Disintegration rate	3.824×10^{10} dis./sec.	2.436×10^{11} dis./sec.
Power generated	3.506×10^{-8} watts	2.218×10^{-4} watts
Quantity of tritium	...	2.571 ml S.T.P.
Average decay energy	5.72 kev	5.68 kev
Half-life	...	12.46 years

with the average energy values of 5.72 and 5.68 kev are ±0.06 kev and ±0.04 kev, respectively. The weighted mean of these values is 5.69±0.04 kev.

Slack *et al.*[11] have pointed out that the accurate determination of the average energy release in tritium enables one to make an equally accurate determination of the maximum beta-energy release. They have carried out a computation using the above value for the average energy and obtained a value of 18.6±0.2 kev for the maximum energy, a result which is in close agreement with the results of proportional counter measurements of the maximum energy.[6,7]

The half-life determined in this study is slightly greater than the value of 12.1±0.5 years reported by Novick,[4] and is considerably greater than the value of 10.7±2 years reported as a preliminary value by Goldblatt *et al.*[2] It does, however, fall within the estimated error associated with each of the previous values.

[11] Slack, Owen, and Primakoff, Phys. Rev. **75**, 1448 (1949).

PHYSICAL REVIEW VOLUME 80, NUMBER 6 DECEMBER 15, 1950

Improved Calculations on Cascade Shower Theory*

I. B. BERNSTEIN**
Brookhaven National Laboratory, Upton, New York
(Received June 8, 1950)

The diffusion equations of cascade shower theory are solved by means of a perturbation method. The first approximation is taken to be that solution obtained by Snyder using the so-called completely screened cross sections for the elementary processes of bremsstrahlung and pair production. The correction to this is then calculated using more refined approximations to the Bethe-Heitler cross sections.

The results, which lend themselves to accurate numerical work only in the case of light elements and high incident energies, indicate with respect to Snyder's solution that (1) the shower maximum is decreased in height and slightly shifted to greater depths, (2) there is a decrease in the average number of electrons present at small absorber depths and a correspondingly larger number at large depths. The magnitude of the correction is larger than had been previously assumed. Numerical results are given so that the correction to the solution under the assumption of completely screened cross sections can be readily calculated for all light elements when the incident particle is either a single photon or a single electron.

I. INTRODUCTION

THE latest and most accurate calculations on the cascade theory of showers are those of Snyder[1] who gave solutions of the diffusion equations of the theory of such a nature that accurate numerical results were readily derivable therefrom. The calculations, however, were based on the assumption of so-called "completely screened" or "asymptotic" cross sections. That is, the cross sections used were those valid for high energy particles, and too high a probability was assigned to those elementary processes associated with the lower energy particles in the shower. The purpose of this paper is to calculate the correction to the Snyder solution introduced by the use of more accurate cross sections.

Efforts to employ more accurate cross sections have already been made by Corben[2] and by Chakrabarty,[3] but their calculations were based on none too numerically accurate solutions of the diffusion equations for the completely screened case, and on none too accurate approximations to the appropriate Bethe-Heitler cross sections.[4] The order of magnitude of the effect of this refinement as here calculated is much greater, and the results are in a more general form than is indicated by the work of these authors.

II. THE DIFFUSION EQUATIONS

The well-known diffusion equations of the cascade shower theory are

$$\frac{\partial P(E,t,E_0)}{\partial t}=\beta\frac{\partial P(E,t,E_0)}{\partial E}+2\int_E^\infty \gamma(E',t,E_0)R(E,E')\frac{dE'}{E'}+\lim_{\delta\to 0}\left[\int_{E+\delta}^\infty P(E',t,E_0)R(E',E'-E)\frac{E'-E}{E'^2}dE'-P(E,t,E_0)\int_\delta^E R(E,E')\frac{E'dE'}{E^2}\right], \quad (1)$$

$$\frac{\partial\gamma(E,t,E_0)}{\partial t}=\int_E^\infty P(E',t,E_0)R(E',E)\frac{EdE'}{E'^2}-\gamma(E,t,E_0)\int_0^E R(E',E)\frac{dE'}{E}. \quad (2)$$

* This paper is based on a dissertation submitted in partial fulfillment of the requirements for the degree of Doctor of Philosophy at New York University. This work was performed at Brookhaven National Laboratory under the auspices of the AEC.

** Now at Westinghouse Research Laboratories.

[1] H. S. Snyder, Phys. Rev. **76**, 1563 (1949).

[2] H. C. Corben, Phys. Rev. **60**, 435 (1941).

[3] S. K. Chakrabarty, Proc. Nat. Inst. Sci. Ind. **9**, 323 (1943).

[4] H. A. Bethe and W. Heitler, Proc. Roy. Soc. **159**, 432 (1937).

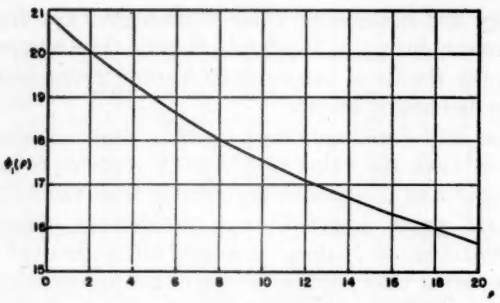

FIG. 1. Cross section modifying function $\phi_1(\rho)$ *vs.* ρ.

$P(E, t, E_0)$ is the number of electrons, $\gamma(E, t, E_0)$ the number of photons per unit energy at thickness t in the energy range between E and $E+dE$. t is distance measured in radiation units Δ,

$$\Delta=[(4z^2N/137)(e^2/mc^2)^2\ln(183z^{-\frac{1}{3}})]^{-1}.\dagger$$

β is the ionization loss per unit length of t. $R(E, E')$ is a factor[4] common to the cross sections for bremsstrahlung and pair production. E_0 is the total energy in the incident spectrum of electrons and photons.

In the "complete screening" approximation one takes

$$\begin{aligned} R(E, E')&=R_0(E, E')=1-a(E/E')+a(E/E')^2,\\ a&=\alpha+4/3,\\ \alpha&=9\ln(183z^{-\frac{1}{3}})\sim\text{const.}=0.025, \end{aligned} \tag{3}$$

in which case the diffusion equations (1) and (2) can be solved by means of a Laplace transform with respect to t and a Mellin transform with respect to E.

More accurately, the cross sections are given by

$$R(E, E')=R_0(E, E')\frac{\phi_1(\rho)-\frac{1}{3}4\ln z}{4\ln 183-\frac{1}{3}4\ln z}, \tag{4}$$

where

$$\rho=(100/z^{\frac{1}{3}})|mc^2E'/E(E-E')| \tag{5}$$

and $\phi_1(\rho)$ is given in Fig. 1.

Equation (4) predicts smaller values of the cross sections for given values of E and E' than does (3), the difference being greater the smaller is E.

Since $\phi_1(\rho)$ is known only numerically, it is not feasible to use (4) directly in a solution of the diffusion equations. It is expedient, however, to use the following empirical expression which fits (4) to within two percent over the whole range of Fig. 1, which is the range of importance in the genesis of a cascade shower.

$$R(E, E')=\frac{R_0(E, E')}{1+K|E'/E(E-E')|}, \tag{6}$$

where

$$K=(mc^2/z^{\frac{1}{3}})255/(15.6-\tfrac{1}{3}4\ln z). \tag{7}$$

In what follows, it is convenient to measure energy in units of K as shown in Table I.

TABLE I. Energy units used *vs.* Z.

Z	1	5	10	20	30	40	50	60	70	80	90
u(Mev)	8.30	5.63	4.81	4.11	3.74	3.53	3.37	3.27	3.15	3.08	3.00

† As kindly pointed out to me by Professor J. A. Wheeler, in the case of light elements, the z^3 appearing in the expression for Δ should be replaced by $z(z+1)$: J. A. Wheeler and W. E. Lamb, Phys. Rev. 55, 858 (1939).

III. THE TRANSFORM METHOD[5-7]

For any admissible function $F(E, t)$ let us define the following:

Laplace transform

$$\mathfrak{L}F(E, s)=\int_0^\infty dt\, e^{-st}F(E, t). \tag{8}$$

Mellin transform

$$\mathfrak{M}F(p, t)=\int_0^\infty d\left(\frac{E}{\beta}\right)\left(\frac{E}{\beta}\right)^p F(E, t). \tag{9}$$

Then

$$\mathfrak{M}\mathfrak{L}F(p, s)=\int_0^\infty d\left(\frac{E}{\beta}\right)\left(\frac{E}{\beta}\right)^p\int_0^\infty dt\, e^{-st}F(E, t). \tag{10}$$

By the Laplace and Mellin inversion theorems

$$F(E, t)=\int_L\frac{ds}{2\pi i}e^{st}\mathfrak{L}F(E, s), \tag{11}$$

$$F(E, t)=\int_M\frac{dp}{2\pi i}\left(\frac{E}{\beta}\right)^{-p-1}\mathfrak{M}F(p, t), \tag{12}$$

where L and M are contours parallel to the respective imaginary axes, running from $-i\infty$ to $+i\infty$, and to the right of all singularities in the respective complex planes. Therefore,

$$F(E, t)=\int_L\frac{ds}{2\pi i}e^{st}\int_M\frac{dp}{2\pi i}\left(\frac{E}{\beta}\right)^{-p-1}\mathfrak{M}\mathfrak{L}F(p, s).$$

In this paper we confine ourselves to a consideration of two initial spectra, a single incident electron of energy E_0, and a single incident photon of energy E_0. In this latter case, the solutions of the diffusion equations will be set off by a dagger. All other incident spectra are but linear combinations of these with appropriate weighting functions. Those solutions obtained by taking $R(E, E')=R_0(E, E')$ (the "complete screening" approximation) will be denoted by a subscript 1, that is, $P_1(E, t, E_0)$ and $\gamma_1(E, t, E_0)$.

[5] L. Landau and G. Rumer, Proc. Roy. Soc. 166, 277 (1938).
[6] W. T. Scott, Phys. Rev. 80, 611 (1950).
[7] G. Doetsch, *Theorie und Anwendung der Laplace Transformation* (Verlag. Julius Springer, Berlin, 1937).

In addition to these it will be necessary, for use in the iteration scheme to follow, to have a solution to the equation obtained from (1) by deleting the term

$$2\int_E^\infty \gamma(E', t, E_0)R(E, E')dE'/E'$$

taking $R(E, E')=R_0(E, E')$, and with the initial condition of one incident electron of energy E_0. This solution will be denoted by $P_0(E, t, E_0)$.

If now one operates on the diffusion equations with

$$\int_0^\infty d\left(\frac{E}{\beta}\right)\left(\frac{E}{\beta}\right)^p\int_0^\infty dt\, e^{-st}$$

the result is

$$G_0(p, s)\mathfrak{MP}P_0(p, s, E_0)+p\mathfrak{MP}P_0(p-1, s, E_0) = (1/\beta)(E_0/\beta)^p, \quad (13)$$

$$G_1(p, s)\mathfrak{MP}P_1(p, s, E_0)+p\mathfrak{MP}P_1(p-1, s, E_0) = (1/\beta)(E_0/\beta)^p, \quad (14)$$

$$\mathfrak{MP}\gamma(p, s, E_0)+[C(p)/(s+D)]\mathfrak{MP}P_1(p, s, E_0), \quad (15)$$

$$G_1(p, s)\mathfrak{MP}P_1{}^\dagger(p, s, E_0)+p\mathfrak{MP}P_1{}^\dagger(p-1, s, E_0) = \frac{B(p)}{s+D}\frac{1}{\beta}\left(\frac{E_0}{\beta}\right)^p, \quad (16)$$

$$\mathfrak{MP}\gamma_1{}^\dagger(p, s, E_0) = \frac{C(p)}{s+D}\mathfrak{MP}P_1{}^\dagger(p, s, E_0)+\frac{1}{s+D}\left(\frac{E_0}{\beta}\right)^p, \quad (17)$$

where

$$G_0(p, s)=s+A(p), \quad (18)$$

$$G_1(p, s)=s+A(p)-B(p)C(p)/(s+D), \quad (19)$$

and

$$A(p)=a[\psi(p+1)-\psi(1)]+\tfrac{1}{2}-1/(p+1)(p+2), \quad (20)$$

$$B(p)=2\left(\frac{1}{p+1}-\frac{a}{p+2}+\frac{a}{p+3}\right), \quad (21)$$

$$C(p)=\frac{1}{p+2}-\frac{a}{p+1}+\frac{a}{p}, \quad (22)$$

$$D=1-\tfrac{1}{6}a, \quad (23)$$

$$\psi(p)=d\ln\Gamma(p)/dp. \quad (24)$$

Equations (13), (14), and (16) are all linear difference equations of the form

$$G(p, s)g(p, s)+pg(p-1, s)=\varphi(p, s). \quad (25)$$

A formal solution of (25) in the form of a complex integral is

$$g(p, s)=-\int_K \frac{d\sigma}{2\pi i}\frac{\pi}{\sin\pi\sigma}\frac{\Gamma(p+1)}{\Gamma(p+\sigma+2)} \times\varphi(p+\sigma+1, s)Q(p+1, \sigma, s), \quad (26)$$

where K is a contour parallel to the imaginary axis, running from $-i\infty$ to $+i\infty$ in the strip $-1<Re\,\sigma<0$ (26) is valid if the integrand is regular in this strip, goes to 0 sufficiently strongly at ∞, and $Q(p+1, \sigma, s)$ satisfies

$$Q(p+1, 0, s)=1, \quad (27)$$

$$G(p, s)Q(p+1, \sigma, s)=Q(p, \sigma+1, s). \quad (28)$$

A formal solution of (27) and (28) is

$$Q(p+1, \sigma, s)=\lim_{N\to\infty}G(N+1, s)^\sigma\prod_{K=1}^{N}\frac{G(p+K, s)}{G(p+\sigma+K, s)}. \quad (29)$$

For those $G(p, s)$ and $\varphi(p, s)$ with which we are concerned, the conditions on the integrand are satisfied, the limit in (29) exists, and (26) is a true solution.

In what follows that solution of (28) in which $G(p, s)=G_0(p, s)$ will be denoted by a subscript 0, that in which $G(p, s)=G_1(p, s)$ by a subscript 1.

One can now write the solutions of the electron diffusion equations as

$$P_0(E, t, E_0)=-\frac{1}{\beta}\int_L\frac{ds}{2\pi i}e^{st}\int_M\frac{dp}{2\pi i}\left(\frac{E}{\beta}\right)^{-p-1}\int_K\frac{d\sigma}{2\pi i}\frac{\pi}{\sin\pi\sigma}\frac{\Gamma(p+1)}{\Gamma(p+\sigma+2)}\left(\frac{E_0}{\beta}\right)^{p+\sigma+1}Q_0(p+1, \sigma, s), \quad (30)$$

$$P_1(E, t, E_0)=-\frac{1}{\beta}\int_L\frac{ds}{2\pi i}e^{st}\int_M\frac{dp}{2\pi i}\left(\frac{E}{\beta}\right)^{-p-1}\int_K\frac{d\sigma}{2\pi i}\frac{\pi}{\sin\pi\sigma}\frac{\Gamma(p+1)}{\Gamma(p+\sigma+2)}\left(\frac{E_0}{\beta}\right)^{p+\sigma+1}Q_1(p+1, \sigma, s), \quad (31)$$

$$P_1{}^\dagger(E, t, E_0)=-\frac{1}{\beta}\int_L\frac{ds}{2\pi i}e^{st}\int_M\frac{dp}{2\pi i}\left(\frac{E}{\beta}\right)^{-p-1}\int_K\frac{d\sigma}{2\pi i}\frac{\pi}{\sin\pi\sigma}\frac{\Gamma(p+1)}{\Gamma(p+\sigma+2)}\left(\frac{E_0}{\beta}\right)^{p+\sigma+1}\frac{B(p+\sigma+1)}{s+D}Q_1(p+1, \sigma, s). \quad (32)$$

The quantity which can be readily calculated however, is not $P(E, t, E_0)$ but rather $N(0, t, E_0)$, where $N(E, t, E_0)$ is the so-called integral spectrum defined by

$$N(E, t, E_0)=\int_E^\infty dE\, P(E, t, E_0). \quad (33)$$

Note that $N(0, t, E_0)$ is the average number of electrons at thickness t and is given in terms of the Mellin transform as

$$N(0, t, E_0)=\beta\mathfrak{M}P(0, t, E_0). \quad (34)$$

In order to show the equivalence of say (31) with the result of Snyder, it is necessary to invert the Laplace transform, To this end we define

$$\mu(p)=-\tfrac{1}{2}[A(p)+D] +\tfrac{1}{2}\{[A(p)-D]^2+4B(p)C(p)\}^{\frac{1}{2}}, \quad (35)$$

$$\nu=(p)=-\tfrac{1}{2}[A(p)+D] -\tfrac{1}{2}\{[A(p)-D]^2+4B(p)C(p)\}^{\frac{1}{2}}. \quad (36)$$

Then

$$G_1(p,s)=[s-\mu(p)][s-\nu(p)]/(s+D). \quad (37)$$

Moreover, one can write

$$Q(p+1,\sigma,s)=\frac{Q(p+\sigma+j,1-j,s)Q(p+1,\sigma+j,s)}{G(p+\sigma+j,s)}, \qquad j=1,2,3,\cdots \quad (38)$$

whence

$$Q_1(p+1,\sigma,s) =\frac{(s+D)Q_1(p+\sigma+j,1-j,s)Q_1(p+1,\sigma+j,s)}{[s-\mu(p+\sigma+j)][s-\nu(p+\sigma+j)]} \quad (39)$$

and it is convenient to invert the Laplace transform in terms of the poles of the integrand of the inversion integral. Hence

$$P_1(E,t,E_0)=-\frac{1}{\beta}\int_K\frac{dp}{2\pi i}\int_M\frac{d\sigma}{2\pi i}\left(\frac{E}{\beta}\right)^{-p-1}\frac{\pi}{\sin\pi\sigma}\frac{\Gamma(p+1)}{\Gamma(p+\sigma+2)}\left(\frac{E_0}{\beta}\right)^{p+\sigma+1}\sum_{j=1}^{\infty}\left\{\frac{[\mu(p+\sigma+j)+D]e^{t\mu(p+\sigma+j)}}{\mu(p+\sigma+j)-\nu(p+\sigma+j)}\right.$$
$$\times Q_1(p+\sigma+j,1-j,\mu(p+\sigma+j))Q_1(p+1,\sigma+j,\mu(p+\sigma+j))+\frac{[\nu(p+\sigma+j)+D]e^{t\nu(p+\sigma+j)}}{\nu(p+\sigma+j)-\mu(p+\sigma+j)}$$
$$\left.\times Q_1(p+\sigma+j,1-j,\nu(p+\sigma+j))Q_1(p+1,\sigma+j,\nu(p+\sigma+j))\right\}. \quad (40)$$

While μ and ν have simultaneous branch points, note that upon going around a branch point the net effect is an interchange of μ and ν. This circumstance leaves the integrand of (40) unchanged since it is symmetric in μ and ν. Therefore, because the integrand is single valued and non-singular over that region of the new σ-plane over which we shift contours, we may let $\sigma+j$ go into σ and then shift all contours to the contour $K+2$. By contour $K+2$ is meant the line obtained by shifting K parallel to itself, 2 units to the right. The result is

$$P_1(E,t,E_0)=\sum_{j=1}^{\infty}\left(-\frac{\beta}{E_0}\right)^{j-1}\int_M\frac{dp}{2\pi i}\int_{K+2}\frac{d\sigma}{2\pi i}\frac{\pi}{\sin\pi\sigma}\frac{\Gamma(p+1)}{\Gamma(p+\sigma+2-j)}\left(\frac{E_0}{\beta}\right)^{p+\sigma}\left(\frac{E}{\beta}\right)^{-p-1}\frac{1}{\mu(p+\sigma)-\nu(p+\sigma)}$$
$$\cdot\{[\mu(p+\sigma)+D]e^{t\mu(p+\sigma)}Q_1(p+\sigma,1-j,\mu(p+\sigma))Q_1(p+1,\sigma,\mu(p+\sigma))$$
$$-[\nu(p+\sigma)+D]e^{t\nu(p+\sigma)}Q_1(p+\sigma,1-j,\nu(p+\sigma))Q_1(p+1,\sigma,\nu(p+\sigma))\}. \quad (41)$$

This is identical with Eq. (38) of Snyder[1] if one makes the following identifications:

$$n=j-1,\quad y=p+\sigma,\quad y+s+1=\sigma,$$
$$K_\mu(y,s)=\Gamma(s+1)Q_1(y+s+1,-s,\mu(y)),$$
$$K_\nu(y,s)=\Gamma(s+1)Q_1(y+s+1,-s,\nu(y)),$$
$$A_n(y)=(-1)^n\frac{\Gamma(y+1)}{\Gamma(y+1-n)}Q_1(y,-n,\mu(y)),$$
$$B_n(y)=(-1)^n\frac{\Gamma(y+1)}{\Gamma(y+1-n)}Q_1(y,-n,\nu(y)).$$

One property of the diffusion equations which must be possessed by any true solution and which, in particular, is possessed by the Snyder solution is

$$\int_0^\infty dt N(0,t,E_0)=\beta\mathfrak{M}\mathfrak{R}P(0,0,E_0)=E_0/\beta. \quad (42)$$

This is a statement of the conservation of energy, namely that all the energy originally in the incident spectrum, in the model used in setting up the diffusion equations, is absorbed by ionization loss.

IV. ITERATION SCHEME

The Mellin transform method depends for its success on the fact that in the "complete screening" approximation the function $R_0(E,E')$ is homogeneous, depending only on the variable E/E'. This is no longer true if one wishes to use Eq. (6). However, since one would not expect the correction to the "complete screening" solution caused by the introduction of (6) to be excessively large, a perturbation method is indicated.

The most convenient perturbation method is arrived at by writing the diffusion equations in the form of a single integral equation. To do this one first solves Eq. (2) in the form

$$\gamma(E,t,E_0)=\gamma(E,0,E_0)\exp[-\mathfrak{D}(E)t] +\int_0^t dx\exp[-(t-x)\mathfrak{D}(E)] \times\int_E^\infty P(E',x,E_0)R(E',E)\frac{EdE'}{E'^2}, \quad (43)$$

where

$$\mathfrak{D}(E)=\int_0^E \frac{dE'}{E}R(E', E) \tag{44}$$

is the gamma-ray absorption coefficient.

The electron diffusion equation (1) can now be written

$$\frac{\partial P(E, t, E_0)}{\partial t}-\beta\frac{\partial P(E, t, E_0)}{\partial E}$$

$$-\lim_{\delta\to 0}\left[\int_{E+\delta}^{\infty} P(E', r, E_0)R_0(E', E'-E)\frac{E'-E}{E'^2}dE'\right.$$

$$\left.-P(E, t, E_0)\int_{\delta}^{E} R_0(E, E')\frac{E'dE'}{E^2}\right]=S(E, t, E_0), \tag{45}$$

where

$$S(E, t, E_0)=\lim_{\delta\to 0}\left[\int_{E+\delta}^{\infty} P(E', t, E_0)R_1(E', E'-E)\frac{E'-E}{E'^2}\right.$$

$$\left.-P(E, t, E_0)\int_{\delta}^{E} R_1(E, E')\frac{E'dE'}{E^2}\right]$$

$$+2\int_E^{\infty}\frac{dE'}{E'}R(E, E')\left\{\gamma(E, 0, E_0)\exp[-\mathfrak{D}(E')t]\right.$$

$$+\int_0^t dx\exp[-(t-x)\mathfrak{D}(E')]$$

$$\left.\times\int_E^{\infty} P(E'', x, E_0)R(E'', E')\frac{E'dE''}{E''^2}\right\} \tag{46}$$

and we have written

$$R(E, E')=R_0(E, E')+R_1(E, R'). \tag{47}$$

Interpreting the left-hand side of (45) as governing the propagation of an electron suffering only ionization loss and bremsstrahlung under the assumption of complete screening and the right side as a source function incorporating the effects of pair production and screening, one can write, since $P_0(E, t, E_0)$ is the Green's function:

$$P(E, t, E_0)=\int_0^t dt'\int_0^{\infty} dE'P_0(E, t-t', E')$$

$$\times S(E', t', E_0)+\pi(E, t, E_0), \tag{48}$$

where $\pi(E, t, E_0)$ is some multiple of $P_0(E, t, E_0)$ satisfying the desired initial condition on $P(E, t, E_0)$.

The integral equation is now in a form suitable for solution by iteration. The first approximation to the solution of the diffusion equations using (6) can be obtained by using $P_1(E, t, E_0)$ in evaluating $S(E, t, E_0)$ according to (44), and substituting this in the right-hand side of (46), and will be denoted by $P_2(E, t, E_0)$. The next approximation is obtained by so using $P_2(E, t, E_0)$, etc.

For calculational purposes it is more convenient to work with the Laplace-Mellin transform of Eq. (36) rather than directly with the equation itself. This is

$$\mathfrak{M}\mathfrak{L}P(p, s, E_0)=\int_0^{\infty} dE'\,\mathfrak{M}\mathfrak{L}P_0(p, s, E')$$

$$\times\mathfrak{L}S(E', s, E_0)+\mathfrak{M}\mathfrak{L}\pi(p, s, E_0), \tag{49}$$

which yields

$$\mathfrak{L}N(0, s, E_0)=\beta\int_0^{\infty} dE'\,\mathfrak{M}\mathfrak{L}P_0(0, s, E')$$

$$\times\mathfrak{L}S(E', s, E_0)+\beta\mathfrak{M}\mathfrak{L}\pi(0, s, E_0). \tag{50}$$

V. THE CORRECTION IN THE CASE OF A SINGLE INCIDENT ELECTRON

Let us calculate the first iteration, based on Eqs. (50) and (6), in the event that the initial condition is a single incident electron. Here $\pi(E, t, E_0)=P_0(E, t, E_0)$.

The Laplace transform of $N_2(0, t, E_0)$ is then, after appropriate changes of variable,

$$\mathfrak{L}N(0, s, E_0)=\mathfrak{L}N_0(0, s, E_0)+\int_M\frac{dp}{2\pi i}\int_K\frac{d\sigma}{2\pi i}$$

$$\times\int\frac{d\sigma'}{2\pi i}\frac{\pi}{\sin\pi\sigma}\frac{\pi}{\sin\pi\sigma'}\frac{1}{\Gamma(\sigma'+2)}\frac{\Gamma(p+1)}{\Gamma(p+\sigma+2)}$$

$$\times\left(\frac{E_0}{\beta}\right)^{p+\sigma+1}\beta^{p-\sigma'-1}Q_0(1, \sigma', s)Q_1(p+1, \sigma, s)$$

$$\times\{2\mathfrak{A}(p, \sigma', s)+\mathfrak{B}(p, \sigma')-\mathfrak{C}(p, \sigma')\}, \tag{51}$$

where

$$\mathfrak{A}(p, \sigma', s)=\int_0^{\infty} d\xi\,\xi^{p-\sigma'-2}$$

$$\times\int_0^1 dx\frac{x^p(1-ax+ax^2)}{\left[\frac{\xi}{1-x}+1\right]\left[s+\mathfrak{D}\left(\frac{1}{x\xi}\right)\right]}$$

$$\times\int^1 d\omega\frac{\omega^{p-1}(\omega^2-a\omega+a)}{\frac{\omega^2x\xi}{1-\omega}+1}, \tag{52}$$

$$\mathfrak{B}(p, \sigma')=\int_0^{\infty} d\xi\,\xi^{p-\sigma'-1}\int_0^1 dx\frac{x^2-ax+a}{1+x(\xi-1)}, \tag{53}$$

$$\mathfrak{C}(p, \sigma')=\int_0^{\infty} d\xi\,\xi^{p-\sigma'-1}\int_0^1 dx\frac{x^p[x^2-(2-a)x+a]}{1+\xi(1-x)}. \tag{54}$$

Note that this result has been obtained by reversing the order of integration from the stepwise inversion of the transforms. This implies, that, while the σ and σ' contours remain as before, the p contour in any term in (51) be parallel to the imaginary axis and in a strip determined by the conditions for convergence on the integrals (52), (53), and (54). But the regions of convergence are as follows:

(52) converges if $-1<Re(p-\sigma'-2)<0$
$0<Re\,p$; (55)

(53) converges if $-1<Re(p-\sigma'-1)<0$; (56)

(54) converges if $-1<Re(p-\sigma'-1)<0$
$-1<Re\,p$, (57)

which conditions follow from a consideration of the several integrands at the limits of integration. The requirements are then that the p contour lie in the strip $-1<Re(p-\sigma'-2)<0$ for the term containing $\mathfrak{N}(p, \sigma', s)$ and in the strip $-1<Re(p-\sigma'-1)<0$ for the other terms.

The next step in the evaluation of the first iteration is an evaluation of the p integral in (51) in terms of the poles of its integrand. Integration by parts of (52) shows that the analytic continuation of the function there defined by the real integral has poles at $p-\sigma'=0, \pm1, \pm2, \cdots; p=0, -1, -2, \cdots$. Moreover, the strength of the first-order pole at $p=\sigma'+1$ is

$$B(\sigma'+1)C(\sigma'+1)/2(s+D) = \tfrac{1}{2}[G_0(\sigma'+1, s)-G_1(\sigma'+1, s)] \quad (58)$$

while the strength of the first-order pole at $p=0$ is

$$h(\sigma', s)=\frac{a}{\sigma'+1}\int_0^\infty d\xi\, \xi^{-\sigma'-1}\frac{\partial}{\partial\xi}\int_0^1 \times\frac{1-ax+ax^2}{\left[\dfrac{\xi}{1+x}+1\right]\left[s+\mathfrak{D}\left(\dfrac{1}{x\xi}\right)\right]}. \quad (59)$$

Therefore, if we deform the path of integration of the $g(p, \sigma', s)$ term to coincide with that of the other terms in the integrand of (51) the contributions of the intervening poles will be

$$I_1=\int_K\frac{d\sigma}{2\pi i}\int_K\frac{d\sigma'}{2\pi i}\frac{\pi}{\sin\pi\sigma}\frac{\pi}{\sin\pi\sigma'}\left(\frac{E_0}{\beta}\right)^{\sigma+\sigma'+2} \times\frac{1}{\Gamma(\sigma+\sigma'+3)}Q_0(1, \sigma', s)Q_1(\sigma'+2, \sigma, s) \times[G_0(\sigma'+1, s)-G_1(\sigma'+1, s)] \quad (60)$$

from the pole $p=\sigma'+1$, and

$$I_2=\int_K\frac{d\sigma}{2\pi i}\int\frac{d\sigma'}{2\pi i}\frac{\pi}{\sin\pi\sigma}\frac{\pi}{\sin\pi\sigma'}\frac{1}{\Gamma(\sigma'+2)}\frac{1}{\Gamma(\sigma+2)} \times\left(\frac{E_0}{\beta}\right)^{\sigma+1}\beta^{-\sigma'-1}Q_0(1, \sigma', s)Q_1(1, \sigma, s)2h(\sigma', s)$$

from the pole at $p=0$. One can write

$$I_2=-\mathfrak{N}N_1(0, s, E_0)\int_K\frac{d\sigma}{2\pi i}\frac{\pi}{\sin\pi\sigma}\frac{1}{\Gamma(\sigma+2)} \times\beta^{-\sigma-1}2h(\sigma, s)Q_0(1, \sigma, s), \quad (61)$$

since

$$\mathfrak{N}N_1(0, s, E_0)=-\int_K\frac{d\sigma}{2\pi i}\frac{1}{\Gamma(\sigma+2)}\left(\frac{E_0}{\beta}\right)^{\sigma+1}Q_1(1, \sigma, s). \quad (62)$$

In order to simplify I_1 we note that, as a result of (29),

$$G_0(\sigma'+1, s)Q_0(1, \sigma', s)=Q_0(1, \sigma'+1, s),$$
$$G_1(\sigma'+1, s)Q_1(\sigma'+2, \sigma, s)=Q_1(\sigma'+1, \sigma+1, s),$$

and therefore

$$I_1=\int_K\frac{d\sigma}{2\pi i}\int_K\frac{d\sigma'}{2\pi i}\frac{\pi}{\sin\pi\sigma}\frac{\pi}{\sin\pi\sigma'}\frac{1}{\Gamma(\sigma+\sigma'+3)} \times\left(\frac{E_0}{\beta}\right)^{\sigma+\sigma'+2}[Q_0(1, \sigma'+1, s)Q_1(\sigma'+2, \sigma, s) -Q_0(1, \sigma', s)Q_1(\sigma'+1, \sigma+1, s)]. \quad (63)$$

In the first term of (63) let σ' go into $\sigma'-1$, and then shift the contour back to the contour K. The pole at $\sigma'=0$ contributes. In the second term let σ go into $\sigma-1$ and shift the contour back to K. The pole at $\sigma=0$ contributes. The result is:

$$I_1=-\int_K\frac{d\sigma}{2\pi i}\int_K\frac{d\sigma'}{2\pi i}\frac{\pi}{\sin\pi\sigma}\frac{\pi}{\sin\pi\sigma'}\frac{1}{\Gamma(\sigma+\sigma'+2)} \times\left(\frac{E_0}{\beta}\right)^{\sigma+\sigma'+1}Q_0(1, \sigma', s)Q_1(\sigma'+1, \sigma, s)$$
$$-\int_K\frac{d\sigma}{2\pi i}\frac{\pi}{\sin\pi\sigma}\frac{1}{\Gamma(\sigma+2)}\left(\frac{E_0}{\beta}\right)^{\sigma+1} \times Q_0(1, 0, s)Q_1(1, \sigma, s)$$
$$+\int_K\frac{d\sigma}{2\pi i}\int\frac{d\sigma'}{2\pi i}\frac{\pi}{\sin\pi\sigma}\frac{\pi}{\sin\pi\sigma'}\frac{1}{\Gamma(\sigma+\sigma'+2)} \times\left(\frac{E_0}{\beta}\right)^{\sigma+\sigma'+1}Q_0(1, \sigma', s)Q_1(\sigma'+1, \sigma, s)$$
$$+\int_K\frac{d\sigma'}{2\pi i}\frac{\pi}{\sin\pi\sigma'}\frac{1}{\Gamma(\sigma'+2)}\left(\frac{E_0}{\beta}\right)^{\sigma'+1} \times Q_0(1, \sigma', s)Q_1(\sigma'+1, 0, s)$$
$$=\mathfrak{N}N_1(0, s, E_0)-\mathfrak{N}N_0(0, s, E_0) \quad (64)$$

since

$$\mathfrak{N}N_0(0, s, E_0)=-\int_K d\sigma\frac{\pi}{\sin\pi\sigma}\frac{1}{\Gamma(\sigma+2)}\left(\frac{E_0}{\beta}\right)^{\sigma+1}Q_0(1, \sigma, s)$$

and in view of (27), and the cancellation of the double integrals.

One can, therefore, write the Laplace transform of the correction to Snyder's solution in the form:

$$\mathfrak{L}N_2(0, s, E_0)-\mathfrak{L}N_1(0, s, E_0)$$

$$=-\mathfrak{L}N_1(0, s, E_0)\int_K \frac{d\sigma}{2\pi i}\frac{\pi}{\sin\pi\sigma}\frac{1}{\Gamma(\sigma+2)}$$

$$\times Q_0(1, \sigma, s)\beta^{-\sigma-1}2h(\sigma, s)+\int_K \frac{d\sigma}{2\pi i}\int_K \frac{d\sigma'}{2\pi i}$$

$$\times\int \frac{dp}{2\pi i}\frac{\pi}{\sin\pi\sigma}\frac{\pi}{\sin\pi\sigma'}\frac{1}{\Gamma(\sigma'+2)}\frac{\Gamma(p+1)}{\Gamma(p+\sigma+2)}$$

$$\times\left(\frac{E_0}{\beta}\right)^{p+\sigma+1}\beta^{p-\sigma'-1}Q_0(1, \sigma', s)Q_1(p+1, \sigma, s)$$

$$\times\{2\mathfrak{A}(p, \sigma', s)+\mathfrak{B}(p, \sigma')-\mathfrak{C}(p, \sigma')\}. \quad (65)$$

The p contour for the triple complex integral in (65) is a line parallel to the imaginary axis in the strip $0<Re(p-\sigma'-1)<0$; $-1<Re\,p<0$. The next singularity to the right of the contour lies at $p=\sigma'$.

The order of magnitude of the contribution of this term can be estimated crudely by considering $p-\sigma'$ to be very nearly zero, and noting that the integral is very roughly $\mathfrak{L}N_1(0, s, E_0)(1/E_0)$. (In the same fashion the single complex integral term is roughly of order $1/\beta$.) But in all cases of interest in shower theory E_0 is greater than 10β. Hence we neglect the contribution of this term.

Therefore, to this order, in virtue of the convolution theorem for Laplace transform one can write:

$$N_2(0, t, E_0)-N_1(0, t, E_0)$$

$$=\int_0^t dx N_1(0, t-x, E_0)F(x), \quad (66)$$

where

$$\mathfrak{L}F(s)=-\int_K \frac{d\sigma}{2\pi i}\frac{\pi}{\sin\pi\sigma}\frac{1}{\Gamma(\sigma+2)}$$

$$\times Q_0(1, \sigma, s)\beta^{-\sigma-1}2h(\sigma, s). \quad (67)$$

To this order the first iteration (66) satisfies the boundary conditions since the correction as calculated in (66) is obviously zero for $t=0$.

It is convenient to evaluate (67) in terms of the poles of its integrand to the right of the σ-contour. The first of these is of the third order and occurs at $\sigma=0$, a $1/\sigma$ contribution coming from the term $\pi/\sin\pi$, a b/σ^2 contribution from the term $h(\sigma,s)$. The pole strength, as determined by integration by parts of (59), is

$$b=-a\left[\frac{1}{s+D}-\frac{D}{(s+D)^2}\right]=\frac{-as}{(s+D)^2}. \quad (68)$$

Equation (67) can now be written as

$$\mathfrak{L}F(s)=-a\left[\frac{1}{s+D}-\frac{D}{(s+D)^2}\right]\frac{\partial^2}{\partial\sigma^2}\left\{\beta^{-\sigma-1}\frac{Q_0(1, \sigma, s)}{\Gamma(\sigma+2)}\right\}$$

$$-\int_{K+1}\frac{d\sigma}{2\pi i}\frac{\pi}{\sin\pi\sigma}\frac{1}{\Gamma(\sigma+2)}\beta^{-\sigma-1}Q_0(1, \sigma, s)2h(\sigma, s). \quad (69)$$

Since the location of the next pole is at $\sigma=1$, the integral in (69) can be estimated to be of order $1/\beta^2$. It is not feasible to evaluate the contribution of the next pole since it is of fourth order and its residue is too complicated for ready numerical calculation. Moreover, it is not even clear that this residue, by itself, is a proper Laplace transform. Therefore, to order $1/\beta$, we can write the correction to the completely screened solution in the form

$$N_2(0, t, E_0)-N_1(0, t, E_0)=a\int_0^t dx N_1(0, t-x, E_0)$$

$$\times\left\{\frac{\ln^2\beta}{\beta}W_1(x)-\frac{2\ln\beta}{\beta}W_2(x)+\frac{1}{\beta}W_3(x)\right\}, \quad (70)$$

where

$$\mathfrak{L}W_1(s)=\frac{Q_0(1, \sigma, s)}{\Gamma(\sigma+2)}\bigg|_{\sigma=0}\frac{-as}{(s+D)^2}$$

$$=-as/(s+D)^2, \quad (71)$$

$$\mathfrak{L}W_2(s)=\frac{\partial}{\partial\sigma}\frac{Q_0(1, \sigma, s)}{\Gamma(\sigma+2)}\bigg|_{\sigma=0}\frac{-as}{(s+D)^2}$$

$$=\frac{-as}{(s+D)^2}\left\{\lim_{N\to\infty}\left(\ln[s+A(N+1)]\right.\right.$$

$$\left.\left.-\sum_{k=1}^{N}\frac{A'(k)}{s+A(k)}\right)-\psi(1)\right\}, \quad (72)$$

$$\mathfrak{L}W_3(s)=\frac{\partial^2}{\partial\sigma^2}\frac{Q_0(1, \sigma, s)}{\Gamma(\sigma+2)}\bigg|_{\sigma=0}\frac{-as}{(s+D)^2}$$

$$=\frac{-as}{(s+D)^2}\left\{\left[\lim_{N\to\infty}\left(\ln[s+A(N+1)]\right.\right.\right.$$

$$\left.\left.\left.-\sum_{k=1}^{N}\frac{A'(k)}{s+A(k)}\right)\right]^2+\sum_{k=1}^{\infty}\left[\frac{A'(k)^2}{[s+A(k)]^2}\right.\right.$$

$$\left.\left.-\frac{A''(k)}{s+A(k)}\right]+\psi(1)^2-\psi'(1)\right\}$$

$$-2\psi(1)\mathfrak{L}W_1(s). \quad (73)$$

Here primes indicate differentiations. $\partial Q_0(1, \sigma, s)/\partial\sigma$ and $\partial^2 Q_0(1, \sigma, s)/\partial\sigma^2$ were calculated by taking logarith-

TABLE II. Tables of the $W(t)$'s for use in numerically effecting the convolutions indicated in Eqs. (70) and (70′).

t	$W_1(t)$	$W_2(t)$	$W_3(t)$	t	$W_1(t)$	$W_2(t)$	$W_3(t)$
0	−1.000	$-\infty$	$-\infty$	5.8	0.039	−0.065	0.121
0.2	−0.724	−0.302	2.051	6.0	0.034	−0.060	0.119
0.4	−0.507	+0.299	1.590	6.2	0.030	−0.055	0.114
0.6	−0.337	0.492	0.756	6.4	0.027	−0.051	0.110
0.8	−0.205	0.521	0.215	6.6	0.024	−0.047	0.106
1.0	−0.104	0.498	−0.154	6.8	0.021	−0.043	0.101
1.2	−0.028	0.431	−0.393	7.0	0.019	−0.039	0.097
1.4	+0.028	0.356	−0.519	7.2	0.017	−0.035	0.091
1.6	0.069	0.279	−0.584	7.4	0.015	−0.032	0.086
1.8	0.097	0.207	−0.590	7.6	0.013	−0.028	0.080
2.0	0.116	0.142	−0.547	7.8	0.012	−0.026	0.075
2.2	0.128	0.087	−0.500	8.0	0.010	−0.023	0.072
2.4	0.134	0.040	−0.416	8.2	0.0094	−0.021	0.064
2.6	0.135	0.002	−0.339	8.4	0.0083	−0.018	0.059
2.8	0.134	−0.028	−0.267	8.6	0.0072	−0.016	0.055
3.0	0.130	−0.052	−0.202	8.8	0.0064	−0.014	0.050
3.2	0.124	−0.069	−0.145	9.0	0.0056	−0.013	0.047
3.4	0.117	−0.080	−0.098	9.2	0.0050	−0.011	0.043
3.6	0.110	−0.091	−0.041	9.4	0.0040	−0.010	0.040
3.8	0.103	−0.096	−0.004	9.6	0.0038	−0.0089	0.037
4.0	0.095	−0.098	0.026	9.8	0.0034	−0.0080	0.034
4.2	0.087	−0.099	0.052	10.0	0.0029	−0.0071	0.031
4.4	0.080	−0.097	0.074	11	0.0029	−0.0041	0.031
4.6	0.073	−0.094	0.092	12	0.0015	−0.0023	0.020
4.8	0.066	−0.091	0.104	13	0.0008	−0.0014	0.011
5.0	0.059	−0.086	0.112	14	0.0004	−0.0007	0.0057
5.2	0.054	−0.080	0.118	15	0.0002	−0.0004	0.0030
5.4	0.048	−0.075	0.121	16		−0.0002	0.0015
5.6	0.044	−0.070	0.122	17		−0.0001	0.0001

mic derivatives of the infinite product representation for $Q_0(1, \sigma, s)$.

The Laplace inverses of (71), (72), and (73) are readily obtainable in terms of single and double series of the Dirichlet type, but it is more convenient for the derivation of a table of values to adopt the following scheme.

Let us define

$$\mathfrak{L}U_1(s)=\lim_{N\to\infty}\left(\ln[s+A(N+1)]-\sum_{k=1}^{N}\frac{A'(k)}{s+A(k)}\right)\frac{1}{s+D}, \tag{74}$$

$$\mathfrak{L}U_2(s)=U_1(s)/(s+D), \tag{75}$$

$$\mathfrak{L}U_3(s)=[\mathfrak{L}U_1(s)]^2, \tag{76}$$

$$\mathfrak{L}U_4(s)=(s+D)\mathfrak{L}U_3(s), \tag{77}$$

$$\mathfrak{L}U_5(s)=\sum_{k=1}^{\infty}\left[\left(\frac{A'(k)}{s+A(k)}\right)^2-\frac{A''(k)}{s+A(k)}\right], \tag{78}$$

$$\mathfrak{L}U_6(s)=\mathfrak{L}U_5(s)/(s+D), \tag{79}$$

$$\mathfrak{L}U_7(s)=\mathfrak{L}U_6(s)/(s+D). \tag{80}$$

The W's can be defined in terms of these, as is done later.

Then

$$U_1(t)=e^{-Dt}\lim_{N\to\infty}\left\{\ln[A(N+1)-D]-\sum_{k=1}^{N}\frac{A'(k)}{A(k)-D}\right\}+\sum_{k=1}^{\infty}\frac{A'(k)}{A(k)-D}e^{-A(k)t}. \tag{81}$$

Expression (81) converges for all $t>0$ and diverges like $-\ln t$ as t approaches zero. The series in (81) can be summed numerically by means of the Euler summation formula,[8] which also permits one to develop an approximation formula for $U_1(t)$ valid near $t=0$. Also one can write

$$U_5(t)=\sum_{k=1}^{\infty}\{tA'(k)^2-A''(k)\}e^{-A(k)t}. \tag{82}$$

Equation (82) too is evaluable numerically by means of the Euler summation formula, the series converging for $t\geq 0$.

The other quantities, both U's and W's, can then be computed numerically, in stepwise fashion, according to the prescription

$$\begin{aligned}
U_2(t)&=\int_0^t dx U_1(t-x)e^{-Dx},\\
U_3(t)&=\int_0^t dx U_1(x)U_1(t-x),\\
U_4(t)&=U_3'(t)+DU_3(t),\\
U_6(t)&=\int_0^t dx U_5(t-x)e^{-Dx},\\
U_7(t)&=\int_0^t dx U_6(t-x)e^{-Dx},\\
W_1(t)&=e^{-Dt}(Dt-1),\\
W_2(t)&=-\psi(1)W_1(t)-U_1(t)+DU_2(t),\\
W_3(t)&=-U_4(t)+DU_3(t)-U_6(t)+DU_7(t)\\
&\quad+2\psi(1)[U_1(t)-DU_2(t)]\\
&\quad+[\psi(1)^2-\psi'(1)]W_1(t).
\end{aligned} \tag{83}$$

The W's are tabulated in Table II and suitable approximation formulas for $t\sim 0$ are given in Table III.

It is now possible to evaluate the correction to $N_1(0, t, E_0)$ to the order of accuracy represented by (70), by carrying out numerically the indicated integrations, using the values of $N_1(0, t, E_0)$ given by Snyder.[1]

It is interesting to note that to this approximation

TABLE III. Approximation formulas for use in effecting part of the convolutions indicated in Eqs. (70) and (70′).

$W_2(t)\sim -\ln t$	$[-1+1.550t-0.60t^2]+1.007-0.881t+0.17t^2$
$W_3(t)\sim \ln^2 t$	$[-1+1.549t-0.30t^2]-\ln t[2.015-1.757t+0.63t^2]$ $+1.276-2.844t+1.85t^2$
	$0<t\leq 0.2$

[8] K. Knopp, *Theory and Application of Infinite Series* (Blackie and Son, Ltd., London, 1928).

condition (42) is satisfied by the corrected solution because

$$\int_0^\infty dtN_2(0,t,E_0)$$

$$=\int_0^\infty dtN_1(0,t,E_0)+\int_0^\infty dt\,a\int_0^t dxN_1(0,t-x,E_0)$$

$$\times\left\{\frac{\ln^2\beta}{\beta}W_1(x)-\frac{2\ln\beta}{\beta}W_2(x)+\frac{1}{\beta}W_3(x)\right\}$$

$$=\mathfrak{L}N_1(0,0,E_0)+aN_1(0,0,E_0)$$

$$\times\left\{\frac{\ln^2\beta}{\beta}\mathfrak{L}W_1(0)-\frac{2\ln\beta}{\beta}\mathfrak{L}W_2(0)+\frac{1}{\beta}\mathfrak{L}W_3(0)\right\}$$

$$=E_0/\beta$$

since

$$\mathfrak{L}N_1(0,0,E_0)=E_0/\beta$$

while the Laplace transforms of all the $W(t)$'s contain as a factor $s/(s+D)^2$ and hence all the $\mathfrak{L}W(0)$'s are zero.

If one examines the case in which the incident spectrum is a single photon of energy E_0, then to order $1/E_0$ the results come out in the same form. The result there is

$$\mathfrak{L}N_2{}^\dagger(0,s,E_0)-\mathfrak{L}N_1{}^\dagger(0,s,E_0)$$
$$=\mathfrak{L}N_1{}^\dagger(0,s,E_0)\mathfrak{L}F(s) \quad (66')$$

and again to order $1/\beta$

$$N_2{}^\dagger(0,t,E_0)-N_1{}^\dagger(0,t,E_0)$$

$$=a\int_0^t dxN_1{}^\dagger(0,t-x,E_0)$$

$$\times\left\{\frac{\ln^2\beta}{\beta}W_1(x)-\frac{2\ln\beta}{\beta}W_2(x)+\frac{1}{\beta}W_3(x)\right\}. \quad (70')$$

Since in the "complete screening" approximation (subscript 1) the solution of (1) and (2) for any initial spectrum is but a linear combination of the solutions for a single incident electron and single incident photon, we see that to order $1/E_0$ in the first iteration the correction introduced by screening is always in the form of a convolution over the "complete screening" solution.

VI. DISCUSSION AND CONCLUSIONS

The introduction of the more accurate cross sections into the diffusion equations means that the probabilities for the various elementary processes (bremsstrahlung and pair production) are decreased, the decrease being larger the smaller is the energy E_0 of the parent particle. This implies that $N(0,t,E_0)$, the average number of electrons at thickness t, must be smaller initially than that calculated under the assumption of complete screening. But, the area under $N(0,t,E_0)$ is E_0/β regardless of the cross sections used. Therefore, there must be a corresponding increase in $N(0,t,E_0)$ for large values of t. These qualitative results are verified by those of the numerical calculations which can be considered to be accurate.

TABLE IV. Representative values of various parameters.

	Air	H_2O	Al	Fe	Pb
β (Mev)	103	115	55.6	25.9	7.00
Δ (cm)	34.2	43.4	9.80	1.84	0.525
K (Mev)	5.15	5.70	4.55	3.85	3.05
β/K	20.0	20.0	12.2	6.72	2.27

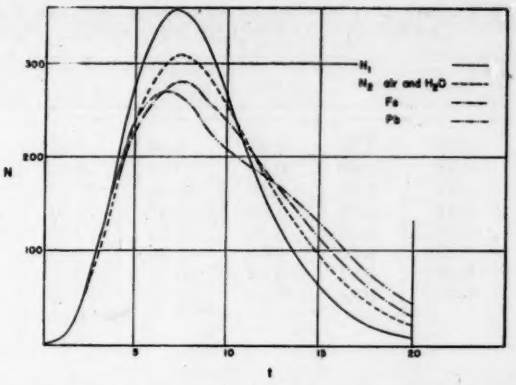

FIG. 2. $N(t)$ the average number of electrons induced by a single incident electron of energy E_0 *vs.* absorber thickness t. β=ionization loss per unit radiation length; Snyder solution $N_1(t)$; corrected solution $N_2(t)\cdot\ln E_0/\beta=8$.

One would expect that the screening correction should depend on the energy of the incident particle in such a way that if this latter is high then the screening correction is low, and vice versa. This property is possessed by both (66) and (70). In both of these the dependence on E_0/β is given through $N_1(0,t,E_0)$, the average number of electrons at thickness t under the assumption of complete screening. The larger E_0/β, the larger is the value of t for which the maximum in $N_1(0,t,E_0)$ occurs. Since in both cases the function with which $N_1(0,t,E_0)$ is convoluted exhibits exponential decrease for sufficiently large values of t, (66) and (70) yield proportionally smaller corrections, the larger is E_0/β.

The dependence on material is introduced essentially through the β (ionization loss per unit length) dependence of the term with which $N_1(0,t,E_0)$ is convoluted. This term, and hence the correction, is an increasing function of $1/\beta$ and, therefore, of Z.

The estimate which led to (66) as a good approximation to the correction as given by the first iteration is crude but plausible. Physically, if we note the origins of the terms $\mathfrak{A}(p,\sigma',s)$, $\mathfrak{B}(p,\sigma')$, and $\mathfrak{C}(p,\sigma')$ in (57), the estimate says that the correction to the Snyder (complete screening) solution is largely due to the correction of the cross section for pair production alone.

For reasonably high incident energies, the correction is only about 10 percent at the maximum of $N_1(0,t,E_0)$.

TABLE V. Part 1. $N_1(t)$ = Snyder solution in the case of a single incident electron, $N_2(t)$ = the corresponding corrected solution. $\epsilon = \ln E_0/\beta$, $N_1{*}W = \int_0^t dx N_1(t-x)W(x)$, $N_2(t) = N_1(t) + 1.358[N_1{*}W_1(\ln^2\beta/\beta) - N_1{*}W_2(2\ln\beta/\beta) + N_1{*}W_3(1/\beta)]$.

t	N_1	$N_1{*}W_1$	$N_1{*}W_2$	$N_1{*}W_3$	N_1	$N_1{*}W_1$	$N_1{*}W_2$	$N_1{*}W_3$	N_1	$N_1{*}W_1$	$N_1{*}W_2$	$N_1{*}W_3$
		$\epsilon=3$				$\epsilon=4$				$\epsilon=5$		
1	3.75	−1.36	−0.44	1.08	4.87	−1.57	−0.69	0.95	5.68	−1.54	−0.87	0.87
2	4.55	−2.00	0.86	0.92	8.86	−3.55	0.55	2.44	14.46	−5.38	−0.25	3.06
3	3.85	−1.47	1.58	−0.96	10.13	−4.00	2.43	0.03	21.17	−8.27	2.91	2.20
4	2.81	−0.44	1.55	−2.37	9.07	−2.84	3.63	−3.08	23.60	−8.55	6.28	−2.13
5	1.94	0.36	0.76	−2.23	7.09	−0.88	3.08	−4.93	22.01	−5.33	7.70	−7.67
6	1.22	0.80	0.03	−1.29	5.23	0.71	1.54	−4.51	18.40	−2.26	6.43	−11.30
7	0.68	0.97	−0.48	−0.30	3.52	1.72	0.10	−2.70	13.97	−1.28	3.60	−10.50
8	0.48	0.88	−0.67	0.55	2.39	2.08	−1.03	−0.60	9.96	−3.64	0.48	−6.50
9					0.90	1.75	−1.56	1.15	4.72	4.57	−3.46	1.59
12					0.31	1.06	−1.32	2.59	1.99	3.55	−0.39	6.55
14									0.79	2.05	−0.20	5.28
16									0.30	1.10	−0.08	3.88
18									0.12	0.55	−0.05	2.21
		$\epsilon=6$				$\epsilon=7$				$\epsilon=8$		
1	6.33	−1.89	−0.99	0.88	6.7	−1.57	−1.22	0.01	8.5	−1.89	−1.60	−0.38
2	26.7	−6.98	−1.38	3.10	33.1	−10.64	−3.70	5.48	44.3	−13.12	−5.67	9.08
3	41.0	−15.26	1.51	5.07	68.7	−25.26	1.43	11.46	115.8	−39.96	−2.99	27.61
4	53.42	−20.22	9.79	2.19	106.3	−38.96	12.79	6.68	201.5	−74.53	15.59	31.64
5	57.33	−18.85	16.28	−9.40	135.0	−46.89	26.71	−6.63	287.5	−102.71	44.70	11.02
6	54.20	−12.79	17.56	−20.08	142.1	−42.46	38.89	−31.19	335.4	−107.34	77.12	−38.33
7	46.42	−4.72	14.55	−23.82	135.2	−28.13	39.92	−48.92	357.5	−93.99	90.89	−84.57
8	37.25	+2.69	7.86	−20.95	119.2	−10.65	31.18	−54.26	346.0	−64.42	89.60	−115.81
10	20.16	10.68	−3.88	−3.44	75.6	−18.22	3.30	−28.66	261.3	6.27	40.83	−118.63
12	9.67	10.70	−9.94	10.77	41.1	27.43	−17.34	12.04	155.2	58.8	−18.32	11.86
14	4.0	7.45	−8.39	15.45	20.2	23.72	−22.30	34.06	85.5	67.4	−53.22	76.72
16	1.67	4.35	−5.62	12.56	9.1	16.11	−18.06	36.01	42.2	51.5	−52.63	98.60
18	0.67	2.14	−3.21	8.10	3.9	9.00	−11.84	26.73	18.9	32.9	−41.13	84.34
20	0.10	1.02	−1.58	4.41	1.6	4.49	−6.62	17.06	8.0	18.8	−29.62	59.56

Hence one might expect that the first iteration is a sufficient approximation. In view of the complicated nature of the functions involved, a more accurate determination of the errors is not feasible.

It is possible to obtain numerical results from (70), but it is prohibitively laborious to calculate a more accurate approximation to (66). However, one can expect that (70) is a good approximation to (66) if β is large. This is true for light elements. Table IV gives values of the various parameters to be used in the calculations.

In view of this discussion we see that the numerical calculations made are applicable only to light elements and moderate or high initial energies. Tables of the convolutions necessary for the calculation in the case of those initial conditions considered in this paper are given in Table V. In these the indices 0 and E_0 are suppressed. They are based on the values for the completely screened solution given by Snyder.[1]

Representative results are given in Figs. 2 and 3.

Figure 4 indicates how well the approximation to the cross sections here used, that is Eq. (6), agrees with the

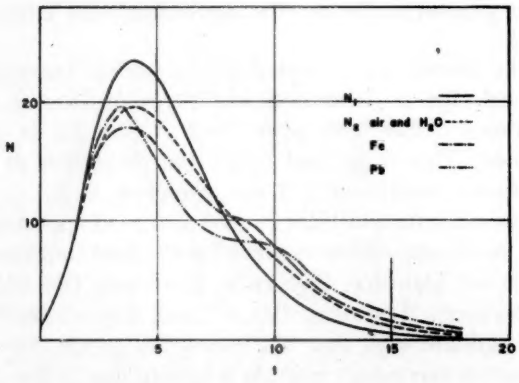

FIG. 3. $N(t)$ the average number of electrons induced by a single incident electron of energy E_0 *vs.* absorber thickness t. β = ionization loss per unit radiation length. Snyder solution $N_1(t)$; corrected solution $N_2(t)\cdot \ln E_0/\beta = 5$.

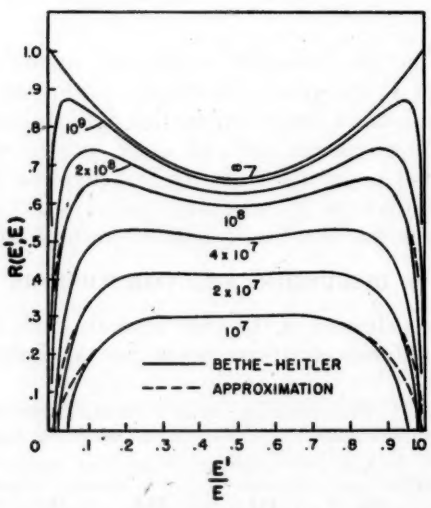

FIG. 4. $R(E, E')$ the differential probability of pair production per unit radiation length *vs.* fractional energy transferred. Labels on solid curves indicate E, the energy in electron volts of the parent particle.

TABLE V. Part 2. $N_1^\dagger(t)$ = Snyder solution in the case of a single incident photon, $N_2^\dagger(t)$ = the corresponding corrected solution. $\epsilon = \ln E_0/\beta$, $N_1^\dagger * W = \int_0^t dx N_1(t-x)W(x)$, $N_2^\dagger(t) = N_1^\dagger(t) + 1.358[N_1^\dagger * W_1(\ln^2\beta/\beta) - N_1^\dagger * W_2(2\ln\beta/\beta) + N_1^\dagger * W_3(1/\beta)]$.

t	$N_1\dagger$	$N_1\dagger * W_1$	$N_1\dagger * W_2$	$N_1\dagger * W_3$	$N_1\dagger$	$N_1\dagger * W_1$	$N_1\dagger * W_2$	$N_1\dagger * W_3$	$N_1\dagger$	$N_1\dagger * W_1$	$N_1\dagger * W_2$	$N_1\dagger * W_3$
		$\epsilon=3$				$\epsilon=4$				$\epsilon=5$		
1	1.88	−0.57	−0.33	0.30	2.27	−0.58	−0.42	0.26	3.1	−0.44	−0.56	0.39
2	3.59	−1.43	0.12	0.89	5.97	−2.15	−0.22	1.19	8.85	−3.13	−0.39	1.71
3	3.86	−1.58	1.06	0.09	8.51	−3.39	1.20	1.13	16.19	−6.03	1.06	2.15
4	3.34	−1.04	1.45	−1.26	9.02	−3.27	2.67	−1.05	20.40	−7.60	4.04	0.16
5	2.49	0.25	1.17	−1.99	8.04	−2.06	3.07	−3.34	21.60	−6.86	6.21	−4.19
6	1.75	0.38	0.52	−1.56	6.51	−0.55	2.34	−4.21	19.96	−4.40	6.53	−8.67
7	1.12	0.71	−0.07	−0.78	4.85	0.73	1.14	−3.53	16.93	−1.33	5.01	−9.11
8	0.80	0.79	−0.45	0.04	3.48	1.51	−0.06	−1.99	13.20	1.44	2.55	−7.75
10	0.29	0.63	−0.61	0.91	1.60	1.78	−1.33	1.07	7.40	4.03	−1.83	−0.61
12					0.65	1.29	−1.40	2.29	3.28	4.01	−3.36	4.24
14									1.32	2.77	−3.11	5.67
									0.52	1.50	−2.05	4.66
									0.19	0.76	−1.13	2.92
		$\epsilon=6$				$\epsilon=7$				$\epsilon=8$		
1	3.2	−0.82	−0.61	0.20	3.6	−0.90	−0.74	0.15	8.5	−2.58	−1.55	1.34
2	13.33	−4.18	−1.54	1.78	13.9	−4.57	−1.28	2.28	24.4	−8.17	−1.29	3.51
3	27.2	−10.19	0.65	4.93	46.0	−14.79	−2.86	5.12	71.0	−23.54	−2.34	8.16
4	42.5	−15.58	5.14	2.68	78.9	−29.78	5.56	12.04	140.2	−49.71	5.46	16.24
5	51.2	−17.96	11.29	−2.99	109.0	−39.60	18.30	1.25	218.2	−78.53	25.79	12.82
6	53.5	−15.57	15.01	−12.71	130.1	−41.79	29.26	−16.48	285.2	−95.01	52.13	−14.38
7	49.9	−9.75	14.88	−18.90	133.9	−35.52	36.41	−33.21	326.0	−97.00	74.22	−51.47
8	43.0	−2.90	11.25	−20.46	126.5	−22.54	34.49	−46.19	342.1	−81.22	83.75	−75.63
10	26.5	7.07	0.01	−9.59	93.5	6.59	13.38	−37.46	291.4	−14.15	59.71	−108.9
12	13.8	10.57	−7.25	5.88	54.5	23.86	−9.18	−3.99	201.2	39.38	4.52	−49.54
14	6.8	7.97	−8.42	13.51	29.4	24.75	−20.75	25.48	113.5	64.34	−37.99	28.52
16	3.5	4.80	−6.32	13.20	13.5	18.58	−19.17	34.54	61.2	57.29	−53.39	81.11
18	1.9	2.80	−4.14	9.32	5.8	11.79	−14.18	29.99	29.9	39.92	−44.06	85.43
20	0.5	1.75	−2.09	5.42	2.6	6.50	−9.18	20.93	9.9	25.64	−29.94	66.55

corresponding Bethe-Heitler values in the case of pair production.

From these, qualitatively, the effect of the correction on $N_1(0, t, E_0)$ is an initial decrease, a decrease in the maximum and slight shift of the maximum to greater depths, and a consequent increase for large t.

The author wishes to express his thanks to Dr. H. S. Snyder, who suggested the problem and gave constant guidance and encouragement; to Dr. W. T. Scott for his many suggestions; and to Miss Theresa Danielson, Mrs. Dale Meyer, and Mrs. Louise Trebing, who did most of the numerical work.

Excitation Functions for Spallation Reactions on Cu*

F. O. Bartell, A. C. Helmholz, S. D. Softky, and D. B. Stewart
Radiation Laboratory, Department of Physics, University of California, Berkeley, California
(Received July 31, 1950)

Excitation functions have been measured for 190-Mev deuterons from the 184-inch Berkeley cyclotron on the natural isotopic mixture of Cu^{63} and Cu^{65}. Chemical separation of Zn, Cu, Ni, Co, Fe, and Mn has been performed and the yields of several of the radioactive isotopes of these elements have been measured as a function of deuteron energy. The results seem to be in agreement with Serber's theory of high energy processes and with other information on the yields of nuclear reactions at these energies.

I. INTRODUCTION

MEASUREMENTS of the yields of nuclear reactions as a function of the energy of the bombarding particles have provided considerable information regarding the mechanics of the nuclear processes involved. At low energies the familiar type of excitation function is one which rises from the threshold to a maximum and then falls off rapidly owing to the competition from other processes. Most of these results are explained satisfactorily by the theory of the compound nucleus formed by the addition of the bombarding particle. Early results with the very high energy particles from the 184-inch cyclotron showed a considerably different behavior in that the yield did not fall off at high energies. Serber[1] has explained these results in terms of the inelastic scattering of the impinging particle leaving in turn an excited nucleus. This excited nucleus is now the compound nucleus and decays by the usual processes. More detailed calculations have been made for the case of $C^{12}(p, pn)O^{11}$ by Heckrotte and Wolff.[2]

II. METHOD

This work was undertaken for the purpose of making a thorough study of the different radioactivities resulting from the deuteron bombardment of a single element, copper. Lindner and Perlman[3] have discussed the factors involved in the spallation reactions from As. These factors will not be reviewed here. Excitation functions have been determined for Zn^{63}, Zn^{62}, Cu^{64}, Cu^{61}, Ni^{65}, Ni^{57}, Co^{58}, Co^{56}, Co^{55}, Fe^{59}, Fe^{52}, Mn^{56}, and Mn^{52}, formed by 194-Mev deuterons on natural isotopic copper. The stacked foil technique, described for the 184-inch cyclotron by Thornton and Senseman,[4] was used. The foils on which the chemical separations were performed were electrolytic copper 0.002 in. thick, 1-in. diameter disks. These were placed in a 2-in. square stack of $\frac{1}{32}$-in. copper absorbers so as to cover the energy ranges desired. It was not practicable to perform the separations on more than 12 foils, so 10 were placed between 194- and 0-Mev energies of the deuterons and 2 beyond the range to give an estimate of the neutron background and of any effect of deuterons scattered into the side of the stack. A 0.001-in. Al foil of the same size as the Cu foils was placed at the high energy edge of the stack and used as a monitor. The $Al^{27}(d, \alpha p)Na^{24}$ cross section of 0.048 barn[5] at 194 Mev was used to estimate the cross sections for the elements formed.

The stack of foils was bombarded in the internally deflected beam of the 184-inch cyclotron for times of the order of one hour. After chemical separations to be described below, the samples were counted with mica end window counters, and the resultant decay curves resolved to determine amounts of different isotopes present. No special attempt was made to determine isotopes with half-lives less than about one hour. The Al monitor was counted under the same geometry, as nearly as possible, in order to minimize effects of backscattering, etc.; that is, if the samples were plated on Pt disks, the monitor was mounted on such a disk, etc. Experiments showed variations in counting rates of as much as 100 percent, depending on the backing and geometry of the sample, so that the estimates of cross section are certainly no more accurate than a factor of 2. Fortunately, the 1.4-Mev β-spectrum of Na^{24} is a reasonable mean of those investigated, though this isotope was chosen because of the convenient half-life

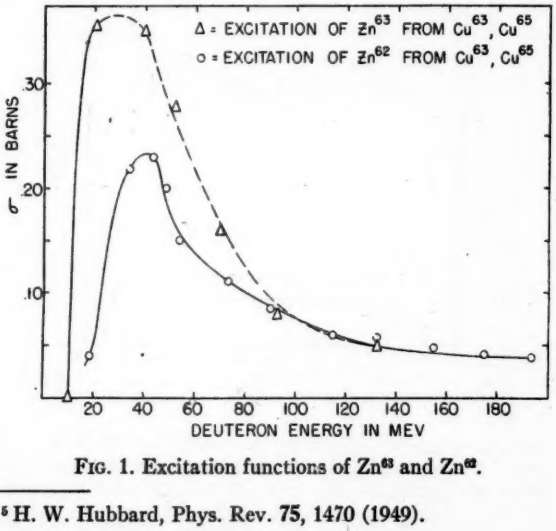

FIG. 1. Excitation functions of Zn^{63} and Zn^{62}.

* This work was performed under the auspices of the AEC.
[1] R. Serber, Phys. Rev. **72**, 1114 (1947).
[2] W. Heckrotte and P. Wolff, Phys. Rev. **73**, 264 (1948).
[3] M. Lindner and I. Perlman, Phys. Rev. **78**, 499 (1950).
[4] R. L. Thornton and R. W. Senseman, Phys. Rev. **72**, 872 (1947).
[5] H. W. Hubbard, Phys. Rev. **75**, 1470 (1949).

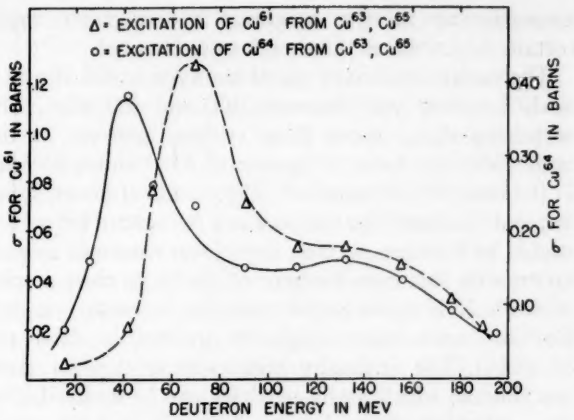
Δ = EXCITATION OF Cu61 FROM Cu63, Cu65
o = EXCITATION OF Cu64 FROM Cu63, Cu65
σ FOR Cu61 IN BARNS
σ FOR Cu64 IN BARNS
DEUTERON ENERGY IN MEV

FIG. 2. Excitation function of Cu^{64} and Cu^{61}.

and absence of other activities. The excitation curve for the reaction $Al^{27}(d, \alpha p)Na^{24}$ was also used as a check on the energy values. It has a peak at approximately 25 Mev, which was the energy at the last Cu foil. The deuterons have passed through 22 g/cm² and the energy straggling is so large that no detail is possible below this.

Experimentally, the major problem was that of getting quantitative chemical separation of the elements near Cu from the 400 mg of Cu in the foils, and using at maximum about 3 mg of carrier. More carrier would have affected β-counting accuracy. The problem was met by special method of separation and duplicate equipment for processes such as ether extraction, etc., so that work on 12 foils could be completed in a few hours. The details are given in the appendix.

III. DISCUSSION OF RESULTS[6]

A. Zn^{63} and Zn^{62}

Zn^{63} is the well-known 38-min. β^+ activity formed in this case by $(d, 2n)$ and $(d, 4n)$ reactions; Zn^{62}, formed by $(d, 3n)$ and $(d, 5n)$, decays 90 percent by K-capture, 10 percent by β^+ emission, and is mainly detected by its daughter,[7] the 10-min Cu^{62}. The yields are shown on Fig. 1. These activities have the advantage that there is no background caused by neutrons, since Zn can be formed only by the addition of a charge. Each curve is presumably a composite of two double humped ones caused by the two reactions, but the energy resolution is not sufficient to show this up. The Zn^{62} curve is displaced to higher energy as would be expected. The fall off at high energies is not as rapid as might be expected from simple compound nucleus theory. This may be the result of exchange collisions between high energy incident protons and neutrons in the nucleus. The cross section at the maximum, 0.4 barn, is also of the expected order of magnitude, the geometrical cross section of a Cu nucleus being about 1 barn.

B. Cu^{64} and Cu^{61}

Cu^{64} is the familiar 12.8-hr. activity whose excitation curve by the reaction (d, p) has been studied by Livingston and Wright[8] and has a maximum below 10 Mev. Clearly, this portion of the curve is not visible in Fig. 2, where the yield of Cu^{64} is plotted. (Note the different ordinates for Cu^{64} and Cu^{61}.) The maximum at approximately 40 Mev is presumably due to the reaction (d, dn), $(d, p2n)$, or $(p, pn)(n, 2n)$ depending on whether one considers the reaction as caused by the deuteron as a whole or by one of its constituents. One might expect the maximum of these reactions to be at about twice the threshold energy[2] or about 20 Mev.

Cu^{61} (Fig. 2) is the well known 3.4-hr. activity. It requires the expulsion of more neutrons and, consequently, the maximum in its curve is at higher energy than that for Cu^{64}. The shape suggests a combination of sharper resonance with slowly varying portion. Why this second portion should decrease above 140 Mev is not at all clear, however. None of the curves calculated by Heckrotte and Wolff show such a decrease, even for the case of C, a much more transparent nucleus. The maximum cross section for the production of Cu^{61} is also smaller than that for Cu^{64}, as would be expected from the additional competition at higher energies.

C. Ni

The two Ni isotopes measured were Ni^{65} and Ni^{57}. The circled points on Fig. 3 were adjusted to fit a smooth Ni^{65} curve. When so adjusted, the Ni^{57} points fit on a smooth curve. This seems to be good evidence that there was chemical loss in these samples. The magnitude of the corrections was about 20 percent. Ni^{65} is formed by the $(d, 2p)$ or (n, p) reactions, and so is present even beyond the range of the deuterons owing to neutrons formed in the stack. The threshold for the reaction is low (2.3 Mev), and since the strag-

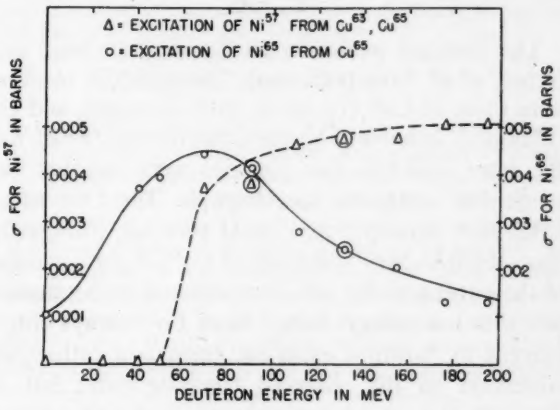
Δ = EXCITATION OF Ni57 FROM Cu63, Cu65
o = EXCITATION OF Ni65 FROM Cu65
σ FOR Ni57 IN BARNS
σ FOR Ni65 IN BARNS
DEUTERON ENERGY IN MEV

FIG. 3. Excitation functions of Ni^{57} and Ni^{65}.

[6] The periods, radiations, etc., of the radioactive isotopes are given in the table of Seaborg and Perlman, Rev. Mod. Phys. 20, 585 (1948).

[7] R. W. Hayward, Phys. Rev. 79, 541 (1950).

[8] R. S. Livingston and B. T. Wright, Phys. Rev. 58, 656 (1940).

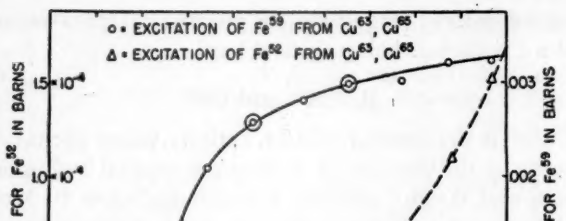

FIG. 4. Excitation functions of Fe^{59} and Fe^{52}.

gling is much greater than 2 Mev, a yield should be observed down to zero energy. The rather broad apparent maximum in the curve at about 60 Mev probably occurs at a somewhat lower energy. This energy is undoubtedly associated with the necessity for ejecting one or two protons over the Coulomb barrier. If the stripping process, in which the neutron enters the nucleus and the proton goes on, gives a large contribution, the necessary deuteron energy will be high because the neutron averages only half of it. In this connection, the yield of the (n, p) reaction as a function of neutron energy would be valuable to know.

The Ni^{57} curve is characteristic of those with high threshold energies. If one calculates the threshold for $Cu^{63}(d, 2p6n)Ni^{57}$ from a semi-empirical mass formula,[9] one gets 62 Mev. The agreement with the curve can be considered satisfactory. As will be seen below, there is evidence that α-particles are ejected as units; but in this case, unless the deuteron is captured to form a Zn compound nucleus, α-ejections cannot give Ni^{57}.

It is probably significant that the decrease of the Ni^{65}, Zn^{62}, and Cu^{61} cross sections sets in at about 60 Mev, when the Ni^{57} and others listed below start to rise.

D. Co

The chemical recoveries on Co were the least satisfactory of all those performed. The activities recovered were those of Co^{58} (72 days), Co^{56} (72 days), and Co^{55} (18 hours). In order to separate the first two, which have the same half-life, the particles were counted in a rough 180° magnetic spectrograph. The Co^{56} with a a 1.5-Mev beta-spectrum could then be distinguished from the 0.47-Mev spectrum of Co^{58}. A pure standard of the latter activity was also prepared by bombarding Mn with low energy alphas. Since Co^{58} decays only 15 percent by positron emission, there is a rather large correction to the observed counting rate; but the measurement in the magnetic spectrograph made certain that none of the x-rays were counted.

The excitation curves are of the type which rise to a fairly constant yield between 100 and 200 Mev. The surprising thing about these curves, however, is the large yield, 0.2 barn in the case of Co^{58} and 0.04 barn in the case of Co^{56} and Co^{55}. The results of Good, Peaslee, and Deutsch[10] on the positron K-capture branching should be accurate, so that there is no reason to suspect an error in this measurement of the large cross section of Co^{58}. It is to be noted that the reactions yielding Co^{58} are ones which might be written $(d, d\alpha n)$ and $(d, d\alpha 3n)$. The unusually high cross section for those reactions in which alpha-particles can be emitted after the excitation of the bombarded nucleus is discussed below.

Co^{57} (270 d.) is undoubtedly formed also in these experiments. Since these activities were weak, it was not possible to detect Co^{57} with certainty. However, the yields of Co^{56} and Co^{58} may be somewhat too high.

E. Fe

The 7.8-hr. Fe^{52}, which is the parent of the 21-m. Mn^{52m}, and the 49-d. Fe^{59} were the iron activities investigated. The results are shown in Fig. 4. Corrections similar to those mentioned for Ni were made on the circled points of the Fe^{59} curve with the resultant good fit to the Fe^{52} curve.

The Fe^{59} yield extends apparently to zero energy; and, while the energy definition is poor in this region, the curve does indicate that the reaction proceeds at low energies. Using the semi-empirical mass formula, one finds that the reaction $Cu^{65}(d, 2\alpha)Fe^{59}$ is exoenergetic by about 2 Mev. At low energies the spread in deuteron beam energy is large compared to the α-barrier height, so that one expects to find a yield at zero energy. The threshold for $Cu^{63}(d, 2p\alpha)Fe^{59}$ is 5 Mev, and because of the barrier for the α-particle this reaction will not become appreciable until higher energies. The rise in the curve beginning at about 50 Mev might

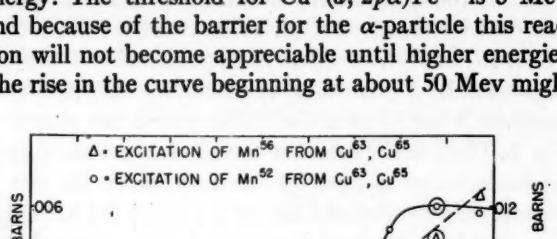

FIG. 5. Excitation functions of Mn^{56} and Mn^{52}.

[9] See Orear, Rosenfeld, and Schluter, "Nuclear Physics, Lectures by E. Fermi," p. 6. No Coulomb barrier energies are included in the threshold calculations.

[10] Good, Peaslee, and Deutsch, Phys. Rev. 69, 313 (1946).

e associated with this reaction or with reactions such s $Cu^{63}(n, p\alpha)$ or $Cu^{63}(n, 3p2n)$. In the latter the threshold is 28 Mev higher, while in both the necessary deuteron energy is increased because the neutron is considered as the particle involved and averages only one-half the deuteron energy. Further work on these reactions using low energy deuterons is projected.

The Fe^{52} exhibits the lowest cross section and the highest threshold measured in this work. The calculated threshold for $Cu^{63}(d, 4p9n)Fe^{52}$ is 104 Mev. The energetic threshold seems to be definitely below this (the energy definition in this region should be good) and would indicate that a reaction such as $Cu^{63}(d, \alpha 2p7n)$ or $Cu^{63}(n, \alpha p7n)$ was participating. Such reactions are particularly necessary if one postulates that only the neutron or the proton gives energy to the nucleus, although it is important to remember that this cross section is very small, and that occasionally a proton or a neutron may impart a large fraction of the deuteron energy to a nucleus.[11]

F. Mn

Mn^{56} (2.56 hr.) and Mn^{52} (6.5 d.) were the two Mn isotopes investigated. The curves are shown in Fig. 5. The 6.5-day activity is the lower of the two Mn^{52} isomeric states and is undoubtedly produced to some extent as a decay product of Fe^{52} through Mn^{52m}. The separations of Fe and Mn were performed on all samples at the same time and within a few hours of the end of the bombardment; and since the excitation curves are not radically different, the curve shown in Fig. 5 should not be much in error. Both Mn curves show the rather steep rise beginning at high energies characteristic of a reaction with high threshold. The calculated threshold for protons and neutrons out $(d, 5p4n)$ for Mn^{56} is 67 Mev, which is slightly above the observed threshold, indicating that probably α's are involved, while the calculated threshold for Mn^{52} from Cu^{63} is 102 Mev, and the observed threshold is definitely lower. In this case it seems certain that α's rather than individual protons and neutrons are emitted.

IV. CONCLUSIONS

The sets of yield curves presented above definitely show that at high energies of the bombarding particle the typical curve predicted by the compound nucleus theory at low energies is not found. The curves are in agreement with what would be expected from the theory presented by Serber. Detailed calculations such as extensions of those of Horning and Baumhoff[12] might be worth while to show whether the agreement is as close as could be expected.

More striking is the alternation of the magnitude of cross sections with the Z of the product isotope superimposed on a decreasing trend. Table I exemplifies this at 190 Mev. Since one cannot measure the yield of every isotope, the data are only fragmentary; but it does seem that the yield of Cu is large, of Ni small, of Co large, etc. A good example seems to be the cases of Fe^{52} and Mn^{52}, in which the latter cross section is a factor of 100 higher although it requires the ejection of an extra proton rather than a neutron. At very high energies one might expect that any barrier effect would be negligible and that the yields would be about equal. If we assume that the incident particle, neutron, proton, or deuteron, does not stick but only leaves the struck nucleus excited, then we notice that Mn^{52} can be formed by the ejection of two alphas and three neutrons from Cu^{63}, while Fe^{52} must be formed by ejection of particles less tightly bound to each other. As was mentioned above, the thresholds seem to indicate that alphas may be emitted; and this alternation in yield seems to be more evidence for the same thing. Such an alternation is evident in the results of Miller, Thompson, and Cunningham[13] with Cu and also, though not so noticeably, of Hopkins and Cunningham[14] working with As.

TABLE I. Maximum cross sections in barns for spallation products from deuterons on Cu. All are for 190 Mev except Cu^{61}.

A ↓ / Z →	Mn	Fe	Co	Ni	Cu
61					0.11
60					
59		0.003			
58			0.200		
57				0.0005	
56	0.006		0.040		
55			0.040		
52	0.012	0.00015			

APPENDIX

The following chemical separations were mostly determined by convenience and the relative amounts of the activities present. The Zn separation had to be good only for Cu removal, since relative amounts of the other activities were small. The Ni, Co, Mn, and Fe separations had to be good from all other activities. The Fe separation was the most rigorous of them all, having to be good to one part in 10^6 from all other elements.

Zinc

The separation of Zn from the elements near it was as follows: Cu target foils were dissolved in the minimum necessary 6N HNO_3 and 2 mg of Zn carrier added as the nitrate or sulfate. One ml of concentrated H_2SO_4 was added and the HNO_3 removed by evaporating to SO_3 fumes. The solution was then diluted to about 3N H_2SO_4 and 500 mg of 20 mesh Al added. This solution was boiled until all the Cu was reduced and for about 5 minutes after the solution appeared water white. The solution was then cooled and filtered through a rapid filter paper, the Cu metal being washed with 0.1N H_2SO_4. The pH was adjusted to about 2 or 3 with NaOH and dilute H_2SO_4. The solution was then saturated

[11] R. Serber, Phys. Rev. **72**, 1008 (1947).
[12] W. Horning and L. Baumhoff, Phys. Rev. **75**, 370 (1949).
[13] Miller, Thompson, and Cunningham, Phys. Rev. **74**, 347 (1948).
[14] H. H. Hopkins and B. B. Cunningham, Phys. Rev. **73**, 1406 (1948).

with H_2S to precipitate ZnS, centrifuged, and the supernatant, which contained Mn, Fe, Co, and Ni, decanted. The precipitate was washed with 0.01N H_2SO_4 containing H_2S and then dissolved in 3 ml concentrated HNO_3. This solution was then evaporated to dryness on a stainless steel dish, flamed to destroy any excess sulfur and water of hydration, and was ready to be counted.

Copper

The Cu target foil was dissolved in a minimum of dilute HNO_3, made up to 250 ml in a volumetric flask and some convenient small fraction (0.8 percent to 4 percent) transferred to an electrolytic cell. Two drops of concentrated H_2SO_4 and a small amount of dilute HNO_3 were added and the solution plated to exhaustion by about ½ to 1 hour plating at about 20 milliamperes out of a volume of 20 ml. Zn, Mn, Fe, Co, and Ni will not plate under these conditions. The plates were quickly removed, washed in alcohol, dried in air, and were ready to count. The Cu was about 2 mg/cm² thick.

Nickel

The separation of Ni from the elements in the region of copper was done as follows: The target foil was dissolved in 6N HCl and a few drops of 30-percent H_2O_2, the excess H_2O_2 then being boiled off. About one-half to one mg of Ni carrier was added as chloride, the solution neutralized with NH_4OH, and then made slightly acid with HCl. NH_4HSO_3 was added to reduce Cu^{++} to Cu^{+} and excess SO_2 boiled off. CuSCN was precipitated from the warm solution with a few crystals of NH_4SCN, and allowed to settle for ten minutes. The solution was filtered and the precipitate washed with a one-percent solution of NH_4SCN containing a little NH_4SO_3. To complex the Fe, one ml of 50-percent tarataric acid was added to the filtrate which was made slightly ammoniacal and brought to near boiling. The Co, Zn, and Cu were thus complexed in the NH_4OH and Ni dimethyl glyoxime was precipitated by adding one to two ml of 1-percent dimethyl-glyoxime in ethanol. The precipitate was filtered and washed with hot water, dissolved in dilute HCl, and reprecipitated twice in order to free it from occluded Zn. Finally, the clean precipitate was dissolved in concentrated HNO_3, evaporated to dryness in a stainless steel dish, flamed, and was ready to count.

Cobalt

The separation of Co from the elements near Cu presented more difficulty than most of the other separations. The method finally evolved essentially consisted of removing all contaminant elements which would plate electrolytically and then plating the remaining Co onto platinum disks out of ammoniacal solution.

The Cu target foil was dissolved in minimum amount of dilute HNO_3, 1 mg each of Co, Ni, and Mn carriers, 2 drops of concentrated H_2SO_4 were added, and the solution diluted to 20 ml. The excess Cu was removed by electrodeposition on a stainless steel strip cathode set into the beaker using about 1 to 2 amp. at 2 to 3 volts. When the solution was water white, the electrodes were removed, 1 ml concentrated H_2SO_4 added and the solution evaporated to SO_3 fumes to destroy HNO_3 present. Then it was diluted to 35 to 50 ml and saturated with H_2S to precipitate the remaining Cu. Most of the Zn occluded on these CuS precipitates. After repetition of the procedure, the filtrate was again boiled to expel H_2S, made slightly ammoniacal, and 1 to 2 ml of 1-percent dimethyl-glyoxime in ethanol added. The Ni and Fe precipitates were filtered off, the filtrate was acidified with HNO_3 and evaporated to SO_3 fumes to destroy the alcohol, a few drops of concentrated HCl were added, and the filtrate was again taken to SO_3 fumes to insure removal of NO_3. The solution was transferred to an electrolysis cell fitted with a Pt disk cathode, made strongly ammoniacal, and Co metal deposited as a smooth, uniform, adherent plate on the cathode by plating for from ½ to 1 hour at about 1 to 2 amperes. MnO_2 was deposited simultaneously on the stirrer anode. Zn does not plate at these voltages. The electrolyte was then removed and replaced by distilled water with the current still on in order to prevent the Co plate from dissolving. The anode was quickly removed and the Co plate washed in alcohol and dried in air.

Manganese

It was found that Mn could be separated as part of the process for Fe isolation. The foils were dissolved in a minimum of 6N HNO_3 and 1 mg Mn carrier was added as the nitrate. The solution was then diluted to about 1N HNO_3, 0.1 g of $KBrO_3$ was added, and the solution was boiled for ten minutes or until the MnO_2 was well coagulated. There was probably some occlusion of Cu, Co, and Zn on this precipitate. The precipitate was filtered and washed with 6N HNO_3 until no Cu blue showed in the wash, then redissolved through the filter paper with concentrated HCl, and and 2 mg Cu carrier added. The solution was made strongly ammoniacal and a few crystals of $(NH_4)_2S_2O_8$ added. Any occluded Cu, Co, and Zn was complexed in the NH_4OH. The excess persulfate was boiled off, and the MnO_2 reprecipitated and centrifuged. After washing with dilute NH_4OH, the precipitate was deposited on a stainless steel dish and dried. This separation was perhaps the least troublesome of all those done in that the time required was a minimum and the degree of purification and percentage recovery excellent.

Iron

The following separation for Fe has the advantages of high purity ($\sim 10^9$) and that a small amount of carrier is necessary. Since the Fe yield was very small, the Fe half-lives relatively long, and the Fe^{59} β^- soft, these advantages turned out to be absolutely essential, even if recovery was not as complete as in some of the other fractions.

Cu foils were dissolved in a minimum 6N HNO_3 and diluted to 1 or 2 N HNO_3. One mg Fe and 1 mg Mn carrier were added as nitrates. The Mn was precipitated as MnO_2 by addition of about 0.1 g $KBrO_3$ and boiling for 10 minutes, filtered and washed. $Fe(OH)_3$ was precipitated from the filtrate by addition of excess NH_4OH and centrifuged. The Cu, Co, Ni, and Zn complexed in the supernatant liquid. The $Fe(OH)_3$ was dissolved in HCl, about 3 mg of $CuCl_2$ added, and the Fe precipitated twice more, this number of sweeps being necessary to get rid of the tremendous excess of Cu activity. The final $Fe(OH)_3$ precipitate was dissolved in three drops of concentrated HCl, and transferred to a separatory funnel with 6N HCl. An equal volume of diethyl ether presaturated with 6N HCl was added and the Fe extracted. Extraction was repeated on the aqueous layer, 1 mg Fe carrier added to this aqueous layer, and extracted again. All ether phases were collected with water and the ether boiled off in a hot water bath, then $Fe(OH)_3$ precipitated from this solution. This was dissolved in several drops concentrated HNO_3, evaporated to dryness on a stainless steel dish, flamed, and was ready for counting.

Total Cross Sections of Be, B, O, and F for Fast Neutrons*

C. K. BOCKELMAN
University of Wisconsin, Madison, Wisconsin
(Received August 22, 1950)

Previous studies of the cross sections of Be and O as functions of neutron energy have been extended to higher energies. Three resonances in oxygen were observed below 1.4 Mev, in agreement with those reported by the Minnesota group. In the range from 0.2 to 1.4 Mev, two resonances were found for Be. For energies below 1 Mev, one level was observed in B, while evidence for at least seven resonances was found for F in the energy interval from 0.01 to 0.7 Mev. The assignment of reduced widths and spin values to the compound states is possible in certain cases.

I. INTRODUCTION

MEASUREMENTS of the total cross sections of light elements are of interest because of the information they offer concerning the energy levels of these nuclei. In the lighter elements the levels are sufficiently broad and widely separated in energy that their true shapes may be obtained with neutron energy spreads which are conveniently attainable. The present paper is concerned with an extension to higher energies of previously[1] published measurements on beryllium and oxygen and also presents the results of measurements of the total cross sections of boron and fluorine.

Cross sections were measured by transmission experiments according to techniques previously described,[1] the neutrons being produced by the Li(p,n)Be reaction. The presence of a small number of neutrons of lower energy at energies above 650 kev for the main group[2] is believed to have a negligible effect in this experiment. If there were a significant number of low energy neutrons present, one would expect maxima observed with the main group to repeat as the energy of the second group passed through a resonance. No such effect was observed. Also, the close agreement of the oxygen data with those of Freier, *et al.*,[3] who used neutron detectors biased against this group, corroborates this argument.

For the interpretation of the observed resonances it will be assumed that elastic scattering is the only process of importance in the energy range and for the nuclei investigated in the present study. The cross section may then be considered to be composed of the contributions of potential scattering and of the resonant interaction of the incident neutrons with the target nuclei. Since at the neutron energies used here the potential scattering is almost entirely s-scattering, resonances produced by s-neutrons should be recognizable by a region of destructive interference between resonance and potential scattering preceding the resonance peak. If all interactions other than elastic scattering are neglected, the variation of the cross section at an isolated resonance is given according to the Breit-Wigner theory by $2\pi k^{-2}(2J+1)/(2I+1)$, where k is the wave number of the incident neutron, J the spin of the compound nucleus, and I the spin of the bombarded nucleus. Thus, the spin of the compound state can be deduced from the measured variation of cross section at a resonance.

A convenient energy-independent parameter for the description of level widths is the reduced width γ^2, defined as

$$\gamma^2=\Gamma/2kT_l,$$

where Γ is the natural width and T_l is the centrifugal barrier penetration factor. The sum of the reduced widths for transitions from a given level in the compound nucleus to all final states has been given by Wigner.[4] In certain cases this sum rule makes possible an assignment of the orbital angular momentum of the neutrons which produce a resonance.

II. BERYLLIUM

Determinations of the total cross section of Be from 0.03- to 0.75-Mev neutron energy were reported in reference 1. The measurements were extended to 1.40 Mev with an energy resolution of 20 kev, and those in the range from 0.20 to 0.85 Mev were repeated with a

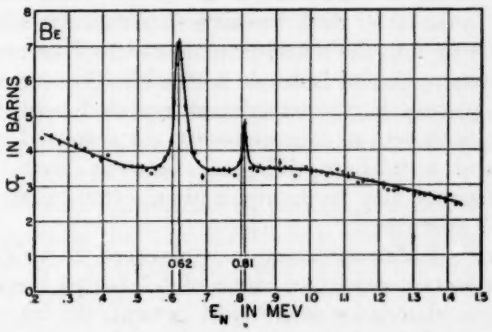

FIG. 1. The total cross section of beryllium. Points denoted by open circles represent data taken with a neutron energy spread of 20 kev; for the solid circles the energy spread was 12 kev. The length of the vertical bars through the points give the standard statistical error.

* This work was supported by the Wisconsin Alumni Research Foundation and by the AEC.

[1] Adair, Barschall, Bockelman, and Sala, Phys. Rev. **75**, 1124 (1949).

[2] Johnson, Wilson Laubenstein, and Richards, Phys. Rev. **77**, 413 (1950).

[3] Freier, Fulk, Lampi, and Williams, Phys. Rev. **78**, 508 (1950).

[4] E. P. Wigner, Am. J. Phys. **17**, 99 (1949).

FIG. 2. The total cross section of boron. The neutron energy spread was 12 kev for energies above 0.13 Mev, and 25 kev for lower energies.

neutron energy spread of 12 kev. The results are shown in Fig. 1.

As might be expected, the shape of the 0.62 Mev resonance did not change appreciably from that described in reference 1, since its experimental width is considerable larger than the neutron energy spread used in either experiment. The peak at 0.81 Mev, however, has a measured width of 12 kev, equal to the experimental energy spread. Thus, it is not felt that the true shape of the resonance is sufficiently well known to specify the angular momenta involved. However, absence of any dips near the peak indicates that it must be caused by neutrons with orbital angular momentum $l>0$, and the height of the resonance is greater than that which would occur if the spin of the compound nucleus were zero.

III. BORON

The neutron flux transmitted through a sample of amorphous boron in a brass container was compared with that transmitted through an identical empty container. For measurements above 0.13 Mev a neutron energy spread of 12 kev was used; below this energy the resolution was about 25 kev. The total cross section is shown in Fig. 2. The results agree reasonably well with those of Wattenberg,[5] but are consistently higher than those of Barschall, *et al.*[6] While the geometry used in the latter work was such that the correction for scattering into the detector amounted to 7 percent on the assumption of isotropic scattering, this correction is 3 percent in the experiment reported here. Even after both sets of measurements are corrected, there remains a 0.7-barn difference between them. This discrepancy may be the result of anisotropic scattering of the neutrons.

At 0.43 Mev a maximum is observed at which the cross section reaches a value of 6.7 barns. Since the isotopic abundance of B^{11} is 81 percent, the resonance is ascribed to this isotope. The lack of any dip in the neighborhood of the peak indicates that it should not be attributed to *s*-neutrons. Since values of l greater than unity yield reduced widths which exceed the limit imposed by the sum rule,[4] the resonance is assigned to *p*-neutrons and has a reduced width of 1.0×10^{-13} Mev-cm, corresponding to the observed width of 45 kev. When it is assumed that inelastic scattering and absorption can be neglected at these energies, application of the single level dispersion formula yields maximum values of 2.2, 3.6, and 5.1 barns as resonance contributions for the spin of the compound nucleus $J=1$, 2, and 3, respectively. These values include a factor of 0.81 to account for the isotopic abundance of B^{11}. If the potential scattering is taken as equal to 3.7 barns in the neighborhood of the resonance, it seems most reasonable to attribute the resonance to interaction with *p*-neutrons forming a compound nucleus with $J=2$ although the value $J=3$ cannot be excluded.

Since an oxygen resonance occurs at very nearly the same energy, it was suspected that this maximum might actually be caused by an oxygen contamination of the sample. Therefore, the boron was tested for presence of the oxide by leaching it with hot water, in which boron oxide is soluble while boron is not. Less than 3 percent of the sample by weight dissolved, so it was concluded that the oxygen contamination was insufficient to affect the measurement significantly. Furthermore, if oxygen were responsible for the resonance, one would expect it to cause an increase in the cross section at the next oxygen resonance around 1 Mev. No such increase was found.

IV. OXYGEN

The oxygen cross section was obtained by comparison of the transmission through a brass container filled with BeO to that through an identical container enclosing a Be disk of such thickness as to match as closely as possible the number of Be atoms. The solid circles in Fig. 3 represent the present measurements, taken with an energy resolution of 20 kev. For the sake of completeness, the results cited in reference 1 are also shown, indicated by open circles. The data are in agreement with those of Freier, *et al.*[3] in the energy range they have in common.

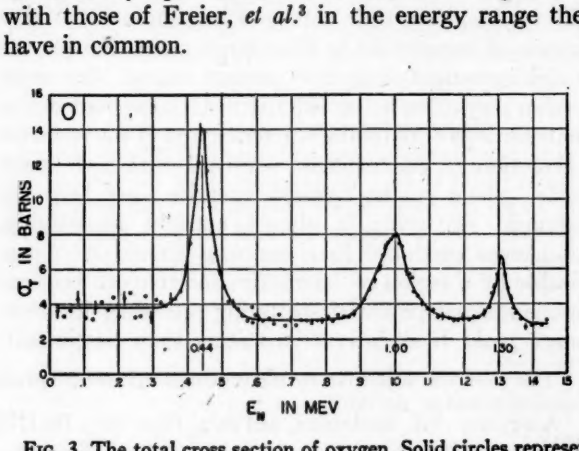

FIG. 3. The total cross section of oxygen. Solid circles represent the present measurements; open circles indicate the results described in reference 1. A neutron energy spread of 20 kev was used.

[5] Fields, Russell, Sachs, and Wattenberg, Phys. Rev. **71**, 508 (1947).

[6] Barschall, Battat, and Bright, Phys. Rev. **70**, 458 (1946).

The three resonances at 0.44, 1.00, and 1.30 Mev have experimental widths at half-maximum of 45, 100, and 40 kev respectively. The observed maxima are best fitted by taking $J=3/2$. This resonance contribution, added to the potential scattering, yields values of 16.8, 8.9, and 7.5 barns at 0.44, 1.00, and 1.30 Mev, respectively, as compared with the experimental values of 14.0, 7.9, and 6.7 barns. By assuming that the neutron energy spread is Gaussian in shape, one can estimate that the true maxima are about 10 percent larger than those observed, so that the agreement between experimental and predicted values is satisfactory. The lack of any dips near the peaks indicates that the resonances should not be assigned to s-neutrons. Since values of l greater than unity yield reduced widths which exceed the limit given by the sum rule[4] by more than 50 percent, the 0.44-Mev peak is attributed to an interaction with p-neutrons, and has a reduced width of 0.76×10^{-13} Mev-cm. Although the experiment does not give any further direct information about the orbital angular momentum of the incident neutrons, it does not seem likely that the maximum at 1.00 Mev would be caused by neutrons with $l>1$, since the reduced width for $l=2$ would amount to 50 percent of the sum. Thus, this resonance is assigned to p-neutrons, on which assumption the reduced width is 0.66×10^{-13} Mev-cm. For both of these levels, the reduced widths are about 4 percent of the sum-rule limit. If these resonances are caused by p-neutrons, the parities of these states are opposite to that of the ground state.

In the case of the resonance at 1.30 Mev it is not possible to choose between values of $l=1$ and $l=2$ for the interacting neutrons. If the compound state is formed by p-neutrons, the reduced width is 0.17×10^{-13} Mev cm; if by d-neutrons, the reduced width is 1.7×10^{-13} Mev cm.

Alvarez,[7] in his study of the neutrons emitted from O^{17} formed by β^- decay of N^{17}, reports the existence of a broad neutron group of 0.92-Mev energy. If neutrons were emitted from the excited states here reported, the energies of these neutrons would be 0.39, 0.89, and 1.16 Mev. The energy of the lowest group would not have been sufficient to have been observed in Alvarez' experiment. While neither the results of Alvarez nor those of Hayward[8] reveal the existence of more than one neutron group in this region, it would be difficult to explain why N^{17} would not decay to both levels since they both have the same spin, unless they differed in parity. However, it seems possible that the two groups were not separated.

If the binding energy of an additional neutron to O^{16} is taken[9] as 4.14 Mev, the resonances here reported arise from levels at 4.56-, 5.08-, and 5.36-Mev excitation. The 4.56-Mev level may correspond to that at 4.49 Mev reported by Burcham and Smith in their study of the $F(d,\alpha)O$ reaction.[10]

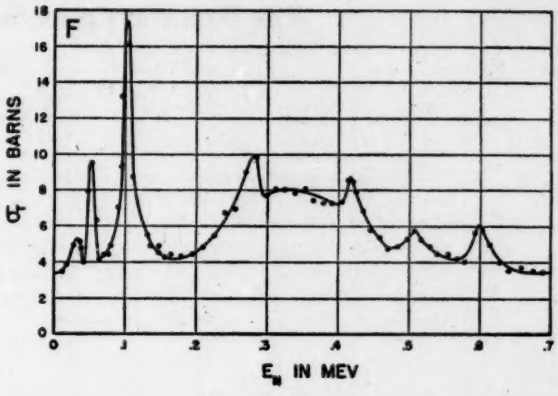

FIG. 4. The total cross section of fluorine. Neutron energy spreads of 20 kev were used for energies above 0.13 Mev and 9 kev for lower energies.

V. FLUORINE

The cross section of fluorine was determined by measuring the cross section of Teflon, $(CF_2)_n$, and subtracting the carbon cross section, which was measured under similar conditions.[11] For energies below 0.13 Mev, neutrons of an estimated energy spread of 9 kev were used, while above this energy the energy resolution was about 20 kev.

Figure 4 shows the results of the measurements. Fluorine has about the same level density as does sodium.[1] Only the 100-kev resonance is sufficiently resolved so that its width and spin can be surmised. If it is caused by the interaction of s-neutrons to form a compound state of spin one in F^{20}, the natural width is about 15 kev, leading to a reduced width of about 0.09×10^{-13} Mev-cm. This width is very much smaller than the reduced widths of the O^{17} levels, but it is of the same order of magnitude as the width of the levels which have been identified in sulfur.[12]

The cross section between 250 kev and 450 kev was further investigated with a neutron energy spread of about 5 kev in order to determine whether the behavior was the result of unresolved resonances. The results were the same as those shown in Fig. 4 which had been obtained with a resolution of 20 kev. It seems, then, most probable that this structure is the result of the superposition of three levels, each with a width of the order of 50 kev.

[7] L. Alvarez, Phys. Rev. 75, 1127 (1949).
[8] E. Hayward, Phys. Rev. 75, 917 (1949).
[9] Rosenfeld, *Nuclear Forces* (Interscience Publishers, Inc., New York, 1948).
[10] W. E. Burcham and Smith, Proc. Roy. Soc. A168, 176 (1938).
[11] D. W. Miller, Phys. Rev. 78, 86 (1950).
[12] Peterson, Barschall, and Bockelman, Phys. Rev. 79, 593 (1950).

The Neutron Cross Section of Mn Below 5000 ev

S. P. HARRIS, C. T. HIBDON, AND C. O. MUEHLHAUSE
Argonne National Laboratory, Chicago, Illinois

(Received August 18, 1950)

Experimental measurements of the neutron scattering and absorption cross sections of manganese at energies less than 5000 ev are shown to fit a two-level Breit-Wigner formula. Only one parameter, the nuclear radius, need be adjusted to do this. This adjustment having been made, it is possible to obtain (a) the total scattering, the coherent scattering, and the absorption cross section for thermal neutrons, (b) the angular momenta of the two low energy resonances, and (c) the proper cross-section behavior in the wing of the lowest energy resonance. The evidence presented demonstrates in detail that the Breit-Wigner formula tion yields the proper neutron scattering cross section as a function of energy.

I. INTRODUCTION

AT neutron energies below 5000 ev two resonances in manganese are known. These are principally scattering resonances,[1] and are located at 345 ev and ~2400 ev, respectively.[2] However, a significant amount of resonance absorption (~2 percent) is observed to be associated with the 345-ev level. Other available data on manganese consist of measurements of the total scattering, the coherent scattering,[3] and the absorption cross section for thermal neutrons. Also, the thermal scattering length of manganese is known to be negative.[4] In the present work, measurements of the resonance scattering integrals of each resonance as well as the resonance absorption integral of the 345-ev resonance are presented. In addition, self-indication measurements at 345 ev are given which determine the total angular momentum of the 345-ev level. A final check is made of the foregoing conclusions from measurements of the total cross section of manganese at specific energies below 150 ev.

Verification of the behavior of a neutron cross section in the wings of a resonance[5] is one of the principal purposes of this paper. Manganese offers an admirable opportunity for such a study, since the low energy wing of the 345-ev level extends to zero energy. In this region, resonance scattering detectors with high energy resolution are available. These enable one to make accurate manganese transmission measurements at definite energies.

II. THEORY

The Breit-Wigner expression for a multi-level scattering cross section[5] is given by

$$\sigma_s/4\pi=\sum_J g_J[R+\sum_r \tfrac{1}{2}\lambda_r\Gamma_{nr}/(\epsilon-\epsilon_r+\tfrac{1}{2}i\Gamma_r)]_J^2, \quad (1)$$

where J=total angular momentum of the compound nucleus ($J=I\pm\frac{1}{2}$ for S neutrons, where I is the total angular momentum of the initial nucleus), $g_J=\frac{1}{2}(2J+1)/(2I+1)$ (statistical weight); R=nuclear radius; λ_r=neutron wave-length (divided by 2π) at exact resonance, r; ϵ_r=resonance (r) energy; Γ_{nr}=neutron resonance width at exact resonance; Γ_r=total resonance width at exact resonance=$\Gamma_{nr}+\Gamma_{\gamma r}$, where $\Gamma_{\gamma r}$ is the radiation resonance width (constant); and ϵ=independent energy variable.

The numerator of the resonance term is actually $\lambda\Gamma_n$, where λ and Γ_n refer to "r" at energies not necessarily equal to E_r. This product can be set equal to the constant $\lambda_r\Gamma_{nr}$ if Γ_n varies directly as the neutron velocity (i.e., inversely as λ). The correctness of this important feature is implicit in the $1/v$ absorption law for thermal energies, but is confirmed experimentally for the scattering case by the present work.

That R be independent of J may seem surprising except for very heavy nuclei.[6] In the present work, however, good agreement with the data is obtained assuming a single radius.

Coherent scattering, σ_{coh}, is given by the square of the sum of all amplitudes.

$$\sigma_{coh}/4\pi=\{\sum_J g_J[R+\tfrac{1}{2}\sum_r \lambda_r\Gamma_{nr}/(\epsilon-\epsilon_r+\tfrac{1}{2}i\Gamma_r)]_J\}^2$$
$$=[R+\textstyle\sum_r g_r\lambda_r\Gamma_{nr}/2(\epsilon-\epsilon_r+\frac{1}{2}i\Gamma_r)]^2. \quad (2)$$

For manganese only two resonances are known. In order to apply formulas (1) and (2) it is important to know whether $J_1=J_2$ or $J_1\neq J_2$ (the subscripts refer to r, i.e., 345 ev and 2400 ev respectively), since only states of the same J mix. In the experimental sections of this paper it is shown that $J_1\neq J_2$, so that Eq. (1) may be written as the sum of two Breit-Wigner one-level terms:

$$\sigma_s/4\pi=g_1[R+\tfrac{1}{2}\lambda_1\Gamma_{n1}/(\epsilon-\epsilon_1+\tfrac{1}{2}i\Gamma_1)]^2$$
$$+g_2[R+\tfrac{1}{2}\lambda_2\Gamma_{n2}/(\epsilon-\epsilon_2+\tfrac{1}{2}i\Gamma_2)]^2. \quad (3)$$

Similarly for (2):

$$\sigma_{coh}/4\pi=[R+g_1\lambda_1\Gamma_{n1}/2(\epsilon-\epsilon_1+\tfrac{1}{2}i\Gamma_1)$$
$$+g_2\lambda_2\Gamma_{n2}/2(\epsilon-\epsilon_2+\tfrac{1}{2}i\Gamma_2)]^2. \quad (4)$$

At thermal energies, $\epsilon-\epsilon_r\simeq-\epsilon_r$. Also, $\epsilon_r\gg\Gamma_r$, and hence:

$$\sigma_{th\ s}/4\pi=g_1(R-a_1)^2+g_2(R-a_2)^2, \quad (5)$$

$$\sigma_{th\ coh}/4\pi=(R-g_1a_1-g_2a_2)^2, \quad (6)$$

[1] Harris, Muehlhause, and Thomas, Phys. Rev. **79**, 11 (1950).
[2] Hibdon, Muehlhause, Selove, and Woolf, Phys. Rev. **77**, 730 (1950).
[3] C. G. Shull and S. Siegel, Phys. Rev. **75**, 1008 (1949).
[4] E. Fermi and L. Marshall, Phys. Rev. **71**, 666 (1947).
[5] H. A. Bethe, Rev. Mod. Phys. **9**, 152 (1937).
[6] C. O. Muehlhause, Phys. Rev. **79**, 1002 (1950).

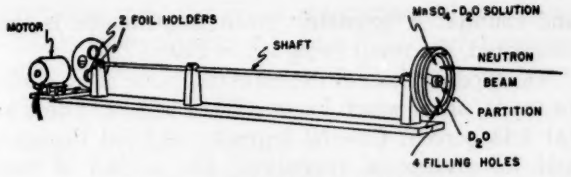

FIG. 1. Rotating cell and foil holders.

where $a_r=\lambda\!\!\!^{-}_r\Gamma_{nr}/2\epsilon_r$ (resonance amp.). The thermal incoherent (spin effect) scattering cross section is given by the difference of (5) and (6):

$$\sigma_{\text{th inc}}/4\pi=g_1g_2(a_1-a_2)^2. \quad (7)$$

Note that g_1g_2 is uniquely given by I, the angular momentum of the target nucleus. Expressions (5) to (7) provide valuable means of determining certain Breit-Wigner resonance parameters.[7] Conversely, they may be taken to evaluate the effective nuclear radius, R.

It is shown in the experimental sections of this paper that the thermal capture cross section of manganese is approximately given by the resonance parameters of the 345-ev level. It is reasonable to expect that the 2400-ev level contributes appreciably to the thermal scattering cross section, $\sigma_{\text{th }s}$, but not to the thermal absorption cross section, $\sigma_{\text{th }a}$. This is true for manganese since Γ_{nr} increases much more rapidly[2] with r ($r=1$ or 2 diff. J) than $\epsilon_r^{\frac{1}{2}}$. The following Breit-Wigner one-level form of the capture cross section illustrates this:

$$\sigma_a/\pi=g_1\lambda\!\!\!^{-}_1{}^2\Gamma_{n1}\Gamma_{\gamma1}(\epsilon_1/\epsilon)^{\frac{1}{2}}/[(\epsilon-\epsilon_1)^2+\tfrac{1}{4}\Gamma_1{}^2], \quad (8)$$

which for thermal energies (0.025 ev) reduces to

$$\sigma_{\text{th }a}/\pi=g_1\lambda\!\!\!^{-}_1{}^2\Gamma_{n1}\Gamma_{\gamma1}(40\epsilon_1)^{\frac{1}{2}}/\epsilon_1{}^2$$
$$\sigma_{\text{th }a}/4\pi=g_1(\Gamma_{\gamma1}/\Gamma_{n1})(40\epsilon_1)^{\frac{1}{2}}\cdot a_1{}^2. \quad (9)$$

Resonance scattering, $\sum_r$, and absorption, $\sum_a$, integral expressions are also obtained from the Breit-Wigner formulation.[1]

$$\sum_{sr}=\tfrac{1}{2}\pi(4\pi\lambda\!\!\!^{-}_r{}^2)g_r\Gamma_{nr}{}^2\Gamma_r/\Gamma_r{}^2\epsilon_r=4\pi^2\lambda\!\!\!^{-}_r(\Gamma_{nr}/\Gamma_r)g_ra_r; \quad (10)$$

$$\sum_{ar}=\tfrac{1}{2}\pi(4\pi\lambda\!\!\!^{-}_r{}^2)g_r\Gamma_{nr}\Gamma_{\gamma r}\Gamma_r/\Gamma_r{}^2\epsilon_r$$
$$=4\pi^2\lambda\!\!\!^{-}_r(\Gamma_{\gamma r}/\Gamma_r)g_ra_r; \quad (11)$$

$$\sum_r=\sum_{sr}+\sum_{ar}=4\pi^2\lambda\!\!\!^{-}_rg_ra_r. \quad (12)$$

It can be seen from Eq. (12) that the total resonance integral (for level r) yields the coherent thermal amplitude, g_ra_r, due to resonance, r.

One more relation of importance is employed in the experimental sections. This is the cross section for self-indication, σ_{self}. The transmission cross section measured by placing a thin resonance filter in a neutron beam wherein neutrons are detected by a thin foil of the same resonance material is given by[5]

$$\sigma_{\text{self}}=\tfrac{1}{2}\sigma_{\max}=2\pi\lambda\!\!\!^{-}_r{}^2g_r\Gamma_{nr}/\Gamma_r \quad (13)$$

$\Gamma_{nr}/\Gamma_r(\sim1$ for Mn) is obtained from the ratio of Eq. (10) to Eq. (12) and $\lambda\!\!\!^{-}_r$ is known from the resonance energy, ϵ_r. Therefore, Eq. (13) determines g_r and consequently J_r of the compound state, r. That $\sigma_{\text{self}}=\frac{1}{2}\sigma_{\max}$ experimentally (Section IV) may be considered as partial proof of the Breit-Wigner formulation. For example, if the resonance shape were Gaussian, $\sigma_{\text{self}}=\sigma_{\max}/\sqrt{2}$.

III. EXPERIMENTAL MEASUREMENT OF Σ_{s1} AND Σ_{s2}

The apparatus and method of measurement of resonance scattering integrals are fully described in a previous paper.[1]

With a very thick sodium filter ($\epsilon_r\sim3000$ ev) and a resonance neutron beam from the Argonne heavy water reactor, a "$1/\epsilon$" neutron flux can be obtained in which neutrons near 2400 ev are removed.[7a] Therefore, the resonance scattering cross section of manganese can be measured with and without the presence of scattering at 2400 ev. After corrections are made for foil thickness and counter sensitivity, it is found that

$$\sum_{s1}=419b, \quad \sum_{s2}=90b,$$

where 1 indicates the resonance at 345 ev, 2 indicates the resonance at 2400 ev, and $b\equiv10^{-24}$ cm^2 barn.

TABLE I. Neutron cross sections of Mn.

ϵ ev	$\sigma_T(\epsilon)$ b	$\sigma_a(\epsilon)$ b	$\sigma_s(\epsilon)$ b
10.0	2.90	0.64	2.26
19.5	2.88	0.51	2.37
120	6.39	0.38	6.01

In Section IV it is shown that

$$\sum_{a1}\simeq14b, \quad \sum_{a2}\simeq0.$$

Therefore,

$$\sum_1=433b, \quad \sum_2\simeq90b,$$

and

$$g_1a_1=0.448b^{\frac{1}{2}}, \quad g_2a_2=0.245b^{\frac{1}{2}}, \quad b^{\frac{1}{2}}\equiv10^{-12}\text{ cm}.$$

The rest of this section will be devoted to the consequences of the above values for the coherent resonance scattering amplitudes. In the case of manganese $I=5/2$ and $g=7/12$ or $5/12$. Therefore,

$$a_1=\begin{cases}0.768b^{\frac{1}{2}}(J_1=3)\\1.075b^{\frac{1}{2}}(J_1=2),\end{cases} \quad a_2=\begin{cases}0.420b^{\frac{1}{2}}(J_2=3)\\0.588b^{\frac{1}{2}}(J_2=2).\end{cases}$$

TABLE II. Neutron scattering cross section of Mn.

E ev	$\sigma_s(\epsilon)$ —barns Measured	Calculated (3, 2)	Calculated (2, 3)
10.0	2.26	2.29	2.36
19.5	2.37	2.46	2.59
120	6.01	6.33	7.68

[7] M. Hamermesh and C. O. Muehlhause, Phys. Rev. **78**, 175 (1950).

[7a] The Na—Mn resonance overlap is about 20 percent. The resonances are probably closer than 600 ev to cause this. ϵ_2(Mn) $=2400\pm500$ ev, and ϵ_1(Na) $=3000\pm600$ ev.

From the experiments of Fermi,[4] Shull,[3] and Bendt[8] it is evident that $\sigma_{\text{th s}} \sim \sigma_{\text{th coh}}$. In an actual neutron crystal diffraction experiment, temperature effects and crystal imperfections increase $\sigma_{\text{th inc}}$ at the expense of $\sigma_{\text{th coh}}$. However, there are two sets of a_r values above that satisfy the condition: $\sigma_{\text{th s}} \sim \sigma_{\text{th coh}}$. This can be expressed by stating that $J_1 \neq J_2$. Application of formula (7) demonstrates the above (a_1 and a_2 would have the same sign if $J_1=J_2$). In Section V of this paper it is shown that any reasonable fit to the total cross-section data yields $\sigma_{\text{th s}}=2.13\pm0.05b$. The two possibilities ($J_1=3$, $J_2=2$) and ($J_1=2$, $J_2=3$) are now to be considered.

Case (3, 2):

$$\sigma_{\text{th inc}}/4\pi = 7/12\times 5/12(0.768-0.588)^2 \sim 7.87\times 10^{-3};$$

i.e., $\sigma_{\text{th coh}} \sim 2.03b$; and

$$-(2.03/4\pi)^{\frac{1}{2}} = R - 0.448 - 0.245;$$

i.e., $R=0.291b^{\frac{1}{2}}$.

Case (2, 3):

$$\sigma_{\text{th inc}}/4\pi = 7/12\times 5/12(1.075-0.420)^2 \sim 0.104;$$

i.e., $\sigma_{\text{th coh}}=0.82b$; and

$$-(0.82/4\pi)^{\frac{1}{2}} = R - 0.448 - 0.245;$$

i.e., $R=0.437b^{\frac{1}{2}}$.

Both cases agree sufficiently well with the values of $\sigma_{\text{th coh}}$ given in the literature. However, the next two experimental sections demonstrate that the case (3, 2) is the correct one.

IV. EXPERIMENTAL MEASUREMENT OF $\sigma_{1\max}$

The peak cross section of the 345-ev resonance is determined by the method of self-indication as outlined in Section II. Two thin manganese foils of mean thickness 7.097×10^{19} atoms/cm^2 serve as activation detectors in a cadmium filtered $1/\epsilon$ distributed pile neutron beam.[1] Two aluminum cells, one filled with D_2O and the other $D_2O-MnSO_4$ (3.28×10^{19} atoms Mn/cm^2) serve as filters for the detectors. The cells and detector foils are mounted on a four-foot long shaft, the axis of which is parallel to the neutron beam. The shaft slowly rotates the cells and foils in and out of the neutron beam, thereby insuring a self-monitoring system. That is, the neutron transmission of the $MnSO_4$ is given by I_1/I_2, where foil #1 is behind the cell containing the $MnSO_4$, and foil #2 is behind the blank cell. Figure 1 illustrates the experimental arrangement.

The foils are bombarded to saturation and are counted simultaneously on two well-matched Geiger counters for three half-lives ($T_{\frac{1}{2}}=2.59$ hr.). To avoid asymmetry in the counting apparatus, the experiment is re-run with the roles of the foils exchanged as to cell and counter. A geometric mean transmission is then calculated, the result being $\sigma_{\text{self}}=1490\pm250b$.

Three corrections to the expected value of σ_{self} must be made, all of which lower it from $\sigma_{\max}/2$. These are (a) 4.43 percent Cu–Ni impurity, (b) foil thickness, and (c) absorption resolution. The second of these depends on which J value is assumed for the 345-ev level, and the third is given by the fraction of resonance absorption to total epi-cadmium absorption (includes $1/v$ absorption). A cadmium ratio[1] measurement of the thin manganese foils standardized by a cadmium ratio measurement of gold and boron ($1/v$ absorber) enables one to evaluate both the resonance absorption integral and the $1/v$ absorption integral. This method is described in a previous paper.[1] The results are

$$\sum_{1/v} = 6.2b \quad (1/v \text{ abs. integral}), \text{ and}$$
$$\sum_a = 14.1b \quad (\text{res. abs. integral});$$

and the resonance absorption fraction, ρ, is given by

$$\rho = \sum_a/(\sum_{1/v}+\sum_a) = 0.694.$$

Making the various corrections indicated permits two possible observable self-indication cross sections:

$$\sigma_{1\text{ self}} = \begin{cases} 1470b (J_1=3) \\ 1070b (J_1=2). \end{cases}$$

In the above it is assumed that negligible absorption occurs at 2400 ev. This assumption is now justified by the fact that the observed value of σ_{self} agrees with the higher predicted value of $\sigma_{1\text{ self}}$. The self-monitoring value of $1490b$ indicates strong preference[9] for $J_1=3$ and, therefore, for the case (3, 2).

That the resonance absorption integral is mainly associated with the 345-ev level is evident from application of formulas (9) and (11). In this calculation, the thermal absorption cross section ($12.1b$) is taken from pile oscillation values,[10] and one obtains $\sum_{a1}=10.2b$. This is about 70 percent of the measured value. The discrepancy may be due either to experimental errors, to a possible failure of Γ_γ to be independent of energy, or to a 2400 ev contribution to $\sum_a$. At any rate, a value of $\sum_{a1}=10.2b$ does not invalidate the above conclusion that $J_1=3$, since the value of ρ cannot change much and consequently neither can σ_{self}. The following resonance widths are also readily computed from formulas (9)–(12):

$$\Gamma_{\gamma 1} \simeq 0.6 \text{ ev}, \quad \Gamma_{n1}=21.6 \text{ ev}, \quad g_1\Gamma_{n1}=12.6 \text{ ev};$$
$$\Gamma_{\gamma 2} \sim 0, \quad \Gamma_{n2}=304 \text{ ev}, \quad g_2\Gamma_{n2}=127 \text{ ev}.$$

If $\Gamma_{\gamma 2} \sim 1$ ev, the contribution to the thermal capture cross section from the 2400 ev resonance is given by Eq. (9), namely, $\sim 2b$. This quantity is significant, but within the experimental error of both σ_{self} and $\sum_a$.

In the following section, it is necessary to know the

[8] P. J. Bendt and I. W. Ruderman, Phys. Rev. 77, 575 (1950).

[9] Seidl, Harris, and Langsdorf, Phys. Rev. 72, 168A (1947).

[10] Harris, Muehlhause, Rasmussen, Schroeder, and Thomas, Phys. Rev. 80, 342 (1950).

absorption cross section of manganese below 150 ev. Since the thermal value of $12.05\pm0.05b$ is well measured and most of this is associated with the 345-ev resonance, it is sufficient to assume

$$\sigma_a=[\sigma_{\text{th }a}/(40\epsilon)^{\frac{1}{2}}][\epsilon_1/(\epsilon_1-\epsilon)]^2 =[12.05/(40\epsilon)^{\frac{1}{2}}][345/(345-\epsilon)]^2. \quad (14)$$

V. EXPERIMENTAL MEASUREMENT OF $\sigma_T(\epsilon)$

The apparatus employed here is the same as that described in Section III. The method consists in using various resonance scattering detectors such as Co^{59} (120 ev), W^{186} (19.5 ev),[11] and Sm^{152} (10.0 ev) in order to select neutron energies at which manganese transmission cross sections can be measured. This method has been described by the authors in connection with similar transmission measurements made on chlorine.[12] The total manganese cross section at the cobalt point is corrected for the fraction of cobalt resonance scattering of the total epi-cadmium cobalt scattering.[13] Formula (14) is used to obtain the net or scattering cross section at the various energies selected. Table I lists the data obtained.

Preliminary fitting of the data in Table I for either case (3, 2) or (2, 3) indicates $\sigma_{\text{th }s}=2.13\pm0.05b$. Now the resonance parameters obtained in Sections III and IV are used to evaluate $\sigma_s(\epsilon)$. To do this the following two-level Breit-Wigner formula is considered ($\Gamma_r\ll[\epsilon_r-\epsilon]$):

$$\sigma_s(\epsilon)/4\pi=R^2+g_1a_1\{[\epsilon_1/(\epsilon_1-\epsilon)]^2a_1 -[\epsilon_1/(\epsilon_1-\epsilon)]2R\}+g_2a_2\{[\epsilon_2/(\epsilon_2-\epsilon)]^2a_2 -[\epsilon_2/(\epsilon_2-\epsilon)]2R\}. \quad (15)$$

Two sets of parameters must be tried in Eq. (15) corresponding to the two cases: (3, 2) and (2, 3). Table II lists the observed and calculated cross sections. It should be observed that both sets of calculated values approach the proper thermal scattering cross section at low energies. The crucial test is at the cobalt point. It is evident by inspection that case (3, 2) fits better than case (2, 3). This is in agreement with Section IV wherein $J_1=3$ is also preferred.

VI. DISCUSSION OF RESULTS

Independent measurements of the resonance scattering properties of manganese can all be fitted to the following two-level Breit-Wigner formula:

$$\sigma_s/4\pi\simeq0.085 +331\{1+(\epsilon-345)/455\}/\{1+[(\epsilon-345)/11.1]^2\} +36.0\{1+(\epsilon-2400)/2430\}/\{1+[(\epsilon-2400)/152]^2\}.$$

Only one parameter, the nuclear radius, need be adjusted to do this. When this is done, it is possible to obtain

(a) the total thermal scattering cross section,
(b) the coherent thermal scattering cross section,
(c) the negative thermal scattering length,
(d) the thermal capture cross section,
(e) the proper behavior of the cross section in the wings of the resonance,
(f) the angular momenta of the two levels, and
(g) justification of $\Gamma_n\propto\epsilon^{\frac{1}{2}}$.

The last conclusion is a necessary consequence of the good fit. One important point remains: Γ_r appears to vary as ϵ_r (though here the r refers to different J). This is also the situation in sodium.[2] If this be true, a_r might decrease sufficiently slowly with increasing r to make it doubtful that enough resonance terms have been included in the expressions for the thermal cross sections. The effect of higher or negative energy levels is to alter the effective value of the nuclear radius. Since bound states (i.e., real levels) should have very little scattering, the most important a_r terms are for r positive; i.e., $\epsilon_r>0$. Such unaccounted-for resonance levels in manganese have the effect of decreasing the apparent nuclear radius, and also of perturbing the calculated thermal coherent scattering cross section in a nonlinear way. The apparent radius deduced in the text is smaller than that obtained by the $A^{\frac{1}{3}}$ rule ($\sim0.52b^{\frac{1}{2}}$). This may or may not be taken seriously.[6] At any rate, if one assumes a higher energy resonance having thermal amplitude a_3, its effect would be to increase R and to lower $\sigma_{\text{th coh}}$. However, in view of the good fit obtained by considering only two levels, the authors believe that a_3 is not of sufficient magnitude to invalidate the essential conclusions drawn from the work.

[11] Argonne Resonance Region Time-of-Flight Velocity Selector, W. Selove.
[12] C. T. Hibdon and C. O. Muehlhause, Phys. Rev. 79, 44 (1950).
[13] C. T. Hibdon and C. O. Muehlhause, Phys. Rev. 76, 100 (1949).

Measurements of Short-Lived Isomers*

W. J. MacIntyre†
Sloane Physics Laboratory,‡ Yale University, New Haven, Connecticut
(Received August 21, 1950)

The half-lives of eight short-lived isomers were investigated by the delayed coincidence method of detecting short-lived excited gamma-states following beta-emission. Of these, the half-life of Hg^{198*} following beta-decay of Au^{198} was measured as 2.3×10^{-8} sec. Excited states of Mg^{24*}, Hg^{199*}, Ca^{42*}, Nd^{142*}, A^{38*}, Te^{122*}, and Fe^{56*} were found to have half-lives shorter than 1 to 2×10^{-8} sec., the lowest value measurable, owing to circuit limitations.

By means of the measured half-lives or upper limits, probable l values, the change in units of angular momentum, were assigned through comparison with the theoretical values of the Segrè-Helmholz formula. Correlation with l values estimated through other methods has resulted in probable assignment of l values for four isomers and upper l values for the remaining four.

I. INTRODUCTION

THE measurement of short-lived nuclear isomers by the method of delayed coincidences has been recently employed by many investigators.[1-3] With the development of scintillation counters of fast decay time, half-lives of the order of 10^{-8} to 10^{-9} second can be measured.[4-6]

The delayed coincidence method refers to the measurement of the time interval between the formation of the excited state and emission of the gamma-ray from the decay of the state. In the following work the time reference for the formation of the state is taken to be the emission of a beta-particle leading to the excited state. The general relationship for the number of coincidences per second as a function of delay time, T, as the pulse from the beta-detector is delayed is thus:

$$C=2\tau N_1N_2\lambda e^{-\lambda T},$$

where τ is the resolving time of the coincidence circuit, λ is the decay constant, N_1 is the counting rate of the beta-particles, and N_2 is the number of gamma-rays per beta-disintegration. This equation neglects the variation of pulses in the detector or assumes that this variation is very small with respect to the delay time.

Van Name[7] has shown the value of the consideration of time of pulse formation in the interpretation of results from delayed coincidence counting. By assuming a triangular distribution of pulses about the mean time of pulse formation, Van Name derived directly the variation of coincidences as a function of delay time. Binder[8] has developed an analysis similar to Van Name's by assuming a Gaussian spread for the pulses. Computations from this assumption are simple, since one expression is valid for the entire range of the curve.

In all three expressions the coincidence rate approximates an exponential function for large delay times, which relationship has also been shown by Newton.[9] The analyses show that a plot of the logarithm of the counting rate *versus* delay time will fall off with a slope of λ, this method being used for calculation of half-life in this work. The entire curve has been fitted by Binder[8] and the upper limit estimated from the constants of the theoretical curve with the shortest half-life that deviates appreciably from the symmetric curve. This limit has been placed at 1 to 2×10^{-8} second, dependent on the resolution. As a measured half-life of 2.3×10^{-8} sec. deviates markedly from the symmetric curve, the writer feels this limit is justified experimentally.

II. CORRELATION WITH THEORETICAL PREDICTION OF ISOMERIC HALF-LIFE

A simple relationship between the decay constant, λ, and l, the change in angular momentum, has been previously derived by Segrè and Helmholz.[10,11] Segrè and Helmholz point out that their assumption that the dimension of the radiation multipole be equal to the nuclear radius ($A^{\frac{1}{3}}\times1.45\times10^{-13}$ cm) is only a crude approximation; but since a change of angular momentum of one unit in l may result in a difference of predicted half-life by a factor of 10^5, this formula is sufficient to assign l values to the gamma-ray transition. With so great a change, a difference in the measured value by as much as a factor of 100 would not prohibit the l assignment. Such assignment is not necessarily definite, but merely the closest fit to the theoretical prediction. This formula in general predicts somewhat too large a value for the half-life; therefore, in half-

* Part of a dissertation presented to the Faculty of the Graduate School of Yale University in candidacy for the degree of Doctor of Philosophy.

† Now at the Atomic Energy Medical Research Project, Western Reserve University, Cleveland, Ohio.

‡ Assisted by the joint program of the ONR and AEC.

[1] S. DeBenedetti and F. K. McGowan, Phys. Rev. **74**, 728 (1948).

[2] Bowe, Goldhaber, Hill, Meyerhof, and Sala, Phys. Rev. **73**, 1219 (1948).

[3] P. T. Bittencourt and M. Goldhaber, Phys. Rev. **70**, 780 (1946).

[4] F. K. McGowan, Phys. Rev. **77**, 138 (1950).

[5] M. Deutsch and W. G. Wright, Phys. Rev. **77**, 139 (1950).

[6] R. E. Bell and R. L. Graham, Phys. Rev. **78**, 490 (1950).

[7] F. W. Van Name, Jr., Phys. Rev. **75**, 100 (1949).

[8] D. Binder, Phys. Rev. **76**, 856 (1949).

[9] T. D. Newton, Phys. Rev. **78**, 490 (1950).

[10] A. C. Helmholz, Phys. Rev. **58**, 48 (1941).

[11] E. Segrè and A. C. Helmholz, Rev. Mod. Phys. **21**, 271 (1949).

lives falling between two l values, the shorter predicted half-life is preferred.

III. DESCRIPTION OF EQUIPMENT

For the detection of beta-particles, cylindrical proportional counters were used. The length measured five-eighths inch, with a one-quarter-inch inside diameter centered about a three-mil coaxial wire. The small size resulted in a low geometrical efficiency, but was designed to keep the random fluctuations at a minimum. These counters were used by Farley[12] in detection of heavy particles (protons, deuterons, tritons, and alpha-particles). By resolution curves, Farley[12] has shown the pulses to be very sharp, rising at least as fast as 5×10^{-8} sec.

For the detection of gamma-rays a scintillation counter with selected 931A electron multiplier tube was used, operating at dry ice temperature. Although naphthalene and calcium fluoride crystals were initially tried as scintillation phosphors, both exhibited decay times which were too long[13] for use. Polystyrene showed the fastest resolving time and a decay time too fast to be detected with this equipment. The pulses from polystyrene were extremely small and hard to detect,[14] but at the time of these measurements the faster organic crystals such as stilbene were not generally available.

As a preamplifier for the electron multiplier tube the cathode follower shown in Fig. 1 was used. This is similar to the cathode preamplifier used by Farley except for the resistance network used to apply voltage steps to the 931A electron multiplier tube. This circuit has a wide band width (over 25 Mc/sec.); and although the gain is low, this is no disadvantage since greater amplification is available in the linear amplifier than is required.

Although a similar cathode follower was originally used with the proportional counter for heavy particle

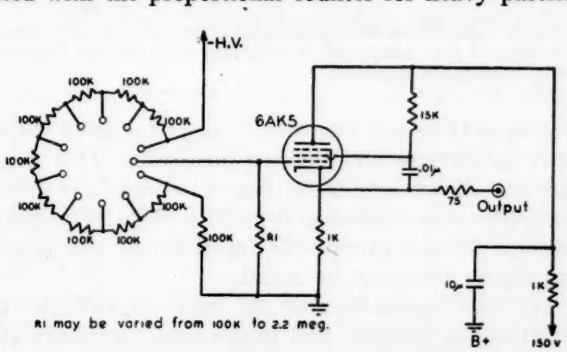

FIG. 1. Electron multiplier preamplifier for scintillation counter. Outputs of both preamplifiers are carried through RG11U coaxial cable to amplifiers of 75-ohm input.

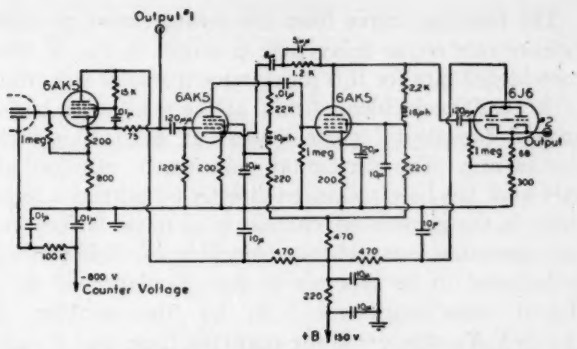

FIG. 2. Preamplifier for proportional counter. Output #1 is used for detection of heavy particles. Output #2 includes one stage of amplification and is used for detection of β-particles.

detection, the smaller pulses from beta-particles made the addition of one section of amplification necessary. After the cathode follower for impedance matching, one section of the wide-band amplifier developed by Schultz[15] was added. The band width of these pairs is 23 to 26 Mc/sec. and, as the output is again a cathode follower for line matching, the entire preamplifier is of this band width. This circuit is shown in Fig. 2. The linear amplifiers themselves consist of sections of these feed-back pairs terminated by the 6J6 cathode-follower output of Fig. 2.

The coincidence circuit was developed by Farley and possesses a threshold delay time of the discriminator of approximately 2×10^{-9} sec. With the counters described, resolution as low as 10^{-8} sec. has been reached; but 3.8×10^{-8} sec. is usual.

For a variable delay, lengths of seventy-ohm coaxial cable (RG 11/U) was used. The velocity of a pulse in this line has been found to be 2×10^{10} cm/sec.; thus, a convenient length of two meters of this cable represents a time delay of 10^{-8} sec.

IV. RESULTS OF ISOMER MEASUREMENTS

A. Na^{24}

While early investigation on the disintegration of Na^{24} gave rise to conflicting reports, most of the later work is in general agreement with Siegbahn,[16] indicating a beta-ray group of 1.39-Mev peak energy and two gamma-rays of 1.38 and 2.76 Mev.

The Na^{24} source was placed between the proportional counter and the polystyrene counter with a brass absorber screening the gamma-scintillation counter from the beta-particles. Since the proportional counter has a low efficiency for gamma-rays, this arrangement resulted in the detection of beta-particles alone by the proportional counter and gamma-rays alone by the scintillation counter. This detection is important for this case, which involves cascaded gamma-rays, since it proves the data obtained are for $\beta-\gamma$ coincidences and not $\gamma-\gamma$.

[12] B. G. Farley (to be published). Ph.D. thesis, Yale University, 1948.
[13] W. J. MacIntyre, Phys. Rev. **75**, 1439 (1949).
[14] G. N. Harding of the Atomic Energy Research Establishment at Harwell, England, has estimated that the pulses from polystyrene were about one-tenth the size of those from naphthalene (private communication).
[15] H. L. Schultz, "High speed counter and short pulse techniques." Brookhaven Conference Report, p. 35, (August 1947).
[16] K. Siegbahn, Phys. Rev. **70**, 127 (1947).

The resulting curve from the measurement of coincidence rate *versus* delay time is shown in Fig. 3. The coincidence rate for this measurement was of the order of 50 to 200 coincidences/min. at the peak, with background (accidental coincidences) at 8 to 40 coincidences/min. The accidental coincidence rate on all this work has been measured directly by putting a large delay in the gamma-ray channel so as to get far beyond the resolution curve of true coincidences. This method is believed to be superior to the calculation of accidental coincidence rate, A, by the relation of $A=2\tau N_1 N_2$, where τ is the resolving time, and N_1 and N_2 are the single rates in both channels. This formula makes assumptions both on the circuit and the invariance of τ.

Although the curve of Fig. 3 shows a slight asymmetry to the trailing edge, it is too fast for this equipment to measure, and gives essentially a resolution curve as obtained by simultaneous stimulation of both counters. Measured states as fast as 2×10^{-8} sec. show a marked asymmetry; in addition, the theoretical work of Binder has shown that states with a half-life as low as 1×10^{-8} sec. can be detected by the change in shape of the coincidence rate curve. From this observation it is estimated that the excited states of Mg^{24*}, formed by beta-decay of Na^{24}, must have a half-life shorter than 1×10^{-8} sec.

The zero point for delay time is arbitrary, since the amplifiers and other circuits are not balanced exactly. Also, the placement and shape of the source may cause shifting of the zero point, which may explain the variation of the zero point in the succeeding resolution curves.

For the gamma-ray of energy 1.38 Mev, the Segrè-Helmholz formula predicts a half-life of 6×10^{-13} sec. for $l=2$; 2×10^{-8} sec. for $l=3$; and 1×10^{-4} sec. for $l=4$,

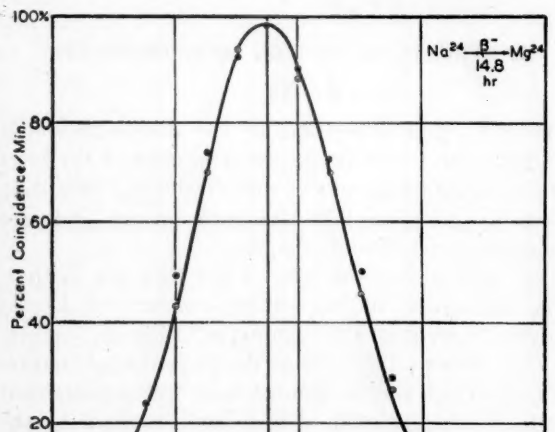

FIG. 3. Coincidence rate *versus* delay time curve for Na^{24} decay. Plus values of delay time refer to delay added to β-channel. Symmetry of the curve indicates the state to be too fast to be measured by this equipment.

indicating an l change of three or less, with three itself doubtful.

From the lack of sharp resonance absorption in scattering experiments on these gamma-rays, Pollard and Alburger[17] have shown that the radiation must involve an l value of two or higher. From a combination of these two experiments, it seems probable that the transition of both gamma-rays is $l=2$. This result is also consistent with the conclusions of Brady and Deutsch,[18] who have measured the angular correlations of the gamma-rays and placed the spin of the levels in Mg^{24*} at 4, 2, and 0, a difference of two between the levels.

B. Cl^{38}

Although the disintegration scheme of Cl^{38} is complex, most measurements have been consistent with the

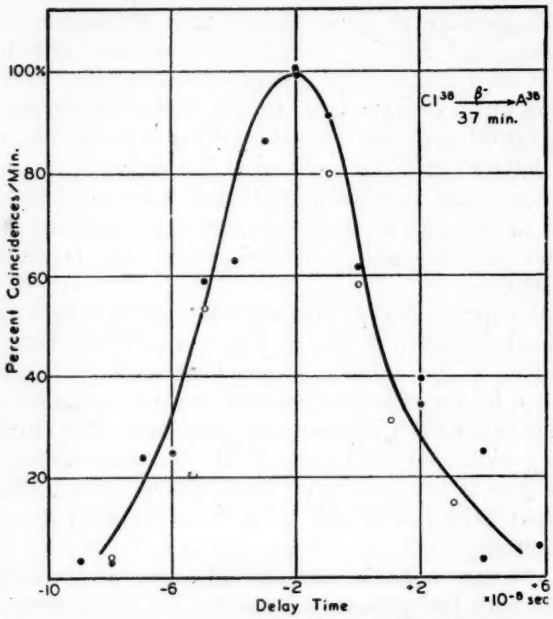

FIG. 4. Coincidence rate *versus* delay time curve for Cl^{38} decay. The point of zero delay time is arbitrary, since the two channels are not necessarily balanced.

scheme of Hole and Siegbahn,[19] except for small variations in energies and relative intensities. This work shows a direct beta-transition, a second beta-group followed by one gamma-ray, and a third beta-group followed by one gamma-ray transition to the second gamma-ray transition in cascade.

The two gamma-transitions have comparable intensities and energies, and thus would contribute approximately equal effects on the curve. In the event a measurable half-life had been found, additional absorption experiments would have been necessary in order to identify to which transition this half-life belonged. Figure 4 is seen to be symmetric, however, which shows

[17] E. C. Pollard and D. E. Alburger, Phys. Rev. 74, 926 (1948).
[18] E. L. Brady and M. Deutsch, Phys. Rev. 74, 1541 (1948).
[19] N. Hole and K. Siegbahn, Arkiv. Mat. Astron. Fys. 33A, No. 9 (1946).

the transition half-lives to be less than 1×10^{-8} sec.

For the 1.60-Mev gamma-ray of A^{38*}, the Segrè-Helmholz equation shows a half-life of 2×10^{-13} sec. for $l=2$; 2×10^{-9} sec. for $l=3$; and 1×10^{-5} sec. for $l=4$. Similarly, for the 2.12-Mev gamma-ray a half-life of 4×10^{-10} sec. for $l=3$ and 6×10^{-7} sec. for $l=4$ is predicted. From this prediction the transitions are assigned an l value of equal to or less than three.

Hole and Siegbahn[19] have assigned spin values for the various levels of A^{38}; and, from the degree of forbiddeness of the beta-particle transitions from Cl^{38} decay, have concluded that both the ground level and the second excited level have spins of zero and the first excited level a spin of one or two. This conclusion leads to an l value equal to or less than two for both gamma-

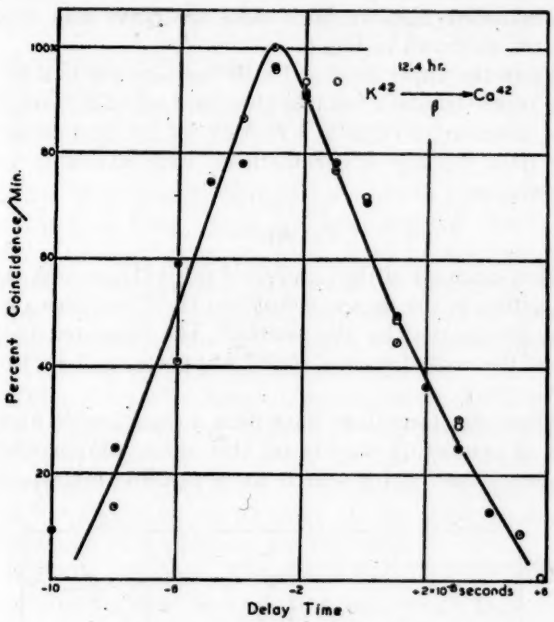

FIG. 5. Coincidence rate *versus* delay time curve for K^{42} decay.

transitions, this value being consistent with the above measurement.

Langer's[20] interpretation from his measurements places the spin of the ground level of A^{38} at zero and the second excited level of A^{38*} at three. This scheme is also consistent with the values obtained from the upper half-life limit.

The curve of Fig. 4 is seen to be less clearly defined than that of Fig. 3. This difference is probably the effect of poorer statistical accuracy, since the short half-life of Cl^{38} necessitated coincidences taken per number of single counts at low counting rates where accidentals were negligible. As the accidentals vary as the second power of the counting rate, it is advantageous to minimize their effect so that decay of the parent state may be easily accounted for.

[20] L. M. Langer, Phys. Rev. **77**, 52 (1950).

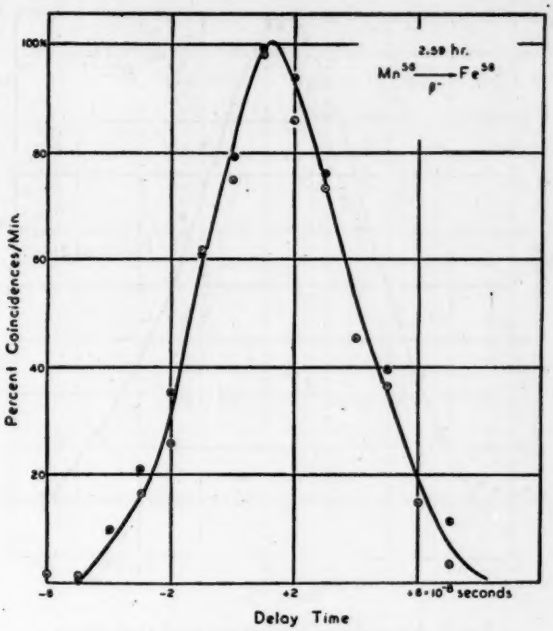

FIG. 6. Coincidence rate *versus* delay time curve for Mn^{56} decay.

C. K^{42}

The decay of K^{42} involves only one gamma-ray of 25 percent intensity as given by Siegbahn.[21] Good counting statistics were hard to obtain, since the strong (75 percent) beta-particle transition to ground state raised the background of accidental coincidences.

The data are plotted in Fig. 5 and show a predominately symmetric curve. The resolution of this curve is not as sharp as the previous curves (probably owing to the strong beta-transition), so that the upper limit of the half-life is placed at less than 2×10^{-8} sec. rather than less than 1×10^{-8} sec., to which the sharper resolution curves can be read.

Theoretical predictions from the Segrè-Helmholz equation show a half-life of 2×10^{-13} sec. for a value of $l=2$; 3×10^{-9} sec. for $l=3$; and 1×10^{-5} sec. for $l=4$. This prediction indicates a value for l of possibly three but more probably two or less.

In an interpretation of K^{42} radioactivity by Shull and Feenberg[22] from an analysis of Siegbahn's data for a characteristic forbidden type of energy distribution of the beta-transition, the value of l for the transition of Ca^{42*} was placed at two. The combination of investigations show that l is probably two.

D. Mn^{56}

In spite of the complexity of the transitions and the varied types of investigations, almost all data obtained on Mn^{56} decay are consistent with the decay scheme advanced by Elliot and Deutsch,[23] and by Siegbahn

[21] K. Siegbahn, Arkiv. Mat. Astron. Fys. **34B**, No. 4 (1948).
[22] F. B. Shull and E. Feenberg, Phys. Rev. **75**, 1768 (1949).
[23] L. G. Elliot and M. Deutsch, Phys. Rev. **64**, 321 (1943).

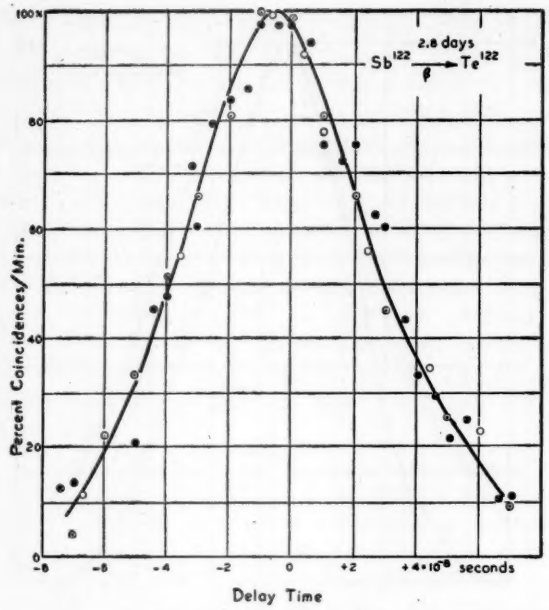

FIG. 7. Coincidence rate *versus* delay time curve for Sb^{122} decay.

and Johannson.[24] This scheme shows all excited levels decaying to the ground state by the path of the 0.822-Mev gamma-transition. The ratio of the intensity of this transition to that of the next strongest transition is then 10:3, so that the measurement will be dominated by this 0.822-Mev gamma-ray.

Good counting statistics were obtained on this measurement with a rate of 1000 to 1500 coincidences/min. This rate is shown by the well-defined curve of Fig. 6, which is also seen to be symmetric and indicates a half-life less than 1×10^{-8} sec. Comparison with the Segrè-Helmholz formula yields a prediction for an l value of two or less.

Elliot and Deutsch,[23] and, independently, Siegbahn and Johannson,[24] have suggested possible angular momentum units for the decay scheme of Mn^{56} which placed the ground state of Fe^{56} at zero and the 0.822-Mev state of Fe^{56*} at one. This value of $l=1$ falls within the l values obtained from the half-life limit.

E. Sb^{122}

The decay scheme of Sb^{122} shows a single gamma-ray of 0.57 Mev as measured by Rall and Wilkinson,[25] by Kern, Zaffarano, and Mitchell,[26] and by Cook and Langer.[27]

The measurements on this state as plotted in Fig. 7 show a symmetric curve and consequently a half-life less than 1×10^{-8} sec. Comparison with the Segrè-Helmholz formula places the l value at two or less. Although internal conversion of the gamma-ray has been noted by Rall and Wilkinson,[25] the coefficient has not yet been measured. This measurement would provide an independent check on the l value, but to date no correlation is possible.

F. Pr^{142}

The exact decay scheme of Pr^{142} is still subject to investigation, but there is reasonable agreement on a gamma-ray emission of low intensity and energy 1.5 to 2.2 Mev. Mandeville[28] has placed this gamma-ray energy at 1.74 Mev and coupled to a soft beta-spectrum (~0.215 Mev) with an occurrence about one-fiftieth of the strong 2.22 Mev beta-particle transition. This observation is reasonably consistent with other findings.

In this measurement both the proportional counter and a second polystyrene scintillation counter were used for beta-detection. In both cases the curve was symmetric, as shown in Fig. 8.

From the upper limit of 1×10^{-8} sec. on the half-life, the Segrè-Helmholz formula gives an l value of three or less, assuming a value of 1.74 Mev for the gamma-ray. No data for any other methods were available for correlation.

G. Au^{198}

Measurement of the half-life of the 0.411 gamma-ray transition in the decay of Au^{198} to Hg^{198} has been previously reported by this writer.[29] The measured half-life of the excited state of Hg^{198*} was placed at 2.3×10^{-8} sec.

Since that time there have been a considerable number of conflicting reports on this state. Mandeville[30] reported that in his search for a possible metastable

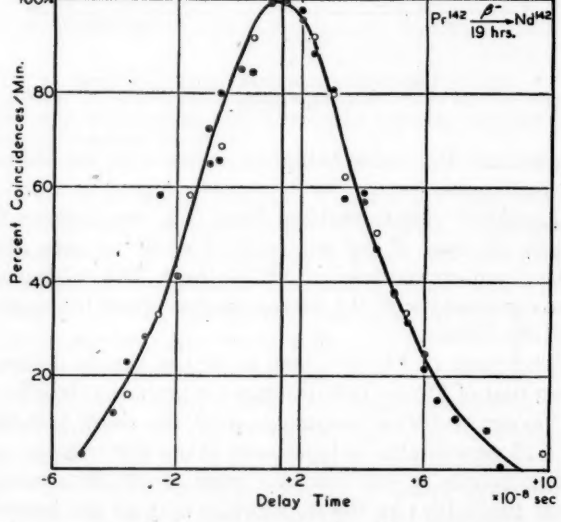

FIG. 8. Coincidence rate *versus* delay time curve for Pr^{142} decay.

[24] K. Siegbahn and Johannson, Arkiv. Mat. Astron. Fys. **34A**, No. 10 (1947).
[25] W. Rall and R. G. Wilkinson, Phys. Rev. **71**, 321 (1947).
[26] Kern, Zaffarano, and Mitchell, Phys. Rev. **73**, 1142 (1948).
[27] C. S. Cook and L. M. Langer, Phys. Rev. **73**, 1149 (1948).
[28] C. E. Mandeville, Phys. Rev. **75**, 1257 (1949).
[29] W. J. MacIntyre, Phys. Rev. **76**, 312 (1949).
[30] C. E. Mandeville, private communication.

TABLE I.

Isomer parent	Measured half-life (seconds)	Theoretical half-lives (Segrè-Helmholz formula) (seconds)			Indicated l value from half-life	Indicated l value from other measurements	Probable l assignment
Mg^{24*}←Na^{24}	$>1\times10^{-8}$	$l=2$ 6×10^{-13}	$l=3$ 2×10^{-8}	$l=4$ 1×10^{-4}	$l\leq2$	$l\geq2$[a]	$l=2$
A^{38*}←Cl^{38}	$>1\times10^{-8}$	$l=2$ 2×10^{-13}	$l=3$ 2×10^{-9}	$l=4$ 1×10^{-5}	$l\leq3$	$l\leq2$[b]	$l\leq2$
Ca^{42}←K^{42}	$>2\times10^{-8}$	$l=2$ 2×10^{-13}	$l=3$ 3×10^{-9}	$l=4$ 1×10^{-5}	$l\leq3$	$l=2$[c]	$l=2$
Fe^{56*}←Mn^{56}	$>1\times10^{-8}$	$l=2$ 3×10^{-12}	$l=3$ 1×10^{-7}		$l\leq2$	$l=1$[d]	$l=1$
Te^{122*}←Sb^{122}	$>1\times10^{-8}$	$l=2$ 6×10^{-12}	$l=3$ 4×10^{-7}		$l\leq2$	...	$l\leq2$
Nd^{142*}←Pr^{142}	$>1\times10^{-8}$	$l=3$ 1×10^{-10}	$l=4$ 1×10^{-7}		$l\leq3$	...	$l\leq3$
Hg^{198*}←Au^{198}	2.3×10^{-8}	$l=2$ 1.7×10^{-11}	$l=3$ 1.4×10^{-6}		$l=2\sim3$	$l=2\sim3$[e] $l=2$[f]	$l=2$
Hg^{199*}←Au^{199}	$>2\times10^{-8}$	$l=2$ 1×10^{-9}	$l=3$ 5×10^{-7}		$l\leq2$	...	$l\leq2$

[a] See references 17 and 18.
[b] See references 19 and 20.
[c] See reference 22.
[d] See references 23 and 24.
[e] D. Saxon and R. Heller, Phys. Rev. 75, 909 (1949).
[f] D. Saxon, private communication.

state in this decay by looking for a loss in beta-gamma coincidences from Au^{198} by reduction of resolving time of their coincidence circuit from 1.0 microsecond to 0.035 ± 0.0002 μsec., a decrease was noticed at the lower limit. This observation indicating a barely measurable lifetime for the Hg^{198*} state, but their statistical limit was too great for an accurate estimate.

Bell and Petch[31] attempted measurement of this state with negative results. With their equipment a completely symmetrical curve was plotted, from which an upper limit of 3×10^{-9} sec. was obtained. Deutsch and Wright[5] also obtained negative results and placed an upper limit of 4×10^{-9} sec. on this state.

Recently, Jastram, Konneker, and Cleland[32] measured this state at $(4\pm1)\times10^{-8}$ sec., which is in fair agreement with this writer's results. Correlation with the Segrè-Helmholz formula has been previously reported.[28]

H. Au^{199}

The decay of Au^{199} involves only one beta-particle of energy, about 0.32 Mev, and several gamma-rays, as reported by Beach, Peacock, and Wilkinson,[33] and by Meem and Maienschein,[34] with the strongest gamma-ray about 0.230 Mev.

The coincidence curve taken on this decay gave poor resolution and poor statistical accuracy. The obtained curve was roughly symmetric, however, and no measurable half-life found. The upper limit of half-life was estimated at less than 2×10^{-8} sec. This placed the transition of the strongest gamma-ray at l equal to or less than two by correlation with the Segrè-Helmholz formula.

A summary of all the above results with prediction of l values from the Segrè-Helmholz formula, correlation with l values obtained from other methods, and probable l assignments is shown in Table I.

The author wishes to express his thanks to Professor Ernest C. Pollard for valuable discussions throughout, and to Professor Howard L. Schultz for numerous discussions on equipment design and coincidence techniques.

[31] R. E. Bell and H. E. Petch, Phys. Rev. 76, 1409 (1949).
[32] Jastram, Konneker, and Cleland, Phys. Rev. 79, 243 (1950).
[33] Beach, Peacock, and Wilkinson, Phys. Rev. 76, 1585 (1949).
[34] J. L. Meem, Jr. and F. C. Maienschein, Phys. Rev. 76, 328 (1949).

The Temperature Dependence of the Self-Diffusion Coefficients of Argon, Neon, Nitrogen, Oxygen, Carbon Dioxide, and Methane*

EDWARD B. WINN**
Department of Physics, University of Minnesota, Minneapolis, Minnesota
(Received August 10, 1950)

The self-diffusion coefficients of A, Ne, N_2, O_2, CO_2, and CH_4 have been measured as functions of the temperature: A, Ne, N_2, and O_2 in the range -196°C to 80°C, CO_2 in the range -78.5°C to 80°C, and CH_4 in the range -183°C to 80°C. The experimental figures have been compared with values calculated on the assumption that the molecular interaction potential is of the form

$$V(r)=4\epsilon[-(r_0/r)^6+(r_0/r)^{12}].$$

With the exception of the lowest point for methane, all figures are in essential agreement with theory.

I. INTRODUCTION

A QUANTITY of considerable interest in the kinetic theory of gases is the coefficient of self-diffusion, which may be defined as a measure of the rate at which a group of gas molecules diffuses into another group composed of identical molecules. It is somewhat difficult to ascribe physical meaning to the process of self-diffusion under this definition, since, as long as the molecules are identical, there is no way of following the process, and hence no process really exists. However, if it be hypothesized that some of the molecules are tagged in such a way that the tagging does not affect the diffusion, then it would be possible actually to observe self-diffusion. Although such a method of tagging cannot exist, there are several devices by which good approximations to the self-diffusion coefficient of a gas may be obtained.

The most important of these devices involves the use of a tracer isotope, in which the mass of the molecule differs only slightly from the mass of the normal molecule. If a stable isotope be used as the tracer, then the diffusion process may be observed with a mass spectrometer; on the other hand, if it be a radioactive isotope, ordinary methods for the detection of radioactivity provide a means for watching the diffusion.

The interdiffusion of gases in general depends, among other factors, on the force fields of the diffusing molecules. Expressions which relate the coefficients of diffusion to these interaction potentials have been derived by Chapman and Cowling.[1] These relations and a knowledge of the values of the coefficients thus make it possible to infer something concerning the nature of the forces between the diffusing molecules.

The case of self-diffusion is by far the more attractive to consider, since only interactions between like molecules are involved. Also, the intermolecular potential for identical molecules is of the greater interest, since it is likewise involved in expressions for the other transport coefficients, as well as in the equation of state.

In the theory of Chapman and Cowling, the transport coefficients are expressed in terms of a set of collision integrals, $\Omega^{l}(n)$, the values of which depend upon the form chosen for the intermolecular potential function. It is practicable to evaluate these integrals analytically only for a few simple molecular models, such as const./r^n, n a positive integer, which have little or no real physical basis.

Recently Hirschfelder, Bird, and Spotz[2] carried out the numerical evaluation of a number of these integrals for the more realistic form of the potential function,

$$V(r)=4\epsilon[-(r_0/r)^6+(r_0/r)^{12}], \quad (1)$$

where r is the separation between the molecules, r_0 is the separation for which the energy of interaction is zero, and ϵ is the energy difference between the separated molecules and the molecules in the configuration for which they have the maximum energy of attraction.

The results are tabulated as the values of the functions $W^{l}(n;x)$, which are related to the $\Omega^{l}(n)$ of Chapman and Cowling by

$$\Omega^{l}(n)=r_0^2[2\pi kT/\mu]^{\frac{1}{2}}W^{l}(n;x), \quad (2)$$

where $x=\epsilon/kT$, k is the Boltzmann's constant, and μ is the reduced mass of the colliding molecules.

In the present paper are reported the results of the experimental determination of the self-diffusion coefficients of argon, neon, nitrogen, oxygen, carbon dioxide, and methane as functions of the temperature, stable isotopes being used as the tracers. These results are compared with the values calculated from the following expression for the first approximation to the self-diffusion coefficient, D_{11}, derived by Hirschfelder *et al.* in a later paper,[3] using the potential model of Eq. (1) and the basic theory of Chapman and Cowling:

$$(D_{11})_1=0.0013140T^{\frac{1}{2}}/[pr_0^2W^{1}(1;kT/\epsilon)M^{\frac{1}{2}}], \quad (3)$$

where p is the pressure in atmospheres, and M is the

* This research was supported by a joint ONR and AEC grant.
** Present address: Acetate Research Division, E. I. du Pont de Nemours and Company, Inc., Waynesboro, Virginia.
[1] S. Chapman and T. G. Cowling, *The Mathematical Theory of Non-Uniform Gases* (Cambridge University Press, London, 1939).
[2] Hirschfelder, Bird, and Spotz, J. Chem. Phys. 10, 968 (1948).
[3] Hirschfelder, Bird, and Spotz, Chem. Rev. 44, 205 (1949).

molecular weight. The second approximation to D_{11} is given by

$$(D_{11})_2=(D_{11})_1/(1-\Delta). \quad (4)$$

For all of the temperatures used in this work Δ is a very small quantity, and the difference between the first and second approximations is less than the experimental error.

The values of the quantities ϵ and r_0 involved in the expression for D_{11} can be determined from experimental measurements of the second virial coefficient. As a result of the numerical evaluation of the integrals in the expression given by Chapman and Cowling for the coefficient of viscosity, using the 6–12 potential model of Eq. (1), the values of ϵ and r_0 for pure gases can also be obtained from viscosity data. This has been done for a number of gases, including those reported here, by Hirschfelder *et al.*[3] The figures so obtained are found to be in close agreement with those computed from equation of state data.

II. APPARATUS

The apparatus in which the diffusions were carried out is illustrated schematically in Fig. 1. The diffusion system is patterned after a device originated by Ney and Armistead,[4] and consists of two identical cylindrical brass bulbs, *A* and *B*, having volumes of 357 cm³, which are mounted on a common axis and connected through a cylindrical brass tube, *C*. The connecting tube has a length of 8.006 cm and an inside diameter of 0.3250 cm, uniform to 0.0003 cm. The diffusions were performed by placing a sample of the normal gas in one bulb and a sample enriched in a tracer isotope in the other. Mixing then occurred by diffusion through the connecting tube, so that the isotopic consistency of the gas in either bulb varied with time.

These bulbs differ from earlier diffusion set-ups in that there is no isolating stopcock in the connecting tube, nor are there any valves in the filling lines immediately at the bulbs. This construction was chosen so that no difficulty would be encountered in the operation of necessary valves when the apparatus was immersed in a bath of extreme temperature.

The absence of a stopcock in the connecting tube necessitated the use of a somewhat more complicated filling system than would otherwise have been required. The bulbs are connected through copper filling capillaries to two Hoke toggle valves, *F* and *G*, mounted just outside of the temperature bath, *E*. The volume of the capillaries is less than 0.3 percent of the total volume of the bulbs, so that only a very small correction is needed to account for the effect of diffusion into and out of the capillary ends. The Hoke valves are set up side by side and connected together with a link so that they may be operated either individually or simultaneously.

[4] E. P. Ney and F. Armistead, Phys. Rev. 71, 14 (1947).

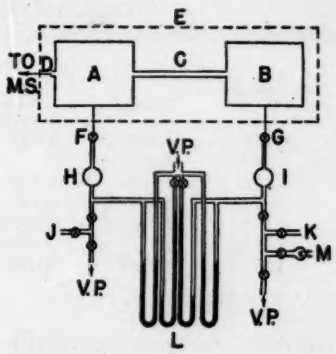

FIG. 1. Schematic diagram of the diffusion apparatus.

To fill the bulbs, samples are attached by means of grinds at *J* and *K*, and the entire system evacuated to a pressure less than 10^{-3} mm Hg, the pressure being indicated by a thermistor gauge attached at *M*. Evacuation is accomplished by a fore pump connected to the points *V. P.* Valves *F* and *G* are closed, and the samples are admitted to the filling reservoirs *H* and *I*, each of which is a glass bulb having a volume of 225 cm³. The sample pressures are matched by means of the comparison manometers, *L*, consisting of two mercury and two oil manometers. The oil manometers are mounted side by side, as shown, and are filled with Octoil, which, at room temperature, gives a magnification over mercury of 14.90 ± 0.03. When the samples are at the proper pressure, the toggle valves are snapped open simultaneously, and the samples in reservoirs *H* and *I* flow into bulbs *A* and *B* respectively. If the sample pressures have been chosen sufficiently near each other, then the observed equilibrium concentration of the tracer isotope is just that which is computed from the initial concentrations in the two samples, with an isolating stopcock assumed to be located at the midpoint of the connecting tube. This indicates that, for equal reservoir pressures, very little initial mixing occurs.

As soon as the equilibrium pressure is attained, within a few seconds after filling, the temperature and pressure are recorded, the toggle valves closed, and the diffusion allowed to proceed. A continuous analysis of the gas in bulb *A* is performed with a 60° Nier-type mass spectrometer, the bulb being connected to the spectrometer vacuum system through a fixed capillary leak, *D*. Since the initial concentrations of the tracer isotope in the two bulbs are not required for a calculation of the diffusion coefficient, any convenient time shortly after the start of the diffusion run may be taken as the time zero, and subsequent points measured from this reference. The final concentration of the tracer, after complete mixing, must be known, however. With an isolating stopcock in the connecting tube it is possible to compute this equilibrium concentration from a knowledge of the initial concentrations in the two bulbs. In the present apparatus, on the other hand, each run must be allowed to proceed to equilibrium, and the final concentration then measured. In theory, infinite time is required for complete mixing. Actually,

TABLE I. D_{11} for A^{40}.

Temperature °C	D_{11}, cm²/sec. Theory	Experiment: Present work	Experiment: Hutchinson
80.0	0.246	0.249 ±0.003	...
53.5	0.213	—	0.212 ±0.002
22.0	0.178	0.178 ±0.003	0.180 ±0.001
0	0.154	0.156 ±0.002	0.158 ±0.002
−78.5	0.0822	0.0830±0.0011	0.0833±0.0009
−183.0	0.0178	0.0180±0.0003	0.0277±0.0010
−195.5	0.0134	0.0134±0.0002	...

however, the error becomes unmeasurably small if the equilibrium concentration determination is made after about seven relaxation times have elapsed. With the temperatures and pressures used, the relaxation time of the system varied from one to three hours for the gases studied in this program.

All of the tracer isotopes used were concentrated by separation of the normal gas in thermal diffusion columns. The purity of the samples was quite good, being in no case less than 99 percent.

Each value tabulated for D_{11} for each gas is the unweighted mean of four runs at that temperature. In two runs of each set, the concentration of the tracer isotope in bulb A increased with time; in the other two runs, it decreased. With the exception of the methane runs at −183.0°C, the four results were always in excellent agreement.

The precision measures assigned to the tabulated results are the most probable errors computed from the scatter of the data over the four runs and from the various known experimental errors.

In calculation of the diffusion coefficients at the various temperatures, account was taken of the effect of the thermal expansion of the apparatus. The correction of the geometrical constant was in no case as large as one percent.

The figure actually measured in this study is the coefficient of diffusion of the tracer isotope into the normal isotope, D_{12}. Although in most cases this is a good approximation to the true self-diffusion coefficient, D_{11}, it would nonetheless seem worth while to calculate D_{11} from D_{12}. Hutchinson has shown[5] that the self-diffusion coefficient of a gas can be obtained from the coefficient of diffusion of one isotope into another

TABLE II. D_{11} for Ne^{20}.

Temperature °C	D_{11}, cm²/sec. Theory	Experiment
80.0	0.668	0.703 ±0.005
25.0	0.504	0.516 ±0.005
0	0.435	0.452 ±0.003
−78.5	0.246	0.255 ±0.004
−195.5	0.0492	0.0492±0.0004

[5] F. Hutchinson, J. Chem. Phys. 17, 1081 (1949).

TABLE III. D_{11} for $N^{14}N^{14}$.

Temperature °C	D_{11}, cm²/sec. Theory	Experiment: Present work	Experiment: Reference 6
80.0	0.273	0.287 ±0.009	...
25.0	0.203	0.212 ±0.005	0.219±0.009
0	0.174	0.185 ±0.006	...
−78.5	0.0946	0.104 ±0.002	...
−195.5	0.0161	0.0168±0.0003	...

by the following relation:

$$D_{11}=[2M_2/(M_1+M_2)]^{\frac{1}{2}}D_{12}, \quad (5)$$

where M_1 and M_2 are the masses of the two isotopes. The figures given for D_{11} in the accompanying tables were obtained from the observed D_{12} by means of this equation.

III. RESULTS

A. Argon

The results for argon, referred to 760 mm Hg pressure, are given in Table I. These results were obtained by observing the diffusion of argon having a 36/40 ratio of 0.051 into tank argon, which is more than 99 percent A^{40}.

The figures recorded in Table I were obtained by multiplying the observed coefficient of diffusion by the mass correction factor of 0.9736.

For purposes of comparison, the results of Hutchinson,[5] obtained from the diffusion of radioactive A^{41} into A^{40}, are reproduced here. It should be mentioned that his result at −183°C is the figure for one run only, after which run the apparatus was damaged, thus precluding further work at this temperature.

B. Neon

The results for neon, referred to 760 mm Hg, are given in Table II. These were obtained by allowing neon having a 22/20 ratio of 0.31 to diffuse into pure Ne^{20}. The coefficients are given as D_{11} for Ne^{20}, the observed figures being multiplied by the mass correction factor 1.0235.

C. Nitrogen

The results for nitrogen, at 760 mm Hg, are given in Table III. The tracer molecule used was $N^{14}N^{15}$, the sample enrichment being such that the 29/28 ratio was

TABLE IV. D_{11} for $O^{16}O^{16}$.

Temperature °C	D_{11}, cm²/sec. Theory	Experiment
80.0	0.279	0.301 ±0.004
25.0	0.206	0.232 ±0.006
0	0.176	0.187 ±0.003
−78.5	0.0944	0.104 ±0.002
−195.5	0.0154	0.0153±0.0002

TABLE V. D_{11} for $C^{12}O^{16}O^{18}$.

Temperature °C	D_{11}, cm²/sec. Theory	Experiment
80.0	0.149	0.153 ±0.003
25.0	0.109	0.113 ±0.002
0	0.0918	0.0974±0.0007
−78.5	0.0475	0.0500±0.0003

0.031. The mass correction applied to the observed D_{12} is 1.0087.

The room temperature value of D_{12} for $N^{14}N^{15}$ into $N^{14}N^{14}$ was reported earlier[6] from work with another apparatus. The data have been recalculated, and the mass correction factor applied, to give the result which is compared to the room temperature figure for D_{11} found in the present work.

D. Oxygen

The results for oxygen, referred to 760 mm Hg, are listed in Table IV. The tracer molecule was $O^{16}O^{18}$, the isotopic enrichment by thermal diffusion giving a 34/32 ratio of 0.56. The mass correction factor applied to the observed values of the diffusion coefficient to obtain those given in the table is 1.0151.

E. Carbon Dioxide

The diffusion coefficients for carbon dioxide, referred to 760 mm Hg, are given in Table V. The tracer molecules were those of mass 45, and were principally $C^{13}O^{16}O^{16}$, although a small amount of $C^{12}O^{17}O^{16}$ was present. Since the theory takes no account of internal degrees of freedom, but treats the molecules as point masses surrounded by spherically symmetrical potentials, no differentiation between the two mass 45 molecules can be made.

The tracer sample was enriched to a 45/44 ratio of 0.038. The heavy CO_2 was not prepared directly by thermal diffusion; rather, it was obtained from $BaCO_3$ enriched in C^{13}, which had in turn been prepared from methane enriched in $C^{13}H_4$ by thermal diffusion.

The mass correction factor applied to the observed figures to obtain D_{11} is 1.0056.

F. Methane

The results for methane, referred to 760 mm Hg, are given in Table VI. The tracer used was $C^{13}H_4$, the sample having a 17/16 ratio of 0.042. The mass correction factor of 1.0151 was applied to the observed figures to obtain those listed for D_{11}.

[6] E. B. Winn, Phys. Rev. 74, 698 (1948).

TABLE VI. D_{11} for $C^{13}H_4$

Temperature °C	D_{11}, cm²/sec. Theory	Experiment: Present work	Experiment: Reference 7
80.0	0.293	0.318 ±0.006	···
25.0	0.215	0.240 ±0.004	0.234±0.006
0	0.183	0.206 ±0.005	···
−78.5	0.0968	0.0992±0.0006	···
−183.0	0.0187	0.0266±0.0023	···

The room temperature figure for D_{12} for $C^{13}H_4$ and $C^{12}H_4$ has already been reported.[7] The data have been recalculated, and the mass correction factor applied, to give the value set forth here. It should be mentioned that the results for nitrogen and methane reported in references 6 and 7 were obtained with the same apparatus at the University of Virginia.

From Table VI it can be seen that the agreement between the observed and calculated values of D_{11} at the lowest temperature is not as close for methane as for the other five gases studied. Some difficulty was encountered in making the runs at −183.0°C, since, to obtain a reasonable relaxation time, pressures of 4 to 5 mm Hg were required. This resulted in the $C^{13}H_4^+$ peak being only a small part of the mass 17 peak, with the result that accurate figures for the methane 17/16 ratio could not be obtained. Despite the unduly large precision measure which must be assigned to the result, however, the D_{11} from each one of the four runs made at this temperature differed significantly from the calculated value.

On the whole, the experimental values agree fairly well with those computed from the theory. With the exception of methane, the agreement is especially good at the lowest temperature.

The author wishes to express his appreciation to Professor Alfred O. C. Nier for his help and encouragement throughout the course of this project, and to Messrs. R. B. Thorness and D. M. Kvanbeck for their praiseworthy job of the machining of the diffusion bulbs. The construction of the mass spectrometer used in this work was made possible by a grant from the American Cancer Society acting through the Committee on Growth of the National Research Council. The research program was aided materially by a grant from the University of Minnesota Technical Research Fund subscribed to by General Mills, Inc., the Minneapolis Honeywell Regulator Company, the *Minneapolis Star and Tribune*, the Minnesota Mining and Manufacturing Company, and the Northern States Power Company.

[7] E. B. Winn and E. P. Ney, Phys. Rev. 72, 77 (1947).

Beta-Decay of Isomeric Cd^{113}

W. L. Carss,* Jane R. Gum, and M. L. Pool
Ohio State University, Columbus, Ohio

(Received August 18, 1950)

A 5.1±0.3-year activity has been assigned as an isomer of the stable Cd^{113} isotope. Instead of the usual decay to the ground state by gamma-rays, beta-rays of 0.5 Mev are emitted to form In^{113}. X-rays are also observed.

I. INTRODUCTION

An activity of about a 5-year half-life has been reported in the cadmium fraction when cadmium was bombarded with deuterons.[1] The decay appeared to be by beta-ray emission.

This activity has now been followed for nearly seven years on a Wulf unifilar electrometer attached to an ionization chamber. As shown in Fig. 1, the half-life is found to be 5.1±0.3 years.

II. MASS ASSIGNMENT

The 5.1-year activity is also obtained when cadmium is irradiated with neutrons from lithium bombarded with 10-Mev deuterons. When palladium is bombarded with 20-Mev alpha-particles, the 5.1-year activity is again obtained. This activity, however, is not obtained when palladium or silver is bombarded with deuterons. These observations then leave mass numbers 105, 112, and 113 as the only ones in cadmium available for assignment.

In order to make a definite mass assignment for this activity, a cadmium sample enriched in isotope 112 from 24 percent to 83.5 percent[2] was bombarded with deuterons. The characteristic radiations of the 5.1-year activity was observed in the cadmium fraction. Cadmium samples enriched in isotopes 113, 114, and 116 were bombarded with deuterons and the cadmium fractions removed.

The observations made on these three fractions showed that the 5.1-year half-life activity, if present, was very weak compared with that produced in the cadmium fraction from the sample enriched in isotope 112. Therefore, this 5.1-year activity is assigned to Cd^{113}.

The previously reported 2.3-minute activity,[3] obtained by bombarding cadmium with fast neutrons and assigned to Cd^{113}, was neither confirmed nor rejected because of the conflicting 1.94-minute activity of oxygen and the 2.4-minute activity of silver.

III. BETA-DECAY

The assignment of the 5.1-year activity as an isomer of the stable cadmium isotope of mass 113 made the possibility of beta-decay extremely interesting. At the time of these experiments all isomers of stable isotopes decay to the stable state by gamma-ray emission.[4]

To determine the energy and nature of the particles emitted in the decay of Cd^{113}, aluminum absorption measurements were undertaken. The results are shown in Fig. 2a. A particle end-point energy of 0.5 Mev is indicated. The shape of the absorption curve resembles one which would be expected from a beta-emitting activity rather than from an internally converted gamma-ray emitter.

The thickness of the source was 24.3 mg/cm². It was first necessary, then, to determine whether self-absorption within the source could so reduce and vary the apparent energy of possibly emitted monoergic electrons that the resulting absorption curve would resemble one obtained from a substance which emitted a continuous spectrum of energies.

Sr^{87} was chosen as a comparison standard for several reasons. It decays with a 2.7-hour half-life. A highly converted gamma-ray of 0.386 Mev is emitted; the ratio of the number of monoergic electrons to unconverted gamma-rays is 0.15. The short half-life permitted without lasting effects the admixture of Sr^{87} with the Cd^{113} sample. In this way the influence of the self-absorption of the 0.370-Mev monoergic electrons on the shape of the absorption curve could be specifically observed.

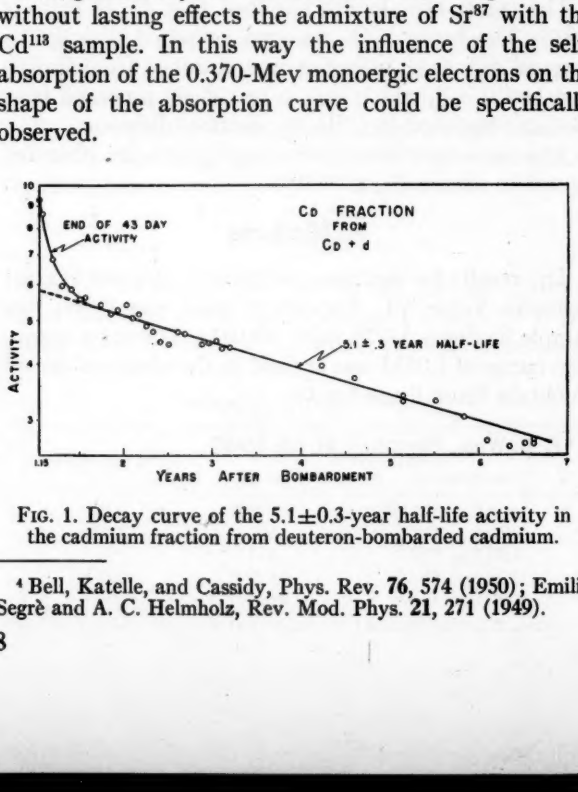

Fig. 1. Decay curve of the 5.1±0.3-year half-life activity in the cadmium fraction from deuteron-bombarded cadmium.

* Major, USAF. Research under auspices of the USAF Institute of Technology, Wright-Patterson A. F. B., Dayton, Ohio.

[1] Gum, Thompson, and Pool, Phys. Rev. **76**, 184 (1949).

[2] Supplied by the Y-12 plant, Carbide and Carbon Chemicals Corporation, through the Isotopes Division U.S.A.E.C., Oak Ridge, Tennessee.

[3] A. C. Helmholz and C. L. McGinnis, Phys. Rev. **74**, 1559 (1948).

[4] Bell, Katelle, and Cassidy, Phys. Rev. **76**, 574 (1950); Emilio Segrè and A. C. Helmholz, Rev. Mod. Phys. **21**, 271 (1949).

Accordingly, chemically pure strontium was bombarded with 10-Mev deuterons in order to produce Y^{87}. After bombardment the yttrium fraction was removed and allowed to decay for a suitable time. When an adequate activity of Sr^{87} was formed by K-capture from Y^{87}, the strontium was removed and thoroughly mixed with the Cd^{113} sample. The mass thus added was less than 2.7 mg/cm².

Absorption measurements were again made, and one is shown in Fig. 2b. At the time of this measurement the admixed strontium activity had decayed to six times the cadmium activity. The downward concavity of the curve is typical for monoergic electron sources. The thickness of the sample, therefore, does not seriously obscure the clear evidence of the 0.370-Mev monoergic electrons. The shape of the absorption curve later, when the strontium activity had died down to nearly that of the cadmium, is shown in Fig. 2c.

Figure 2d shows the final absorption curve taken after the 2.7-hour Sr^{87} had decayed to a negligible intensity. The shape of this absorption curve again clearly shows the characteristics of a true beta-absorption. The intensity of the sample also has essentially returned to that before the addition of the strontium. Since the thickness of the Cd^{113} sample was not sufficient to cause by self-absorption an appreciable distortion in the shape of the absorption curve of 0.370-Mev monoergic electrons, it is concluded that the more energetic particles, 0.5 Mev, emitted by the decay of Cd^{113} must therefore be considered beta-particles.

The decay of the 5.1-year isomeric state of Cd^{113}, then, is not primarily to the stable state of Cd^{113}, but to In^{113}.

IV. X-RAYS

X-rays were also observed in the decay of Cd^{113}. The relative sensitivities of the measuring instruments to beta-particles and to x-rays were determined by using the 2.7-hour Sr^{87} activity. The number of monoergic electrons and the number of x-rays emitted by this activity per unit of time are equal.[5] After making corrections for the difference in the ionizing effects of the x-rays of the cadmium region over those of the strontium, the absorption measurements indicated that there are approximately eleven particles emitted per x-ray in the decay of Cd^{113}.

The presence of x-rays suggests at least two possibilities. In the ratio of about 10:1 the 5.1-year activity decays competitively to the ground state of In^{113} and to either the ground state of Cd^{113} or the excited state (1.74-hour) of In^{113}. The final decision must await the knowledge of whether the emitted x-rays are those characteristic of cadmium or of indium.

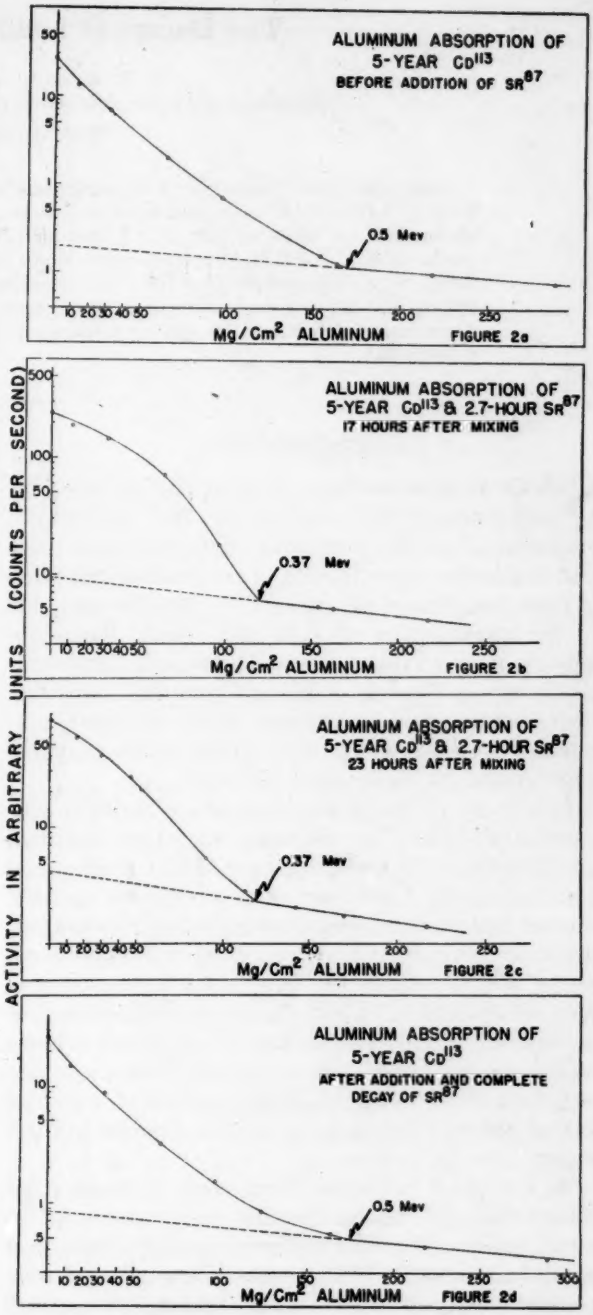

FIG. 2. Aluminum absorption curves taken: (a) of the 5.1-year activity alone, (b) 17 hours after addition of 2.7-hour Sr^{87} activity, (c) 23 hours after the addition, and (d) after the complete decay of the added strontium activity.

The authors are grateful for the support received from the Ohio State University Development Fund and the Graduate School.

[5] A. C. Helmholz, Phys. Rev. **60**, 415 (1941).

The Decays of Luminescent KBr and LiF

A. H. Morrish and A. J. Dekker
Department of Physics, University of British Columbia, Vancouver, Canada
(Received June 29, 1950)

A photo-multiplier, together with electronic pulse techniques, has been used to investigate the luminescent decay of KBr and LiF after irradiation with x-rays, at various temperatures. Decay curves plotted on a log-log scale are linear for KBr at 21°C and for LiF at 21°C and 0°C, with an average slope of 1.2. The curves for KBr at 0°C and the temperature of dry ice and acetone have linear upper and lower parts, connected by an intermediate curved part. It is suggested that the upper linear part is due to the decay of F' centers, and the lower part to the decay of F centers. The emission spectrum of KBr consists of 2 bands, a strong one centered at 4550A and a weaker one at 5300A, while that of LiF extends into the ultraviolet below 3000A.

I. INTRODUCTION

SEVERAL authors[1] have pointed out the need for experimental data concerning the luminescent properties of simple substances, since such data may lead to a better understanding of the processes involved in more complicated phosphors. The alkali halides, due to the investigations of Pohl and others,[2] have contributed much to the understanding of photo- and semiconductors in general. Little information concerning their luminescence can be found in the literature, presumably because of the low intensity which makes measurement of decay times difficult.

In a study of the phosphorescence of thallium activated alkali-halides, low intensities have been measured by Pringsheim[3] by using a Geiger-Müller counter and a scaling circuit. A few months ago the present authors[4] showed that modern photo-multiplier pulse techniques, developed in connection with scintillation counter work, can be used to measure the decay of the luminescence of pure alkali halides. In fact, the decay of the afterglow of these substances can be observed for periods of hours after x-ray excitation. The experimental technique and some results obtained for single crystals of KBr and LiF at different temperatures will be described in this paper.

At this point it may be worth while to make a few remarks on the possible electron energy levels in the alkali halides. The Bloch energy scheme of the pure alkali halides at $T=0°K$ consists of a number of completely filled and empty energy bands. The optical activation energy corresponding to an electron transition from the upper filled band (outer electrons of the negative ions) to the conduction band varies between about 5.5 and 8 ev for this group of compounds. Upon irradiation with x-rays, a number of new absorption bands appear, the most pronounced being the F band. It is now generally accepted that these bands are associated with the presence of vacant lattice points which exist in any crystal in thermodynamic equilibrium. These vacancies may occur as single ones, in pairs, or in larger clusters, depending on the temperature and history of the crystal. The x-rays will release photoelectrons which move through the lattice with high velocity, thereby producing secondary electrons and holes. The electrons may either recombine with the holes or be trapped by lattice points where negative ions are missing. Electrons trapped by single negative ion vacancies give rise to the F band. Similarly, holes may be trapped by lattice points where positive ions are missing. The field around an F center is of such a form that a second electron may be trapped, thereby leading to the F' band at the longer wave-length side of the F band. Various combinations of vacant lattice points and their consequences on the electron levels are discussed in the review article by Seitz.[2]

II. EXPERIMENTAL TECHNIQUE

The measurements were carried out on clear KBr and LiF single crystals of high purity.[5] Several crystals, not all of the same size, were used. They were polished with alcohol prior to the irradiation with x-rays. The crystals were irradiated with 55-kv 3-ma x-rays at a distance of 4 cm from the source for various periods of time. A simple technique, using a small dead air space, was developed such that the crystal could be irradiated at room, 0°C, and dry ice and acetone temperatures with no formation of a visible film of condensed water vapor. Also, it was arranged so that at the end of the excitation the crystal could be placed quickly in a dead air space in front of a photo-multiplier tube. The entire operation was performed in a dark room to prevent bleaching of the crystal, since it was found that bleaching gave results which were not reproducible.

The photo-multiplier used was the RCA 5819 which has a large (about $1\frac{3}{4}''$ diameter) photo-sensitive cathode. Curves supplied by the company show that the tube is most sensitive about 5000A. It cuts off at about 6500A at the low energy side, and at 3000A at the high

[1] See for example the discussions in Cornell Symposium, *Solid Luminescent Materials* (John Wiley and Sons, Inc., New York, 1948), and G. F. J. Garlick, *Luminescent Materials* (Clarendon Press, Oxford, 1949).
[2] For reviews of this work see N. F. Mott and R. W. Gurney, *Electronic Processes in Ionic Crystals* (Clarendon Press, Oxford, 1940) and F. Seitz, Rev. Mod. Phys. 18, 384 (1946).
[3] P. Pringsheim, Rev. Mod. Phys. 14, 135 (1942).
[4] A. J. Dekker and A. H. Morrish, Phys. Rev. 78, 301 (1950).
[5] Obtained from Harshaw Chemical Company, Cleveland, Ohio.

energy side. The tubes were operated with a total of 1200 to 1300 volts across the ten multiplying and cathode and collector electrodes. At room temperature, the signal-to-noise ratio can be made very large and, consequently, it was not found necessary to cool the tube.

The pulses were fed into a two-tube head amplifier, consisting of an amplifier and cathode follower. The input circuit had a 10^4-ohm resistor and it is estimated that the capacity of the final electrode and leads was about 20 $\mu\mu$f. The gain of the head amplifier was about 20. Further amplification was necessary and a three-tube linear amplifier with attenuator and a diode clipping circuit was constructed. It was found that a total gain of 60 was sufficient to give suitable pulse size. A commercial sale of 64 followed by a decade unit and mechanical register counted the pulses.

A suitable bias was used so that the noise pulses gave about 0.1 in the scale of 640 counts/min. It was found that with a suitably sized crystal and time of irradiation and a selected RCA 5819 the number of pulses produced by the luminescence could be made very large compared with the number of noise pulses. Counting rates were used that were not large enough to make scaling losses appreciable.

The noise and luminescence pulse distributions were determined, the latter being difficult to obtain because of the decay of the luminescence. It was found, for example, that the ratios of the number of pulses with heights above 5 volts to the number above 10 volts was about the same for the noise and signal pulses. If anything, there were more smaller pulses per large pulse in the luminescence distribution. Also, it was found that the maximum pulse size of noise and signal was about the same, a few signal pulses being found with a 20 percent higher voltage than any noise pulse in a reasonable counting time. Of course, to obtain good statistics for the noise distribution an intolerably long counting time would be necessary at the higher discriminator voltages.

Since the signal pulse distribution was roughly a noise distribution, it is suggested that they are due to single photons. This assumes that noise pulses are due to single electrons, with of course a few pulses being produced by the emission of two electrons from the cathode in a time interval equal to or shorter than the integrating time of the input circuits (about 0.2 μsec.). The work of Allen[6] with a Be-Cu multiplier tube, used as an electron counter, shows that electrons of about 100 volts (the voltage between the cathode and the first multiplying stage) are counted with an efficiency of the order of 80 percent. Comparison of bias curves of the 5810 and the Be-Cu tube seem to indicate, together with measurements of the photo-sensitivity of the Be-Cu tube,[7] that this assumption is correct. The mechanism by which the photons are produced by the alkali-halides is discussed later.

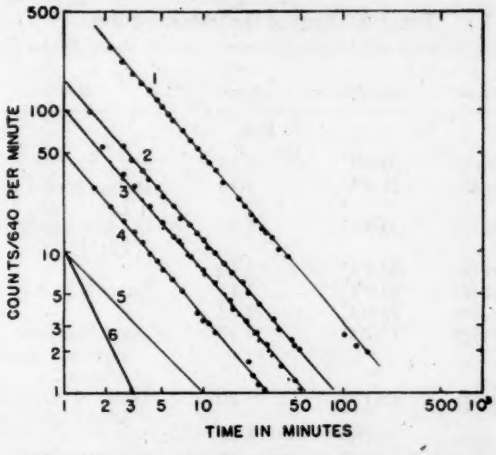

FIG. 1. Luminescent decays of KBr are shown by curves 1, 3, and 4, and that for LiF is shown by curve 2. Curve 5 shows a slope of 1 and curve 6 a slope of 2; the slopes of the decay curves are clearly different from these. The time refers to time in minutes after x-irradiation.

Because of the nature of the distribution, it is important to use a photo-multiplier tube that is highly stable. It is perhaps worth noting that we have had two tubes, which worked satisfactorily for a time, become unstable inasmuch as the noise started to fluctuate widely. Also some tubes had a low signal-to-noise ratio and were unusable, indicating that the quantum efficiency of the photo-cathode can vary by a factor 10^2.

III. EXPERIMENTAL RESULTS

(a) At Room Temperature

A number of runs were taken with two different KBr crystals (20×20×3 mm each) at room temperature for different periods of irradiation. A plot of the intensity *versus* the time after irradiation yields a straight line in a log-log scale, as can be seen from a few examples as given in Fig. 1. The slopes obtained are summarized in Table I. The average value is 1.17.

Curve 3 in Fig. 1 shows two separate runs after 1-minute irradiation, the circles being one run, the dots the other. These runs were taken a day apart, and it is believed that conditions were very nearly the same. Curve 4 also shows a KBr decay after 1-minute irradiation, but made about 3 weeks later. The slope is the same within the experimental error, but the curve is displaced with respect to curve 3. This illustrates what was generally found in these experiments; the slopes were very reproducible but the absolute values were difficult to reproduce. One of the reasons is the strong dependence of the pulse size on the high voltage applied to the photo-multiplier tube. Other sources of error in this respect are the variations in the emission of the x-ray tube, the position of the crystal, etc. Some of them can be eliminated by refinements of the experimental technique. Curve 1 was taken about the time

[6] J. S. Allen, Rev. Sci. Inst. 18, 739 (1947).
[7] Morrish, Williams, and Darby, Rev. Sci. Inst. 21, 884 (1950).

TABLE I. Slopes of the intensity curves.

Time of irradiation	Temperature	Slope		Remarks
		KBr		
30 seconds	20.6°C	1.18		
1 minute	21.0°C	1.16		Dots, curve 3 in Fig. 1.
1 minute	20.9°C	1.16		Circles, curve 3 in Fig. 1.
1 minute	20.8°C	1.16		
1 minute	20.9°C	1.13		Curve 4 in Fig. 1.
5 minutes	20.0°C	1.22		
5 minutes	17.7°C	1.16		Slope increases slightly after 45 minutes.
5 minutes	19.1°C	1.20		More scattering of points than usual.
5 minutes	20.7°C	1.14		
15 minutes	21.0°C	1.18		Curve 1 in Fig. 1.
	Average	1.17		
		Upper	Lower	
5 minutes	0°C	1.46	1.20	
5 minutes	0°C	1.44	1.20	
6 minutes	0°C	1.45	—	Time of experiment too short to observe lower slope, but bend was observed.
20 minutes	0°C	1.51	1.08	Shown in Fig. 3.
	Average	1.46	1.16	
1 second	dry ice and acetone	—	1.13	Upper part still curving upwards. See Fig. 4.
1 second	dry ice and acetone	—	1.06	
15 seconds	dry ice and acetone	1.44	—	Very high counting rate. No bend appeared after 100 minutes.
	Average	1.44	1.10	
		LiF		
1 minute	20.4°C	1.16		
5 minutes	20.8°C	1.15		Curve 2 of Fig. 1.
5 minutes	0°C	1.22		Some scatter.
10 minutes	0°C	1.15		Curve 2 of Fig 3.
	Average	1.17		

curve 3 was obtained and represents the decay of KBr after 15 minutes x-irradiation. It is displaced upwards, presumably because greater numbers of electrons were excited.

For convenience, a slope 1 is shown by curve 5 and a slope 2 by curve 6. It appears clear, from the data, that slopes of 1 or 2 are ruled out for the decay process.

Figure 2 shows four runs with different irradiation times. Experimental conditions were believed to be approximately constant during the collection of these data. The individual curves show the counting rate after a specified time after the x-ray excitation. They indicate a saturation effect for the formation of color centers.

Similar measurements to those just described were carried out with two LiF blanks (10 mm diam., 4 mm thick) at room temperature. The reproducibility was similar to that of KBr and the average slope obtained in a log-log scale was 1.16 (see Table I). An example is shown by curve 2 in Fig. 1. It is worth noting that the slope is the same as for KBr within the experimental error.

(b) At 0°C

Figure 3 shows sample curves for KBr and LiF irradiated and measured at 0°C (melting ice). The LiF decay (curve 2) shows an average slope of 1.18 and is equal to that at room temperature within the experimental error. The KBr curves, however, show a break as shown by the sample curve 1 in Fig. 3. They start off with a relatively steep slope (A) and ultimately end as a straight line with a slope (B) about equal to that of LiF and those at room temperature. Although it must be admitted that, due to the break, the slopes A and B cannot be determined as accurately as those of the room temperature curves, one is probably justified in giving the approximate values $A=1.46$ and $B=1.16$. The details of the data are shown in Table I.

(c) At Dry Ice and Acetone Temperature

Figure 4 shows the decay of a KBr crystal irradiated for about 1 second at the temperature of dry ice and acetone; the measurements were carried out at the same temperature. The curve shows a break similar to that obtained at 0°C. It should be noted that part A may be increased by using a longer period of irradiation. However, an irradiation time of 15 seconds produced such an enormous counting rate that measurements with the same gain settings could be started not earlier

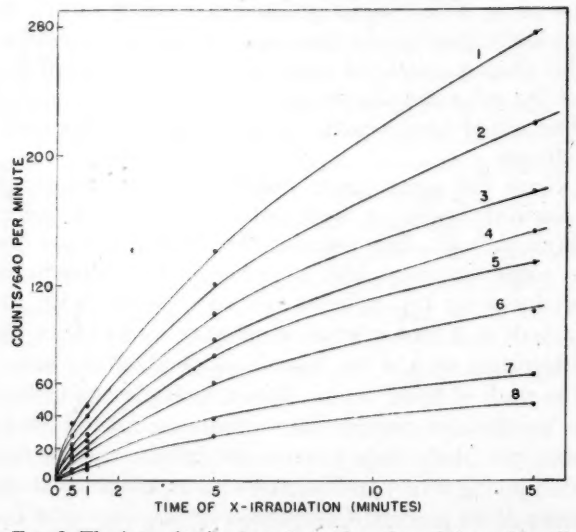

FIG. 2. The intensity is plotted as a function of time of irradiation for KBr in four runs in which other experimental conditions were believed to be very constant. They were taken at room temperature, and curve 1 refers to points taken two minutes after x-irradiation, curve 2 to 2.5 minutes after, curve 3 to 3.0 minutes after, curve 4 to 3.5 minutes after, curve 5 to 4 minutes, curve 6 to 5 minutes, curve 7 to 7.5 minutes, and curve 8 to 10 minutes after irradiation.

than 10 minutes after the x-irradiation, due to the limit of 30,000 counts per minute set by the mechanical counter. The slope of part *B* in Fig. 4 can be determined more accurately than that in Fig. 3 and gives a value of 1.13. This again is the same as the slopes obtained at room temperature. A slope for part *A* cannot be obtained from Fig. 4. However, as already mentioned, by using longer irradiation times this part can be extended and a curve (for 15 seconds irradiation) yielded a slope of 1.44. This is practically the same as the slope of part *A* in Fig. 3.

(d) Miscellaneous Experiments

Some runs were made by irradiating the KBr crystals at room temperature and then cooling to 0°C. The resultant decay gave points on a log-log plot that fluctuated widely from a straight line. A rough average slope was about 0.3. The absolute value of the counting rates, even immediately after the irradiation, was low, being of the order of one or two percent of that for KBr measured at room temperature.

An attempt to detect the decay of KBr and LiF in the ultraviolet was made using an electron multiplier whose electrodes, including the photo-cathode, were constructed from a Be-Cu alloy.[6] The tube is sensitive to u.v. photons below 2900A. No counting rate was observed for the KBr, but a small counting rate was observed for the LiF. However, the counting statistics were so bad that preliminary attempts to determine the slope of the decay curve were unsuccessful.

To investigate the emission spectrum of KBr further, a Hilger medium quartz spectrograph was used. The crystal was placed as close to the slit as possible. Because of the low intensity of the luminescence, a slit width of 0.5 mm was used. An exposure time of 3 hours, during which period the crystal was irradiated with x-rays, was necessary to obtain a satisfactory blackening on the photographic plate (Kodak F II). The spectrum consists

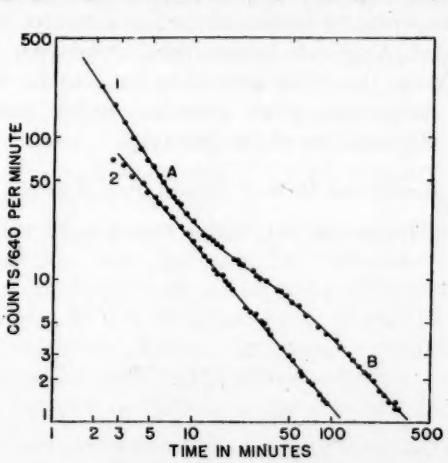

FIG. 3. Decay of KBr at 0°C is shown in curve 1 for KBr and curve 2 for LiF. The slopes *A* and *B* are clearly different, while *B* has approximately the same slope as curve 2, and the curves taken at room temperature shown in Fig. 1.

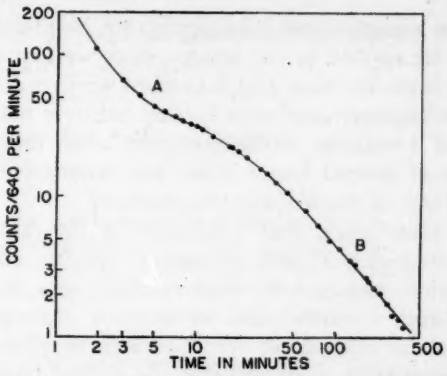

FIG. 4. Decay of KBr at dry ice and acetone temperature. The time of x-irradiation was one second. Curves *A* and *B* have approximately the same slope as *A* and *B* of Fig. 3.

of a band at about 4550A and a much weaker one at about 5300A. A similar attempt to obtain the LiF spectrum failed, presumably because of the low intensity of emission.

IV. DISCUSSION

One can divide phosphors, according to their decay laws, roughly into two classes. The first group gives a decay described by a differential equation of the type

$$dn/dt = -\alpha n, \tag{1}$$

where n is the number of centers excited at time t and α is the transition probability. Upon integration, one obtains the expression

$$I(t) = I_0 e^{-\alpha t}, \tag{2}$$

for the intensity. This temperature independent exponential decay is found in phosphors when the excited levels are non-metastable and localized in the heighborhood of the absorbing centers. The alkali halides do not belong to this group, since they exhibit photo-conductivity and a temperature dependent luminescence.

The second group of phosphors have a decay satisfied by an equation of the type

$$I(t) = I_0/(1+\beta t)^p. \tag{3}$$

For $\beta t \gg 1$ this leads to a t^{-p} power decay. In case $p=2$, the corresponding differential equation is of the form

$$dn/dt = -\gamma n^2, \tag{4}$$

where $\gamma = \beta^2/I_0$.

Boyd[8] has investigated the thermoluminescence of LiF. He obtained curves with $p=2$ in the temperature regions 155 to 195°C and 371 to 419°C. In the region 195 to 371°C his curves ($I^{-\frac{1}{2}}$ plotted *versus* t) were convex. In deriving equations for the analysis of his experiment, he assumed a single trap depth and proportionality between the trapped and free electrons. He then arrived at an equation of type (4). From his results he found the depths of the traps in the two tem-

[8] C. A. Boyd, J. Chem. Phys. 17, 1221 (1949).

perature regions where p was equal to 2. Boyd's analysis cannot be applied to our results, since we found in all cases a slope less than 2. It is perhaps worth noting that Boyd's measurements were carried out over periods of at most 4 minutes, while ours were often taken over periods of several hours. Also, our experiments were carried out at much lower temperatures.

Our observation that irradiation of the crystals at room temperature, and subsequent cooling after the irradiation, greatly lowers the counting rate, indicates that direct recombination of trapped electrons and holes is not responsible for the observed photons. It seems justifiable to assume that the excited crystal can return to its ground state only after release of the electrons or holes from traps. The observed photons would then be produced by recombination of a free electron (hole) and a hole (electron). This assumption was also used by Boyd in his analysis of the thermoluminescence of LiF. The fact that the recombination just referred to produces a visible photon, whereas the absorption lies in the u.v., may be due to the Frank-Condon principle.

Since our experiments were carried out at comparatively low temperatures, it seems reasonable to assume that the intensity of the luminescence is mainly determined by the rate at which electrons are released from traps.

The number of F and F' absorption centers formed on irradiation with x-rays will depend on their stability at the particular temperature at which irradiation took place. Since the electron levels responsible for the F' band are not as far below the conduction band as those giving rise to the F band, one would expect the relative number of F' centers to increase with decreasing temperature. Also, one would expect the shallow traps to be emptied first.[9] Therefore, we are inclined to believe that the upper part of the curves that consist of two straight lines and an intermediate part is associated with the release of F' centers. The lower part will then correspond to the release of electrons from F centers. Since only one straight line was observed for KBr at room temperature, it appears that the temperature is too high for the formation of F' centers. The upper part of the curve extends for a greater time, for a given irradiation time, at the temperature of dry ice and acetone than at 0°C, as the formation of F' centers is favored at the lower temperature. The above interpretation is strengthened by the equality of the slopes of the lower parts of the low temperature curves with that observed at room temperature (about 1.2), and the higher (about 1.5) slope for the upper parts of the low temperature curves.

Power decays with $p<2$ have been observed in many other substances. These deviations have been explained in the literature by assuming a certain energy distribution for the traps.[10] There are more traps in alkali halides besides the F and F' centers, but the details are not sufficiently well known to enable one to suggest a mathematical expression for such a distribution.

Ellickson and Parker,[11] studying the decay of infrared sensitive phosphors, explained a deviation from $p=2$ by taking into account absorption of both the exciting and emitted radiation inside the crystal. These authors used an absorption coefficient, characteristic of the unexcited crystal, for the emitted light. In our case, however, the unexcited crystal is transparent to the visible luminescence and only trapped electrons could act as absorbing centers. If this type of "self-absorption" actually exists, light emitted in a certain part of the crystal would excite trapped electrons in other parts, leading to a very complicated mechanism. This is further complicated, since x-rays of the energy used are almost entirely absorbed in the first mm of the crystal, giving rise to a non-uniform discoloration.

There are reasons to believe that "self-absorption" is not a determining factor in the decay laws we observe. First, we find that the emission spectrum of KBr consists of a strong band around 4550A, and a comparatively weak band around 5300A, whereas the F absorption band has a peak at 6300A. The F' absorption band has a maximum value at about 8000A. Secondly, we did not find any change in the power of the decay for different irradiation times.

Attempts to explain the slopes of the decay curves on the basis of present models of the luminescence process have failed. A private communication from Dr. F. A. Kröger states that Wise believes he has found a mathematical formalism which explains similar problems existing in phosphors of the ZnS type.

[9] To give a numerical example: for an activation energy of 1 ev the probability for an electron to be released per second is about 10^{-6}. For 0.5 ev it is about 10^{3}.

[10] J. T. Randall and M. H. F. Wilkins, Proc. Roy. Soc. A 184, 366 (1945).

[11] R. T. Ellickson and W. L. Parker, Phys. Rev. 70, 290 (1946).

The Angular Distributions of the Alpha-Particles and of the Gamma-Rays from the Disintegration of Fluorine by Protons*

C. Y. CHAO†
Kellogg Radiation Laboratory, California Institute of Technology, Pasadena, California
(Received August 14, 1950)

The theoretical angular distributions of the alpha-particles and of the gamma-rays from the fluorine +proton reactions are given. They are compared with the experimental data, and the following results are obtained: (1) Both angular distributions of the α_π-group and of the α_0-group favor the assumption of even parity of F^{19}. (2) If the parity of F^{19} is taken as even, then (a) the isotropic angular distribution of the gamma-rays at the resonances of 340 and 669 kev can be interpreted as due to the formation of Ne^{20} compound states of $J=1^+$ by the capture of s-protons, (b) the slightly anisotropic angular distribution of the gamma-rays at the resonances of 598, 874, and 1381 kev can be interpreted as due to the formation of Ne^{20} states of $J=1^+$ by a mixture of s- and d-protons, or of $J=2^-$ by p-protons, (c) the highly anisotropic distribution of the gamma-rays observed at 1290 and 1355 kev can be interpreted as due to the formation of Ne^{20} states of $J=3^+$, and (d) the experimental data of the gamma-ray angular distribution and of the ratio $I(\alpha)_{140°}/I(\gamma)_{90°}$ are compatible with the assignment $j'=3^-$ for the γ_1-level of O^{16}. In general it is possible to make spectroscopic assignments consistent with the experimental data but unique assignments will await further experimental results.

I. INTRODUCTION

ENERGY, spin, and parity are three important properties of a nuclear state. The energy of a nuclear state, especially of an excited state, is normally determined by measuring the energies of the products, both particles and gamma-rays, of a nuclear reaction which involves that state. In a similar way, information about the spin and parity of a nuclear state can be obtained by studying the relative angular momenta of the reaction products. A number of methods are available for this purpose. The simplest is the one of observing the level width, which, in favorable cases, reveals the relative orbital angular momentum of the products of one of the nuclear processes, or the multipole nature of the radiation emitted. While this method is simple, it is usually not very conclusive. The most suitable method is no doubt that involving the measurement of angular distributions. The angular distributions of the reaction products and the angular correlations between the successively emitted products are determined theoretically by the symmetry properties of the nuclear states involved. When measured accurately, they give the most extensive information about the spin and parity of the nuclear states. The information is especially unambiguous when only one level of the intermediate nucleus is involved in the reaction.

In the following we shall first give the theoretical formulas and then the result of calculation for the angular distributions of the alpha-particles and of the gamma-rays from the fluorine+proton reactions. Five alpha-groups are known for these reactions:[1] the α_0-group which leads to the ground state of O^{16} and the α_π, α_1, α_2, and α_3-groups, in the order of decreasing energy, corresponding to one electron-pair level and three gamma-ray levels, respectively. The angular distributions of the α_0-group and of the gamma-rays have been measured at several proton energies. For other groups and at other energies information is only available indirectly. Comparison will be made between the calculated result and the experimental data, but the conclusions so far reached are of preliminary nature because of the scarcity of the available data.

While this work was going on, Arnold[2] obtained very interesting results for the angular correlation between the alpha-particles and the gamma-rays of the reaction $F^{19}(p,\alpha\gamma)O^{16}$. His results help to clarify several points which were unsettled in our original analysis.

II. THEORETICAL FORMULAS

The theoretical formulas for the calculation of the angular distributions of the reaction products have been given in a number of papers.[3] In some of the papers, the formulas were developed by assuming Russell-Saunders coupling. Since there is no definite evidence that such coupling is prevalent in nuclear reactions, we adopt the general treatment which includes the Russell-Saunders coupling as a special case. In the general treatment the spin of the initial nucleus is first combined with that of the incident particle giving a resultant **S**. **S** is then combined with the relative orbital angular momentum **l** of the incident particle to give the total angular momentum of the system. A transition from any sub-state of the two-particle system with an angular momentum (**l**+**S**) to a sub-state of the compound nucleus with an angular momentum **J** is considered possible if the parity is conserved and if $\mathbf{J}=\mathbf{l}+\mathbf{S}$ and $M=\lambda+\sigma$, where M,

* This work was assisted by the joint program of the ONR and AEC.
† On leave from Institute of Physics, Academia Sinica, China.
[1] A summary of the experimental results is to be found in a recent article by Chao, Tollestrup, Fowler, and Lauritsen, Phys. Rev. 79, 108 (1950).
[2] W. R. Arnold, Phys. Rev. 80, 34 (1950). The author is also indebted to Professor D. R. Inglis for this information.
[3] R. D. Meyer, Phys. Rev. 54, 361 (1938); E. Gerjuoy, Phys. Rev. 58, 503 (1940); D. R. Inglis, Phys. Rev. 74, 21 (1948); also E. R. Cohen, Ph.D. thesis at California Institute of Technology (1949).

λ, and σ are the projections of **J**, **l**, and **S** in the direction of the incident particles, which is taken as the direction of quantization. In this section, we shall give the formulas to be used in convenient forms and supplement them with necessary explanations.

(A) Angular Distributions of the Emitted Particles

Suppose that a bombarding particle P is captured by a target nucleus A with the result of formation of a compound nucleus C and that a particle Q subsequently escapes leaving a residual nucleus B. Consider the general case in which several levels of the compound nucleus contribute to the capture process. Let **J**, **l**, **S**, M, λ, and σ have the meanings as explained in the foregoing, λ being always zero and $M=\sigma$. Let **l**′ and λ' be the relative orbital angular momentum and its projection in the direction of quantization of the outgoing particle Q, and **S**′ and σ' be the combined spin and its projection of the system $B+Q$. Then the angular distribution of the outgoing particle Q is given by:

$$I_Q(\theta)=K\sum_{SS'}\sum_{\sigma\sigma'}\left|\sum_{Jll'}\frac{H^{CJM}_{lOS\sigma}H^{*CJM}_{l'\lambda'S'\sigma'}P_{l'\lambda'}(\theta)}{(E-E_J)+(i\Gamma/2)}\right|^2 \qquad (1)$$

with $\mathbf{J}=\mathbf{S}+\mathbf{l}=\mathbf{S}'+\mathbf{l}'$, $M=\sigma=\lambda'+\sigma'$. It is to be noted that amplitudes contributed by different levels or by different **l** or **l**′ interfere among themselves, while amplitudes due to states of different spin orientations give no interference. Both **S** and **S**′ may assume different values and have different orientations. These are taken care of by the summations over S, S', σ, and σ'. It is also to be noted that summation over λ' is not necessary, since $\lambda'=\sigma-\sigma'$. $P_{l'\lambda'}(\theta)$ is the normalized associated Legendre polynomial, which represents the wave of the outoing particle specified by **l**′ and λ'. We have omitted the factor $\exp(i\lambda'\phi)$, which should accompany $P_{l'\lambda'}(\theta)$, because the interference effect between states belonging to different values of λ', i.e., to different values of σ or σ', vanishes.

The matrix elements H and H^* can be written as:

$$H^{CJM}_{lOS\sigma}=\alpha^{JM}_{lOS\sigma}\phi(l)u^{CJ}_{JlS},$$
$$H^{*CJM}_{l'\lambda'S'\sigma'}=\alpha^{JM}_{l'\lambda'S'\sigma'}\phi(l')u^{*CJ}_{Jl'S'}. \qquad (2)$$

In the expression for H, α is the transformation coefficient between the representation labeled by J, M and that labeled by l, λ, and S, σ of the same system $A+P$, $\phi(l)$ is the square root of the barrier penetration factor of the incoming particle of relative orbital angular momentum **l**, and the product $\phi(l)u$ is the matrix element for the transition between the sub-state JM of the compund nucleus C and the sub-state JM of the system $A+P$, formed by the vector addition of **l** and **S**. In the present treatment, u is supposed to be dependent on **l** and **S** but independent of M. Numerical factors appearing during the expansion of the incident wave function are absorbed in the functions u's. Similar explanations hold for the expression of H^*. The coefficients α's can be found in the book by Condon and Shortley.[4]

We shall now consider the special form of (1) when it is applied to the alpha-particles of the reactions $F^{19}(p,\alpha)O^{16}$ and $F^{19}(p,\alpha\gamma)O^{16}$ and treat the case of α_γ-groups and of α_0-group separately.

1. *The α_γ-Groups*

Since the resonance levels for the α_γ-groups are narrow and the background is low, we have here a fair approximation for most of these resonances by treating them as a one-level problem. The Ne^{20} compound states which yield the α_γ-groups do not give the α_0-group. Hence they are supposed to have $J=0^-, 1^+, 2^-, \cdots$, as are usually assumed, where the $+$ or $-$ sign indicates the even or odd parity of the level. The value of S which can give the above set of J's depends on the spin and parity of F^{19}. The spin of F^{19} is known[5] to be $\frac{1}{2}$. Hence $S=0$ or 1. If the parity of F^{19} is even, the Ne^{20} levels with $J=0^-, 1^+, 2^-, \cdots$ can only be formed with $S=1$, i.e., with the parallel spin of F^{19} and H^1; if the parity of F^{19} is odd, these levels can be formed with $S=1$ or 0, i.e., with parallel or antiparallel spin combinations, except the level with $J=0^-$ which only be formed with $S=0$. Since the outgoing alpha-particle has no spin, there is only one value of S' and it is equal to the spin j' of the residual nucleus O^{16}. $\phi(l)$ decreases rapidly as l increases when the energy of the incident particle is below the barrier. In general we consider only the lowest l which satisfies the conservation laws but we do consider admixtures of d-waves ($l=2$) when s-waves ($l=0$) are possible. Throughout most of the calculation, we take the lowest possible value of l'. At exact resonance, $E=E_J$. Writing

$$A_{lS}=\phi(l)\phi(l')u^{CJ}_{JlS}u^{*CJ}_{Jl'S'}/(\tfrac{1}{2}i\Gamma), \qquad (3)$$

we have, from (1),

$$I_{\alpha\gamma}(\theta)=K\sum_{S}\sum_{\sigma\sigma'}\left|\sum_{l}\alpha^{JM}_{lOS\sigma}\alpha^{JM}_{l'\lambda'S'\sigma'}A_{lS}P_{l'\lambda'}(\theta)\right|^2, \qquad (4)$$

where $\sum_{l'}$ is replaced by its value for the minimum allowable l'. The quantity A_{lS} is complex. It may be called the partial amplitude of the compound nuclear state. In the case of narrow resonance, the phase factor in A_{lS} can be evaluated.[6] If the parity of F^{19} is even, Ne^{20} compound states of $J=1^+$ can be formed by combining $l=0$ or 2 with $S=1$. We set, in this case,

$$X=A_{2S}/A_{0S}. \qquad (5)$$

If the parity of F^{19} is odd, Ne^{20} compound states of

[4] E. U. Condon and G. H. Shortley, *Theory of Atomic Spectra* (The Macmillan Company, New York, 1935), pp. 76–77.
[5] J. E. Mack, Rev. Mod. Phys. **22**, 64 (1950).
[6] E. P. Wigner and L. Eisenbud, Phys. Rev. **72**, 29 (1947).

$J=1^+, 2^-, 3^+$, etc., can be formed combining $l=1, 2, 3$, etc., with $S=1$ or 0. We set, in these cases,

$$t=|A_{11}/A_{10}|^2. \tag{6}$$

X may be called the ratio of the partial amplitudes due to the d-wave and the s-wave components of protons and t the ratio of the contributions due to the triplet combination and the singlet combination. X and t are the arbitrary constants occurring in the final expression of the angular distribution.

2. *The α_0-Group*

In this case the resonance levels are not very sharp and the background is appreciable. Hence we have to take into account the effect of several levels at one proton energy. We let, now,

$$A^J_{ll'SS'}=\phi(0)\phi(l')u^{cJ}_{JlS}u^{*cJ}_{Jl'S'}/[(E-E_J)+\tfrac{1}{2}i\Gamma], \tag{7}$$

where $\phi(0)$ is the square root of the barrier penetration factor for $l=0$. Then

$$I_{\alpha_0}(\theta)=K\sum_{SS'}\sum_{\sigma\sigma'}\times\left|\sum_{Jll'}\alpha^{JM}_{lOS\sigma}\alpha^{JM}_{l'\lambda'S'\sigma'}\frac{\phi(l)}{\phi(0)}A^J_{ll'SS'}P_{l'\lambda'}(\theta)\right|^2. \tag{8}$$

We have purposely separated $\phi(l)/\phi(0)$ from A in order to facilitate the comparison of different A's. Formula (7) can be simplified further because the spin of the residual nucleus, i.e., of the ground state of O^{16}, is zero and hence $S'=0$, $l'=J$, $\lambda'=M$, and the second transformation coefficient α equals unity. Thus, we need only three indices to label A and have

$$I_{\alpha_0}(\theta)=K\sum_S\sum_\sigma\left|\sum_{Jl}\alpha^{JM}_{lOSM}\frac{\phi(l)}{\phi(0)}A_{JlS}\exp(i\omega_{JlS})P_{l\lambda'}(\theta)\right|^2, \tag{9}$$

where we have separated the phase factor $e^{i\omega}$ from A_{JlS}. A_{JlS} and ω_{JlS} are now the arbitrary constants occurring in the final expression of the angular distribution.

(B) Angular Distribution of the Gamma-Rays

The formula for the angular distribution of the gamma-rays from the reaction $F^{19}(p,\alpha\gamma)O^{16}$ is similar to (4). It can be written as

$$I_\gamma(\theta)=K\sum_S\sum_{\sigma\sigma'}\left\{\left|\sum_l\alpha^{JM}_{lOS\sigma}\alpha^{JM}_{l'\lambda'S'\sigma'}A_{lS}\right|^2 f_{S'\sigma'}(\theta)\right\}, \tag{10}$$

where A_{lS} is the quantity defined in (3) and $f_{S'\sigma'}(\theta)$ is the angular distribution of the radiation due to the transition $\Delta j'=S'$, $\Delta m'=\sigma'$ of O^{16}. Formula (10) is much simpler than the general formula for the gamma-rays from such reactions because (a) we consider only one level of the Ne^{20} compound nucleus, (b) the outgoing particle has zero spin and hence the spin of the excited O^{16} nucleus is equal to S', and (c) the spin of the ground state of O^{16} is zero. We can use here also the quantities X and t defined in (5) and (6) in the final expression. It is to be noted that the probability for an alpha-particle emitted in the direction (θ, ϕ) and a gamma-ray subsequently emitted in the direction (θ', ϕ') is a function $P(\theta, \phi, \theta', \phi')$ and that the intensity of the gamma-ray in the direction (θ', ϕ') is, in general, given by:

$$I_\gamma(\theta', \phi')=\int P(\theta, \phi, \theta', \phi')d\omega_\alpha. \tag{11}$$

When the outgoing α-particles may have more than one value of l', Eq. (11) is to be used[7] instead of Eq. (10).

The function $f_{S'\sigma'}(\theta)$ gives the angular distributions of the dipole, quadrupole, and octupole radiations for $S'=1$, 2, and 3, respectively. These angular distributions are given below:[8]

(a) Dipole radiation:

$$\begin{aligned} f_{10}(\theta)&=3(1-\cos^2\theta),\\ f_{11}(\theta)&=3(1+\cos^2\theta)/2. \end{aligned} \tag{12}$$

(b) Quadrupole radiation:

$$\begin{aligned} f_{20}(\theta)&=15(\cos^2\theta-\cos^4\theta),\\ f_{21}(\theta)&=\tfrac{1}{2}5(1-3\cos^2\theta+4\cos^4\theta),\\ f_{22}(\theta)&=5(1-\cos^4\theta)/2. \end{aligned} \tag{13}$$

(c) Octupole radiation:

$$\begin{aligned} f_{30}(\theta)&=(7/32)\cdot 12(1-11\cos^2\theta+35\cos^4\theta-25\cos^6\theta),\\ f_{31}(\theta)&=(7/32)(1+111\cos^2\theta-305\cos^4\theta+225\cos^6\theta),\\ f_{32}(\theta)&=(7/32)\cdot 10(1-3\cos^2\theta+11\cos^4\theta-9\cos^6\theta),\\ f_{33}(\theta)&=(7/32)\cdot 15(1-\cos^2\theta-\cos^4\theta+\cos^6\theta). \end{aligned} \tag{14}$$

TABLE I. Observed angular distributions of the α_γ-groups and of the gamma-rays.

Levels	$I_\gamma(\theta)\sim 1+a\cos^2\theta$ Coefficient a D.H.	Kellogg	$\frac{I(\alpha)_{140^\circ}}{I(\gamma)_{90^\circ}}$
340	0		0.88+
598	0.2		0.90+
669	0		0.97
874	0.1	0.10	0.90
935		0	0.88
1290		0.67	0.99
1355		0.25	0.97
1381		−0.07	0.88

III. THEORETICAL ANGULAR DISTRIBUTIONS AND THEIR COMPARISON WITH THE EXPERIMENTAL DATA

(A) Angular Distributions of the α_γ-Groups and of the Gamma-Rays

The angular distribution of the α_γ-groups have not been measured; those of the gamma-rays have been

[7] The author is indebted to Professor R. F. Christy for pointing out this fact.

[8] D. R. Hamilton, Phys. Rev. **58**, 122 (1940); D. S. Ling, Jr. and D. L. Falkoff, Phys. Rev. **76**, 1639 (1949).

TABLE II. Angular distributions of the $\alpha\gamma$-groups and of the gamma-rays under the assumption of even parity of F^{19}.

	$Ne^{20}(J=0^-)$	$Ne^{20}(J=1^+)$	$Ne^{20}(J=2^-)$	$Ne^{20}(J=3^+)$
$O^{16}(j'=1^-)$	$I_\alpha=0$	$I_\alpha\sim 1+\frac{0.95x}{1-0.32x}\cos^2\theta$	$I_\alpha\sim 1+\cos^2\theta$	$I_\alpha\sim 1+1.2\cos^2\theta+1.0\cos^4\theta$
		$I_\gamma\sim 1-\frac{0.47x}{1+0.16x}\cos^2\theta$	$I_\gamma\sim 1+0.64\cos^2\theta$	$I_\gamma\sim 1+0.82\cos^2\theta$
			$I_\alpha'/I_\gamma'=1.4$	$I_\alpha'/I_\gamma'=1.64$
$O^{16}(j'=1^+)$	$I_\alpha\sim 1$	$I_\alpha\sim 1$	$I_\alpha\sim 1+1.62\cos^2\theta$	$I_\alpha\sim 1-0.33\cos^2\theta+3.0\cos^4\theta$
	$I_\gamma\sim 1$	$I_\gamma\sim 1+\frac{0.95x}{1-0.32x}\cos^2\theta$	$I_\gamma\sim 1-0.45\cos^2\theta$	$I_\gamma\sim 1-0.44\cos^2\theta$
	$I_\alpha'/I_\gamma'=1$		$I_\alpha'/I_\gamma'=1.08$	$I_\alpha'/I_\gamma'=0.99$
$O^{16}(j'=2^-)$	$I_\alpha\sim 1$	$I_\alpha\sim 1-\frac{0.19x}{1+0.063x}\cos^2\theta$	$I_\alpha\sim 1$	$I_\alpha\sim 1+1.6\cos^2\theta$
	$I_\gamma\sim 1$			
	$I_\alpha'/I_\gamma'=1$	$I_\gamma\sim 1-\frac{0.47x}{1+0.16x}\cos^2\theta$	$I_\gamma\sim 1+\cos^2\theta$	$I_\gamma\sim 1+2.9\cos^2\theta-2.0\cos^4\theta$
			$I_\alpha'/I_\gamma'=1.33$	$I_\alpha'/I_\gamma'=2.0$
$O^{16}(j'=2^+)$	$I_\alpha=0$	$I_\alpha\sim 1+\frac{0.95x}{1-0.32x}\cos^2\theta$	$I_\alpha\sim 1-0.78\cos^2\theta$	$I_\alpha\sim 1+4.6\cos^2\theta-4.7\cos^4\theta$
		$I_\gamma\sim 1+\frac{0.47x}{1-0.16x}\cos^2\theta$	$I_\gamma\sim 1+0.43\cos^2\theta$	$I_\gamma\sim 1-1.4\cos^2\theta+1.8\cos^4\theta$
			$I_\alpha'/I_\gamma'=0.83$	$I_\alpha'/I_\gamma'=1.18$
$O^{16}(j'=3^-)$	$I_\alpha=0$	$I_\alpha\sim 1+\frac{0.95x}{1-0.32x}\cos^2\theta$	$I_\alpha\sim 1-\frac{2}{3}\cos^2\theta$	$I_\alpha\sim 1-0.9\cos^2\theta$
		$I_\gamma\sim 1+\frac{0.71x}{1-0.24x}\cos^2\theta$	$I_\gamma\sim 1+0.24\cos^2\theta$	$I_\gamma\sim 1+1.27\cos^2\theta+0.15\cos^4\theta$
			$I_\alpha'/I_\gamma'=0.83$	$I_\alpha'/I_\gamma'=0.96$
$O^{16}(j'=3^+)$	$I_\alpha\sim 1$	$I_\alpha\sim 1-\frac{0.27x}{1+0.09x}\cos^2\theta$	$I_\alpha\sim 1+\frac{1}{3}\cos^2\theta$	$I_\alpha\sim 1$
	$I_\gamma\sim 1$			
	$I_\alpha'/I_\gamma'=1$	$I_\gamma\sim 1-\frac{0.57x}{1+0.19x}\cos^2\theta$	$I_\gamma\sim 1+1.3\cos^2\theta$	$I_\gamma\sim 1+1.2\cos^2\theta+\cos^4\theta$
			$I_\alpha'/I_\gamma'=1.55$	$I_\alpha'/I_\gamma'=1.6$

measured by Devons and Hine[9] at the resonances below 900 kev of the proton energy and are being studied more extensively in this laboratory.[10] Devons and Hine found that the angular distribution of the gamma-rays so far obtained can be expressed in the form,

$$I_\gamma(\theta)=1+a\cos^2\theta, \tag{15}$$

with a equal to zero or a small fraction (≤ 0.2). The preliminary result of the gamma-ray angular distribution obtained in this laboratory does not show appreciable asymmetry between the forward and backward direction, and it yields a value of a as high as 0.67 at 1290 kev when the intensity is expressed in the form (15). Information about the angular distribution can also be obtained indirectly from the measured ratio of the alpha-intensity at 140° in the center-of-mass system to the gamma-intensity[1] at 90°. Table I gives the experimental values of the coefficient a and of the ratio $I(\alpha)_{140°}/I(\gamma)_{90°}$ at various gamma-ray resonances, the values of the coefficient a marked with D. H. being taken from reference 9.

As was mentioned before, the Ne^{20} compound states giving rise to the $\alpha\gamma$-groups are supposed to have $J=0^-$, 1^+, $2^-\cdots$. We consider only those levels with $J\leq 3$. Of the three gamma-rays, the intensity of γ_1 is strongest. The γ_1-level of O^{16} is expected to have $j'=1^-$ according to the shell structure model of the nucleus and to have $j'=3^-$ or to be a doublet with $j'=2^-$ and 2^+ according to the alpha-particle model. On the other hand, Devons and Hine suggested $j'=1^+$ for the γ_1-level taking the F^{19} parity to be odd. By means of formulas (4) and (10), we have calculated the theoretical angular distributions of the $\alpha\gamma$-group and of the corresponding gamma-rays for various transitions which are derived from different assignments of the compound state of Ne^{20} and of the excited state of O^{16} and with even parity of F^{19}. We shall see later on that the assumption of even parity of F^{19} is favored by the observed angular distributions of the α_x- and α_0-groups. Also even parity is indicated by the filling of $2s$-levels between O^{16} and Ne^{20}. The results of our calculation are given in Table II, where I_α and I_γ are the angular distributions of the alpha-particles and of the gamma-rays, respectively, I_α'/I_γ' is the theoretical ratio of the alpha-intensity at 140° to the gamma-intensity at 90° and x is the real part of the quantity X, which is defined in Eq. (5).

[9] S. Devons and M. G. N. Hine, Proc. Roy. Soc. **199A**, 56 (1949).
[10] Day, Chao, Fowler, and Perry, Phys. Rev. **80**, 131 (1950).

Comparison between the experimental data of Table I and the theoretical expressions of Table II now gives the following interpretations:

(a) The isotropic angular distribution of the gamma-rays at the resonances of 340, 669, and 935 kev can be interpreted as due to the capture of protons of $l=0$ or to the formation of Ne^{20} compound nuclei of $J=0^-$.

(b) The slightly anisotropic angular distribution of the gamma-rays at the resonance of 1381 kev can be interpreted as due to the formation of a Ne^{20} compound state of $J=1^+$ by a mixture of s- and d-protons. The observed value of the coefficient a is -0.07 at this resonance. From the barrier effect and the phase difference between the s- and d-protons we would expect a value of $x\sim-0.06$ at the proton energy of 1381 kev. This is found to be quite close to the values of x, which the assignments $j'=1^+$, 2^+, and 3^- require in order to have $a=-0.07$. Furthermore, with the values of x corresponding to $a=-0.07$ the assignments $j'=1^+$, 2^+ and 3^- give $I_\alpha'/I_\gamma'=0.98$, 0.94, and 0.95, respectively. They are all close to the observed ratio 0.88 at this resonance.

(c) The resonance at 598 kev gives a gamma-ray angular distribution with $a=0.2$. This can be interpreted by the assignment $J=2^-$ for the Ne^{20} compound nucleus and $j'=3^-$ for the γ_1-level. The resonance at 874 kev can be interpreted in the same way as the one at 598 kev or as that at 1381 kev.

(d) The large values of the coefficient a at the resonances of 1290 and 1355 kev can be interpreted as caused by (i) the formation of Ne^{20} compound states of $J=2^-$, or (ii) the formation of Ne^{20} states of $J=3^+$. It is seen in Table II, that with $J=2^-$ all transitions which give $a>0.5$ lead to values of I_α'/I_γ' greater than unity. Since the observed values of I_α'/I_γ' at these two resonances are 0.99 and 0.97, we must assume in this case that the intensities of the three gamma-ray components are just of the right proportion to make the average value of this ratio approximately equal to unity. If, on the other hand, we take $J=3^+$, the assignment with $j'=3^-$ leads to $I_\alpha'/I_\gamma'=0.96$, which is very close to the observed ratios. The coefficient a given by this assignment is now considerably higher than the observed coefficients at these two resonances. But this is to be expected from the effect of the background and of averaging over the three gamma-ray components. The small $\cos^4\theta$ term in I_γ required by this assignment would be inappreciable in the preliminary measurement in this laboratory.

(e) Arnold[2] found his results of correlation measurement between the alpha-particles and the gamma-rays at 340-kev proton energy to be in good agreement with the assignment $J=1^+$ for the Ne^{20} compound state and $j'=3^-$ for the γ_1-level of O^{16}. The assignment $j'=3^-$ is just the one required in (c) and (d). If we take $j'=3^-$ for the γ_1-level, the interpretation for the isotropic and slightly anisotropic angular distributions of the gamma-rays in (a) and (b) would be the same except that the assignment $J=0^-$ to the Ne^{20} compound state must be dropped for the gamma-ray resonances so far observed, because a state of $J=0^-$ could not transit to one of $j'=3^-$ by alpha-emission only. Hence, in addition to the levels at 340 and 1381 kev, which have been given the assignment $J=1^+$, the levels at 669 and 935 kev would have also $J=1^+$ on this basis. The fact that the α_1-group is present at all observed gamma-ray resonances might be an indication that transitions from a compound state of $J=0^-$ to all the three gamma-levels of O^{16} are forbidden. If this be the case, it might be still possible to detect a compound state of $J=0^-$ by the proton scattering experiment.

We give now in Table III our tentative assignment to the compound nucleus, the relative orbital angular momentum of the captured proton, and the calculated and observed proton widths for each resonance discussed in the foregoing. The values of the calculated proton width are obtained from the curves given by Christy and Latter,[11] and are normalized here to 1 kev at 1-Mev proton energy without barrier. The values of the observed proton width are taken from reference 1. They are calculated from the gamma-ray yields under the assumption that the alpha-width is large compared with the proton width. It is seen in Table III that the ratio of the observed to the calculated proton width varies considerably. Since the assumption $\Gamma_p\ll\Gamma_\alpha$ is only a trial one, some of the irregularities might be due to the breakdown of this assumption.

For some assignments of J and j' more than one value of l' satisfy the conservation laws of the angular momentum and the parity. Furthermore, the square roots of the relative barrier penetration factors of the α_1-group at the proton energy of 874 kev are: $\phi'=0.26$, 0.20, 0.10, 0.03, and 0.006 for $l'=0$, 1, 2, 3, and 4, respectively. Alpha-emission with a value of l' greater by two units than the lowest value might therefore produce an appreciable interference effect. When two or more values of l' are possible, it is found that the corresponding partial amplitudes give interference only on

TABLE III. Assignments to the Ne-levels giving rise to the gamma-ray resonance.

Level (kev)	J(Ne)	l_p	$(\Gamma_p)_{cal}$* (kev)	$(\Gamma_p)_{ob}$ (kev)	$\frac{(\Gamma_p)_{ob}}{(\Gamma_p)_{cal}}$†
340	1^+	0	0.0002	0.043	210
598	2^-	1	0.0020	0.044	22
669	1^+	0	0.014	0.13	9
874	2^-	1	0.013	1.13	87
874	1^+	0,2	0.042	1.13	27
935	1^+	0	0.060	0.63	11
1290	3^+	2	0.007	0.14	20
1355	3^+	2	0.008	0.21	26
1381	1^+	0,2	0.230	2.9	13

* $(\Gamma_p)_{cal}$, normalized to 1 kev at 1-Mev proton energy without barrier.
† This column gives widths without barrier in kev, when the proton energy is reduced to 1 Mev.

[11] R. F. Christy and R. Latter, Rev. Mod. Phys. **20**, 185 (1948).

TABLE IV. Angular distribution of the α_π-group.

Proton wave	$Ne(J=1^-)$	$Ne(J=2^+)$
$l=0$	$F^{19}(+)$ $I(\alpha_\pi)=0$ $F^{19}(-)$ $I(\alpha_\pi)\sim 1$	$F^{19}(+)$ $I(\alpha_\pi)=0$ $F^{19}(-)$ $I(\alpha_\pi)=0$
$l=1$	$F^{19}(+)$ $I(\alpha_\pi)\sim\cos^2\theta+(t/2)(1-\cos^2\theta)$ $t=0\to\infty$ $I_{140°}/I_{Av}=1.8\to 0.6$ $F^{19}(-)$ $I(\alpha_\pi)=0$	$F^{19}(+)$ $I(\alpha_\pi)=0$ $F^{19}(-)$ $I(\alpha_\pi)\sim 1+3\cos^2\theta$ $I_{140°}/I_{Av}=1.40$
$l=2$	$F^{19}(+)$ $I(\alpha_\pi)=0$ $F^{19}(-)$ $I(\alpha_\pi)\sim 1+3\cos^2\theta$ $I_{140°}/I_{Av}=1.40$	$F^{19}(+)$ $I(\alpha_\pi)\sim 1+(6t-6)\cos^2\theta+(9-6t)\cos^4\theta$ $t=0\to\infty$ $I_{140°}/I_{Av}=0.8\to 1.8$ $F^{19}(-)$ $I(\alpha_\pi)=0$

the alpha-intensity but not on the gamma-intensity. Hence, the calculated angular distributions of the gamma-rays, in particular, the coefficients of the $\cos^2\theta$ and $\cos^4\theta$ terms and the coefficients of x in the expressions of I_γ in Table II are not appreciably changed by considering more than one value of l'. The foregoing conclusions (a), (b), (c), (d), and (e) are therefore still valid when two values of l' are taken into consideration. The interference of two partial amplitudes corresponding to different values of l' might give appreciable change to the alpha-intensity. Detailed investigation about this change is, however, omitted because of the scarcity of the observed data.

(B) Angular Distribution of the α_π-Group

The resonance levels for the pair excitation are not very narrow compared to their spacing. Strictly speaking, we ought to consider the interference effect of the neighboring levels. Since, however, no data are available for the angular distribution of the α_π-group except some indirect information, for the sake of simplicity, we made calculation for this group also by means of formula (4). The excitation of the pairs is usually attributed to the formation of Ne^{20} compound states with $J=0^+, 1^-, 2^+, \cdots$. The assignment of the pair level is assumed to be $j'=0^+$. The calculated angular distributions of the α_π-group together with the ratio $I(\alpha_\pi)_{140°}/I(\alpha_\pi)_{Av}$ are given in Table IV.

Two sources of information are available for the angular distribution of the α_π-group: (a) the ratio of the yield of the α_π-group per unit solid angle at 140° with the incident beam to that of the pairs at 13° is found to be about 2 at the pair resonances 843 and 1236 kev in this laboratory.[1,12] Since the angular distribution of the pairs is expected to be isotropic, this value can be taken as the observed value of $I(\alpha_\pi)_{140°}/I(\alpha_\pi)_{Av}$. (b) The relative yield of α_0/α_π at the neighborhood of 1236 kev as measured at 90° by Van Patter *et al.*[13] is almost four times larger than the relative yield of α_0/pairs obtained at 90° by Streib *et al.*,[14] or $I(\alpha_\pi)_{90°}/I(\alpha_\pi)_{Av}\sim\frac{1}{4}$. Comparing the results (a) and (b) with the corresponding ratios which are given in Table IV or derivable therefrom, we find that the experimental results can be best interpreted as due to the capture of p-protons or d-protons by F^{19} with even parity.

(C) Angular Distribution of the α_0-Group

The Ne^{20} compound states giving rise to the high energy α_0-group ought to have $J=0^+, 1^-, 2^+, \cdots$. We shall limit our discussion to incident protons with orbital angular momenta up to $l=2$. The angular distributions will be different according to which parity F^{19} has. For convenience in discussion, we give in Table V the values of l and S for each value of J under the assumption of even or odd parity for F^{19}. The combination $(lSJ)=(3\ 1\ 2)$ is omitted under the odd parity of F^{19} because l is greater than 2 in that case.

At low proton energies the angular distribution of the α_0-group has been measured by Mclean *et al.*,[15] and analyzed by Gerjuoy[3] under the assumption of even parity of F^{19}. Rubin[16] has measured the angular distribution of the α_0-group at various proton energies and with great care at the two energies 1155 and 1348 kev.[17] He obtained:

$$I(\theta)=1-\tfrac{1}{3}\cos\theta+\cos^2\theta-\cos^3\theta \text{ at 1155 kev} \quad (16)$$

and

$$I(\theta)=1-\cos\theta+6\cos^2\theta+\cos^3\theta-5\cos^4\theta \text{ at 1348 kev.} \quad (17)$$

He also observed that the result at 1348 kev is in fair agreement with the theoretical angular distribution expected from the formation of a compound state of $J=2$ plus a background under the assumption of even parity of F^{19}.

TABLE V. Compound Ne states for the α_0-group.

$F^{19}(+)$			$F^{19}(-)$		
l	S	J	l	S	J
0	0	0^+	1	1	0^+
1	0	1^-	0	1	1^-
1	1	1^-	2	1	1^-
2	0	2^+	1	1	2^+
2	1	2^+	2	1	3^-

[12] Rasmussen, Hornyak, Lauritsen, and Lauritsen, Phys. Rev. **77**, 617 (1950).

[13] Strait, Van Patter, and Buechner, Phys. Rev. **78**, 337 (A) (1950); Van Patter, Sperduto, Strait, and Buechner, Progress Report of Laboratory for Nuclear Science and Engineering, MIT, p. 57, April (1950) (unpublished).

[14] Streib, Fowler, and Lauritsen, Phys. Rev. **59**, 253 (1941).

[15] Mclean, Ellett, and Jacobs, Phys. Rev. **58**, 500 (1940).

[16] S. Rubin, Phys. Rev. **72**, 1176 (1947).

[17] These values are a little higher than those originally given in Rubin's paper because of a change of the voltage scale.

We have calculated the two angular distributions of the α_0-group corresponding to both parities of F^{19} by means of formula (9). As the ratios of the square roots of the barrier penetration factors in (9), we take their values at the proton energy 1200 kev, i.e.,

$$\phi(0):\phi(1):\phi(2)=1:0.58:0.18. \quad (18)$$

In the following, we shall compare the observed angular distributions at 1155 and 1348 kev with each of the two theoretical angular distributions corresponding to the even and odd parity of F^{19}.

(1) *Angular Distribution of the α_0-Group under the Assumption of Even Parity of* F^{19}

In this case, we consider the contributions from three levels of $J=0^+$, 1^-, and 2^+. J is always equal to l. Hence we need only two indices l and S to specify the partial amplitude A and we can write A_{lS} instead of A_{JlS}. With this convention, we have, by applying formula (9) and dropping the constant K,

$$\begin{aligned}I_{\alpha_0}(\theta)=&\{0.50(A_{00})^2+0.021(A_{20})^2+0.25(A_{11})^2\\&-0.20A_{20}A_{00}\cos\omega_{20}\}\\&+\{A_{10}A_{00}\cos\omega_{10}+0.35A_{21}A_{11}\cos(\omega_{21}-\omega_{11})\\&-0.20A_{20}A_{10}\cos(\omega_{20}-\omega_{10})\}\cos\theta\\&+\{0.50(A_{10})^2-0.125(A_{20})^2\\&+0.60A_{20}A_{00}\cos\omega_{20}-0.25(A_{11})^2\\&+0.125(A_{21})^2\}\cos^2\theta\\&+\{0.60A_{20}A_{10}\cos(\omega_{20}-\omega_{10})\\&-0.35A_{21}A_{11}\cos(\omega_{21}-\omega_{11})\}\cos^3\theta\\&+\{0.187(A_{20})^2-0.125(A_{21})^2\}\cos^4\theta, \quad (19)\end{aligned}$$

ω_{00} being set equal to zero. The above formula is similar to the one given by Gerjuoy[3] with only two differences: (1) he used the barrier penetration factors at 400 kev; (2) he had separated the expansion coefficient $(2l+1)^{\frac{1}{2}}$ of the incident wave from the partial amplitude.

Let us now compare the observed angular distribution (16) and (17) with the theoretical expression (19). In doing this we indicate the partial amplitudes at 1155 and 1348 kev by A_{lS}' and A_{lS}'', respectively. The results obtained are as follows:

(a) The coefficient -5 of the $\cos^4\theta$ term at 1348 kev requires $A_{21}''\geq 6.3$ and $A_{21}''>A_{20}''$. It is seen in (19) that this high amplitude A_{21}'' is sufficient to account for the large coefficient of $\cos^2\theta$ at that resonance and hence makes the main contribution of the intensity, indicating a level with $J=2^+$ at 1348 kev.

(b) The presence of the $\cos\theta$ and $\cos^3\theta$ terms at 1348 kev requires an additional level $J=1^-$ to interfere with the level $J=2^+$. The angular distribution (17) could be interpreted as due to two levels $J=1^-$ and 2^+ only. But the position of the level $J=1^-$ cannot be established by (17) alone. Furthermore, (17) does not exclude the possibility of any influence of a third level $J=0^+$.

(c) The $\cos^3\theta$ term at 1155 kev requires the interference of two levels $J=1^-$ and 2^+, while the absence of the $\cos^4\theta$ term indicates small values of A_{21}' and A_{20}'. This is to be expected if we assume that a level $J=1^-$ is at 1155 kev and that interference is produced by the level $J=2^+$ at 1348 kev.

(d) If the assumption made in (c) is true, it is found by comparing the coefficients of the $\cos\theta$ powers of (16) and (19) that the observed angular distribution at 1155 kev can be better explained by assuming another level $J=0^+$ in addition to the two levels $J=1^-$ and 2^+. The level $J=0^+$ might be a broad one which constitutes the background.

(2) *Angular Distribution of the α_0-Group under the Assumption of Odd Parity of* F^{19}

If the parity of F^{19} is odd, four values of J are possible with $l\leq 2$. The $\cos^4\theta$ term at 1348 kev can be contributed only by the interference of the levels $J=1^-$ and 3^-. In order to account for the $\cos\theta$ and $\cos^3\theta$ term, there must be at least one level with even parity, which might have $J=0^+$ or 2^+. Because the resonance at 1348 kev is narrow and that at 1155 kev is broad, it seems reasonable to assume a level $J=3^-$ at 1348 kev, a level $J=1^-$ at 1155 kev, and a broad level $J=0^+$ as the background. We take now these three levels to calculate the angular distribution of the α_0-group in this case. Since S has the same value 1 for all the partial amplitudes, we write $A_{J,l}$ (with a comma between J and l) instead of A_{JlS}. By applying formula (9) and Eq. (18), we obtain now:

$$\begin{aligned}I_{\alpha_0}(\theta)=&\{1.5(A_{1,0})^2+0.056(A_{0,1})^2+0.005(A_{1,2})^2\\&+0.018(A_{3,2})^2+0.17A_{1,0}A_{1,2}\cos\omega_{1,2}\\&-0.32A_{1,0}A_{3,2}\cos\omega_{3,2}\\&-0.019A_{1,2}A_{3,2}\cos(\omega_{1,2}-\omega_{3,2})\}\\&+\{-0.58A_{1,0}A_{0,1}\cos\omega_{0,1}\\&+0.067A_{0,1}A_{1,2}\cos(\omega_{0,1}-\omega_{1,2})\\&+0.19A_{0,1}A_{3,2}\cos(\omega_{0,1}-\omega_{3,2})\}\cos\theta\\&+\{0.015(A_{1,2})^2-0.035(A_{3,2})^2\\&-0.52A_{1,0}A_{1,2}\cos\omega_{1,2}\\&+0.98A_{1,0}A_{3,2}\cos\omega_{3,2}\\&+0.22A_{1,2}A_{3,2}\cos(\omega_{1,2}-\omega_{3,2})\}\cos^2\theta\\&+\{0.31A_{0,1}A_{3,2}\cos(\omega_{0,1}-\omega_{3,2})\}\cos^3\theta\\&+\{0.088(A_{3,2})^2-0.28A_{1,2}A_{3,2}\\&\times\cos(\omega_{1,2}-\omega_{3,2})\}\cos^4\theta. \quad (20)\end{aligned}$$

By comparing (17) and (20), the coefficients of $\cos^4\theta$ now give

$$0.088(A_{3,2})^2-0.28A_{1,2}A_{3,2}\cos(\omega_{1,2}-\omega_{3,2})=-5$$

or

$$0.088(A_{3,2})^2-0.28A_{1,2}A_{3,2}+5\leq 0. \quad (21)$$

The last equation gives a minimum value of $A_{1,2}=4.7$, for which $A_{3,2}=7.5$. Since $A_{1,2}$ and $A_{1,0}$ are the partial amplitudes of the state $J=1^-$ due respectively to d-protons and s-protons with the factor $\phi(l)/\phi(0)$ taken out, $A_{1,2}$ and $A_{1,0}$ are expected to be of the same order of magnitude. Now, a value of $A_{1,0}$ of the order of 5 would result in a very large constant term of the order of 20 in the expression (20). This is incompatible with the observed constant term 1 in (17). The above con-

clusion is independent of the fact that we have omitted the possibility of a level $J=2^+$, because: (a) Eq. (21) will not change, and (b) the constant term might be even greater, if we introduce a level $J=2^+$ in addition to the three levels already assumed. The only way to avoid the above difficulty is to assume $A_{1,2} \gg A_{1,0}$. This might be possible if the capture proton fills a d-orbit inside the nucleus in forming the compound state $J=1^-$ and if an incoming d-proton has a much larger cross section for this process than an s-proton. The coefficient 6 of the $\cos^2\theta$ term in (17) also requires a high value of $A_{1,2}$ of the order of 20 if the resonance peak at 1348 kev is not mainly produced by interference. This in turn would make the level $J=1^-$ the main contributor of intensity and hence the resonance level at 1348 kev. While all the requirements mentioned above might not be impossible, the explanation given in (1) seems to be much more natural.

IV. CONCLUSIONS

Direct information on the angular distribution of the alpha-particles is available only for the α_0-group. The analysis of the data of this group is, however, rendered difficult by the interference effects. On the other hand, data about the angular distribution of the gamma-rays are still meager. Hence, most of the foregoing conclusions can be considered as only preliminary. We shall now summarize them as follows:

(a) The angular distribution of the α_π-group as well as that of the α_0-group favors the assumption of even parity for F^{19}.

(b) The isotropic gamma-ray angular distribution at some of the resonances can be interpreted as due to the capture of s-protons. The level at 340 kev which gives a strong resonance at low proton energy can be taken as one of $J=1^+$, formed by the capture of an s-proton, capture of d-protons being negligible at this energy. The levels at 669 and 935 kev which also give isotropic angular distribution of gamma-rays are probably formed in the same way.

(c) The gamma-ray angular distribution with a small coefficient of $\cos^2\theta$ can be interpreted as due to the formation of a compound state of $J=1^+$ by a mixture of s- and d-protons. This is probably the case with the level at 1381 kev, and possibly with some other levels.

(d) The level at 598 kev is probably one of $J=2^-$, formed by p-protons. The level at 874 kev can be interpreted as one of $J=1^+$ or of $J=2^-$.

(e) The levels at 1290 and 1355 kev, which give relatively large coefficients of the $\cos^2\theta$ term in the gamma-ray angular distribution, are probably those of $J=3^+$, formed by the capture of d-protons.

(f) The experimental data of the gamma-ray angular distribution and of the ratio I_α'/I_γ' are all in conformity with the assignment $j'=3^-$ for the γ_1-level of O^{16}.

It is to be mentioned that with the assignments of the three gamma-levels of O^{16} limited to the values of j' listed in Table II it is still difficult to explain the observed intensity ratios of the three α_γ-groups as given in reference (1). For further progress, it will be necessary to extend the correlation measurement between the alpha-particles and the gamma-rays and to measure the angular distributions of the separate α-groups.

In conclusion, the author wishes to thank Professor C. C. Lauritsen for his encouragement during the course of this investigation and to thank Professor W. A. Fowler and Professor R. F. Christy for their valuable suggestions and criticisms.

Second Sound in He^3-He^4 Mixtures

ERNEST A. LYNTON* AND HENRY A. FAIRBANK
Sloane Physics Laboratory, Yale University,† New Haven, Connecticut
(Received July 31, 1950)

Second sound has been investigated in He^3-He^4 mixtures for He^3 concentrations between 0.09 percent and 0.80 percent in the temperature range between 1.24°K and 1.95°K. The velocity of second sound was found to increase markedly with increasing concentration; e.g., at 1.26°K, the velocity with the 0.80 percent concentration was 26.52 meters/second as compared to 19.08 meters/second for pure He^4. The results of these experiments are compared with the theoretical predictions of Pomeranchuk.

I. INTRODUCTION

THE current theories of liquid He II[1,2] regard it as a mixture of two components, the normal fluid and the superfluid. As the temperature decreases from the λ-point, the ratio of the normal fluid to the super fluid density decreases very sharply, until at 1.4°K, e.g., only about six percent of the total liquid is in the normal phase.[3] Now, since it is one of the peculiarities of He II that only the atoms of the normal fluid can exchange momentum with other atoms, any extraneous particles in He II, such as atoms of He^3, are associated with the normal component. This reasoning has been verified experimentally by different investigators.[4-6] Any concentration of extraneous particles, large or small, of course, remains constant with decreasing temperature, so that even a very small percentage of such particles affects the normal density very strongly at lower temperatures.

Thus, even small amounts of He^3 constitute a very effective parameter in the study of any of those properties of liquid He II which depend strongly on the ratio of normal to superfluid density. One of these properties is second sound, the propagation of a temperature wave through liquid He II. A heat pulse sent into the liquid in one place creates there an excess of normal fluid. The equilibrium ratio of normal fluid and superfluid densities is re-established by a counterflow of the two fluids, which in turn disturbs the equilibrium elsewhere, and in this fashion the disturbing heat pulse is propagated through the liquid. Extensive experimental investigations of second sound[7-9] have shown it to be one of the most clear-cut and most accurately measurable phenomena of liquid He II. Because of this, and because of the strong dependence of the second sound velocity on the ratio of normal to superfluid densities and thus also on the concentration of He^3, we have felt that significant results could be obtained even with the small amount of He^3 which we had available.

A preliminary report of measurements of the second sound velocity with a 0.09 percent concentration of He^3 in He^4 has already appeared.[10] This article discusses in greater detail the experimental procedure used, and lists results for various concentrations between 0.09 and 0.80 percent, the highest concentration which we could achieve with the 3 cm^3 NTP of He^3 obtained from the AEC.

II. APPARATUS

The choice of the method and the design of the apparatus used in this series of experiments were determined primarily by two considerations. First of all, only a very small amount of He^3 was available, and thus every attempt had to be made to minimize the volume of the apparatus in order to obtain concentrations of reasonable magnitude. Furthermore, the isotope equilibrium in the liquid mixture could easily have been upset by any appreciable heat flux setting up internal convection of the normal and superfluid components of He II.[5,6] In such a process the normal component flows away from the source of heat and, since it alone can exchange momentum with other atoms, carries along most of the He^3. To avoid this, the heat input both at the transmitter and the receiver of the second sound had to be kept to a very low value.

As is shown schematically in Fig. 1, the cavity assembly consisted of a set of closely fitting Lucite parts, L, holding two circular carbon strip resistors,[11] R_1 and R_2, at either end of a cavity 3.0 mm in diameter and 10.0 mm in length. To each resistor were soldered two Kovar wires, one of which in turn was connected to a Kovar tube which, together with the other wire, formed a coaxial lead. The wire and the coaxial tube were separated by glass, and both in turn passed through Kovar-glass seals, K_1 and K_2. The whole assembly was made helium-tight by a stainless steel sleeve, S, which was soldered at both ends to the Kovar-glass seals, and the cavity was filled by means of a copper tube, F, 0.025″ in diameter, which was soldered to a 0.015″

* Dupont Predoctoral Fellow. This work is part of a thesis to be submitted by E. A. L. in partial fulfillment of the requirements for the Ph.D. degree at Yale University.
† Assisted by the ONR.
[1] L. Tisza, J. de phys. et rad. 1, 165, 350 (1940).
[2] L. Landau, J. Phys. U.S.S.R. 5, 71 (1941); 8, 1 (1944).
[3] E. L. Andronikashvili, J. Exp. Theor. Phys. 18, 424 (1948).
[4] Daunt, Probst, Johnson, Aldrich, and Nier, Phys. Rev. 72, 502 (1947).
[5] Lane, Fairbank, Aldrich, and Nier, Phys. Rev. 73, 256 (1948).
[6] Reynolds, Fairbank, Lane, McInteer, and Nier, Phys. Rev. 76, 64 (1949).
[7] V. Peshkov, J. Phys. U.S.S.R. 8, 381 (1944); 10, 389 (1946).
[8] Lane, Fairbank, and Fairbank, Phys. Rev. 71, 600 (1947).
[9] J. R. Pellam, Phys. Rev. 75, 1183 (1949).
[10] E. A. Lynton and H. A. Fairbank, Phys. Rev. 79, 735 (1950).
[11] H. A. Fairbank and C. T. Lane, Rev. Sci. Inst. 18, 525 (1947).

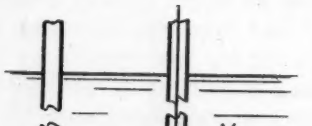

FIG. 1. Schematic diagram of the cavity assembly, showing resistors, R_1 and R_2, lucite pieces, L, Kovar-glass seals, K_1 and K_2, stainless steel sleeve, S, and filling tube, F.

stainless steel tube just above the cavity. The diameter of the cavity was smaller than that of the resistors; this difference ensured that the second sound propagation was essentially one-dimensional.

The second sound measurements were carried out by the pulse method,[9,12] in which the time of flight of a heat pulse between a transmitter and a receiver a known distance apart is measured by standard radar techniques. By feeding single pulses of heat into the transmitter and simultaneously pulsing the current through the receiver, it was possible to keep the input of heat to a very low value. The actual electronic arrangement is shown in block diagram in Fig. 2. A pulse generator triggered the sweep of an A/R radar range scope and, after an adjustable delay, sent into the transmitter a 60-volt signal of length variable up to 250 μsec. Simultaneously, a small steady current of about 1 milliampere through the receiver was pulsed manually for about half a second. The values of the transmitter and receiver resistance values were, respectively, about 17000 and 300 ohms. The input signal sent a current of about 3 milliampere through the transmitter, so that the total heat input into both resistances remained very small.

As the temperature pulse reached the receiver, the voltage signal resulting from the resistance change was sent to the vertical plates of the scope through a high gain amplifier. Since direct pick-up within the electronic circuit rendered visible the input pulse into the transmitter, the transit time could be directly determined from the scope picture. This was recorded photographically, superimposed on a calibrating signal of 50 kc, and the final measurements were made on a projection of the developed film.

The cavity was filled with mixtures of He^3 and He^4 of varying concentrations by means of a gas-handling system which included bulbs of He^3 and of He^4, manometers, and two Toepler pumps, with which any desired amount of the two isotopes could be mixed together and pushed into the cavity. Temperatures were measured by the vapor pressure of the helium bath using the latest vapor pressure tables.[13] Before a set of readings were taken, the bath was kept at a fixed temperature for about ten minutes to ensure temperature equilibrium, and this was checked by measurement of the vapor pressure of the mixture with a manometer attached to the filling tube of the cavity.

III. PROCEDURE AND RESULTS

Both previous calculations and preliminary experimentation indicated that with the values of resistance used and the single pulse transmitted to the pulsed receiver circuit, any heat flux effect was small enough to be negligible. Thus, we could take several readings at any one temperature in fairly rapid succession, and this was done for the various mixtures used throughout the temperature range between 1.24°K and 1.70°K. As will be discussed in greater detail below, the results of all the readings at any one temperature agreed very well to within the experimental error. At temperatures above 1.70°K, however, such multiple measurements could not be taken. Since the ratio of the amplitude of the heat pulse to the power input into the transmitter varies inversely with the specific heat of liquid helium, this temperature amplitude began to decrease sharply at about 1.70°K. In this region, therefore, the steady current through the receiver had to be increased to render the signal visible. This also increased the effect of heat flux, and so it was deemed advisable to take only a few readings, at rather long intervals, at each temperature. Here again the results were entirely consistent to within the experimental error, but the reliability of the values is necessarily somewhat lower that at the lower temperatures.

When the temperature for a certain set of readings was reached by raising the bath temperature from a lower value, heat would flow into the cavity. Conversely, when the temperature was attained after a previously higher value, heat would flow out of the cavity. Measurements were taken under both conditions, and their

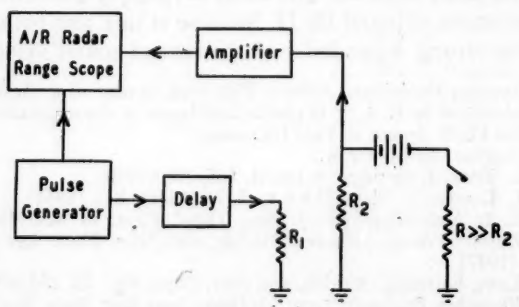

FIG. 2. Schematic block diagram of electronic apparatus. R_1 and R_2 are the transmitter and receiver resistors, respectively.

[12] D. V. Osborne, Nature 162, 213 (1948).

[13] H. van Dijk and D. Shoenberg, Nature 164, 151 (1949).

complete consistency showed that any disturbance of isotope equilibrium due to such heat flow was negligible. As a further check on the reproducibility of our results, some of the measurements with the 0.80 percent concentration were repeated on different days. Here again the values differed by less than the experimental error, indicating that our precautions to attain temperature equilibrium were sufficient. It must be noted, however, that in spite of all precautions isotope equilibrium may not have been established in the cavity. The only way to obtain such equilibrium with certainty is to stir the liquid, and that could not be done with the present apparatus.

The different concentrations of He^3 were obtained by first measuring the volume, pressure, and temperature of the 89 percent pure He^3, and then diluting it successively with known amounts of pure He^4. The necessary pressure measurements were made on a mercury manometer in a way which may have introduced an error in the concentration values as large as five percent. More accurate determinations of the concentrations in a mass spectrometer were intended; but, unfortunately, the spectrometer in this laboratory was found to be unsuitable for this type of measurement without calibration. Since no calibrating mixture was available, this difficulty has not yet been resolved.

TABLE I. Second sound velocity in liquid helium.

Temperature (°K)	Velocity (m/sec.)	Temperature (°K)	Velocity (m/sec.)
	A. Pure He^4		
1.26	19.08	1.545	20.33
1.30	19.28	1.60	20.50
1.40	19.71	1.65	20.46
1.45	19.97	1.70	20.33
1.50	20.12		
	B. 0.09 percent He^3		
1.26	20.68	1.60	20.92
1.39	20.58		
	C. 0.21 percent He^3		
1.25	22.02	1.50	21.16
1.395	21.29	1.59	21.13
	D. 0.41 percent He^3		
1.24	24.04	1.50	21.90
1.42	22.35	1.60	21.68
	E. 0.60 percent He^3		
1.24	25.71		
	F. 0.80 percent He^3		
1.24	27.09	1.55	23.02
1.26	26.52	1.575	22.96
1.26	26.66	1.58	22.94
1.27	26.44	1.60	22.88
1.28	25.84	1.61	22.72
1.33	25.32	1.65	22.31
1.38	24.63	1.66	22.16
1.40	24.40	1.70	21.87
1.40	24.36	1.75	21.47
1.425	24.22	1.80	21.12
1.46	23.78	1.85	20.42
1.50	23.45	1.895	19.51
1.545	23.13	1.93	18.76

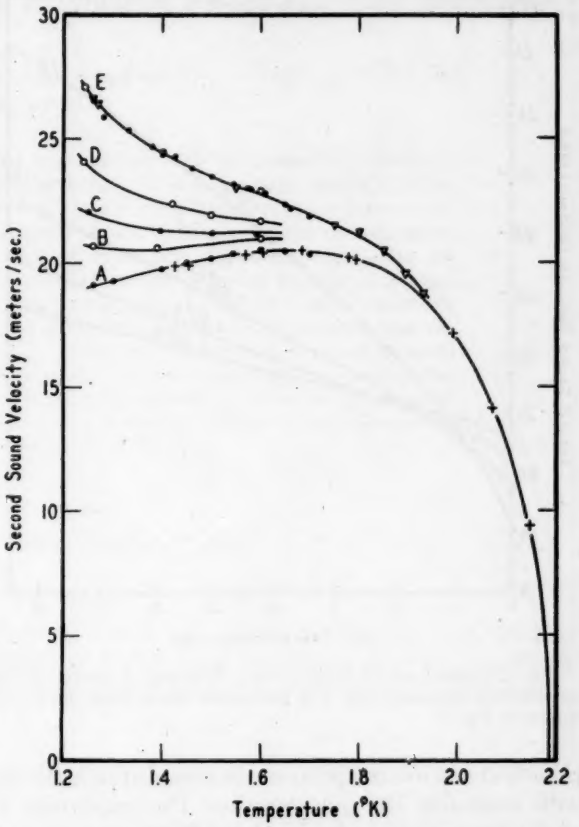

FIG. 3. Second sound velocity as a function of temperature for different concentrations: A, Pure He^4; B, 0.09 percent He^3; C, 0.21 percent He^3; D, 0.41 percent He^3; E, 0.80 percent He^3. In curve A the dots are the measurements taken in these experiments, the crosses those of reference 8. In curve E the open and closed dots are measurements taken with the same apparatus on different days. The triangles are the points taken with increased receiver current.

The combined results of the various runs are shown in Table I, and are also plotted in Figs. 3 and 4. As mentioned above, all values for temperatures below 1.70°K are the averages of a group of measurements, none of which deviate from their average by more than one-half of one percent. The measurements at 1.70°K with the 0.80 percent concentration were also taken with the low receiver current, allowing a whole series of readings; here, however, the signal received had already become very small with a corresponding decrease in the accuracy of the measurements. The value cited at this point, therefore, is an average from which the individual measurements deviate by almost one percent. In the temperature region between 1.75°K and 2.0°K, with the 0.80 percent concentration, only one or two readings were taken at any one temperature, all sets of two readings agreeing with each other to within one-half of one percent or better.

With the same transmitter pulse width and height and the same receiver current, the receiver signal am-

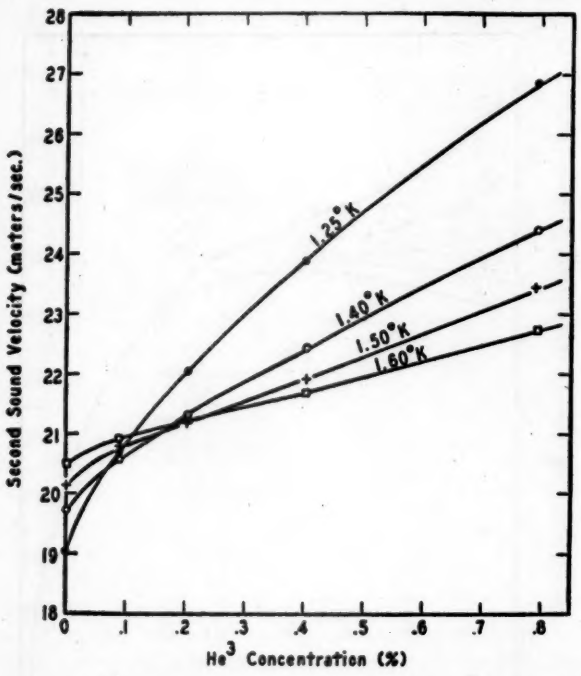

FIG. 4. Second sound velocity as a function of concentration for different temperatures. The points are taken from the curves shown in Fig. 3.

plitude at any one temperature decreased systematically with increasing He^3 concentration. The amplitude, T, of the temperature pulse is related to the power input, W, at the transmitter by the relation,

$$T/W = 1/\rho c u_2$$

(see e.g., reference 12), where ρc is the specific heat per unit volume of the liquid, and u_2 the second sound velocity. This equation is simply a statement of energy conservation with the assumption of negligible heat capacity in the transmitter.

A comparison of the height of the direct signal with that of the first echo showed that there was no appreciable increase in attenuation with increasing concentration. We therefore could use this equation to obtain values of the specific heat of the mixtures relative to that of pure He^4 from the respective signal amplitudes, and the known values of u_2 and W. With constant W, the product of T and u_2 decreased with increasing concentration by as much as a factor of about two for the 0.80 percent concentration at 1.25°K. Since there is no increase in attenuation to explain this effect, a corresponding increase in specific heat is implied. The magnitude of this increase is quite unexpected, and since the amplitude measurements could be in error by about ten percent, more precise experiments are being carried out before quantitative conclusions are drawn.

IV. DISCUSSION

The only theoretical treatment of the problem of second sound velocity in mixtures of He^3 and He^4 is that by Pomeranchuk in a paper[14] in which he treats the effect of small amounts of extraneous particles on the thermodynamic relations for He II and on the second sound velocity. He derives for the second sound velocity under these conditions the expression,

$$u_2^2 = (T/C)(\rho_s/\rho_n)[(S_0 + k\epsilon/m)^2 + k\epsilon C/m],$$

where ϵ is the concentration of the extraneous particles, and where C, the specific heat, and ρ_n, the normal component density, are themselves functions of ϵ. According to Pomeranchuk's theory, the first terms containing ϵ to become appreciable as the temperature decreases from the λ-point are those in $k\epsilon/m$, so that at first the second sound velocity for mixtures exceeds that for pure He^4. At lower temperatures the normal component density begins to exceed that of pure He^4 very markedly, reversing the trend of the effect caused by the He^3, until ultimately the velocity for mixtures is far lower than that for pure He^4.

Pomeranchuk treats two cases, one for which the minimum energy of the extraneous particles occurs for zero particle momentum ($p_0 = 0$), and the other where the energy minimum occurs at some value of momentum, $p_0 \neq 0$. The main difference between the two cases in relation to the second sound velocity lies in the behavior of the normal component density, ρ_n; in the first case Pomeranchuk obtains,

$$\rho_n = \rho_{n0} + \rho\epsilon/m,$$

and in the second,

$$\rho_n = \rho_{n0} + (\rho/m)(p_0/3kT)\epsilon.$$

He calculates second sound velocities for different concentrations at various temperatures for the case $p_0 = 0$, and points out that the difference between the two cases is not very great for $T > 1.1$°K, and concentrations of 0.1 percent or less. For the 0.09 percent concentration our values for the fractional increase of the second sound velocity for mixtures over that for pure He^4 agree very closely with the theoretical predictions, but are lower than Pomeranchuk's values for our higher concentrations. According to the theory this would indicate that for He^3, $p_0 \neq 0$.

We wish to thank Professor Howard L. Schultz for his help in designing the electronic equipment. We are also grateful to Professor William W. Watson and Mr. John Donaldson for devoting much time and effort to the problem of determining the He^3 concentration with the mass spectrometer.

[14] I. Pomeranchuk, J. Exp. Theor. Phys. U.S.S.R. 19, 42 (1949).

Quantum Theory of Non-Local Fields. Part II. Irreducible Fields and their Interaction*

HIDEKI YUKAWA†
Columbia University, New York, New York
(Received August 7, 1950)

General properties of non-local operators are considered in connection with the problem of invariance with respect to the group of inhomogeneous Lorentz transformations. It is shown that irreducible fields can be classified by the eigenvalues of four invariant quantities. Three of these quantities can be interpreted, respectively, as the mass, radius, and magnitude of the internal angular momentum of the particles associated with the quantized non-local field in question. Further, space-time displacement operators are introduced as a particular kind of non-local operator. As a tentative method of dealing with the interaction of non-local fields, an invariant matrix is defined by the space-time integral of a certain invariant operator, which is a sum of products of non-local field operators and displacement operators. It is shown that the matrix thus constructed satisfies the requirements that it be unitary and invariant and that the matrix elements are different from zero only if the initial and final states had the same energy and momentum. However, the remaining conditions of correspondence and convergence cannot be fulfilled simultaneously, in general, by the S-matrix for the non-local fields. It is yet to be investigated whether all of these requirements are satisfied by an appropriate change in the definition of the S-matrix.

I. ELEMENTARY NON-LOCAL SYSTEMS

THE notion of an elementary particle has been intimately connected with the procedure of decomposing a quantized field into its irreducible parts. Accordingly, if the concept of the field itself is so extended as to include the non-local field, the definition of the elementary particle will be altered in its turn. In Part I,[1] we confined our attention to certain types of non-local fields which satisfied a set of operator equations and were supposed to represent assemblies of elementary particles with finite radii. Our problem is now to decompose more general non-local fields into irreducible parts. Again we start from an arbitrary unquantized non-local scalar field U, which can be represented by an arbitrary matrix $(x'|U|x'')$, where x' and x'' stand for x_μ' and x_μ'' ($\mu=1, 2, 3, 4$), respectively. The matrix $(x'|U|x'')$ can be regarded as a function $U(X, r)$ of two sets of real variables,

$$X_\mu=\tfrac{1}{2}(x_\mu'+x_\mu''), \quad r_\mu=x_\mu'-x_\mu'' \tag{1}$$

as in Part I. Then an arbitrary function $U(X, r)$ can be expanded in the form

$$U(X, r)=\int\cdots\int u(k, r)\exp(ik_\mu X^\mu)(dk_\mu)^4 \tag{2}$$

and further in the form

$$U(X, r)=\int\cdots\int u(k, l)\exp(ik_\mu X^\mu)\times\prod_\mu\delta(r_\mu-l_\mu)(dk_\mu)^4(dl_\mu)^4, \tag{3}$$

where $u(k, r)$ and $u(k, l)$ are arbitrary functions of parameters k, r and k, l, respectively.

Now, if we perform an arbitrary homogeneous Lorentz transformation,

$$x_\mu'=a_{\mu\nu}x_\nu, \tag{4}$$

where x_μ' ($\mu=1, 2, 3, 4$) denote this time the space-time operators in the new coordinate system. Therewith, two sets of parameters, X and r, are transformed into

$$X_\mu'=a_{\mu\nu}X_\nu, \quad r_\mu'=a_{\mu\nu}r_\nu \tag{5}$$

and $U(X, r)$ becomes

$$U(X', r')=\int\cdots\int u'(k', l')\exp(ik_\mu'X'^\mu)\times\prod_\mu\delta(r_\mu'-l_\mu')(dk_\mu')^4(dl_\mu')^4, \tag{6}$$

where $u'(k', l')=u(k, l)$. k', l' are connected with k, l just as X', r' are connected with X, r. In order that Eq. (6) retain the same form as Eq. (3) for an arbitrary Lorentz transformation (4), either one of the following two requirements must be satisfied:

(i) $u(k, l)$ is a function of k and l, which retains its form under an arbitrary Lorentz transformation;

(ii) $u(k, l)$ is not a mere function of k and l, but is an ensemble of quantities, which are distinguished by the parameters k and l and which are to be subject to second quantization.

In the first case, it is required that

$$u(k', l')=u(k, l) \tag{7}$$

for an arbitrary transformation

$$k_\mu'=a_{\mu\nu}k_\nu, \quad l_\mu'=a_{\mu\nu}l_\nu, \tag{8}$$

so that $u(k, l)$ must be the function of invariant quantities such as $k_\mu k^\mu$, $l_\mu l^\mu$ and $k_\mu l^\mu$ alone. In many cases, however, we can confine our attention to the subgroup of the homogeneous Lorentz group which does not include the reversal of the time, so that $u(k, l)$ may depend also on $k_4/|k_4|$, provided that k_μ is a time-like vector, and similarly for l_μ. Thus $U(X, r)$ can be

* Publication assisted by the Ernest Kempton Adams Fund.
† On leave of absence from Kyoto University, Kyoto, Japan.
[1] H. Yukawa, Phys. Rev. 77, 219 (1950). See also B. Kwal, J. de phys. et rad. 11, 213 (1950).

written, in general, in the form

$$U(X,r)=\int\cdots\int w(K,L,M)\delta(k_\mu k^\mu-K)\delta(l_\mu l^\mu-L)\times\delta(k_\mu l^\mu-M)\exp(ik_\mu X^\mu)\prod_{\mu=1}^{4}\delta(r_\mu-l_\mu)\times(dk_\mu)^4(dl_\mu)^4dKdLdM, \quad (9)$$

where $w(K,L,M)$ is an arbitrary function of the real parameters K, L, and M, which can be positive, negative, or zero. If we restrict the transformations to those belonging to the subgroup mentioned above, w may depend also on $k_4/|k_4|$ (and on $l_4/|l_4|$). In any case, the operator U of this type has nothing to do with the quantized non-local field, because there is no room for the application of the method of second quantization. However, an important family of space-time displacement operators belongs to this category as will be shown later on.

The case (ii) is the more important, because the field operator U can be quantized as in the usual theory. Namely, the coefficients $u(k,l)$ can be regarded as an ensemble of creation and annihilation operators for the quanta associated with the field U. The requirement of invariance is fulfilled simply by identifying $u(k,l)$ $[=u'(k',l')]$ with the creation or annihilation operator for a particle in the quantum state characterized by k and l according as k_4 is positive or negative. The only effect of a transformation of the type (4) or (8) is to give a new notation $u'(k',l')$ to the operator $u(k,l)$, owing to the change in name for the same quantum states caused by the change of the reference system. Thus, there is the one-to-one correspondence between $u(k,l)$ and $u'(k',l')$ in two representations, (3) and (6), of the same operator U. Since $k_\mu k^\mu$, $l_\mu l^\mu$, and $k_\mu l^\mu$ are invariant with respect to any Lorentz transformation, the one-to-one correspondence remains, even if the domain of integrations on the right-hand side of Eq. (3) is restricted to definite values K, L, M of these invariant quantities $k_\mu k^\mu$, $l_\mu l^\mu$, and $k_\mu l^\mu$, respectively. In such a case, $U(X,r)$ reduces to

$$U(X,r)=\int\cdots\int u(k,l)\exp(ik_\mu X^\mu)\prod_\mu\delta(r_\mu-l_\mu)\times\delta(k_\mu k^\mu-K)\delta(l_\mu l^\mu-L)\delta(k_\mu l^\mu-M)(dk_\mu)^4(dl_\mu)^4. \quad (10)$$

It is now clear that the scalar non-local field, which was dealt with in detail in Part I, is a particular example with

$$K\equiv-\kappa^2,\quad L\equiv+\lambda^2,\quad M\equiv 0. \quad (11)$$

More generally, L and M can be either positive or negative including zero, but K can only be negative or zero, because a positive K has no correspondence with the classical model of particles with real mass. Positive values of L correspond to the assembly of elementary particles with a finite dimension which is extended to space-like directions, whereas negative values of L corresponds to that which is extended to time-like directions.

It should be noticed, however, that the field characterized by a set of values of K, L, and M can be decomposed further into irreducible parts, each of which corresponds to a definite value for the absolute magnitude of the internal angular momentum. Namely, as shown in Part I, the non-local scalar field U with a given set of values K, L, M can be expanded in the form

$$U=\sum_{k_1k_2k_3}\sum_{l,m}(2\pi/L)^3[\lambda/4\kappa(k^2+\kappa^2)^4]\times[u(k,l,m)U(k,l,m)+v^*(k,l,m)U^*(k,l,m)], \quad (12)$$

provided that K is negative, L is positive, and M is zero, where u, v^*, U, U^* are defined by the expressions (43) and (44) in Part I. The parameter l in (12) is the quantum number which characterizes the magnitude of the internal angular momentum in the coordinate system moving with the particle with a given wave vector k_1, k_2, k_3. Since l thus defined is invariant with respect to Lorentz transformations, each part of U with a definite value of l transforms into itself and constitutes an irreducible representation of the non-local scalar field. Thus, it is possible that the elementary particles with the integer spins are classified by the value of four constants K, L, M, and l, provided that they are represented by irreducible representations of the non-local scalar field. Among these four constants, $-K$, L, and l can be interpreted, apart from the numerical factors depending on $\hbar$ and c alone, as the mass, radius, and magnitude of the internal angular momentum of the particle, whereas M has no immediate physical meaning.[2]

As was pointed out recently by Fierz,[3] each of these irreducible representations of the non-local scalar field finds its counterpart in the usual field theory of elementary particles with arbitrary integer spin, so far as the behavior with respect to Lorentz transformations is concerned. The essential difference between local and non-local fields will be clear only when the interaction between fields is taken into account. In the case of the non-local spinor field, however, the situation is somewhat different. Namely, a non-local spinor operator ψ_i $(i=1,2,3,4)$ is equivalent to a set of four functions $\psi_i(X,r)$, which can be expanded in the form

$$\psi_i(X,r)=\int\cdots\int u_i(k_\mu,l_\mu)\exp(ik_\mu X^\mu)\times\prod_\mu\delta(r_\mu-l_\mu)(dk_\mu)^4(dl^\mu)^4. \quad (13)$$

This can be decomposed into parts in an invariant manner by giving each of $k_\mu k^\mu$, $l_\mu l^\mu$, $k_\mu l^\mu$ a definite value. Each part can further be regarded as a sum of operators, which differ from one another by their behaviors with respect to space rotations in the rest

[2] D. Yennie, Phys. Rev., following paper.
[3] M. Fierz, Phys. Rev. 78, 184 (1950); Helv. Phys. Acta 23, 412 (1950).

system. Each of these operators thus obtained is not yet irreducible in general, because it is a mixture of two types of fields belonging to the same resultant (half-integral) spin. For instance, the operator corresponding to the resultant spin 1/2 may have an internal orbital angular momentum of either zero or unity. In the usual local field theory, however, a spinor field with the spin 1/2, for example, is already irreducible. Thus the difference between the non-local spinor field and the local spinor fields with arbitrary half-integral spins is apparent without taking into account the interaction between the fields.[4]

So far we have considered the problem of invariance of non-local operators with respect to homogeneous Lorentz transformations. Now we go over to the more general inhomogeneous Lorentz transformation of the type

$$x_\mu' = a_{\mu\nu}(x_\nu + b_\nu) \tag{14}$$

or

$$x_\mu' = a_{\mu\nu}x_\nu + b_\mu', \tag{15}$$

with $b_\mu' = a_{\mu\nu}b_\nu$, X and r are transformed thereby into

$$X_\mu' = a_{\mu\nu}(X_\nu + b_\nu), \quad r_\mu' = a_{\mu\nu}r_\nu. \tag{16}$$

Accordingly, we have

$$k_\mu' = a_{\mu\nu}k_\nu, \quad l_\mu' = a_{\mu\nu}l_\nu, \tag{17}$$

and

$$u'(k', l') = \exp(-ik_\mu b^\mu)u(k, l), \tag{18}$$

in order that U be invariant with respect to the transformation (14). The implication of the relation (18) must be considered for the cases (i) and (ii) separately.

In case (i), relation (18) is compatible with the assumption that $u(k, l)$ is an invariant function of k and l, only if $u(k, l)$ is zero for all values of k_μ except $k_\mu = 0$ ($\mu = 1, 2, 3, 4$). This is equivalent to the following statement:

(i)′ A non-local operator U which satisfies requirement (i) is invariant with respect to the whole group of inhomogeneous Lorentz transformations only if $U(X, r)$ is an invariant function of r alone.

It will be shown in the next section that some of the invariant operators satisfying the requirement (i)′ will be of importance in constructing the S-matrix for the interacting non-local fields.

In case (ii), relation (18) reflects the situation that the creation or annihilation operator $u(k, l)$ or $u^*(k, l)$ is defined unambiguously except for an arbitrary phase factor. In spite of this ambiguity or complication, the operator $u^*(k, l)u(k, l)/|k_4|$, which is to be identified with the occupation operator for particles in the quantum state characterized by k_μ and l_μ apart from the purely numerical factor, is defined uniquely and is invariant with respect to the whole group of inhomogeneous Lorentz transformations. So are the commutation relations for $u(k, l)$ and $u^*(k, l)$ as given by Eq. (37) of Part I, for example. Of course, it must always be kept in mind that the time-reversal is associated with the interchange of the annihilation operator $u(k, l)$ and the creation operator $u^*(k, l)$.

These arguments can be applied to non-local spinor fields without essential change. In this way we arrive at the following suggestion: according to the non-local field theory it is possible that there are only two kinds of elementary particles, Bose-Einstein particles and Fermi-Dirac particles, which are described by a scalar field and a spinor field, respectively. The customary discrimination of particles with spins 0, 1, 2, etc., among Bose-Einstein particles, for instance, may well be reduced to the difference in the quantum number l for the internal motion of the same kind of particles.

II. S-MATRIX IN NON-LOCAL FIELD THEORY[5]

Now we must undertake the problem of interaction between non-local fields. In the usual field theory we could always start from the Schrödinger equation for the total system. The Hamiltonian in the Schrödinger equation is derived from the Lagrangian which, in turn, is so chosen as to give the correct field equations for unquantized fields, when the classical variation principle was applied to the system consisting of unquantized fields. In the non-local field theory, however, it is difficult to follow the same procedure as in local field theories for two reasons. Firstly, even in the case of the free field, it is difficult to deduce all of the field equations, (4), (5), and (12), for example, for the scalar non-local field from an invariant operator which is supposed to correspond to the Lagrangian in the usual theory. Moreover, the procedure of variation itself is ambiguous.[6] Secondly, it is rather dubious whether the differentiation of the Schrödinger function with respect to time will play an important role in non-local field theory because other operators, in general, are related to two time instants, which differ from each other by a finite amount. Even the existence of the Schrödinger function in the same sense as in the local field theory is not at all certain.

Although it is not yet clear whether these difficulties could be overcome without renouncing the fundamental principles of quantum mechanics, there seems to exist a tentative solution which retains many of the characteristics of the present field theory. Namely, we can start from the so-called interaction representation in the usual theory, laying aside for the moment the question of whether the free field equations in non-local field theory can be deduced from the Lagrangian formalism or not. Furthermore, we can adopt the integral formalism of the usual theory, which has been

[4] Detailed discussions of non-local spinor field will be made elsewhere.

[5] A preliminary account of the subject was published by H. Yukawa, Phys. Rev. 77, 849 (1950).

[6] Variation principles in the non-local field theory were discussed by C. Bloch, Kgl. Danske Vid. Sel. Math.-Fys. Medd. See also C. Gregory, Phys. Rev. 78, 67, 479 (1950).

proved to be equivalent to the differential formalism and in which the S-matrix, instead of the Schrödinger wave function, came in the foreground. Then the S-matrix for local fields can be transformed in the following manner so as to be easily extended to the case of non-local fields. We consider a system of local fields, for which the interaction Hamiltonian density $H'(x, y, z, t)$ is invariant and is equal to $-L'(x, y, z, t)$, where L' is the interaction part in the Lagrangian density for the system. In the usual one-time formalism, the Schrödinger equation has the form

$$i\hbar\partial\Psi(n', t)/\partial t=\sum_{n''}(n'|\bar{H}'(t)|n'')\Psi(n'', t), \quad (19)$$

where each of n' and n'' stands for a set of eigenvalues of occupation operators of various types of particles in the system in various quantum states. $\bar{H}'(t)=-\bar{L}'(t)$ is the space integral of the Hamiltonian density $H'(x, y, z, t)$ or $-L'(x, y, z, t)$. The differential equation (19) can be integrated with respect to time, at least formally, by the method of successive approximation and we obtain

$$\Psi(n', +\infty)=\Psi(n', -\infty)$$
$$+(i/\hbar)\int_{-\infty}^{+\infty}\sum_{n''}(n'|\bar{L}'(t)|n'')dt\cdot\Psi(n'', -\infty)$$
$$+(i/\hbar)^2\int\int_{t>t'}\sum_{n'', n'''}(n'|\bar{L}'(t)|n'')(n''|\bar{L}'(t')|n''')$$
$$\times dtdt'\Psi(n''', -\infty)+\cdots, \quad (20)$$

where $\Psi(n', +\infty)$ and $\Psi(n', -\infty)$ are Schrödinger wave functions in the infinite future and infinite past, respectively. Thus the S-matrix for this case is given by

$$(n'|S|n'')=(n'|1|n'')+(i/\hbar)\int(n'|\bar{L}'(t)|n'')dt$$
$$+(i/\hbar)^2\int\int_{t>t'}\sum_{n'''}(n'|\bar{L}'(t)|n''')(n'''|\bar{L}'(t')|n'')$$
$$\times dtdt'+\cdots. \quad (21)$$

In order to generalize this expression for the S-matrix to the case of the system of non-local fields, we introduce an invariant Hermitian non-local operator L' which is represented by a matrix $(n', x'|L'|n'', x'')$ and which reduces to

$$(n', x'|L'|n'', x'')=(n'|L'(x')|n'')\prod_{\mu}\delta(x'^{\mu}-x''^{\mu}) \quad (22)$$

in the limiting case of the system of local fields, where each of x' and x'' stands for a set of eigenvalues of space-time operators $x^1=x$, $x^2=y$, $x^3=z$, $x^4=ct$. With the help of Eq. (22) and of another non-local operator ϵ which is represented by the matrix

$$(n', x'|\epsilon|n'', x'')$$
$$=\tfrac{1}{2}\{[(x'^4-x''^4)/|x'^4-x''^4|]+1\}(n'|1|n^4). \quad (23)$$

Equation (21) can be written in the form

$$(n'|S|n'')=(n'|1|n'')$$
$$+(i/\hbar c)\int\int(n', x'|L'|n'', x'')(dx')^4(dx'')^4$$
$$+(i/\hbar c)^2\int\cdots\int\sum_{n''', n^{\mathrm{IV}}}(n', x'|L'|n''', x''')$$
$$\times(n''', x'''|\epsilon|n^{\mathrm{IV}}, x^{\mathrm{IV}})(n^{\mathrm{IV}}, x^{\mathrm{IV}}|L'|n'', x'')$$
$$\times(dx')^4(dx'')^4(dx''')^4(dx^{\mathrm{IV}})^4+\cdots. \quad (24)$$

If we define $\{A\}$ for an arbitrary non-local operator A by

$$(n'|\{A\}|n'')$$
$$=\int\cdots\int(n', x'|A|n'', x'')(dx')^4(dx'')^4, \quad (25)$$

the S-matrix with matrix elements as given by Eq. (24) can be written symbolically in the form

$$S=1+(i/\hbar c)\{L'\}+(i/\hbar c)^2\{L'\epsilon L'\}$$
$$+(i/\hbar c)^3\{L'\epsilon L'\epsilon L'\}+\cdots. \quad (26)$$

This could be used as the definition of the S-matrix in non-local field theory as well as in local field theory. Alternatively, we can define S or $S-1$ by

$$S-1=\{R\}, \quad (27)$$

where

$$R=(i/\hbar c)L'+(i/\hbar c)^2L'\epsilon L'+(i/\hbar c)^3L'\epsilon L'\epsilon L'+\cdots. \quad (28)$$

Incidentally, the non-local operator R satisfies a linear operator equation

$$R=(i/\hbar c)L'+(i/\hbar c)L'\epsilon R. \quad (29)$$

The physical interpretation of the S-matrix remains the same as in the usual theory in spite of the fact that the S-matrix is non-local field theory is defined directly by Eq. (26) or by Eqs. (27) and (28) without recourse to the Schrödinger equation of type (19). Thus, $|(n'|S|n'')|^2$ is the probability that the system will be in the state characterized by n' in the infinite future provided that it was in the state characterized by n'' in the infinite past. In fact, the S-matrix as defined by (26) satisfies two conditions:

(i) S is a unitary matrix which satisfies the relation

$$S^*S=SS^*=1. \quad (30)$$

(ii) The matrix element $(n'|S|n'')$ is different from zero only if the states characterized by n' and n'', respectively, have the same total energy and momentum.

Before going into the proof of these statements, we have to take into account the third condition:

(iii) S must be an invariant matrix.

In local field theories, the S-matrix defined above is

invariant, in spite of the fact that the operator ϵ as defined by Eq. (23) is not invariant with respect to Lorentz transformations. This is due to the fact that the Hamiltonian density $H'(x')$ at a point x' is commutative with the density $H'(x'')$ at any other point x'', which is located in a space-like direction with respect to x'. It is not so, in general, in non-local field theory. An obvious way of guaranteeing the invariance of the S-matrix in such a case is to replace the operator ϵ in Eq. (26) by a suitable invariant non-local operator D_+ such that conditions (i) and (ii) are still fulfilled. Thus the S-matrix for the system of non-local fields takes the form

$$S=1+(i/\hbar c)\{L'\}+(i/\hbar c)^2\{L'D_+L'\}+(i/\hbar c)^3\{L'D_+L'D_+L'\}+\cdots. \quad (31)$$

The actual form of the operator D_+ can be determined in the following manner. If we assume that the invariant operator L' is a sum of products of non-local field operators, condition (ii) is satisfied for any displacement operator D_+ whose matrix element $(x'|D_+|x'')\equiv D_+(X, r)$ is an invariant function of r_μ alone. The proof is simple. Any non-local operator A can be represented by a matrix $(x'|A|x'')$ or a function $A(X, r)$ and Eq. (25) can be written alternatively in the form

$$(n'|\{A\}|n'')=\int\int (n'|A(X, r)|n'')(dX)^4(dr)^4. \quad (32)$$

If the operator A consists of a sum of products of L' and D_+, $(n'|A(X, r)|n'')$ can be expanded into a series with the typical term

$$(n'|a(k_\mu^{(i)}, r_\mu)|n'')\exp(iK_\mu X^\mu), \quad (33)$$

where

$$K_\mu=\sum_i n''^{(i)}k_\mu^{(i)}-\sum_i n'^{(i)}k_\mu^{(i)}. \quad (34)$$

Evidently $\hbar K$ is the difference in momenta between the initial state n'' and the final state n' and $-\hbar cK_4$ is the difference in energies of the states n'' and n'. If we insert Eq. (33) into Eq. (32) and integrate with respect to X, we find that each term of $(n'|\{A\}|n'')$ contains a factor $\prod_\mu \delta(K_\mu'-K_\mu'')$, so that $(n'|\{A\}|n'')$ is different from zero only if the states n' and n'' have the same energy and momentum. It should be noticed, however, that we mean by the energy and momentum of a particle the energy and momentum of its center of mass. Thus the energy of internal motion is supposed to be included already in the mass $\hbar\kappa/c$. In other words, κ must be, in general, a function of other constants such as λ and l. The problem of determining the form of such a function is still completely open.

The condition (i) is also fulfilled, if we further imply the condition

$$D_+ + D_+^* = E \quad (35)$$

on D_+, where D_+^* is the Hermitian conjugate of D_+ and E is an invariant displacement operator with the matrix element

$$(n', x'|E|n'', x'')=(n'|1|n''). \quad (36)$$

for any values of x' and x''. In order to prove this, we have only to multiply S as given by Eq. (31) by

$$S^*=1-(i/\hbar c)\{L'\}+(i/\hbar c)^2\{L'D_+^*L'\}-(i/\hbar c)^3\{L'D_+^*L'D_+^*L'\}+\cdots. \quad (37)$$

Then the condition of unitarity

$$\sum_{n'''}(n'|S^*|n''')(n'''|S|n'')=\sum_{n'''}(n'|S|n''')(n'''|S^*|n'')=(n'|1|n'') \quad (38)$$

comes out by the help of Eq. (32) and the relation

$$\{AEB\}=\{A\}\{B\}, \quad (39)$$

which holds for any two non-local operators A and B.

The operators D_+^* and D_+ which satisfy all of these conditions are given by matrices

$$(n', x'|D_+|n'', x'')=(n'|1|n''),\ \tfrac{1}{2}(n'|1|n''),\text{ or } 0;$$
$$(n', x'|D_+^*|n'', x'')=0,\ \tfrac{1}{2}(n'|1|n''),\text{ or } (n'|1|n''), \quad (40)$$

according as $x'-x''$ is future-like, space-like, or past-like.

This modification of the definition of S-matrix gives rise to the new question: does it reduce to the usual definition (21) in the limit of local fields? This question is very intimately connected with another, and probably the most important, question: is the S-matrix for non-local fields convergent? In order to answer these questions, we begin with the investigation of the particular matrix element $(0|S|0)$ of $(n'|S|n'')$, where both the initial state n'' and the final state n' are complete vacua; i.e., all eigenvalues n' and n'' are zero. Now $(0|S|0)$ has the general form

$$(0|S|0)=1+(i/\hbar c)(0|\{L'\}|0)+(i/\hbar c)^2(0|\{L'D_+L'\}|0)+\cdots. \quad (41)$$

Let us consider a very simple case of a system consisting of a complex non-local scalar field V, V^* and a real non-local scalar field U with the interaction of the form

$$L'=gV^*UV. \quad (42)$$

We have first

$$(0|\{L'\}|0)=0 \quad (43)$$

because L' is linear in U and hence has no term which connects the state 0 with itself. As for the third term in Eq. (38), we have the relation

$$(0|\{L'D_+L'\}|0)=\tfrac{1}{2}\sum_{n'}(0|\{L'\}|n')(n'|\{L'\}|0)+\tfrac{1}{2}(0|\{L'DL'\}|0) \quad (44)$$

on account of relations (32) and (36), where the operator D is defined by

$$D=D_+-D_+^* \quad (45)$$

with the matrix element

$$(n', x'|D|n'', x'')=(n'|1|n''),\ \ 0,\ \ -(n'|1|n''), \quad (46)$$

according as $x'-x''$ is future-like, space-like, or past-like.[7] The first term on the right-hand side of (44)

[7] This operator was introduced by Koba independently. See Z. Koba, Prog. Theor. Phys. 5, 139 (1950).

vanishes on account of the fact that $(n'|\{L'\}|0)$ is zero provided that $\kappa_U<2\kappa_V$ and the second term also vanishes for the following reason: first we expand U, V, V^*, and D in Fourier series and integrate each of the terms of $(0|\{L'DL'\}|0)$ with respect to all of the space-time parameters. Actually we have eight sets of such parameters. Then we are left with the expression of the form

$$\int\int\int f(k_\mu^{(1)}, k_\mu^{(2)}, k_\mu^{(3)})\delta'(K_\mu K^\mu) \times (dk_\mu^{(1)})^4(dk_\mu^{(2)})^4(dk_\mu^{(3)})^4, \quad (47)$$

where $K_\mu=\sum_i k_\mu^{(i)}$ and $k_\mu^{(1)}$, $k_\mu^{(2)}$, $k_\mu^{(3)}$ are the wave vectors of the three particles created in the intermediate state. The first of them is a particle of U-type and the other two are particles of $V-V^*$-type. $f(\cdots)$ is a function of $k_\mu^{(1)}$, $k_\mu^{(2)}$, $k_\mu^{(3)}$, which could be determined by elementary calculations, but it is not necessary for our purpose to write it explicitly. δ' denotes the derivative of the δ-function with respect to the argument, which comes from the Fourier transform of the operator D, as discussed in detail by Yennie.[2] Thus, $(0|\{L'DL'\}|0)$ must be zero, unless the condition

$$K_\mu K^\mu=0 \quad (48)$$

is fulfilled. The condition (48) can be satisfied by certain sets of $k_\mu^{(1)}$, $k_\mu^{(2)}$, $k_\mu^{(3)}$ only if both types of particles have the rest mass zero.

The above arguments can be applied to local fields as well as to non-local fields. According to the usual theory of local fields, the third term on the right-hand side of Eq. (41) must be the divergent self-energy of the vacuum, whereas it is actually zero according to our formalism, except for the very particular case of particles both with the rest mass zero. The same argument can be applied to the case of charged particles interacting with the electromagnetic field, and according to our formalism the self-energy of the vacuum is zero, at least up to the second order, if we assume that there is no charged particle with the rest mass zero. Thus, the discrepancy between our formalism and the usual theory is already clear; they give different answers to the same problem for local fields.

Next we consider the matrix element $(1|S|1)$ of S, where only one particle of the same type in the same state exists in the initial and final states. The second-order term of $(1|S|1)$ corresponds to the divergent self-energy of the particle in local field theory. As discussed by Yennie in detail,[2] if we start from a system of two non-local scalar fields of U-type and $V-V^*$-type with the interaction operator L' as given by Eq. (42), the self-energy term is again divergent. However, the fields U and $V-V^*$ can be decomposed further into positive frequency and negative frequency parts without destroying the invariance with respect to the subgroup of Lorentz transformation, in which the direction of time is not reversed. Namely, we can write

$$U=U_++U_-, \quad V=V_++V_-, \quad V^*=V_+^*+V_-^*, \quad (49)$$

where U_+, U_- are positive and negative frequency parts of U, while V_+, V_+^* and V_-, V_-^* are corresponding parts of V and V^*. If we take the new interaction operator

$$L'=g\{V_+^*UV_++V_-UV_-^*+V_+^*UV_-+V_-^*UV_+\} \quad (50)$$

instead of Eq. (39), the self-energy terms for the U-type particle as well as the $V-V^*$-type particles are convergent, although there still remains an undesirable feature, as discussed by Yennie.[2]

Now, in order to remove the discrepancy between the present formalism and the usual formalism in the limit of local fields, we may imagine that D-operator above defined is a limit of the operator with the matrix element, which is a function of r_μ and is different from zero in a narrow region outside the light cone in r-space. Then the correspondence between the present formalism and the usual formalism in the limit of local fields is restored up to the second order, but the essential difference between ϵ- and D-operators remains in the third- and higher order terms. Moreover, the divergences reappear in the case of non-local fields. It is very difficult to construct an S-matrix which is convergent and which reduces to the usual S-matrix in the limit of local fields. It is not yet clear whether the S-matrix formalism itself is not adequate for dealing with the problem of interaction of non-local fields. It might be possible that the S-matrix as defined by Eq. (24) is invariant, if the interaction operator L' has an appropriate form, even in the case of non-local fields. However, it is more probable that the clean-cut separation of the free fields from their interaction is justified only if we are dealing with the weak coupling between local fields. If so, we must go back in search of the Lagrangian formalism for the whole system of non-local fields interacting with one another. In any case, the compatibility conditions for the field equations or the integrability conditions for any substitute for the Schrödinger equation will be of fundamental importance.

In this connection it should be noticed that so far we have not been able to find any relation between the mass and other constants. It is clear that a relation which connects the mass of an elementary particle with other constants such as the radius, the internal angular momentum, and the constants of coupling with other particles will be of vital importance in any future theory of elementary particles. Again this is closely related to the problem of finding the Lagrangian operator for the whole system or any substitute for it.

The author wishes to express his appreciation to Columbia University, where this work was done, for the hospitality shown to him, and to the Rockefeller Foundation for financial support. He is indebted also to Mr. Yennie for his useful criticism and elucidation of some of the important consequences of the formalism.

Some Remarks on Non-Local Field Theory†

D. R. YENNIE*
Columbia University, New York, New York
(Received August 7, 1950).

The S-matrix formalism introduced by Yukawa for non-local field theory is considered. For suitable types of non-local fields and interactions it is shown that the S-matrix is convergent through the second order of interaction. In the limiting case in which the non-local fields become local, it is found that the S-matrix formalism yields results inconsistent with the usual formalism unless a certain limiting process is introduced. The limiting process brings agreement between the two formalisms only through the second order of interaction; and the higher orders will, in general, disagree. Unfortunately, the limiting process also destroys the convergence of the S-matrix in the general case of non-local fields. These results suggest that the S-matrix formalism will need to be revised, but no definite recommendations for doing this are made here. An internal angular momentum operator for non-local fields is introduced; this operator aids in the decomposition of the field into irreducible parts of different spins.

I. INTRODUCTION

RECENTLY Yukawa considered the possibility of extending ordinary (local) field theory by introducing the concept of non-local fields which were supposed to represent elementary particles having a finite extension in space-time.[1] In local field theory we associate a field quantity with each space-time point x^μ ($x^1=x_1=x$, $x^2=x_2=y$, $x^3=x_3=z$, $x^4=-x_4=ct$); for example, a local scalar field is represented by $U(x)$. In non-local field theory, however, we consider the field to be a matrix element of a non-local operator, the rows and columns of the matrix being characterized by space-time coordinates; for example, a non-local scalar field would be written as $(x'|U|x'')$. A local field is then a special case of a non-local field in which the matrix is diagonal:

$$(x'|U|x'')=U(x')\delta(x'-x''), \tag{1}$$

where

$$\delta(x)=\delta(x^1)\delta(x^2)\delta(x^3)\delta(x^4).$$

The problem of introducing interactions between non-local fields seems to be much more difficult than in local field theory, since it does not seem to be possible to extend the concept of the Schrödinger wave functional and Schrödinger equation in any simple manner. Yukawa[2,3] suggested, however, that it might be possible to introduce interactions between fields by extending the formalism of the S-matrix to the case of non-local fields. To do this he defined a space-time average for an arbitrary operator A by

$$\{A\}\equiv\int\cdots\int(x'|A|x'')(dx')^4(dx'')^4, \tag{2}$$

where

$$(dx)^4=dx^1dx^2dx^3dx^4.$$

The proposed S-matrix then has the form

$$S=1+(i/\hbar c)\{L'\}+(i/\hbar c)^2\{L'D_+L'\}+(i/\hbar c)^3\{L'D_+L'D_+L'\}+\cdots, \tag{3}$$

where L' is an invariant Hermitian operator characterizing the interaction and is expressed as a sum of products of non-local and local field quantities. D_+ is an invariant displacement operator with the matrix elements

$$(x'|D_+|x'')=D_+(x'-x'')=1,\ \tfrac{1}{2},\ 0, \tag{4}$$

as $(x'-x'')$ is time-like in the future, space-like, or time-like in the past. As shown by Yukawa,[3] this S-matrix has the following properties: (i) it is relativistically invariant; (ii) it is unitary; and (iii) it is diagonal with respect to total energy and momentum.

The question of the convergence of the S-matrix will be considered in Sec. II. No general investigation will be attempted, but a simple example will be considered and it will be shown that for a suitable choice of L' the S-matrix is convergent through the second order of interaction. In Sec. III, the limiting case in which L' is made up of local field quantities will be discussed, and it will be shown that the present S-matrix does not yield the same results as the usual formulation of field theory. This difference can be eliminated in second order by introducing a certain limiting process to be applied to the operator D_+. Unfortunately, however, if this same limiting process is applied to the general case in which L' is composed of non-local fields, the S-matrix will no longer be convergent. Because of this difficulty the S-matrix (3) is not completely satisfactory, but, of course, it may still be possible to modify it in some way so that it will satisfy all the desired conditions.

Yukawa has discussed the problem of decomposing arbitrary non-local fields into irreducible parts, each of which is characterized by four constants referring to the mass, internal radius, internal angular momentum, and another quantity which has no immediate physical meaning.[3] These irreducible parts are eigenfunctions of an invariant internal angular momentum operator, and

† Publication assisted by the Ernest Kempton Adams Fund for Physical Research of Columbia University.
* This work was performed partly while the author was a Columbia University Fellow and partly while he was an AEC Predoctoral Fellow in the Physical Sciences.
[1] H. Yukawa, Phys. Rev. **76**, 300 (1949); **76**, 1731 (1949); **77**, 219 (1950).
[2] H. Yukawa, Phys. Rev. **77**, 849 (1950).
[3] H. Yukawa, Phys. Rev., preceding paper.

the corresponding eigenvalues of this operator may be taken to be $\hbar^2 l(l+1)$. This internal angular momentum operator, along with operators for the components of internal angular momentum, will be derived and discussed in Sec. IV.

II. SELF-ENERGY CALCULATION

It is of course impossible to make a general investigation of the convergence of the S-matrix, so that we shall content ourselves with the consideration of a particularly simple example. Although the term "self-energy" may not have a meaning in the same sense here as in local field theory, we shall carry out the calculation which in the limit of local field theory would be called a self-energy calculation. For this purpose we introduce two non-local fields, U and V; U is a real field and V is a complex field. We assume the interaction between them to be given by

$$L' = gV^*UV, \tag{5}$$

where V^* is the Hermitian conjugate of V. Using the notation

$$X = \tfrac{1}{2}(x'+x''), \quad r = (x'-x''), \tag{6}$$

and

$$ab = a_\mu b^\mu = a_1 b^1 + a_2 b^2 + a_3 b^3 + a_4 b^4, \quad a^2 = a_\mu a^\mu, \tag{7}$$

the matrix form of these fields is

$$\begin{aligned}(x'|U|x'') &= (\hbar/(2\pi)^3 c)^{\frac{1}{2}}(\kappa_u/2\pi\lambda_u) \\ &\times \int\cdots\int \delta(q^2+\kappa_u^2)\delta(r^2-\lambda_u^2) \\ &\times \delta(rq)u(q)\exp(iqX)(dq)^4, \end{aligned} \tag{8}$$

with

$$u^*(q) = u(-q), \tag{9}$$

and

$$\begin{aligned}(x'|V|x'') &= [\hbar/(2\pi)^3 c]^{\frac{1}{2}}(\kappa_v/2\pi\lambda_v) \\ &\times \int\cdots\int \delta(k^2+\kappa_v^2)\delta(r^2-\lambda_v^2) \\ &\times \delta(rk)v(k)\exp(ikX)(dk)^4, \\ (x'|V^*|x'') &= [\hbar/(2\pi)^3 c]^{\frac{1}{2}}(\kappa_v/2\pi\lambda_v) \\ &\times \int\cdots\int \delta(k^2+\kappa_v^2)\delta(r^2-\lambda_v^2) \\ &\times \delta(rk)v^*(k)\exp(ikX)(dk)^4 \end{aligned} \tag{10}$$

These non-local fields are less general than those introduced by Yukawa in that the expansion coefficients $u(k)$ and $v(k)$ are not functions of r; this corresponds to using just the spherical harmonic of order $l=0$ in his expansion in terms of spherical harmonics. In the rest system ($k_1=k_2=k_3=0$), we see that the internal structure is given by $r^4=0$, $r_1^2+r_2^2+r_3^2=\lambda^2$, and that there is no dependence on angle.

By analogy with local field theory, we take the non-vanishing commutation relations to be

$$\delta(q^2+\kappa_u^2)[u^*(q), u(q')] = -(q^4/|q^4|)\delta(q-q'), \tag{11}$$

$$\delta(k^2+\kappa_v^2)[v^*(k), v(k')] = -(k^4/|k^4|)\delta(k-k'), \tag{12}$$

where

$$[A, B] \equiv AB - BA. \tag{13}$$

These commutation relations lead to the following definitions for occupation, creation, and annihilation operators:

U-type particles: $q_0 = q^4 = (\mathbf{q}^2+\kappa_u^2)^{\frac{1}{2}}$ ($\mathbf{q}$ is the space vector part of q and $\mathbf{q}^2 = \mathbf{q}\cdot\mathbf{q}$)
- Occupation operator: $M(\mathbf{q}) = (1/2q_0)u^*(\mathbf{q}, q_0)u(\mathbf{q}, q_0)$
- Creation operator: $(1/2q_0)^{\frac{1}{2}}u^*(\mathbf{q}, q_0)$
- Annihilation operator: $(1/2q_0)^{\frac{1}{2}}u(\mathbf{q}, q_0)$

V_+-type particles: $k_0 = k^4 = (\mathbf{k}^2+\kappa_v^2)^{\frac{1}{2}}$
- Occupation operator: $N^+(\mathbf{k}) = (1/2k_0)v^*(\mathbf{k}, k_0)v(\mathbf{k}, k_0)$
- Creation operator: $(1/2k_0)^{\frac{1}{2}}v^*(\mathbf{k}, k_0)$
- Annihilation operator: $(1/2k_0)^{\frac{1}{2}}v(\mathbf{k}, k_0)$

V_--type particles: $k_0 = k^4 = -(\mathbf{k}^2+\kappa_v^2)^{\frac{1}{2}}$
- Occupation operator: $N^-(\mathbf{k}) = (1/2k_0)v(\mathbf{k}, k_0)v^*(\mathbf{k}, k_0)$
- Creation operator: $(1/2k_0)^{\frac{1}{2}}v(\mathbf{k}, k_0)$
- Annihilation operator: $(1/2k_0)^{\frac{1}{2}}v^*(\mathbf{k}, k_0)$

In addition we have the following vacuum expectation values which can be derived from the commutation rules and the creation and annihilation properties of the operators:

$$\delta(q^2+\kappa_u^2)\langle u(q)u^*(q')\rangle_0 = \delta(q-q'), \quad q_0>0; \tag{14}$$

$$\delta(k^2+\kappa_v^2)\langle v(k)v^*(k')\rangle_0 = \delta(k-k'), \quad k_0>0; \tag{15}$$

$$\delta(k^2+\kappa_v^2)\langle v^*(k)v(k')\rangle_0 = \delta(k-k'), \quad k_0<0. \tag{16}$$

We shall consider the second-order contribution of Eq. (5) to the S-matrix. Higher orders of interaction will not be discussed because of the difficulty of calculation and because the results of Sec. III indicate that Eq. (3) is probably not correct in higher orders. The second-order contribution can be written as

$$S^{(2)} = (ig/\hbar c)^2\{V^*UVD_+V^*UV\}. \tag{17}$$

For simplicity, we assume that

$$\{V^*UV\} = 0. \tag{18}$$

This is always valid for $\kappa_u < 2\kappa_v$, since then it is never possible to satisfy the energy-momentum conservation laws derived from Eq. (18). For the same reason it is also valid (regardless of the ratio κ_u/κ_v) when the initial or final state consists of a single V-type particle. Assuming Eq. (18), we may simplify Eq. (17) by replacing D_+ by $\frac{1}{2}D$, where D is defined by

$$D(x) = 1, 0, -1 \tag{19}$$

as x is time-like in the future, space-like, or time-like in the past. This replacement does not alter $S^{(2)}$ because the omitted part can be written as

$$\begin{aligned}&\tfrac{1}{2}(ig/\hbar c)^2\{V^*UVEV^*UV\} \\ &\qquad = \tfrac{1}{2}(ig/\hbar c)^2\{V^*UV\}^2 = 0. \end{aligned} \tag{20}$$

$S^{(2)}$ can now be written out in the following form:

$$S^{(2)}=\tfrac{1}{2}(ig/\hbar c)^2\int\cdots\int\{(x'+r_1+r_2|\,V^*\,|x'+r_2)\times(x'+r_2|\,U\,|x')(x'|\,V\,|x'-r_3)\times(x'-r_3|\,D\,|x''+r_4)(x''+r_4|\,V^*\,|x'')\times(x''|\,U\,|x''-r_5)(x''-r_5|\,V\,|x''-r_5-r_6)\}\times(dx')^4(dx'')^4\prod_{i=1}^{6}(dr_i)^4. \quad (21)$$

In Eq. (21) the variables of integration have been chosen to facilitate integration over the internal coordinates r; the remaining integrations over x then correspond to the usual local field theory except that they contain certain convergence factors introduced by the integration over the internal structure. To carry out the integrations we use the Fourier integral representations (8) and (10). In addition we need the Fourier expansion of $D(x)$ which is shown in the Appendix to be

$$D(x)=(-i/\pi^2)P\int\cdots\int\delta'(p^2)(p^4/|\,p^4\,|)\times\exp(ipx)(dp)^4, \quad (22)$$

where δ' is the derivative of the δ-function with respect to its argument and P represents a principal value which must be taken when performing the integral. In carrying out the integrations over r, we find the following simple integrals:

For r_1 and r_6,

$$(\kappa_v/2\pi\lambda_v)\int\cdots\int\delta(r^2-\lambda_v^2)\delta(rk)(dr)^4=1; \quad (23)$$

For r_2 and r_5,

$$F(kq)=(\kappa_u/2\pi\lambda_u)\int\cdots\int\delta(r^2-\lambda_u^2)\delta(rq)\exp(ikr)(dr)^4=(\sin\lambda_u Q)/\lambda_u Q, \quad (24)$$

where

$$Q=[k^2-(kq)^2/q^2]^{\frac{1}{2}}=[(kq/\kappa_u)^2-\kappa_v^2]^{\frac{1}{2}}; \quad (25)$$

For r_3 and r_4,

$$G(k'p)=(\kappa_v/2\pi\lambda_v)\int\cdots\int\delta(r^2-\lambda_v^2)\delta(rk')\times\exp(ipr)(dr)^4=(\sin\lambda_v K)/\lambda_v K, \quad (26)$$

where

$$K=[p^2-(k'p)^2/(k')^2]^{\frac{1}{2}}=k'p/\kappa_v. \quad (27)$$

These integrals are invariant functions of their arguments and are most easily evaluated by using special Lorentz frames to simplify the calculation; for example, Eq. (24) would be evaluated by using the reference system in which $\mathbf{q}=0$, $q^4=\pm\kappa_u$. In Eq. (27) we have set p^2 equal to zero because of the factor $\delta'(p^2)$ occurring in the remainder of the integrand; this is not strictly correct, but should introduce little error into our later semi-quantitative arguments.[4]

The expressions (24) and (26) are responsible for making $S^{(2)}$ convergent, and accordingly they will be called convergence factors. They are of the form $x^{-1}\sin x$, a function whose properties are well known. To see the nature of these convergence factors, let us suppose in Eqs. (24) and (25) that $\mathbf{q}=0$, $q^4=\pm\kappa_u$; then $Q=|\mathbf{k}|$ and $F=(\lambda_u|\mathbf{k}|)^{-1}\sin(\lambda_u|\mathbf{k}|)$. If $\lambda_u|\mathbf{k}|$ is small compared to unity, F will be close to unity; accordingly, if λ_u is small enough, the factor F will affect the S-matrix only for a very large momentum $|\mathbf{k}|$. For real processes, the effect of the factor F would be detected only at high energies; for virtual processes, F becomes a cut-off factor which helps produce convergence in the integrations over the intermediate momenta. For later work, it will be useful to express Q and K in different forms, so that at least one of the momenta in each expression represents the momentum of a real particle. This is possible because the momenta are always connected by an expression of the form

$$k-q-k'-p=0,$$

from which we can derive

$$kq=-k'p-\tfrac{1}{2}\kappa_u^2-\tfrac{1}{2}p^2=-k'p-\tfrac{1}{2}\kappa_u^2, \quad (28)$$

where we again have set p^2 equal to zero.[4] Thus Q and K can be expressed in terms of kq or $k'p$ and some constants; at least one of the momenta k, q, or k' is the momentum of a real particle.

Making use of these results, $S^{(2)}$ becomes

$$S^{(2)}=(i\hbar g/4\pi^3c^5)\int\cdots\int\prod_{i=1}^{4}(dk_i)^4\delta(k_i^2+\kappa_v^2)\times\prod_{j=1}^{2}(dq_j)^4\delta(q_j^2+\kappa_u^2)(dp)^4\{(p^4/|\,p^4\,|)\delta'(p^2)\times\delta(k_1-q_1-k_2-p)\delta(k_3+q_2-k_4+p)\times v^*(k_1)v(k_2)v^*(k_3)v(k_4)u(q_1)u^*(q_2)\times F(k_1q_1)F(k_4q_2)G(k_2p)G(k_3p)\}. \quad (29)$$

Except for the convergence factors F and G and the use of the Fourier transform of $D(x)$, this expression is much like the one which would be obtained from local field theory. There are three different self-energy terms in Eq. (29), one for each type of particle. Owing to the way in which we have chosen the interaction, the self-energy of the V_+-particle differs from that of the V_--particle; in fact, as we shall see, the self-energy of

[4] This implies neglecting the derivatives of F and G with respect to p, which is reasonable since these functions are slowly varying compared with the other functions in the integrand of Eq. (21).

the V_+-particle is finite, while that of the V_--particle is infinite. This arises from the particular choice of L' given by Eq. (5). By splitting the V field into positive and negative frequency parts, and using a slightly different interaction, it is possible to eliminate this asymmetry between V_+- and V_--particles (see below, Eq. (36)).

We shall consider the self-energy calculation for the V_+-particle in detail, and indicate briefly the results for the other two types of particles. There are two possible contributions to this self-energy which are given by[5]

$$v^*(k_1)v(k_4)\langle v(k_2)v^*(k_3)\rangle_0\langle u(q_1)u^*(q_2)\rangle_0, \quad (30)$$

$$v(k_2)v^*(k_3)\langle v^*(k_1)v(k_4)\rangle_0\langle u(q_1)u^*(q_2)\rangle_0. \quad (31)$$

As a matter of fact, the contribution from Eq. (31) vanishes because it is impossible to satisfy simultaneously the relations

$$\begin{gathered}(k_3+q_2-k_4)^2=p^2=0,\\ (q_2)_0>0, \quad (k_3)_0>0, \quad (k_4)_0<0.\end{gathered} \quad (32)$$

This is connected with the fact, mentioned by Yukawa in the preceding paper,[3] that with this S-matrix formalism there is no self-energy of the vacuum.

Using Eq. (29), we find for the self-energy of V_+-particles

$$(\cdots, N_{k_1}{}^+=1, \cdots|S^{(2)}|\cdots, N_{k_4}{}^+=1, \cdots)$$

$$=(i\hbar g^2/4\pi^3c^5)\delta(k_1-k_4)\delta(k_1{}^2+\kappa_v{}^2)\delta(k_4{}^2+\kappa_v{}^2)I_1(k_4), \quad (33)$$

where

$$I_1(k_4)=\int_{k_0>0,\ q_0>0}\cdots\int(dk)^4(dq)^4(dp)^4 \times\{\delta(k+q-k_4+p)\delta(k^2+\kappa_v{}^2)\delta(q^2+\kappa_u{}^2) \times(p^4/|p^4|)\delta'(p^2)[F(k_4q)G(kp)]^2\}. \quad (34)$$

We note that $I_1(k_4)$ is an invariant function of k_4 and can therefore depend only on $k_4{}^2=-\kappa_v{}^2$, accordingly we simplify further considerations by setting $\mathbf{k}_4=0$, $(k_4)_0=\kappa_v$. We also use Eq. (28) to express G as a function of k_4q. The integrals over k and p in Eq. (34) are then easily performed since they are independent of the convergence factors; the details of this calculation will be found in the Appendix. The resulting expression for I_1 is

$$I_1(k_4)=\pi\int_{q_0>0}\cdots\int\delta(q^2+\kappa_u{}^2)A(q_0) \times\{[1/(l^2+\kappa_v{}^2)]-(1/2l^2)\} \times[F(\kappa_vq_0)G(k_vq_0-\tfrac{1}{2}\kappa_u{}^2)]^2(dq)^4, \quad (35)$$

where

$$A(q_0)=\begin{cases}\tfrac{1}{2}\text{ for } q_0>(\kappa_u{}^2+\kappa_v{}^2)/2\kappa_v\\ 1\text{ for } q_0<(\kappa_u{}^2+\kappa_v{}^2)/2\kappa_v,\text{ if } \kappa_u<\kappa_v\\ 0\text{ for } q_0<(\kappa_u{}^2+\kappa_v{}^2)/2\kappa_v,\text{ if } \kappa_u>\kappa_v\end{cases}$$

and

$$l^2=-\kappa_u{}^2-\kappa_v{}^2+2\kappa_vq_0.$$

The integrand of Eq. (35) has a singularity at just the value of q_0 at which $A(q_0)$ has a discontinuity; consequently, the integral is not convergent. This divergence of the integral will be ignored at present, however, because the discussion of Sec. III and the Appendix will show that it is a consequence of the structure of the S-matrix rather than of the particular properties of the fields. A suitable modification of the S-matrix should eliminate divergences occurring at finite intermediate momenta. We are more interested here in the convergence of Eq. (35) at the upper limit of integration. At this limit, the combined convergence factors produce a factor of the order of $|\mathbf{q}|^{-4}$, so convergence of Eq. (35) is secured; we shall accordingly consider Eq. (35) to be convergent.

Having seen that the self-energy of the V_+-particle is finite, we consider briefly the other two types of particles. The self-energy of the V_--particle involves an integral of the form (34) except that the integration is over k_4, while k is a fixed vector. Making use of Eq. (28) then, the convergence factors are found to depend only on kp. Since the integration over p is convergent without the convergence factors, we see that the value of the integral is essentially independent of these factors, and the integral will diverge. The self-energy in this case diverges linearly; this is in contrast to the ordinary field theory, where the divergence is only logarithmic. This difference arises because in the present calculation there is a contribution from Eq. (31) but not from Eq. (30). In ordinary field theory both of these terms contribute and partially cancel in such a way that the order of the divergence is reduced. The self-energy of the U-particle is found to be finite because the convergence factor for that calculation can be written as $[F(k_4q)\times G(-k_4q-\frac{1}{2}\kappa_u{}^2)]^2$. Since q is fixed, integration over k_4 will always be convergent.

The asymmetry between the V_+-particle and the V_--particle can be removed by revising the interaction operator L'.[6] We separate the field V into two parts: V_+ and V_-. V_+ corresponds to $k_0>0$, and V_- to $k_0<0$. We may then take L' to be

$$L'=g\{V_+{}^*UV_+ + V_-UV_-{}^* + V_+{}^*UV_- + V_-{}^*UV_+\}, \quad (36)$$

or we may symmetrize the last two terms:

$$L'=g\{V_+{}^*UV_+ + V_-UV_-{}^* + \tfrac{1}{2}(V_+{}^*UV_- + V_-UV_+{}^* + V_-{}^*UV_+ + V_+UV_-{}^*)\}. \quad (36')$$

Using either one of these interactions, we have the two

[5] Operators referring to different momenta may be freely commuted.

[6] The author is indebted to Prof. Yukawa for suggesting the following scheme.

self-energies given by

$\frac{1}{2}(ig/\hbar c)^2\{V_+^*UV_+DV_+^*UV_+\}$ for the V_+-particle,
$\frac{1}{2}(ig/\hbar c)^2\{V_-UV_-^*DV_-UV_-^*\}$ for the V_--particle.

Because of the creation and annihilation properties given previously, it is seen that these two expressions are symmetrical in the two types of particles and both are convergent (provided that we again ignore the divergence occurring at finite intermediate momenta). This procedure seems to be quite arbitrary at present, but it may turn out that this, or something similar, will be necessary in the future development of the non-local field theory.

The calculations of this section seem to indicate that when a satisfactory method of introducing interactions is found, the non-local field theory will be convergent. The present S-matrix seems to be unsatisfactory for various reasons, but the non-local character of the fields introduces convergence factors which eliminate the usual divergences of local field theory. These convergence factors should be carried over into the more correct formulation when it is found.

III. THE LIMIT OF LOCAL FIELD THEORY

If we let λ_u and λ_v approach zero in Eqs. (8) and (10), we find that U and V become local fields $U(x)$ and $V(x)$ with the following non-vanishing commutation relations:

$$[V^*(x'), V(x'')]=(\hbar/ic)\Delta_v(x'-x''), \tag{37}$$

$$[U(x'), U(x'')]=(\hbar/ic)\Delta_u(x'-x''), \tag{38}$$

where Δ_v and Δ_u are the usual invariant functions of local field theory and are given by

$$\Delta=[-1/(2\pi)^3i]\int\cdots\int\delta(k^2+\kappa^2)(k_0/|k_0|)\times\exp(ikx)(dk)^4. \tag{39}$$

We have now to compare the results of calculations using the S-matrix given by Eq. (3) with the results from the usual field theory. In the usual theory, the S-matrix takes the form[7]

$$S'=1+(i/\hbar c)\{L'\}+(i/\hbar c)^2\{L'\epsilon_+L'\}+(i/\hbar c)^3\{L'\epsilon_+L'\epsilon_+L'\}+\cdots, \tag{40}$$

where ϵ_+ is a non-invariant operator given by[8]

$$(x'|\,\epsilon_+\,|x'')=\epsilon_+(x'-x'')=\begin{cases}1 & \text{for } x'^4>x''^4\\ 0 & \text{for } x'^4<x''^4\end{cases}. \tag{41}$$

The relativistic invariance of Eq. (40) is a result of the condition of integrability

$$[L'(x'), L'(x'')]=0 \text{ for } (x'-x'') \text{ space-like}. \tag{42}$$

We thus see that the relativistic invariance of Eq. (3) has been obtained by purely kinematical means while invariance of Eq. (40) depends on the dynamical properties of the field and the form of the interaction.

The second-order contributions to the S-matrix in the two cases are found to be[9]

$$S^{(2)}=\tfrac{1}{4}(i/\hbar c)^2\int\cdots\int D(x'-x'')\times[L'(x'), L'(x'')](dx')^4(dx'')^4, \tag{43}$$

$$S^{(2)}=\tfrac{1}{4}(i/\hbar c)^2\int\cdots\int\epsilon(x'-x'')\times[L'(x'), L'(x'')](dx')^4(dx'')^4, \tag{44}$$

where

$$\epsilon(x'-x'')=\begin{cases}1 & \text{for } x'^4>x''^4\\ -1 & \text{for } x'^4<x''^4\end{cases}. \tag{45}$$

These two expressions appear to be equivalent for the following reason: the integrands are equivalent for $(x'-x'')$ time-like, and they both vanish for $(x'-x'')$ space-like. This equivalence is only apparent, however, for the commutator $[L'(x'), L'(x'')]$ has a singularity of the δ-function type when $(x'-x'')$ lies on the light cone. (For spinor fields the singularity would be even stronger.) In Eq. (43), $D(x'-x'')$ changes discontinuously as $(x'-x'')$ crosses the light cone; the δ-function from the commutator averages out this discontinuity in D so that the contribution from the light cone is only half as great as in Eq. (44), where ϵ is continuous across the light cone. The effect of this will be seen in more detail with the aid of an example.

Using the previous interaction (5) we have

$$\begin{aligned}&[L'(x'), L'(x'')]\\ &=g^2\{V^*(x')V(x')V^*(x'')V(x'')[U(x'), U(x'')]\\ &\quad+U(x'')U(x')V^*(x')V(x')[V(x'), V^*(x'')]\\ &\quad+U(x'')U(x')V^*(x'')V(x')[V^*(x'), V(x'')]\}.\end{aligned} \tag{46}$$

To compare Eqs. (43) and (44), we may use for example the first term of Eq. (46); this amounts to comparing

$$A(x)=\tfrac{1}{2}D(x)\Delta_u(x) \tag{47}$$

with

$$A'(x)=\tfrac{1}{2}\epsilon(x)\Delta_u(x). \tag{48}$$

Equation (48) is the function $\bar{\Delta}_u$ defined by Schwinger[10] and is known to have the Fourier expansion

$$A'(x)=\bar{\Delta}_u(x)=(1/(2\pi)^4)P\int\cdots\int\exp(ikx)(dk)^4/(k^2+\kappa_u^2). \tag{49}$$

We shall compare the two expressions (47) and (48) by finding the Fourier transform of Eq. (47). This is most easily done by means of a theorem of Fourier trans-

[7] F. J. Dyson, Phys. Rev. 75, 486 (1949).

[8] More generally, ϵ_+ is based on the ordering in time of space-like surfaces on which x' and x'' are situated (reference 7), but we may specialize to constant time surfaces for the present application.

[9] A similar result has been given by F. Koba, Prog. Theor. Phys. 5, 139 (1950).

[10] J. Schwinger, Phys. Rev. 75, 651 (1949).

forms,[11] which gives the Fourier transform of $A(x)$ in terms of the transforms of $D(x)$ and $\Delta_u(x)$:

$$A(x)=\int\cdots\int f(k)\exp(ikx)(dk)^4, \tag{50}$$

where

$$f(k)=(1/16\pi^5)P\int\cdots\int\delta[(k-p)^2+\kappa_u{}^2]$$
$$\times[(k^4-p^4)/|k^4-p^4|]\delta'(p^2)(p^4/|p^4|)(dp)^4. \tag{51}$$

This is the integral J_2 which is calculated in the Appendix; the result for $f(k)$ is, therefore,

$$f(k)=[1/(2\pi)^4]\{[1/(k^2+\kappa_u{}^2)]-(1/2k^2)\}. \tag{52}$$

In using this result in further integrations, it is implied that a principal value is to be taken whenever this part of the integrand becomes singular.[11] The first term of Eq. (52) obviously agrees with Eq. (49), while the second term is a consequence of the combination of the δ-function with a discontinuity on the light cone.

The result (52) shows that we must modify the S-matrix (3) if that expression is to reduce properly in the limit of local field theory. This can be accomplished by a modification of the D function such that the discontinuity occurs outside the light cone. Since D is an odd function of x^4, this cannot be done in an invariant manner; but we can do the calculations with the modified D function and then let the discontinuity approach the light cone. The result will be that the last term of Eq. (52) will disappear, thus bringing about agreement of the two S-matrices in second order. The calculations are given in the Appendix.

We must now re-examine the self-energy calculations in terms of the limiting process. We now find that both Eq. (30) and Eq. (31) contribute to the self-energy; in terms of the interaction (36), the additional terms to be added to the self-energy are

$$\tfrac{1}{2}(ig/\hbar c)^2\{V_-{}^*UV_+DV_+{}^*UV_-\}$$
for the V_+- or the V_--particle.

In the self-energy calculation of Sec. II, there was a divergence due to a singularity in the integrand at a finite value of the intermediate momentum. The addition of the second type of self-energy process and the use of the limiting process on D serves to eliminate this difficulty; the calculations are discussed in the Appendix. For the V_+-particle, the operator V_+ corresponds to a fixed momentum; from the considerations of Sec. II, it is therefore apparent that this contribution to the self-energy is not convergent. For the V_--particle, the operator V_- corresponds to a fixed momentum, and this contribution to the self-energy is convergent. Using the interaction (36′) makes the self-energy of both types of particles divergent. The self-energies calculated with the S-matrix (3) and with the modified D_+ function are accordingly divergent. For this reason, the S-matrix (3) will have to be modified or replaced by another method of introducing interactions; but when this has been done, it seems likely that a convergent theory can be obtained with the use of non-local fields.

In higher orders it becomes more difficult to make a comparison between the two S-matrices. We can note, however, some further difficulties with Eq. (3); for example, the third-order term is given by

$$S^{(3)}=(i/\hbar c)^3\int\cdots\int L'(x')D_+(x'-x'')L'(x'')$$
$$\times D_+(x''-x''')L'(x''')(dx')^4(dx'')^4(dx''')^4. \tag{53}$$

The presence of the D_+ functions insures that $(x'-x'')$ and $(x''-x''')$ must be space-like, or time-like in the future. These functions do not directly impose conditions on the character of $(x'-x''')$, however; in fact, it is even possible for this vector to be time-like in the past. No such situation occurs in the case of Eq. (40), where all of the interactions have a definite ordering in time.

The conclusion of this section would seem to be that the proposed method of introducing interactions in non-local field theory is not correct in its present form, but that an approach along this line is not yet ruled out. The essential difficulty is that the commutation relations for two non-local fields depend not only on their properties as creation and annihilation operators, but also on their matrix character with respect to space-time coordinates. It may be that the matrix character of non-local fields has been overemphasized; that is, it may perhaps be better to consider them simply as fields depending on a center-of-mass coordinate (X) and an internal structure coordinate (r).

IV. INTERNAL ANGULAR MOMENTUM OPERATOR

In the preceding paper[3] Yukawa has discussed the process of decomposing general non-local fields into irreducible parts. The reduced fields $U(X,r)$ were eigenfunctions of the operators

$$\alpha=\partial^2/\partial X_\mu\partial X^\mu, \tag{54}$$
$$\beta=r_\mu r^\mu, \tag{55}$$
$$\gamma=r_\mu\partial/\partial X_\mu, \tag{56}$$

with eigenvalues $-K$, L, and iM, respectively. For correspondence to particles with real mass, $-K$ must be positive, but L and M are unrestricted in value (except that they must be real). In addition, the field may be further decomposed into separate parts characterized by the internal angular momentum. It will be the purpose of this section to produce an operator for the

[11] This theorem is briefly:
Given $G(x)=\int g(k)\exp(ikx)dk$; $H(x)=\int h(k)\exp(ikx)dk$, then $G(x)H(x)=\int f(x)\exp(ikx)dk$, where $f(k)=\int g(k-l)h(l)dl$. When this is applied to Eq. (50), it is necessary to use care in handling the limiting processes implied by the principal value in the definition of D. These limiting processes are to be left as the last step of the successive integrations in Eq. (50); the result of this is that we have an ordinary principal value implied for the singularities which occur in $f(k)$.

internal angular momentum. This operator should satisfy the following conditions: (i) it should be an invariant operator; (ii) it should commute with the previous three operators. Except for a multiplicative factor and an additive constant depending only on α, β, and γ, the desired operator is determined by these two requirements. The calculation is a little lengthy, but it is completely straightforward. We shall merely sketch in the procedure here.

Using the operator $(\partial/\partial r_\mu)$ along with r_μ and $(\partial/\partial X_\mu)$, we can form three new invariant operators.

$$\partial^2/\partial r_\mu \partial r^\mu, \quad r_\mu \partial/\partial r_\mu, \quad \partial^2/\partial r_\mu \partial X^\mu. \tag{57}$$

No linear combination of the elements (57) commutes with α, β, and γ; we therefore form from elements (57) an operator δ, which is the most general linear differential operator of second order in r, with arbitrary coefficients depending only on α, β, and γ.

$$\begin{aligned}\delta\alpha=&(\partial^2/\partial r_\mu\partial r^\mu)a+(r_\mu\partial/\partial r_\mu)^2 b+(\partial^2/\partial r_\mu\partial X^\mu)c\\&+(r_\mu\partial^2/\partial r_\mu\partial r_\lambda\partial X^\lambda)d\\&+(r_\mu\partial/\partial r_\mu)e+(\partial^2/\partial r_\mu\partial X^\mu)f+g.\end{aligned} \tag{58}$$

Equation (58) satisfies the condition of invariance (i). The commutation conditions (ii) are

$$[\delta, \alpha]=0, \quad [\delta, \beta]=0, \quad [\delta, \gamma]=0. \tag{59}$$

The relations (59) determine the first six coefficients of Eq. (58) except for a common factor; at this stage, the operator takes the form

$$\begin{aligned}\delta\alpha=&\{(\partial^2/\partial r_\mu\partial r^\mu)(\alpha\beta-\gamma^2)-(r_\mu\partial/\partial r_\mu)^2\alpha\\&-(\partial^2/\partial r_\mu\partial X^\mu)^2\beta-2r_\mu(\partial^3/\partial r_\mu\partial r_\lambda\partial X^\lambda)\gamma\\&-7r_\mu(\partial/\partial r_\mu)\alpha+8(\partial^2/\partial r_\mu\partial X^\mu)\gamma+g'\alpha\}a'.\end{aligned} \tag{60}$$

If $-K=\kappa^2$; the rest system is characterized by

$$\partial/\partial X_\mu=i\kappa\delta_4{}^\mu. \tag{61}$$

Using Eq. (61), we have the following reductions in the rest system

$$\begin{aligned}(\beta\alpha-\gamma^2)=\sum_{i=1}^{3} r_i{}^2\alpha, \quad (\partial^2/\partial r_\mu\partial X^\mu)^2=(\partial^2/\partial r_4\partial r^4)\alpha,\\(\partial^2/\partial r_\mu\partial X^\mu)\gamma=(\partial/\partial r_4)r_4\alpha,\end{aligned} \tag{62}$$

so that δ reduces to

$$\delta=\left\{\frac{1}{2}\sum_{i,j=1}^{3}\left(r_i\frac{\partial}{\partial r_j}-r_j\frac{\partial}{\partial r_i}\right)^2+12+g'\right\}a'. \tag{63}$$

This will reduce to the usual form for an angular momentum operator if we choose the arbitrary constants to be

$$g'=-12, \quad a'=-\hbar^2. \tag{64}$$

This result can be put into simpler and more compact form by introducing a new operator by

$$\alpha r_\mu{}'=\alpha r_\mu-\gamma\partial/\partial X^\mu. \tag{65}$$

The meaning of this operator is somewhat clearer if we note that in the rest system

$$\alpha r_\mu{}'=\begin{cases}\alpha r_\mu & \text{if } \mu=1,2,3\\ 0 & \text{if } \mu=4\end{cases}, \tag{66}$$

so that Eq. (65) represents, in a sense, a translation of coordinates. Using Eq. (65), the internal angular momentum operator becomes

$$\begin{aligned}\alpha^2\delta=&-\tfrac{1}{2}\hbar^2[(r_\mu{}'\partial/\partial r_\nu)-(r'^\nu\partial/\partial r^\mu)]\\&\times[(r'^\mu\partial/\partial r^\nu)-(r_\nu{}'\partial/\partial r_\mu)]\alpha^2\\&-\hbar^2(\partial^2/\partial r_\mu\partial X^\mu)^2(\gamma^2-\alpha\beta).\end{aligned} \tag{67}$$

As is well known, the eigenfunctions of δ in the rest system are the spherical harmonics and the corresponding eigenvalues are $\hbar^2 l(l+1)$ (where $l=1,2,3,\cdots$). Thus α, β, and γ have continuous eigenvalues and δ has discrete eigenvalues. These four operators allow us to decompose completely a general non-local field into irreducible parts because an expansion in terms of simultaneous eigenfunctions of these operators is unique and no further decomposition is possible. Each irreducible part is characterized by the four quantities κ^2, L, M, and l. This justifies the procedure of Sec. II, in which the non-local fields had $L=\lambda^2$, $M=0$, and internal angular momentum given by $l=0$.

We have yet to show that there are no other independent invariant operators which are functions of elements (57) and which commute with α, β, and γ. We shall prove this for operators which are finite polynomials of the operators (57). The most general operator of this form may be written as

$$d=\sum_{n=0}^{N}\sum_{m=0}^{M}(r_\mu\partial/\partial r_\mu)^n(\partial^2/\partial r_\lambda\partial X^\lambda)^m a_{nm}, \tag{68}$$

where the a_{nm} are functions of α, β, γ, and δ; the operator $(\partial^2/\partial r_\mu\partial r^\mu)$ does not appear explicitly because it can be expressed in terms of $(r_\mu\partial/\partial r_\mu)$, $(\partial^2/\partial r_\mu\partial X^\mu)$, and δ. Commuting Eq. (68) with β and γ, we find terms of the form

$$\begin{aligned}[(r_\mu\partial/\partial r_\mu)^n(\partial^2/\partial r_\lambda\partial X^\lambda)^m, \beta]\\=2n(r_\mu\partial/\partial r_\mu)^{n-1}(\partial^2/\partial r_\lambda\partial X^\lambda)^m\beta\\+2m(r_\mu\partial/\partial r_\mu)^n(\partial^2/\partial r_\lambda\partial X^\lambda)^{m-1}\gamma+\cdots,\end{aligned} \tag{69a}$$

$$\begin{aligned}[(r_\mu\partial/\partial r_\mu)^n(\partial^2/\partial r_\lambda\partial X^\lambda)^m, \gamma]\\=n(r_\mu\partial/\partial r_\mu)^{n-1}(\partial^2/\partial r_\lambda\partial X^\lambda)^m\gamma\\+m(r_\mu\partial/\partial r_\mu)^n(\partial^2/\partial r_\lambda\partial X^\lambda)^{m-1}\alpha+\cdots.\end{aligned} \tag{69b}$$

The dots indicate terms in lower powers of the operators $(r_\mu\partial/\partial r_\mu)$ and $(\partial^2/\partial r_\mu\partial X^\mu)$. Applying Eq. (69) to d and investigating the highest order terms, we find that it is necessary to take $N=M=0$; thus d is a function of α, β, γ, and δ.

We can easily write a tensor operator $J_\mu{}^\nu$ whose components may be considered to be the components of the internal angular momentum; this operator is

$$\alpha J_\mu{}^\nu=(\hbar/i)[(r_\mu'\partial/\partial r_\nu)-(r'^\nu\partial/\partial r'^\mu)]\alpha$$
$$-(\hbar/i)[(r_\mu'\partial/\partial X_\nu)-(r'^\nu\partial/\partial X^\mu)]\partial^2/\partial r_\lambda\partial X^\lambda. \quad (70)$$

In the rest system, this reduces to

$$J_\mu{}^\nu=\begin{cases}0 & \text{if } \mu \text{ or } \nu=4\\ (\hbar/i)[(r_\mu\partial/\partial r_\nu)-(r^\nu\partial/\partial r_\mu)] & \text{if } \mu,\nu=1,2,3.\end{cases} \quad (71)$$

The total internal angular momentum is easily seen to be given by

$$\delta=\tfrac{1}{2}J_\mu{}^\nu J_\nu{}^\mu. \quad (72)$$

The components of the internal angular momentum also commute with α, β, and γ:

$$[J_\mu{}^\nu,\alpha]=[J_\mu{}^\nu,\beta]=[J_\mu{}^\nu,\gamma]=0. \quad (73)$$

We also have the following commutation relations between the components of the internal angular momentum and the total internal angular momentum:

$$\alpha[J_\mu{}^\nu,J_\sigma{}^\lambda]=(\hbar/i)\{J_\mu{}^\lambda[g_\sigma{}^\nu\alpha-(\partial^2/\partial X_\nu\partial X^\sigma)]$$
$$-J_\sigma{}^\nu[g_\mu{}^\lambda\alpha-(\partial^2/\partial X_\lambda\partial X^\mu)]$$
$$-g_{\sigma\alpha}J_\mu{}^\alpha[g^{\nu\lambda}\alpha-(\partial^2/\partial X_\lambda\partial X_\nu)]$$
$$+g^{\lambda\alpha}J_\alpha{}^\nu[g_{\sigma\mu}\alpha-(\partial^2/\partial X^\sigma\partial X^\mu)]\}, \quad (74)$$
$$[J_\mu{}^\nu,\delta]=0, \quad (75)$$

where the $g_{\nu\lambda}$ are the components of the metrical tensor:

$$g_{\nu\lambda}=g^{\nu\lambda}=\begin{cases}0 & \nu\neq\lambda\\ +1 & \nu=\lambda=1,2,3\\ -1 & \nu=\lambda=4\end{cases} \quad (76)$$
$$g_\mu{}^\nu=g_{\mu\lambda}g^{\nu\lambda}.$$

For convenience, we note the following relations which are useful in proving Eqs. (72)–(75):

$$\alpha\partial^2r_\mu'/\partial X^\lambda\partial r_\lambda=0,\quad \alpha r_\mu'r'^\mu=\alpha\beta-\gamma^2,$$
$$r_\mu'\partial/\partial X_\mu=0,\quad J_\mu{}^\nu\partial/\partial X_\mu=0. \quad (77)$$

The author wishes to express his appreciation to Professor H. Yukawa for suggesting this work and for many stimulating discussions on the subject of this paper. He also wishes to thank Professor G. Yevick who assisted with valuable discussion and advice, and Dr. V. Hughes and Mr. J. Weneser for their constructive criticism of the manuscript.

APPENDIX

1. Fourier Expansion of $D(x)$

The desired expansion of D is

$$D(x)=-(i/\pi^3)P\int\cdots\int(p^4/|p^4|)\delta'(p^2)\exp(ipx)(dp)^4. \quad (A\text{-}1)$$

In Eq. (A-1), the symbol P standing before the integral denotes that a principal value must be taken when performing the integral. We define this principal value in the following manner. Delete from the region of integration a small volume about $p_\mu=0$; the volume deleted is to contain the point $p_\mu=0$ and to be invariant under the reflection $p_\mu\to-p_\mu$. As this deleted volume shrinks to zero, the integral approaches a limit which is the desired principal value. For definiteness, we assume that a similar sort of limiting process is implied for $p_\mu\to\infty$.

To show that Eq. (A-1) is correct, we note first that the quantity on the right is an invariant function of x and therefore depends only on x^2 and $x^4/|x^4|$. (Note that $(p^4/|p^4|)$ is really an invariant quantity because p must lie on the light cone, and also that the volume of integration is invariant in the limit.) In addition, owing to the factor $(p^4/|p^4|)$, the integral is an odd function of x^4. Because of these two conditions, the integral must vanish for space-like distances x. For time-like x, we specialize to that Lorentz frame in which $\mathbf{x}=0$, $x^4=a$. The integral becomes

$$(-4i/\pi)P\int_{-\infty}^{\infty}dp_0\int_0^\infty p^2dp(p_0/|p_0|)$$
$$\times\exp(-ip_0a)\partial\delta(p^2-p_0^2)/2p\partial p.$$

Integration by parts with respect to p, yields

$$(2i/\pi)P\int_{-\infty}^{\infty}dp_0\int_0^\infty dp(p_0/|p_0|)\delta(p^2-p_0^2)\exp(-ip_0a).$$

The integrated part does not vanish, but is rapidly oscillating in a (before the limit is taken) and would average to zero in any application. Integrating over p makes

$$D=(i/\pi)P\int_{-\infty}^{\infty}dp_0\exp(-ip_0a)/p_0.$$

P now stands for the ordinary principal value, and we have

$$D(0,0,0,a)=\begin{cases}1 & \text{for } a>0\\ -1 & \text{for } a<0\end{cases}$$

This verifies that Eq. (A-1) is the correct Fourier expansion of $D(x)$.

2. Evaluation of Certain Integrals

Consider the integral (34), which arises in the self-energy calculation; after the integration over k is performed, the integration with respect to p becomes

$$J_1=P\int_{(l-p)^4>0}\cdots\int\delta((l-p)^2+\kappa_0^2)\delta'(p^2)(p^4/|p^4|)(dp)^4, \quad (A\text{-}2)$$

where

$$l=k_4-q.$$

This integral is an invariant function of l and is therefore most easily carried out by using special Lorentz frames to simplify the calculation. For l time-like, we choose $\mathbf{l}=0$, $l^4=l'$; J_1 then becomes

$$J_1=4\pi P\int_{-\infty}^{l'}dp_0\int_0^\infty p^2dp\delta(p^2-p_0^2-l'^2+2l'p_0+\kappa^2)$$
$$\times(p_0/|p_0|)\delta'(p^2-p_0^2),$$
$$=2\pi P\int_{-\infty}^{l'}dp_0(p_0^2+l'^2-2l'p_0-\kappa_0^2)^{\frac{1}{2}}(p_0/|p_0|)\delta'(l'^2-2l'p_0-\kappa_0^2)$$
$$=(\pi/l')P\int_{-\infty}^{l'}dp_0(1-l'/p_0)\delta(2l'p_0-l'^2+\kappa_0^2)$$
$$=\begin{cases}0 & \text{if } l'<0\\ \pi\{[1/(-l'^2+\kappa_0^2)]+1/2l'^2\} & \text{if } l'>0.\end{cases}$$

For l space-like, we take $l^4=0$, and we take the vector $\mathbf{l}$ of magnitude l'' as the direction of the polar axis for a set of spherical coordinates in the three-dimensional space part of $(dp)^4$. J_1 then becomes

$$J_1=-2\pi\int_{-\infty}^{0}dp_0\int_0^\pi\sin\theta d\theta\int_0^\infty p^2dp\delta(l''^2-2l''p\cos\theta$$
$$+p^2-p_0^2+\kappa_0^2)\delta'(p^2-p_0^2).$$

Integrating over p_0 and making the substitution $\cos\theta=\mu$ gives

$$J_1=-\pi\int_{-1}^{1}d\mu\int_0^\infty p^2dp\delta'(2l''p\mu-l''^2-\kappa_v^2)/(p^2+l''^2-2l''p\mu+\kappa_v^2)^{\frac{1}{2}}$$
$$=-(\pi/2l'')\int_0^\infty dp\delta(2l''p-l''^2-\kappa_v^2)+(\pi/4l'')\int_{(l''^2+\kappa_v^2/2l'')}^\infty dp/p^2$$
$$=\pi/2\{[1/(l''^2+\kappa_v^2)]-1/2l''^2\}.$$

We can express both of these results in terms of a function

$$J=\pi\{[1/(l^2+\kappa^2)]-1/2l^2\}. \tag{A-3}$$

Then

$$J_1=\begin{cases}\frac{1}{2}J_v & \text{for } l \text{ space-like}\\ 0 & \text{for } l \text{ time-like, } l^4<0\\ J_v & \text{for } l \text{ time-like, } l^4>0.\end{cases} \tag{A-4}$$

The space- or time-like character of l depends on the sign of

$$l^2=-\kappa_u^2-\kappa_v^2+2\kappa_v q_0. \tag{A-5}$$

If l is time-like, it is easy to see that

$$\begin{aligned}&l^4>0 \text{ if } \kappa_v>\kappa_u,\\ &l^4<0 \text{ if } \kappa_v<\kappa_u.\end{aligned} \tag{A-6}$$

These are the relations which determine the factor $A(q_0)$ occurring in Eq. (35).

The integral J_2 occurring in Eq. (51) is:

$$J_2=P\int\cdots\int\delta[(k-p)^2+\kappa_u^2]\delta'(p^2)$$
$$\times[(k^4-p^4)p^4(dp)^4/|k^4-p^4||p^4|]. \tag{A-7}$$

Using the results of the J_1 integration, this integral is readily evaluated. It is an even function of k^4; and for k time-like with $k^4>0$, it is easy to see that $J_2=J_1$. Also, for k space-like, J_2 has an integrand which is an even function of p_0, and, therefore, $J_2=2J_1$. In general, then

$$J_2=J_u. \tag{A-8}$$

3. Limiting Process for D Function

The D function is to be modified so that its discontinuity occurs outside the light cone; such a function is D', defined by

$$D'(x)=-(i/\pi^2)P\int\cdots\int(p^4/|p^4|)\delta'(p^2)\exp(ip\cdot\mathbf{x}-i\rho p^4x^4)(dp)^4, \tag{A-9}$$

where

$$\rho>1$$

In some Lorentz frame we may take ρ to be a constant; in this system the discontinuity occurs outside the light cone at $|\mathbf{x}|=\rho|x^4|>|x^4|$. With a change of variable Eq. (A-9) can be written as

$$D'(x)=-(i/\pi^2)P\int\cdots\int(p^4/|p^4|)\delta'(\mathbf{p}^2-\sigma p_0^2)$$
$$\times\exp(ipx)(1/\rho)(dp)^4, \tag{A-10}$$

where

$$\sigma=1/\rho^2<1.$$

We shall illustrate the use of this modified D function by a calculation of the modified J' function when k is time-like. Take $\mathbf{k}=0$, $k^4=k'$; then this integral becomes

$$J'=4\pi P\int_{-\infty}^\infty dp_0\int_0^\infty p^2dp\delta(p^2-p_0^2-k'^2+2k'p_0+\kappa^2)$$
$$\times[p_0(k'-p_0)/|p_0||k'-p_0|]\delta'(p^2-\sigma p_0^2)(1/\rho)$$
$$=2\pi P\int_{-\infty}^\infty\sigma^{\frac{1}{2}}dp_0(p_0^2+k'^2-2k'p_0-\kappa^2)^{\frac{1}{2}}$$
$$\times[p_0(k'-p_0)/|p_0||k'-p_0|]\delta'[p_0^2(1-\sigma)+k'^2-2k'p_0-\kappa^2]$$
$$=\pi P\int_{-\infty}^\infty\sigma^{\frac{1}{2}}dp_0\left\{\frac{k'}{[k'-p_0(1-\sigma)]^2}-\frac{k'}{p_0[k'-p_0(1-\sigma)]}\right\}\frac{k'-p_0}{|k'-p_0|}$$
$$\times\delta'[p_0^2(1-\sigma)+k'^2-2k'p_0-\kappa^2].$$

The argument of the δ-function vanishes at two points:

$$p_0^{(1)}=(k'^2-\kappa^2)/2k';\quad p_0^{(2)}=2k'/(1-\sigma).$$

The contribution to J' from the singularity at $p_0^{(1)}$ is simply J (if we let $\sigma\to1$, $\sigma<1$). The contribution to J' from the singularity at $p_0^{(2)}$ turns out to be $(-\pi/2k'^2)$, so that we have

$$J'=\pi/(k^2+\kappa^2). \tag{A-11}$$

This result is true for both space-like and time-like k. This shows that the use of the modified D-function does eliminate the undesirable term from J.

We wish to discuss finally the effect of the limiting process on the self-energy calculation. This will be done for small intermediate momenta so that the effect of the convergence factors may be neglected. In calculating the self-energy of the V_+-particle, we must now add in the contribution from Eq. (31), which no longer vanishes; after the momenta have been renamed in a suitable manner, this contribution may be written

$$I_2(k_4)=-\int_{k_0<0,\,q_0<0}\cdots\int(dk)^4(dq)^4(dp)^4\{\delta(k+q-k_4+p)$$
$$\times\delta(k^2+\kappa_v^2)\delta(q^2+\kappa_u^2)(p^4/|p^4|)\delta'(p^2-\sigma p_0^2)\}. \tag{A-12}$$

This may be combined with $I_1(k_4)$, Eq. (34), by inserting under the integral sign a factor $\frac{1}{2}(k^4/|k^4|+q^4/|q^4|)$. The resulting integral can be expressed in terms of the modified J' function just calculated, so that we have for the contribution to the self-energy

$$I(k_4)=(\pi/2)\int\cdots\int\delta(q^2+\kappa_u^2)/[(k_4-q)^2+\kappa_v^2](dq)^4$$
$$+(\pi/2)\int\cdots\int\delta(k^2+\kappa_v^2)/[(k_4-k)^2+\kappa_u^2](dk)^4. \tag{A-13}$$

In Eq. (A-13), it is to be understood that a principal value is to be taken at all singular points of the integrand.[11] This eliminates the difficulty of Sec. II, in which a singularity in the integrand was coincident with a discontinuity. For higher momenta, this procedure is no longer valid because the convergence factors in I_1 and I_2 may be different. The two processes are then to be considered separately.

Gamma-Neutron Cross Sections

H. E. JOHNS, L. KATZ, R. A. DOUGLAS, AND R. N. H. HASLAM
Betatron Group, University of Saskatchewan, Saskatoon, Saskatchewan, Canada

(Received July 17, 1950)

A method is outlined for determining the total number of photons at each energy for a given irradiation from a betatron, assuming the bremsstrahlung photon distribution to be represented by an equation of Schiff and the response of an r-meter to be proportional to the absorption cross section for photons in the wall material.

The resulting activities produced by gamma-neutron reactions in Cu^{63}, Cu^{65}, Sb^{121}, Sb^{123}, and Ta^{181} have been measured as functions of the maximum photon energy of the betatron. In each case the activity was normalized to saturation per gram for 100 roentgens of radiation.

A method is also outlined whereby these activation curves may be analyzed to give the photo-neutron cross section as a function of energy. The cross section for Cu^{63} obtained by this method has its maximum at 17.5 Mev with a resonance half-width of 6 Mev and an integrated area of 0.7 Mev—barn. Maxima for the other nuclides are at somewhat lower energies and have essentially the same half-width.

I. INTRODUCTION

PHOTO-NEUTRON disintegrations were produced by x-rays from a betatron operating with peak energies from 9 to 26 Mev. Dosage rates up to 160 r.p.m. at the samples were used. The maximum energy of the betatron was stabilized within 0.1 Mev by an integrator-expander developed by Katz *et al.*[1] Calibration was based on the threshold[2] of $Cu^{63}(\gamma, n)Cu^{62}$ at 10.9 Mev, and $C^{12}(\gamma, n)C^{11}$ at 18.7 Mev.

The energy distribution in the forward direction of the betatron beam is given by a theoretical equation of Schiff,[3,4] which is plotted on Fig. 1 for maximum photon energies of 4.5, 7.5, 11.5, 15.5, 19.5, and 24.5 Mev. This distribution is in essential agreement with the theoretical work of Heitler[5] and of Rossi and Greisen.[6]

Koch and Carter[7,8] have obtained an experimental energy distribution by measuring the radius of curvature of positron and negatron tracks in a cloud chamber. Their results compare reasonably well with the Schiff distribution.

Experimental results are given for (γ, n) reactions in the following parent isotopes: Cu^{63}, Cu^{65}, Sb^{121}, Sb^{123}, and Ta^{181}. Satisfactory agreement with the work of McElhinney *et al.*[2] is obtained for Cu^{63}, approximate agreement for Ta^{181}, and exact agreement with the recent work of Almy and Diven.[9] The results differ rather widely from the work of Baldwin and Klaiber.[10] Our results indicate a broader "resonance width" than that postulated by Goldhaber and Teller,[11] though not in disagreement with the theoretical work of Levinger and Bethe.[12]

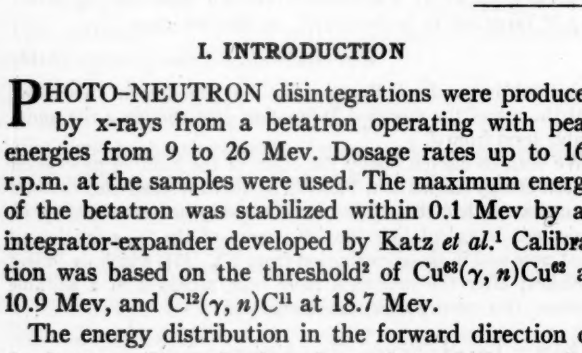

FIG. 1. Relative intensity of the bremsstrahlung in the forward direction as given by Eq. (1).

II. THEORETICAL CALCULATIONS

The intensity in the forward direction, according to Schiff[4] is proportional to

$$\Gamma = 8[2(1-z)(\ln\alpha - 1) + z^2(\ln\alpha - \tfrac{1}{2})], \quad (1)$$

where

$$\alpha^2 = \alpha_1^2\alpha_2^2/(\alpha_1^2+\alpha_2^2),$$
$$\alpha_1 = 2E_0(1-z)/\mu z,$$

and

$$\alpha_2 = 191/Z^{\frac{1}{3}}.$$

Here μ is the rest energy of the electron, k is the energy of the photon, $z=k/E_0$, E_0 is the total energy of the electron, and Z is the atomic number of the target material.

[1] Katz, McNamara, Forsyth, Haslam, and Johns, Can. J. Research **28**, 113 (1950).
[2] McElhinney, Hanson, Becker, Duffield, and Diven, Phys. Rev. **75**, 542 (1949).
[3] I. Schiff, Phys. Rev. **70**, 87 (1946).
[4] G. D. Adams, Phys. Rev. **74**, 1707 (1948).
[5] W. Heitler, *The Quantum Theory of Radiation* (The Clarendon Press, Oxford, 1936).
[6] B. Rossi and K. Greisen, Rev. Mod. Phys. **13**, 240 (1941).
[7] H. W. Koch and R. E. Carter, Phys. Rev. **75**, 1950 (1949).
[8] H. W. Koch and R. E. Carter, Phys. Rev. **77**, 165 (1950).
[9] B. C. Diven, G. M. Almy, Phys. Rev. **80**, 407 (1950).
[10] G. C. Baldwin and G. S. Klaiber, Phys. Rev. **73**, 1156 (1948).
[11] M. Goldhaber and E. Teller, Phys. Rev. **74**, 1046 (1948).
[12] J. S. Levinger and H. A. Bethe, Phys. Rev. **78**, 115 (1950).

TABLE I. Thickness and chemical composition of the absorbers in the photon beam.

		Thickness g/cm²	Chemical composition H	C	O	Al	Si	K
Donut		2.53	...	...	0.48	0.14	0.28	0.10
Monitor	Bakelite	0.625	0.07	0.56	0.37	...	...	...
	Aluminum	0.132	...	...	...	1.00	...	...
Lucite		4.13	0.08	0.60	0.32	...	...	...

Figure 2 shows the arrangement of the experimental apparatus. The wall of the donut, the monitor, and the wall of the Lucite block affect the spectral distribution because the absorption coefficients depend upon the energy and because secondary radiation is produced. However, the probability that the secondary radiation has an energy greater than the threshold for a nuclear reaction is very small, and therefore it does not contribute to the observed activity. Unfortunately, this radiation may be recorded by the Victoreen r-meter, which is used to monitor the dose given to the samples. In general, only a small fraction of these secondary photons are emitted exactly in the forward direction, so that an r-meter subtending a small solid angle at the absorber will not be affected appreciably. This condition, known as "good geometry," is satisfied for both the donut and the monitor; but not for the Lucite block. Figure 3 shows the effect of these factors upon the theoretical distribution as follows:

A. Theoretical Schiff distribution for a maximum photon energy of 24.5 Mev.

B. Curve A modified by the absorption of the donut and monitor using total absorption coefficients.

C. Curve B modified by the absorption of the Lucite block using real absorption coefficients. This distribution assumes that all the secondary scattered radiation from the Lucite block is detected.

D. Curve B modified by the absorption of the Lucite block using total absorption coefficients. This curve neglects the secondary radiation and gives the distribution which produces photodisintegration. The Victoreen will respond to some distribution lying between C and D, but C is probably a closer approximation and so has been used in all subsequent calculations. In any case, the percentage difference is small. Table I gives the data for these calculations.

The energy flux in ergs/cm² is obtained by measuring the ionization which the beam of photons produces in the cavity of a material with known absorption coefficients. The ionization J_v in a cavity filled with air and completely surrounded by this material is given by the

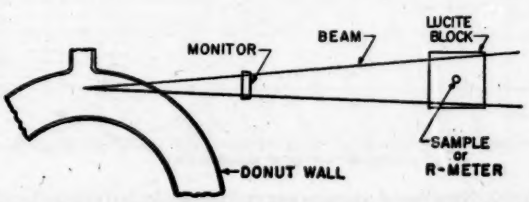

FIG. 2. Sketch of the apparatus showing the relative positions of the donut, monitor, and sample.

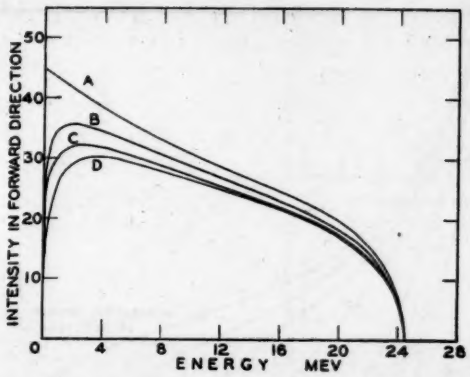

FIG. 3. Effect of absorption on the photon distribution: *A*. Theoretical Schiff distribution for a maximum photon energy of 24.5 Mev. *B*. Curve A modified by the absorption of the donut and monitor using total absorption coefficients. *C*. Curve B modified by the absorption of the Lucite block using real absorption coefficients. *D*. Curve B modified by the absorption of the Lucite block using total absorption coefficients.

well-known formula of Gray:[13]

$$J_v = (E_v/\rho W) \text{ e.s.u./cm}^3, \qquad (2)$$

where E_v is the energy truly absorbed per unit volume of wall in ergs/cm³, ρ is the ratio of the loss of energy suffered by a beta-particle in traversing 1 cm of the wall compared to the loss in 1 cm of air, and W is the average energy per e.s.u. required to produce a pair of ions.

This equation is correct only if the wall thickness is sufficient to produce equilibrium between the electromagnetic radiation and the corpuscular radiation arising from its absorption. The actual wall thickness is of the

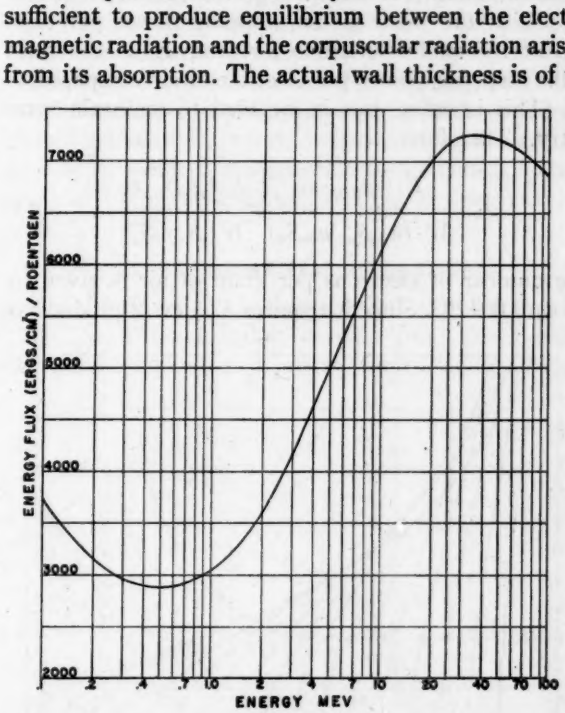

FIG. 4. Energy flux required to produce one "roentgen" measured in an air cavity in Lucite, as a function of the energy of the radiation.

[13] L. H. Gray, Proc. Roy. Soc. **A156**, 578 (1936).

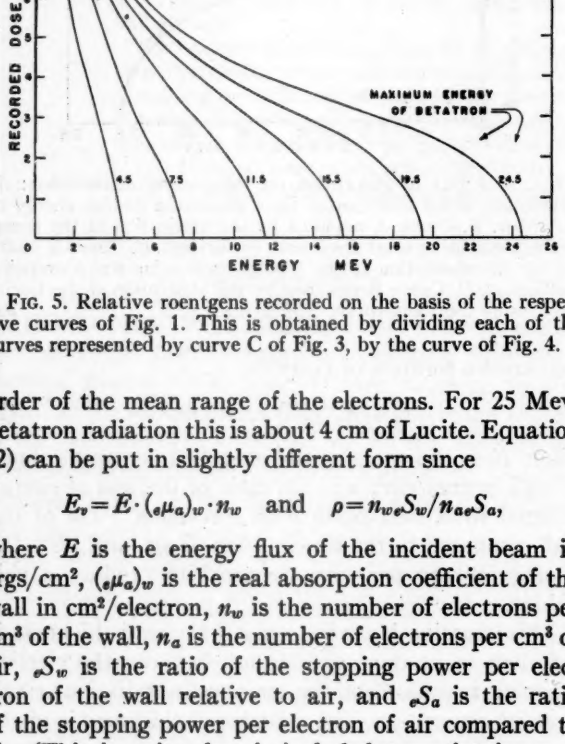

FIG. 5. Relative roentgens recorded on the basis of the respective curves of Fig. 1. This is obtained by dividing each of the curves represented by curve C of Fig. 3, by the curve of Fig. 4.

order of the mean range of the electrons. For 25 Mev, betatron radiation this is about 4 cm of Lucite. Equation (2) can be put in slightly different form since

$$E_v = E \cdot ({}_e\mu_a)_w \cdot n_w \quad \text{and} \quad \rho = n_w {}_eS_w / n_a {}_eS_a,$$

where E is the energy flux of the incident beam in ergs/cm², $({}_e\mu_a)_w$ is the real absorption coefficient of the wall in cm²/electron, n_w is the number of electrons per cm³ of the wall, n_a is the number of electrons per cm³ of air, ${}_eS_w$ is the ratio of the stopping power per electron of the wall relative to air, and ${}_eS_a$ is the ratio of the stopping power per electron of air compared to air. (This is unity, but is included to maintain symmetry.) Therefore,

$$J_v = \frac{E \cdot ({}_e\mu_a)_w \cdot n_w}{W \cdot (n_w {}_eS_w / n_a {}_eS_a)} = \frac{E \cdot ({}_e\mu_a)_w \cdot n_a}{W({}_eS_w / {}_eS_a)}. \tag{3}$$

The number of electrons per gram of air is given by $n = n_a/0.001293$. Since it requires 32.5 ev to produce an ion pair, Eq. (3) can be written as

$$J_v = \frac{E \cdot ({}_e\mu_a)_w \cdot n}{83({}_eS_w / {}_eS_a)}. \tag{4}$$

Figure 4 is a plot of E/J_v, using $n = 3.007 \times 10^{23}$ electron/g and[13]

$${}_eS_w / {}_eS_a = 1.02 \quad \text{(Lucite)}.$$

In this paper the dose as measured in a Lucite block will be referred to as the dose in "roentgens." This does not correspond exactly to the formal definition of the roentgen because the ionization is produced in the walls surrounding the cavity, which do not have the same absorption coefficients as air. In actual fact, the dose in true roentgens would be 2 to 15 percent greater, depending on the photon energy, for the same exposure if a true air wall material were used.

Figure 4 thus gives the energy flux at each energy which is required to record a dose of one "roentgen" for an r-meter placed in a Lucite block. Above 40 Mev the response curve begins to drop, owing to the increase in the real absorption coefficient of Lucite through pair production. The minimum at 0.5 Mev corresponds to the peak in the real Compton absorption at this energy. Below 0.1 Mev the curve rises slightly and then falls to zero as zero photon energy is approached, owing to the very large photoelectric absorption at low energies.

To normalize the distribution curves, the series of curves represented by curve C of Fig. 3 is divided by the response curve of the r-meter (Fig. 4), giving the curves of Fig. 5.

The area under each one of the curves of Fig. 5 is proportional to the number of recorded "r." Normalizing each of these to 100 r will determine the actual ordinates of Fig. 1 and Fig. 3. Using this normalization factor, the curves of Fig. 3 have been redrawn to give Fig. 6, where the ordinate is now in photons per Mev region per cm², per 100 roentgen.

In Fig. 7 the number of photons in any given Mev region is plotted as a function of the maximum energy

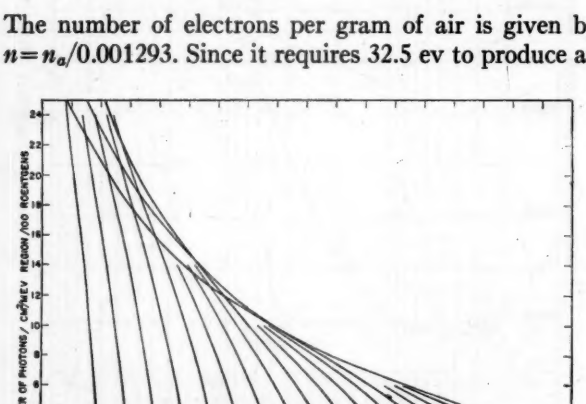

FIG. 6. Absolute photon distribution at the sample as a function of photon energy normalized to 100 "roentgens" (100 r) measured in lucite.

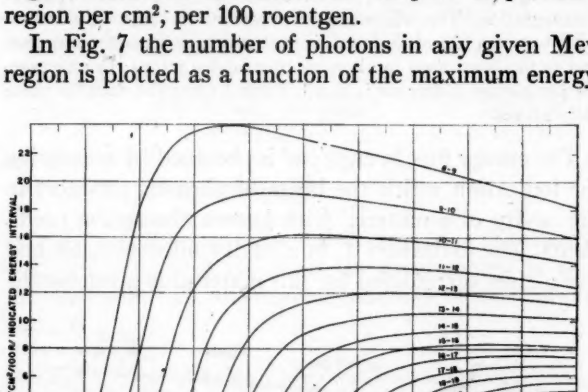

FIG. 7. Number of photons per cm² per indicated energy interval per 100 r measured in Lucite as a function of the maximum photon energy of the betatron.

of the betatron. For example, the number of photons between 8 and 9 Mev is given by the uppermost curve for different maximum energies of the betatron. The falling of this curve at higher energy is caused by normalization to the same dose. These curves are used directly to calculate the cross section.

Experimentally, several samples of the chosen element are irradiated at various maximum energies of the betatron. The number of product nuclei present at any time t_2 following the irradiation is given by

$$N=B/\lambda(1-e^{-\lambda t_1})\exp[-\lambda(t_2-t_1)], \qquad (5)$$

where B is the rate of production of product nuclei in the sample, λ is the decay constant of the product nured from the start of irradiation.

Using this formula, the observed activity may be normalized to saturation at an irradiation rate of 100 r/min. Figure 8 shows the normalized activity curves of Cu^{63}, Ta^{181}, and Sb^{121}.

The method by which the activity curves of Fig. 8 can be resolved into cross-section curves is illustrated in Fig. 9. Figure 9(a) shows an assumed cross-section curve, where σ_1 refers to the average cross section from 11 to 12 Mev, etc. Figure 9(b) is a sketch approximating Fig. 7, and Fig. 9(c) is a sketch representing Fig. 8. When the maximum energy of the betatron is 12 Mev, the activity $k=\sigma_1 a$. We can thus represent the activities k, l, m, etc., of Fig. 9(c) by the following set of equations:

$$\begin{aligned} k&=\sigma_1 a_1, \\ l&=\sigma_1 a_2+\sigma_2 b_1, \\ m&=\sigma_1 a_3+\sigma_2 b_2+\sigma_3 c_1, \text{ etc.} \end{aligned} \qquad (6)$$

These linear equations can be solved for the unknowns, $\sigma_1, \cdots, \sigma_n$, yielding the desired cross-section curve.

The method is complicated by experimental error in $k, l, m, \cdots$ of the order of 2 percent. Because the computation involves the difference of two numbers of nearly the same magnitude, the error in some values of σ may be 50 percent. In general, because of the nature of the curves, if the calculated value of σ_j is too large, the value of σ_{j+1} will be too small by a greater percentage. This results in an oscillating, rather than a smooth, cross-section curve particularly if the uncertainty in the activity curve is large. However, approximate values can be calculated and progressive smoothing used to obtain a smooth curve. At higher energies the calculation of a negative cross section is an indication that some of the earliest estimated cross sections were too large.

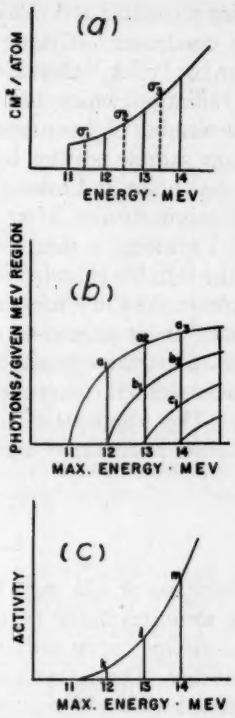

FIG. 9. (a) Sketch of a hypothetical cross section. (b) Sketch of Fig. 7. (c) Sketch of a saturated activity curve.

III. EXPERIMENTAL PROCEDURE

The dose given to a sample is recorded by the monitor (Fig. 2). The ionization current from the monitor charges a condenser to a predetermined value, at which

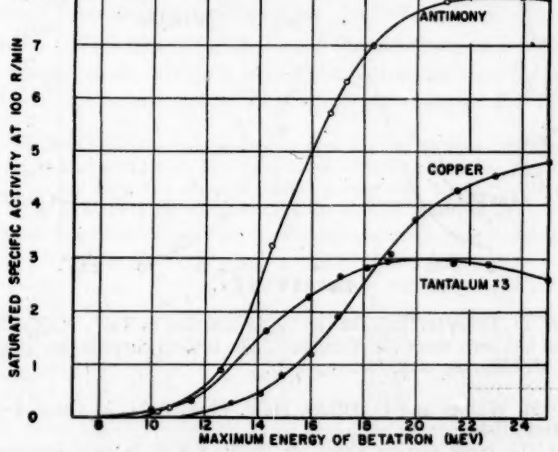

FIG. 8. Activity induced in 1 g of the isotopes Cu^{63}, Sb^{121}, and Ta^{181} if irradiated at 100 r.pm.. until saturation, after corrections have been applied for geometry, self-absorption, etc.

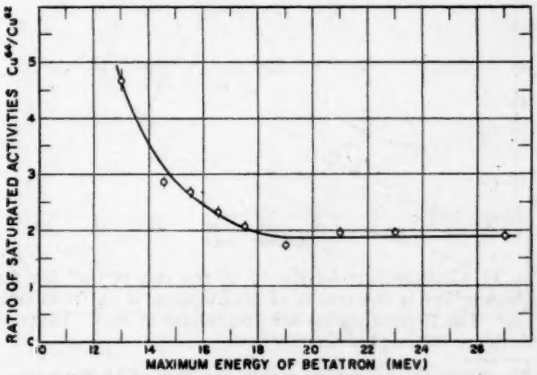

FIG. 10. Ratio of the saturated activity of Cu^{64} to that of Cu^{62} after a correction has been applied for the decay scheme of Cu^{64}.

point a counter and relay operate. The relay discharges the condenser, allowing the process to repeat. Each count or "click," therefore, represents a definite amount of radiation which has passed through the monitor. The number of "roentgens" per click can be determined in any sample position by placing the Victoreen r-meter at that point and taking several measurements.

Experimentally, after the monitor is calibrated with the Victoreen, a sample of cross-sectional area similar to the thimble chamber is placed in the holder and given a known dose in a measured time. After irradiation it is placed under an end-on counter and the activity measured. Separate experiments are performed to measure geometrical efficiency, self-absorption, and backscattering. The application of these corrections gives the absolute normalized activity curve shown in Fig. 8.

IV. RESULTS

A. Copper

Samples of 425 mg/cm² thickness and 1.1 by 2 cm size were irradiated between $\frac{1}{16}$-in. sheets of cadmium. The decay curve indicated 10.1 min. and 12.8 hour activities. The latter was negligible if the sample was counted within 20 minutes of the end of irradiation.

The Cu^{64} activity curve was found by measuring the ratio of the 12.8 hour to the 10.1 min. activities. Figure 10 shows the ratio of the saturated activities. Cu^{64} has a rather complex decay scheme,* some of the atoms going to Zn^{64} by β^- (36.5 percent) emission while others go to Ni^{64} by positron emission (17.5 percent) or K-capture (46 percent). The activity measured was corrected for the loss of counts due to K-capture by multiplying all measured counting rates by 1.85.

Figure 11 shows the absolute cross sections of Cu^{63} and Cu^{65}. The broken curve is due to McElhinney *et al.*[2] for Cu^{63}. A recent determination by Almy and Diven,[9] in excellent agreement with this work, is also shown. Wäffler and Hirzel[14] give $1.2\pm0.3\times10^{-25}$ cm² at 17.5 Mev. Our value of 1.1×10^{-25} is within their probable error.

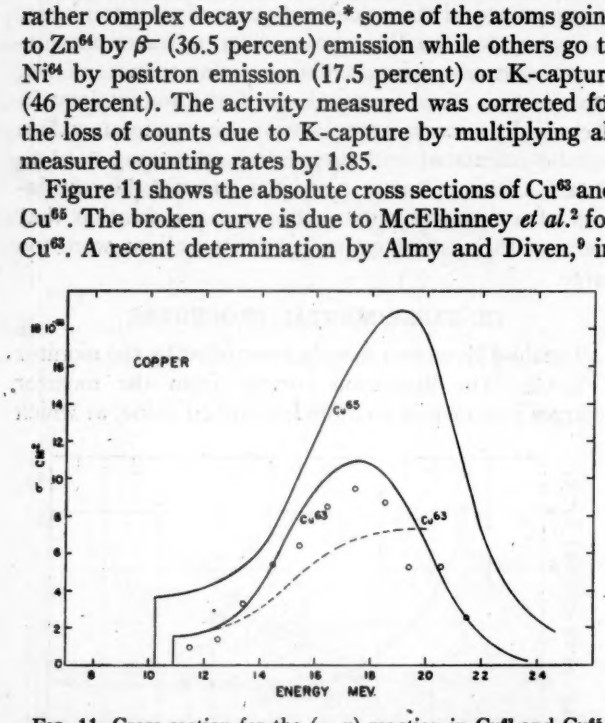

FIG. 11. Cross section for the (γ, n) reaction in Cu^{63} and Cu^{65}. The broken line is the results of McElhinney *et al.* (reference 2) for Cu^{63}. The plotted points are the results of B. C. Diven and G. M. Almy (to be published).

* To obtain the branching ratios, the data of H. Brandt et al. Helv. Phys. Acta 19, 219 (1946) was combined with that of R. Bouchez and G. Kayes, J. de phys. et rad. (Ser. 8) 10, 110 (1949).

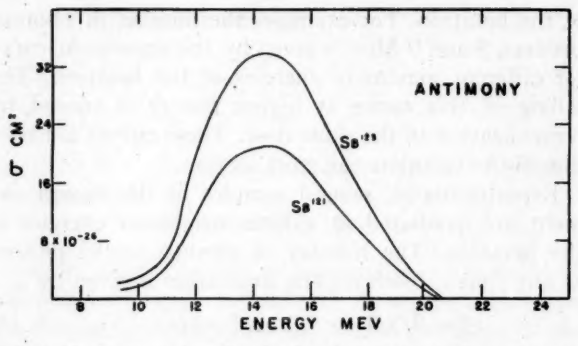

FIG. 12. Cross sections for the (γ, n) reaction in Sb^{122} and Sb^{121}. The cross section of Sb^{121} is only for those reactions which lead to the 16.4-min. isomeric state.

B. Antimony

Powdered antimony was irradiated in a cadmium thimble the same size as the Victoreen thimble chamber.

The decay showed 16.4±0.1-min. and 66-hour activities. When the longer activity is not subtracted, a 17.0-min. activity, which has previously been mentioned in the literature, is obtained. The authors believe the 16.4±0.1-min. half-life to be correct.

The Sb^{123} activity curve was determined independently, but found to be approximately 1.62 times the Sb^{121} after all corrections were applied.

Figure 8 shows the Sb^{121} activity curve and Fig. 12† the Sb^{121} and Sb^{123} cross-section curves.

C. Tantalum

Samples of 260 mg/cm² thickness and 1.1 cm by 2 cm size were irradiated and counted on thin plastic film. The decay curve showed a pure 8.0-hour activity.

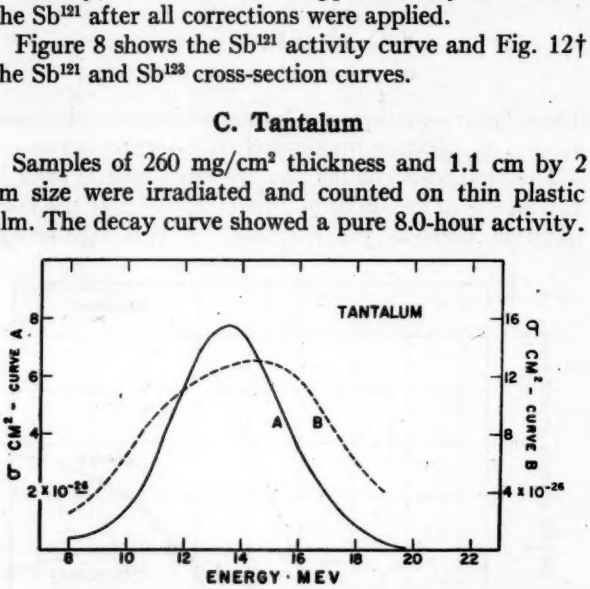

FIG. 13. Cross sections for the (γ, n) reaction in Ta^{181}. No correction has been made for *K*-capture. The broken curve is the results of McElhinney *et al.* (reference 2).

[14] H. Wäffler and O. Hirzel, Helv. Phys. Acta. 21 (Nos. 3–4), 200–3 (1948).

† The cross section given for $Sb^{121}(\gamma h)Sb^{120}$ is only for those reactions which lead to the 16.4-min. isomeric state. To obtain the total cross section for reactions going directly to the ground state of Sb^{120}.

TABLE II. Summary of the results of the cross-section measurements.

Parent isotope	Threshold Mev	Energy of maximum σ Mev	Maximum σ Barn	Half-width Mev	Integrated cross section Mev-Barn
Cu^{63}	10.9	17.5	0.11	6.0	0.70
Cu^{65}	10.2	19.0[a]	0.18	6.0	1.40
Sb^{121}	9.3	14.5	0.21	5.5	1.2
Sb^{123}	9.3	14.5	0.34	5.5	2.0
Ta^{181}	8.0	13.5	0.078	4.5	0.39

[a] The position of this maximum is not believed to be as accurately located as to the other substances.

Figure 8 shows the normalized activity curve and Fig. 13 the calculated cross section.‡ The result of McElhinney *et al.*[2] is indicated by the broken line.

V. DISCUSSION OF RESULTS

Table II shows the significant features of these cross-section measurements.

The most striking feature of the (γ, n) curves obtained in this work is their broadness. They give a "resonance width" of about 5.5 Mev, which is considerably broader than that found by Baldwin and Klaiber, though in good agreement with the measurements of McElhinney *et al.* and the more recent work of Almy and Diven. The cross-section *vs.* energy values obtained by these latter workers are plotted on top of our smooth curve in Fig. 11, the agreement being much better than one would expect from the estimated accuracy of the measurements.

Although the theory of Levinger and Bethe does not say anything about the expected "resonance width" in these reactions, it does predict the mean energy for photon absorption. According to their Eq. (40) and (42), this mean energy cannot be lower than 16 Mev. The values for this quantity are given in Table III and are seen to be less than 16 Mev in the case of antimony and tantalum. Competing reactions with relatively large integrated cross sections may raise these values considerably and bring them in closer agreement with theory. According to Levinger and Bethe, the integrated total cross section $\int \sigma dE$ should vary as NZ/A, or nearly as A, where σ is the total cross section for all reactions, $(\gamma, n)(\gamma, p)(\gamma, x)$, etc., at energy E. The

TABLE III. Harmonic mean energies of the various reactions involved and a check on the validity of assuming that the photon distribution over the energy region giving rise to the activity varies as $1/E$. $\bar{E}$ is the mean energy for photon absorption.

Parent isotope	$\bar{E}$ Mev	E_H Mev	$\int \sigma(\gamma, n)dE/E$ Barn	$\frac{C_{24}}{P_m E_m}$ Barn
Cu^{63}	17.5	17.0	0.041	0.52
Sb^{121}	14.5	14.3	0.084	0.084
Sb^{123}	14.5	14.5	0.137	0.136
Ta^{181}	13.5	13.3	0.029	0.027

‡ No correction has been applied for undetected activity due to K-capture and internal conversion since the decay scheme of Ta^{180} is not known.

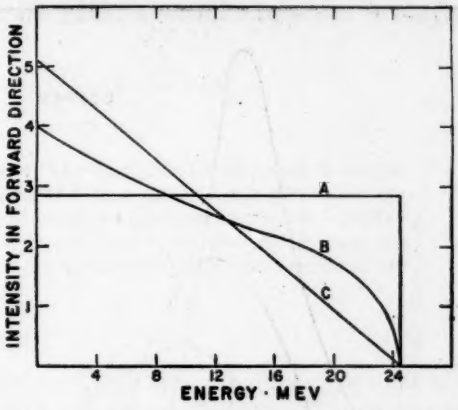

FIG. 14. Intensity in the forward direction for the assumed distributions: *A*. *A* $1/E$ photon distribution with a finite number of photons at the maximum energy. *B*. Schiff distribution. C. *A* $(E^{-1}-E_0^{-1})$ photon distribution with zero photons at the maximum energy.

values of this integral for the (γ, n) reactions only are listed in Table II and, as can be seen, are not linear in A. In order to retain the theory one would have to postulate a very large competing reaction in the case of tantalum or a large correction for K-capture.

If we assume that $P(E, E_0)$ gives the number of photons per cm² per Mev interval, then the number of active atoms produced in a given sample during an irradiation is

$$\int_0^{E_0} \sigma_{(\gamma, n)} P dE = C_{E_0}, \tag{7}$$

where E_0 is the maximum energy of the bremsstrahlung from the betatron. In our determination of cross section the systems of linear equations (6) express such sets of integrals with the integral being evaluated in each case by the trapezoidal rule. If $E_0 = 24$ Mev, then the area under the σP *vs.* E curve is actually made in our computation to be equal to the measured value of C_{24}.

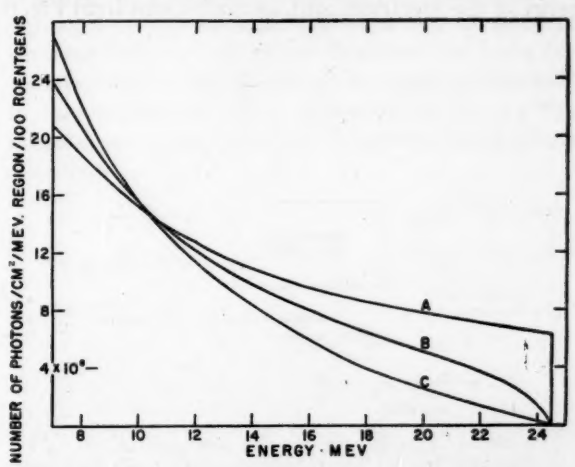

FIG. 15. Absolute photon distributions at the sample corresponding to the assumptions shown on Fig. 14. These have been normalized to 100 "roentgens" measured in Lucite.

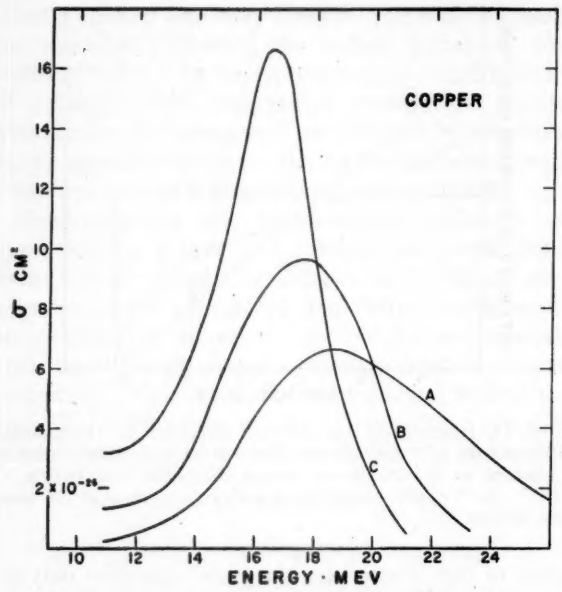

FIG. 16. Cross sections of copper which result from the three distributions of Fig. 14.

Assuming that the photon spectrum varies as $1/E$ we can write

$$P=P_mE_m/E, \tag{8}$$

where E_m is the energy at which $\sigma_{(\gamma,n)}$ has its maximum value and P_m is the value of P at this energy. Then to a fair approximation,

$$\int_0^{24}\sigma_{(\gamma,n)}dE/E=C_{24}/P_mE_m. \tag{9}$$

The actual values of the integral were determined by graphical integration and are listed in Table III. Their difference from C_{24}/P_mE_m values which are listed is an indication of the validity of Eq. (8). The disagreement is large in the case of copper because the peak of the cross-section curve is in this case too near the maximum energy of the spectrum, and, as can be seen from Fig. 6, the assumed equation does not give a good fit in this region.

The harmonic mean energy defined by Levinger and Bethe,

$$E_H=\left(\int\sigma_{(\gamma,n)}dE\right)\Big/\left(\int\sigma_{(\gamma,n)}dE/E\right),$$

is also listed in Table III.

The authors wish to express their appreciation for a grant from the N.R.C. and a bursary held by one of them (R.D.) which made this project possible. They also wish to thank L. Pease who measured the ratio of the Cu^{64}/Cu^{62} activity and S. B. Mauchel, betatron technician, for his untiring assistance.

APPENDIX

The dependence of the calculated cross-section shape upon the assumed photon distribution was investigated. Figure 14 shows the intensity in the forward direction for a maximum photon energy of 24.5 Mev for three assumed intensity distributions. Figure 15 shows the corresponding photon distributions normalized to give 100 "roentgens" as shown previously. These distributions are:

A. A $1/E$ photon distribution with a finite number of photons at the maximum energy.

B. Schiff distribution.

C. A $(E^{-1}-E_0^{-1})$ photon distribution with zero photons at the maximum energy.

Figure 16 shows the cross sections calculated using these assumed photon distributions.

Going from assumptions A to C it is seen that the maximum of the cross-section curve is shifted to lower energies, the half-width decreases and $\int\sigma_{(\gamma,n)}dE$ decreases. This indicates, however, that the cross section is only moderately sensitive to the assumed distribution, since relatively large variations in it do not produce correspondingly large variations in the cross-section shape and especially in $\int\sigma_{(\gamma,n)}dE$. Therefore, we would not expect smaller corrections to the Schiff formula to affect our results appreciably.

The resolving power of this method was also investigated. It was found that it would not resolve two rectangular cross sections 1 Mev in width and separated by 2 Mev. Thus, these results give only the general features of the cross section and do not indicate what the finer structure, if any, may be.

On the Photo-Disintegration of the Deuteron by Lithium and Fluorine γ-Rays

P. V. C. HOUGH*
Laboratory of Nuclear Studies, Cornell University, Ithaca, New York
(Received July 7, 1950)

The photographic emulsion has been used to measure the differential cross section for the photo-disintegration of the deuteron by 6.1- and 7.0-Mev γ-rays, and by 14.8- and 17.6-Mev γ-rays. A new method for the absolute measurement of γ-ray intensities leads to an absolute value for the total cross section at 17.6 Mev of $(7.2\pm1.5)\times10^{-28}$ cm². The results are in agreement with the theory for a "free" deuteron *P*-wave, but are not sufficiently accurate to fix with greater precision any of the parameters in the neutron-proton potential.

I. INTRODUCTION

IT was first pointed out by Powell[1] in 1940 that the photographic plate allows a new measurement of the cross section for the photo-disintegration of the deuteron. Since the war Gibson, Green, and Livesey,[2] and Goldhaber[3] have exploited the technique, using deuteron-loaded emulsions. They employed for their source the 6.1-Mev and 7.0-Mev gamma-radiation which results from the bombardment of fluorine by protons. The present paper (Section II) reports an extension of their work which yields an angular distribution of the photo-disintegration protons at the mean energy of the fluorine γ-rays.

The use of deuteron-loaded emulsions for recording disintegrations by higher energy γ-rays is complicated by the onset of competing (γ, p) processes in other elements in the emulsion. Fast neutrons, produced by (γ, n) reactions in surrounding material, also contribute to the background through collision with emulsion protons and deuterons. As described in Section III, both background components have been eliminated, and differential and absolute total cross-section measurements have been made from the 14.8- and 17.6-Mev γ-rays obtained by the bombardment of lithium with protons. The absolute cross-section measurement depends on a new method for the absolute measurement of γ-ray intensities which was suggested by R. R. Wilson and is described in Section IV.

While these experiments were in progress, Waffler and Younis[4] reported an absolute measurement of the total cross section for the photo-disintegration by lithium γ-rays. Also, Fuller[5] published preliminary results for the differential cross section at various γ-ray energies as well as a measurement of the relative total cross section as a function of energy, using the bremsstrahlung beam from a 22-Mev betatron. Since then Goldhaber[6] has reported measurements of the differential cross section using fluorine γ-rays, and Barnes, Stafford, and Wilkinson,[7] total cross sections for γ-rays from both fluorine and lithium. The measurements of these experimenters are compared with the present results, and the experiments compared with the theory, in Section V.

II. DISINTEGRATION BY FLUORINE γ-RAYS

As was first demonstrated by Goldhaber,[3] nuclear emulsions can absorb large amounts of heavy water and still record low energy proton tracks. In the present investigation two Kodak NTB 100-micron plates were loaded with 34 mg/cm² of D_2O and 33 mg/cm² of H_2O respectively. The plates were then irradiated with γ-rays produced by the bombardment of a thick sodium fluoride target with 1.1-Mev protons from the Cornell cyclotron. Vapor-tight aluminum cassettes supported the plates, with their emulsions in the plane of the cyclotron target plate. With the geometrical arrangement in this plane shown in Fig. 1, an exposure from 100μ amp.-hrs. of protons was found to be satisfactory. The plates were processed by standard techniques, except that the usual pre-soak in water was already accomplished during the exposure.

For observation, the emulsion area was divided by light scratches into squares about 2 mm on a side. The provision of small, definite search areas which can be examined in a single observation period has many advantages. It allows different observers to work conveniently on a single plate. It allows the plate to be removed and replaced without introducing uncertainty in the coordinates. Most important of all, it permits unambiguous comparison of the accuracies of different observers.

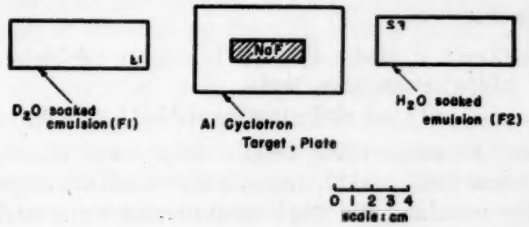

FIG. 1. Arrangement of the photographic emulsions with respect to the sodium fluoride target for the exposure to the fluorine γ-rays.

* Now at the University of Michigan, Ann Arbor, Michigan.
[1] C. F. Powell, Nature **145**, 155 (1940).
[2] Gibson, Green, and Livesey, Nature **160**, 534 (1947).
[3] G. Goldhaber, Phys. Rev. **74**, 1725 (1948).
[4] H. Waffler and S. Younis, Helv. Phys. Acta **22**, 414 (1949).
[5] E. G. Fuller, Phys. Rev. **76**, 576 (1949); **77**, 647 (1950); **79**, 303 (1950).
[6] G. Goldhaber, Phys. Rev. **77**, 753 (1950).
[7] Barnes, Stafford, and Wilkinson, Nature **165**, 70 (1950).

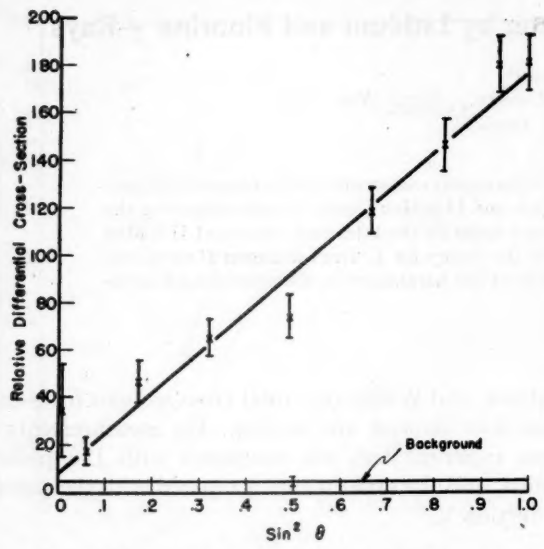

FIG. 2. Relative differential cross section at the mean energy of the fluorine γ-rays.

The search of a 1.3-cm² area of the D_2O-loaded emulsion yielded 1034 tracks beginning and ending in the emulsion, or an area density of about 800 tracks/cm². The H_2O-loaded emulsion showed an area density of similar tracks which was 4 percent of this number.

In determination of the angular distribution of the photo-protons, tracks of very great dip angle are rejected because of the unknown and probably smaller efficiency for their detection. (The dip angle of a track is the complement of the angle the track makes with the normal to the emulsion surface. The polar angle, θ, and azimuthal angle, α, used here and in Section IV, refer to a spherical coordinate system, with the polar axis parallel to the emulsion surface and in the direction of propagation of the gamma-radiation.) If δ_0 is the maximum dip angle considered, tracks of polar angle $\delta_0<\theta<\pi-\delta_0$ are selected only if they lie in a range of azimuthal angle compatible with the restricted dip angle. Furthermore, for the larger values of $\sin\theta$, a few tracks are lost because they pierce the emulsion surface. This loss is small (always less than 5 percent) because the average track length is only about one-sixth of the wet emulsion thickness.

A simultaneous consideration of both of these effects shows that the fraction $f(\theta)$ of tracks recorded at polar angle θ is

$$\begin{aligned} f(\theta)&=1-(\lambda/\pi)\sin\theta, && \theta<\delta_0 \\ &=(2/\pi)\arcsin(\sin\delta_0/\sin\theta) \\ &\quad -(\lambda/\pi)[\sin\theta-(\sin^2\theta-\sin^2\delta_0)^{\frac{1}{2}}], && \theta>\delta_0, \quad (1) \end{aligned}$$

where λ=mean track length (65μ)÷wet emulsion thickness (385μ)=0.17, and δ_0 is the cut-off dip angle.

The searching and track measurement were carried out by three observers, with concordant results. All tracks observed were recorded and selections made afterward to form a group of dip less than $4\mu/35\mu$, and another of dip less than $6\mu/35\mu$. The reduction of measured dip angles to true unprocessed wet-emulsion dip angles requires a knowledge of the emulsion thickness under the conditions of the exposure. Micrometer measurements on other plates of the same emulsion number established that water and emulsion volumes add to within 5 percent. Thus, the measured weight of D_2O added to the emulsion gives for its thickness during the exposure $385\pm20\mu$. The true maximum dip angles for the two groups of tracks considered are 56° and 67°.

The detection efficiency of the observers was found by the Rutherford method of coincidence observing to be only about 70 percent. This low efficiency is a consequence of the wet emulsion exposure, which gave weak tracks. However, possible forward or 90° observer bias was removed by the survey of half the total emulsion area with the plate at right angles to its usual position. Also, no evidence was found for any systematic variation in detection efficiency with dip angle (up to the maximum values accepted).

As a check, the length of each track was recorded. The distribution in range obtained showed a strong peak at 65μ and a smaller peak, not completely resolved, at about 90μ. The corresponding energies deduced for the fluorine γ-ray lines are 6.2 and 7.0 Mev, in agreement, within experimental error, with the more accurate measurements of Walker and McDaniel.[8]

The results of the angular distribution measurement are shown in Table I. The second column gives the number of tracks of dip angle less than 67° and with polar θ relative to the γ-ray in the range shown in column 1. (The group with $\delta_0=56°$ was found to give an angular distribution in agreement within statistics, but is not shown because it is not statistically independent and is of less statistical weight.) Column 3 is column 2 divided by $f(\theta)$ and thus gives the total numbers of tracks which occur in the various ranges of θ. Column 4 is column 3 divided by $(10/2\pi)$ times the solid angle available for the photo-protons in each angular range and hence is proportional to the differential cross section for the photo-disintegration. Throughout, tracks at angle $\pi-\theta$ are grouped with those at angle θ, because in most cases it was impossible to determine the direction of motion of the proton. Figure 2

TABLE I. The angular distribution of photo-protons at the mean energy of the fluorine γ-rays.

Polar angle θ°	Observed number of tracks $\delta_0=67°$	Corrected number of tracks	Relative differential cross section
0–9	4	4	34±20
10–19	7	7	17± 6
20–29	30	30	46± 9
30–39	56	58	65± 8
40–49	79	82	74± 9
50–59	144	151	119±10
60–69	194	209	147±11
70–79	208	275	181±12
80–90	227	321	182±12

[8] R. L. Walker and B. D. McDaniel, Phys. Rev. 74, 315 (1948).

shows the relative differential cross section plotted against $\sin^2\theta$. The background, measured on the H_2O-loaded plate and assumed to be isotropic, is also indicated. The straight line through the data points was determined by least squares. If we write the differential cross section in the form,

$$\sigma(\theta)=\sigma_t(a+\sin^2\theta)/4\pi(a+\tfrac{2}{3}), \qquad (2)$$

where σ_t is the total cross section, the least squares line gives

$$a=0.02^{+0.04}_{-0.02}.$$

The lower limit of error is determined by the fact that a is non-negative, and the upper limit is the r.m.s. deviation from the mean.[9]

The ratio, τ, of the photo-magnetic to photoelectric total cross section is simply $(3a/2)$,[10] provided the contribution of the tensor force to the isotropic component in the differential cross section is negligible.[11] On this assumption we have at the mean fluorine γ-ray energy of 6.4 Mev,

$$\tau=0.03^{+0.06}_{-0.03}. \qquad (3)$$

The theoretical value[10] for τ at this energy is 0.02, neglecting P-state forces entirely.

III. DISINTEGRATION BY LITHIUM γ-RAYS

The well-known lithium γ-rays, of energies 14.8 and 17.6 Mev, were obtained by the bombardment of a thick lithium metal target with 0.75-Mev protons from the Cornell cyclotron. D_2O- and H_2O-loaded emulsions were exposed to this radiation, as in the work described above. Now, however, preliminary measurements showed no significantly larger number of tracks in the D_2O-loaded emulsion.

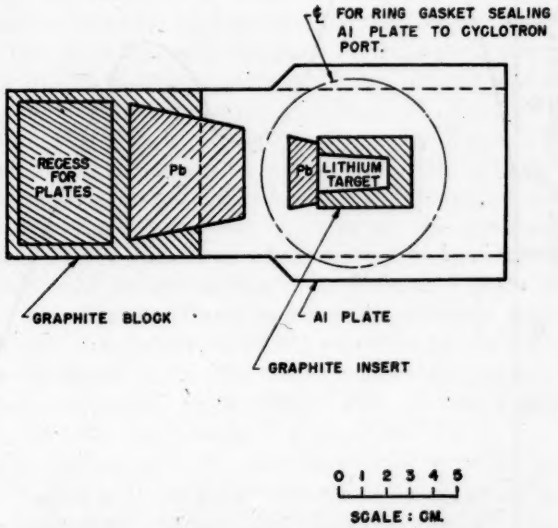

FIG. 3. Combination cyclotron target plate and plate holder for the exposure to the lithium γ-rays.

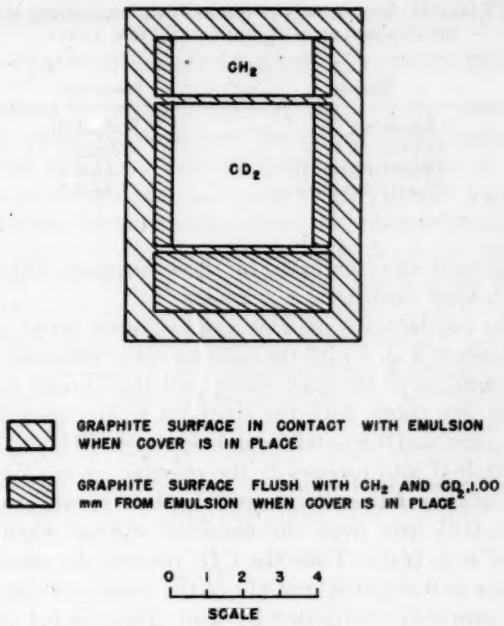
CH_2
CD_2
GRAPHITE SURFACE IN CONTACT WITH EMULSION WHEN COVER IS IN PLACE
GRAPHITE SURFACE FLUSH WITH CH_2 AND CD_2, 1.00 mm FROM EMULSION WHEN COVER IS IN PLACE
0 1 2 3 4
SCALE

FIG. 4. Graphite cover for the plate holder shown in Fig. 3.

It was decided, therefore, to shield the emulsion from the direct gamma-radiation and to study the disintegrations occurring in a thin slab of deuterated paraffin (CD_2), placed parallel to the emulsion and a few millimeters away in the full γ-ray beam. In this way (γ, p) processes occurring in the emulsion are suppressed, while photo-protons from the CD_2 can cross the short air space to the emulsion to be recorded. A minimum emulsion range of 53μ was required for acceptance of a track for measurement, and this criterion excludes all tracks from the reaction $C^{12}(\gamma, p)B^{11}$. The plate holder itself was made of graphite, so that the possibility of a background due to (γ, p) reactions is eliminated.

The possibility remains, however, that some tracks entering the emulsion from the CD_2 slab are fast deuterons resulting from the impact of photo neutrons. To investigate this point, a section of the CD_2 "radiator" was replaced with CH_2. Since the (n, p) scattering cross section is slightly larger than the (n, d) cross section over the relevant neutron energy range, the number of tracks from the CH_2 gives a (close) upper bound to the number of recoil deuterons. It was found in this way that in an early arrangement about 20 percent of the tracks originating in the CD_2 were actually deuteron recoils. The photo-neutron flux was then reduced by introducing a graphite insert into the cyclotron aluminum target plate where the γ-ray intensity is high, by decreasing the thickness perpendicular to the γ-ray beam of the lead sheet which shields the emulsion, and by surrounding the plate holder with a several-foot thick paraffin shield. The recoil deuteron

[9] Whittaker and Robinson, *The Calculus of Observations* (Blackie and Son, London, 1924), Chapter IX.
[10] H. A. Bethe, *Elementary Nuclear Theory* (Wiley, 1947).
[11] W. Rarita and J. Schwinger, Phys. Rev. 59, 436, 556 (1941).

TABLE II. Area density of tracks in various regions of the emulsion after exposure to lithium γ-rays.

Region	Tracks/cm²
Opposite CD_2	17.0±1.0
Opposite CH_2	2.6±0.6
Opposite graphite	2.7±0.7
Unexposed plate	3.3±1.5

component was eliminated by these measures, although which were essential is not known.

The combination cassette and cyclotron target plate is shown in Fig. 3 with the cassette cover removed. The top surfaces of the lead shield and the lithium target are in one plane, with the emulsion surface parallel to this plane and 0.50±0.05 mm below. The CH_2 and CD_2 are melted into recesses in the cassette cover (Fig. 4), so that their free surfaces are in a plane parallel to and 1.00±0.05 mm from the emulsion surface when the cover is in place. Thus the CD_2 nearest the emulsion surface is 0.50±0.08 mm above the surface of the lead and definitely unshielded by lead. There is 6.4 cm of paraffin, 1.2 cm of graphite, and 1.2 cm of rubber between the source and the CD_2 during the exposure. One region of the emulsion surface faces simply graphite, and it is this part which is scanned to verify that (γ, p) reactions in the emulsion are really eliminated. The completeness of the background eradication may be judged from the track area densities given in Table II.

As in the work with fluorine γ-rays, the detection sensitivity of the arrangement is not independent of the angle of motion of the proton and must be calculated. To formulate the problem precisely, we choose rectangular coordinates in the surface of the CD_2 radiator with the x-axis in the direction of the gamma-radiation. The thickness of the radiator is greater than the maximum range of the disintegration protons. If θ is the polar angle relative to the x-axis and α is the azimuth angle, the number of recorded tracks in solid angle $\sin\theta d\theta d\alpha$ coming from the radiator area element $dxdy$ is

$$d^4n=\epsilon G(x)\sigma(\theta)\sin\theta d\theta d\alpha\cdot Nz(\theta,\alpha)dxdy, \qquad (4)$$

where ϵ is the detection efficiency of the observer, $G(x)$ is the total number of γ-rays/cm² at position (x, y) (to sufficiently good approximation G is independent of y), $\sigma(\theta)$ is the differential cross section for the photodisintegration, and N is the number of deuterons per cm³ of heavy paraffin. $z(\theta, \alpha)$ denotes the total thickness of paraffin in which a proton can originate and cause a track at angles θ, α, whose projected length in the emulsion is at least 53μ and which stops before entering the glass. (The first criterion is designed to assure a high observer efficiency, and the second to eliminate from consideration the many cosmic-ray tracks which traverse the emulsion completely.) Since momentum and energy conservation determines the energy of a disintegration proton, and therefore also its range in paraffin and in the emulsion, it is a matter of geometry to determine $z(\theta, \alpha)$. The integration of (4) over α and over x and y is elementary, and without giving further details we write the result as follows:

$$dn=\epsilon\Gamma tNAZ(\theta)\sigma(\theta)\sin\theta d\theta/4\pi x_1x_2. \qquad (5)$$

Here dn represents the observed number of tracks in the range $d\theta$ at θ, Γ is the total number of γ-rays emitted by the source during the exposure, t represents the transmission of the material between the source and the radiator (0.85), x_1 is the distance from the center of the source to the nearest edge of the CD_2 radiator (13.6 cm), x_2 is the distance to the farthest edge (17.4 cm), and A is the area of the radiator (14.5 cm²). Evidently $Z(\theta)$ can be interpreted as the average thickness of the radiator times the average range of azimuth angle for which disintegration protons at polar angle θ are recorded.

Actually, for the two lithium γ-rays, we must replace $Z\sigma$ in Eq. (5) by $Z_1\sigma_1[I_1/(I_1+I_2)]+Z_2\sigma_2[I_2/(I_1+I_2)]$, where I_1, I_2 are the intensities of the low and high energy lines respectively. If we define

$$\bar{Z}=Z_1[\sigma_1I_1/(\sigma_1I_1+\sigma_2I_2)]+Z_2[\sigma_2I_2/(\sigma_1I_1+\sigma_2I_2)],$$
$$\bar{\sigma}=\sigma_1[I_1/(I_1+I_2)]+\sigma_2[I_2/(I_1+I_2)], \qquad (6)$$

this replacement gives simply

$$dn=\epsilon\Gamma tNA\bar{Z}(\theta)\bar{\sigma}(\theta)\sin\theta d\theta/4\pi x_1x_2. \qquad (7)$$

Using the measured intensity ratio[12] $I_1/I_2=0.52$ and the Bethe-Peierls theoretical ratio[10] $(\sigma_1/\sigma_2)=1.24$, one

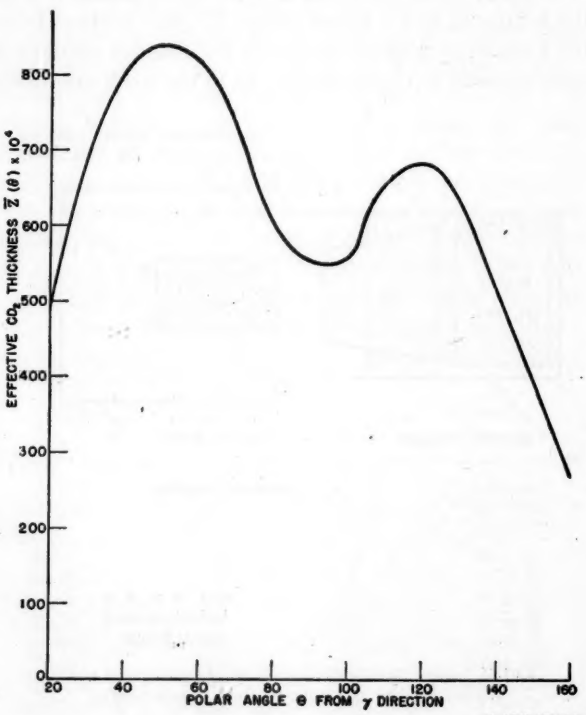

FIG. 5. Effective thickness, $\bar{Z}(\theta)$, of the CD_2 radiator (see text).

[12] Obtained by graphical integration of the dotted curves of Fig. 4b, reference 8.

TABLE III. The differential cross section at the mean energy of the lithium γ-rays.

Polar angle $\theta°$	Number of tracks opposite CD_2	Background	Differential cross section $\bar{\sigma}(\theta)\times10^{29}$ cm²/steradian
20–29	4	1	2.2±1.3
30–39	15	2	5.6±1.6
40–49	17	3	4.3±1.3
50–59	24	3	5.6±1.3
60–69	42	3	9.8±1.6
70–79	51	3	13.4±2.0
80–89	27	4	7.2±1.4
91–100	31	6	8.0±1.6
101–110	29	5	7.4±1.4
111–120	24	5	5.6±1.3
121–130	21	5	5.2±1.3
131–140	9	3	2.5±1.1
141–150	3	1	1.3±0.9
151–160	3	1	2.5±1.8

obtains for $\bar{Z}(\theta)$ the result shown in Fig. 5. The main features of the curve are readily understood. The decrease in the "effective thickness" of the radiator for θ near 0° and 180° occurs because at these angles only protons originating near the radiator surface will have sufficient projected range in the emulsion to be recorded. The depression near $\theta=90°$ is chiefly the result of the loss of the tracks so nearly normal to the emulsion surface that complete penetration of the emulsion cannot give sufficient projected range. The forward peak is larger than the backward one because the forward protons have somewhat higher energy.

The final plates were exposed for about 20 hours with an average cyclotron beam current of 75 μamp. Three lead-encased Geiger counters served to integrate the γ-ray intensity. The counters were checked from time to time with a radium source, and were calibrated absolutely 12 days after the run (see Sec. IV).

The use of dry emulsions made the subsequent searching and track measurement much less difficult and led to an observer efficiency, $\epsilon=0.91\pm0.05$. The results obtained from a survey of two 1-inch by 3-inch NTB 200-micron plates are shown in Table III. Column 2 gives the number of tracks found in the emulsion region opposite the CD_2 radiator which satisfy the acceptance criteria given above and which fall within the range of polar angle shown in column 1. Column 3 gives the number of similar tracks found in the emulsion region opposite the graphite and CH_2, corrected for the difference in search areas. The fourth column gives the absolute differential cross section $\bar{\sigma}(\theta)$ calculated from Eq. (7) with the value for Γ given in Sec. IV.

For comparison with the theory, the experimental cross section is averaged over the 30° angular ranges centered on 60°, 90°, and 120°, and over the 25° ranges centered on $32\frac{1}{2}°$ and $147\frac{1}{2}°$. (The point at 90° is raised above the average cross section by 0.1×10^{-28} cm² to take account of the curvature in the experimental curve.) The laboratory system cross sections are then reduced to center-of-mass system cross sections by use of the relation

$$\sigma_{CM}(\theta+4.0°\sin\theta)=\sigma_{lab}(\theta)/[1+(8/57)\cos\theta].$$

Denoting the angle of disintegration in the center-of-mass system by ϕ, we plot the experimental values for $\sigma_{CM}(\phi)$ in Fig. 6. The solid curve also shown is that calculated by Marshall and Guth[13] (their Fig. 4) normalized to give a total cross section $\bar{\sigma}_t=7.6\times10^{-28}$ cm². This value for $\bar{\sigma}_t$ corresponds to a total cross section at 17.6 Mev of 7.0×10^{-28} cm², which is the value calculated from Eq. (6) of Bethe and Longmire[14] with the new experimental triplet effective range,[15] $r_0=1.74\times10^{-13}$ cm. It is to be noted that there is no adjustable parameter in either the experimental or the theoretical results.

The cross section averaged forward and back, $(\frac{1}{2})[\sigma_{CM}(\phi)+\sigma_{CM}(\pi-\phi)]$ is found to be well represented by Eq. (2), with θ replaced by ϕ and with

$$a=0.02^{+0.14}_{-0.02}.$$

The laboratory differential cross section is integrated numerically by use of the data of Table III and yields for $\bar{\sigma}_t$ the value,

$$\bar{\sigma}_t=(7.8\pm1.5)\times10^{-28}\text{ cm}^2. \quad (8)$$

From Eq. (6) and the intensity and cross-section ratios given after Eq. (7), we find for the total cross section at 17.6 Mev,

$$\sigma_{2t}=(7.2\pm1.5)\times10^{-28}\text{ cm}^2. \quad (9)$$

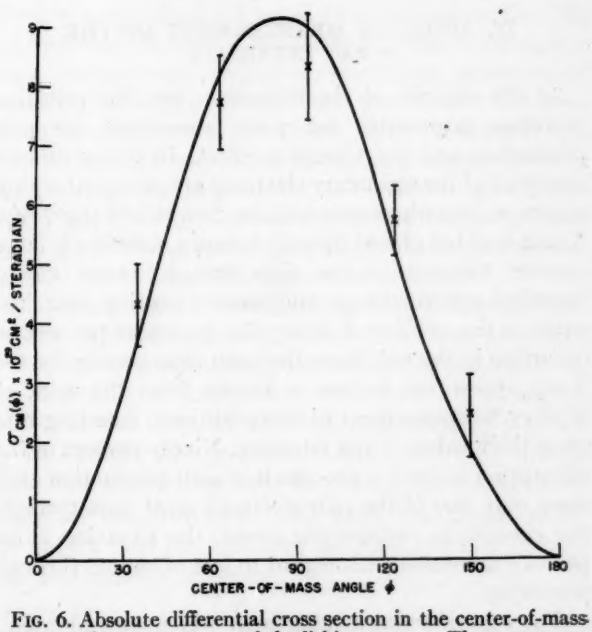

FIG. 6. Absolute differential cross section in the center-of-mass system at the mean energy of the lithium γ-rays. The crosses are the experimental values, and the solid curve is that calculated by Marshall and Guth.

[13] J. F. Marshall and E. Guth, Phys. Rev. **78**, 738 (1950).
[14] H. A. Bethe and C. Longmire, Phys. Rev. **77**, 647 (1950).
[15] D. J. Hughes, Phys. Rev. **78**, 315 (1950). Hughes, Burgy, and Ringo, Phys. Rev. **77**, 291 (1950).

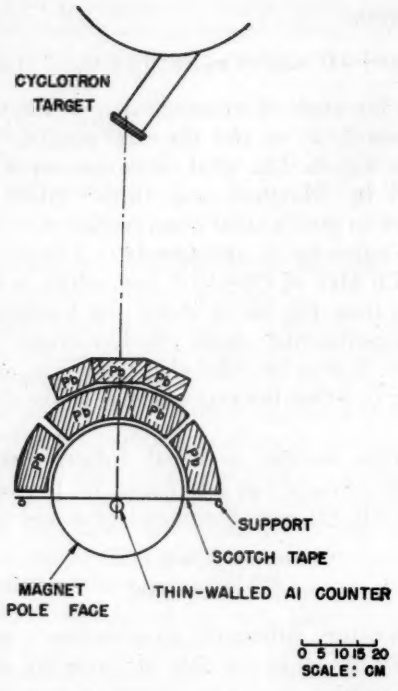

FIG. 7. Experimental arrangement for the absolute measurement of the intensity of the lithium gamma-radiation.

The essential limitation in the measurement is in the finite[17] γ-ray source size, which means that the source-radiator distances x_1 and x_2 in Eq. (7) are known only to about 10 percent.

IV. ABSOLUTE MEASUREMENT OF THE γ-RAY INTENSITY

At the energies of the lithium γ-rays, the principal processes responsible for γ-ray absorption are pair production and the Compton effect. In either process nearly all of the secondary electrons are produced within a narrow cone whose axis is in the direction of the γ-ray. A thin lead foil placed directly before a sufficiently large counter exposed to the high energy γ-rays should therefore contribute an additional counting rate just equal to the number of absorption processes per second occurring in the foil. Since the total cross section for the γ-ray absorption in lead is known from the work of Walker,[16] measurement of this additional counting rate gives the incident γ-ray intensity. Ninety percent of the absorption in lead is the result of pair production and, since only one of the pair electrons must pass through the counter to register the event, the situation is especially favorable with regard to loss of counts through scattering.

The experimental arrangement which was adopted[17] is shown in Fig. 7. The γ-ray beam from the cyclotron target is collimated and enters a magnetic field of about 3000 gauss which sweeps out electrons originating in the collimator. A Victoreen aluminum Geiger counter of wall thickness 30 mg/cm^2 and sensitive area about 2 cm$\times$5 cm is mounted vertically in the magnetic field with Scotch Tape. Thin lead foils of lateral dimensions 1 cm$\times$2 cm are attached to the front of the counter, also with Scotch tape. Calling the counting rate of the Victoreen counter V, we may write

$$V=V_0+(N_0w/A)\bar{\sigma}_e g, \tag{10}$$

where V_0 is the counting rate with no foil, N_0 is Avogadro's number, w is the foil weight in grams, A is the atomic weight of lead, and g is the number of γ-rays per cm^2-sec. at the foil.

$\bar{\sigma}_e$ is the average non-nuclear absorption cross section of lead for the lithium γ-rays and is calculated in the following way. Walker[16] gives for the total cross section of lead at 17.6 Mev $\sigma=20.56\pm0.12$ barns. If we subtract the (γ, n) cross section in lead, estimated[18] to be 0.3 barn, we obtain a non-nuclear absorption cross section, $\sigma_e=20.3\pm0.1$ barns. Using the theoretical ratio[19] $\sigma_e(14.8)/\sigma_e(17.6)=0.940$ and assuming the intensity ratio of the two lines given after Eq. (7), we get $\bar{\sigma}_e=\sigma_e(14.8)[I_1/(I_1+I_2)+\sigma_e(17.6)[I_2/(I_1+I_2)]$ $=19.6\pm0.1$ barns.

Equation (10) applies only for w so small that scattering and absorption of the secondary electrons and absorption of the primary gamma-radiation are negligible. These effects will contribute a negative term in Eq. (10) proportional to w^2 (for small w) and are negligible as long as the experimental curve of V against w is straight.

The quantity actually determined experimentally is not V, but

$$V/m_3=(V_0/m_3)+(N_0\bar{\sigma}_e/A)(g/m_3)w, \tag{11}$$

where m_3 denotes the counting rate of one of the lead-encased monitor counters (see Section III). V/m_3 is shown as a function of w in Fig. 8. The foil weight, $w=1.5$ grams, where the curve begins to deviate from linearity, corresponds to a 4 percent absorption of the primary beam. The measured slope of the straight line portion is $(1.35\pm0.10)\times10^{-2}$ (gram)$^{-1}$. With the value for $\bar{\sigma}_e$ given above, we obtain $g/m_3=0.238\pm0.019$.

(One measurement was made using an aluminum foil instead of lead. For equal values of N_0w g/A, the two materials gave counting rates above background in the ratio of their cross sections, $\bar{\sigma}_e$ at the mean lithium energy, to within the statistical error of 5 percent in the counting rate ratio. McDaniel[18] has compared lead, aluminum, and copper, with similar results. Since the relative absorption cross sections of the three elements

[16] R. L. Walker, Phys. Rev. 76, 527 (1949).

[17] A similar arrangement was used first by M. Camac (private communication). The general method was proposed by R. R. Wilson.

[18] McDaniel, Walker, and Gorman (to be published.) Our estimate, which does not need to be accurate, is taken from their preliminary measurements. I wish to thank these authors for making their results available before publication.

[19] P. V. C. Hough, Phys. Rev. 73, 266 (1948). W. Heitler. *Quantum Theory of Radiation* (Oxford University Press, London. 1936).

vary strongly with energy, these results serve to rule out any large proportion of degenerated γ-rays in the beam leaving the collimator. The aluminum-lead comparison shows, for example, that less than 8 percent of the γ-rays leaving the collimator have energies betwen 1 and 5 Mev; similar limits are obtained for other energy ranges.)

Now let M_3 represent a total number of monitor counts, and Γ the corresponding total number of lithium γ-rays emitted at the cyclotron target. Since the emission is known to be isotropic,[20] we have $g/m_3 = T(\Gamma/M_3)/4\pi R^2$, where R is the cyclotron target-Victoreen counter distance, and $T=0.96$ is the calculated transmission of the $\frac{1}{8}$ inch of aluminum and $\frac{1}{2}$ inch of water which intervene. For the exposure of the plates described in Section III, $M_3=3.61\times10^6$ and, taking $R=1$ meter, we find $\Gamma=(1.12\pm0.10)\times10^{11}$. Through error, the monitor counters were moved before R was measured precisely, and it is necessary to increase the error to ±0.2. A completely independent earlier calibration of the monitor counters by Walker[21] using the pair spectrometer leads to the value $\Gamma=(0.9\pm0.2)\times10^{11}$. We adopt $\Gamma=(1.01\pm0\ 15)\times10^{11}$ as the final value for the source strength used in Section III.

It seems likely that the above method for the absolute measurement of γ-ray intensity is capable of an accuracy of better than 5 percent.

V. COMPARISON WITH OTHER EXPERIMENTS AND WITH THE THEORY

Table IV gives the results of all the recent published measurements of the isotropic component, a, in the differential cross section, and of the total cross section, σ_t, at the γ-ray energies of 6.13 and 17.6 Mev. (For an estimate of a at some intermediate energies, see reference 5.) The theoretical results quoted assume a free P-wave, and are calculated as described before Eq. (8).

TABLE IV. The isotropic component a in the differential cross section and the total cross section σ_t for the photo-disintegration of the deuteron.

γ-ray energy (Mev)	a (experiment)	a (theory)	$\sigma_t\times10^{28}$ cm^2 (experiment)	$\sigma_t\times10^{28}$ cm^2 (theory)
6.13	0.1[a]	0.03[c]	21.5±1.2[d]	21.2[c]
	$0.02^{+0.04}_{-0.02}$[b]			
17.6	~0.2[f]	0.01[c]	8 ±3[g]	7.0[c]
			8.5±1.2[d]	
	$0.02^{+0.14}_{-0.02}$[b]		7.2±1.5[b]	

[a] G. Goldhaber, Phys. Rev. **74**, 1725 (1948).
[b] Present work.
[c] H. A. Bethe, *Elementary Nuclear Theory* (John Wiley and Sons, New York, 1947).
[d] Barnes, Stafford and Wilkinson, Nature **165**, 69 (1950).
[e] H. A. Bethe and C. Longmire, Phys. Rev. **77**, 647 (1950). A triplet effective range, $r_0=1.74\times10^{-13}$ cm, is used.
[f] E. G. Fuller, Phys. Rev. **79**, 303 (1950).
[g] H. Waffler and S. Younis, Helv. Phys. Acta **22**, 414 (1949).

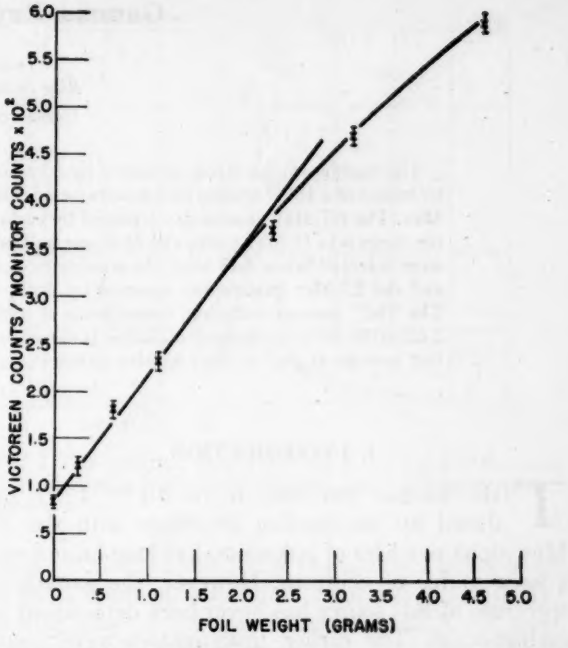

FIG. 8. Showing the counting rate of the Victoreen thin-walled aluminum Geiger counter, relative to the counting rate of a monitor counter, as a function of the weight of a lead foil attached to the front of the Victoreen counter.

Since most of these experiments were undertaken the high energy neutron-proton scattering experiments at Berkeley[22] have shown that the P-state force is much smaller than the S-state force. Consequently, very precise measurements of the photo-disintegration cross section are required at 17.6 Mev to give independent evidence for the nature of the neutron-proton interaction. The present experiments are in good agreement with the simple theory of the process.

I wish to thank Professor Robert R. Wilson for suggesting this problem and for his continuing help and encouragement throughout the work. For assistance in the searching of plates and measurement of tracks I owe thanks to Mrs. M. R. Keck and especially to Mr. T. E. Palfrey, who gathered most of the high energy data. Mr. Bruce Dayton's help with the cyclotron is gratefully acknowledged. This work was begun while the author held the Eastman Kodak Company fellowship at Cornell University.

[20] Ageno, Amaldi, Bocciarelli, and Trobacchi, Ricerca Scient. **12**, 139 (1941).
[21] R. L. Walker, private communication.
[22] See, for example, R. S. Christian and E. W. Hart, Phys. Rev. **77**, 441 (1950).

Gamma-Rays from $Be^9(\alpha,n)$ *

JAMES TERRELL†
Rice Institute, Houston, Texas
(Received August 4, 1950)

The gamma-ray spectrum produced by bombarding Be^9 with polonium alpha-particles has been analyzed by means of a 180° focusing pair spectrometer. The spectrum shows a single gamma-ray of energy 4.45±0.09 Mev. The 6.7-Mev gamma-ray reported by earlier observers is not detected: no gamma-rays are present in the range 6 to 11 Mev to the extent of one-half percent of the 4.45-Mev intensity. Although no gamma-rays were detected below 4.45 Mev, the sensitivity of the spectrometer is much smaller in this low energy region, and the 2.7-Mev gamma-ray reported by Bothe and Dzelepov would probably not be detected if present. The Th*C″* gamma-radiation, investigated as a check on the operation of the spectrometer, is measured as 2.62±0.06 Mev; no gamma-radiation is detectable in the vicinity of 3.2 Mev with intensity as great as one-half percent of that of the 2.62-Mev gamma-ray.

I. INTRODUCTION

THE nuclear reaction $Be^9(\alpha,n)C^{12}$, C^{12*}, produced by bombarding beryllium with the 5.3-Mev alpha-particles of polonium, has long been a well-known source of neutrons. However, the gamma-ray spectrum of this source has never been determined unambiguously. The earlier investigators were unable to obtain strong polonium-beryllium sources; furthermore, the presence of the neutrons is a complicating factor.

Bothe,[1] investigating this gamma-ray spectrum with a 180° focusing electron spectrometer, found three gamma-rays, of energies 2.7, 4.2, and 6.7 Mev, and of roughly equal intensities. Maier-Leibnitz[2] reported neutron-gamma- and gamma-gamma-coincidences due to this source, and concluded that the two lower energy gamma-rays are the product of a cascade transition from a 6.7-Mev level in C^{12}, which is also the source of the highest energy gamma-ray. A second investigation of the gamma-ray spectrum was performed by Dzelepov[3] by means of a 180° focusing pair spectrometer. Dzelepov found gamma-rays of energy 2.7, 4.7, and 7.0 Mev, with the middle line 14 times as intense as the high energy line. The intensity of the lowest line was not estimated because of the unfavorable conditions for detecting it. Unfortunately, all of these early determinations of the gamma-ray spectrum were limited in accuracy by statistical factors owing to the relative weakness of the sources.

The neutron spectrum from polonium-beryllium has not been examined with precision; however, Bradford and Bennett,[4] using 1.4-Mev alpha-particles to bombard beryllium, found two well-resolved neutron groups, from the ground level of C^{12} and from an excited level at 4.45 Mev. A level at 7 Mev would not have been excited at this bombarding energy.

II. DESCRIPTION OF THE APPARATUS

The pair production spectrometer used in this work is similar to that used by Walker and McDaniel,[5] but has been designed for high intensity, with some necessary loss of resolution. A uniform magnetic field is used to produce 180° focusing of the pairs produced in a thin radiator by collimated gamma-radiation from the source (Fig. 1). The electrons and positrons are counted by four Geiger-Müller counters on either side of the radiator. Coincidences between the counters, in all 16 possible combinations, can be measured as a function

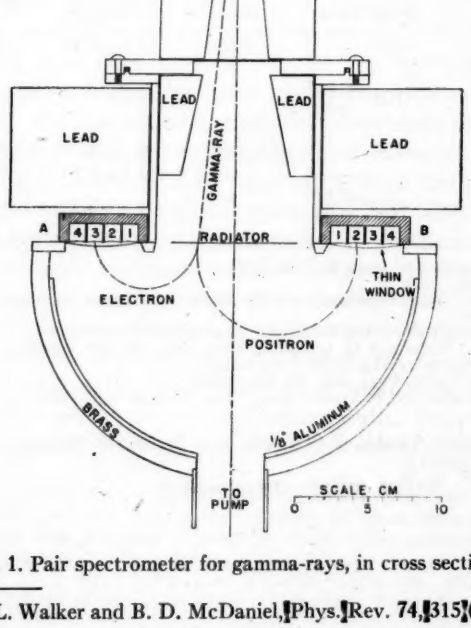

FIG. 1. Pair spectrometer for gamma-rays, in cross section.

* This paper is condensed from part of a Ph.D. thesis presented to the faculty of the Rice Institute in May, 1950. A preliminary report of this work was presented at the April, 1950, meeting of the American Physical Society [Phys. Rev. 79, 239 (1950)]. This work was supported by the joint program of the ONR and AEC.

† AEC Predoctoral Fellow. Now at Laboratory of Physics, Western Reserve University, Cleveland, Ohio.

[1] W. Bothe, Zeits. f. Physik **100**, 273 (1936).
[2] H. Maier-Leibnitz, Zeits. f. Physik **101**, 478 (1936).
[3] B. S. Dzelepov, Comptes Rendus U.R.S.S. **23**, No. 1, 24 (1939).
[4] C. E. Bradford and W. E. Bennett, Phys. Rev. **78**, 302 (1950).
[5] R. L. Walker and B. D. McDaniel, Phys. Rev. **74**, 315 (1948).

of magnetic field. The use of the large radiator and banks of counters is made possible by the fact that the total momentum of a pair (algebraic sum) is nearly independent of the manner in which the energy of the gamma-ray is divided between the two particles.

The vacuum box, counters, and lead shielding are shown in cross section in Fig. 1, in a plane perpendicular to the magnetic field. The brass box, 4 in. deep in the direction of the field, is lined with $\frac{1}{8}$-in. aluminum to reduce scattering effects; with this in place the distance between interior walls is $3\frac{1}{4}$ in. The radiator is 8.7 cm square, but the area effective for pair production is smaller, approximately 8.1×5.4 cm, the short dimension being parallel to the magnetic field. The distance from source to radiator is 25.5 cm. The thin windows soldered to the vacuum box and to the counter blocks are brass shim stock, 0.004 and 0.002 in. thick, respectively. The counters are milled out of Muntz metal, four in each block, separated by 0.05-cm walls. Each counter is 1.14 cm wide and 1.20 cm deep; the average distance from the radiator center is 8.86 cm. The counter wires are 5-mil tungsten, with an effective length, between Kovar seals, of 9.0 cm ($3\frac{1}{2}$ in.); the filling mixture is argon-alcohol at 23 cm pressure (22 cm of argon and 1 cm of alcohol).

The circular pole pieces are $10\frac{1}{2}$ in. in diameter, the center of the pole pieces nearly coinciding with the center of the cylindrical part of the magnet box. Slots are cut into the pole faces to receive the ends of the counters. The magnetic field is found to be sufficiently uniform in the region of the desired electron paths; it is uniform within one percent for most of this region, dropping off by two percent from its maximum value for portions of the outermost paths. In the region between the vacuum wall of the spectrometer and the radiator, the magnetic field serves as a clearing field, removing secondary particles produced in the vacuum wall. The electronically regulated magnet current, furnished by a 25-kw generator, does not fluctuate more than one percent for the smallest currents used, and is constant to better than one-half percent for larger current values. The magnetic field has been measured with flip coils and fluxmeter to a relative accuracy considerably better than one percent; the absolute value of the field is thought to be known within approximately two percent. Hysteresis effects are small, and are found to be entirely negligible when a standard cycle of current settings is followed.

The amplification and coincidence circuits are such that each counter is placed in coincidence with each of the four counters in the other block; the outputs of the 16 coincidence circuits are grouped according to the distance between counters, in order to simplify the taking of data. There are thus seven channels, with statistical weights of 1, 2, 3, 4, 3, 2, 1 (number of pairs of counters) in order of increasing distance of separation. The circuits are arranged such that the individual counting rates of the counters can also be determined,

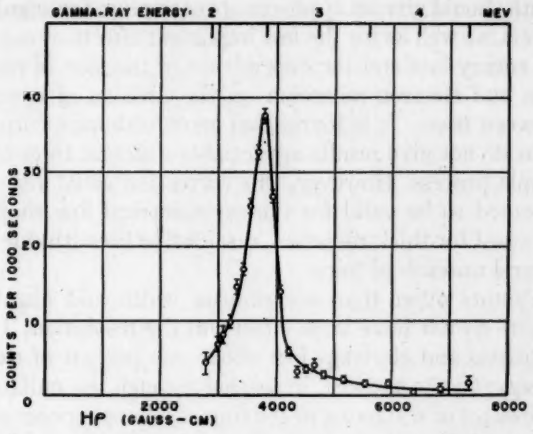

FIG. 2. Pair spectrum from ThC″, using 20.7-mg/cm² tin radiator. The ordinate scale is the counting rate for a single pair of counters.

both to check the operation of the counters and to allow the calculation of accidental coincidence rates. The resolving time of the coincidence circuits is 0.5 μsec., small enough to make the accidental correction a minor and sometimes negligible factor.

III. RESOLUTION AND YIELD

The most important of the factors affecting the resolution are the width of the counters and the angular distribution of the pairs leaving the radiator. The counters, with an effective width of 1.19 cm, are at an average distance of 8.86 cm from the radiator center. In the idealized case of particles leaving the radiator in the direction normal to the surface, the counting rate for pairs as a function of $H\rho$ is a triangular curve of 6.7 percent width at half-height, with the peak of the triangle corresponding to the true momentum of the pairs. The effect of an angular distribution differing from this ideal is to broaden and round the triangular shape and to shift the peak toward lower momentum values.

The angular distribution of electrons and positrons leaving the radiator is determined by two independent factors in addition to the initial directions of the gamma-rays: the pair production process, and multiple scattering in the radiator. For the radiators used in this work the angular effects due to multiple scattering are more important than those due to pair production. No accurate theory exists for either effect, for the large average angles involved at these energies of a few Mev. Thus the peak shift and half-width due to angular effects cannot be calculated directly with any precision.

However, the yield of pairs as a function of $H\rho$ has been calculated by numerical integration for several assumed Gaussian angular distributions, and it is found that the peak shift is approximately equal to half of the width at half-height due to angular effects, this width in excess of 6.7 percent being calculated by the difference of squares. Calculation of the peak shift from the

width should give an approximate correction for angular effects, as well as for the less important effects of radiator energy loss and the dependence of the sum of positron and electron momenta on the division of energy between them. It is found that more elaborate corrections do not give results appreciably different from this simple process. However, this correction could not be expected to be valid for the asymmetrical line shapes obtained for thick radiators, nor for line breadth due to several unresolved lines.

Factors other than the counter width and angular effects do not have large effects on the resolution. The positrons and electrons lose about one percent of their energy, on the average, in passing through the radiator. The effect of scattering in the thin windows between the magnet box and the counters is minimized by making the distance between box window and counter as small as possible; in the present case the average distance is about $\frac{1}{16}$ in. The effects on the resolution of slight inhomogeneities and fluctuations in the magnetic field should be very small, considerably less than one percent.

The numerical integrations used in the calculation of peak shifts also give the spectrometer efficiency (fraction of pairs formed in the radiator which are counted) for an assumed angular distribution. This efficiency is of the order of 6.7 percent per pair of counters when angular effects are negligible, at high energies; for energies of several Mev the efficiency is much lower and must be found experimentally.

The coincidence rate for a pair of counters depends on the distance between them as well as on the value of $H\rho$; counter pairs which are farther apart than the average have somewhat better resolution and lower counting rates than the average. This has been taken into account by modifying the channel weights somewhat empirically by a $1/\rho^2$ factor, taken as unity for the central channel, which is found to give good agreement between the channels. In the most important regions of the gamma-ray spectra the magnetic field settings are taken at 3.5 percent intervals, overlapping all four channels used for each value of $H\rho$. Since these four counting rates are simply added, and the sum divided by the total channel weight, the shape of the curve is unaffected by the choice of weights. Weighting factors would be unnecessary were it not that some points of the data do not represent the overlap of all four channels.

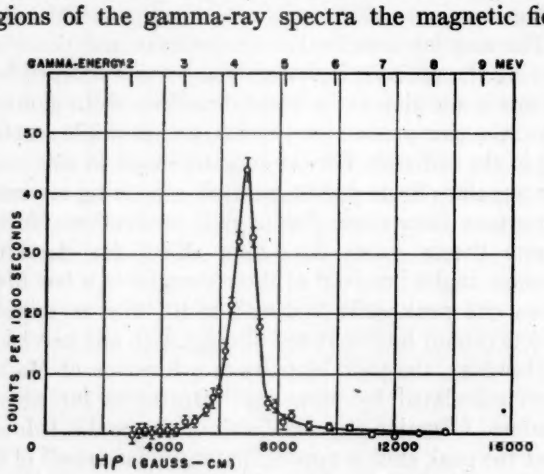

FIG. 3. Pair spectrum from polonium-beryllium source, using 31.0-mg/cm² tin radiator. The ordinate scale is the counting rate for a single pair of counters.

IV. EXPERIMENTAL RESULTS

A. Mesothorium Source

As a check on the operation of the spectrometer, pairs were observed from the 2.62-Mev gamma-ray of ThC''. The source was a MsThI salt, with gamma-radiation equivalent to about 9 mg of radium. The pair counting rate obtained in the most carefully done of several runs using a 20.7-mg/cm² tin radiator is plotted as a function of $H\rho$ (value for one particle) in Fig. 2. Standard statistical errors are indicated for all the points. The counting rates have been divided by channel weights to reduce the data to the counting rate for a single pair of counters, and have been corrected for accidental counts (about four percent of the peak counting rate) and for a small background (also about four percent) independent of the presence of the radiator, which was measured as a function of $H\rho$. The pair yield curve shows a single peak, with a long low tail at high energy. The long tail is probably due in part to pairs, one member of which has been scattered from an interior wall of the spectrometer; another probable source is coincidences between Compton electrons produced in the radiator and the scattered quanta. The peak is located at $H\rho = 3800$ gauss-cm, and has a height of 34.4 counts per 1000 sec. above the low background tail. The width at half-height is 13.8 percent of 3800 gauss-cm; the high energy edge is somewhat steeper than the low energy edge. Allowing for 6.7 percent counter resolution, we find a width of 12.0 percent due to angular distribution effects and to energy loss in the radiator (about 28 kev average for the pair). Applying a peak shift correction of 6.0 percent, we obtain 2.62 Mev as the energy of the gamma-ray from ThC''. The fact that this is accurately known to be the energy[6] indicates that no correction is necessary to the measured value of the magnetic field. The order of magnitude of the error involved in this energy measurement is probably not less than two percent; thus we write the energy of the ThC'' gamma-ray as 2.62 ± 0.06 Mev, as determined in this pair spectrometer. This serves more as a calibration for the spectrometer than as an absolute measurement of the gamma-ray energy.

There is no evidence in Fig. 2 for any gamma-ray in the neighborhood of 3.2 Mev, which has been suspected on the basis of the disintegration scheme. Statistical fluctuations here are of the order of two

[6] G. D. Latyshev, Rev. Mod. Phys. 19, 132 (1947); J. L. Wolfson, Phys. Rev. 78, 176 (1950).

percent of the peak counting rate, and, allowing for increased spectrometer efficiency and higher pair cross section at this energy, we may be reasonably sure that no gamma-ray exists in this region with intensity greater than about one-half percent of the intensity at 2.62 Mev. This is in agreement with the data of Bell and Elliott,[7] who set a maximum of 0.2 percent for any possible gamma-radiation at 3.2 Mev.

A Th*C''* source of 9-mC strength should emit about 3.4×10^8 gamma-rays/sec.; comparing this with the observed counting rate of 0.034 pair/sec./pair of counters, we find that the spectrometer counts one pair for each 10^{10} gamma-rays emitted, per pair of counters, using a 20.7-mg/cm² tin radiator. This sensitivity is 340 times lower than that calculated on the basis of no angular distribution losses, giving a loss factor of about 18 for each side of the spectrometer due to this angular distribution; the spectrometer is very insensitive at this low energy.

The Th*C''* gamma-ray was also observed, less carefully, using a tin radiator twice as thick as in the work just described. The width (14.9 percent) was slightly larger, and the yield of pairs was increased by 33 percent. The small increase in pair yield is undoubtedly due to the poorer angular distribution from the source side of the radiator, causing the added thickness to be relatively ineffective in producing pair counts. The high energy tail was just twice as high as for the thinner radiator.

B. Polonium-Beryllium Source

After this preliminary work with Th*C''*, the pair spectrometer was used to observe the gamma-rays from a strong polonium-beryllium source loaned by Los Alamos Scientific Laboratory. The source emitted $4.86\pm0.40\times10^6$ neutrons/sec. on November 26, 1949, according to a calibration performed at Los Alamos. Since the source decayed with a half-life of 140 days, the data obtained have been corrected to the value which would have been obtained on the calibration date. The pair counting rates observed from this source have been plotted in Fig. 3, as obtained from a 31.0-mg/cm² tin radiator. The data has been corrected for accidental counts with a rate about three percent of the maximum counting rate, and for a no-radiator background which is about 13 percent of the maximum pair counting rate in the vicinity of the peak, and rises to about 40 percent of the maximum pair rate in the vicinity of 3000 gauss-cm. The observed maximum counting rate for pairs was 41.8 counts/1000 sec./pair of counters, at 6880 gauss-cm, and the width at half-height was observed to be 11.9 percent. The peak shift may be calculated to be 4.9 percent, giving a gamma-ray energy of 4.45 ± 0.09 Mev. No other gamma-rays are apparent in the spectrum, but the sensitivity is very much lower below the 4.45-Mev peak, so that gamma-rays in this region are not ruled out. Statistical deviations in the region between 6 and 8 Mev are of the order of one percent of the peak yield, and a consideration of the increase in efficiency and pair cross section cuts the maximum intensity which might not be detected to about one-half percent of the 4.45-Mev gamma-ray strength.

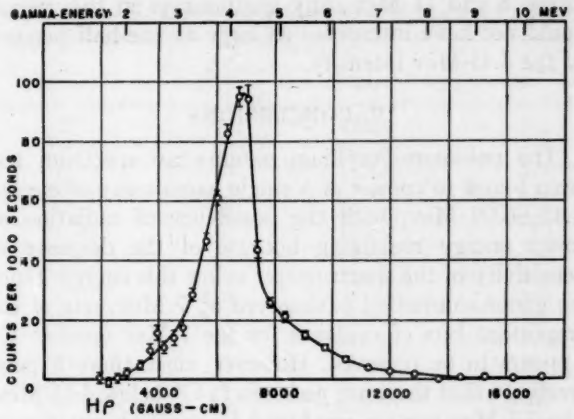

FIG. 4. Pair spectrum from polonium-beryllium source, using 273-mg/cm² tungsten radiator. The ordinate scale is the counting rate for a single pair of counters.

Estimating the number of 4.45-Mev gamma-rays emitted by the source as 3×10^6 quanta/sec., we calculate that this pair spectrometer counts one pair (per unit channel weight) for 7×10^7 gamma-quanta emitted, when a 31.0-mg/cm² tin radiator is used. This figure is of course only roughly determined. If we take the value for 2.62 Mev as 8×10^9 gamma-quanta/pair count for the same radiator thickness, we find the sensitivity to be about 110 times higher at the higher energy. Thus a 2.7-Mev gamma-ray would probably not be detected even if present with intensity several times larger than that of the 4.45-Mev gamma-ray (statistical fluctuations in the region of 2.7 Mev are of the order of three percent of the maximum counting rate).

The polonium-beryllium gamma-rays have also been observed with a much thicker radiator, partly to observe the effect of such a radiator. The results obtained with a 273-mg/cm² tungsten radiator are plotted in Fig. 4. Such a radiator is about 340 kev thick for the pairs, as compared to 42 kev for the 31-mg/cm² tin radiator, and should yield 12.4 times as many pairs. The actual peak intensity observed was only 77 percent higher than for the tin radiator, or 74 counts/1000 sec. above a wide, low background. This background, which is due to the radiator, is proportionately higher than for the tin target by the ratio of radiator weights (8.8). The width at half-height of the peak is 18.7 percent; the peak cannot be located accurately, but does not appear to be shifted from the location observed with the tin radiator. The curve is markedly asymmetrical, so that the peak shift cannot be estimated from the width. This thick-radiator data gives information as to the absence of gamma-radiation in the region be-

[7] R. E. Bell and L. G. Elliott, Can. J. Research **26A**, 379 (1948).

tween 8 and 11 Mev; any gamma-rays in this region could not have intensities as large as one-half percent of the 4.45-Mev intensity.

V. CONCLUSIONS

The polonium-beryllium gamma-ray spectrum has been found to consist of a single gamma-ray of energy 4.45 ± 0.09 Mev, with the possibility of radiation at lower energy remaining because of the decrease in sensitivity of the spectrometer below this energy. Since no gamma-radiation is observed at 7 Mev, one of the important bits of evidence for the 7-Mev level in C^{12} appears to be removed. However, since there is good evidence that there are no levels in C^{12} below 4.45 Mev, the 2.7-Mev gamma-ray found by early observers cannot be accounted for except by postulating the 7-Mev level. Thus it seems possible that this low energy gamma-ray may also not exist, the evidence for it being of the same statistical accuracy as the evidence for the 7-Mev gamma-ray. Further doubt is cast on the existence of this level by recent experimental results[8] on the inelastic scattering of protons by carbon nuclei, which indicate levels in C^{12} only at 4.8 and 10.1 Mev.

The author wishes to thank Professor T. W. Bonner for guidance and assistance in all phases of this work, and to express his indebtedness to the Los Alamos Scientific Laboratory for the loan of the polonium-beryllium source.

[8] Levinthal, Martinelli, and Silverman, Phys. Rev. 78, 199 (1950).

PHYSICAL REVIEW VOLUME 80, NUMBER 6 DECEMBER 15, 1950

On the Deep Configurations of V I and Cr II

ABRAHAM A. SCHWEIZER
Department of Physics, Hebrew University, Jerusalem, Israel
(Received July 5, 9950)

The theoretical formulas for d^3s^3, d^4s, and d^5 are compared with the experimental data of V I and Cr II; the Cr II terms are assigned to configurations. The agreement remains practically unimproved by taking into account the interactions between configurations.

I. INTRODUCTION

THIS study constitutes a direct continuation of Many's work[1] on 3- and 4-electron spectra in the iron group, applied to 5-electron spectra. The procedure adopted is essentially the same in our case, and the reader is referred to Many's article for abbreviations, designations, etc., In both spectra, we may still presume that we are confronted with *LS* coupling.

Following Many's example, we first compared the theoretical formulas with the experimental term values, not taking into account any configuration interactions. Thereafter we repeated our calculations allowing for interactions between configurations. In either case, we calculated the Slater-Condon F's and G's by means of least squares, evaluated the terms, and, finally, compared the agreements in both cases.

All theoretical formulas are taken from Racah.[2]

II. V I

This spectrum is well known for its clean *LS* coupling. The experimental term values are taken from Meggers and Russell.[3] The two lowest configurations d^3s^2 and d^4s are moderately well mixed up. Of their 32 terms 17 are found experimentally; besides a high lying ^6S term, a still higher ^4F assigned to d^5 is given in the new tables of Moore.[4] Both are excluded from our calculations and dealt with separately afterward.

At first, separate calculations for d^4s and d^3s^2 were carried out, although there is but little theoretical justification for such a procedure, and then the calculations for d^4s and d^3s^2 combined were made. Finally, the configuration interactions were taken into account. It is seen from Table I that, on the one hand, the small lowering of the mean deviation and the rise of the mean error in the case of d^3s^2, when taking separate parameters B and C in d^4s and d^3s^2 (see column 1) do not warrant this procedure; on the other hand, the mean error rises also when taking into account the electrostatic interactions between d^4s and d^3s^2 (see column 3). Therefore, the best result is obtained by calculating with the same B and C in both configurations and neglecting the interactions between configurations (see column 2). As regards d^3s^2 and d^4s, there is no possibility of interchanging the assignments of any two terms.

Concerning the two d^5 terms, there can be no doubt about the identity of the ^6S. Computing $A(d^5)$ from this latter term and taking the values of B and C from our previous calculation, we can compute the theoretical

[1] A. Many, Phys. Rev. 70, 511 (1946).
[2] G. Racah, Phys. Rev. 62, 438 (1942); 63, 367 (1943).
[3] H. N. Russell and W. F. Meggers, J. Research Nat. Bur. Stand. 17, 125 (1936).
[4] C. E. Moore, *Atomic Energy Levels* (National Bureau of Standards, 1949), Vol. I.

TABLE I. The deep configurations of V I. Column (1). Neglecting configuration interactions, separate parameters in the two configurations. Column (2). Neglecting configuration interactions. Same B and C in both configurations. Column (3). With configuration interactions.

Term		Obs.	(1) Calc.	(1) Diff.	(2) Calc.	(2) Diff.	(3) Calc.	(3) Diff.
d^3s^2	^4F	319	377	+58	1593	+1274	1699	+1380
d^4s	^6D	2297	2217	−80	1651	−646	1683	−614
$d^4(^5D)s$	^4D	8596	8743	+147	8186	−410	8344	−252
d^3s^2	^4P	9715	9857	+142	10269	+554	10157	+442
d^3s^2	^2G	11008	10868	−140	10727	−281	10702	−306
d^3s^2	^2P	13805	14027	+222	13619	−186	13497	−308
d^3s^2	$^2D^-$	14535	15425	+890	14743	+208	14670	+135
d^4s	^4H	14992	14282	−710	14365	−627	14315	−677
d^3s^2	^2H	15192	14027	−1165	13619	−1573	13628	−1564
$d^4(^3P^-)s$	^4P	15389	15506	+117	15779	+390	15937	+548
$d^4(^3F^-)s$	^4F	15725	15902	+177	16076	+351	16042	+317
d^4s	^4G	17166	17193	+17	17257	+91	17217	+51
$d^4(^3P^-)s$	^2P	19061	19422	+361	19700	+639	19869	+808
$d^4(^3H)s$	^2H	19090	18198	−892	18286	−804	18376	−714
$d^4(^3F^-)s$	^2F	19056	19817	+761	19997	+941	19667	+611
$d^4(^3D)s$	^4D	20789	21269	+480	21301	+517	21281	+492
$d^4(^3G)s$	^2G	21622	21109	−513	21178	−444	21276	−346
d^5	^6S	20202						
d^5	^4F	37032						
d^4s	^2I						21297	
$d^4(^1G^-)s$	^2G						22287	
d^3s^2	^2F						22592	
$d^4(^1S^-)s$	^2S						25231	
$d^4(^3D)s$	^2D						25285	
$d^4(^1D^-)s$	^2D						26586	
$d^4(^1F)s$	^2F						30151	
$d^4(^3F^+)s$	^4F						33288	
$d^4(^3P^+)s$	^4P						33643	
d^3s^2	$^2D^+$						34117	
$d^4(^3F^+)s$	^2F						37282	
$d^4(^3P^+)s$	^2P						37615	
$d^4(^1G^+)s$	^2G						38675	
$d^4(^1D^+)s$	^2D						50611	
$d^4(^1S^+)s$	^2S						64343	
			d^3s^2	d^4s				
$A(d^3s^2)$			9757	—	10269		10443	
$A(d^4s)$			—	19664	19025		19202	
$A(d^5)$			—	—	—		(40537)	
$B=F_2-5F_4$			632	582	578		581	
$C=35F_4$			2654	2108	2273		2244	
G_2			—	1305	1307		1332	
$H_2=R^2(dd,ds)/35$			—	—	—		106	
Mean error			±864	±607	±828		±850	
Mean deviation			±611	±484	±696		±684	

term value of the ^4F belonging to d^5; this is found to be 48692 cm^{-1}. Since the experimentally found ^4F lies at 37032 cm^{-1}, this term can hardly be assigned to d^5. On the other hand, it is pretty close to $d^4(^3F^+)s^4F$ to be found at 33288 cm^{-1} (see Table I), and this new assignment corresponds, therefore, much better to the facts. Furthermore, the separations between the levels of ^4F are rather big for a d^5 term; the two intervals $J:2\frac{1}{2}$–$3\frac{1}{2}$ and $J:3\frac{1}{2}$–$4\frac{1}{2}$ obey the Landé interval rule pretty well.

TABLE II. Comparison between V II[a] and V I.

V II Term		Calc.-obs.	V I Term		Calc.-obs.
d^3s	$\frac{1}{2}((4)^3F+{}^5F)$	+1495	d^3s^2	^4F	+1274
d^3s	$\frac{1}{2}((4)^3P+{}^5P)$	+776	d^3s^2	^4P	+554
d^3s	$\frac{1}{2}(^3G+{}^1G)$	+104	d^3s^2	^2G	−281
d^3s	$\frac{1}{2}((2)^3P+{}^1P)$	+177	d^3s^2	^2P	−186
d^3s	$\frac{1}{2}(^3D^-+{}^1D^-)$	+421	d^3s^2	$^2D^-$	+208
d^3s	$\frac{1}{2}(^3H+{}^1H)$	−980	d^3s^2	^2H	−1573
d^4	^5D	−1342	d^4s	$\frac{1}{2}(^6D+(3)^4D)$	−528
d^4	^3H	−1512	d^4s	$\frac{1}{2}(^4H+{}^2H)$	−716
d^4	$^3P^-$	+231	d^4s	$\frac{1}{2}(^4P^-+{}^2P^-)$	+515
d^4	$^3F^-$	−135	d^4s	$\frac{1}{2}(^4F^-+{}^2F^-)$	+646
d^4	^3G	−517	d^4s	$\frac{1}{2}(^4G+(3)^2G)$	−177
d^4	^3D	+177	d^4s	$(3)^4D$	+517

[a] See reference 1.

TABLE III. Experimental Landé factors in d^4s of Cr II.

Term	$(E_J-E_{J-1})/J=\zeta(SL)$	$\zeta(SL)/\alpha$	ζ_{3d}
$(^5D)^6D$	43	43×5	215
$(^5D)^4D$	66	666/3	222
$(^3D)^4D$	−18	18×18	324
$(^3D)^2D$	−35	35×9	315
$(^3G)^4G$	25	25×10	250
$(^3G)^2G$	12	12×5	60
$(^3H)^4H$	14	14×15	210
$(^3H)^2H$	30	30×7.5	225
$(^3P^-)^4P$	230	230×1	230
$(^3P^-)^2P$	465	465/2	232
$(^3F^-)^4F$	14	14×15	210
$(^3F^-)^2F$	11	11×7.5	83
$(^3P^+)^4P$	−24	24×1.5	36
$(^3F^+)^4F$	80	−80×90	−7200

TABLE IV. The deep configurations of Cr II. Column (1). Neglecting configuration interactions. Column (2). With configuration interactions.

Term		Obs.	(1) Calc.	(1) Diff.	(2) Calc.	(2) Diff.
d^5	a^6S	00000	−1616	−1616	−1524	−1524
$d^4(^5D)s$	a^6D	12281	14258	+1977	14164	+1883
$d^4(^5D)s$	a^4D	19833	21553	+1720	21230	+1397
d^5	a^4G	20521	19473	−1048	19443	−1078
d^5	a^4P	21829	22870	+1041	22779	+950
d^5	b^4D	25046	24513	−533	24973	−73
d^5	a^2I	30155	28528	−1627	28588	−1567
d^4s	a^4H	30292	29708	−584	29692	−600
$d^4(^3P^-)s$	b^4P	30535	31410	+875	31582	+1047
$d^4(^3F^-)s$	a^4F	31172	31813	+641	31540	+368
d^5-	a^2D	31432	32725	+1293	32346	+914
d^5-	a^2F	32471	33364	+893	33277	+806
d^5	b^4F	32857	33669	+812	33863	+1006
d^4s	b^4G	33598	33308	−290	33319	−279
$d^4(^3H)s$	a^2H	34740	34086	−654	34150	−590
$d^4(^3P^-)s$	a^2P	35132	35787	+655	35985	+853
$d^4(^3F^-)s$	b^2F	35601	36190	+589	35601	−0
d^5	b^2H	35673	35524	−149	35733	+60
d^5-	a^2G	36206	36446	+244	35375	−831
$d^4(^3D)s$	c^4D	38324	38347	+23	38316	−8
$d^4(^3G)s$	b^2G	38549	37686	−863	38243	−306
$d^4(^1G^-)s$	c^2G	39773	39386	−387	39929	+156
d^5+	c^2F	39829	39326	−503	39882	+53
d^4s	b^2I	40225	38164	−2061	38234	−1991
$d^4(^3D)s$	b^2D	42944	42724	−220	42949	+5
$d^4(^1D^-)s$	c^2D	45718	44738	−980	44587	−1131
d^5+	d^2G	52325	53521	+1196	53456	+1131
$d^4(^3F^+)s$	c^4F	53656	53215	−441	53002	−654
$d^4(^3P^+)s$	c^4P	55062	(53618)	(−1444)	(53398)	(−1664)
$d^4(^1S^-)s$	^2S				40898	
d^5	^2S				45685	
d^5	^2D				48663	
$d^4(^1F)s$	^2F				49081	
$d^4(^3P^+)s$	^2P				57446	
$d^4(^3F^+)s$	^2F				57710	
$d^4(^1G^+)s$	^2G				59585	
d^5	^2P				65948	
d^5+	^2D				70900	
$d^4(^1D^+)s$	^2D				74354	
$d^4(^1S^+)s$	^2S				91185	
$A(d^4s)$				35211		35192
$A(d^5)$				23579		23317
$B=F_2-5F_4$				720		710
$C=35F_4$				2778		2790
G_2				1459		1531
$H_2=R^2(dd,ds)/35$				—		150
Mean error				±1116		±1073
Mean deviation				±1011		±952

The mean error of ± 850 cm^{-1} on a configuration width of 22000 cm^{-1} constitutes an accuracy of four percent.

For a further comparison we show in Table II the differences between theoretical and experimental term values in V I and their parents in V II as taken from Many.[1] It is important to note that, for related terms, the differences in question are mostly of the same order of magnitude and have the same signs.

III. Cr II

The recent classification of this spectrum by Kiess appears to be still unpublished. Therefore, we had to compile the experimental term values from the classification of the Cr II spectrum as given by Moore.[5]

Since Moore did not assign the terms to specific configurations, the problem of assignments naturally arose. After several calculations best agreement was reached by ascribing all of the 29 terms given by Moore to d^5 and d^4s, d^3s^2 being apparently too high. d^5 and d^4s combined should theoretically contain 40 different terms. Our most powerful means for testing these assignments was the check-up on the Landé splittings, which, according to theory, should vanish for all d^5 terms and all doublets of d^4s which are based on singlets. In Table III we evaluated ζ_{3d} from the experimental splittings of each term assigned to d^4s.

It should be noted that the values of α shown against the last six terms in Table III, which are non-linear, are approximate only. As the average, resulting from this calculation, we obtained roughly $\zeta_{3d}=220$ cm^{-1}. Most of the poor agreements can be explained. With $(^3D)^4D$, it suffices to use instead of an average value of 18 cm^{-1} the least one, namely, 12.5 cm^{-1}, in order to reach agreement with the above-quoted value of ζ_{3d}. The unsatisfactory values in the cases of $(^3G)^2G$ and $(^3F^-)^2F$ can be explained qualitatively by spin interactions with neighboring terms.

On the other hand, we can make, starting from $\zeta_{3d}=220$ cm^{-1}, rough calculations for the presumably not weak spin interactions in the two cases of $d^5(^2D_{5/2}-{}^2F_{5/2})$ and $d^5(^2G_{9/2}-{}^2H_{9/2})$. The results obtained are 270 and 170 cm^{-1}, respectively, in pretty good agreement with the actual splittings found in these four d^5 terms; according to theory the latter, belonging to a half-filled shell, should show no splittings at all. The agreement is very bad in the case of c^4F, and it is interesting to note here that, taking the hypothetical case of c^4F as the lowest term of d^3s^2, we should receive the much better result, $\zeta_{3d}=240$ cm^{-1}.

Finally, the usual calculations have been carried out, first disregarding electrostatic interactions and, thereafter, taking them into account. In both cases c^4P has been neglected because of its uncertainty. The results are compiled in Table IV. The improvement, when allowing for electrostatic interactions, is but insignificant. The mean error of ± 1076 cm^{-1} on a configuration width of 53000 cm^{-1} constitutes an accuracy of two percent.

I am deeply grateful to Professor G. Racah for suggesting this problem and for his constant assistance throughout my work.

[5] C. E. Moore, *A Multiplet Table of Astrophysical Interest* (Princeton University Press, Princeton, New Jersey, 1945).

PHYSICAL REVIEW VOLUME 80, NUMBER 6 DECEMBER 15, 1950

The Electromechanical Behavior of $BaTiO_3$ Single-Domain Crystals*

M. E. CASPARI AND W. J. MERZ
Laboratory for Insulation Research, Massachusetts Institute of Technology, Cambridge, Massachusetts

(Received August 14, 1950)

The electromechanical response of $BaTiO_3$ single-domain crystals was investigated as a function of temperature from room temperature to above the Curie point. It was found that when we eliminate domain effects, either by using a perfect single-domain crystal or by aligning the domains by an external electric field, we are dealing with a true linear piezoeffect. The linear piezoeffect was measured by both a static and a dynamic method. The values of the d_{31} piezoelectric coefficient were compared with those calculated from the dielectric constant and the spontaneous polarization. The behavior of the piezoelectric resonance frequency was observed also through the same temperature range. Although the crystal is cubic above the Curie point and has a center of symmetry, the piezoelectric response persisted under the application of an external d.c. field because the external field will induce a tetragonal crystal structure through the electrostrictive effect, so that the crystal becomes piezoelectric again above the Curie point. Optical and dielectric measurements were found to verify these results.

I. INTRODUCTION

THE practical importance of $BaTiO_3$ as transducers makes it essential to know the electromechanical response of this substance. A number of measurements of the electromechanical coupling have been made on ceramics and also on multidomain crystals by Mason,[1] Jaffe,[2] and Rzhanov.[3] However,

* Sponsored by the ONR, the Army Signal Corps, and the USAF.

[1] W. P. Mason, Phys. Rev. 74, 1134 (1948).
[2] H. Jaffe, Ind. Eng. Chem. 42, 264 (1950), and a private communication.
[3] A. V. Rzhanov, J. Exp. Theor. Phys. U.S.S.R. 19, 502 (1949).

for a true understanding of $BaTiO_3$, the electromechanical behavior of single-domain crystals must be investigated in detail. Such experiments have been carried out from room temperature through the Curie region with static and dynamic methods. Since the interpretation of the electromechanical effects of $BaTiO_3$ crystals in the ferroelectric region is more complicated than for ordinary piezoelectric crystals, a brief discussion of the electromechanical coupling of ferroelectrics follows.

II. ELECTROMECHANICAL COUPLING OF FERROELECTRIC CRYSTALS

The relation between strain (x_h), stress (X_h), electric field (E_h), and electric polarization (P_h) for nonferroelectric, piezoelectric crystals is given by the following equations:

$$x_h(E, X)=\sum_{i=1}^{3} d_{ih}E_i+\sum_{i=1}^{3} g_{ih}E_i^2-\sum_{i=1}^{6} s_{ih}X_i+\cdots, \quad h=1\cdots 6, \quad (1)$$

$$P_h(E, X)=\sum_{i=1}^{3} \chi_{ih}E_i-\sum_{i=1}^{6} d_{hi}X_i+\cdots, \quad h=1, 2, 3. \quad (2)$$

Here, χ_{ih} are the components of the electric susceptibility, s_{ih} the elastic compliance coefficients, while d_{ih} and g_{ih} are known as the first- and second-order piezoelectric coefficients, respectively. The first term on the right-hand side of Eq. (1) represents the linear converse piezoeffect, while the second term represents the second-order effect, which is quadratic and is called the electrostrictive effect. In our experiments we are concerned with the converse effect without external stress, where the external field is applied in the z-direction (along the polar axis).

For a crystal of tetragonal symmetry such as $BaTiO_3$ in the ferroelectric region between 5° and the Curie temperature θ at 120°C, Eq. (1) reduces to

$$x_x=d_{31}E_{z,\text{ext.}}+g_{31}E^2_{z,\text{ext.}}, \quad (3)$$

$$z_z=d_{33}E_{z,\text{ext.}}+g_{33}E^2_{z,\text{ext.}}, \quad (4)$$

where x_x and z_z are the strain components along the x- and z-axes, respectively. These equations hold also for $BaTiO_3$ above the Curie point; however, in this cubic range the d_{ih} coefficients are zero, since the crystal structure has a center of symmetry. The ferroelectricity of barium titanate complicates the situation, as compared with other piezoelectric crystals, in two ways. In the first place, there is now a spontaneous polarization, the magnitude of which depends on the temperature and the applied external field; and thus the piezoelectric coefficients are dependent on these parameters. Secondly, a domain structure exists in these crystals, which changes with the applied field and thus causes additional changes in the strain components.

The effect of the spontaneous polarization can be taken into account in the following way: calling P_0 the spontaneous polarization which is directed along the z-axis of the crystal and $(z_z)_0$ and $(x_x)_0$ the spontaneous

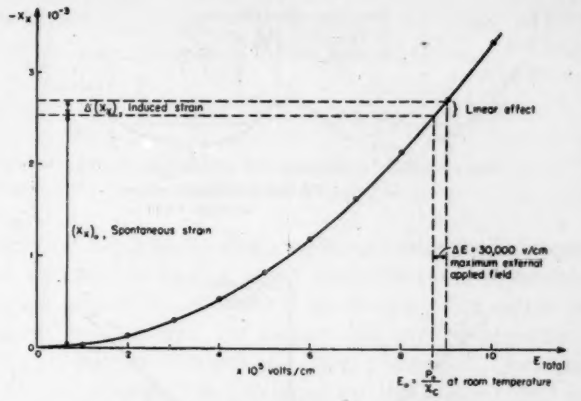

FIG. 1. Total strain as function of total field.

strain components along the z- and x-directions, respectively, taken relative to the dimensions of the crystal at the Curie point, it has been demonstrated[4] that the following relations hold:

$$(x_x)_0=\mu P_0^2, \quad (5)$$

$$(z_z)_0=\rho P_0^2, \quad (6)$$

where μ and ρ are constants. Here $(x_x)_0$ corresponds to a contraction and $(z_z)_0$ to an elongation. Using the values of $(x_x)_0$ and $(z_z)_0$ calculated from Megaw's x-ray measurements,[5] and our values[4] of P_0 as a function of temperature, we obtain the following values for μ and ρ:

$$\mu=-10.5\times 10^6 \text{ cm}^4/\text{coul}^2=-1.17\times 10^{-12} \text{ c.g.s.},$$
$$\rho=+24.0\times 10^6 \text{ cm}^4/\text{coul}^2=+2.67\times 10^{-12} \text{ c.g.s.}$$

When an external field is applied along the z-axis, resulting in an additional "external" polarization $P_{z,\text{ext.}}$, we obtain a further change $\Delta(x_x)$ and $\Delta(z_z)$ in the respective strain components. Then Eqs. (5) and (6) become

$$x_x=(x_x)_0+\Delta(x_x)=\mu(P_0+P_{z,\text{ext.}})^2, \quad (7)$$

$$z_z=(z_z)_0+\Delta(z_z)=\rho(P_0+P_{z,\text{ext.}})^2. \quad (8)$$

Expanding the first of these equations, we have

$$x_x=(x_x)_0+\Delta(x_x)=\mu P_0^2+(2\mu P_0)P_{\text{ext.}}+\mu P^2_{\text{ext.}}. \quad (9)$$

Thus

$$\Delta(x_x)=(2\mu P_0)P_{\text{ext.}}+\mu P^2_{\text{ext.}}. \quad (10)$$

For $P_{\text{ext.}}$ we can write $\chi_c E_{\text{ext.}}$, where χ_c is the susceptibility in the z-direction. Thus, the additional contractional strain component in the x-direction becomes

$$\Delta(x_x)=(2\mu\chi_c P_0)E_{z,\text{ext.}}+(\mu\chi_c^2)E^2_{z,\text{ext.}}. \quad (11)$$

Similarly, the additional z-component of the strain caused by the external field in the z-direction is

$$\Delta(z_z)=(2\rho\chi_c P_0)E_{z,\text{ext.}}+(\rho\chi_c^2)E^2_{z,\text{ext.}}. \quad (12)$$

[4] W. J. Merz, Phys. Rev. **76**, 1221 (1949).
[5] H. D. Megaw, Proc. Roy. Soc. A189, 261 (1947).

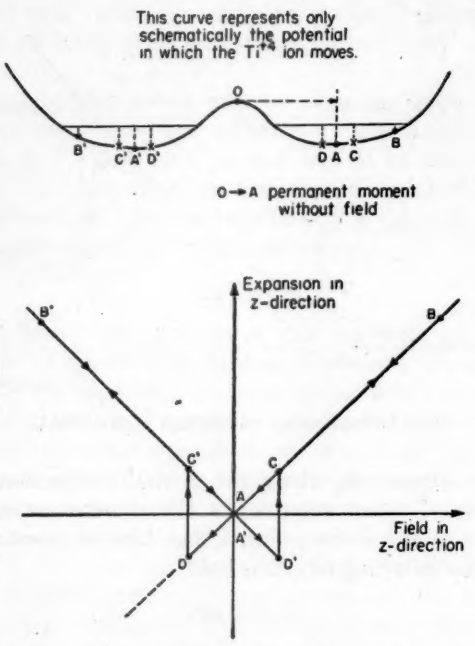

FIG. 2. Piezoelectric response of ideal $BaTiO_3$ "single-domain" crystal.

Comparison with Eqs. (3) and (4) shows that

$$d_{31}=2\mu\chi_e P_0, \quad d_{33}=2\rho\chi_e P_0;$$

while

$$g_{31}=\mu\chi_e^2, \qquad g_{33}=\rho\chi_e^2. \tag{13}$$

If we take for χ_e the initial electric susceptibility as measured earlier,[4] we can calculate the coefficients from Eqs. (13) at any temperature. At room temperature we have ($\chi_e=16$; $P_0=15.5\times10^{-6}$ coul/cm^2)

$$d_{31}=-173\times10^{-8}\text{ c.g.s.}, \quad d_{33}=+396\times10^{-8}\text{ c.g.s.},$$
$$g_{31}=-300\times10^{-12}\text{ c.g.s.}, \quad g_{33}=683\times10^{-12}\text{ c.g.s.}$$

Since, at the field strength which we have applied (max. 30,000 v/cm), the quadratic effect is much smaller than the linear, it can be neglected.

In the above argument we have tacitly assumed that the spontaneous polarization does not depend on the "external" polarization; that is, when the external field is applied, the spontaneous polarization remains constant as long as the temperature is kept constant. This is not strictly true, of course, since there is no inherent difference between the two types of polarization. The assumption is justified, however, since the internal field is very much larger than the externally applied field. The internal field is of the order of P_0/χ_e. Taking the values of the initial susceptibility for χ_e, we get for the internal field at room temperature 8.7×10^5 v/cm, which is about 30 times the largest applied field. Again, using Megaw's[5] value of the lattice constant *vs.* temperature, we find that a spontaneous polarization at room temperature of the value of 15.5×10^{-6} coul/cm^2 produces, according to Eq. (5), a spontaneous strain component in the x-direction of about -2.65×10^{-3}, while the strain component produced by an externally applied field of 20,000 v/cm is about -7×10^{-5}. It is thus justifiable to speak of a linear piezoeffect at any specified temperature, at least at temperatures not too near the Curie temperature, when an external field is applied (Fig. 1).

The effect of the domains on the electromechanical response is quite complicated. The alignment of the domains by an external field contributes towards the total strain effect. This, as we shall show later, is at least of the same order of magnitude as the true linear piezoeffect. Without an external field not all domains are parallel, and thus their polar axes do not point in the same direction throughout the crystal. When the domains are aligned and these axes turned into the same direction, the dimensions of the crystal will change, since the polar axis is about 1 percent longer than the other axes at room temperature. In order to minimize domain effects, we have worked consistently with single-domain crystals grown by the method first used by Matthias *et al.*[6] It is known that these crystals consist of closely spaced parallel and antiparallel domains[4,7] which can be aligned parallel by an external field.

In this truly aligned state the situation is as follows (Fig. 2): without an external field the Ti^{+4} ions rest in their equilibrium positions, A, somewhat off-center in the TiO_6 octahedra, thus forming permanent electric dipoles. An external field will vary the moments of these

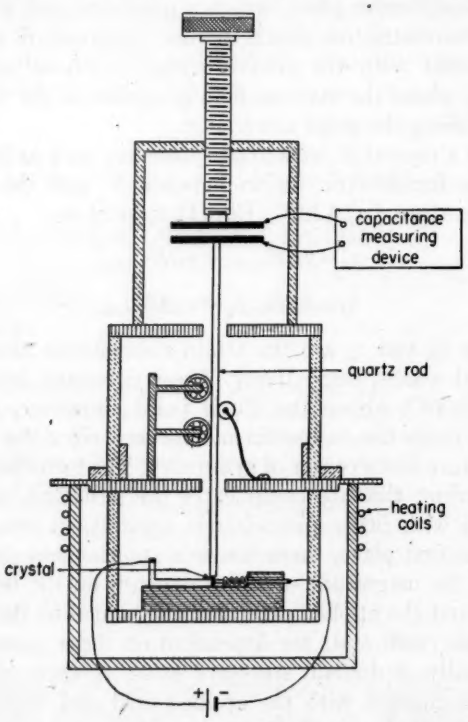

FIG. 3. Apparatus for static measurement of the electromechanical response of $BaTiO_3$ single-domain crystals.

[6] Danielson, Matthias, and Richardson, Phys. Rev. **74**, 986 (1948).
[7] W. J. Merz, Phys. Rev. **78**, 52 (1950).

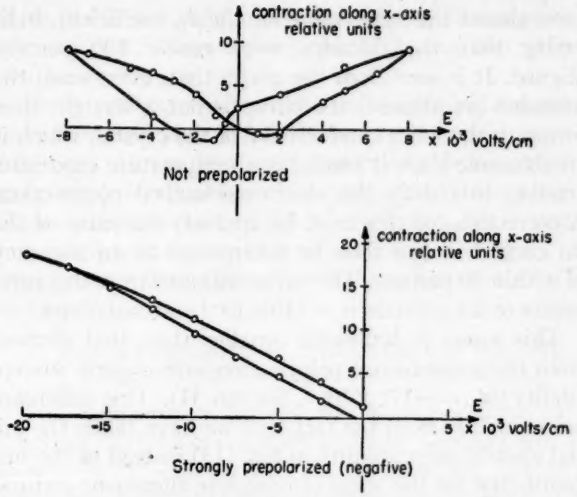

FIG. 4. Piezoelectric contraction of actual $BaTiO_3$ single-domain crystals.

dipoles by moving the Ti^{+4} ions to B and thus cause an elongation in the z-direction. As explained above, this effect is almost linear when the applied fields are much smaller than the internal field. In a normal piezoelectric material, when the field along the z-direction is reduced to zero and then increased in the opposite direction, the crystal will contract along the line B–C–D and beyond D. Since in our ferroelectric crystal the domain can be turned through an angle of 180°, the permanent dipole moments will at some point D reverse their directions and the Ti^{+4} ions will jump from D to C' on the other side of the octahedron center. This will cause a sudden expansion, as indicated in the graph, followed by a continuous expansion C' to B' as the reverse field is increased. Similarly, when the field is again reversed, another domain switch will take place at D' to C. If the Ti^{+4} ions jump from A to A', no change of length would be observed; but, since under the action of the field the jump carries the Ti^{+4} ions from D to C' or from D' to C, a sudden expansion in the z-direction and a sudden contraction in the x-direction results. In an actual crystal where parallel and antiparallel domains can exist, not a single abrupt change will take place, but small jumps distributed over a wide field-strength range. To eliminate domain effects, one has therefore to operate at high field strengths or have a truly single-domain crystal when measurements of the true piezoelectric effect are observed.

We may thus summarize the situation: besides the spontaneous strain caused by the spontaneous polarization (expressed in the tetragonality of the crystal),

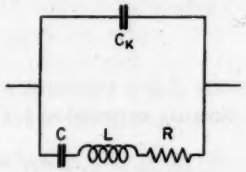

FIG. 5. Equivalent circuit of a piezoelectric crystal.

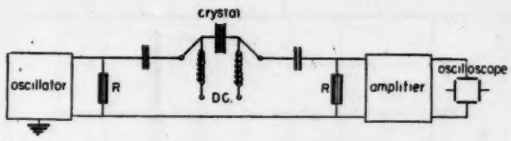

FIG. 6. Apparatus for measuring resonance and antiresonance frequencies.

which is a quadratic effect, we have, under the influence of an external field, a linear piezoeffect and a second-order piezoeffect, which is quadratic. The latter is much smaller than the former and can be neglected. We are allowed to speak of a linear piezoeffect, since the external polarization produced by the applied field is always much smaller than the spontaneous polarization. In addition, we have strains caused by domain changes, which can be very large, even in our so-called single-domain crystals.

III. STATIC MEASUREMENT OF THE d_{31} COEFFICIENT

The piezoelectric coefficient d_{31} of $BaTiO_3$ was measured statically by the converse piezoeffect. An electric field was applied in the z-direction; and the resulting contraction, and thus the strain component in the x-direction, was measured. Apart from the strain caused by the linear piezoeffect, there is a contribution to the strain from the domains. Thus, the total strain component in the x-direction at zero external stress is given by the equation,

$$\begin{aligned}\Delta(x_x)_{\text{total}} &= \Delta(x_x)_{\text{piezo}} + \Delta(x_x)_{\text{domain}}, \\ &= d_{31}E_{z,\text{ext.}} + \Delta(x_x)_{\text{domain}},\end{aligned} \tag{14}$$

from which d_{31} can be evaluated as soon as domain effects can be eliminated. The strain component $\Delta(x_x)$ was measured as a capacity change produced by the change in spacing of a parallel plate condenser (Fig. 3). The crystals used were single-domain crystal plates *ca.* 3 mm² in area and 0.2 mm thick, the polar axis (z-direction) of which was perpendicular to the plate. A very light quartz rod with a thin aluminum plate attached to its upper end rested on the crystal. When the crystal contracted, the capacity of the condenser formed by the two aluminum plates changed.

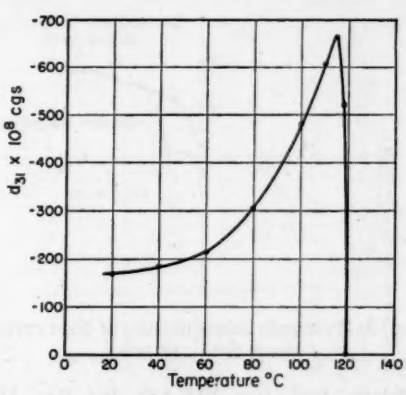

FIG. 7. d_{31} coefficient as a function of temperature (calculated).

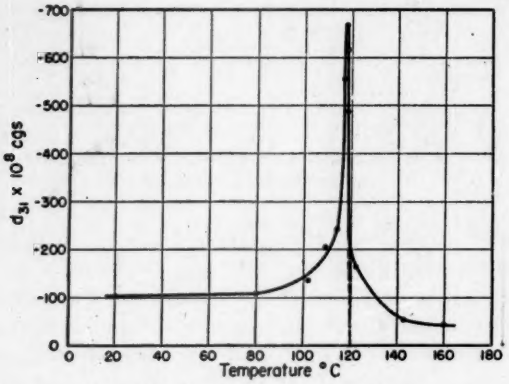

FIG. 8. d_{31} coefficient as a function of temperature by the static method.

This change was measured on a beat frequency apparatus.[8] This apparatus has an ultimate sensitivity of better than 0.001 $\mu\mu$fd and about the same accuracy. By converting this sensitivity to measurable changes of length it is found that over-all displacements up to 1×10^{-7} cm can be accurately measured by using condenser plates 1 in. diam. and a spacing of 0.1 mm.

Figure 4 shows graphs of field strength *vs.* actual contraction for two different crystals. The values given for the contraction are only relative; they are of the order of magnitude of 10^{-6} to 10^{-5} cm. The upper graph is the characteristic of a non-prepolarized crystal taken through a complete cycle at relatively low field strengths. We can here recognize the well-known butterfly hysteresis loop.[1,2] This can be explained on the basis of the arguments pertaining to Fig. 2 in Section II if it is borne in mind that our crystals consist of many parallel and antiparallel domains which can be turned at various field strengths. The lower graph shows the curve of a strongly prepolarized crystal (10,000 v/cm applied for 2 days); the curve is much smoother, and the loop is repeatedly reproducible. Although some hysteresis effects are still present at high field strengths, a reversible behavior is found when the field strength is taken up and down between 17 and 20 kv/cm. At these fields all effects of domains are minimized, and the magnitude of the d_{31} coefficient can be measured. All good crystals gave almost the same value for the d_{31} coefficient, indicating that the domains were nearly 100 percent aligned. It is seen from the graph that, even when the domains are aligned, the curve is not a straight line, owing to the finite conductivity of the crystal, which is troublesome since it produces a temperature expansion tending to nullify the electromechanical contraction. A correction for this must be applied; the value of the d_{31} coefficient can then be determined to an accuracy of within 10 percent. The value obtained from measurements of six crystals is -110×10^{-8} statcoul/dyne.

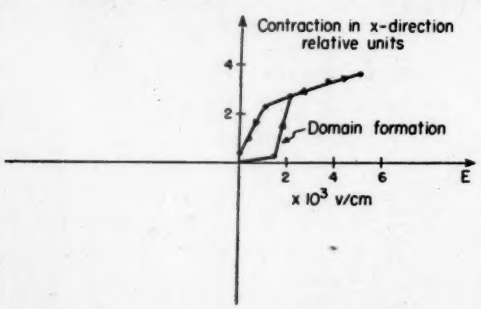

FIG. 9. Hysteresis characteristics of good crystal above the Curie point.

This value is somewhat smaller than that derived from the spontaneous polarization and electric susceptibility ($d_{31}=-173\times10^{-8}$, Section II). This difference arises mainly from the fact that we have taken the initial electric susceptibility in Eq. (13) instead of the susceptibility for the state of complete alignment (saturation). This value could not be obtained directly from the hysteresis loops with satisfactory accuracy. However, it is evident that the values of the initial susceptibility are larger than those of true saturation susceptibility, and hence the measured electromechanical coefficients must be smaller than the calculated ones.

IV. DYNAMIC METHOD

It is known that a vibrating piezoelectric crystal can be represented by the equivalent network of Fig. 5. From the resonance frequency, the antiresonance frequency, and the dielectric constant of the crystal, it is possible, by using this equivalent network, to calculate the piezoelectric coefficients.

In order to carry out this experiment, the conventional apparatus was used, which consists of a generator, an amplifier, and a cathode-ray oscilloscope (Fig. 6).

In terms of the elements of the equivalent network, the resonance frequency can be expressed by the formula,

$$\nu_R=1/2\pi(LC)^{\frac{1}{2}}, \tag{15}$$

and the antiresonance frequency by

$$\nu_A=(C+C_k)^{\frac{1}{2}}/2\pi(LCC_k)^{\frac{1}{2}}. \tag{16}$$

The capacitances, C and C_k, are related to the piezoelectric coefficients by the following equations:

$$C=\alpha d_{31}^2 a/sd, \tag{17}$$

$$C_k=\kappa' a/4\pi d, \tag{18}$$

where α is a constant, d_{31} is the piezoelectric coefficient, a the area, s the elastic compliance coefficient, d the thickness of the crystal plate, and κ' the dielectric constant in the z-direction.

Letting

$$\nu_R=\beta(1/s\rho)^{\frac{1}{2}}, \tag{19}$$

where β is a constant and ρ the density, we obtain the following expression for the d_{31} piezoelectric coefficient:

$$d_{31}^2=G\Delta\nu\cdot\kappa_e'/\nu_R^3. \tag{20}$$

[8] J. G. Jelatis, Tech. Rep. VII, Lab. Ins. Res., M.I.T., September, 1947.

Here, $\Delta\nu$ is the difference between the resonance and antiresonance frequencies, and G a constant which contains α, β, ρ, a, and d.

Unfortunately, the crystals used were small rectangular plates and the width of the crystal could not be neglected. Hence it was impossible to determine the exact mode of vibration of the crystal and the constant, G. An absolute value of the d_{31} coefficient could therefore not be determined by this method. However, the temperature dependence of the coefficient could be measured.

V. THE TEMPERATURE DEPENDENCE OF THE ELECTROMECHANICAL RESPONSE

The temperature dependence was measured as a function of temperature from room temperature to above the Curie point (120°C). By using Eq. (13) it is possible to calculate the d_{31} coefficient as a function of temperature from the measured P and χ_c characteristics. The result is shown in Fig. 7, where we have taken our values of P_0 for the spontaneous polarization and χ_c for the initial susceptibility from our data.[4] It can be seen that the d_{31} coefficient increases slowly at first and at higher temperatures more rapidly towards a sharp maximum a few degrees below the Curie point. It then drops suddenly to zero at the Curie point since the crystal is not piezoelectric above this temperature. The maximum value obtained lies between -600 and -700×10^{-8} statcoul/dyne.

A direct measurement by the static method (Fig. 8) shows a very similar behavior. This experimental characteristic was obtained at field strengths between 5000 and 6000 v/cm. It is important to use such high fields, since near the Curie point even good single-domain crystals tend to break up into many domains if the external field does not keep them aligned.

The maximum values in Figs. 7 and 8 agree well. This closer agreement near the Curie point is to be expected because in this region the value of the electric susceptibility does not change much with field strength. However, the experimental value does not go to zero at the Curie point. There is a definite piezoelectric response above the Curie point which decreases only slowly as the temperature increases. At 160°C the value is still about half that at room temperature.

The electromechanical response of the crystal above the Curie point is indicated in detail in Fig. 9. As the field strength is raised, the response is at first small; but at some critical field strength a sudden contraction takes place. At higher field strengths the characteristic flattens out again. The better the crystal, the higher the critical field strength and the smaller this contraction.

The dynamic method leads to the following results: the piezoelectric resonance frequency, ν_R, stays constant for a considerable range of temperature and drops to a sharp minimum a few degrees below the Curie point, as already seen by earlier observers.[9] At the same temperature the difference $\Delta\nu$ between resonance frequency ν_R and antiresonance frequency ν_A reaches a maximum (Fig. 10). The better the crystal, the nearer the extrema approach the Curie temperature as determined by the maximum of the dielectric constant. The crystals also show a slight piezoelectric response above the Curie point. However, when very good crystals are used with a minimum of internal strains and absolutely free of domains perpendicular to the thickness of the crystal plate, the behavior becomes different. The resonance frequency again drops sharply near the Curie point, but shows no minimum. It does not rise again, and there is no piezoelectric response above the Curie point (Fig. 11).

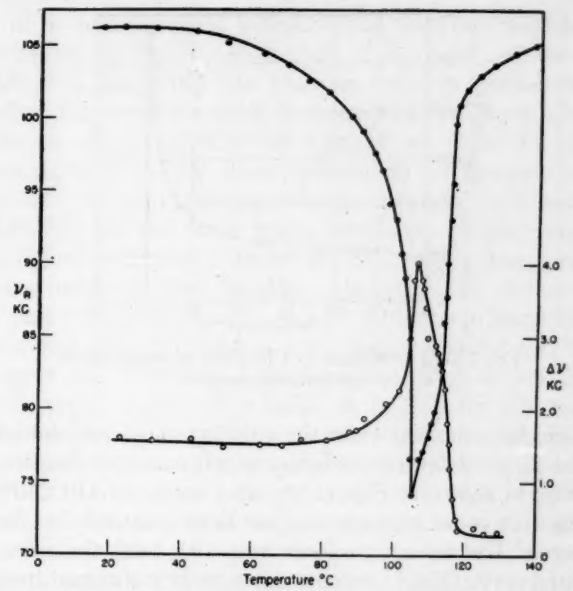

FIG. 10. Resonance frequency ν_R and $\Delta\nu=\nu_A-\nu_R$ *vs.* temperature.

From the results for ν_R and $\Delta\nu$ and the values of the

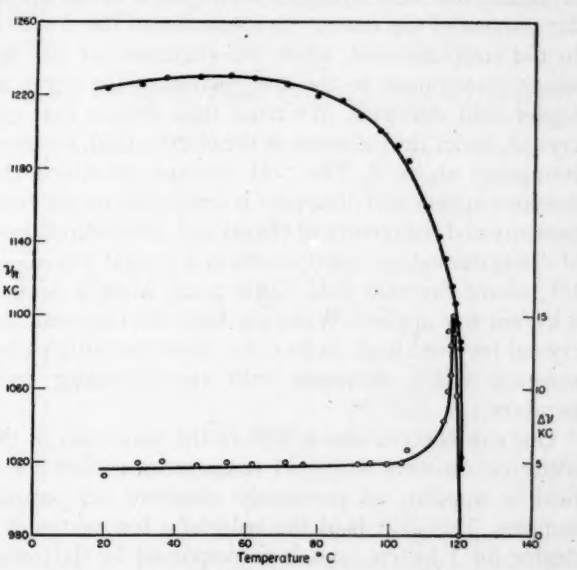

FIG. 11. Resonance frequency ν_R and $\Delta\nu=\nu_A-\nu_R$ *vs.* temperature.

[9] Blattner, Känzig, and Merz, Helv. Phys. Acta 22, 35 (1949).

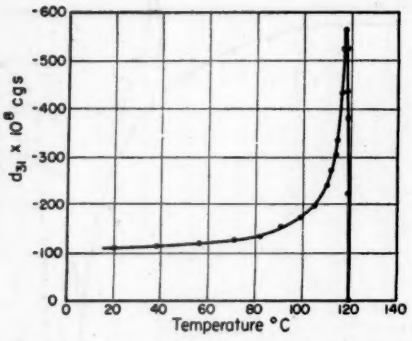

FIG. 12. d_{31} coefficient as a function of temperature by the dynamic method.

dielectric constant κ' for the good crystals,[4] one obtains the d_{31} piezoelectric coefficient as a function of temperature, as shown in Fig. 12. A value for d_{31} of 110×10^{-8} c.g.s. at room temperature has been assumed for this curve. The behavior agrees well with both the calculated curve (Fig. 7) and the characteristic obtained from static measurements (Fig. 8). However, there is no piezoelectric response above the Curie point, in contrast to the static method.

VI. OPTICAL AND DIELECTRIC OBSERVATIONS

Optical observations have shown that at and immediately above the Curie temperature the cubic $BaTiO_3$ crystals become birefringent when an external d.c. field is applied. We observed that when the field strength is increased, the crystal lighted up and at somewhat higher field strengths domain patterns could be observed that are similar to those below the Curie point. At even higher field strengths the domain pattern again disappeared because of the alignment of the domains, but the crystal remained birefringent. This is in agreement with the hysteresis curve obtained by the static method above θ (Fig. 9). The lighting up of the crystal at low field strengths corresponds to the initial flat portion of the curve, the formation of the domains to the steep increase, while the alignment of the domains corresponds to the flat portion of the curve at higher field strengths. We must thus deduce that the crystal, under the influence of the electric field, becomes tetragonal above θ. The field strength at which the domains appear and disappear is dependent on the temperature and the quality of the crystal. The temperature of disappearance of the domains in a crystal was about 1°C above the zero field Curie point when a field of 1 kv/cm was applied. When the field was removed, the crystal reverted back to its cubic structure with a time constant which decreases with the increasing temperature.

One can observe also a shift of the maximum of the dielectric constant to higher temperatures when a d.c. field is applied, as previously observed on ceramic samples. This shift is of the order of a few tenths of a degree for 1 kv/cm, and is accompanied by flattening out of the peak of the characteristic.

VII. DISCUSSION

The drop in the resonance frequency with increasing temperature can be explained in the following way: it is known that, apart from the geometry of the crystal, the resonance frequency depends on the elastic constants (s_{ih}) such that $\nu_R \sim s^{-\frac{1}{2}}$. However, it is necessary to distinguish between the compliance coefficients of a shorted and of an insulated crystal. The former, s_{ih}^E, corresponds to the condition of constant field, while in the latter s_{ih}^P corresponds to that of constant polarization. The relation between the various coefficients in the two cases is[10]

$$s_{ih}^E = s_{ih}^P + (4\pi d_{ni} d_{nh}/\kappa_n'), \tag{21}$$

with κ_n' the dielectric constant. For $BaTiO_3$ we have

$$\begin{aligned} s_{11}^E &= s_{11}^P + (4\pi d_{31}^2/\kappa_c'), \\ s_{12}^E &= s_{12}^P + (4\pi d_{31}^2/\kappa_c'), \end{aligned} \tag{22}$$

since $d_{31}=d_{32}$. By replacing one of the d_{31} coefficients according to Eq. (13),

$$\begin{aligned} s_{11}^E &= s_{11}^P + 2\mu P_0 d_{31}, \\ s_{12}^E &= s_{12}^P + 2\mu P_0 d_{31}. \end{aligned} \tag{23}$$

The elastic coefficient, s_{ih}^P, of the insulated crystal changes only slightly and almost linearly with temperature. Thus, when $d_{31}P_0$ has a maximum value, s_{ih}^E will have a maximum, and hence the resonance frequency of the plated crystals will drop to a minimum. Since P_0 decreases much more slowly than d_{31} increases with temperature very near the Curie point, the maximum of d_{31} and of $\Delta\nu$ occurs at nearly the same temperature as the minimum of the resonance frequency.

Optical observations showed that most of the crystals split up into many domains immediately below the Curie temperature. It could be verified that the maximum in the d_{31} coefficient, and thus also the minimum in the resonance frequency, occurs exactly at this temperature where the single-domain state of the crystal breaks up into multiple domains. Crystals with much internal strain show this domain change at a lower temperature than do good crystals, since the formation of these domains is the result of residual strain effects. In most of the crystals used, some domains were present even at room temperature, which is substantiated by the fact that such poor crystals have a dielectric constant along the thickness (z-direction) of the order of 1200, while in a very good crystal this value is 200 to 300 at room temperature. An ideal crystal completely free of strains changes suddenly at the Curie temperature from the tetragonal to the cubic crystal structure, and then there is no more piezoeffect. In poor crystals we can expect that owing internal strains the various domains of the crystal become cubic at different temperatures, so that the transitions take place over a wide temperature range. It seems likely that the cubic re-

[10] W. G. Cady, *Piezoelectricity* (McGraw-Hill Book Company, New York, 1946), p. 271.

gions of the crystal are harder and have smaller compliance coefficients. In this case the resonance frequency of the plated crystal should increase again above the minimum, as was observed. Since in this case there is no really sharply defined Curie temperature, and the Curie temperature which we have indicated is determined from the maximum of the dielectric constant (which measures an average behavior over all domains), it is to be expected that even above this temperature a slight piezoelectric response can be obtained. Thus, the peculiar behavior obtained from most of our crystals (Fig. 10), in contrast to that of a very good crystal (Fig. 11), may be explained by domain effects.

That a piezoelectric response is obtained by the static method even for the very best crystals is caused by the tetragonality induced by the external field. This must be explained by the fact that even in the best crystal some Ti^{+4} ions are shifted to an eccentric position by the external field through the electrostrictive effect, which thus induces a piezoelectric effect, at least in parts of the crystal. As the temperature is increased, this effect is greatly reduced; but, up to about 180°C in fields of 6 kv/cm, it was never found to disappear completely.

It is now possible to compare our results with those of Mason[1] and Jaffe.[2] Both obtained the butterfly hysteresis characteristics similar to our Fig. 4. They interpreted their results as a quadratic effect which they call electrostrictive. This quadratic effect is caused by the domain changes and is not electrostrictive in the usual sense. As soon as the domain effect is suppressed by prepolarization with an external field, the behavior becomes linear, as can be seen for single-domain crytals in Fig. 4, and for multi-domain crystals and ceramics[2] when all the domains are aligned. Thus, we can speak of a true linear piezoeffect. Our absolute values are smaller than those obtained by Mason and Jaffe, presumably because we have been able to eliminate domain effects to a large extent. They are in rather close agreement, however, with the values obtained by Rzhanov[3] on ceramics.

It is interesting to compare the electromechanical behavior of $BaTiO_3$ with that of Rochelle salt and KH_2PO_4. The latter two show no butterfly characteristics, but have the usual hysteresis loops. There, the domain effects (Barkhausen jumps) are much larger compared with the linear piezoeffect[11,12] (saturation branch of the hysteresis loop). Rochelle salt and KH_2PO_4, on the other hand, have only parallel and antiparallel domains, unlike $BaTiO_3$, which may also have perpendicular domains. However, the domain jumps from antiparallel to parallel positions in Rochelle salt and KH_2PO_4 cause a shear strain of about half a degree and, therefore, a considerable change in length will result. On the other hand, in $BaTiO_3$ the domain change from antiparallel to parallel will give no change in length without an external field (Section II); and perpendicular domains are not present in our single-domain crystals. In ceramics only a relatively small percentage (about 10 percent according to Mason[1]) of the domains switch into the parallel position.

The shape of the curve of the temperature dependence of the d_{31} piezoelectric coefficient obtained by Rzhanov[3] on ceramics is very similar to ours. His values have been obtained by static measurements of the direct piezoeffect, and thus no response above the Curie temperature could be observed.

We have confined our measurements to those on the d_{31} coefficient. The temperature dependence of the d_{33} coefficient should be, according to Eq. (13), identical to that of the d_{31} coefficient, while its absolute value should be about 2.3 times as large as the d_{31}. This value is in agreement with the measurements of Jaffe.[2]

The authors are grateful to Professor A. von Hippel for many helpful discussions during the course of this work. They would also like to acknowledge the valuable help of J. G. Jelatis in the construction of the static apparatus, and of S. R. Arnold for his optical measurements.

[11] H. Hinz, reference 10, p. 541.
[12] A. von Arx and W. Bantle, Helv. Phys. Acta 17, 298 (1944).

Studies of the Propagation Velocity of a Ferromagnetic Domain Boundary*

H. J. Williams, W. Shockley, and C. Kittel
Bell Telephone Laboratories, Murray Hill, New Jersey

(Received August 4, 1950)

Experimental results are given on the velocity of propagation of a single domain boundary in a crystal of silicon iron with a simple domain structure. In weak applied magnetic fields (~0.003 oersted) the velocity is given by a relation of the form $v=G(H-H_0)$, where G is a constant ~4 cm/sec./oersted in this crystal, and $H_0\cong 0.003$ oersted is the *starting field*. Calculation of the eddy current losses accompanying the motion of a plane boundary gives a theoretical expression for G in good agreement with experimental values; the predicted linear dependence on the resistivity was approximately verified by measurements at 78°, 194°, and 293°K. In stronger fields (>5 oersteds) there is evidence that the wall closes on itself, and the experimental velocity of collapse of the wall as deduced from flux changes agrees with the theoretical result based on a model of eddy current losses accompanying a collapsing cylindrical boundary. The results have a bearing on the well-known *eddy current anomaly*, namely, the fact that the total loss in a ferromagnetic material undergoing a.c. magnetization is often two or three times larger than the eddy-current and hysteresis losses calculated in the usual way assuming a spatially uniform and isotropic classical permeability.

I. INTRODUCTION

THIS paper discusses the results and interpretation of measurements of the propagation velocity of a ferromagnetic domain boundary in the single crystal of silicon iron with a simple domain structure employed previously by Williams and Shockley.[1] The experiment is similar in principle to the Sixtus-Tonks experiment,[2] with the important difference that in the present experiment the eddy current configuration is amenable to exact mathematical calculation, thereby enabling a quantitative comparison with observation. Experiments and analysis similar to those described in III and V below have been carried out by K. H. Stewart[2a] and were reported at the Grenoble Conference on Ferromagnetism and Antiferromagnetism as were the principal results of this article. However, it appears from Stewart's hysteresis loops unlikely that his specimen had as simple a domain structure as that encountered in our experiments.

II. DESCRIPTION OF SPECIMEN

The specimen was cut from a single crystal of 4 weight percent silicon iron so as to form a hollow rectangle (Fig. 1) having all surfaces parallel to [100] planes. The outside dimensions of the rectangle are 1.34×1.71 cm and the cross section of a leg is 0.114 ×0.152 cm.

Figure 1 shows the domain structure of the crystal. The broken lines represent domain boundaries or Bloch walls. There is a boundary at each corner and one extending completely along the length of the specimen, forming a total of eight domains. If the four inner domains carry flux around the crystal in a clockwise manner the four outer domains carry flux in a counterclockwise manner. The net flux depends on the position of the boundary which can be moved by an applied field. The field is obtained by winding a number of turns of wire around the specimen and then passing a current through the wire. The change in flux is measured by a secondary winding connected to a fluxmeter.

III. LOW FIELD MEASUREMENTS

With this specimen there is a direct correlation between the position of the boundary and the net magnetization in the specimen, so that the velocity of the boundary movement for low fields can be measured by timing the deflections on a Cioffi recording fluxmeter with a stop watch. When the magnetization changes from saturation in one direction to saturation in the other direction the boundary moves the width of a leg in the hollow rectangle. At low fields the boundary is thought to be plane, as shown in Fig. 2a, the surface tension of the boundary overcoming the tendency of the eddy current drag to make it curve. The effective driving field was taken to be the difference between the applied field and the minimum value of the field which would make the boundary move. First a hysteresis loop was traced using the smallest value of the field that would move the boundary. This value of the field was not constant but varied somewhat as the boundary moved across the crystal perhaps due to different imperfections that the boundary encountered in various places. Then another loop was traced keeping the excess field constant by manipulating the current control in the magnetizing circuit. This was done by observing the loop as it was being traced and keeping the recording pen a constant distance away from the side of the previous loop. A series of such loops was traced with constantly increasing field and the times for the deflections measured. Then the velocity was plotted as a function of the field. The maximum excess field was 0.003 oersted. A linear relation was obtained; the slope of the line gave the velocity per oersted. Sets of measurements were made at 78°, 194°, and 293°K.

* A preliminary report was presented at the New York Meeting, Phys. Rev. 78, 341 (1950).

[1] H. J. Williams and W. Shockley, Phys. Rev. 75, 178 (1949).

[2] K. J. Sixtus and L. Tonks, Phys. Rev. 37, 930 (1931); 39, 357 (1932); 42, 419 (1932); 43, 70, 931 (1933).

[2a] K. H. Stewart, Proc. Phys. Soc. 63A, 761 (1950).

These results are compared with the theoretical values in Fig. 3.

The criterion for low fields is that the effect of surface tension for appreciable curvature of the wall be large compared to the driving field. A surface tension γ of 2 ergs/cm^2 and a field H of 0.003 oersted correspond to a radius of $r=\gamma/2IH=2/2\times1500\times0.003=0.22$ cm or more than twice the edge of the rectangle cross section. For such a condition, no matter what forces tended to hold the wall back, the applied field could not deform it appreciably from a plane. On the other hand, for the high field conditions described below, the H values are 1000 times larger and consequently surface tension forces are negligible for the curvatures that are expected to occur, such as those in Fig. 2(b), for example.

IV. HIGH FIELD MEASUREMENTS

Some preliminary work was done in which a condenser was discharged through the primary winding and the deflections observed on a galvanometer scale to determine the extent of the boundary movement. During these tests it was observed that if a reversing field was applied to the specimen in an initially saturated condition the net change in flux increased uniformly with condenser voltage up to about the point at which half the flux was reversed. For larger discharges it was observed that the ballistic kick was followed by a slow motion which proceeded with gradually increasing velocity until the specimen became spontaneously magnetized to saturation in the reverse direction. This was interpreted as meaning that under high fields the eddy currents tend to retard the motion of the boundary more in the middle of the crystal than near the surface so that the boundary curves and finally forms a cylinder which collapses due to its surface tension as is shown in Fig. 2b. This idea was checked by making a series of measurements at comparatively high fields.

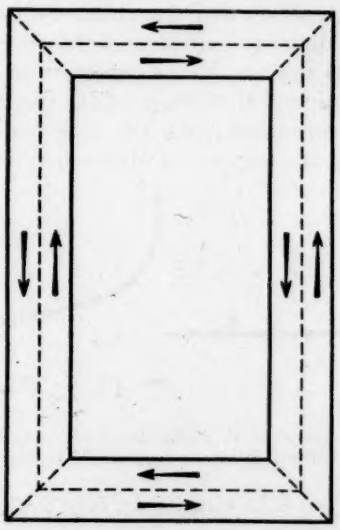

FIG. 1. Simple domain structure in Si-Fe single crystal in form of hollow rectangle.

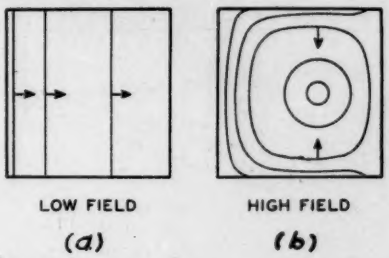

FIG. 2. Boundary motion in low and high fields.

For high field measurements secondary voltage pulses were photographed on a type 304H Dumont cathode-ray oscillograph using a 5C PA tube. A variable delay circuit was used so that the field was applied after the sweep had been triggered. The secondary voltage pulses were photographed with a Leica camera having an f/3.5 lens and using a super xx panchromatic film. Figure 4 shows a typical voltage pulse.

Voltage pulses were obtained for fields ranging from 5 to 80 oersteds. For each pulse values of V/H were plotted as a function of the corresponding values of $T\times H$ as shown in Fig. 5, which also shows the theoretical curve for a collapsing cylindrical boundary. The experimental results are in good agreement with theory.

We go on to derive the theoretical expressions for the low and high field situation.

V. EXACT SOLUTION OF EDDY CURRENT LOSSES FOR PLANE WALL IN RECTANGULAR BAR

This calculation is intended to apply at low fields. The width of the bar in the x-direction is $2L$, and in the y-direction is d. The origin of coordinates is at the center of the cross section, and the wall is in the plane $x=0$. We neglect H in comparison with B_s, as is readily justified. We employ Gaussian units.

We require solutions of the following equations for the current density $\mathbf{i}$:

$$\nabla^2\mathbf{i}=0; \tag{1}$$

$$\text{curl}\,\mathbf{i}=0; \tag{2}$$

$$\text{div}\,\mathbf{i}=0; \tag{3}$$

except within the wall, where

$$\text{curl}\,\mathbf{i}=-(1/\tau c)(d\mathbf{B}/dt), \tag{2a}$$

τ being the electrical resistivity. The boundary conditions are

$$\mathbf{i}_n=0 \tag{4}$$

on all outer surfaces, and at the wall position

$$\pm i_y=B_s v/\tau c, \tag{5}$$

where v is the wall velocity. We suppose that the wall is moving sufficiently uniformly so that dissipation of energy by purely local eddy currents caused by structural irregularities may be neglected. This appears to

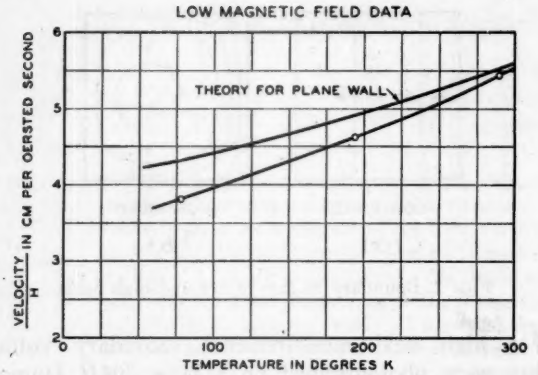

FIG. 3. Comparison of experimental and theoretical values of the wall velocity in low fields. The theoretical calculation, based on eddy current losses for a plane wall in uniform motion, does not contain any disposable constants. The deviations between the two curves are within the estimated accuracy of the measurements.

be a valid supposition in our experiments, but in the case of cold worked materials the local losses may be appreciable, and we have in these circumstances a probable explanation of the effects of cold-working reported by Dijkstra and Snoek[3] in their work on the Sixtus-Tonks experiment.

The solution may be verified to be of the form:

$$i_z = -\sum_{\substack{\text{odd}\\ n}} D_n \sin(n\pi y/d)\sinh[(L-x)n\pi/d]; \quad (6)$$

$$i_y = \sum_{\substack{\text{odd}\\ n}} D_n \cos(n\pi y/d)\cosh[(L-x)n\pi/d], \quad (7)$$

where

$$D_n = \pm 4(B_s v/\tau c)/[n\pi \cosh(Ln\pi/d)], \quad (8)$$

the plus sign obtaining for $n=1, 5, 9, \cdots$, and the minus sign for $n=3, 7, 11, \cdots$.

We denote by P the power loss per unit length in the z-direction, and find

$$P = 4\tau \int_0^L \int_0^{d/2} (i_z^2 + i_y^2)\,dx\,dy, \quad (9)$$

which comes out after carrying out the indicated integrations, to be

$$P = (16d^2 B_s^2 v^2/\pi^3 \tau c^2) \sum_{\substack{\text{odd}\\ n}} n^{-3} \tanh(n\pi L/d). \quad (10)$$

The series is rapidly converging, and for a square rod $d=2L$ is equal to 0.97, while for the actual dimensions of the crystal employed the sum is 1.00.

If we set the eddy current losses equal to the rate $2HI_s vd$ at which work is done by the applied field on the specimen, per unit length, we find, taking the sum as equal to unity, the result

$$v = (\pi^2 \tau c^2/32 B_s d)H, \quad (11)$$

which is in excellent (±20 percent or less) agreement with the experimental results shown in Fig. 3. The observed velocities are slightly lower, and this is in the expected direction as we have not considered purely relaxation effects on the wall motion. In the experiments $v/H \approx 4$ cm/sec./oersted.

Landau and Lifshitz[4] in their classic paper on domains show that relaxation effects alone will give the following relation:

$$v = (\gamma^2 I_s \Delta/\Lambda)H, \quad (12)$$

where Λ is the relaxation frequency, γ is the magnetomechanical ratio and $\Delta = (A/K)^{\frac{1}{2}}$ is the usual wall thickness parameter; in Si-Fe we have $\Delta \approx 3\times 10^{-6}$ cm; $\gamma \approx 2\times 10^7$ radians/sec./oersted; $I_s \approx 1600$; $\Lambda \approx 3\times 10^9$ sec.$^{-1}$ as estimated from microwave resonance results; so that $v/H = 600$ cm/sec./oersted. This is much higher than the actual velocity, which is apparently limited almost entirely by eddy currents. But in very thin sheets or in high resistivity material (such as ferrites) we may expect to find that relaxation processes[5] are important in determining wall velocities. Further, in the case of experiments of the Sixtus-Tonks type the wall makes a small glancing angle with the propagation direction, so that the effective value for Δ to be used in Eq. (12) may be greater by a factor of the order of 100 than the normal wall thickness. This is the explanation which we offer to account for the high values (~50000 cm/sec./oersted) for v/H reported, for example, by Dijkstra and Snoek[3] in a Sixtus-Tonks experiment.

VI. STUDY OF COLLAPSING CYLINDRICAL DOMAIN WALL IN CYLINDRICAL SPECIMEN

This calculation is intended to apply at high fields; we approximate the rectangular cross section of a crystal leg by a circle of equal area. We consider a long cylinder of magnetic material of radius R, and suppose that within and concentric with this there is a tube-like domain boundary of radius ρ separating two domains running in the direction of the cylinder axis, but antiparallel to each other. We suppose that the wall is collapsing under the action of an external field H alone, and neglect the surface tension of the wall,

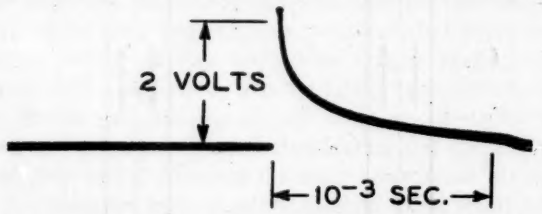

FIG. 4. Photograph of voltage pulse resulting from collapse of Bloch wall in strong fields (~10 oersteds).

[3] L. J. Dijkstra and J. L. Snoek, Philips Res. Rep. 4, 334 (1949).

[4] L. Landau and E. Lifshitz, Physik. Zeits. Sowjetunion 8, 153–169 (1935).

[5] C. Kittel, Proceedings of Grenoble Conference, 1950 (to be published); Phys. Rev. 79, 214 (1950).

which is quite legitimate. We study the voltage induced in an external winding which is concentric with the cylinder.

The flux associated with the collapsing wall induces at radius r a field E_θ:

$$2\pi r E_\theta = -\frac{1}{c}\frac{d\varphi}{dt} = -\frac{1}{c}8\pi M_s \cdot \frac{d}{dt}\pi\rho^2 = -\frac{16\pi^2}{c}M_s\rho v_r, \quad (13)$$

where $v_r = d\rho/dt$ is the radial velocity of the wall. We have

$$E_\theta = -(8\pi/c)M_s v_r \rho/r. \quad (14)$$

Dropping the minus sign, the eddy current density is

$$j_\theta = 8\pi M_s v_r \rho/\tau c r, \quad (15)$$

where τ is the electrical resistivity. The total current per unit length of cylinder is

$$i_\theta = \int_\rho^R j_\theta dr = (8\pi/\tau c)M_s v_r \rho \ln(R/\rho). \quad (16)$$

We have again neglected secondary eddy current effects, as is quite justified in our velocity range.

The longitudinal field inside the wall is

$$H = 4\pi i_\theta/c,$$
$$H = (32\pi^2/\tau c^2)M_s v_r \rho \ln(R/\rho). \quad (17)$$

The velocity of the wall is determined by the energy balance $A = B$,

where

A = energy dissipation by eddy currents,
B = energy release by magnetization change.

$$A = \int_\rho^R jE 2\pi r dr = \int_\rho^R (64\pi^2/\tau c^2)M_s^2 v_r^2 \rho^2 \cdot 2\pi dr/r$$
$$= (128\pi^3/\tau c^2)M_s^2 v_r^2 \rho^2 \ln(R/\rho); \quad (18)$$
$$B = 4\pi H M_s \rho v_r. \quad (19)$$

Equation (19) gives for the velocity

$$v_r = H\tau c^2/[32\pi^2 M_s \rho \ln(R/\rho)] \quad (20)$$

and, for the voltage,

$$V = H\tau c N/2 \ln(R/\rho), \quad (21)$$

where N is the number of turns on the secondary winding. The comparison with experiment is shown in Fig. 5.

VII. THE EDDY CURRENT ANOMALY

The calculation of eddy current losses in ferromagnetic materials is a standard engineering calculation in connection with transformer cores and rotating electrical machinery. It is well known that the calculation does not give correct results in ferromagnetic materials, even when hysteresis effects are considered: the observed losses are always greater than the calculated

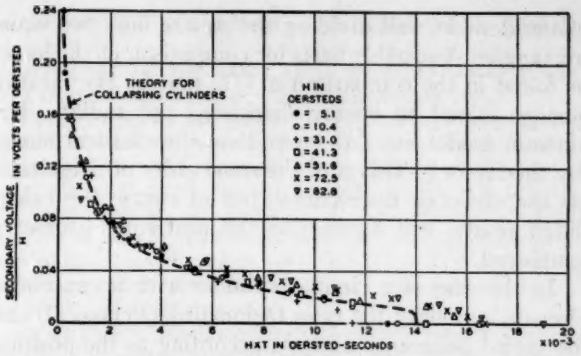

FIG. 5. Comparison of experimental and theoretical values of the voltage pulse arising from the wall collapse at high fields. The theoretical calculation is based on eddy current losses for a circular cylinder and does not contain any disposable constants.

losses, often by a factor of two or three. The discrepancy is known as the eddy current anomaly.[6]

At the basis of the standard calculation lies the assumption that the permeability is homogeneous and isotropic; that is, it is assumed that every element of volume of the specimen is characterized by a scalar permeability μ_0. Actually we know that the important magnetization changes in ferromagnetic materials are associated with domain rotation and domain boundary displacement. We are concerned in this paper only with domain boundary displacement. Here the effective local permeability is very inhomogeneous. In the case of a field applied parallel to a 180 degree boundary the local permeability is unity away from the boundary, but assumes extremely high values within the boundary. It is obvious that the values inside the boundary must be very high if the average of the permeability over the entire volume is to account for the high average permeabilities observed in transformer materials.

It is reasonable to expect that such an inhomogeneous distribution of permeability will lead in general to higher eddy current losses than one would calculate on the basis of an equivalent uniform average permeability. A given flux change will cause a definite e.m.f. $\int E \cdot dl$ around a fixed path, independent of the origin of the flux change. But the power dissipation is proportional to E^2, and the average value of E^2 will be higher for an inhomogeneous distribution of flux change than for a uniform distribution, even though the total flux change may be equal in both cases. Therefore, we expect on this qualitative reasoning to find that the uniform permeability assumption leads to calculated losses lower than observed losses.

We give below exact calculations for the comparison of losses on the classical and domain models for the case of a square rod in an a.c. field parallel to the axis of the rod. For the domain structure we assume a single

[6] F. Brailsford, J. Inst. Elec. Eng. 95, II, 38 (1948); O. I. Butler and C. Y. Mang, J. Inst. Elec. Eng. 95, II, 25 (1948); R. Feldtkeller, Frequenz 3, 229 (1949); V. E. Legg, Bell Sys. Tech. J. 15, 39 (1936); L. W. McKeehan and R. M. Bozorth, Phys. Rev. 46, 527 (1934).]

plane domain wall dividing the square into two equal rectangles. A suitable basis for comparison of the losses is found in the comparison of Q's, that is, the ratio of energy stored to energy dissipated per radian. The domain model has a Q lower than the classical model by the factor $\frac{1}{3}$. This is of the same order of magnitude as the observed discrepancy, but of course the calculated results will depend on the particular geometry employed.

In the case of a circular cylinder with a concentric domain boundary the ratio Q(domain)/Q(classical) can be varied between 0 and ∞, according to the position of the domain boundary. This situation is rather special, however, and in general one would expect the domain Q to be lower, on the basis of the qualitative argument given above relating to the average values of E^2 and E.

There are theoretical grounds for believing that the eddy current anomaly may be larger in thin sheets of material than in thicker sheets, if we suppose the number of domain boundaries to be constant. The thinner the sheet, the more concentrated are the lines of E about each domain boundary, thus leading to a high average value of E^2 and high eddy current loss.

VIII. CLASSICAL THEORY OF EDDY CURRENT LOSSES IN SQUARE ROD

We consider the eddy current losses in a square rod of side a, permeability μ, and conductivity σ. The rod is situated in a uniform field of amplitude H_0 parallel to the axis and varying with angular frequency ω. We treat first the low frequency limit at which the skin depth δ is $\gg a$. The field then penetrates the rod without significant change in amplitude, so that we have

$$(\text{curl } \mathbf{E})_z = -j\omega\mu H_0/c, \tag{22}$$

or

$$(\text{curl } \mathbf{i})_z = -j\omega\mu\sigma H_0/c. \tag{23}$$

This equation is satisfied by

$$i_x = Fy; \quad i_y = -Fx, \tag{24}$$

if

$$F = j\omega\mu\sigma H_0/2c. \tag{25}$$

The time-average power loss per unit length of rod is

$$P = \frac{1}{2\sigma}\int\int (i_x^2 + i_y^2)\,dx\,dy$$

$$= 4(F^2/2\sigma)\int_0^{a/2}\int_0^{a/2} (x^2+y^2)\,dx\,dy \tag{26}$$

$$= \sigma\omega^2\mu^2 H_0^2 a^4/48c^2. \tag{27}$$

The maximum energy stored is $\mu H_0^2 a^2/8\pi$, so that the Q is

$$Q = 12(\delta/a)^2. \tag{28}$$

At the high frequency limit $a \gg \delta$, and we employ appropriate approximations to find for the average power

$$P = \omega(\mu H_0^2/16\pi)(4a\delta), \tag{29}$$

while the maximum energy stored is $\mu H_0^2 4a\delta/16\pi$, giving

$$Q = 1. \tag{30}$$

The effective permeability may be written as

$$\mu(1 + jQ^{-1}), \tag{31}$$

which is consistent with the familiar equation $Q = \omega L/R$.

IX. DOMAIN THEORY OF EDDY CURRENT LOSSES IN SQUARE ROD

We treat a model in which there is a single plane wall running parallel to the axis of a square rod, and parallel to two of the sides. We suppose that the equilibrium position of the wall is at the midpoint of the rod; the losses will depend somewhat on the choice of equilibrium position. If there is a restoring force $-qx$ per unit area of wall the permeability at sufficiently low frequencies will be real and given by

$$\mu_0 = B_s^2/\pi q a, \tag{32}$$

where a is the side of the square, and we suppose that $\mu \gg 1$.

We suppose that in the absence of restoring force there is a relation of the form

$$v = GH \tag{33}$$

connecting the wall velocity and the applied field. It is shown in Section V above that

$$G^{-1} = (32B_s a/\tau c^2\pi^2) \sum_{\substack{\text{odd} \\ n}} n^{-3} \tanh(n\pi/2), \tag{34}$$

where the sum is approximately equal to 0.97.

The complete force equation now is

$$2HI_s = qx + j2\omega I_s x/G, \tag{35}$$

which gives

$$\mu = \mu_0[1 + j(B_s\omega/2\pi Gq)]^{-1}. \tag{36}$$

We have

$$B_s\omega/2\pi Gq = (8/\pi^3)(a/\delta)^2(0.97), \tag{37}$$

where the effective skin depth δ is defined in the classical way, using μ_0 as the permeability.

At low frequencies $\delta \gg a$, and

$$Q = (\pi^3/7.76)(\delta/a)^2$$
$$\approx 4(\delta/a)^2, \tag{38}$$

which is only one-third of the value of the classical Q given by Eq. (28).

At high frequencies $\delta \ll a$, and

$$\mu \approx -4j(\delta/a)^2\mu_0 \tag{39}$$

so that the material behaves as a resistive element. The calculation is valid only so long as the skin depth for permeability unity is greater than the side of the specimen, or when $\mu_0\delta^2 > a^2$. It is seen that also at high frequencies the domain model gives lower Q's than the classical mode.

We wish to thank Mr. H. R. Moore for electronics assistance and Mr. J. G. Walker for general technical assistance.

Letters to the Editor

PUBLICATION of brief reports of important discoveries in physics may be secured by addressing them to this department. The closing date for this department is five weeks prior to the date of issue. No proof will be sent to the authors. The Board of Editors does not hold itself responsible for the opinions expressed by the correspondents. Communications should not exceed 600 words in length.

Angular Distributions of Protons from the Reaction $O^{16}(d,p)O^{17}$

HANNAH B. BURROWS
University of Liverpool, Liverpool, England
W. M. GIBSON
University of Bristol, Bristol, England
AND
J. ROTBLAT
Medical College of St. Bartholomew's Hospital, London, England
October 30, 1950

THE reaction $O^{16}(d,p)O^{17}$ gives a number of groups of protons, of which the two corresponding to the ground state and first excited state of O^{17} have Q-values of 1.925 Mev and 1.049 Mev (Buechner *et al.*[1]). The intensities of these two groups have been measured at seven angles by Heydenburg and Inglis,[2] using deuteron energies between 0.65 Mev and 3.05 Mev.

We have used the 8-Mev deuteron beam from the University of Liverpool cyclotron, and a scattering camera in which photographic plates record particles emitted from a gas target at all angles from 10° to 165°, to obtain detailed angular distributions for the charged particles emitted in a number of deuteron-induced reactions. A full account of the method and results will be published elsewhere, but because of their theoretical interest (Butler[3]), the angular distributions of the two groups of protons from the reaction $O^{16}(d,p)O^{17}$ are presented here.

Tracks of protons from the two groups were identified by their ranges in the photographic emulsion, and the number of protons in each group, found in a given area, was determined for a series of angles from 10° to 160°. Ordinarily, measurements were made at 5° intervals, but at the more critical angles the interval was reduced to 2.5° or even to 1.25°. Using these numbers and the geometry of the apparatus, we calculated the angular distributions of the two proton groups in the center-of-mass system. These are shown in Fig. 1, in which the ordinates are proportional to the cross sections per unit solid angle in the center-of-mass system, at a center-of-mass angle ϕ, and the abscissae are $\cos\phi$.

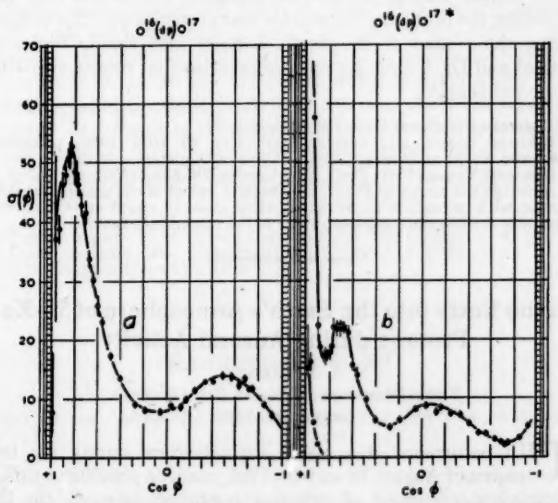

FIG. 1. $O^{16}(d,p)O^{17}$ angular distributions in the center-of-mass (c.m.) system: ϕ = c.m. angle, $\sigma(\phi)$ = c.m. differential cross section in arbitrary units. Curve *a* is for formation of O^{17} in the ground state, and curve *b* is for the 0.88-Mev excited state.

Figure 1a shows that when the O^{17} nucleus is formed in its ground state, there is a definite maximum in the intensity at $\cos\phi=0.83$ ($\phi=34°$). At higher angles, the intensity falls to a minimum at about 85°, rises to a smaller maximum at 120°, and falls again towards 180°. Below 34° the intensity falls, apparently tending to zero in the forward direction, although it is not excluded that it may rise again at very small angles; it is hoped that further experiments will show the behavior at angles too small to be studied with this apparatus.

In contrast to this, the intensity of protons from the formation of O^{17} in its excited state at 0.88 Mev (Fig. 1b) has a peak at $\cos\phi=0.7$ ($\phi=45°$) and a minimum at $\cos\phi=0.84$ ($\phi=33°$), rising steeply as the angle decreases from 33°.

The most interesting feature of these results is the difference in behavior of the two groups at angles below 50°. Butler[3] has shown that a stripping process, in which no compound nucleus is formed, can give one of several characteristic angular distributions, according to the spins and parities of the reacting nuclei. The observed results for small angles fit very well with the theoretical predictions, and it appears that (d,n) and (d,p) angular distributions may be of use in determining the spins and parities of ground and excited states in many nuclei.

[1] Buechner, Strait, Sperduto, and Malm, Phys. Rev. **76**, 1543 (1949).
[2] N. P. Heydenburg and D. R. Inglis, Phys. Rev. **73**, 230 (1948).
[3] S. T. Butler, Phys. Rev. **80**, 1095 (1950). Following letter.

On Angular Distributions from (d,p) and (d,n) Nuclear Reactions

S. T. BUTLER*
Department of Mathematical Physics, University of Birmingham, Birmingham, England
October 30, 1950

THE purpose of this note is to report the results of calculations which show how information regarding the spins and parities of nuclear energy levels can be obtained from angular distributions from nuclear reactions of the type $X(d,p/n)Y$ without the necessity of assuming properties of resonance levels of a compound nucleus. This work was commenced, at the suggestion of Professor Peierls, when experimental angular distributions for certain (d,p) reactions[1] were made available to him some time ago by Professor Rotblat. All exhibited a pronounced structure at small angles, and the work of Holt and Young[2] gives similar results. Such a structure must arise from contributions from high incident angular momenta of classical impact parameters larger than the nuclear radius. The obvious conclusion is that the reactions proceed, at least in part, by a stripping process in which one of the particles of the deuteron is absorbed into the nucleus, while the other merely carries off the balance of energy and momentum. Such a process is possible in the case of (d,p) and (d,n) reactions because of the low binding energy and large diameter of the deuteron.

I have calculated angular distributions resulting from such a stripping process by equating, at the nuclear surface, the exact wave function for a particle outside the nucleus to the interior wave function. After some simplification the resulting boundary equations can be solved in such a way that unknown properties of the nuclear wave functions affect the important parts of the distributions merely as a constant multiplying factor. The resulting curves show a pronounced maximum near the forward direction, the position of which is determined in each case by the spins and parities of the nuclear states involved. This is due to the fact that the requirements of conservation of angular momentum and of parity allow the nucleus to accept a particle (say a neutron) with only very limited values of angular momenta l_n, and the angular distribution depends very sensitively on these

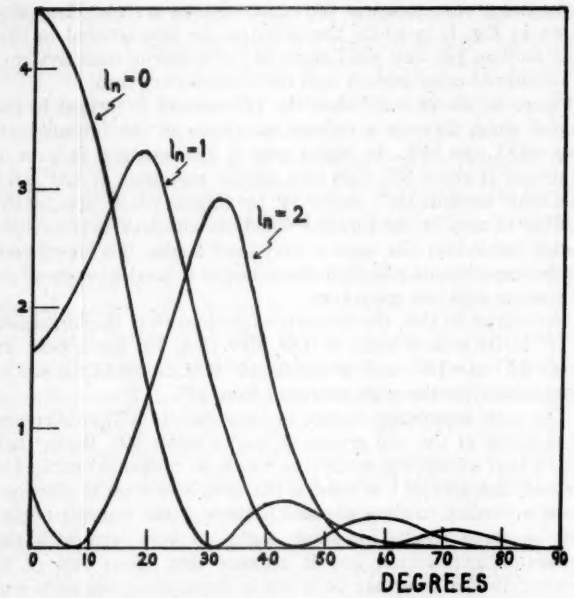

FIG. 1. Theoretical angular distributions for (d, p) and (d, n) reactions for different angular momentum transfers to the initial nucleus.

values. For deuteron energies above the Coulomb barrier, the distributions for the different values 0, 1, and 2 of l_n are generally of the form shown[3] in Fig. 1.

The possibility that the whole deuteron may enter the nucleus has been neglected. This is justified for large impact parameters, and hence the results should be reliable at small angles which are important for the present analysis. It is found that in any one case the experimental distribution agrees extremely well at small angles with one of the possible theoretical curves. We can thus identify the angular momentum transferred to the nucleus, and hence determine the spin and parity of the final nucleus from that of the initial nucleus.

For example, from the experimental angular distributions[1] for the reaction $O^{16}(d, p)O^{17}$ with 7.9-Mev incident deuterons, it is found that the theoretical curve required to obtain coincidence with the experimental one at small angles is, for the ground state of O^{17} that for $l_n=2$, and for the first excited state (0.88 Mev above ground) that for $l_n=0$. This agreement is illustrated in Figs. 2 and 3. Since the ground state of O^{16} has spin 0 and even parity, this implies that the ground state of O^{17} has spin 5/2 or 3/2

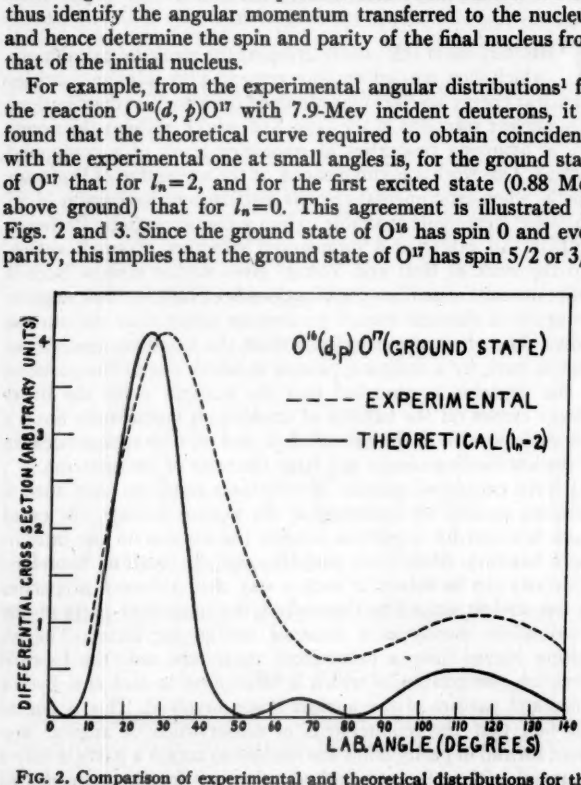

FIG. 2. Comparison of experimental and theoretical distributions for the ground-state transition of the reaction $O^{16}(d, p)O^{17}$ with 7.9-Mev incident euterons. The theoretical curve is that for $l_n=2$.

and even parity, and that the first excited state of O^{17} has spin 1/2 and even parity.

Table I gives spin and parity assignments which have so far been made from the experimental evidence of Burrows, Gibson,

TABLE I. Spin and parity assignments.

Reaction	Ground state initial nucleus	Final nucleus: Ground state	Final nucleus: First excited state
$O^{16}(d, p)O^{17}$ [a]	0+	(5/2 or 3/2)+	1/2+
$N^{14}(d, p)N^{15}$ [a]	1+	(1/2, 3/2, or 5/2)−	
$C^{13}(d, p)C^{14}$ [a]	0+	(1/2 or 3/2)−	
$Al^{27}(d, p)Al^{28}$ [b]	5/2+	(2 or 3)+	(0, 1, 4, or 5)+

[a] See reference 1.
[b] See reference 2.

and Rotblat, and of Holt and Young. For the ground states of C^{13} and N^{15} the assignments are consistent with what is already known.

Full details of these calculations, together with further assignments of spins and parities, will be published elsewhere.

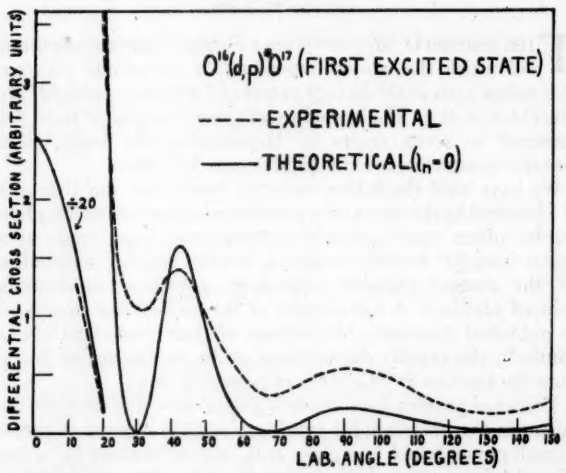

FIG. 3. Comparison of experimental and theoretical distributions for the transition to the 0.88-Mev excited state of O^{17} in the reaction $O^{16}(d, p)O^{17}$ with 7.9-Mev incident deuterons. The theoretical curve is that for $l_n=0$.

My sincere thanks are due to Professor Peierls not only for suggesting the problem, but also for many very helpful discussions during the course of the work. I must also thank Professor Rotblat and Dr. Gibson for making experimental results available before publication.

* Australian National University Scholar.
[1] Burrows, Gibson, and Rotblat, Phys. Rev. **80**, 1095 (1950), preceding letter, and report at Harwell Nuclear Physics Conference, 1950.
[2] Holt and Young, Proc. Phys. Soc. London **78**, 833 (1950).
[3] Although not shown in Fig. 1, the absolute values of the maxima usually decrease with increase of l_n, so that in those cases in which more than one value of l_n is allowed, the lowest value is the most important.

On the Entry into the Earth's Atmosphere of 57-Kev Protons during Auroral Activity

A. B. MEINEL
Yerkes Observatory, Williams Bay, Wisconsin
October 27, 1950

THE occurrence of a major auroral storm during the two nights of August 18 and 19, 1950, made it possible to utilize a grating spectrograph of sufficient resolution to study the Hα wave-length region. The spectrograph was pointed toward the magnetic zenith for three spectra and toward the north magnetic horizon for five spectra. Some spectra from both orientations

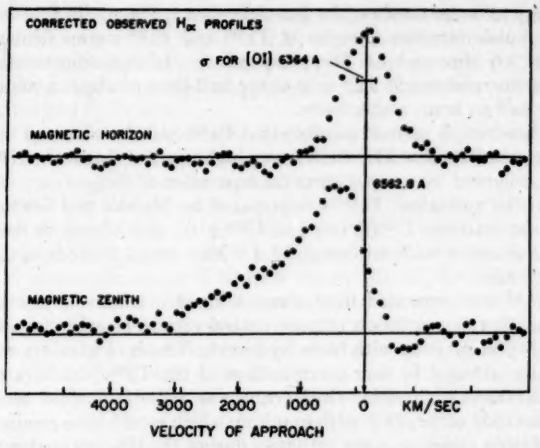

FIG. 1. Corrected observed profiles for Hα in the auroral spectrum for two magnetic orientations.

showed Hα in considerable intensity. A spectrum of a flaming feature which did not show Hα in appreciable intensity was used as a comparison for the effect of the first positive bands of N_2 that are adjacent to Hα.

Previous observations by Vegard,[1] Gartlein,[2] and others, of diffuse hydrogen emissions had been interpreted as scattering of rapidly moving incident protons. No Doppler displacement, however, was established. The current spectra, obtained with respect to the geomagnetic coordinates, have enabled an unambiguous evaluation of the nature of auroral hydrogen. The profile of Hα observed from the magnetic zenith is very asymmetrical, with the entire line shifted to the violet. The profile of Hα in the magnetic horizon is symmetrical but broadened. Figure 1 shows the mean of four separate microphotometer traces for each magnetic orientation after correction for the first positive bands of N_2.

The velocity profile of Hα in the zenith cannot indicate a real velocity spread of the incident protons because of their nearly simultaneous arrival in the auroral zone. The profile, therefore, must be a consequence of the loss of energy of the protons upon entering the upper atmosphere. The violet wing indicates that the velocity of the protons before entering the atmosphere is greater than 3300 km/sec., corresponding to an energy of 57 kev. This velocity is considerably greater than has been deduced from indirect correlations.

It has been pointed out by J. R. Platt[3] that protons moving with these velocities have a small probability of emitting Hα-radiation through electron capture. The probability increases to a maximum when the velocity of the proton is equal to the Bohr orbital velocity for the 3*s* shell (730 km/sec.). As a consequence, it would be difficult to detect protons moving with much higher velocities than those currently observed; hence, the velocity of 3300 km/sec. represents only a lower limit to the velocity of the auroral protons.

[1] Vegard, report to the Gassiot Comm., Phys. Soc. London, p. 82 (1948).
[2] Gartlein, Trans. Am. Geophys. Union 31, No. 1, 7 (1950).
[3] J. R. Platt, private communication.

Radioactivity of F^{17}

V. PEREZ-MENDEZ AND P. LINDENFELD
Pupin Physics Laboratories, Columbia University, New York, New York*
October 23, 1950

FLUORINE[17] has long been known to be a positron emitter. Early cloud-chamber investigations by Kurie, Richardson, and Paxton[1] showed that the maximum energy of the transition was approximately 2.1 Mev. An excess of positrons at the low energy end of the spectrum was interpreted by Bethe, Hoyle, and Peierls[2] as possibly being due to a low energy beta-group followed by a gamma-ray of approximately 900-kev energy.

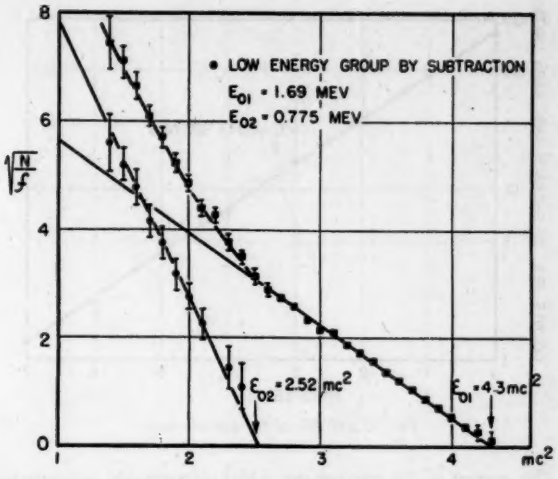

FIG. 1. β-spectrum of F^{17}.

The beta-ray spectrum of F^{17} has recently been investigated in this laboratory, using the technique of bombarding gases in the cyclotron and transporting them by a circulating pump to the source chamber of a semicircular focusing spectrometer as described previously.[3] The F^{17} was produced by a (d, n) reaction on O^{16}. A Fermi plot of the spectrum (Fig. 1) shows that it is of the allowed shape down to 2.5 mc^2, where it deviates considerably from linearity. The end-point energy (average of several such runs and corrected for window absorption) is $E_{01}=4.35\ mc^2$ which corresponds to a maximum energy of 1.72±0.03 Mev. On subtracting the high energy spectrum a low energy group of the allowed shape is obtained, having an end-point energy of $E_{02}=0.78$ Mev.

The relative intensity of the two groups was calculated from the intercepts of the two Fermi plot lines on the vertical and horizontal axes. The data obtained indicate that the low energy group is 33±5 percent as intense as the high energy group. The partial lives for the two transitions are found to be $t_1=93$ sec. and $t_2=285$ sec. (based on an observed half-life[4] of 70.0 sec.) with the corresponding ft values $ft_1=3240$ sec. and $ft_2=350$ sec.

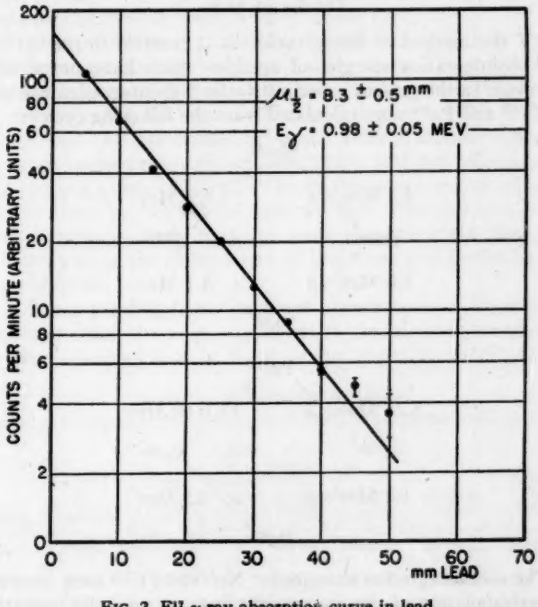

FIG. 2. F^{17} γ-ray absorption curve in lead.

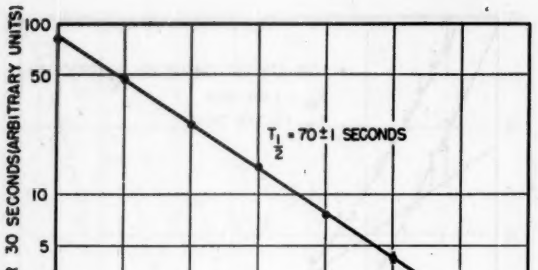

FIG. 3. Half-life of F^{17} gamma-ray.

The energy of the gamma-ray which presumably accompanies the low energy transition was measured. Figure 2 shows an absorption curve in lead of the gamma-rays from F^{17}. A photomultiplier tube with an anthracene crystal was used as detector. The 0.51-Mev annihilation radiation is not seen on this curve since the discriminator was set to detect only the larger pulses produced by the higher energy gamma-rays. The half-thickness for absorption shows that the energy of this gamma-ray is 0.98 ±0.05 Mev.

A decay curve of the gamma-ray (Fig. 3), taken with the same geometry and discriminator setting shows that its half-life is 70±1 sec., in good agreement with the half-life for the β^+ decay.

We wish to thank Professor W. W. Havens for his constant help and encouragement. Our thanks are also due to the AEC which aided materially in the performance of this research.

* Assisted by the AEC.

[1] Kurie, Richardson, and Paxton, Phys. Rev. **49**, 368 (1936).
[2] Bethe, Hoyle, and Peierls, Nature **143**, 200 (1939).
[3] H. Brown and V. Perez-Mendez, Phys. Rev. **78**, 649 (1950).
[4] H. W. Newson, Phys. Rev. **48**, 790 (1935).

Preparation of Th^{235} and Pa^{235}

B. G. HARVEY AND B. I. PARSONS*
National Research Council of Canada, Atomic Energy Project, Chalk River, Ontario, Canada
October 30, 1950

BY the method of decay cycles[1] it is possible to predict the disintegration energies of nuclides which have never been observed. In the present experiment, the β-disintegration energies of Th^{235} and Pa^{235} were calculated from the following cycles:

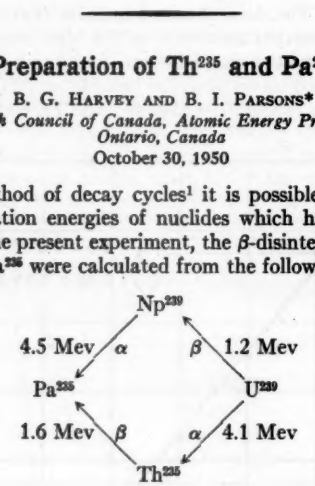

The α-disintegration energies for Np^{239} and U^{239} were obtained by extrapolation of the appropriate lines on an α-disintegration energy *vs.* mass number plot (see reference 1, Fig. 1). In this way, the β-disintegration energies of Th^{235} and Pa^{235} were calculated to be 1.6 Mev and 1.4 Mev, respectively. It was expected that these energies would lead to β-decay half-lives of about a minute and half an hour, respectively.

Therefore, it seemed possible that Pa^{235} could be obtained by a short irradiation of Th^{234} (UX_1) at a high neutron flux in the NRX pile, followed by a rapid chemical separation of Pa.

In the meantime, Pa^{235} was prepared by Meinke and Seaborg[2] by the reactions $U^{238}(d, \alpha n)$ and $U^{238}(p, \alpha)$, and shown to decay by β-emission with an energy of 1.4 Mev and a half-life of 23.7 ±0.5 min.

Th^{234} was separated from about 1 kg of uranium by aqueous extraction of a solution of pure uranyl nitrate in ether followed by co-precipitation with ferric hydroxide. Traces of uranium were finally removed by four precipitations of the Th^{234} with a carrier of lanthanum fluoride. Great care was taken to avoid recontamination of the Th^{234} with uranium, which would have produced confusing fission product activities during the pile irradiation.

The Th^{234} was finally dissolved in 6 M nitric acid and Pa isotopes were removed by three extractions with di-isopropyl ketone.[3] The Th^{234} solution was immediately evaporated in a small silica tube, sealed, and irradiated for 45 min. in a thermal neutron flux of 6×10^{13} neutrons/cm²/sec. in the NRX pile. The preliminary removal of Pa isotopes reduced the contamination of the Pa^{235} by 6.7-hr. Pa^{234}.

After the irradiation, the silica tube was smashed, and Pa extracted as before with di-isopropyl ketone to separate it from the Th^{234} and La^{140}. The Pa was further purified from La^{140}, Th^{234}, and any traces of uranium fission products by washing the di-isopropyl ketone solution twice with equal volumes of a solution of 1 M nitric acid and 3 M ammonium nitrate. The Pa was then extracted back into 0.1 M nitric acid. A half-volume of concentrated nitric acid was added to the aqueous solution, and Pa was finally purified by extracting it into an equal volume of 0.4 M

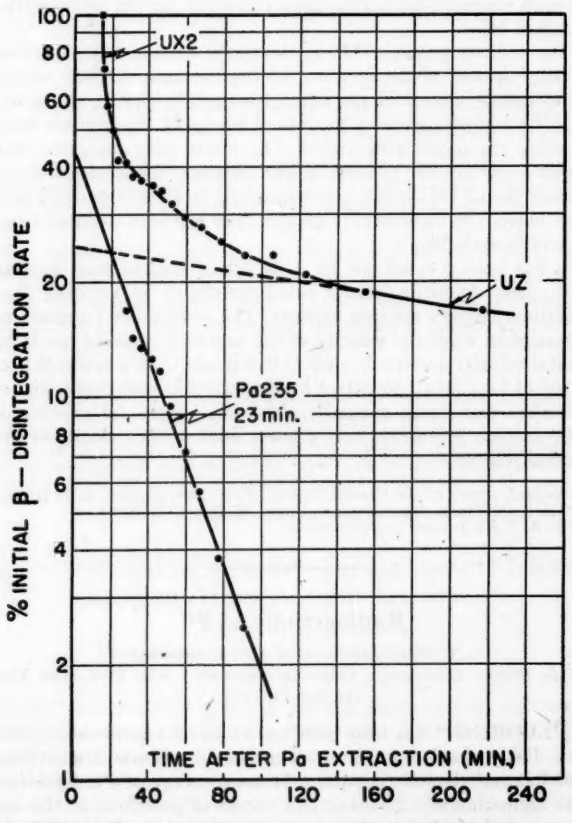

FIG. 1. Decay of Pa fraction from neutron-irradiated UX_1.

thenoyltrifluoroacetone in benzene. The benzene solution was washed once with 4 M nitric acid to remove any of the aqueous phase which had been carried over with it, and evaporated on to an aluminum counting tray. The chemical separation of Pa was completed in 12 min.

The decay of the sample was observed with an end-window Geiger counter, using a 50-mg/cm² aluminum absorber to reduce the counting rate due to the 6.7-hr. Pa^{234}.

Three components were observed (Fig. 1), decaying with half-lives of about 1 min., 23±1.5 min., and 6 hr. These activities are attributed to 1.14-min. Pa^{234} (UX_2), Pa^{235}, and 6.7-hr. Pa^{234} (UZ).

A second extraction of Pa from the irradiated Th^{234} was carried out in one case 10 min. after, and in another case 25 min. after, the first. In neither case was any of the 23-min. activity observed. It is therefore concluded that substantially all of the Th^{235} had decayed to Pa^{235} during the 12-min. interval between removal of the samples from the pile and the first chemical separation of Pa.

Since the 6.7-hr. Pa^{234} could be used as a tracer for the Pa^{235}, it was not necessary to know either the initial amount of Th^{234} or the chemical yield in order to calculate the (n, γ) cross section of Th^{234} for the formation of Th^{235}. Values of 1.7 and 1.8 barns were obtained in two irradiations. The possibility that the Pa^{235} was produced directly by (n, γ) reaction in the small amount of 6.7-hr. Pa^{234} present or in 1.14-min. Pa^{234} is not considered likely, because the (n, γ) cross sections of the two Pa^{234} isomers would need to have the unusually large values of about 1.1×10^6 and 5×10^4 barns, respectively, to account for the quantity of Pa^{235} observed.

* Present address: McGill University, Montreal, Canada.
[1] Perlman, Ghiorso, and Seaborg, Phys. Rev. 77, 26 (1950).
[2] W. W. Meinke and G. T. Seaborg, Phys. Rev. 78, 475 (1950).
[3] W. W. Meinke, AECD-2750, December 2, 1949, unpublished.

Evidence Concerning the Existence of the New Unstable Elementary Neutral Particle

V. D. HOPPER AND S. BISWAS
Department of Physics, University of Melbourne, Melbourne, Australia
October 30, 1950

ROCHESTER and Butler[1] in 1947 observed tracks in a Wilson cloud chamber which could be interpreted as the spontaneous decay of new types of elementary particles. They found two events selected from five thousand photographs, one of which consisted of two tracks which were copunctal, the particles producing the tracks having opposite signs and their momenta about 340 and 350 Mev/c, respectively. The second event consisted of a forked track produced by two positively charged particles of momenta 600 and 770 Mev/c. The first event could be interpreted as the decay of a neutral particle into two charged particles of opposite signs and the second event as the decay of a charged particle into a neutral and a charged particle. Recently Seriff *et al.*[2] have obtained similar results in cloud-chamber observations taken at a maximum altitude of 10,000 ft., and from a study of 11,000 cloud-chamber photographs they have obtained 34 forked tracks, 30 of which corresponded to the first event and 4 to the second event described by Rochester and Butler. In 15 of the results of the first kind the neutral particle could have originated in a nuclear disintegration, the plane of the decay tracks being approximately coplanar with the position of nuclear impact. It has recently been reported[3] that Butler using the cloud chamber has observed at an altitude of 9000 ft. an additional 9 events of the first and one of the second kind.

A result similar to the first event, a two-pronged star produced by a neutral particle, has been observed in a 400μ-thick Ilford G5 nuclear emulsion flown to an altitude of 70,000 ft.; and, fortunately, both tracks were of sufficient length to enable the masses of both particles to be identified. This has not been possible with the cloud-chamber observations. A facsimile drawing showing the position of the two-pronged star in relation to a large star of 29 prongs is shown in Fig. 1. The plane of the pair of tracks does not coincide with the center of the star, so it is concluded that if

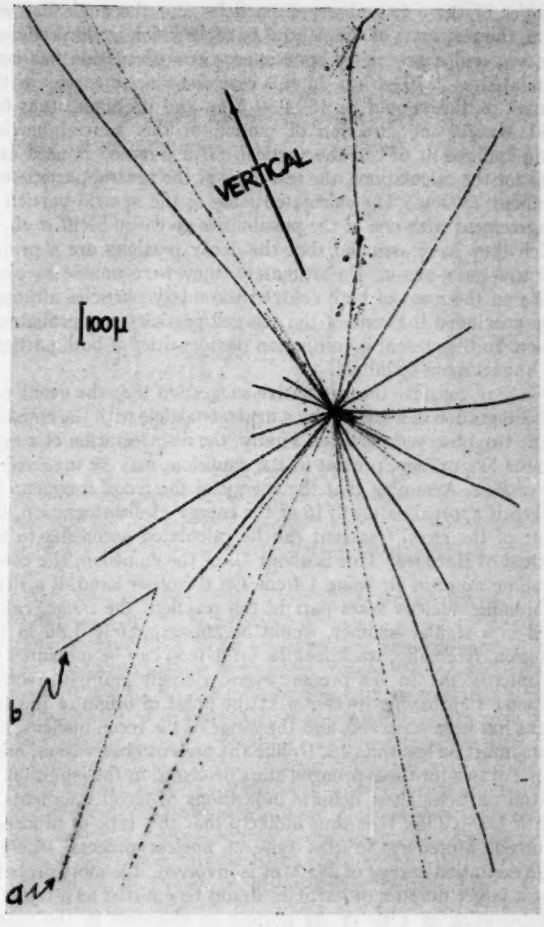

FIG. 1. Facsimile drawing which shows position of the two-pronged star relative to a large star. The plane of the two-pronged star does not coincide with the center of the large star. Track (a) corresponds to a meson and track (b) to a proton.

a high energy neutral particle disintegrated into the two-pronged star, it did not emanate from the large star. A summary of the data for the two prongs is given in Table I.

Neither of the tracks ended in the emulsion and there was no significant change in grain density along them. The grain-density of track (a) was slightly above the value of the grain-density corresponding to the minimum ionization particles for this emulsion which was 14.0 grains/50μ. $\alpha°$ is the average angular deviation between successive chords 100μ in length and was calculated by the method given by Fowler.[4] From the above results with the curves given by Fowler[4] the particles were identified as a meson and a proton. Both particles have approximately the same momenta as in the observations of Rochester and Butler for this type of event.

It is not possible from the above observations to identify the meson as either the π- or μ-type, but in the following calculations we have assumed it to be the π-meson. From the momenta and

TABLE I. Data on the two prongs.

Prong	Length in emulsion	Mean grain-density	Angle between the tracks	$\alpha°$, Mean-deviation/100μ	Type of particle	Energy Mev	Momentum Mev/c
(a)	2600μ	16.3/50μ	40°	0.10°	Meson	215±30	329±30
(b)	400μ	50/50μ		0.3°	Proton	62±20	335±50

energies of these two observed particles and the angle between them, the rest mass of the neutral particle which could produce a π-meson and a proton by spontaneous transformation has been calculated as $2370\pm60m_e$. In this case the kinetic energy of the neutral particle would be 150 ± 30 Mev and its momentum 620 ± 80 Mev/c, the direction of motion of this neutral particle being inclined at 65° to the vertical. (If a μ-meson is used as a basis for the calculations, the rest mass of the neutral particle will be about $2300m_e$.) The calculated mass of the neutral particle is in agreement with one of the possibilities given by Seriff *et al.*, in which they have assumed that the decay particles are a proton and a π- or μ-meson. Unfortunately, they were unable to place limits on the mass of both charged secondary particles although they concluded that one of the charged particles was probably a meson. In the present investigation the identities of both particles are known more definitely.

We may consider the alternative suggestion that the event was a disintegration of a nucleus by a neutral particle with the emission of the two observed particles. Firstly, the disintegration of a light nucleus like oxygen, present in the emulsion, may be involved in the process. Assuming that the energy of the recoil fragment for oxygen is approximately 1/16 of the energy of disintegration, the range of the recoil fragment can be calculated according to the method of Harding.[5] This is about 7μ in the emulsion, the corresponding range in air being 1.4 cm. On the other hand, if a silver or bromine nucleus takes part in the reaction, the range, calculated in a similar manner, would be approximately 1.8μ in the emulsion. Normally, track lengths up to 0.5μ can be measured by the microscope. In the present event a single grain of average diameter 1.5μ having its center at the point of origin of the two tracks has been observed, and the range of the recoil nucleus, if it exists, must be less than 1μ. Unlike the present observation, other events of two- or three-pronged stars produced in the emulsion by neutral particles show definite indications of recoil fragments of length 1.0 to 2.0μ. It is thus unlikely that this type of process is involved. Moreover, in this type of nuclear process, where a large excitation energy of 275 Mev is involved, it is more probable that a larger number of particles would be emitted as a result of disintegration of a Br or Ag nucleus as observed in the many-pronged high energy stars. Further, in the observations of similar events with the Wilson cloud chamber, where the heaviest nucleus present is oxygen, the range of recoil fragment in this assumed process of nuclear disintegration would have been 1.4 cm of air. This, too, is against the assumption of the disintegration of a nucleus by a neutral particle. Thus, all the arguments seem to favor the process of decay of a neutral particle into two charged secondary particles, the mass of the neutral particle being $2370\pm60m_e$, assuming the decay products are solely the proton and π-meson observed.

Finally, we may consider to what extent some of the unusual nuclear reactions fit the present event. These may be:

$$\gamma+n=p^++\pi^-, \quad (1)$$

$$\pi^\circ+n=p^++\pi^-, \quad (2)$$

$$n+\pi^\circ=p^++\pi^-. \quad (3)$$

The first two processes do not satisfy the energy and momentum conditions, while the third process, the neutron colliding with a π°-meson satisfies these relations. Such a reaction is difficult to imagine since the π°-meson does not exist free in nature.

The authors would like to express their gratitude to the Commonwealth Meteorological Service for assistance in exposing the nuclear plates at high altitudes, and to Professor L. H. Martin for helpful discussions. One of the authors (S.B.) is grateful to the Commonwealth Government of Australia for the award of a UNESCO fellowship which enabled him to carry on the work.

[1] G. D. Rochester and C. C. Butler, Nature **160**, 855 (1947).
[2] Seriff, Leighton, Hsiao, Cowan, and Anderson, Phys. Rev. **78**, 290 (1950).
[3] P. M. S. Blackett, Proceedings of the Harwell Nuclear Physics Conference (AERE G/M 68), 20, September, 1950.
[4] P. H. Fowler, Phil. Mag. **41**, 169 (1949).
[5] J. B. Harding, Phil. Mag. **40**, 530 (1949).

Radioactive Nuclei Emitted in Cosmic-Ray Stars

E. Pickup and L. Voyvodic
Division of Physics, National Research Council, Ottawa, Canada
October 27, 1950

In a survey[1] of cosmic-ray stars formed in electron-sensitive photographic emulsions (Ilford G5) at about 85,000 feet we find that, in addition to ${}_3Li^8$ nuclei, characterized by the "hammer tracks," about an equal number of short range radioactive fragments are emitted. These are identified by the tracks of decay electrons with energies of a few Mev, originating from the end of the fragment. Unless heavy fragments are radioactive, it is difficult to distinguish their tracks from those of protons or α-particles in the emulsion unless they are of sufficiently long range to show either δ-rays or the characteristic thinning down in track width towards the end of the path. A mosaic of photo-micrographs illustrating a typical radioactive fragment is shown in Fig. 1.

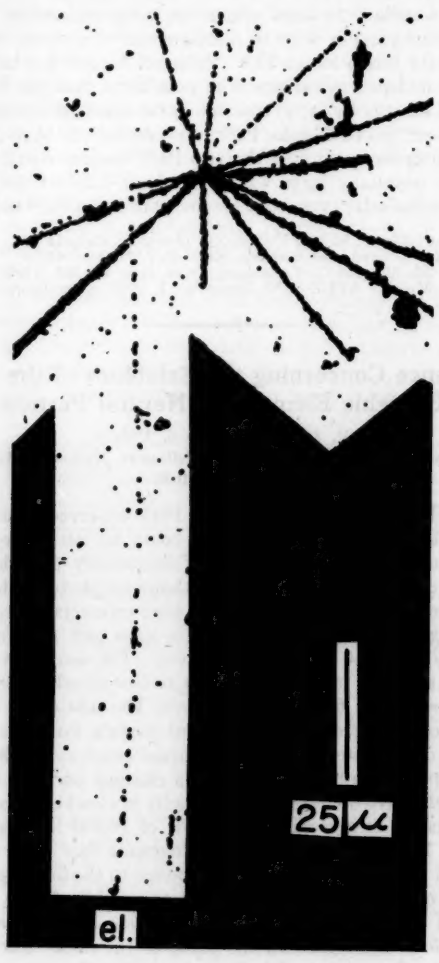

FIG. 1. Fifteen-pronged star with nucleus, from the end of which originates a decay electron.

Out of a total of about 4300 stars with more than 5 prongs[2] there were 31 stars with Li^8 fragments, and 32 with other radioactive fragments of ranges from a few microns to about 50 microns. The average range of the Li^8 nuclei was about 50 microns, being greater than the average range of the other radioactive nuclei. In one case of a 35-pronged star, two Li^8 nuclei were ejected; and in some cases there was at least one other non-radioactive nucleus, heavier than an α-particle.

There were also about 20 cases[3] in which electrons with energies

TABLE I. Energies of electrons from radioactive fragments (N = number of prongs, E = electron energy in Mev).

N	14	21	10	19	11	9	12
E	7.2±1	6.0±1	4.0±7	7.0±1.5	6.9±1	2.0±0.3	5.0±1.0
	25	24	21	16	6	21	16
	8.7±2	0.8±0.2	7.0±0.4	2.7±1	1.3±0.2	3−6	13.5±1.5

of a few Mev appeared to originate at the star center, these probably being decay electrons from residual nuclei. In some, but not all, of these stars, there were short tracks, 1 or 2 microns in range, presumably due to residual recoil nuclei; and the electrons could have come from them.

Table I shows the energy values for some of the electrons from radioactive fragments, as measured by the multiple Coulomb scattering method. The rather wide spread in energy values is not indicative of any one β-emitting nucleus. In the case of Li^8 electrons (end point ~13 Mev), 7 electrons out of 8 measured had energies between 5 and 8 Mev. It is, in any case, to be expected that the radioactive nuclei observed will comprise several different types.

It can be seen from the data in Table I that there are 7 nuclei with β-ray energies >5 Mev and 4 with energies >7 Mev. This means that these nuclei are probably to be identified as either N^{16}, N^{12}, or B^{12}, since the end points of most other known β-ray emitters are too low for them to have contributed these electrons. There are considerably more possibilities for the remaining examples. Most of the stars observed must be ascribed to Ag or Br disintegrations because of the numbers of prongs they have; and, in general, there is an appreciable mass excess left which could account for a variety of nuclei. These would, however, have relatively low β-ray energies if they were radioactive. The energies of the electrons which appeared to originate at the star centers seemed, on the whole, to be lower than those from the ends of visible fragments.

It would appear from the above results that the probability of emission of Li^8 nuclei is greater than that for other radioactive nuclei, although the certainty of identification of the event is greater in the former case. Also, as has been pointed out,[4] the apparent scarcity of a radioactive residue in stars means that there must be appreciable neutron emission in the disintegrations.

We are greatly indebted to Mr. I. B. McDiarmid, who carried out many of the scattering measurements. Further details of this work will be submitted for publication in the *Canadian Journal of Research.*

[1] The emulsions were exposed through a collaborative program of cosmic-ray investigations by the Bartol Research Foundation and the National Research Council of Canada, with the cooperation of the ONR project, "Skyhook."
[2] This criterion is given, since an appreciable number of the smaller stars would be missed with the low microscope magnification used for searching most of these emulsions.
[3] In the case of large stars, the center is often not too clear, and some examples may have been missed.
[4] K. J. LeCouteur, Proc. Phys. Soc. (London) 63, 259 (1950).

The Isomeric Transition of Tc^{95}

HEINRICH A. MEDICUS* AND PETER PREISWERK
Swiss Federal Institute of Technology, Zurich, Switzerland
October 24, 1950

THE isotope of technetium with mass number 95 decays with two half-lives of 20 hr. and 60 days. The assignment of these half-lives to Tc^{95} is based on the production of technetium by bombardment of enriched Mo isotopes. Previously, we had investigated in detail the transition of these two isomeric states.[1] It was found that K-capture (and a small fraction of positron emission) with the two cited periods does not result in the excitation of the same levels of the daughter nucleus Mo^{95}. This observation raised some questions regarding the assignment of both half-lives to the same isotope. However, the transitions were explained by consideration of the difference in angular momentum between these isomeric states. On this basis we had concluded that the two states of Tc^{95} exist with a difference in angular momentum of 4 units and different parities.

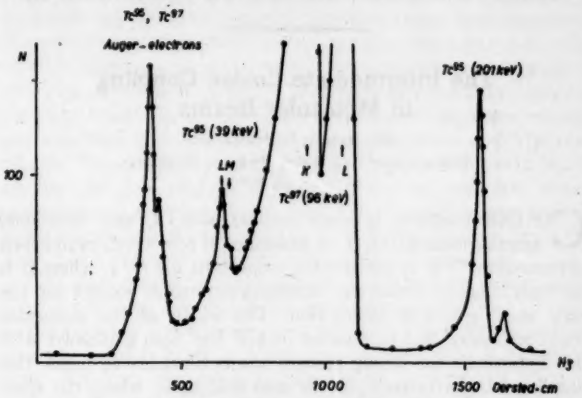

FIG. 1. Low energy electron lines of Tc^{95} and Tc^{97}.

We have now succeeded in observing the direct transition from the 60-day level to the 20-hr. level by means of a magnetic lens spectrometer and thus have substantiated the assumed decay scheme. We examined the low energy region of conversion electrons and observed, in addition to the intense conversion lines of the 96-kev isomeric transition of the 90-day Tc^{97}, a new line with an energy of 35.9 kev. (Fig. 1.) This line must be interpreted as an L-conversion line of an isomeric transition with $\Delta E = 39.0 \pm 0.7$ kev from the 60-day Tc^{95} level. The intensity of the line decreases with a half-life of 60±10 days. If the line were the result of a K-conversion, the associated L-conversion line should have been found, since a careful search was conducted for it. The K-conversion line of a 39-kev transition unfortunately happens to coincide with that formed by Auger electrons and therefore, could not be observed separately. Further support for the assignment to an isomeric transition is gained by estimating the intensity of this transition relative to the K-capture of the 60-day period. For this purpose, the intensity of the 36-kev line was compared with that due to the 201-kev transition. It is known that 70 percent of the decays of 60-day Tc^{95} go by way of the 201-kev level in Mo^{95}. Moreover, the conversion ratio of this transition is known to be 4 percent. The relative probabilities of K- and L-conversion in the isomeric transition are not known, however. If one assumes

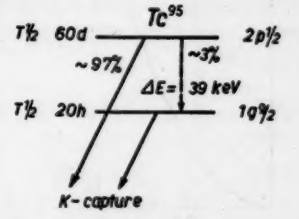

FIG. 2. Scheme of the isomeric transition in Tc^{95}.

that they are equal (this conjecture is probably correct to within a factor of 2), one obtains for the branching ratio of the 60-day level between K-capture and isomeric transition 30:1 and, therefore, for the partial half-life of the isomeric transition $\tau_{\frac{1}{2}} = 5$ years. This value is in agreement with that which was to be expected for an isomeric transition of 39 kev and an order of transition $A = 5$. (Fig. 2.)

Thus the above-mentioned assumptions regarding the spin and parity relations are substantiated and it is shown that the state with a half-life of 60 days is the excited one, and that with the period of 20 days is the ground state of Tc^{95}.

It is noteworthy that another technetium isotope (mass assignment uncertain) has an isomeric state with almost the same

excitation energy (34.4 kev) as the one under discussion.[1] Its half-life of 51.5 min. and the $K:L$ conversion ratio, however, point to its assignment to the next lower transition order.

* Present address: Radiation Laboratory, University of California, Berkeley, California.

[1] Medicus, Preiswerk, and Scherrer, Helv. Phys. Acta 23, 299 (1950).

The Intermediate Cosine Coupling in Molecular Beams

WILLIAM A. NIERENBERG
University of California, Berkeley, California
October 26, 1950

COSINE coupling between nuclear spin, **I**, and rotational angular momentum, **J**, in molecules, is now a well established phenomenon.[1-9] It is particularly important for $I=\frac{1}{2}$, where it is the only angular dependent interaction possible except for the very small spin-spin interaction. The width of the molecular beam resonance line in fluorine in LiF has been explained with this hypothesis for strong enough magnetic fields to break this coupling.[2] Unfortunately, in the zero-field limit, where the spectrum has been discussed theoretically, the observations were obscured by experimental difficulties.

It has therefore been considered desirable to calculate the molecular beam line shape for diatomic molecules and large J for all values of the magnetic field so that experimental verification can be performed to nearly zero field for $I=\frac{1}{2}$. This calculation has been completed. The line shape is given by:

$$dN/dx=(w/2)^{\frac{1}{2}}(x/x_I)[\mathrm{erf}(x+x_I)-\mathrm{erf}|x-x_I|].$$

The notation of reference 2 is used $x=h\alpha\nu/c$. Here ν is the radio-frequency, c is the coefficient of the $\mathbf{I}\cdot\mathbf{J}$ coupling in the Hamiltonian, $x_I=h\alpha\nu_I/c$, where ν_I is the Larmor frequency of the uncoupled nucleus. $\alpha=(h^2/8\pi^2KkT)^{\frac{1}{2}}$, where K is the moment of inertia of the molecule. x_I is therefore the correct measure of the coupling. For large values of the magnetic field $x_I\to\infty$ and the limiting value of dN/dx agrees with the result found previously. If $x_I\to 0$, we have the Zeeman effect and the limiting value of dN/dx for $x_I=0$ also agrees with the earlier results.

Figure 1 is the line shape for $x_I=1$. It is clear that the line

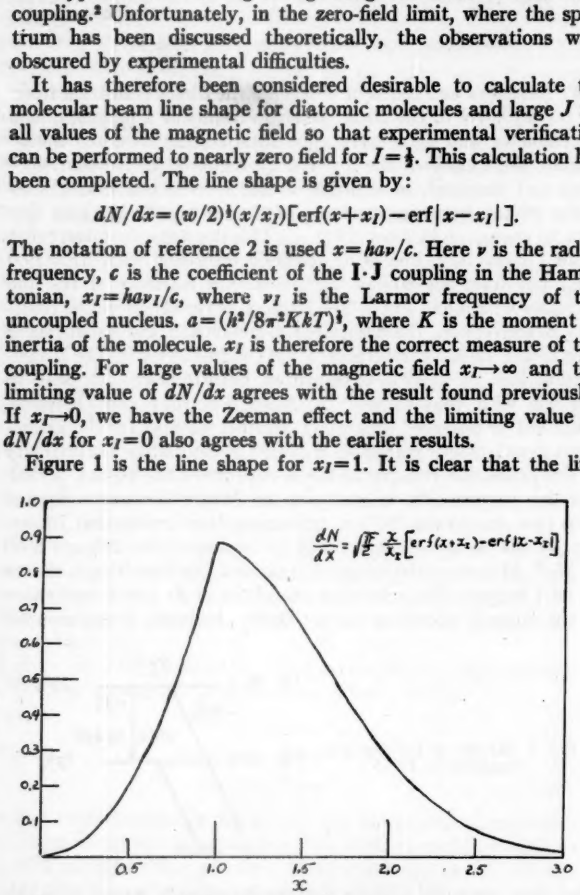

FIG. 1. Line shape for $x_I=1$.

shape has become highly asymmetric. The calculation ignored the transition probabilities, the quadrupole coupling of **J** to the other nucleus and the resolution of the apparatus. These effects can be estimated and can usually be ignored.

[1] N. F. Ramsey, Jr., Phys. Rev. 58, 226 (1940).
[2] W. A. Nierenberg and N. F. Ramsey, Phys. Rev. 72, 1075 (1947).
[3] G. C. Wick, Zeits. f. Physik 85, 25 (1933).
[4] G. C. Wick, Phys. Rev. 73, 51 (1948).
[5] H. M. Foley, Phys. Rev. 72, 504 (1947).
[6] Nierenberg, Rabi, and Slotnick, Phys. Rev. 73, 1430 (1948).
[7] J. W. Trischka, Phys. Rev. 74, 718 (1948).
[8] A. Roberts, Phys. Rev. 76, 1723 (1949).
[9] L. Grabner and V. Hughes, Phys. Rev. 79, 819 (1950).

Half-Life of Fe^{55} and Co^{60}

G. L. BROWNELL AND C. J. MALETSKOS
Radioactivity Center, Laboratory for Nuclear Science and Engineering, Department of Physics, Massachusetts Institute of Technology, Cambridge, Massachusetts*
October 23, 1950

THE half-life of Fe^{55} is listed in the 1948 Seaborg and Perlman table[1] as about 4 years, and this value is ascribed to a personal communication from Van Voorhis. As this entry is identical with that in the 1940 Livingood and Seaborg table,[2] it can be assumed that the measurements were made prior to this date. With the exception of the estimates made in the discovery paper of Livingood and Seaborg,[3] this value is the only published report which has been found on the half-life of Fe^{55}.

The original observation of the long-lived Co^{60} activity was made by Sampson, Ridenour, and Bleakney[4] in 1936. Livingood, Fairbrother, and Seaborg[5] in 1937 estimated the half-life to be greater than 1 year, and in the same year, Risser[6] measured the half-life as 2.0 ± 0.5 years. The value reported in the 1940 table[2] was 7.0 years based on unpublished work of Livingood and Seaborg. This value was later changed by Livingood and Seaborg[7] to 5.3 years, and the latter value appears in their 1948 table.[1]

Measurements have been made over a period of 18 months on the decay of a sample of Fe^{55} and Co^{60}. The iron sample was electroplated on a copper planchet from a sample of a cyclotron-produced stock solution of iron chloride which contained no Fe^{59}. The activity of this sample was 1.4×10^5 c.p.m. as measured with a G-M x-ray counter, and the true disintegration rate was perhaps one hundred times this value. The sample was sealed in an ionization chamber of about one liter active volume, and the chamber was filled to atmospheric pressure with tank argon from which water vapor had been removed by passing the gas rapidly through a liquid nitrogen trap. A brass plate controlled externally to the chamber covered the sample for background measurements. The cobalt sample was prepared by sealing about 15 microcuries of Co^{60} in the form of cobalt chloride in a glass vial. The activity was measured by placing the sample adjacent to the chamber. A radium standard was also measured to correct for small changes in the measuring equipment. The standard consisted of 25 microcuries of radium in the form of radium chloride sealed in a glass ampoule. The standard was measured in a manner similar to the cobalt sample. During and between measurements the standard was kept in a vertical position.

The ionization current was measured with a vibrating reed electrometer by the rate of charge method. Time measurements were read from an Esterline-Angus recording ammeter tape, and the voltage decrement was determined with a potentiometer and standard cell. The capacitance of the feed-back condenser in the vibrating reed electrometer was determined by comparison with calibrated resistors. The current produced in the chamber by the two samples and the radium standard was of the order of 1.5×10^{-13} amp., while the background current was 2.5×10^{-15} amp. At each determination five measurements were made with two positionings of each sample.

After a period of 12 months, the argon was removed and analyzed by passing slowly through a liquid nitrogen trap. No CO_2 was observed, but 0.5 percent of water vapor was found. This vapor could possibly have entered from gradual leakage into the chamber as a result of changes in atmospheric pressure or from insufficient outgassing of the short length of vacuum hose which allowed rotation of the background plate. It is very improbable that this amount of water vapor could produce oxidation of the iron sample. Although the O_2 content was not determined, the fact that no CO_2 was observed also makes oxidation very unlikely. The chamber was refilled with water-free argon, and the measurements continued.

After eighteen months of measurements, the chamber was disassembled. The appearance of the iron sample was the same as at assembly, and there was no evidence of oxidation. The portion of the copper planchet surrounding the iron sample was slightly tarnished, and this was attributed to the action of sulfur from

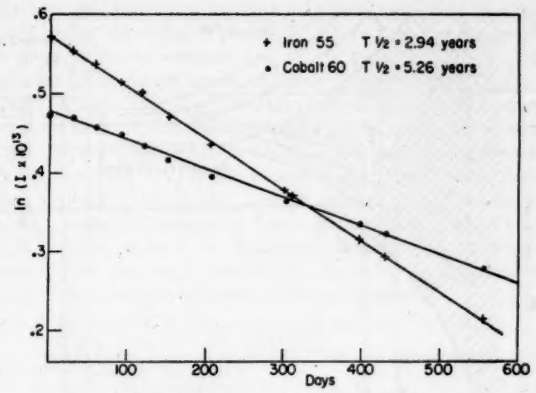

FIG. 1. Decay curves of Fe^{55} and Co^{60}.

the vacuum tubing. A search was made over the interior of the chamber for Fe^{55} activity with a G-M x-ray counter, and none was found.

The results of eleven determinations made over the 18-month period are shown on Fig. 1. The data are corrected for background and for small changes indicated by the radium standard (about two percent). The data have been analyzed by the method of least squares,[8] and the resultant values of half-lives of Fe^{55} and Co^{60}, and standard errors are shown in Table I. The 2.94-year

TABLE I. Half-lives of Fe^{55} and Co^{60}.

Isotope	Half-life	Standard error of half-life	Standard error per determination
Fe^{55}	2.94 years	0.98 percent	0.34 percent
Co^{60}	5.26 years	3.32 percent	0.65 percent

half-life of Fe^{55} is somewhat less than the presently accepted value of about 4 years, but the measured half-life of Co^{60}, 5.26 years, is in excellent agreement with the value of Livingood and Seaborg. The errors derived from this calculation provide a lower limit to the uncertainty in the half-life values, but since no gross instrumental errors have been detected, this error will be considered the total uncertainty in the half-life measurements. The larger standard error per determination for the Co^{60} results from inaccuracies in positioning of the external sample.

* This work has been assisted by the joint program of the ONR and AEC.
[1] G. T. Seaborg and I. Perlman, Rev. Mod. Phys. 20, 585 (1948).
[2] J. J. Livingood and G. T. Seaborg, Rev. Mod. Phys. 12, 30 (1940).
[3] J. J. Livingood and G. T. Seaborg, Phys. Rev. 55, 1268 (1939).
[4] Sampson, Ridenour, and Bleakney, Phys. Rev. 50, 382 (1937).
[5] Livingood, Fairbrother, and Seaborg, Phys. Rev. 52, 135 (1937).
[6] J. R. Risser, Phys. Rev. 52, 768 (1937).
[7] J. J. Livingood and G. T. Seaborg, Phys. Rev. 60, 913 (1941).
[8] W. E. Deming, *Statistical Adjustment of Data* (John Wiley and Sons, Inc., New York, 1938).

Conversion Coefficient of the 35-Kev Gamma-Ray of Te^{125}

G. FRIEDLANDER, M. L. PERLMAN, AND G. SCHARFF-GOLDHABER
Chemistry Department and Physics Department, Brookhaven National Laboratory, Upton, Long Island, New York*
October 23, 1950

THE 58-day isomer[1] of Te^{125} is known to decay by a two-step transition.[2] A 109.7-kev transition which is at least 99 percent converted[1] is followed by a partially converted 35.4-kev gamma-ray. The K/L ratio for the 109.7-kev transition was measured by two groups[3,4] as 1.5 and 1.2; the L/M ratio has been reported[3] to be 3.5. The L and M conversion electrons of the 35.4-kev transition were observed in a spectrograph.[5] The K conversion electrons have escaped detection because of their low energies. By a coincidence method, the fraction of the 35.4-kev transitions internally converted (c) was estimated[2] as 0.80 to 0.85, the fraction of the transitions converted in the K shell (c_K) as 0.6 to 0.8. The unconverted 35.4-kev gamma-ray was observed by means of Geiger counters with critical fluorescence and absorption methods.[2]

With the use of a proportional counter and pulse-height analyzer[6] the 35.4-kev gamma-rays have now been measured directly from a pure Te^{125} source prepared by separation from Sb^{125}. Preliminary observations of these gamma-rays were made with an argon-filled counter. For the measurements, a 4-in. diameter brass counter was used which had a beryllium window and was filled to 3 atmos. with 97 percent krypton and 3 percent ethane. The observed pulse-height distribution with peaks representing the $K\alpha$- and $K\beta$-x-rays of tellurium and the 35-kev gamma-ray is shown in Fig. 1. An I^{126} source which gave a Te K x-ray intensity due to K-capture comparable to that from the Te^{125} had a negligible counting rate in the 35-kev region.

The relative peak heights for the K x-rays and the gamma-rays, after corrections for the x-ray fluorescence yield of tellurium, counter window transmission, counter efficiency, and peak position give a ratio of K holes to 35-kev gamma-rays of 17.2. From this ratio and from the previously measured[3,4] conversion fractions $c_{K109}=0.51$, $c_{L109}=0.38$, and $c_{M109}=0.11$ of the 109-kev gamma-ray one can calculate the unconverted fraction $c_{\gamma 35}$ and the K conversion fraction c_{K35} of the 35.4-kev transition provided an assumption is made about the ratio of c_{K35} to the total c_{35}. It will be seen that the value of $c_{\gamma 35}$ is not sensitive to the value assumed for this ratio. If c_{35} is assumed to be $1.1c_{K35}$, then

$$1.1c_{K35}+c_{\gamma 35}=1=c_{109}=1.95c_{K109}. \quad (1)$$

From the measurements above,

$$c_{K35}+c_{K109}=17.2c_{\gamma 35}. \quad (2)$$

Combining (1) and (2) one obtains

$$c_{\gamma 35}=0.153c_{K109}=0.078,$$

and

$$c_{K35}=(1-c_{\gamma 35})/1.1=0.84.$$

If c_{35} is assumed to be $3c_{K35}$, then $c_{\gamma 35}=0.048$ and $c_{K35}=0.32$.

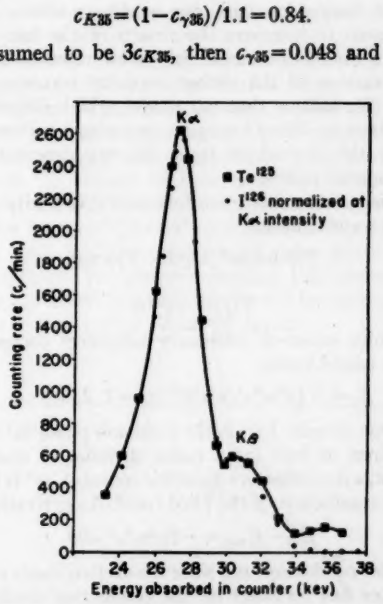

FIG. 1. Proportional counter pulse-height distribution for Te^{125} and I^{126} radiations.

These values and the approximate theoretical values[7,8] for various types of transitions are listed in Table I.

The present experiments establish that the unconverted fraction of the 35.4-kev transitions cannot exceed 0.08 ± 0.01 even if there is no conversion outside of the K shell. According to the theory of internal conversion, the transition therefore is not

TABLE I. Conversion fractions.

	c_{3s}/c_{K3s}	$c_{\gamma 3s}$	c_{K3s}
Electric dipole	1.13[a]	0.23	0.68
Magnetic dipole	1.10[a]	0.12	0.80
Electric quadrupole	3.16[a]	0.018	0.31
Present work	(1.1)[b]	0.078	0.84
Present work	(3)[b]	0.048	0.32

[a] For these calculations conversion in shells higher than the L shell has been neglected.
[b] Assumed values.

electric dipole, but would appear to be a mixture of magnetic dipole and electric quadrupole. This is in agreement with the shell structure model of M. G. Mayer,[9] which predicts a spin change of one unit without parity change.

We wish to thank Miss E. Wilson for valuable assistance.

* Research carried out under the auspices of the AEC.

[1] Friedlander, Goldhaber, and Scharff-Goldhaber, Phys. Rev. 74, 981 (1948).
[2] J. C. Bowe and G. Scharff-Goldhaber, Phys. Rev. 76, 437 (1949).
[3] Hill, Scharff-Goldhaber, and Friedlander, Phys. Rev. 75, 324 (1949).
[4] Kern, Mitchell, and Zaffarano, Phys. Rev. 76, 94 (1949).
[5] R. D. Hill, Phys. Rev. 76, 333 (1949).
[6] Bernstein, Brewer, and Rubinson, Nucleonics 6, No. 2, 39 (1950).
[7] M. H. Hebb and E. Nelson, Phys. Rev. 58, 486 (1940).
[8] S. D. Drell, Phys. Rev. 75, 132 (1949).
[9] M. G. Mayer, Phys. Rev. 75, 1969 (1949).

On the Mechanism of Impurity Band Conduction in Semiconductors

CAVID ERGINSOY
High Voltage Laboratory, Queen Mary College, London, England
October 16, 1950

IN recent letters Hung and Gliessman[1] and Hung[2] have reported on the anomalous low temperature behavior of the resistivity and the Hall coefficient of germanium. Similar anomalies have previously been observed in silicon carbide by Busch and Labhart.[3] In connection with our work[4] on silicon carbide we have attempted to interpret the results of the last authors on the basis of a conduction mechanism in an impurity band formed by the interaction of the *excited* impurity states at high concentrations. We believe that our model, which differs somewhat from that given by Hung,[2] may be used also for germanium and can explain the deviations from the experimental curves of Hung's calculated values.

In a semiconductor with non-interacting impurity centers the Schrödinger wave equation

$$\nabla^2\psi+(2m^*/\hbar^2)(E-V)\psi=0, \tag{1}$$

where

$$V(r)=-e^2/\kappa r \tag{2}$$

has an infinite series of stationary solutions[5] corresponding to the discrete bound states

$$E_n=-2\pi^2m^*e^4/n^2\kappa^2\hbar^2 \quad (n=1, 2, 3, \cdots) \tag{3}$$

of the electron or hole. $V(r)$ is the Coulomb potential between the bound electron or hole (at a radial distance r) and the corresponding ion, κ is an effective dielectric constant, m^* is the effective mass in the conduction or the filled band. An activation energy

$$Ea_0=E_{n=1}=-2\pi^2m^*e^4/\kappa^2\hbar^2 \tag{4}$$

is required for conduction and since the excited states are localized, their presence has no effect on the conduction mechanism. The right-hand portion of Fig. 1 shows the discrete levels of a donor-type impurity atom in a n-type semiconductor.

A wave function ψ_n corresponds to each energy level E_n, whose radial extent increases with n. As the impurity concentration is increased, neighboring atoms approach each other and overlapping begins between ψ_n's of the excited states. These states broaden into quasi-continuous band-like series which partly overlap each other and the conduction band in a manner shown in the central portion of Fig. 1.

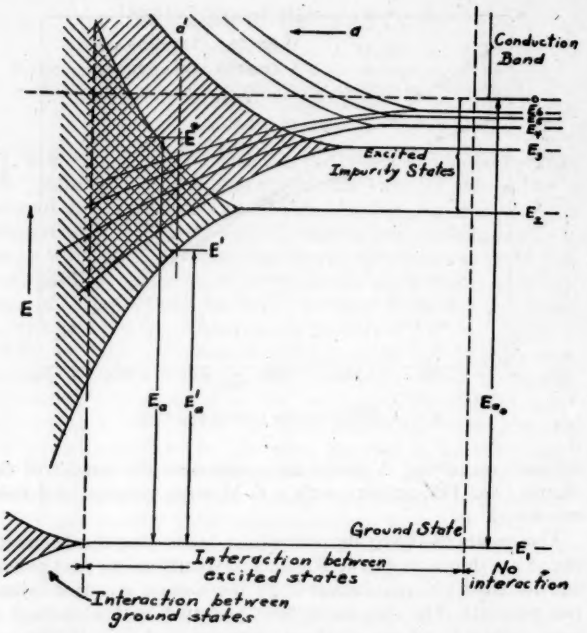

FIG. 1. Schematic representation of the broadening of the discrete impurity states with increasing concentration of donor-type impurity atoms in a n-type semiconductor. The average distance a between neighboring centers decreases in the direction of the arrow. E_a' is the low temperature activation energy giving low mobility electron conduction in the impurity band, E_a is the normal activation energy.

For a given concentration corresponding to an average distance a' between neighboring atoms, *a low temperature activation energy* E_a' may be defined, which is sufficient to take the bound electron from its ground state into a level E' where it can contribute to the conduction with a high but finite effective mass $m'>m^*$ and therefore a low mobility. At higher temperatures a greater number of electrons have higher energies and one can define the *normal activation energy* E_a as that required to take the bound electron into a level E^* (lower for higher impurity concentrations) where the density of the states is such that the effective mass of the electrons approximates to m^*.

The decrease of the normal activation energy E_a with increasing impurity concentration, first recognized theoretically by Shifrin,[6] has been observed in a large number of semiconductors including silicon[7] and germanium[8] but no satisfactory theory has been put forward so far. The existence of a lower activation energy E_a' affecting the low temperature behavior has not previously been considered. Hung and Gliessman's experimental curves of logρ *vs.* $1/T$ and log$R$ *vs.* $1/T$ at very low temperatures show small but definite slopes which indicate the presence of an activation energy. In Hung's interpretation of the impurity band conduction this energy is neglected and the calculated curves of the resistivity ρ and the Hall coefficient R are both flat. The approximate agreement obtained by Hung is based on the assumption that the carriers in the impurity band in an n-type crystal are electrons and those in a p-type crystal are holes. In our model this is explained by the fact that the impurity band formed by the excited states in an n-type crystal is empty at 0°K and partially filled at higher temperatures, so that conduction is of the electron type. The objections to a model which attributes conducting properties to a donor band in such a crystal are that: (a) the broadening of the ground states into a donor band requires very strong interaction between neighboring centers, i.e. very high concentrations, and (b) since such a donor band is completely filled at 0°K, any conduction at higher temperatures must be of the hole type.

A further point which our model may clear up in the case of germanium is the source of the extra scattering ions which Hung and Johnson[9] introduce in order to explain the resistivity curves at temperatures above that at which the anomaly begins. They

attribute this resistivity to the Rutherford scattering by impurity ions[10] of concentration $N_s=n+N_0$, where n is the concentration of the conduction carriers and N_0 is provided by the loss of electrons from donor levels to lower lying acceptor levels. This model requires that the concentrations of donors and acceptors in a high resistivity sample should be nearly equal. This condition is not necessarily satisfied in practice. Such an assumption is not needed, however, if it is considered that in germanium, due to a small activation energy E_a', a large number of carriers are found in the conducting impurity band described above, so that an equal number of ions are provided which can act as scattering centers. The resistivity curves may therefore be explained satisfactorily on the basis of a single type of impurity.

[1] C. S. Hung and J. R. Gliessman, Phys. Rev. 79, 726 (1950).
[2] C. S. Hung, Phys. Rev. 79, 727 (1950).
[3] G. Busch, Helv. Phys. Acta 19, 167 (1946). G. Busch and H. Labhart, Helv. Phys. Acta 19, 463 (1946).
[4] C. Erginsoy (to be published).
[5] N. F. Mott and R. W. Gurney, *Electronic Processes In Ionic Crystals*, 2nd Ed. (Oxford University Press, London, 1948), p. 81.
[6] K. Shifrin, J. Phys. U.S.S.R. 8, No. 4,242 (1944); J. Tech. Phys. U.S.S.R. 14, No. 1–2, 43 (1944).
[7] G. L. Pearson and J. Bardeen, Phys. Rev. 75, 865 (1949).
[8] G. L. Pearson and W. Shockley, Phys. Rev. 71, 142 (1947).
[9] C. S. Hung and V. A. Johnson, Phys. Rev. 79, 535 (1950).
[10] E. Conwell and V. F. Weisskopf, Phys. Rev. 77, 388 (1950).

X-Ray Study of the Phase Transition in Lead Titanate

GEN SHIRANE, SADAO HOSHINO, AND KAZUO SUZUKI
Tokyo Institute of Technology, Oh-okayama, Tokyo, Japan
October 23, 1950

IN a preceding note,[1] we have reported that the solid solution of $BaTiO_3$ and $PbTiO_3$ has the same type of crystal structure as that of $BaTiO_3$, and its tetragonality increases with lead contents, accompanying the rise of Curie temperature. Lead titanate has a larger tetragonality and a higher Curie temperature (*ca.* 490°C) compared with those of $BaTiO_3$. It may be expected that this crystal also transforms to cubic structure at the Curie point as in the case[2] of $BaTiO_3$. To examine this behavior precisely, we have performed an x-ray study on the temperature change of lattice parameters.

We used the ceramic specimens prepared by sintering the mixture of PbO and TiO_2 at about 1100°C. These ceramics were pulverized to fine powder and sealed in a very thin capillary tube made of hard glass (diameter=0.5 mm). The Debye photographs were taken at temperatures from 30 to 535°C, using CuK_α-radiation. The camera length is 55.5 mm. The precise lattice constants and the axial ratio were calculated mainly from (143) and (134) lines on photographs taken by the back reflection method. These results are shown in Figs. 1 and 2.

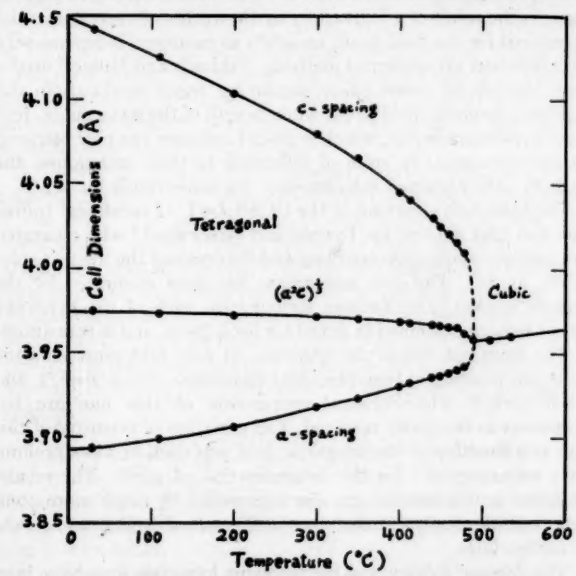

FIG. 1. Lattice parameters as a function of temperature.

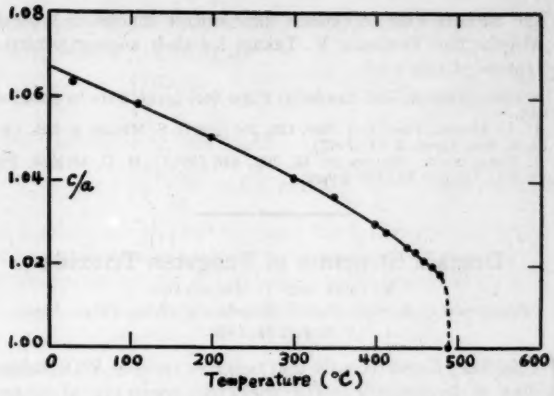

FIG. 2. Axial ratio as a function of temperature.

The photograph at 30°C clearly shows the tetragonal structure with $a=3.894$A, $c=4.140$A, and $c/a=1.063$. These results are in agreement with those of other authors.[3] When the temperature is raised, this axial ratio decreases gradually until the structure changes to a cubic lattice at about 490°C, in accordance with our permittivity measurement. At 535°C, the lattice constant $a=3.960$A.

It is remarkable that, as is shown in Fig. 3, the volume of unit cell does not increase but decreases slightly with the temperature rise, and during the transitional region it diminishes nearly discontinuously by the amount $\Delta v/v=4.4\times10^{-3}$; i.e., 0.27A³ per unit cell. It seems reasonable to suppose that the thermal expansion of $BaTiO_3$-type ferroelectrics is a superposition of the normal expansion and abnormal contraction which is caused by the temperature change of polarization. It seems that in this crystal the latter effect is large enough to cover the former. The volume expansion coefficient of this crystal is given approximately by $\alpha=-1.6\times10^{-6}$/deg. in the tetragonal region, and $\alpha=2.5\times10^{-6}$/deg. in the cubic region. A preliminary dilatometric measurement is in good agreement with the x-ray data.

After all, it will probably be said that the phase transition in $PbTiO_3$ is of the barium titanate type, but is more drastic in several points. In addition, we have measured the permittivity at temperatures from −170 to 550°C, and found only one transition, in contrast with $BaTiO_3$, which shows three transitions in this temperature range. We are now studying the anomalous specific heat at this transition. Detailed results will be reported shortly in the *Journal of the Physical Society of Japan*.

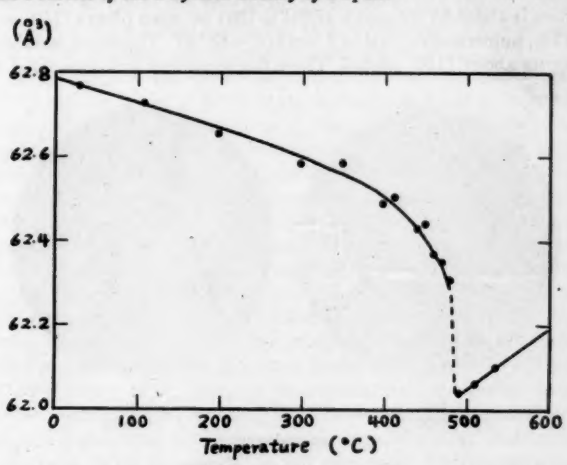

FIG. 3. Unit cell volume as a function of temperature.

The authors wish to express their sincere thanks to Professor S. Miyake and Professor Y. Takagi for their encouragement in the course of this work.

[1] Shirane, Hoshino, and Suzuki, J. Phys. Soc. Japan 5 (to be published) (1950).
[2] H. D. Megaw, Proc. Roy. Soc. 189, 261 (1947). S. Miyake and R. Ueda, J. Phys. Soc. Japan 2, 93 (1947).
[3] I. Naray-Szabo, Naturwiss. 31, 202, 446 (1943). H. D. Megaw, Proc. Phys. Soc. London 58, 133 (1946).

Domain Structure of Tungsten Trioxide

R. UEDA AND T. ICHINOKAWA
Department of Applied Physics, Waseda University, Tokyo, Japan
August 22, 1950

IT has been found recently that tungsten trioxide, WO_3, behaves like a ferroelectric.[1] The dielectric constants of sintered ceramics or monocrystals are high compared with those of ordinary solid materials, being 100 to 300 at low temperature and of the order of 10^3 at room temperature. Though the tartrate, dihydrogenphosphate, and barium titanate are found to be analogous to a ferromagnetic, for example, to obey the Curie-Weiss law and to show the multiple domain structure, it is not certain whether WO_3 corresponds to this case.

The present authors obtained single crystals of WO_3 from the melt and were able to observe the details of the multiple domain structure which exhibits phenomena similar to those of $BaTiO_3$.[2] Optical and x-ray observation showed that the crystal has a pseudo-orthorhombic symmetry; $a=7.278$A, $b=7.460$A, $c=3.838$A, and $\beta\sim 90°$ which coincide with the values reported earlier.[3] The flat plate of monocrystal obtained was usually smaller than $1\times 1\times 0.1$ mm^3 in dimensions, with the orthorhombic c-axis parallel to the shortest edge. In many cases each crystal is composed of multiple domains divided by parallel stripes which are oriented at an angle 45° to the plate edges, or sometimes parallel to them.

In some cases, however, the crystal appears almost transparent with faint lines. These domain patterns, which are very like the twinned structure of $BaTiO_3$, are shown in Fig. 1a.

A microscopic inspection reveals that the neighboring twin components show pleochroism when observed by rotating the microscopic stage. When the direction of vibration of the polarized light coincides with one of the plate edges of the monocrystal, the contrast between light and dark fields is largest. This indicates the orthogonality of X'-directions for the neighboring twins.

Between crossed Nicols, an extinction effect is observed at positions at which one of the plate edges coincides with the directions of vibration of the polarized light. That is, the a- (or b-) axis in one domain component is perpendicular to the a- (or b-) axis in the neighboring components. In addition, there exist many fine striations parallel to the plate edges, which are nearly orthogonal with each other for neighboring twins (Fig. 1a). The angle between them is about 88°30′ and is equal to that between planes (110) and $(1\bar{1}0)$, numerically equal to $2\tan(b/a)=88°36'$. Therefore, twininng occurs about {110} planes. These fine striations are considered to be a kind of the crystal habit which specify the a- or b-axis in the orthorhombic lattice.

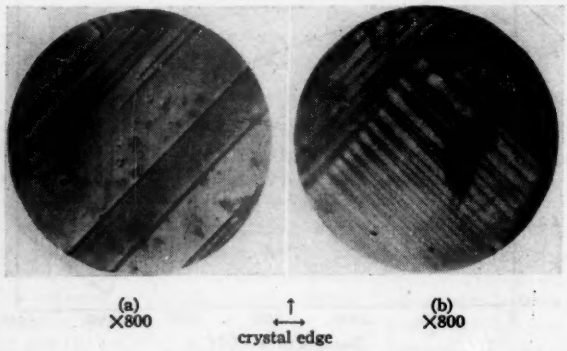

FIG. 1. Multiple domain structure of WO_3. (a) Domains divided by parallel strips. (b) Wedge-shaped domains.

Wedge-shaped domains like those of $BaTiO_3$ are also observed (Fig. 1b). In addition there exists fork- or scissors-shaped domains which are variable in shape, corresponding to the stress existing in the crystal. The breadth of the parallel components is about 0.01 to 0.004 mm, which is comparable to those of $BaTiO_3$.

When an unidirectional pressure is applied along one of the plate edges, some twins grow in volume by a migration of the twin boundary and wedge-shaped domains disappear gradually. At a fairly large pressure, irreversible boundary migration occurs, giving a crystal without domains. Temperature and electric field seemed to have no distinct effect upon the domain pattern.

X-ray studies of the powder samples and single crystals indicate that there exists no remarkable change in reflections above room temperature, except slight change in intensity above 120°C in the region of high Bragg angle.

It seems that there is no phase change like that of $BaTiO_3$ for which a transition occurs from a low symmetry type to a high symmetry one at the Curie temperature.

The details of the investigation will be reported elsewhere.

[1] B. T. Matthias, Phys. Rev. 76, 430 (1949).
[2] Recently Hirakawa reported the microscopic observation of the domain structure for WO_3. Busseiron-Kenkyu (in Japanese), No. 26 (1950).
[3] H. Breakken, Zeits. f. Krist. 78, 484 (1931).

Nuclear Magnetic Moment of S^{33}

J. R. ESHBACH AND R. E. HILLGER
Research Laboratory of Electronics, Massachusetts Institute of Technology, Cambridge, Massachusetts*
AND
C. K. JEN
Cruft Laboratory,† Harvard University, Cambridge, Massachusetts
October 20, 1950

SEVERAL attempts have been made[1-4] to determine the nuclear magnetic moment of S^{33} by the Zeeman effect on the microwave rotational spectra of OCS^{33}. Jen[1,2] first set for $\mu(S^{33})$ a broad range between 0.6 and 0.9 n.m., but there has not been good agreement on a more exact value. The difficulties encountered appeared to lie principally in the low intensities of the hyperfine lines at the low natural abundance of S^{33} and the uncertainty of the sign of the OCS rotational g-factor.

Recently, a sample of sulfur containing an isotopic abundance of 5.54 percent of S^{33} (7.5 times natural abundance), loaned by the Isotopes Division of the AEC, has made possible a re-examination of the problem under much more favorable conditions. The present paper is the result of a joint effort by the authors to reach essential agreement for the final result on $\mu(S^{33})$ as measured independently with different experimental methods. Eshbach and Hillger[4] used a short section of wave guide employing Stark modulation and applied a magnetic field to the whole length of the wave guide. Jen[5] used a resonant cavity, which is placed between the pole pieces of an electromagnet. In spite of difference in their techniques, the authors have obtained substantially the same result for $\mu(S^{33})$.

The hyperfine structure of the OCS^{33} $J=1\rightarrow 2$ rotational transition was first studied by Townes and Geschwind,[6] who measured the nuclear quadrupole coupling and determined the nuclear spin, $I(S^{33})$, as 3/2. The spin assignment has been confirmed by the present studies. The Zeeman splitting for each of the hyperfine lines has been examined in detail for both the π- and σ-transitions.

The strongest line in the spectrum at zero field represents the joint contribution of two coincident transitions: $F=3/2\rightarrow 5/2$, and $F=5/2\rightarrow 7/2$. The Zeeman components of this line are too numerous to be clearly resolved. The variation of intensity of this line as a function of the magnetic field was used in some preliminary experiments[2,4] for the determination of $\mu(S^{33})$. The results obtained in this manner are now superseded by much more accurate results derived from the well-resolved splittings of the hyperfine lines.

The Zeeman splittings of the following hyperfine lines have been examined: $F=1/2\rightarrow 3/2$, $5/2\rightarrow 5/2$, $1/2\rightarrow 1/2$, $3/2\rightarrow 3/2$, and

3/2→1/2. In each instance, there were at least two strong and well-resolved components. The frequency differences between these components have been measured with good accuracy.

It has been found that the observed Zeeman spectra of the OCS^{33} $J=1\rightarrow2$ hyperfine structure are completely consistent with theory[5,7] if $|g_N|=0.421$, $|g_{mole}|=0.026$, and g_{mole} and g_N have opposite signs. Here, g_N is the S^{33} nuclear g-factor and g_{mole} is the rotational g-factor for OCS. The quantity g_{mole} determined here is consistent with the value of g_{mole} determined directly from the OCS^{32} Zeeman spectrum.

In an attempt to establish the absolute signs of the g-factors, Eshbach[8] has used an arrangement providing a circularly polarized wave and succeeded in proving that the absolute signs of g_N and g_{mole} are respectively positive and negative.

Using $g(N_{33})=0.421$ and $I=3/2$, the final result for the nuclear magnetic moment of S^{33} is

$$\mu(S^{33})=0.632\pm0.010 \text{ n.m.}$$

This result is within the Schmidt limits and is in agreement with the prediction of the single particle model of nuclear shell structure.

The authors acknowledge their indebtedness to the Isotopes Division of the U. S. Atomic Energy Commission for the loan of the S^{33}—enriched sample.

* This work was supported in part by the Signal Corps, the Air Materiel Command, and ONR.
† This work was supported by the U. S. Navy, Signal Corps, and Air Force under ONR contract.

[1] H. L. Poss, *The Properties of Atomic Nuclei*, Brookhaven National Laboratory, October, 1949, p. 11, unpublished.
[2] C. K. Jen, Phys. Rev. **78**, 339 (1950).
[3] J. E. Mack, Rev. Mod. Phys. **22**, 65 (1950).
[4] J. R. Eshbach and R. E. Hillger, Quarterly Progress Report, Research Laboratory of Electronics, M.I.T., pp. 42–43, July, 1950, unpublished.
[5] C. K. Jen, Phys. Rev. **74**, 1396 (1948); Phys. Rev. **76**, 1494 (1949).
[6] C. H. Townes and S. Geschwind, Phys. Rev. **74**, 626 (1948).
[7] F. Coester, Phys. Rev. **77**, 454 (1950).
[8] A complete report of this work will be published later.

Angular Dependence of Hyperfine Structure for the Copper Ion

E. F. Carr and C. Kikuchi
Department of Physics and Astronomy, Michigan State College, East Lansing, Michigan
October 25, 1950

SHORTLY after the discovery of hyperfine structure in solids by Penrose, it was found by a number of independent workers[1] that the experimental results are not in agreement with the theoretical deductions, if one assumes that the electron-orbit-nuclear spin and electron-spin-nuclear spin terms are responsible for the hyperfine separation. A careful experimental investigation by Ingram[2] has accentuated the discrepancy between theory and experiment. Recently Abragam[3] has proposed a theory to account for the experimental results. We would like to suggest in this note another term which is perhaps partly responsible for the angular dependence of hyperfine structure.

A new interaction term was suggested to us by the recent work of England and Schneider[4] who investigated the absorption properties of the Mn^{++} ion as activators in zinc sulfide phosphors. The spectroscopic ground state of the ion is ${}^6S_{5/2}$, and therefore the interaction terms used for the Cu^{++} ion will give no contribution to the separation. To account for the observed hyperfine splitting it is necessary to use a term[5] of the form $a_2\mathbf{S}\cdot\mathbf{I}$. Since the d electrons are responsible for the spin in both copper and manganese, we have investigated the consequences of assuming that a_2 is approximately the same for copper and manganese. We have used the interaction potential

$$H'=-a_1\mathbf{L}\cdot\mathbf{I}+a_1\left\{\frac{3(\mathbf{S}\cdot\mathbf{r})(\mathbf{I}\cdot\mathbf{r})}{r^2}-\mathbf{I}\cdot\mathbf{S}\right\}-a_2\mathbf{S}\cdot\mathbf{I}+\gamma\mathbf{H}\cdot\mathbf{I}.$$

This expression differs from that taken by others in that the signs of the first two terms are different, and that the additional $\mathbf{S}\cdot\mathbf{I}$ term is introduced.

It follows from fairly general group-theoretical considerations that for a doubly degenerate electron ground state the above interaction potential leads to the following term values:

$$E^+=(g_{\parallel}^2\cos^2\theta+g_{\perp}^2\sin^2\theta)^{\frac{1}{2}}\mu_BH+\left[\left(\frac{\Delta\nu_{\parallel}g_{\parallel}}{2g}+\gamma H\right)^2\cos^2\theta+\left(\frac{\Delta\nu_{\perp}g_{\perp}}{2g}+\gamma H\right)^2\sin^2\theta\right]^{\frac{1}{2}}m_I,$$

$$E^-=-(g_{\parallel}^2\cos^2\theta+g_{\perp}^2\sin^2\theta)^{\frac{1}{2}}\mu_BH-\left[\left(\frac{\Delta\nu_{\parallel}g_{\parallel}}{2g}-\gamma H\right)^2\cos^2\theta+\left(\frac{\Delta\nu_{\perp}g_{\perp}}{2g}-\gamma H\right)^2\sin^2\theta\right]^{\frac{1}{2}}m_I.$$

The symbols $\Delta\nu^{\parallel}$ and $\Delta\nu^{\perp}$ represent the hyperfine structure component separations in a parallel and perpendicular magnetic field. For the particular case of Cu^{++} these quantities are given by

$$\Delta\nu_{\parallel}=2a_1[-4p+(2/7)-3q/7]+a_2,$$
$$\Delta\nu_{\perp}=2a_1[-q-(1/7)+3q/14]+a_2/2,$$

where the p and q are certain coefficients appearing in Polder's[6] wave functions and are related to the g values by $g_{\parallel}=2(1-4p)$ and $g_{\perp}=2(1-q)$.

The results of the above equation can be used to determine the relative values of a_1 and a_2. For the g values we take $g_{\parallel}=2.44$ and $g_{\perp}=2.06$. Ingram gives $\Delta\nu_{\parallel}/\Delta\nu_{\perp}=g_{\parallel}\Delta H_{\parallel}/g_{\perp}\Delta H_{\perp}=8.3$. These numerical values lead to $a_1=0.88a_2$. The average separation of adjacent lines in manganese is 68 gauss which corresponds to an energy separation of $2\mu_B\Delta H=1.25\times10^{-15}$ erg. For a copper ion in a parallel field $\Delta\nu_{\parallel}=g_{\parallel}\mu_B\Delta H=a_1+a_2$. Assuming that a_2 is the same for both copper and manganese we obtain $\Delta H=118$ gauss, which gives an over-all separation of 354 gauss. This value is in good agreement with Ingram's value of 350 gauss.

After completing this investigation we have heard indirectly that J. M. Jauch has come to similar conclusions.

[1] Penrose, Abragam, and Pryce, Nature **163**, 992 (1949); L. J. F. Broer, Physica **15**, 673 (1949); C. Kikuchi and R. D. Spence, Am. J. Phys. **18**, 167 (1950).
[2] D. J. E. Ingram, Proc. Phys. Soc. London **A62**, 664 (1949).
[3] A. Abragam, Phys. Rev. **79**, 534 (1950).
[4] T. S. England and E. E. Schneider, Nature **166**, 437 (1950).
[5] H. A. Bethe, *Handbuch der Physik*, second edition Vol. **24/1**, p. 386 (1933).
[6] D. Polder, Physica **9**, 709 (1942).

Spin-Spin Interaction within Paramagnetic Ions

M. H. L. Pryce*
Clarendon Laboratory, Oxford, England
October 30, 1950

THAT the magnetic spin-spin interaction (W_{SS}, say) between pairs of electrons in an atom can cause deviations from the Landé interval rule is well known in spectroscopy. The effect is usually relatively small, although in helium it completely distorts the triplet terms. The purpose of this letter is to point out its possible role in the microwave resonance behavior of certain paramagnetic salts. The cases of interest occur where the splitting of the lowest spin multiplet of the paramagnetic ion, due to the combined action of the crystalline potential V and the spin-orbit interaction W_{LS}, either vanishes to second order in W_{LS}, or is very small. The splitting may then be dominated by W_{SS}.

In the salts of the iron transition group the ions Mn^{++} and Fe^{+++}, which are in a $3d^5$ ${}^6S$ state, furnish examples of interest. Their splitting has been studied by Van Vleck and Penney,[1] who consider various higher order processes involving V and W_{LS} through intermediate excited electronic states, using order of magnitude arguments to estimate the resulting splitting: but detailed calculation shows that their estimates are too high and that the mechanisms they propose are inadequate to explain the observed splittings. The important mechanisms would actually appear to be (a) a second-order process involving the first powers of W_{SS} and $V_2=H'(2z^2-x^2-y^2)$ via the intermediate state $3d^44s$ ${}^6D$, giving a contribution DS_z^2 to the sub-Hamiltonian, and (b) a fifth-order process, quartic in W_{LS} and linear in $V_4=-G'(x^4+y^4+z^4+3y^2z^2-3z^2x^2-3x^2y^2)$, through intermediate states formed from $3d^5$, giving a contribution $(a/6)(S_x^4+S_y^4+S_z^4)$. Experimental evidence indicates that (a) dominates in manganous salts,[2] and (b) in ferric salts.[3] This changeover is not surprising, for (b) increases with a very high power of the effective nuclear charge of the ion.

TABLE I. Values of ρ from spectroscopic data.

Ion	State	ρ/cm^{-1}	Reference
Ti^{++}	$3d^2\ ^3F$	0.24 ± 0.03	a
V^{++}	$3d^3\ ^4F$	$0.4\ \pm0.1$	a
V^{+++}	$3d^2\ ^3F$	0.24 ± 0.05	a
Cr^{++}	$3d^4\ ^5D$	0.42 ± 0.05	b
Cr^{+++}	$3d^3\ ^4F$	0.44 ± 0.05	c
Mn^{+++}	$3d^4\ ^5D$	$0.8\ \pm0.2$	c
Fe^{++}	$3d^6\ ^5D$	0.95 ± 0.1	d
Co^{++}	$3d^7\ ^4F$	1.50 ± 0.05	e
Ni^{++}	$3d^8\ ^3F$	5.31 ± 0.03	e

[a] Atomic Energy Levels, Circular 467, National Bureau of Standards (1949).
[b] F. L. Moore, Princeton thesis (1950).
[c] I. S. Bowen, Phys. Rev. 52, 1153 (1937).
[d] B. Edlen and P. Swings, Astrophys. J. 95, 532 (1942).
[e] A. G. Shenstone, unpublished.

Detailed calculation shows that the coefficient D arising from (a) is given by

$$D=\frac{6}{25}\left(\frac{eh}{mc}\right)^2\frac{eH'}{\Delta E}(3w-2v)\int r^4\psi_d(r)\psi_s(r)dr, \qquad (1)$$

where

$$v=\int_0^\infty\frac{1}{r}\psi_d(r)\psi_s(r)\int_0^r r'^2\psi_d^2(r')dr'dr,$$

$$w=\int_0^\infty\frac{1}{r^3}\psi_d^2(r)\int_0^r r'^4\psi_d(r')\psi_s(r')dr'dr.$$

Here ψ_d and ψ_s are the radial wave functions of the $3d$ and $4s$ electrons, and ΔE is the energy of $3d^44s\ ^6D$ above $3d^5\ ^6S$. It is difficult to estimate the integrals, which depend strongly on the overlap of ψ_d and ψ_s, but reasonable assumptions give the right order of magnitude ($D\sim0.02\ \text{cm}^{-1}$).

In the other ions of the iron group W_{SS} has diagonal elements within the ground term, representable by a sub-Hamiltonian quadratic in S, and which from arguments of rotational covariance must have the form

$$W_{SS}=-\rho\{\tfrac{1}{2}L_iL_j+\tfrac{1}{2}L_jL_i-\tfrac{1}{3}L(L+1)\delta_{ij}\}S_iS_j$$
$$=-\rho\{(\mathbf{L}\cdot\mathbf{S})^2+\tfrac{1}{2}(\mathbf{L}\cdot\mathbf{S})-\tfrac{1}{3}LS(L+1)(S+1)\}. \qquad (2)$$

One finds, for the lowest term,

$$\rho=\frac{1}{7S(2L-1)}\left(\frac{eh}{mc}\right)^2\left\{(4S-5)p+\frac{1}{7}(100-62S)q\right\}, \qquad (3)$$

where

$$p=\int_0^\infty\frac{1}{r}\psi_d^2(r)\int_0^r r'^2\psi_d^2(r')dr'dr,$$

$$q=\int_0^\infty\frac{1}{r^3}\psi_d^2(r)\int_0^r r'^4\psi_d^2(r')dr'dr.$$

If hydrogen-like wave functions with effective nuclear charge Z' are used to calculate p and q, the result is

$$p=12q/7=(11/25920)(Z'me^2/\hbar^2)^2.$$

Second-order effects from W_{LS} via other terms of the $3d^n$ configuration will also give contributions of the form (2), which will add to (3), and in the second half of the transition series they may be larger than the W_{SS} contribution.

In chromous and manganic salts ($3d^4\ ^5D$) the splitting of the spin quintet which is left lowest by the crystalline field is probably mainly determined[4] by W_{SS}. In chromic and vanadous salts ($3d^3\ ^4F$), and nickel salts ($3d^8\ ^3F$), the term in ρ, and also a mechanism analogous to (a), may contribute appreciably to the splitting, and previous estimates of the magnitude of V_2 from the splitting should be treated with reserve.

In some cases ρ can be inferred from the departures from the interval rule in spectroscopic data. These are listed in Table I.

I wish to thank Mr. Martin Redlich for help in the calculations of the coefficients in (1) and (3).

* Present address: Palmer Physical Laboratory, Princeton University, Princeton, New Jersey.
[1] J. H. Van Vleck and W. G. Penney, Phil. Mag. 17, 961 (1934).
[2] B. Bleaney and D. J. E. Ingram, Proc. Roy. Soc. A (to be published).
[3] Weidner, Weiss, Whitmer, and Blosser, Phys. Rev. 76, 1727 (1949); D. Bijl, Leiden thesis, Excelsiors Foto Offset, s'Gravenhagen (1950).
[4] A. Abragam and M. H. L. Pryce, Proc. Roy. Soc. A (to be published).

The New Isotope Pu^{242} and Additional Information on Other Plutonium Isotopes

S. G. THOMPSON, K. STREET, JR., A. GHIORSO, AND F. L. REYNOLDS
Radiation Laboratory and Department of Chemistry, University of California, Berkeley, California*
October 20, 1950

INVESTIGATION of the higher isotopes of plutonium produced by neutron irradiation has revealed the existence and properties of a new plutonium isotope, namely Pu^{242}, and has also yielded some additional information about the previously reported isotopes Pu^{240} and Pu^{241}. This letter will give only a brief report of these new results and a detailed description of the experiments will be deferred until a later date. The investigation of these isotopes was made possible by the intensive irradiation with neutrons of plutonium and americium samples originally consisting essentially completely of the isotopes Pu^{239} and Am^{241}, respectively. The production of Pu^{240} and Pu^{241} by the neutron irradiation of Pu^{239} has been reported previously.[1] Following the irradiation of the samples, which occurred over periods up to a few years, the plutonium, americium, and curium were chemically separated from each other and from fission products and impurities. The isotopic composition of each plutonium sample was then determined by use of a mass spectrograph which employed a thermal ionization source. Lines corresponding to plutonium isotopes of masses 241 and 242 produced by (n,γ) reactions were observed in addition to lines due to the other well-known plutonium isotopes (Pu^{238}, Pu^{239}, and Pu^{240}).

Pu^{240}.—Using very thin samples formed by volatilization from a hot filament, the width of the observed alpha-pulse analysis peak corresponding to the alpha-particles in a sample containing the two isotopes Pu^{239} and Pu^{240} was such that there is not more than about 20-kev difference in the alpha-particle energies of these two isotopes. Therefore, the alpha-particle energy[2] of Pu^{240} is 5.16 ± 0.02 Mev.

Pu^{241}.—A low abundance group of alpha-particles at the energy 4.91 ± 0.03 Mev was observed in neutron-bombarded plutonium using the 48-channel differential alpha-energy pulse analyzer. This group is present in the amount expected if it is due to the isotope Pu^{241}, i.e., best agreement with the alpha-decay systematics[3] is obtained if it is due to Pu^{241}, and it cannot be due to Pu^{242} in view of the results discussed below. To be a low energy alpha-group of the isotope, Pu^{240}, its abundance would apparently be greater by a factor[4] of 5 to 10. If this alpha-particle group is ascribed to Pu^{241}, its alpha-intensity and isotopic abundance lead to a partial half-life of Pu^{241} for alpha-particle decay of roughly 4×10^5 years in agreement with previous results.[5]

The half-life of Pu^{241} for beta-particle decay was estimated from the growth of the daughter Am^{241} using tracer Cm^{242} to determine chemical yield in the separations of the Am^{241} from the plutonium. The separations were made with measured amounts of plutonium in which the daughter had been allowed to grow over successively measured intervals of time. Using the mass spectrographically determined value for the isotopic abundance of Pu^{241} in the plutonium, and a value of 475 years for the half-life[6] of Am^{241}, the half-life of the Pu^{241} for beta-decay was calculated as 14 years, which is in rough agreement with the previous value[5] ($\sim$10 years).

A rough estimate of the cross section for the reaction $Pu^{241}(n,\gamma)Pu^{242}$ with pile neutrons was obtained using an estimated value for the neutron flux and the isotopic compositions determined in the mass spectrograph. The cross section so obtained was very roughly 250 barns, but it is subject to large error owing to uncertainty in the estimation of the neutron flux.

Pu^{242}.—The isotope Pu^{242} was observed in a mass spectrographic analysis of neutron-bombarded plutonium, but its abundance was too small to make it possible to identify the radioactive decay properties in such samples. However, O'Kelley, Crane, Barton, and Perlman[7] have observed that the 16-hour Am^{242m} undergoes appreciable branching decay through the electron capture process. Advantage was taken of this by separating a plutonium fraction from a sample of americium (Am^{241}) which had been bombarded

with neutrons for several months. Mass spectrographic analysis of the total plutonium produced during the irradiation showed that it consisted of about 50 percent Pu^{242} and 50 percent Pu^{238}, the former produced by the electron capture decay of Am^{242m} and the latter through the decay chain $Am^{242m}(\beta^-/16\text{ hr.}) > Cm^{242}(\alpha/162\text{ days}) > Pu^{238}$. Alpha-pulse analysis of this plutonium showed the presence of alpha-particles of 4.88 Mev in abundance corresponding to a half-life of roughly 5×10^6 years for Pu^{242}. This energy and half-life agrees well with those expected for Pu^{242} from the alpha-decay systematics, which also indicate that this isotope should be beta-stable. A smaller sample of daughter plutonium containing a higher proportion of Pu^{242} with respect to Pu^{238} was obtained by separating plutonium from a sample of 16-hour Am^{242m} which was initially free of plutonium and which was allowed to decay for about a day. The alpha-pulse analysis of this sample also showed the 4.88-Mev alpha-particle of Pu^{242}, in this case present in greater relative abundance as expected.

We wish to acknowledge the advice and assistance of Professor Glenn T. Seaborg, whose help contributed greatly to the success of this work.

The successful handling in a safe manner of the radioactivity involved was made possible through the operation and use of remote control equipment and excellent protective devices provided by Nelson Garden and the members of his Health Chemistry group. In this connection we especially wish to thank C. M. Gordon, W. G. Ruehle, and J. M. Davis for assistance during the experiments.

* This work was performed under the auspices of the AEC.

[1] Ghiorso, James, Morgan, and Seaborg, Phys. Rev. **78**, 472 (1950).
[2] G. T. Seaborg and I. Perlman, Rev. Mod. Phys. **20**, 585 (1948).
[3] Perlman, Ghiorso, and Seaborg, Phys. Rev. **77**, 26 (1950).
[4] I. Perlman and T. Ypsilantis, Phys. Rev. **79**, 30 (1950).
[5] Seaborg, James, and Morgan, *The Transuranium Elements: Research Papers* (McGraw-Hill Book Company, Inc., New York, 1949), Paper No. 22.1, National Nuclear Energy Series, Plutonium Project Record, Vol. 14B.
[6] Cunningham, Thompson, and Lohr, unpublished work (1949).
[7] O'Kelley, Barton, Crane, and Perlman, Phys. Rev. **80**, 293 (1950).

The *S*-Matrix in Meson Theory

NING HU
National Research Council, Ottawa, Canada
September 6, 1950

IT has been shown by Dyson[1] that there are only a few types of "primitive divergent graphs" in quantum electrodynamics (different types being specified by different values of E_n and E_m defined below). This result leads to the separation of the divergence from the *S*-matrix obtained by conventional perturbation method. We shall now extend the investigation to the meson theory. We first consider the pseudoscalar meson under pseudovector coupling with the nucleons. Let us consider any primitive graph with n vertices, E_n external nucleon lines, and E_m external meson lines. The numbers of internal nucleon and meson lines are respectively $F_n=n-E_n/2$ and $F_m=(n-E_m)/2$. The contribution of this graph to the *S*-matrix is an integral M which contains F_n factors of the form $S_F(\mathbf{k}_i)=(\mathbf{k}_i+m)/(\mathbf{k}_i^2-m^2)$ and F_m factors of the form $D_F(\mathbf{k}_j)=1/(\mathbf{k}_j^2-\kappa^2)$ and $n-E_m$ factors $g\gamma_5\mathbf{k}_j$ integrated over $d^4k_1d^4k_2\cdots d^4k_F$, where $F=F_n+F_m-n+1$, g is the interaction constant, κ and m are the masses of the meson and nucleon. The bold type letter $\mathbf{k}$ stands for $\gamma_\mu k_\mu$. M will be convergent if

$$2E_m+\tfrac{3}{2}E_n-n-4\geqslant 1. \tag{1}$$

(1) will always be violated for any given values of E_n and E_m if n is big enough. This means that the number of types of primitive divergent graphs is infinite. It is the aim of the present note to show that we can still separate the divergence from the *S*-matrix.

The self-energy integral of the meson of the lowest order g^2 is

$$M_s=-\frac{g^2}{\pi i}\int Sp\left[\gamma_5\mathbf{k}\frac{\mathbf{p}-\frac{1}{2}\mathbf{k}+m}{(\mathbf{p}-\frac{1}{2}\mathbf{k})^2-m^2}\gamma_5\mathbf{k}\frac{\mathbf{p}+\frac{1}{2}\mathbf{k}+m}{(\mathbf{p}+\frac{1}{2}\mathbf{k})^2-m^2}\right]d^4p. \tag{2}$$

For free meson we have $\mathbf{k}^2=\kappa^2$. For virtual mesons k_μ are four independent variables of integration. We shall consider the general case in which $\mathbf{k}^2\neq\kappa^2$. Noticing that γ_5 anti-commutes with γ_μ and $\gamma_5\gamma_5=1$, we have

$$M_s=-\frac{g^2}{\pi i}k_\mu k_\nu\int Sp\left[\gamma_\mu\frac{\mathbf{p}-\frac{1}{2}\mathbf{k}-m}{(\mathbf{p}-\frac{1}{2}\mathbf{k})^2-m^2}\gamma_\nu\frac{\mathbf{p}+\frac{1}{2}\mathbf{k}+m}{(\mathbf{p}+\frac{1}{2}\mathbf{k})^2-m^2}\right]d^4p. \tag{3}$$

Since the spur of an odd number of factors of γ_μ vanishes, the term linear in m must vanish. Equation (3) can therefore be written as

$$M_s=k_\mu k_\nu K_{\mu\nu}+\frac{2g^2}{\pi i}k_\mu k_\nu\int Sp(\gamma_\mu\gamma_\nu)\times\frac{m^2d^4p}{[(\mathbf{p}-\frac{1}{2}\mathbf{k})^2-m^2][(\mathbf{p}-\frac{1}{2}\mathbf{k})^2-m^2]}, \tag{4}$$

where

$$K_{\mu\nu}=-\frac{g^2}{\pi i}\int Sp\left[\gamma_\mu\frac{\mathbf{p}-\frac{1}{2}\mathbf{k}+m}{(\mathbf{p}-\frac{1}{2}\mathbf{k})^2-m^2}\gamma_\nu\frac{\mathbf{p}+\frac{1}{2}\mathbf{k}+m}{(\mathbf{p}+\frac{1}{2}\mathbf{k})^2-m^2}\right]d^4p \tag{5}$$

is the vacuum polarization integral obtained in electrodynamics. The integral in (5) and the second term of (4) have been evaluated by Feynman[2] using his regularization method. We have

$$K_{\mu\nu}=-\frac{g^2}{\pi}(k_\mu k_\nu-\delta_{\mu\nu}\mathbf{k}^2)\left[-\tfrac{1}{3}\ln\frac{\lambda^2}{m^2}-\frac{4m^2+\mathbf{k}^2}{3\mathbf{k}^2}\left(1-\frac{\theta}{\tan\theta}\right)+\tfrac{1}{9}\right], \tag{6}$$

where $\mathbf{k}^2=4m^2\sin^2\theta$. It is seen that $k_\mu k_\nu K_{\mu\nu}$ vanishes identically. The second term of (4) gives

$$M_s=\frac{g^2}{\pi}\mathbf{k}^2\left[4m^2\left(1-\frac{\theta}{\tan\theta}\right)-\tfrac{1}{3}\mathbf{k}^2+2(\lambda^2+m^2)\ln\left(\frac{\lambda^2}{m^2}+1\right)\right]. \tag{7}$$

For free mesons, $\mathbf{k}^2=\kappa^2$, M_s is equal to the mass renormalization

$$\Delta\kappa=\frac{g^2}{\pi}\kappa^2\left[4m^2\left(1-\frac{\theta_0}{\tan\theta_0}\right)-\tfrac{1}{3}\kappa^2+2(\lambda^2+m^2)\ln\left(\frac{\lambda^2}{m^2}+1\right)\right], \tag{8}$$

$$\kappa^2=4m^2\sin^2\theta_0.$$

We have

$$M_s=\Delta\kappa+(\mathbf{k}^2-\kappa^2)\frac{g^2}{\pi}\left[4m^2-\tfrac{1}{3}\kappa^2+2(\lambda^2+m^2)\ln\left(\frac{\lambda^2}{m^2}+1\right)\right]+\frac{g^2}{\pi}\left[\tfrac{1}{3}\mathbf{k}^2(\kappa^2-\mathbf{k}^2)+4m^2\left(\kappa^2\frac{\theta_0}{\tan\theta_0}-\mathbf{k}^2\frac{\theta}{\tan\theta}\right)\right]. \tag{9}$$

The second term on the right-hand side of (9) is the renormalization of the mesic charge, g. The first and second terms in (9) should be omitted if we use the observed values of κ and g. The only observable effect in (9) is the third term

$$D_C(\mathbf{k})=\frac{g^2}{\pi}\left[\tfrac{1}{3}\mathbf{k}^2(\kappa^2-\mathbf{k}^2)+4m^2\left(\kappa^2\frac{\theta_0}{\tan\theta_0}-\mathbf{k}^2\frac{\theta}{\tan\theta}\right)\right], \tag{10}$$

which will contribute to the radiative effect of more complicated processes involving this virtual meson. Let us consider any internal meson line of a given graph. It can be seen easily that the total radiative effect from the self-energy parts of the meson is obtained by replacing the $D_F(\mathbf{k})$ function by

$$D_F'(\mathbf{k})=D_F(\mathbf{k})+D_F(\mathbf{k})D_C(\mathbf{k})D_F(\mathbf{k})+D_F(\mathbf{k})D_C(\mathbf{k})D_F(\mathbf{k})D_C(\mathbf{k})D_F(\mathbf{k})+\cdots=D_F(\mathbf{k})/[1-D_C(\mathbf{k})D_F(\mathbf{k})], \tag{11}$$

where the first term is the original D_F function with no radiative correction, the second term is the radiative correction when one self-energy part is inserted into the meson line, and the third term is the radiative correction when two self-energy parts are inserted, and so on. All of the self-energy parts thus inserted are of the lowest order in g, and no self-energy part of higher order has been inserted. At large values of $\mathbf{k}^2$, $D_F'(\mathbf{k})$ behaves as $1/(\mathbf{k}^2)^2$, while $D_F(\mathbf{k})$ behaves only like $1/\mathbf{k}^2$. After the replacement has been introduced into every internal meson line, the degree of the integrand of M is decreased by $2F_m=(n-F_m)$. Therefore, the condition of convergence (1) is now replaced by

$$E_m+\tfrac{3}{2}E_n-4\geqslant 1, \tag{12}$$

which is the same condition as is obtained in electrodynamics. Therefore, the divergence in our case is the same as in the case of electrodynamics after the renormalizations of charge and mass of the meson have been taken care of. As in electrodynamics, the only possible types of divergences are the self-energy of the nucleon, the self-energy of the meson (of order higher than g^2), the radiative

correction to the scattering of the nucleon, by an external field, and the scattering of meson by meson. We can easily see that the integral M for the last process converges, since its divergent part is identical with that of the scattering of light by light which has been shown to vanish by cancellation. The conventional perturbation method can now be used again, the only precaution being that the graph should not contain any meson self-energy part of order g^2.

Similar calculations applied to scalar meson with vector coupling shows that the corresponding expression (10) vanishes, since M_s is given only by the first term of (4) owing to the absence of the γ_5 factor; therefore, the divergence cannot be removed in this case by renormalizaion of meson mass and charge. It would be of interest to apply the present theory to investigate the nuclear potential and the nucleon magnetic moments. Further details will be published later.

The author is indebted to Professor T. Y. Wu and Dr. J. Pirenne for the helpful discussions.

[1] F. J. Dyson, Phys. Rev. 75, 1736 (1949). This paper contains many terms and concepts used in the present note.
[2] R. P. Feynman, Phys. Rev. 76, 769 (1949). This paper also gives the explanation of most of the notation used in the present note.

Preparation of Co^{58m} by a (γ, n) Reaction*

DARLEANE CHRISTIAN AND DON S. MARTIN, JR.
Institute for Atomic Research and Department of Chemistry, Iowa State College, Ames, Iowa
October 25, 1950

RECENTLY Strauch has reported the preparation and identification of a radioactivity, Co^{58m}, with a half-life of 8.8 hr.[1] The identification was based on evidence of its formation from manganese by a (α, n) reaction. It was also produced by bombardment of cobalt and nickel by deuterons and fast neutrons, and by irradiation of copper with deuterons in the 184-in. cyclotron. He showed that the isomer decayed by the emission of a highly converted gamma-ray with an energy of 25 kev to the well-known 72-day Co^{58} activity which undergoes positron emission and K-capture.[2] Counting of the principal radiation, which consists primarily of 17-kev and 24-kev conversion electrons, requires a sample of high specific activity and use of a windowless counter.

We have prepared Co^{58m} by a (γ, n) process in irradiations in the Iowa State College synchrotron. The necessary high specific activity was obtained by a Szilard-Chalmers-type decomposition of a Co^{III} complex induced by the recoil from the nuclear reaction. In this process the radioactive atoms were converted to the Co^{II} oxidation state, which could then be separated chemically from the target material. To accomplish this separation, 5 g of crystals of the complex salt, $K_3Co(C_2O_4)_3 \cdot 3H_2O$, were placed in a test tube with a 1-cm diameter. The sample tube was carefully aligned with the 65-Mev beam of the synchrotron and irradiated for one hour. After irradiation the target salt was dissolved in water, and the Co^{II} was separated from the $[Co(C_2O_4)_3]^{---}$ anion by adsorption on IRC-50 cation exchange resin. The radioactive Co^{II} was eluted from the resin with HCl and samples were prepared for counting by electroplating cobalt metal on platinum disks. The recovery of cobalt appeared to be better than 95 percent. From the weight of the deposits it was estimated that about three percent of the complex decomposed during irradiation, so that the enrichment amounted to a factor of about 30.

The decay was followed with a windowless, gas-flow G-M counter. A half-life of 9.2±0.2 hr. was observed for the short-lived component. This radiation was completely stopped by a 2 mg/cm² aluminum absorber. Intensities have not yet been satisfactory for the identification of the Co^{58} daughter activity.

A portion of the target salt was mounted for counting under standard conditions and the decay of the C^{11} was followed. The half-life checked the previously reported value,[3] 20.5±0.5 min. By use of the C^{11} as an "internal standard," a tentative ratio for the cross section for the formation of Co^{58m} to the cross section for C^{11} was estimated to be 2.5. Rather large uncertainties in this value were due to the large correction for the self-absorption in the cobalt sample. It is intended to obtain a more accurate value for this quantity, and if possible to evaluate the cross-section ratio for Co^{58}.

We wish to acknowledge our appreciation to Dr. L. J. Laslett and Dr. D. J. Zaffarano for their assistance in providing the synchrotron irradiations.

* Contribution No. 130 from the Institute for Atomic Research and Department of Chemistry, Iowa State College, Ames, Iowa. This work was performed in the Ames Laboratory of the AEC.
[1] K. Strauch, Phys. Rev. 79, 487 (1950).
[2] G. J. Seaborg and I. Perlman, Rev. Mod. Phys. 20, 585 (1948).

The Possible Existence of a Constant Third-Order Difference among the Nuclear Magic Numbers

FRANK A. VALENTE
746 South Florida Street, Arlington, Virginia
October 13, 1950

IT has been called to the writer's attention that the results published in a previous Letter to the Editor under this same title[1] are identical with those given in an earlier note by E. Bagge.[2] Although the writer's considerations were made independently of those of Bagge, it is desired to acknowledge the priority of Bagge's work.

[1] F. A. Valente, Phys. Rev. 78, 77 (1950).
[2] E. Bagge, Naturwiss. 35, 375 (1948).

Evidence Concerning Equality of n-n and p-p Forces

G. BREIT
Yale University, New Haven, Connecticut*
and
Los Alamos Scientific Laboratory,† Los Alamos, New Mexico
November 2, 1950

COULOMB energies of light nuclei offer strong evidence of equality of proton-proton (p-p) and neutron-neutron (n-n) forces. Comparison of neutron-deuteron (n-d) with proton-deuteron (p-d) scattering, which results, respectively, from the work of Wantuch[1] and Rosen[2] leads to similar conclusions. While the observations of Rosen have been made by bombarding ordinary hydrogen with 10.5-Mev deuterons, they are equivalent to the observation of the scattering of 5.25-Mev protons by stationary deuterons. This energy is comparable with neutron energies of 4.5 and 5.5 Mev in Wantuch's work. The interference effect between the Rutherford and the specifically nuclear waves is too high to make the comparison completely quantitative. Upper limits of the effect of the cross-product term between these two waves may be calculated as in Table I.

Here θ is the scattering angle in the center-of-mass system, and the last row in the table gives the ratio of the absolute value of the interference term $2|\psi\psi^c|$ to the square of the absolute value of the wave function ψ. The Coulomb wave is denoted by ψ^c. Rosen's values were used to obtain $|\psi|$.

In Table I no explicit account is taken either of the two independent spin orientations of the colliding particles or of the phase differences between ψ and ψ^c. It is not likely from a statistical viewpoint that the phase relations for both spin orientations are such as to give a maximum possible interference effect and it is not surprising, therefore, that the two sets of data show very similar values, as may be seen from Table II. The agreement is best, on the whole, around the minimum which is close to $\theta=90°$. A 5 percent Coulomb interference effect would remove an appreciable part of the discrepancy at $\theta=160°$. It will be noted

TABLE I. Values of maximum fractional interference with Coulomb wave.

$\theta=$	60°	90°	120°	150°	180°
$2\|\psi^c/\psi\|=$	0.23	0.16	0.12	0.055	0.041

TABLE II. Values of collision cross section per unit solid angle in barns.

$\theta=$	70°	80°	100°	110°	120°	140°	160°	180°	E (Mev)
(p-d)	0.115	0.095	0.060	(0.052)	0.055	0.105	0.230		5.25
(n-d)	0.125	0.088	0.050		0.055	0.105	0.200	0.235	5.5
(n-d)		0.095	0.050		0.055	0.130	0.210	0.275	4.5

that for $\theta=130°$ the difference between the values of σ at 5.5 and 4.5 Mev is sufficiently large to make reasonable an estimate of errors of the order of 10 percent in the n-d measurements. The outstanding differences at $\theta=160°$ may not be real, therefore.

On account of effects in the interior of the nucleus one may expect the phase shifts to be affected when a neutron is changed into a proton. An exact correspondence cannot be expected, therefore, even apart from the interference with Coulomb scattering. The author is indebted to Dr. Louis Rosen for helpful discussion of his data.

* Assisted by the joint program of the ONR and AEC.
† Released by declassification authorities following request of September 25, 1950.
[1] E. Wantuch, Phys. Rev. **79**, 729 (1950).
[2] J. C. Allred and L. Rosen, Phys. Rev. **79**, 227 (1950).

A Note on the Classical Spin-Wave Theory of Heller and Kramers*

MARTIN J. KLEIN AND ROBERT S. SMITH
Department of Physics, Case Institute of Technology, Cleveland, Ohio
October 30, 1950

IN 1934 Heller and Kramers[1] obtained the Bloch energy levels[2] for a ferromagnet by starting with a classical theory of spin-waves and then quantizing this theory. Certain obscurities remained in the theory, however, as recognized by Heller and Kramers, and it is the purpose of this note to clarify these obscure points. We shall discuss particularly the physical and mathematical origin of the apparent zero-point energy, which HK had to omit, and the canonical nature of the variables used. Reference will be made to the quantal spin-wave theory as given by Holstein and Primakoff.[3]

The Hamiltonian for the simplest case, a linear chain of N atoms with nearest-neighbor interactions, is

$$\mathcal{H}=-2\beta H\sum_{l=1}^{N}S_{l,z}-2J\sum_{l=1}^{N}\mathbf{S}_l\cdot\mathbf{S}_{l+1}, \tag{1}$$

where $\mathbf{S}_l$ is the spin vector (operator in the quantal case) of the lth atom in units of $\hbar$, β the Bohr magneton, J the exchange integral, and H the z-directed magnetic field.

Considering $\mathbf{S}_l$ as a classical vector, HK observe that near saturation $S_{l,x}$ and $S_{l,y}$ are small and, therefore,

$$S_{l,z}=[\check{S}^2-(S_{l,x}^2+S_{l,y}^2)]^{\frac{1}{2}}\cong\check{S}[1-(S_{l,x}^2+S_{l,y}^2)/2\check{S}^2], \tag{2}$$

where $\check{S}$ is the magnitude of the spin vector. In a quantal treatment $\check{S}$ is to be replaced by $[S(S+1)]^{\frac{1}{2}}$, where S is now the maximum z component of the spin.

Using Eq. (2) causes the Hamiltonian to become

$$\mathcal{H}\cong\mathcal{H}_{\rm HK}(\check{S})=-2N\check{S}[\beta H+J\check{S}]+2J\sum_{l=1}^{N}\times\{(1+\alpha)(S_{l,x}^2+S_{l,y}^2)-(S_{l,x}S_{l+1,x}+S_{l,y}S_{l+1,y})\}, \tag{3}$$

where $\alpha=\beta H/2J\check{S}$.

We may compare Eq. (3) with the quantal Hamiltonian obtained[4] by HP after introduction of approximations appropriate near saturation. In the same notation:

$$\mathcal{H}_{\rm HP}=\mathcal{H}_{\rm HK}(S)+2J(1+\alpha)i\sum_{l=1}^{N}(S_{l,x}S_{l,y}-S_{l,y}S_{l,x}). \tag{4}$$

We notice that the quantal Hamiltonian has an additional sum of commutators, which vanish classically, and that it is S rather than $\check{S}$ which appears. We shall discuss this below.

An orthogonal transformation is now made by HK to make H a sum of squares. The new variables P_λ, Q_λ after renormalization are determined by

$$S_{l,x}=(S)^{\frac{1}{2}}\sum_{\lambda=0}^{N-1}a_{l\lambda}P_\lambda;\quad S_{l,y}=(S)^{\frac{1}{2}}\sum_{\lambda=0}^{N-1}a_{l\lambda}Q_\lambda, \tag{5a}$$

where

$$a_{l\lambda}=(2/N)^{\frac{1}{2}}\cos[(2\pi\lambda/N)+(\pi\lambda/2N)]\quad(\lambda\neq0)$$
$$a_{l0}=(1/N)^{\frac{1}{2}}. \tag{5b}$$

The variables P_λ, Q_λ are obviously wave-like in nature.

Quantization of the HK theory is now possible, since the classical Poisson bracket is

$$\{P_\lambda,Q_\lambda\}_{\rm P.B.}=(\delta_{\lambda\lambda'}/S)\{S_{l,x},S_{l,y}\}_{\rm P.B.}=\delta_{\lambda\lambda'}S_{l,z}/S\cong\delta_{\lambda\lambda'} \tag{6}$$

from Eq. (5) and with $S_{l,z}/S$ approximately equal to unity, corresponding to conditions near saturation. Hence, $P_\lambda^2+Q_\lambda^2$ has eigenvalues $2(n_\lambda+\frac{1}{2})$ with $n_\lambda=0,1,2,\cdots$.

The energy levels for $\mathcal{H}_{\rm HK}$ are:

$$E_{\rm HK}(n_\lambda,\check{S})=-2N\check{S}[\beta H+J\check{S}]+4JS\sum_{\lambda=0}^{N-1}\left(1+\alpha-\cos\frac{2\pi\lambda}{N}\right)(n_\lambda+\tfrac{1}{2}), \tag{7}$$

a result differing from the quantal energy levels in the appearance of $\check{S}$ and the additional $\frac{1}{2}$ in the factor $(n_\lambda+\frac{1}{2})$ as will now be shown. For the additional terms in Eq. (4) can readily be calculated using the HP approximations[5] to be

$$S_{l,x}S_{l,y}-S_{l,y}S_{l,x}=iS. \tag{8}$$

(Equation (8) indicates that the same approximation is made in the quantal theory as in Eq. (6); i.e., $S_{l,z}$ is replaced by S.) It follows that, using the same orthogonal transformation and quantizing the result, we obtain

$$E_{\rm HP}(n_\lambda)=E_{\rm HK}(n_\lambda,S)-2JS\sum_\lambda(1+\alpha)$$
$$=E_{\rm HK}(n_\lambda,S)-2JS\sum_\lambda\left(1+\alpha-\cos\frac{2\pi\lambda}{N}\right), \tag{9}$$

which verifies the statement made above.

The physical origin of the extra $\frac{1}{2}$ is not hard to see. It arises from Eq. (2): in the HK theory the distinction between S and $[S(S+1)]^{\frac{1}{2}}$ is not maintained, so that, in effect, the expression $S-S_z$, the deviation of the z component of the spin from its maximum value, is replaced by $[S(S+1)]^{\frac{1}{2}}-S_z$. Now the former quantity has, rigorously, integral values, while the latter is approximately $S-S_z+\frac{1}{2}$ (expanding $[S(S+1)]^{\frac{1}{2}}$). The $\frac{1}{2}$ comes from the fact that, quantum-mechanically, the spin vector never lies along the z axis and $S_x^2+S_y^2$ is never rigorously zero. In the formal theory this is expressed by the appearance of the commutator of S_x and S_y as mentioned above.

* Supported in part by the ONR.
[1] G. Heller and H. A. Kramers, Proc. Amst. Acad. Sci. **37**, 378 (1934), referred to as HK.
[2] See A. Sommerfeld and H. Bethe, *Handbuch der Physik*, Vol. 24, Part 2, p. 601.
[3] T. Holstein and H. Primakoff, Phys. Rev. **58**, 1098 (1940), referred to as HP. See also D. Polder, Phil. Mag. **40**, 99 (1949).
[4] Reference 3, Eq. (7).
[5] $S_{l,x}+iS_{l,y}\cong(2S)^{\frac{1}{2}}a_l$, $S_{l,x}-iS_{l,y}\cong(2S)^{\frac{1}{2}}a_l^*$,
$S_{l,z}=S-a_l^*a_l$, $a_la_{l'}^*-a_{l'}^*a_l=\delta_{ll'}$.
See reference 3, Eqs. (3) to (6) and following discussion.

The Scattering Lengths of the Deuteron and p-d Scattering*

M. M. GORDON**
Washington University, St. Louis, Missouri
October 31, 1950

AN analysis of the S-wave scattering of nucleons by deuterons has been carried out by means of a spin-dependent, "effective" two-body model of the nucleon-deuteron interaction.[1] This analysis was begun by considering the deuteron as a single structureless particle so that the actual nucleon-deuteron interaction could be replaced by an "effective" two-body interaction.

The ^3S and ^1S effective two-body neutron-deuteron interactions were represented by square-well central potentials having depths V_2 and V_4, respectively, and the same range r_0. It was then assumed that[2]

$$r_0=(5.0\pm2.0)\times10^{-13}\text{ cm}. \quad (1)$$

The analysis proceeded with the deduction of a theorem to the effect that the binding energy of the ^3S or ^1S ground state of H^3, calculated on the basis of such an effective two-body model, is not greater than the actual binding energy of a neutron to a deuteron in forming that state. The existence of H^3 in a ^3S ground state of known binding energy and with no bound excited states consequently places a restriction on the maximum values of V_2 and V_4 for a given value of r_0.

The value of V_x ($x=2$ or 4) can now be calculated *uniquely*, for a given value of r_0, from the corresponding scattering length of the deuteron a_x ($x=2$ or 4) by means of the relationship:

$$\tan(K_xr_0)/K_xr_0=1-a_x/r_0, \quad (2)$$

where

$$K_x^2=4MV_x/3\hbar^2,$$

provided the above-mentioned restrictions on V_2 and V_4 are considered. At the time this work was undertaken, the experimental results on the scattering of slow neutrons from deuterons provided only two fairly definite conclusions regarding the values of a_2 and a_4;[3-5] namely: a_2, $a_4>0$; and Eq. (5) below. From the fact that $a_4>0$, it was then concluded from (2) that V_4 cannot be greater than zero, and consequently,

$$0<a_4<r_0. \quad (3)$$

From the fact that $a_2>0$, it was deduced from (2) that, for any given value of r_0 in the range of (1),

$$a_2\geqq(a_2)_{\min}\geqq0.4\times10^{-13}\text{ cm}. \quad (4)$$

Corresponding to four different values of r_0 in the range of (1), sixteen sets of values for V_2 and V_4 were then calculated from Eq. (2) by using values of (a_2, a_4) consistent with (3), (4), and the experimental value of

$$\sigma_D=(4\pi/3)(a_2^2+2a_4^2)=3.44\text{ barns}, \quad (5)$$

which was assumed to be correct. It proved convenient to combine (5) with (2), and consider a_2 and r_0 as the independent variables for the functions V_2 and V_4. On the assumption that the specifically nuclear n-n and p-p interactions are the same, these sets of potentials were then used to calculate the angular distributions obtained in p-d scattering at 250 and 275 kev,[6] and the 90° (center-of-mass system) cross sections obtained for p-d scattering from 1.5 to 3.0 Mev.[7] It was found (as was to be expected) that the fit of the calculated values to the experimental data was relatively insensitive to the value of r_0 within the range of (1) (or even to the assumption of two different values of r_0, in that range, for the ^3S and ^1S effective interactions). It was found, however, that a good fit to the data could be obtained only for

$$a_2\approx0.8\times10^{-13}\text{ cm}, \quad a_4\approx0.3\times10^{-13}\text{ cm}, \quad (6)$$

a_4 being obtained from a_2 via (5). These values, moreover, provided this fit over the entire energy range of the p-d data considered.

This work was carried out before the accurate results obtained at Chalk River for the scattering of slow neutrons from D_2 became available.[8] These latter results, together with (3), (4), and (5), give

$$a_2=(0.826\pm0.012)\times10^{-13}\text{ cm}, \quad a_4=(0.26\pm0.02)\times10^{-13}\text{ cm}, \quad (7)$$

which is in excellent agreement with (6) above, deduced from the analysis of p-d scattering. This agreement implies that an effective two-body model of the nucleon-deuteron interaction is indeed a practical means of correlating the low energy nucleon-deuteron scattering data, and, that the hypothesis of the equality of the n-n and p-p interactions is corroborated under these conditions.

A detailed report on the above work will be submitted for publication shortly.

* Assisted by the joint program of the ONR and AEC.
** Present address: Physics Department, University of Florida, Gainesville, Florida.
[1] M. M. Gordon, thesis, Washington University, 1950.
[2] H. A. Bethe, Rev. Mod. Phys. 9, 180 (1937).
[3] E. Fermi and L. Marshall, Phys. Rev. 75, 578 (1949).
[4] Shull, Wollan, Morton, and Davidson, Phys. Rev. 73, 842 (1948).
[5] Rainwater, Havens, Jr., Dunning, and Wu, Phys. Rev. 73, 733 (1948).
[6] R. Taschek, Phys. Rev. 61, 13 (1942).
[7] Sherr, Blair, Kratz, Bailey, and Taschek, Phys. Rev. 72, 662 (1947).
[8] D. G. Hurst and N. Z. Alcock, Phys. Rev. 80, 117 (1950).

Asymptotic Solutions of Ordinary Linear Differential Equations of the Second Order

ISAO IMAI
Department of Physics, Faculty of Science, University of Tokyo, Tokyo, Japan
October 9, 1950

IN a recent paper[1] Kuhn has applied the WKB method to the calculation of the cohesive energies of monovalent metals. His analysis is based on a new procedure proposed by the writer.[2] In consideration of the possibility that this method may be capable of wide applicability, it will be justifiable to present it here in a more explicit form.

We consider the asymptotic solutions of the second-order linear differential equation

$$(d^2\Phi/dx^2)+a^2P(x)\Phi=0 \quad (\text{for } a\to\infty), \quad (1)$$

where

$$P(x)=a_1x+a_2x^2+\cdots \quad (a_1\neq0).$$

We make the transformations

$$z=\int_0^x[P(y)]^{1/2}dy,$$
$$Q=P^{-1/4}d^2P^{1/4}/dz^2=-P^{-3/4}d^2P^{-1/4}/dx^2$$
$$=-[(5/36)z^{-2}+\lambda z^{-2/3}+\lambda_0+\lambda_1z^{2/3}+\cdots], \quad (2)$$
$$Q_1(z)=\int^z Q(y)dy.$$

It can be shown that the two independent solutions Φ_1, Φ_2, can be expressed in the form

$$\Phi_{1,2}=P^{-1/4}\Psi_{1,2} \quad (3)$$

with

$$\Psi_{1,2}=\exp[\pm iaz\pm(i2a)^{-1}Q_1(z)+(4a^2)^{-1}Q(z)]+O(a^{-3}) \quad (4)$$
for $z\neq0$, and

$$\Psi_{1,2}=(\tfrac{1}{2}\pi a)^{1/2}i^{\pm5/6}\exp\Big\{\mp(i2a)^{-1}\times\int_0^\infty[Q+(5/36z^2)]dz\Big\}\cdot z^{1/6}\zeta H_{1/3}^{(1,2)}(\eta)+O(a^{-3}) \quad (5)$$
for $z=O(a^{-1})$.

Here

$$\zeta=[\xi-\tfrac{1}{3}\lambda_1\kappa^{-2}\xi^2]^{1/2}, \quad \eta=\kappa[\xi+\tfrac{1}{3}\lambda_1\kappa^{-2}\xi^2]^{3/2}, \quad (6)$$
$$\xi=z^{2/3}+\lambda\kappa^{-2}, \quad \kappa^2=a^2+\lambda_0,$$

and the symbol H stands for the Hankel functions.

As an example, the asymptotic formula for the Hankel functions for the "transition region" can be written in the form

$$H_a^{(1,2)}(a\sec\theta)=i^{\pm1/3}\cot^{1/2}\theta\cdot z^{1/6}\zeta H_{1/3}^{(1,2)}(\eta)+O(a^{-\eta/2}), \quad (7)$$

where

$$z=\tan\theta-\theta, \quad \lambda=-3^{1/3}/105, \quad \lambda_0=2/75, \quad \lambda_1=-(69/13475)3^{2/3}.$$

This is to be compared with Langer's formula,[3] which can be obtained from the above by setting $\lambda=\lambda_0=\lambda_1=0$, giving

$$H_a^{(1,2)}(a\sec\theta)=i^{\pm1/3}\cot^{1/2}\theta\cdot z^{1/2}\cdot H_{1/3}^{(1,2)}(az)+O(a^{-5/3})$$

and Watson's formula[4]

$$H_a^{(1,2)}(a\sec\theta)\doteq i^{\pm1/3}3^{-1/2}\tan\theta\cdot H_{1/3}^{(1,2)}(\tfrac{1}{3}a\tan^3\theta)+O(a^{-1}).$$

One of the merits of the new formula is that it permits the easy computation of the zeros of Φ (for example, of $J_a(x)$), from those of the Bessel functions of order 1/3.

[1] T. S. Kuhn, Phys. Rev. 79, 515 (1950).
[2] I. Imai, Phys. Rev. 74, 113 (1948).
[3] R. E. Langer, Trans. Am. Math. Soc. 33, 23 (1931).
[4] G. N. Watson, *Bessel Functions* (Cambridge University Press, London, 1922), p. 252.

Statistical Limitations on the Resolving Time of a Scintillation Counter*

R. F. POST AND L. I. SCHIFF
Stanford University, Stanford, California
October 16, 1950

SCINTILLATION counters are being used increasingly for applications that require extremely short resolving times. In this letter, we discuss the limitations on resolving time that arise from fluctuations in the emission, transmission, and collection of scintillation photons. For this purpose we assume that following excitation of the scintillator by an energetic event, the photo-multiplier multiplies the primary photo-electrons without time spread, and that the resulting pulses are fed into a discriminator that gives a signal when it has accumulated a definite number, say Q, of pulses. We ask for the fluctuation in time of these signals. Except for the neglect of time spread in the photo-multiplier, this model contains the essential features of actual counting systems.

The average or expected number of photo-multiplier pulses between the initial excitation of the scintillator at zero time (allowing for a possible constant time delay in the photo-multiplier) and time t is $f(t)$, where $f(0)=0$, f is a continuous monotonically increasing function[1] of t, and df/dt is piecewise continuous. It is assumed that the probability that N pulses occur between 0 and t is given by the Poisson distribution:

$$P_N(t)=[f(t)]^N e^{-f(t)}/N!. \tag{1}$$

This means that either (a) a relatively small, randomly selected, sample of the emitted photons is converted into output pulses, or (b) the magnitude of the initial excitation is randomly distributed,[2] or both. Then the probability that the Qth pulse occurs between t and $t+dt$ is[3]

$$W_Q(t)dt=P_{Q-1}(t)[df(t)/dt]dt. \tag{2}$$

The total probability that the Qth pulse occurs between 0 and ∞ is

$$\int_0^\infty W_Q(t)dt=\frac{1}{(Q-1)!}\int_0^R f^{Q-1}e^{-f}df$$
$$=1-e^{-R}\left[1+R+\frac{R^2}{2!}+\cdots+\frac{R^{Q-1}}{(Q-1)!}\right]\equiv I_Q(R), \tag{3}$$

where $R\equiv f(\infty)$ is the average total number of primary photo-electrons. It is readily verified by comparison of Eqs. (1) and (3) that $I_Q(R)$ is the probability that Q or more pulses occur between 0 and ∞, as it should be. $I_Q(R)$ can be evaluated from Eq. (2), or found from tables of the incomplete gamma-function.[4]

The variance of the signal time is

$$v\equiv\langle t^2\rangle_{Av}-\bar{t}^2=\frac{1}{I_Q(R)}\int_0^\infty t^2W_Q(t)dt-\left[\frac{1}{I_Q(R)}\int_0^\infty tW_Q(t)dt\right]^2.$$

It may also be calculated from a generating function:[5]

$$G(x)=\int_0^\infty x^t W_Q(t)dt, \tag{4}$$
$$v=\left[\frac{1}{G}\left(\frac{\partial^2 G}{\partial x^2}+\frac{\partial G}{\partial x}\right)-\left(\frac{1}{G}\frac{\partial G}{\partial x}\right)^2\right]_{x=1}.$$

If we define the inverse function to $f(t)$ as $t=g(f)$, then Eq. (4) becomes

$$G(x)=\frac{1}{(Q-1)!}\int_0^R x^{g(f)}f^{Q-1}e^{-f}df.$$

As a simple example,[6] we consider the case $f(t)=\lambda t$ (not applicable to scintillation counters), in which case $R=\infty$ and $g(f)=f/\lambda$:

$$G(x)=(1-\lambda^{-1}\ln x)^{-Q},\quad \bar{t}=(\partial G/\partial x)_{x=1}=Q/\lambda,$$
$$v=Q/\lambda^2=\bar{t}^2/Q. \tag{5}$$

For a scintillator, R must be finite, and $g(f)$ has a singularity at the point $f=R$. It is apparent, however, that the integral over f that gives $\langle t^n\rangle_{Av}$ diverges if and only if the nth moment of the probability function (2) diverges, so that any difficulties caused by the singularity can easily be traced.

When R is finite, $G(x)$ and v cannot be written in simple closed forms. However, in the physically useful case $R\gg 1$, $R\gg Q$, Eq. (3) shows that we can put $I_Q(R)\cong 1$, and simple asymptotic expressions can be obtained that involve only the behavior of $f(t)$ near $t=0$. Suppose that

$$f(t)=a_1t+a_2t^2+\cdots;$$

then

$$t=g(f)=b_1f+b_2f^2+\cdots,$$

where

$$b_1=1/a_1,\quad b_2=-a_2/a_1^3,\quad \cdots.$$

In general, a_1, a_2, $\cdots$ are proportional to R, so that $b_1\propto 1/R$, $b_2\propto 1/R^2$, etc., and the series that follow are expansions in powers of Q/R; these are convergent if the series for $g(f)$ converges inside the circle $f=R$, and are otherwise asymptotic. We find that

$$\bar{t}=[1/I_Q(R)][b_1QI_{Q+1}(R)+b_2Q(Q+1)I_{Q+2}(R)+\cdots],$$
$$v=[1/I_Q^2(R)]\{b_1^2[Q(Q+1)I_Q(R)I_{Q+2}(R)-Q^2I_{Q+1}^2(R)]$$
$$+2b_1b_2[Q(Q+1)(Q+2)I_Q(R)I_{Q+3}(R)$$
$$-Q^2(Q+1)I_{Q+1}(R)I_{Q+2}(R)]+\cdots\}.$$

With the approximation $I_Q(R)\cong 1$, these become asymptotic series:

$$\bar{t}\cong b_1Q+b_2Q(Q+1)+\cdots=\frac{Q}{a_1}\left[1-\frac{a_2(Q+1)}{a_1^2}+\cdots\right],$$
$$v\cong b_1^2Q+4b_1b_2Q(Q+1)+\cdots=\frac{Q}{a_1^2}\left[1-\frac{4a_2(Q+1)}{a_1^2}+\cdots\right],$$
$$\frac{v}{\bar{t}^2}\cong\frac{1}{Q}\left[1-\frac{2a_2(Q+1)}{a_1^2}+\cdots\right];$$

the last of these agrees with Eq. (5) to lowest order, as expected.

For an exponentially decaying scintillator:

$$f(t)=R(1-e^{-\lambda t}),\quad a_1=R\lambda,\quad a_2=-\tfrac{1}{2}R\lambda^2,\quad \cdots.$$

In this case:

$$\bar{t}\cong(Q/R\lambda)\{1+[(Q+1)/2R]+\cdots\},$$
$$v\cong\frac{Q}{R^2\lambda^2}\left[1+\frac{2(Q+1)}{R}+\cdots\right]\cong\frac{\bar{t}^2}{Q}\left(1+\frac{Q+1}{R}+\cdots\right). \tag{6}$$

To see the order of magnitude of the r.m.s. signal time deviation in a practical case, we calculate $v^{\frac{1}{2}}$ when $Q=10$, $\lambda=5\times10^8$ sec.$^{-1}$, and $R=75$, which corresponds roughly to the excitation of a fast liquid scintillator[7] by a 1-Mev electron and the conversion of 1 percent of the emitted photons into photo-multiplier pulses, when the spread in photon collection time can be neglected. In this case, the first two terms of Eq. (6) give $v^{\frac{1}{2}}\cong10^{-10}$ sec., with an error of a few percent. With slower scintillators and less energetic events, $v^{\frac{1}{2}}$ can be substantially larger, of the order of 10^{-8} sec. in a typical case. The time $v^{\frac{1}{2}}$ represents a loss of resolution that is superposed on any losses owing to the electronic circuits.

* The work reported herein was performed under a contract between Stanford University and the ONR.

[1] The case in which f is not monotonic, which might be of interest in connection with the time fluctuations in the disintegrations of radioactive chains, could also be treated by a straightforward extension of the formalism.

[2] L. I. Schiff, Phys. Rev. **50**, 88 (1936).

[3] C. H. Westcott, Proc. Roy. Soc. **A194**, 508 (1948).

[4] K. Pearson, *Tables of the Incomplete Gamma Function* (H. M. Stationery Office, London, 1922).

[5] For a discussion of generating functions, see for example F. Seitz and D. W. Mueller, Phys. Rev. **78**, 605 (1950).

[6] W. C. Elmore, Nucleonics **6**, No. 1, 26 (1950), has considered this problem from a somewhat different point of view.

[7] R. F. Post, Phys. Rev. **79**, 735 (1950).

Author Index to Volume 80

References with (A) are to abstracts of papers presented at meetings of the American Physical Society, and those with (T) designate title only. References with (L) are to Letters to the Editor.

Aamodt, Lee (see Panofsky, Wolfgang K. H.)—94(L)
——, **James Hadley, and Wolfgang Panofsky.** Gamma-ray spectrum from the absorption of π^--mesons in deuterium—282(L)
Abraham, B. M., D. W. Osborne, and B. Weinstock. Vapor pressure, critical point, heat of vaporization, and entropy of liquid He^3—366
Adamson, R. E., Jr., W. W. Buechner, W. M. Preston, Clark Goodman, and D. M. Van Patter. Neutron yield from the $C^{13}(p,n)N^{13}$ reaction—985
Addario, M. M. and S. Tamburino. Nuclear disintegrations at 29,000 meters above sea level—749(L)
Adem, J. and M. Moshinsky. Vector boundary value problems and their applications—128(A)
Akeley, Edward (see Caplan, David)—125(A)
—— (see Keenan, Thomas)—125(A)
Alba, Fernando. Potentials of a rotating spherical shell in Birkhoff's theory of gravitation—127(A)
Albrecht, H. O. (see Mandeville, C. E.)—117(L), 299(L), 300(L)
Alburger, D. (see Friedlander, G.)—30
Alcock, N. Z. (see Hurst, D. G.)—117(L)
Allen, K. W. and J. T. Dewan. Emission of long-range charged particles in the slow neutron fission of heavy nuclei—181
Allen, Roland A. Verification of Bragg's law by the use of microwaves—927(A)
Allison, S. K. Experimental programme of the Institute for Nuclear Studies at the University of Chicago—122(T)
Allred, John C., Darol Froman, Alvin Hudson, and Louis Rosen. $D-He^4$ interaction for 10.3-Mev deuterons—136(A)
Almy, G. M. (see Diven, B. C.)—407
Alvarez, Luis W. Three new delayed alpha emitters of low mass—519
Anderson, C. D. Particles in penetrating showers—127(T)
Anderson, Herbert L. Resonance capture of neutrons by uranium—499
—— (see Smaller, B.)—137(A)
Anderson, P. W. Pressure broadening of the ammonia inversion line by foreign gases: quadrupole-induced dipole interactions—511
—— Two comments on the limits of validity of the P. R. Weiss theory of ferromagnetism—922(L)
Anderson, Wallace E. (see Simmons, James W.)—338
Andrews, D. H. (see Bodmer, Max)—122(A)
Appleton, G. L. (see Warshaw, S. D.)—288(L)
Arnold, Wayne R. Angular correlation in the reaction $F^{19}(p,\alpha)O^{16*}(\gamma)O^{16}$—34
Asaro, Frank (see Martin, A. B.)—123(A)
Atteberry, R. W. (see Cobble, James W.)—917(L)
Axel, Peter. Isomers and shell structure—104(L)
—— (see Mann, L. G.)—759(L)

Bailey, F. M. Recent developments in electric servo power drive systems—927(A)
Bak, Børge, Raymond Sloan, and Dudley Williams. Microwave investigation of SCSe—101(L)
Band, William. On the origin of the lighter elements—813
Barber, W. C. Short-lived isomers of Ta^{181}—332
Bardeen, John. Wave functions for superconducting electrons—567
—— **and W. Shockley.** Deformation potentials and mobilities in non-polar crystals—72
—— **and W. Shockley.** Scattering of electrons in crystals in the presence of large electric fields—69
Barker, E. C. (see Snell, Arthur H.)—637
Barschall, H. H. (see Henkel, R. L.)—145
—— (see Johnson, C. H.)—818
Bartell, F. O., A. C. Helmholz, S. D. Softky, and D. B. Stewart. Excitation functions for spallation reactions on Cu—1006
Bartholomew, G. A. (see Kinsey, B. B.)—918(L)
Barton, G. W., Jr. (see O'Kelley, G. D.)—293(L)
Bateson, William O. Proton groups from the deuteron bombardment of boron—982
Beckham, Walter C. and M. L. Pool. Krypton bombardments: radioactive Rb 84—125(A)
Beers, Y. (see Korff, S. A.)—489(L)
Beiser, Arthur. Thermal mechanism for residual latent image fading in nuclear emulsions—112(L)
Bergmann, Peter G., Robert Penfield, Ralph Schiller, and Henry Zatzkis. Hamiltonian of the general theory of relativity with electromagnetic field—81
Bergstralh, T. A. (see Perlow, G. J.)—133(A)
—— **and C. A. Schroeder.** Cosmic-ray diurnal effect measurements—134(A)
Bergström, Ingmar. On the isomerism of Xe^{131}—114(L)
Beringer, Robert (see Castle, J. G., Jr.)—114(L)
Berlman, Isadore B. Grain counts and corrected α-particle range-energy curve for Ilford E-1 emulsions—96(L)
—— On the bombardment of Li_2O and C by alpha-particles and deuterons—775
Bernardini, G., E. T. Booth, L. Lederman, and J. Tinlot. Nuclear interaction of π^--mesons—924(L)
——, **E. T. Booth, and S. J. Lindenbaum.** Stars induced by 350–400 Mev protons—905(L)
Bernstein, Ira B. Improved calculations on cascade shower theory—134(A), 995
Bethe, H. A., L. Tonks, and H. Hurwitz, Jr. Neutron penetration and slowing down at intermediate distances through medium and heavy nuclei—11
Birge, R. W. Proton-proton scattering at 100 Mev—490(L)
Bishop, A. S., J. Steinberger, and Leslie J. Cook. Photoproduction of mesons from hydrogen—136(A)
——, **J. Steinberger, and Leslie J. Cook.** Production of positive mesons by photons on hydrogen—291(L)
Bishop, G. R., C. H. Collie, H. Halban, A. Hedgran, K. Siegbahn, S. du Toit, and R. Wilson. Cross section for photodisintegration of the deuteron at low energies—211
Bishop, M. E. (see Liebson, S. H.)—907(L)
Biswas, S. (see Hopper, V. D.)—1099(L)
Blachman, Nelson M. Synchrotron-oscillation resonance—125(A)
Bloch, Felix (see Meyerhof, W. E.)—132(A)
—— **and C. D. Jeffries.** Direct determination of the magnetic moment of the proton in nuclear magnetons—305(L)
Bloch, I. Normal modes of vibration of nuclei—138(A)
——, **M. H. Hull, Jr., A. A. Broyles, W. G. Bouricius, B. E. Freeman, and G. Breit.** Methods of calculation of radial wave functions and new tables of Coulomb functions—553
Bloembergen, N. (see Kohn, W.)—913(L)
Bloomer, R. O. Application of physics to geology—927(T)
Bockelman, C. K. Total cross sections of Be, B, O, and F for fast neutrons—1011
Bodansky, David. Neutron energy distribution in proton bombardment of beryllium—481(L)
Bodmer, Max, Jean V. Lebacqz, and D. H. Andrews. Superconducting niobium nitride at microwave frequencies—122(A)
Bohm, David and David Pines. Screening of electronic interactions in a metal—903(L)
Bol, Kees. Determination of the speed of light by the resonant cavity method—298(L)

Boorse, H. A. (see Cook, D. B.)—737
Booth, E. T. Report on the cyclotron at Nevis—122(T)
—— (see Bernardini, G.)—905(L), 924(L)
Boothroyd, S. L. Physics principles illustrated in astronomy—927(T)
Boswell, F. W. C. Standard substance for precise electron diffraction measurements—91(L)
Bouricius, W. G. (see Bloch, I.)—553
Bouwkamp, C. J. On Sommerfeld's surface wave—294(L)
Bowers, R., B. S. Chandrasekhar, and K. Mendelssohn. Pressure measurement in superflow—856
Bradner, H. and B. Rankin. Large angle scattering of π^--mesons—916(L)
Bradt, H. L. On the nature of the primary cosmic rays—127(T)
—— (see Peters, B.)—133(A)
—— **and B. Peters.** Abundance of lithium, beryllium, boron and other light nuclei in the primary cosmic radiation and the problem of cosmic-ray origin—943
Branson, Herman (see Donfor, Anthony)—129(A)
—— **and Woodfin Lewis.** Self-diffusion of cobalt in gelatin as measured with Co^{60}—123(A)
Branyan, C. E. (see Cork, J. M.)—286(L)
Brattain, W. H. and G. L. Pearson. Changes in conductivity of germanium induced by alpha-particle bombardment—846
Breit, G. Evidence concerning equality of n-n and p-p forces—1110(L)
—— (see Bloch, I.)—553
—— **and M. H. Hull, Jr.** Asymptotic expansion of irregular Coulomb function for angular momentum zero—392
—— **and M. H. Hull, Jr.** Asymptotic expansion of the irregular Coulomb function—561
Brode, R. B. Abundance and masses of cosmic-ray particles at low elevations—127(T)
Brosi, A. R. (see Ketelle, B. H.)—485(L)
Brown, Harrison (see Inghram, Mark G.)—916(L)
Browne, C. P. (see Richards, H. T.)—524
Brownell, G. L. and C. J. Maletskos. Half-life of Fe^{55} and Co^{60}—1102(L)
Broxon, James W. Barometric and out-door temperature coefficients of frequency of small cosmic-ray bursts—135(A)
Broyles, A. A. (see Bloch, I.)—553
Bube, Richard H. Effect of infrared on emission and trapping in ZnS:Cu phosphors—764(L)
—— Luminescence and trapping in zinc sulfide phosphors with and without copper activator—655
Buckingham, M. J. Surface photoelectric effect—704
Buechner, W. W. (see Adamson, R. E., Jr.)—985
—— (see Malm, Robert)—771
—— (see Sperduto, A.)—769(L)
Buerger, M. J. The photography of atoms in crystals—123(A)
Bunker, Merle E. and Robert Canada. Radiations from Mo^{99} and Tc^{99m}— 961
——, **Robert Canada, and Allan C. G. Mitchell.** Radiations from Os^{185}, Os^{191}, and Os^{193}—126(A)
——, **L. M. Langer, and R. J. D. Moffat.** Beta-disintegration of Th^{233}—468(L)
Burditt, W. F. (see McMahon, Allen J.)—157
Burgess, John S. Rotation-vibration spectra of methane—927(T)
Burgy, M. T. (see Hughes, D. J.)—481(L)
——, **D. J. Hughes, J. R. Wallace, R. B. Heller, and W. E. Woolf.** Double transmission and depolarization of neutrons—953
Burnett, Clyde R. Isotope shift in the atomic spectrum of carbon—494(L)
Burrows, Hannah B., W. M. Gibson, and J. Rotblat. Angular distributions of protons from the reaction $O^{16}(d,p)O^{17}$—1095(L)
Butler, S. T. On angular distributions from (d,p) and (d,n) nuclear reactions—1095(L)
Cameron, A. G. W. and L. Katz. Half-life of Cu^{64}—904(L)
Canada, Robert (see Bunker, Merle E.)—126(A), 961
Caplan, David and Edward Akeley. Axial motion of an electron in a constant wave velocity section of a linear accelerator—125(A)
Carr, E. F. and C. Kikuchi. Angular dependence of hyperfine structure for the copper ion—1107(L)
Carrillo, Nabor. Soil mechanics of the City of Mexico—135(T)
Carss, W. L., Jane R. Gum, and M. L. Pool. Beta-decay of isomeric Cd^{113}—1028
Case, K. M. Singular potentials—797
—— **and A. Pais.** On spin-orbit interactions and nucleon-nucleon scattering—138(A), 203
Caspari, M. E. and W. J. Merz. Electromechanical behavior of $BaTiO_3$ single-domain crystals—1082
Castle, J. G., Jr. and Robert Beringer. Microwave magnetic resonance absorption in nitrogen dioxide—114(L)
Ceccarelli, M., G. Quareni, and A. Rostagni. On the radioactivity of potassium—909(L)
Chandrasekhar, B. S. (see Bowers, R.)—856
Chao, C. Y. Angular distributions of the alpha-particles and of the gamma-rays from the disintegration of fluorine by protons—1035
—— (see Day, R. B.)—131(A)
Chen, Joses J. L. (see Warshaw, S. D.)—97(L), 288(L)
Chew, Geoffrey F. Inelastic scattering of high energy neutrons by deuterons according to the impulse approximation—196
Childs, W. J. (see Cork, J. M.)—286(L)
Christian, Darleane and Don S. Martin, Jr. Preparation of Co^{58m} by a (γ,n) reaction—1110(L)
Cini, Marcello and Luigi A. Radicati. Variational principle for time-dependent problems—300(L)
Cobble, James W. and R. W. Atteberry. Precision determination of some half-lives—917(L)
Cochran, R. G. (see Schelberg, A. D.)—574
Cohen, Bernard L. Theory of natural alpha-radioactivity—105(L)
Cohen, Robert S., Lyman Spitzer, Jr., and Paul McR. Routly. Electrical conductivity of an ionized gas—230
Coles, Donald K. (see Lide, David R.)—911(L)
Colli, Laura, Ugo Facchini, and Emilio Gatti. Pulses in argon counters—92(L)
Collie, C. H. (see Bishop, G. R.)—211
Collins, T. L. Nuclear magnetic resonance for K^{39}—103(L)
Cook, C. Sharp (see Ter-Pogossian, Michel)—294(L), 360
Cook, D. B., M. W. Zemansky, and H. A. Boorse. Super conductivity of columbium—737
Cook, Leslie J. (see Bishop, A. S.)—136(A), 291(L)
Cook, Richard K. and Pearl G. Weissler. Piezoelectric constants of alpha- and beta-quartz at various temperatures—712
Coomes, E. A. (see Munick, R. J.)—887
Coon, J. H. Disintegration of He^3 by fast neutrons—488(L)
Cooper, John N. (see Grove, G. Richard)—107(L), 131(A)
——, **Warren E. Taylor, J. C. Harris, and G. Richard Grove.** Gamma-resonances in magnesium bombarded with protons—131(A)
Copeland, Paul L. and Delbert N. Eggenberger. Electric field at a thermionic cathode as a function of space current—298(L)
Cork, Bruce. Energy dependence of proton-proton scattering, 18.8 to 31.8 Mev—321
Cork, J. M., W. C. Rutledge, C. E. Branyan, A. E. Stoddard, W. J. Childs, and J. M. LeBlanc. Gamma-rays from Ag^{110}—286(L)
Corson, Dale R. Multiple scattering of fast electrons in nuclear emulsions—303(L)
Craig, D. Norman and James I. Hoffman. New method for determining the value of the faraday—487(L)
Crane, W. W. T. (see O'Kelley, G. D.)—293(L)
Crawford, M. F. (see Kelley, F. M.)—295(L)

——, **H. L. Welsh, J. C. F. MacDonald, and J. L. Locke.** Infra-red absorption of hydrogen induced by foreign gases—469(L)
Cross, William G. and Norman F. Ramsey. Conservation of energy and momentum in Compton scattering—929
Crowe, Kenneth M. and Evans Hayward. Cascade showers in lead—40
Cüer, P. On the π-meson absorption and emission mechanisms in nuclei—906(L)
Cutler, C. C. and C. F. Quate. Experimental verification of space charge and transit time reduction of noise in electron beams—875

Dale, E. Brock (see Zimmerman, E. L.)—908(L)
—— **and J. D. Kurbatov.** Gamma-ray spectrum of the 2,3 day isomer of cadmium 115—126(A)
——, **E. D. Richert, T. A. Redfield, and J. D. Kurbatov.** Gamma-radiation of Ba^{131}—763(L)
Darling, B. T. Irreducible volume character of events. I. A theory of the elementary particles and of fundamental length—460
Darrow, Karl E. El átomo desde Lucredio hasta ahora—124(T)
Dart, Francis E. (see Webb, Lyman A.)—129(A)
Das Gupta, K. Soft x-ray valence band spectra and the heat of formation of chemical compounds and alloys—281(L)
Daunt, J. G. Empirical correlation among superconductors—911(L)
Davis, Leo R., C. W. Kissinger, and G. J. Perlow. Proportional counter technique—132(A)
Davis, William O. Energy and density distribution of cosmic-ray neutrons—150
Day, R. B., C. Y. Chao, W. A. Fowler, and J. E. Perry, Jr. Angular distribution of gamma-rays from fluorine—131(A)
de Hoffmann, F. and E. Teller. Magneto-hydrodynamic shocks—692
DeJuren, James. Nuclear cross sections for 270-Mev neutrons—27
—— **and B. J. Moyer.** Variation of high energy neutron collision cross sections with energy—132(A)
Dekker, A. J. (see Leverton, W. F.)—732
—— (see Morrish, A. H.)—1030
de Oyarzábal, Juan. Polarization of vacuum by meson fields—138(A)
—— (see Juárez, A. Romero)—133(A)
de-Shalit, A. Magnetic moments of odd nuclei—103(L)
Devore, Lloyd T., Surindra N. Kalra, and William J. Fry. Generation of coherent electromagnetic radiation—128(A)
Dewan, J. T. (see Allen, K. W.)—181
Dickey, J. E. and E. A. Taft. Photoelectric changes induced in SrO and BaO by ultraviolet irradiation—308(L)
Dickinson, W. C. Hartree computation of the internal diamagnetic field for atoms—563
Dieke, G. H. and Eugene Sant Robinson. Molecular spectrum of He^3—1
Dienes, G. J. Frequency factor and activation energy for the volume diffusion of metals—123(A)
Distad, Merril F. Equilibrium currents induced in zincblende by electron bombardment of negative electrode—879
Diven, B. C. and G. M. Almy. Photo-disintegration of silver and aluminum—407
Donfor, Anthony, Webster Kendrick, and Herman Branson. Mass spectrometric studies of two series of organic compounds—129(A)
Douglas, R. A. (see Johns, H. E.)—1062
—— (see Katz, L.)—131(A)
Duncan, D. B. and J. E. Perry, Jr. Study of the $N^{14}(p,\gamma)O^{15}$ reaction—136(A)
Dunlap, W. C. (see Hall, R. N.)—467(L)
du Toit, S. (see Bishop, G. R.)—211
Dybvig, H. Talman and M. L. Pool. Re^{182} and Re^{183} by relative cross sections—126(A)

Eggenberger, Delbert N. (see Copeland, Paul L.)—298(L)
Ekstein, H. Perturbation treatment of Heisenberg's model of ferromagnetism—122(A)
Elliot, J. O. (see Liebson, S. H.)—907(L)
el Nadi, M. Are mesons complex particles?—754(L)
Emerson, W. H. (see Rado, G. T.)—273
Erginsoy, Cavid. On the mechanism of impurity band conduction in semiconductors—1104(L)
Eshbach, J. R., R. E. Hillger, and C. K. Jen. Nuclear magnetic moment of S^{33}—1106(L)
Etkin, Bernard and Victor G. Szebehely. Comments on Truesdell's paper on Bernoulli's theorem for viscous compressible fluids—767(L)
Extermann, C. R. (see Lacroix, R. P.)—763(L)

Facchini, Ugo (see Colli, Laura)—92(L)
Fainberg, Joseph (see Lord, J. J.)—970
Fairbank, Henry A. (see Lynton, Ernest A.)—1043
Faul, Henry (see Tittle, C. W.)—908(L)
Ferguson, W. F. C. and J. H. Greig. New mounting for an echelette diffraction grating—130(A)
Fernández, Carlos Graef. Perfectly symmetrical universe in flat space-time—127(T), 127(A)
Feynman, R. P. Mathematical formulation of the quantum theory of electromagnetic interaction—440
Finkelnburg, W. and S. M. Segal. High temperature plasma properties from high current arc stream measurements—258
Foldy, L. L. (see Sachs, R. G.)—824
—— **and F. J. Milford.** On the deviations of nuclear magnetic moments from the Schmidt limits—751(L)
Foley, H. M. Nuclear moment discrepancies in gallium and indium—288(L)
Fowler, W. A. (see Day, R. B.)—131(A)
—— (see Schardt, A W.)—136(A)
Fox, R., C. Leith, L. Wouters, and K. R. MacKenzie. Total cross sections of nuclei for 280-Mev neutrons—23
Frazer, B. C. and Ray Pepinsky. Low temperature x-ray diffraction goniometer—124(A)
Freeman, B. E. (see Bloch, I.)—553
Freier, G. D. (see Lampi, E. E.)—853
Fretter, W. B. Penetrating showers from carbon and lithium—127(T)
—— Penetrating showers from lithium—921(L)
—— (see Green, John R.)—134(A)
Friedlander, G., M. L. Perlman, D. Alburger, and A. W. Sunyar. Measurements of absolute electron capture rates with an application to the decay of Ni^{57}—30
——, **M. L. Perlman, and G. Scharff-Goldhaber.** Conversion coefficient of the 35 kev gamma-ray of Te^{125}—1103(L)
Fritz, James J., Oscar D. Gonzalez, and Herrick L. Johnston. Magnetic moments and eddy currents in spheres of superconducting tin—894
Fröberg, Carl-Erik. On the determination of the P-P interaction from scattering experiments—105(L)
Froman, Darol (see Allred, John C.)—136(A)
Fry, William J. (see Devore, Lloyd T.)—128(A)
—— (see Kalra, Surindra N.)—128(A)
Furuichi, J. and T. Mitsui. Domain structure of rochelle salt—93(L)

Galt, J. K. (see Yager, W. A.)—744
Gatti, Emilio (see Colli, Laura)—92(L)
Gellman, H., B. A. Griffith, and J. P. Stanley. Internal conversion in the L_I-shell—866
Germain, Lawrence S. Auger effect in astatine—937
—— Differential range spectrum of cosmic-ray mesons—616
Ghiorso, A. (see Rasmussen, J. O.)—475(L)
—— (see Thompson, S. G.)—781, 790, 1108(L)
Ghormley, J. A. (see Jenks, G. H.)—990
Ghoshal, S. N. Experimental verification of the theory of compound nucleus—939

Gião, Antonio. On the general motion of matter at the cosmological scale—755(L)
Gibson, W. M. (see Burrows, Hannah B.)—1095(L)
Giddings, Glenn W. Industry's views as to type of physics education desirable—927(T)
Gilbert, W. S. (see Peterson, J. M.)—135(A)
Gill, P. S., C. E. Mandeville, and E. Shapiro. Some properties of the 43-day isomer of Cd^{115}—284(L)
Gilvarry, J. J. and D. F. Rutland. General theory of voltage stabilizers—129(A)
Glaser, Donald A., Bernard Hamermesh, and George Safonov. Momentum distribution of charged cosmic-ray particles at sea level—625
Goldman, J. E. Single crystal magnetostriction constants of an iron-cobalt alloy—302(L)
—— **and R. Smoluchowski.** Theory of magnetic anisotropy in Alnico V—302(L)
Goldstein, L. and D. W. Sweeney. On the theory of slow neutron scattering by solid and liquid helium—141
Gómez, C. (see Juárez, A. Romero)—133(A)
Gonzalez, Oscar D. (see Fritz, James J.)—894
Gonzalez-Berredo, J. M. (See Rice, Bernard)—129(A)
Goodman, Clark (see Adamson, R. E., Jr.)—985
—— (see Stelson, P. H.)—287(L)
Gordon, M. M. Scattering lengths of the deuteron and *p-d* scattering—1111(L)
Grebenkemper, C. J. and John P. Hagen. Dielectric constant of liquid helium—89(L)
Green, John R. Penetrating showers in carbon—832
—— **and W. B. Fretter.** Penetrating showers in carbon—134(A)
Greig, J. H. (see Ferguson, W. F. C.)—130(A)
Greisen, K. (see Walker, W. D.)—546
——, **W. D. Walker, and S. P. Walker.** *N* component in extensive air showers—535
Griffith, B. A. (see Gellman, H.)—866
Groetzinger, Gerhart and David Kahn. New evidence for the existence of positively charged particles appearing near beta-ray emitters—108(L)
Gross, Leonard and Donald R. Hamilton. Beta-spectrum of sulfur 35 in the range of 0–30 kilovolts—484(L)
Grove, G. Richard (see Cooper, John N.)—131(A)
——, **John N. Cooper, and J. C. Harris.** Gamma-ray resonances produced by the bombardment of phosphorus with protons—107(L)
——, **John N. Cooper, and J. C. Harris.** Gamma-rays induced by the proton bombardment of phosphorus—131(A)
Gum, Jane R. (see Carss, W. L.)—1028
—— **and M. L. Pool.** Radioactive isotopes of Ag and Cd—315
Gutenberg, Benno. Low velocity layers in the earth's interior, the ocean and the atmosphere—130(T)
Gutowsky, H. S. and C. J. Hoffman. Chemical shifts in the magnetic resonance of F^{19}—110(L)

Hadley, James (see Aamodt, Lee)—282(L)
—— (see Panofsky, Wolfgang, K. H.)—94(L)
—— **and Herbert York.** Protons and deuterons ejected from nuclei by 90-Mev neutrons—345
Hagen, John P. (see Grebenkemper, C. J.)—89(L)
Hahn, E. L. Spin echoes—580
Halban, H. (see Bishop, G. R.)—211
Hall, R. N. and W. C. Dunlap, *P-N* junctions prepared by impurity diffusion—467(L)
Halpern, J. (see Mann, A. K.)—470(L)
Halteman, Eber K. Electron diffraction line broadening in thin nickel films—927(T)
Hamermesh, Bernard. Neutron capture gamma-ray spectra —131(A), 415
—— (see Glaser, Donald A.)—625
Hamilton, Donald R. (see Gross, Leonard)—484(L)
Hamilton, J. G. (see Miller, J. F.)—486(L)
Hanna, G. C. Distintegration of boron by slow neutrons—530
Hanna, S. S. (see Krone, R. W.)—603
Harris, G. G. and T. J. B. Shanley. On the μ-meson decay—474(L)
Harris, J. C. (see Cooper, John N.)—131(A)
—— (see Grove, G. Richard)—107(L), 131(A)
Harris, Sigmund P. Neutron scattering cross sections of the noble gases—20
——, **C. T. Hibdon, and C. O. Muehlhause.** Neutron cross section of Mn below 5000 ev—1014
——, **C. O. Muehlhause, S. Rasmussen, H. P. Schroeder, and G. E. Thomas.** Pile neutron absorption cross sections —342
Harrison, F. B. (see Reynolds, G. T.)—129(A)
Harvey, B. G. and B. I. Parsons. Preparation of Th^{235} and Pa^{235}—1098(L)
Haslam, R. N. H. (see Johns, H. E.)—1062
—— (see Katz, L.)—131(A)
——, **L. Katz, H. J. Moody, and H. M. Skarsgard.** Decay scheme of Cl^{39}—318
Hauptman, H. and J. Karle. Relations among the crystal structure factors—244
Havens, W. W., Jr. (see Tittman, J.)—903(L)
Haworth, F. E. Experiments on the initiation of electric arcs —223
Haymond, H. R. (see Miller, J. F.)—486(L)
Hayward, Evans (see Crowe, Kenneth M.)—40
Heaps, C. W. Magnetoresistance of bismuth at 3000 megacycles—892
Hedgran, A. (see Bishop, G. R.)—211
Heidmann, J. Production of high energy deuterons by energetic nucleons bombarding nuclei—171
Heller, R. B. (see Burgy, M.)—953
Helmholz, A. C. (see Bartell, F. O.)—1006
Henderson, Joseph E., Charles E. Miller, David S. Potter, and Jay Todd, Jr. Relative intensities at 3.4 kilometers and sea level of the cosmic-ray proton component—133(A)
Henkel, R. L. and H. H. Barschall. Capture cross sections for fast neutrons—145
Henry, Allan F. Hyperfine structure of Zeeman levels in nitric oxide—549
—— Zeeman effect in oxygen—396
Henry, C. O. (see Sidhu, S. S.)—123(A)
Hess, David C. (see Inghram, Mark, G.)—916(L)
Heydenburg, N. P. (see Hudspeth, Emmett L.)—643
Hibdon, C. T. (see Harris, S. P.)—1014
Hicks, Harry G. (see Wilkinson, Geoffrey)—491(L)
Hildebrand, Roger H. and Cecil E. Leith. Total cross sections of nuclei for 42 Mev neutrons—842
Hill, J. E. (see Roberts, L. D.)—6
Hill, R. D. Erratum: nuclear isomerism and shell structure—906(L)
Hillger, R. E. (see Eshbach, J. R.)—1105(L)
Hine, G. J. and F. E. Senftle. Neutron yield from $Be^9(\gamma,n)Be^8$ reaction—904(L)
Hipple, J. A. (see Sommer, H.)—487(L)
Hoffman, C. J. (see Gutowsky, H. S.)—110(L)
Hoffman, James I. (see Craig, D. Norman)—487(L)
Hofstadter, R. and J. A. McIntyre. Measurement of gamma-ray energies with crystals of NaI(Tl)—131(A)
—— **and J. A. McIntyre.** Measurement of gamma-ray energies with single crystals of NaI(Tl)—631
Holland, S. S., Jr. (see Sperduto, A.)—769(L)
Hollander, J. M. and R. F. Leininger. On the half-life of actinium—915(L)
Holmes, John R. Isotope shift in the C^{14} atomic spectrum for $2p^1S_0$-$3s^1P_0$—130(A)
Holt, R. B. (see Johnson, R. A.)—376
Hopper, V. D. and S. Biswas. Evidence concerning the existence of the new unstable elementary neutral particle—1099(L)

Hornbeck, John A. Mobilities of molecular and atomic rare gas ions in the parent gases: helium, neon, and argon—297(L)
Horváth, J. I. Geometrical model for the unified theory of the physical fields—901(L)
Hoselitz, K. and M. McCaig. Theory of magnetic properties of anisotropic permanent magnet alloys—757(L)
Hoshino, Sadao (see Shirane, Gen)—1105(L)
Hough, P. V. C. On the photo-disintegration of the deuteron by lithium and fluorine γ-rays—1069
Houston, W. V. Forces on a supraconductor in a magnetic field—135(T)
Hu, Ning. *S*-matrix in meson theory—1109(L)
Hudis, J. (see Ter-Pogossian, M.)—360
Hudson, Alvin (see Allred, John C.)—136(A)
Hudspeth, Emmett L., Charles P. Swann, and N. P. Heydenburg. Deuteron bombardment of C^{14}—643
Hughes, D. J. (see Burgy, M.)— 953
——, **M. T. Burgy, and W. E. Woolf.** Scattering and polarization of neutrons in an iron single crystal—481(L)
Hulet, E. K. (see Reynolds, F. L.)—467(L)
Hull, M. H., Jr. (see Bloch, I.)—553
—— (see Breit, G.)—392, 561
Hulm, J. K., B. T. Matthias, and E. A. Long. Erratum: a ferroelectric Curie point in $KTaO_3$—490(L)
Humphreys, R. F. (see Motz, H. T.)—595
Hurst, D. G. and N. Z. Alcock. Scattering lengths of the deutron—117(L)
Hurwitz, H., Jr. (see Bethe, H. A.)—11

Ichinokawa, T. (see Ueda, R.)—1106(L)
Imai, Isao. Asymptotic solutions of ordinary linear differential equations of the second order—1112(L)
Inghram, Mark G., Harrison Brown, Clair Patterson, and David C. Hess. Branching ratio of K^{40} radioactive decay—916(L)
Inglis, D. R. (see Krone, R. W.)—603
Isenberg, Irvin. Virial theorem and the variation principle—917(L)

Jacobs, John E. Performance of cadmium sulphide as a detector of x-radiation—124(A)
James, J. A., C. J. Milner, and B. N. Watts. Structure of lead sulfide films—298(L)
Jaumot, Frank E., Jr. (see Nix, Foster C.)—119(L)
Jech, C. Double development of nuclear emulsions—759(L)
Jeffries, C. D. (see Bloch, F.)—305(L)
Jen, C. K. (see Eshbach, J. R.)—1106(L)
Jenks, G. H., F. H. Sweeton, and J. A. Ghormley. A precise determination of the half-life and average energy of tritium decay—990
Jennings, B., K. H. Sun, and H. A. Leiter. Neutron production by proton bombardment below the (p,n) threshold—109(L)
Jensen, Erling N., L. Jackson Laslett, and D. J. Zaffarano. Disintegration of praseodymium 142—862
Johns, H. E. (see Katz, L.)—131(A)
——, **L. Katz, R. A. Douglas, and R. N. H. Haslam.** Gamma-neutron cross sections—1062
Johns, M. W. (see Petch, H. E.)—478(L)
Johnson, C. H. and H. H. Barschall. Interaction of fast neutrons with nitrogen—818
Johnson, C. Y. (see Perlow, G. J.)—133(A)
Johnson, E. O. and L. Malter. Floating double probe method for measurements in gas discharges—58
Johnson, M. H. Ionic mobilities and the electric quadrupole moment of N_2—101(L)
Johnson, R. A., B. T. McClure, and R. B. Holt. Electron removal in helium afterglows—376
Johnston, Herrick L. (see Fritz, James J.)—894
Jost, R., J. M. Luttinger, and M. Slotnick. Distribution of recoil nucleus in pair production by photons—189
Juárez, A. Romero. Motion of charges in magnetic fields—138(A)
——, **J. de Oyarzábal, C. Gómez, and F. Medina.** On the albedo of cosmic radiation—133(A)
Jungerman, J. Energy barrier for asymmetric fission in the static liquid drop model—285(L)

Kaenzig, W. Atomic positions and vibrations in the ferroelectric $BaTiO_3$ lattice—94(L)
Kahn, David (see Groetzinger, Gerhart)—108(L)
Kalra, Surindra N. (see Devore, Lloyd T.)—128(A)
—— **and William J. Fry.** Effect of space charge on pulsed electron beams—128(A)
Karle, J. (see Hauptman, H.)—244
Karplus, Robert and Maurice Neuman. Non-linear interactions between electromagnetic fields—380
Karraker, D. G. and D. H. Templeton. Radioactive isotopes of rubidium—646
Kato, Tosio. Variational methods in collision problems—475(L)
Katz, L. (see Cameron, A. G. W.)—904(L)
—— (see Haslam, R. N. H.)—318
—— (see Johns, H E)—1062
——, **H. E. Johns, R. A. Douglas, and R. N. H. Haslam.** Gamma-neutron cross section of some isotopes for γ-ray energies up to 27 Mev—131(A)
Keenan, Thomas and Edward Akeley. Longitudinal motion of electrons in a linear accelerator—125(A)
Keepin, George R., Jr. Search for Be^7 states using the Li^6 technique—768(L)
Kelly, F. M., R. Richmond, and M. F. Crawford. Spectroscopic value of the magnetic moment of $_{83}Bi^{209}$—295(L)
Kendrick, Webster (see Donfor, Anthony)—129(A)
Kenty, Carl. New form of discharge in gas mixtures: the flashing discharge—96(L)
—— Role of metastable ($^3P_2$) Hg atoms in low current discharges in Hg rare gas mixtures—95(L)
Kessler, Karl G. and William F. Meggers. Nuclear spin of $_{43}Tc^{99}$—905(L)
Ketelle, B. H. Ca^{45} beta-distribution obtained in a split crystal scintillation spectrometer—758(L)
——, **A. R. Brosi, and H. Zeldes.** Two-day Xe^{133} isomer—485(L)
Kettner, M. E. (see Lagergren, C. R.)—102(L)
Kikuchi, C. (see Carr, E. F.)—1107(L)
Kikuchi, Seishi. Stars initiated by gamma-rays—492(L)
Kimura, Motoharu. Temperature effect in Geiger-Müller counters—761(L)
Kinsey, B. B. and G. A. Bartholomew. Radiative capture of neutrons in deuterium—918(L)
Kissinger, C. W. (see Davis, Leo R.)—132(A)
Kittel, C. Note on the inertia and damping constant of ferromagnetic domain boundaries—918(L)
—— (see Williams, H. J.)—1090
Klein, Martin J. and Robert S. Smith. Note on the classical spin-wave theory of Heller and Kramers—1111(L)
Knipp, Julian K. (see Ling, Rufus C.)—106(L)
——, **R. B. Leachman, and R. C. Ling.** Ionization defects of fission fragments—478(L)
Koehler, J. S. (see Peach, M.)—436
Kohn, W. (see Silverman, R. A.)—912(L)
—— **and N. Bloembergen.** Remarks on the nuclear resonance shift in metallic lithium—913(L)
Kojima, Shoji and Kazuo Takayama. Noise temperature of a d.c. gas discharge plasma—907(L)
Kojima, Yūzō (see Okamura, Tosihiko)—910(L)
Kolsky, H. G., T. E. Phipps, Jr., N. F. Ramsey, and H. B. Silsbee. Radiofrequency spectrum of D_2 in a magnetic field—483(L)
Korff, S. A. Neutrons in the cosmic rays—127(T)

—— **and Y. Beers.** Solar atmosphere and the origin of radio-frequency radiation—489(L)
Krone, R. W., S. S. Hanna, and D. R. Inglis. Angular yield of both proton groups from $Li^6(d,p)Li^7$—603
Krueger, H. H. A., D. Meneghetti, G. R. Ringo, and L. Winsberg. Small angle scattering of thermal neutrons—507
Kruger, P. Gerald (see Phillips, J. A.)—326
Kundu, D. N. and M. L. Pool. Excitation function for the 6.7-hr. Cd^{107} by (p,n) and $(d,2n)$ reaction from Ag^{107}—126(A)
Kurath, Dieter. Effect of finite range interactions in the (jj) coupling shell model—98(L)
Kurbatov, J. D. (see Dale, E. Brock)—126(A), 763(L)
—— (see Zimmerman, E. L.)—908(L)

LaBerge, W. B. (see Munick, R. J.)—887
Lacroix, R. P., Ch. E. Ryter, and C. R. Extermann. Method for measuring paramagnetic absorption on small samples—763(L)
Lagergren, C. R. and M. E. Kettner. Isotopic constitution of thulium—102(L)
Lampi, E. E., G. D. Freier, and J. H. Williams. Total scattering cross section of neutrons by hydrogen and carbon—853
Landé, Alfred. On advanced and retarded potentials—283(L)
Langer, Lawrence M. (see Bunker, M. E.)—468(L)
—— **and R. Douglas Moffat.** Radioactivity of Ga^{66}—651
——, **R. D. Moffat, and H. C. Price, Jr.** Forbidden shape beta spectrum of Sb^{124}—126(A)
Langsdorf, Alexander, Jr. Experiments upon anisotropic and inelastic scattering with a highly collimated neutron beam—132(A)
Laslett, L. Jackson (see Jensen, Erling N.)—862
Laubenstein, R. A. (see Mobley, R. C.)—309
Laurikainen, K. V. (see Nilsson, S. B.)—291(L)
Lauritsen, C. C. (see Schardt, A. W.)—136(A)
Lawson, J. S., Jr. (see Phillips, J. A.)—326
Lax, Melvin. Neutron refraction in ferromagnets—299(L)
Leachman, R. B. (see Knipp, J. K.)—478(L)
Lebacqz, Jean V. (see Bodmer, Max)—122(A)
LeBlanc, J. M. (see Cork, J. M.)—286(L)
Le Compte, G. (see Verhaeghe, J.)—758(L)
Lederman, L. (see Bernardini, G.)—924(L)
Leighton, R. B. Some properties of the new unstable cosmic-ray particles—127(T)
Leininger, R. F. (see Hollander, J. M.)—915(L)
Leiter, H. A. (see Jennings, B.)—109(L)
Leith, Cecil E. (see Fox, R.)—23
—— (see Hildebrand, Roger H.)—842
Leng, Herta R. Modern physics in modern medicine—927(T)
Leverton, W. F. and A. J. Dekker. Hall coefficient and resistivity of thin films of antimony prepared by distillation—732
Lewis, Woodfin (see Branson, Herman)—123(A)
Li, Yin-Yuan. Natural spread of the conic distribution of the Čerenkov radiation—104(L)
—— On the ordering effect of antiferromagnetism—457
Libby, W. F. (see Martell, E. A.)—977
Lide, David R. and Donald K. Coles. Microwave spectroscopic evidence for internal rotation in methyl silane—911(L)
Liebson, S. H., M. E. Bishop, and J. O. Elliot. Fluorescent decay of scintillation crystals—907(L)
Lindenbaum, S. J. (see Bernardini, G.)—905(L)
Lindenfeld, P. (see Perez-Mendez, V.)—1097(L)
Linder, E. G. Sheath formation in ion-neutralized electron beams—99(L)
Ling, Rufus C. (see Knipp, J. K.)—478(L)
—— **and Julian K. Knipp.** Ionization by recoil particles from alpha-decay—106(L)
Lipkin, H. J. and M. G. White. Erratum: scattering of positrons and electrons by nuclei—770(L)
Little, D. E. and G. M. Shrum. Correlation of auroral observations in the Northern and Southern Hemispheres—135(A)
Little, R. N. (see Moore, J. J.)—137(A)
Lloyd, Stuart P. Angular correlation: a general proof of the method of D. R. Hamilton—118(L)
Locke, J. L. (see Crawford, M. F.)—469(L)
Long, E. A. (see Hulm, J. K.)—490(L)
Lord, J. J., Joseph Fainberg, and Marcel Schein. Evidence for the multiple production of mesons in a single nucleon-nucleon collision—970
—— **and Marcel Schein.** Diurnal variation of primary cosmic-ray heavy nuclei—304(L)
Low, W. and C. H. Townes. Evidence from nuclear masses on proposed closed shells at 20 nucleons—608
Lukesh, Joseph S. On the symmetry of graphite—226
Lundby, Arne. Scintillation decay times—477(L)
Luttinger, J. M. Note on Tisza's theory of superconductivity—727
—— (see Jost, R.)—189
Lynton, Ernest A. and Henry A. Fairbank. Second sound in He^3-He^4 mixtures—1043

Ma, S. T. Quantum theory of the longitudinal electromagnetic field—729
MacDonald, J. C. F. (see Crawford, M. F.)—469(L)
MacIntyre, W. J. Measurements of short-lived isomers—1018
MacKenzie, K. R. (see Fox, R.)—23
Macnamara, J. and H. G. Thode. Isotopes of xenon and krypton in pitchblende and the spontaneous fission of U^{238}—471(L)
—— **and H. G. Thode.** Relative neutron capture cross sections of the istotopes of krypton and xenon—296(L)
Maletskos, C. J. (see Brownell, G. L.)—1102(L)
Malm, Robert and W. W. Buechner. Proton groups from the $N^{14}(d,p)N^{15}$ and $N^{15}(d,p)N^{16}$ reactions—771
Malpica, Jose Mireles. Electrostatic direct current transformer of 300 kilovolts—124(A), 130(T)
Malter, L. (see Johnson, E. O.)—58
Mandeville, C. E. (see Gill, P. S.)—284(L)
—— **and H. O. Albrecht.** Crystals and Geiger counters for scintillation counting—299(L)
—— **and H. O. Albrecht.** Detection of beta-induced scintillations from crystals with a photo-sensitive Geiger-Mueller counter—117(L)
—— **and H. O. Albrecht.** Detection of gamma-ray-induced scintillations from crystals in a photo-sensitive Geiger-Müller counter—300(L)
—— **and E. Shapiro.** Characteristic radiations of rhodium (105)—125(A)
Mann, A. K. and J. Halpern. Excitation function of the reaction $C^{12}(\gamma,p)B^{11}$—470(L)
Mann, L. G. and Peter Axel. Decay of Y^{87} and Sr^{87m}—759(L)
Marais, E. J. and H. Verleger. Rotational structure of the ultraviolet band system of the P_2 molecule—429
Marshak, R. E. (see Tamor, S.)—766(L)
——, **S. Tamor, and A. S. Wightman.** Further remarks on the absorption of π^--mesons in hydrogen—765(L)
Martell, E. A. and W. F. Libby. Natural radioactivity of In^{115}—977
Martin, A. B. and Frank Asaro. Rate of diffusion of gold into copper at low gold concentrations—123(A)
Martin, Don S., Jr. (see Christian, Darleane)—1110(L)
Martin, E. V. (see Morey, D. R.)—927(A)
Marton, L. (see Reverdin, D.)—128(A)
——, **J. A. Simpson, and A. Van Bronkhorst.** Further observations on domain fringe fields—122(A)
Matthews, P. T. Spinless mesons and nucleons in the electromagnetic field—292(L)
—— Spinless mesons in the electromagnetic field—292(L)
Matthias, P. T. (see Hulm, J. K.)—490(L)
McCaig, M. (see Hoselitz, K.)—757(L)
McCammon, G. (see Roberts, L. D.)—6
McClure, B. T. (see Johnson, R. A.)—376

McDaniel, B. D., R. L. Walker, and M. B. Stearns. Neutron yields from photo-disintegration by gamma-rays from lithium—807
McGowan, F. K. 1.7×10^{-9} sec. isomeric state in $_{68}Er^{166}$—923(L)
—— 3×10^{-9} sec. isomeric state in $_{63}Eu^{122}$—482(L)
McIntyre, J. A. (see Hofstadter, R.)—131(A), 631
McMahon, Allen J., Bruno Rossi, and W. F. Burditt. Altitude and latitude dependence of bursts in a lead-shielded ionization chamber—157
McMillan, Edwin M. Artificial production of mesons—122(T)
—— Relation between phase stability and first-order focusing in linear accelerators—493(L)
McQueen, John H. Isotopic separation due to settling in the atmosphere—100(L)
McR. Routly, Paul (see Cohen, Robert S.)—230
Medicus, Heinrich A. and Peter Preiswerk. Isomeric transition of Tc^{95}—1101(L)
Medina, Alejandro. Scattering of mesons by nucleons—138(A)
Medina, F. (see Juárez, A. Romero)—133(A)
Meggers, William F. (see Kessler, Karl G.)—905(L)
Meinel, A. B. On the entry into the earth's atmosphere of 57-kev protons during auroral activity—1096(L)
Mendelssohn, K. (see Bowers, R.)—856
—— **and J. L. Olsen.** Anomalous heat flow in superconductors—859
Meneghetti, D. (see Krueger, H. H. A.)—507
Menzel, D. H. El sol y el universo—130(T)
—— Magnetic field of the sun—127(T)
Merritt, F. R. (see Yager, W. A.)—744
Merritt, J. (see Richman, C.)—900(L)
Merz, W. J. (see Caspari, M. E.)—1082
Meyerhof, W. E., D. B. Nicodemus, and Felix Bloch. Polarization effects of scattered neutrons—132(A)
Milford, F. J. (see Foldy, L. L.)—751(L)
Miller, Charles E. (see Henderson, Joseph E.)—133(A)
Miller, J. F., J. G. Hamilton, T. M. Putnam, H. R. Haymond, and G. B. Rossi. Acceleration of stripped C^{12} and C^{13} nuclei in the cyclotron—486(L)
Millikan, R. A. Evolution of modern physics—130(T)
Milner, C. J. (see James, J. A.)—298(L)
Mitchell, Allan C. G. (see Bunker, Merle E.)—126(A)
Mitsui, T. (see Furuichi, J.)—93(L)
Miyatake, O. (see Yasaki, T.)—754(L)
Mobley, R. C. and R. A Laubenstein. Photo-neutron thresholds of beryllium and deuterium—309
Moffat, R. Douglas (see Bunker, M. E.)—468(L)
—— (see Langer, Lawrence M.)—126(A), 651
Montgomery C. G. (see Wei, J. P. N.)—480(L)
—— **and D. D. Montgomery.** Scintillations produced by cosmic rays—757(L)
Montgomery, D. D. (see Montgomery, C. G.)—757(L)
Moody, H. J. (see Haslam, R. N. H.)—318
Moon, M. L. (see Waggoner, M. A.)—420
Moore, J. J. and R. N. Little. Production of deuterium-zirconium targets—137(A)
Morey, D. R. and E. V. Martin. Optical dichroism from adsorbed dyes and its correlation with orientation of the substrate—927(A)
Morganstern, K. H. (see Ter-Pogossian, M.)—360
Morrish, A. H. and A. J. Dekker. Decays of luminescent KBr and LiF—1030
Morrison, H. L. (see Rogers, F. T., Jr.)—128(A)
Moseley, H. M. and Nathan Rosen. Meson as a composite particle—177
Moshinsky, Marcos. Boundary conditions for the description of nuclear reactions—137(A)
—— Interaction of Birkhoff's gravitational field with the electromagnetic and pair fields—139(A)
—— On the interactions of Birkhoff's gravitational field with the electromagnetic and pair fields—514
—— (see Adem, J.)—128(A)
Motz, H. T. and R. F. Humphreys. Protons from the deuteron bombardment of enriched silicon and related atomic masses—595
Moyer, B. J. (see DeJuren, J.)—132(A)
Mozley, R. F. Production of π^+-mesons by x-rays as a function of atomic number—493(L)
Mrozowski, S. Anomalous diamagnetism of graphite—123(A)
Muehlhause, C. O. (see Harris, S. P.)—342, 1014
Muether, Herbert R. and Stuart L. Ridgway. Shape of the low energy beta-spectrum of Rb^{86}—750(L)
Munick, R. J., W. B. LaBerge, and E. A. Coomes. Periodic deviations in the Schottky effect for tantalum—887

Nakajima, S. and M. Shimizu. Two fluid theory of liquid helium II below 1°K—923(L)
Naudé, S. M. and H. Verleger. Perturbations in the ultraviolet band spectrum of the phosphorus molecule P_2—432
Nesbitt, E. A. and H. J. Williams. Mechanism of magnetization in Alnico V—112(L)
Nesbitt, L. B. (see Serin, B.)—761(L)
Neuman, Maurice (see Karplus, Robert)—380
Newell, G. F. Magnetic shielding constant of H_2—476(L)
Newman, M. M. (see Stickley, E.)—128(A)
Ney, E. P. Energies and nuclear interactions of heavy primary rays—127(T)
Nicodemus, D. B. (see Meyerhof, W. E.)—132(A)
Niday, J. and A. Turkevich. Fission yield curve of Th^{232} with pile neutrons—136(A)
Nierenberg, William A. Intermediate cosine coupling in molecular beams—1102(L)
Nilsson, S. B. and K. V. Laurikainen. On the gravitational self-energy of light—291(L)
Nix, Foster C. and Frank E. Jaumot, Jr. Self-diffusion in cobalt—119(L)
Nowick, Arthur S. Variation of amplitude-dependent internal friction in single crystals of copper with frequency and temperature—249

Oda, Yukiyasu, Jumpei Sanada, and Shotaro Yamabe. On the angular distribution of 3.1-Mev neutrons scattered by protons—469(L)
Okamura, Tosihiko, Yosiharu Torizuka, and Yūzō Kojima. Microwave resonance absorption of $NiOFe_2O_3$—910(L)
O'Kelley, G. D., G. W. Barton, Jr., W. W. T. Crane, and I. Perlman. Radioactivity of Am^{242}—293(L)
Olsen, J. L. (see Mendelssohn, K.)—859
O'Neill, G. F. and W. T. Scott. On range-momentum measurements for electrons in gases—473(L)
Osborne, D. W. (see Abraham, B. M.)—366
Ourom, L. (see Wu, Ta-You)—129(A)

Pais, A. (see Case, K. M.)—138(A), 203
Paneth, Heinz R. Mechanism of self-diffusion in alkali metals—708
Panofsky, Wolfgang K. H. (see Aamodt, Lee)—282(L)
——, **Lee Aamodt, James Hadley, and Robert Phillips.** γ-ray spectrum resulting from capture of negative π-mesons in hydrogen—94(L)
Parkash, Om. On the temperature variations in alcohol-argon filled G-M counters—303(L)
Parker, E. and B. Peters. Large meson showers produced by primary cosmic-ray particles—133(A)
Parsons, B. I. (see Harvey, B. G.)—1098(L)
Parzen, George. On the scattering theory of the Dirac equation—261
—— Scattering of 100-Mev electrons from a heavy nucleus—355
Pasternack, Simon and Hartland S. Snyder. High energy neutron scattering by nuclei—921(L)
Patterson, Clair (see Inghram, Mark G.)—916(L)

Paul, Ronald S. (see Webb, Lyman A.)—129(A)
Peach, M. and J. S. Koehler. Forces exerted on dislocations and the stress fields produced by them—436
Pearson, G. L. (see Brattain, W. H.)—846
Penfield, Robert (see Bergmann, Peter G.)—81
Penfold, A. S. Apparent error in the measured mass of S^{32}—116(L)
Pepinsky, Ray. Modern developments in x-ray crystal-structure analysis—136(T)
—— X-RAC and the feasibility of automatic crystal structure analyses—124(A)
—— (see Frazer, B. C.)—124(A)
Perez-Mendez, V. and P. Lindenfeld. Radioactivity of F^{17}—1097(L)
Perlman, I. (see O'Kelley, G. D.)—293(L)
Perlman, M. L. (see Friedlander, G.)—30, 1103(L)
Perlow, G. J. (see Davis, Leo R.)—132(A)
——, **T. A. Bergstralh, C. Y. Johnson, and J. D. Shipman, Jr.** Rocket measurement of cosmic-ray ionization and range—133(A)
Perry, J. E., Jr. (see Day, R. B.)—131(A)
—— (see Duncan, D. B.)—136(A)
Petch, H. E. and M. W. Johns. Nuclear spins of the 2.62-Mev and 3.20-Mev excited states of thorium D—478(L)
Peters, B. (see Bradt, H. L.)—943
—— (see Parker, E.)—133(A)
—— **and H. L. Bradt.** On the abundance of light nuclei (Li to Si) in the primary cosmic radiation—133(A)
Peterson, J. M., R. S. White, and W. S. Gilbert. Photo-mesons from carbon—135(A)
Peterson, Vincent Z. Positive mesons produced by 345-Mev protons in liquid hydrogen—136(A)
Phillips, G. C. Long-range protons from the disintegration of carbon by deuterons and a study of the competing reactions—164
Phillips, J. A., J. S. Lawson, Jr., and P. Gerald Kruger. Photo-disintegration of the deuteron—326
Phillips, Robert (see Panofsky, Wolfgang K. H.)—94(L)
Phipps, T. E., Jr. (see Kolsky, H. G.)—483(L)
Piccioni, O. (see Walsh, T. G.)—619
Pickup, E. and L. Voyvodic. Radioactive nuclei emitted in cosmic-ray stars—1100(L)
—— **and L. Voyvodic.** Relativistic increase in ionization of charged particles in photographic emulsions—89(L)
Pines, David (see Bohm, David)—903(L)
Pontius, R. B. Application of the theory of reaction rates to studies of dye diffusion in a gel system—927(A)
Pool, M. L. (see Beckham, Walter C.)—125(A)
—— (see Carss, W. L.)—1028
—— (see Dybvig, H. Talman)—126(A)
—— (see Gum, Jane R.)—315
—— (see Kundu, D. N.)—126(A)
Porter, Fred T. (see Ter-Pogossian, Michel)—294(L), 360
Post, R. F. and L. I. Schiff. Statistical limitations on the resolving time of a scintillation counter—1113(L)
Potter, David S. (see Henderson, Joseph E.)—133(A)
Pratt, William W. Disintegration of Hf^{181}—289(L)
Preiswerk, Peter (see Medicus, Heinrich A.)—1101(L)
Present, R. D. Note on the Li^7 quadrupole moment—43
Preston, Melvin A. Photo-disintegration of O^{16}—307(L)
Preston, W. M. (see Adamson, R. E., Jr.)—985
—— (see Stelson, P. H.)—287(L)
Price, H. C., Jr. (see Langer, L. M.)—126(A)
Prieto, Fernando. On the self-energy of mesons—138(A)
Pringle, R. W. and S. Standil. Gamma-rays from neutron activated gold—762(L)
Pryce, M. H. L. Spin-spin interaction within paramagnetic ions—1106(L)
Pugh, Emerson M., N. Rostoker, and A. Schindler. On the Hall effect in ferromagnetics—688
Putnam, T. M. (see Miller, J. F.)—486(L)
Quareni, G. (see Ceccarelli, M.)—909(L)
Quate, C. F. (see Cutler, C. C.)—875

Radicati, Luigi A. (see Cini, Marcello)—300(L)
Rado, G. T., R. W. Wright, and W. H. Emerson. Ferromagnetism at very high frequencies. III. Two mechanisms of dispersion in a ferrite—273
Rainwater, J. (see Tittman, J.)—903(L)
Ramsey, Norman F. (see Cross, William G.)—929
—— (see Kolsky, H. G.)—483(L)
Rankin, B. (see Bradner, H.)—916(L)
Rasmussen, J. O., F. L. Reynolds, S. G. Thompson, and A. Ghiorso. Mass assignments of alpha-active isotopes in the rare-earth region—475(L)
Rasmussen, S. (see Harris, S. P.)—342
Rau, R. Ronald. Nature of wide angle sprays. I—914(L)
—— **and A. S. Wightman.** Nature of wide angle sprays. II—914(L)
Redfield, T. A. (see Dale, E. B.)—763(L)
Reverdin, D. and L. Marton. Space charge distribution in a d.c. cut-off magnetron—128(A)
Reynolds, C. A. (see Serin, B.)—761(L)
Reynolds, F. L. (see Rasmussen, J. O.)—475(L)
—— (see Thompson, S. G.)—1107(L)
——, **E. K. Hulet, and K. Street, Jr.** Mass-spectrographic identification of Cm^{243} and Cm^{244}—467(L)
Reynolds, G. T. and F. B. Harrison. Scintillation properties of solutions—129(A)
Rice, Bernard, J. M. Gonzelez-Berredo, and T. F. Young. Raman spectra at low temperatures. The Raman spectrum of tetramethyl diborane—129(A)
Richard-Foy, R. Camaras para rayos cosmicos—132(A)
Richards, H. T., R. V. Smith, and C. P. Browne. Proton-neutron reactions and thresholds—524
Richardson, J. E. High energy neutrons from the disintegration of C^{13} by deuterons—850
Richardson, J. Reginald (see Ruby, Lawrence)—760(L)
Richert, E. D. (see Dale, E. B.)—763(L)
Richman, C., M. Skinner, J. Merritt, and B. Youtz. Production of a π^+-meson beam using the deflected proton beam of the 184-inch synchro-cyclotron—900(L)
Richmond, R. (see Kelly, F. M.)—295(L)
Ridgway, Stuart L. (see Muether, Herbert R.)—750(L)
Ringo, G. R. (see Krueger, H. H. A.)—507
Robb, J. D. (see Stickley, E.)—128(A)
Roberts, A. (see Waggoner, M. A.)—420
Roberts, L. D., J. E. Hill, and G. McCammon. Study of the slowing down distribution of Sb^{124}-Be photo-neutrons in graphite, and of the use of indium foils—6
Robertson, H. P. Theories of gravitation—127(T)
Robinson, Eugene Sant (see Dieke, G. H.)—1
Rogers, F. T., Jr. (see Rogers, Marguerite M.)—126(A)
—— **and H. L. Morrison.** Un cero de una cierta función de las funciónes de bessel—128(A)
Rogers, Marguerite M. and F. T. Rogers, Jr. Los espectros continuous de los β-rayos de los gases radioactivos en la cámara de C. T. R. Wilson—126(A)
Rohrlich, F. Quantum electrodynamics of charged particles without spin—666
Rose, D. C. Meson spectrum and meteorological variations in cosmic-ray intensity—106(L)
Rosen, Louis (see Allred, John C.)—136(A)
Rosen, Nathan (see Moseley, H. M.)—177
Rossi, Bruno (see McMahon, Allen J.)—157
Rossi, G. B. (see Miller, J. F.)—486(L)
Rostagni, A. (see Ceccarelli, M.)—909(L)
Rostoker, N. (see Pugh, Emerson M.)—688
Rotblat, J. (see Burrows, Hannah B.)—1095(L)
Ruby, Lawrence and J. Reginald Richardson. Internal conversion electrons and other radiations from Cl^{34}—760(L)
Rutland, D. F. (see Gilvarry, J. J.)—129(A)

Rutledge, W. C. (see Cork, J. M.)—286(L)
Ryter, Ch. E. (see Lacroix, R. P.)—763(L)

Sachs, R. G. and L. L. Foldy. Scattering of gamma-rays by nucleons—824
Safonov, George (see Glaser, Donald A.)—625
Salant, E. O. Disintegrations and meson production by relativistic particles at different latitudes—127(T)
Sampson, M. B. (see Schelberg, A. D.)—574
Sanada, Jumpei (see Oda, Yakuyasu)—469(L)
—— **and Shotaro Yamabe.** On the forward scattering of 3.1-Mev neutrons by the deuteron—750(L)
Sard, R. D. Neutron production by cosmic rays at three depths—134(A)
Sawaguchi, Etsuro (see Shirane, Gen)—485(L)
Schardt, A. W., W. A. Fowler, and C. C. Lauritsen. Transmutation of N^{15} by protons—136(A)
Scharff-Goldhaber, G. (see Friedlander, G.)—1103(L)
Schein, Marcel. Nuclear collisions between high energy cosmic-ray particles—127(T)
—— (see Lord, J. J.)—304(L), 970
Schelberg, A. D., M. B. Sampson, and R. G. Cochran. Angular distribution of the $Al^{27}(d,\alpha)Mg^{25}$ reaction and energy levels in Mg^{25}—574
Schiff, L. I. Nuclear saturation and magic numbers in terms of a non-linear meson theory—137(A)
—— (see Post, R. F.)—1113(L)
Schiller, Ralph (see Bergmann, Peter G.)—81
Schindler, A. (see Pugh, Emerson M.)—688
Schorr, Marvin G. and Franklin L. Torney. Solid, non-crystalline scintillation phosphors—474(L)
Schroeder, C. A. (see Bergstralh, T. A.)—134(A)
Schroeder, H. P. (see Harris, S. P.)—342
Schweizer, Abraham A. On the deep configurations of V I and Cr II—1080
Scott, W. T. On a difference equation method in cosmic-ray shower theory—611
—— (see O'Neill, G. F.)—473(L)
Seaborg, G. T. (see Thompson, S. G.)—781, 790
Segal, S. M. (see Finkelnburg, W.)—258
Seitz, Frederick. Influence of plastic flow on the electrical and photographic properties of the alkali halide crystals—239
—— Lattice imperfections and plastic flow in metals—130(T)
Selove, W. Spin dependence of neutron scattering by Na^{23}—290(L)
Senftle, F. E. (see Hine, G. J.)—904(L)
Serin, B., C. A. Reynolds, and L. B. Nesbitt. Mass dependence of the superconducting transition temperature of mercury—761(L)
Shanley, T. J. B. (see Harris, G. G.)—474(L)
Shapiro, E. (see Gill, P. S.)—284(L)
—— (see Mandeville, C. E.)—125(A)
Shapiro, Maurice M. and Herman Yagoda. Collimated and wide-angle meson groups in a hard-shower star—283(L)
Sheer, C. (see Tittman, J.)—903(L)
Shimizu, M. (see Nakajima, S.)—923(L)
Shipman, J. D., Jr. (see Perlow, G. J.)—133(A)
Shirane, Gen, Sadao Hosino, and Kazuo Suzuki. X-ray study of the phase transition in lead titanate—1105(L)
——, **Etsuro Sawaguchi, and Akitsu Takeda.** On the phase transition in lead zirconate—485(L)
Shockley, W. (see Bardeen, J.)—69, 72
—— (see Williams, H. J.)—1090
Shrum, G. M. (see Little D. E.)—135(A)
Sidhu, S. S. and C. O. Henry. Effect of high energy neutron bombardment on crystal lattice of beryllium, graphite, diamond, and aluminum—123(A)
Siegbahn, K. (see Bishop, G. R.)—211
Silsbee, H. B. (see Kolsky, H. G.)—483(L)
Silverman, R. A. and W. Kohn. On the cohesive energy of metallic lithium—912(L)
Simmons, James W. and Wallace E. Anderson. Microwave determination of the centrifugal distortion constants of CH_3Cl, CH_3Br, CH_3I, BrCN, and ICN—338
—— **and William O. Swan.** Structure of methyl bromide from microwave spectra—289(L)
Simpson, J. A. Change of intensity of the nucleonic component during magnetic storms—135(A)
—— (see Marton, L.)—122(A)
Singer, S. F. Primary specific ionization and intensity of the cosmic radiation above the atmosphere at the geomagnetic equator—47
—— (see Van Allen, J. A.)—116(L), 133(A)
—— **and J. A. Van Allen.** Knee in the primary cosmic-ray spectrum—133(A)
Skarsgard, H. M. (see Haslam, R. N. H.)—318
Skinner, M. (see Richman, C.)—900(L)
Sloan, Raymond (see Bak, Børge)—101(L)
Slotnick, M. (see Jost. R.)—189
Smaller, B., E. Yasaitis, and H. L. Anderson. Precise determination of the ratio of the deuteron to proton magnetic moment—137(A)
Smith, Lloyd P. Education offered by an engineering physics curriculum—927(T)
Smith, R. V. (see Richards, H. T.)—524
Smith, Robert S. (see Klein, Martin J.)—1111(L)
Smoluchowski, R. (see Goldman, J. E.)—302(L)
Snell, Arthur H., E. C. Barker, and R. L. Sternberg. Photodisintegration cross sections of deuterium and beryllium for the gamma-rays of sodium 24 and gallium 72—637
Snoek, Jacob L. Cation distribution in copper zinc ferrite—299(L)
Snow, George and Hartland S. Snyder. On the self-energies of quantum field theory—987
Snyder, Hartland S. (see Pasternack, Simon)—921(L)
—— (see Snow, George)—987
Softky, S. D. (see Bartell, F. O.)—1006
Sommer, H., H. A. Thomas, and J. A. Hipple. Values of μ_p, F, and M_p/m_e using the omegatron—487(L)
Sondheimer, E. H. Influence of a transverse magnetic field on the conductivity of thin metallic films—401
Sperduto, A., S. S. Holland, Jr., D. M. Van Patter, and W. W. Buechner. Excited state of C^{14} from the $C^{13}(d,p)C^{14*}$ reaction—769(L)
Spiers, J. A. On the directional correlation of successive nuclear radiations—491(L)
Spitzer, Lyman, Jr. (see Cohen, Robert S.)—230
Spruch, Larry. On the space exchange magnetic moments of light nuclei—372
Staker, William P. Determination of the high altitude latitude dependence in cosmic-ray neutron intensity—52
Standil, S. (see Pringle, R. W.)—762(L)
Stanley, J. P. (see Gellman, H.)—866
Stearns, M. B. (see McDaniel, B. D.)—807
Steffen, Rolf M. Angular correlation of the gamma-rays emitted from the excited states of A^{38}—115(L)
Steinberger, J. (see Bishop, A. S.)—136(A), 291(L)
Stelson, P. H., W. M. Preston, and Clark Goodman. $V^{51}(p,n)$ Cr^{51} neutron spectrum—287(L)
Sternberg, R. L. (see Snell, Arthur H.)—637
Sternglass, E. J. Secondary electron emission and atomic shell structure—925(L)
Sternheimer, R. On nuclear quadrupole moments—102(L)
Stewart, D. B. (see Bartell, F. O.)—1006
Stickley, E., M. M. Newman, and J. D. Robb. Electrostatic charging of aircraft glass during flight—128(A)
Stinchcomb, Thomas G. Barometric effect for large cosmic-ray bursts under thick absorbers at 11,500 feet elevation and the absorption mean free path for very high energy nuclear collisions—479(L)
Stoddard, A. E. (see Cork, J. M.)—286(L)

Stover, Betsy Jones. Os^{182} and Os^{183}, new radioactive osmium isotopes—99(L)
Street, K., Jr. (see Reynolds, F. L.)—467(L)
—— (see Thompson, S. G.)—790, 1108(L)
Sun, K. H. (see Jennings, B.)—109(L)
Sunyar, A. W. (see Friedlander, G.)—30
Suryan, G. New method of integration of weak nuclear magnetic resonance signals—119(L)
Suzuki, Kazuo (see Shirane, Gen)—1105(L)
Swan, William O. (see Simmons, James W.)—289(L)
Swann, Charles P. (see Hudspeth, Emmett L.)—643
Sweeney, D. W. (see Goldstein, L.)—141
Sweeton, F. H. (see Jenks, G. H.)—990
Szebehely, Victor G. (see Etkin, Bernard)—767(L)

Taft, E. A. (see Dickey, J. E.)—308(L
Takayama, Kazuo (see Kojima, Shoji)—907(L)
Takeda, Akitsu (see Shirane, Gen)—485(L)
Tamburino, S. (see Addario, M. M.)—749(L)
Tamor, S. (see Marshak, R. E.)—765(L)
—— **and R. E. Marshak.** On the absorption of π^--mesons in deuterium—766(L)
Taylor, Julius H. Pressure dependence of resistance of germanium—919(L)
Taylor, Warren E. (see Cooper, John N.)—131(A)
Teller, E. (see de Hoffmann, F.)—692
Templeton, D. H. (see Karraker, D. G.)—646
Ter-Pogossian, Michel, C. S. Cook, F. T. Porter, K. H. Morganstern, and J. Hudis. Disintegration of Ti^{48}—360
——, **Fred T. Porter, and C. Sharp Cook.** On the transport of aluminum atoms by a gas—294(L)
Terrell, James. Gamma-rays from $Be^9(\alpha,n)$—1076
Thode, H. G. (see Macnamara, J.)—296(L), 471(L)
Thomas, D. G. (see Zimmerman, E. L.)—908(L)
Thomas, G. E. (see Harris, S. P.)—342
Thomas, H. A. Diamagnetic correction for protons in water and mineral oil—901(L)
—— (see Sommer, H.)—487(L)
Thomas, R. G. Excited states of N^{13} and C^{13}—136(A)
—— Multipole order of the 3.1-Mev gamma-ray from carbon 13—138(A)
Thompson, S. G. (see Rasmussen, J. O.)—475(L)
——, **A. Ghiorso, and G. T. Seaborg.** New element berkelium (atomic number 97)—781
——, **K. Street, Jr., A. Ghiorso, and F. L. Reynolds.** New isotope Pu^{242} and additional information on other plutonium isotopes—1108(L)
——, **K. Street, Jr., A. Ghiorso, and G. T. Seaborg.** New element californium (atomic number 98)—790
Tinlot, J. (see Bernardini, G.)—924(L)
Tisza, L. Theory of superconductivity—717
Tittle, C. W. Depression of the thermal neutron density by a detecting foil—756(L)
—— Thermal neutron diffusion length of paraffin—756(L)
—— **and Henry Faul.** Thermal neutron absorption cross section of silicon—908(L)
Tittman, J., C. Sheer, J. Rainwater, and W. W. Havens, Jr. Slow neutron resonant scattering of gold—903(L)
Todd, Jay, Jr. (see Henderson, Joseph E.)—133(A)
Tonks, L. (see Bethe, H. A.)—11
Torizuka, Yosiharu (see Okamura, Tosihiko)—910(L)
Torney, Franklin L. (see Schorr, Marvin G.)—474(L)
Townes, C. H. (see Low, W.)—608
Turkevich, A. (see Niday, J.)—136(A)
Twiss, R. Q. On Bailey's theory of growing circularly polarized waves in a sunspot—767(L)
Tyson, J. K. Gyroscopic stabilization of a free body—129(A)

Ueda, R. and T. Ichinokawa. Domain structure of tungsten trioxide—1106(L)
Urey, Harold C. Structure and chemical composition of Mars—295(L)

Vachaspati. Scattering of mesons by nuclear particles—973
Valente, Frank A. Possible existence of a constant third-order difference among the nuclear magic numbers—1110(L)
Vallarta, Manuel Sandoval. Geomagnetic analysis of the primary spectrum—127(T)
—— Scientific cooperation in action—138(T)
Van Allen, J. A. (see Singer, S. F.)—133(A)
—— **and S. F. Singer.** Erratum: on the primary cosmic-ray spectrum—116(L)
—— **and S. F. Singer.** On the primary cosmic-ray spectrum—133(A)
Van Bronkhorst, A. (see Marton, L.)—122(A)
van den Bosch, J. C. Some remarks on the analysis of the first U-spark spectrum—100(L)
Vandermeerssche, G. (see Verhaeghe, J.)—758(L)
Van Patter, D. M. (see Adamson, R. E., Jr.)—985
—— (see Sperduto, A.)—769(L)
van Wyk, C. B. Selection rules for closed loop processes—487(L)
Verhaeghe, J., G. Vandermeerssche, and G. Le Compte. Susceptibility and magnetic anisotropy of indium single crystals—758(L)
Verleger, H. (see Marais, E. J.)—429
—— (see Naudé, S. M.)—432
Voisin, André G. Penetrating showers of cosmic rays—920(L)
Voyvodic, L. (see Pickup, E.)—89(L), 1100(L)

Waggoner, M. A. Internal conversion of gamma-ray from Cs^{137}—489(L)
——, **M. L. Moon, and A. Roberts.** Internal conversion of gamma-rays from Co^{60}, Cs^{134}, Zn^{65}—420
Walker, R. L. (see McDaniel, B. D.)—807
Walker, S. P. (see Greisen, K.)—535
—— (see Walker, W. D.)—546
Walker, W. D. (see Greisen, K.)—535
——, **S. P. Walker, and K. Greisen.** Mean free path of penetrating shower producers—546
Wallace, J. R. (see Burgy, M.)—953
Walsh, T. G. and O. Piccioni. Latitude and altitude dependence of the local hard showers of cosmic rays—619
Wangsness, Roald K. On the magnetic moments of the proton and neutron—769(L)
Ward, J. C. Quantum effects in the interaction of electrons with high frequency fields—119(L)
Warshaw, S. D. β-spectrum of C^{14}—111(L)
—— **and Joses J. L. Chen.** Probable energy loss of electrons in matter—97(L)
——, **Joses J. L. Chen, and G. L. Appleton.** Beta-spectrum of P^{32}—288(L)
Watson, W. W. (see Zucker, A.)—966
Watts, B. N. (see James, J. A.)—298(L)
Way, Harold E. Education offered by curriculum leading to B.S. in physics—927(T)
Weaver, Boyd. Mass assignment of natural activity of samarium—301(L)
Webb, Lyman A., Ronald S. Paul, and Francis E. Dart. Detection of soft x-rays with a scintillation counter—129(A)
Wei, J. P. N. and C. G. Montgomery. Narrow air showers of cosmic rays. III. Further absorption measurements—480(L)
Weinstock, B. (see Abraham, B. M.)—366
Weissler, Pearl G. (see Cook, Richard K.)—712
Welsh, H. L. (see Crawford, M. F.)—469(L)
White, Gladys R. Penetration and diffusion of Co^{60} gamma-rays in water using spherical geometry—154
White, M. G. (see Lipkin, H. J.)—770(L)
White, R. S. (see Peterson, J. M.)—135(A)
Wick, G. C. Evaluation of the collision matrix—268
Wightman, A. S. (see Marshak, R. E.)—765(L)

—— (see Rau, R. Ronald)—914(L)
Wilkinson, Geoffrey. Neutron deficient radioactive isotopes of tantalum and wolfram—495
—— **and Harry G. Hicks.** Note on neutron deficient europium activities—491(L)
Williams, Dudley (see Bak, Børge)—101(L)
Williams, Ferd E. Calculation of the absorption and emission spectra of the thallium activated potassium chloride phosphor—306(L)
Williams, H. J. (see Nesbitt, E. A.)—112(L)
——, **W. Shockley, and C. Kittel.** Studies of the propagation velocity of a ferromagnetic domain boundary—1090
Williams, J. H. (see Lampi, E. E.)—853
Wilson, H. A. Energy levels of atomic nuclei—137(A)
Wilson, Richard. Neutron capture γ-rays from Cd, Cl, and C—90(L)
—— (see Bishop, G. R.)—211
Wilson, W. S. Surface ozone in Arctic regions—135(A)
Winckler, J. R. Geomagnetic effects at the top of the atmosphere—127(T)
Winn, Edward B. Temperature dependence of the self-diffusion coefficients of argon, neon, nitrogen, oxygen, carbon dioxide, and methane—1024
Winsberg, L. (see Krueger, H. H. A.)—507
Wood, E. A. (see Yager, W. A.)—744
Woolf, W. E. (see Burgy, M.)—953
——, (see Hughes, D. J.)—481(L)
Wouters, L. (see Fox, R.)—23
Wright, R. W. (see Rado, G. T.)—273
Wu, Ta-You and L. Ourom. Probability of auto-ionization in light atoms—129(A)
Yager, W. A., J. K. Galt, F. R. Merritt, and E. A. Wood. Ferromagnetic resonance in nickel ferrite—744
Yagoda, Herman. Cascade processes recorded in an emulsion chamber exposed in the stratosphere—753(L)
—— (see Shapiro, Maurice M.)—283(L)
Yamabe, Shotaro (see Oda, Yukiyasu)—469(L)
—— (see Sanada, Jumpei)—750(L)
Yasaitis, E. (see Smaller, B.)—137(A)
Yasaki, T. and O. Miyatake. On the probability of asymmetric and symmetric fission—754(L)
Yennie, D. R. Some remarks on non-local field theory—1053
York, Herbert (see Hadley, James)—345
Young, T. F. (see Rice, Bernard)—129(A)
Youtz, B. (see Richman, C.)—900(L)
Yukawa, Hideki. Quantum theory of non-local fields. Part II. Irreducible fields and their interaction—1047

Zaffarano, D. J. (see Jensen, Erling N.)—862
Zatzkis, Henry (see Bergmann, Peter G.)—81
Zeeman, P. B. Spectrum of the boron monosulphide (BS) molecule—902(L)
Zeldes, H. (see Ketelle, B. H.)—485(L)
Zemansky, M. W. (see Cook, D. B.)—737
Zimmerman, E. L., E. B. Dale, D. G. Thomas, and J. D. Kurbatov. Gamma-ray spectrum of Ba^{131}—908(L)
Zinnes, Irving. Polarization correlation of mixed multipoles—386
Zucker, A. and W. W. Watson. Concentration of A^{36} and A^{38} and study of the $A^{36}(d,p)A^{37}$ reactions and the beta activity of A^{39}—966

PHYSICAL REVIEW VOLUME 80, NUMBER 6 DECEMBER 15, 1950

Analytic Subject Index to Volume 80

References with (A) are to abstracts of papers presented at meetings of the American Physical Society. References with (L) are to Letters to the Editor.

Absorption of radiation
Penetration and diffusion of Co^{60} gamma-rays in water, Gladys R. White—154
Arcs (see **Discharge of electricity in gases**)
Astrophysics
Circularly polarized waves in sunspot. R. Q. Twiss—767(L)
Solar atmosphere and radiofrequency radiation, S. A. Korff and Y. Beers—489(L)
Structure and composition of Mars, Harold C. Urey—295(L)
Atmosphere (see **Meteorology**)
Atomic mass (see **Isotopes**)
Atomic structure (see also **Spectra**)
Secondary electron emission, E. J. Sternglass—925(L)
Aurora
Entry of 57-kev protons during activity, A. B. Meinel—1096(L)
Observations in Northern and Southern Hemispheres, D. E. Little and G. M. Shrum—135(A)

Broadening of spectral lines
Ammonia inversion line, P. W. Anderson—511

Conductivity, electrical (see **Electrical conductivity and resistance; Discharge of electricity in gases**)
Constants, physical standards
Speed of light by resonant cavity method, Kees Bol—298(L)

Cosmic radiation
Albedo of radiation, A. Romero Juárez, J. de Oyarzábal, C. Gómez, and F. Medina—133(A)
Barometric effect for large bursts, Thomas G. Stinchcomb—479(L)
Bursts in lead chamber, altitude and latitude dependence, Allen J. McMahon, Bruno Rossi, and W. F. Burditt—157
Camaras para rayos cosmicos, R. Richard-Foy—132(A)
Cascade processes in stratosphere, Herman Yagoda—753(L)
Cascade shower theory, Ira B. Bernstein—134(A), 995
Cascade showers in Pb, synchrotron x-rays, Kenneth M. Crowe and Evans Hayward—40
Difference equation in shower theory, W. T. Scott—611
Disintegrations at 29,000 meters, M. M. Addario and S. Tamburino—749(L)
Diurnal effect measurements, T. A. Bergstralh and C. A. Schroeder—134(A)
Energy and density distribution of neutrons, William O. Davis—150
Extensive air showers, N component, K. Greisen, W. D. Walker, and S. P. Walker—535
Intensity of nucleonic component during magnetic storms, J. A. Simpson—135(A)
Light nuclei (Li to Si) in primary radiation, B. Peters and H. L. Bradt—133(A)
Meson groups in hard-shower star, Maurice M. Shapiro and Herman Yagoda—283(L)

Meson range spectrum, Lawrence Germain—616
Meson showers produced by primary particles, E. Parker and B. Peters—133(A)
Meson spectrum and meteorological variations, D. C. Rose —106(L)
Momentum distribution of charged particles at sea level, Donald A. Glaser, Bernard Hamermesh, and George Safonov—625
Multiple production of mesons, J. J. Lord, Joseph Fainberg, and Marcel Schein—970
Narrow showers, absorption measurements, J. P. N. Wei and C. G. Montgomery—480(L)
Neutron intensity, latitude dependence at high altitudes, William P. Staker—52
Neutron production at three depths, R. D. Sard—134(A)
Penetrating shower producers, mean free path, W. D. Walker, S. P. Walker, and K. Greisen—546
Penetrating showers, André G. Voisin—920(L)
Penentrating showers from Li, W. B. Fretter—921(L)
Penetrating showers in C, John R. Green and W. B. Fretter —134(A); John R. Green—832
On the primary cosmic-ray spectrum, erratum, J. A. Van Allen and S. F. Singer—116(L)
Primary heavy nuclei, diurnal variation, J. J. Lord and Marcel Schein—304(L)
Primary radiation, abundance of light nuclei and origin, H. L. Bradt and B. Peters—943
Primary specific ionization above the atmosphere, S. F. Singer—47
Primary spectrum, J. A. Van Allen and S. F. Singer—133(A)
Primary spectrum, knee, S. F. Singer and J. A. Van Allen— 133(A)
Proportional counter technique, Leo R. Davis, C. W. Kissinger, and G. J. Perlow—132(A)
Radioactive nuclei in stars, E. Pickup and L. Voyvodic— 1100(L)
Relative intensities of protons at 3.4 kilometers and sea level, Joseph E. Henderson, Charles E. Miller, David S. Potter, and Jay Todd, Jr.—133(A)
Rocket measurement of ionization and range, G. J. Perlow, T. A. Bergstralh, C. Y. Johnson, and J. D. Shipman, Jr. —133(A)
Scintillations, C. G. Montgomery and D. D. Montgomery —757(L)
Showers, latitude and altitude dependence, T. G. Walsh and O. Piccioni—619
Small bursts, barometric and temperature coefficients, James W. Broxon—135(A)
Sprays, R. Ronald Rau—914(L); R. Ronald Rau and A. S. Wightman—914(L)

Cosmology
Symmetrical universe in flat space-time, Carlos Graef Fernández—127(A)

Cross section, measurements, theory (see also **Scattering of electrons, mesons, neutrons, protons, and ions**)
Of Be, B, O, and F for fast neutrons, C. K. Bockelman—1011
Capture of neutrons in deuterium, B. B. Kinsey and G. A. Bartholomew—918(L)
For $C^{13}(d,n)N^{14}$, J. E. Richardson—850
Of Cu for (γ,n) reaction, B. D. McDaniel, R. L. Walker, and M. B. Stearns—807
D—He^4 interaction, John C. Allred, Darol Froman, Alvin Hudson, and Louis Rosen—136(A)
Of F, V, Cu^{65}, Ag, I, In^{115}, and Au for fast neutrons, R. L. Henkel and H. H. Barschall—145
For 42 Mev neutrons, Roger H. Hildebrand and Cecil E. Leith—842
γ-d, P. V. C. Hough—1069
Gamma-neutron cross section, L. Katz, H. E. Johns, R. A. Douglas, and R. N. H. Haslam—131(A)
For γ-n reaction, H. E. Johns, L. Katz, R. A. Douglas, and R. N. H. Haslam— 1062
Of Kr and Xe, relative neutron capture, J. Macnamara and H. G. Thode—296(L)
Of Mn for neutrons, S. P. Harris, C. T. Hibdon, and C. O. Muehlhause—1014
Neutron absorption by Si, C. W. Tittle and Henry Faul— 908(L)
Neutron scattering at high energies, Simon Pasternack and Hartland S. Snyder—921(L)
Neutron scattering by Au, J. Tittman, C. Sheer, J. Rainwater, and W. W. Havens, Jr.—903(L)
Of neutrons by H and C, E. E. Lampi, G. D. Freier, and J. H. Williams—853
Neutrons by In, L. D. Roberts, J. E. Hill, and G. McCammon—6
Neutrons in noble gases, Sigmund P. Harris—20
Of Ni^{60} and Cu^{63}, compound nucleus Zn^{64}, S. N. Ghoshal—939
For $N^{14}(n,p)C^{14}$ and $N^{14}(n,\alpha)B^{11}$ reactions, C. H. Johnson and H. H. Barschall—818
Of nuclei for 280-Mev neutrons, R. Fox, C. Leith, L. Wouters, and K. R. MacKenzie—23
Of nuclei for 270-Mev neutrons, James DeJuren—27
Pile neutron absorption, S. P. Harris, C. O. Muehlhause, S. Rasmussen, H. P. Schroeder, and G. E. Thomas—342
Resonance capture of neutrons by U^{238}, Herbert L. Anderson —499
Variation of high energy neutron collision cross sections, J. DeJuren and B. J. Moyer—132(A)

Crystal structure
Atomic positions in ferroelectric $BaTiO_3$ lattice, W. Kaenzig —94(L)
Automatic structure analyses, Ray Pepinsky—124(A)
Cation distribution in copper zinc ferrite, Jacob L. Snoek —299(L)
Domain boundary, propagation velocity, H. J. Williams, W. Shockley, and C. Kittel—1090
Domain structure of rochelle salt, J. Furuichi and T. Mitsui —93(L)
Domain structure of WO_3, R. Ueda and T. Ichinokawa— 1106(L)
Neutron bombardment, effect of, S. S. Sidhu and C. O. Henry—123(A)
Phase transition in lead titanate, Gen Shirane, Sadao Hoshino, and Kazuo Suzuki—1105(L)
Phase transition in lead zirconate, Gen Shirane, Etsuro Sawaguchi, and Akitsu Takeda—485(L)
Self-diffusion in alkali metals, Heinz R. Paneth—708
Structure factors, relations among, H. Hauptman and J. Karle—244
Symmetry of graphite, Joseph S. Lukesh—226

Crystalline state
Antiferromagnetism, ordering effect, Yin-Yuan Li—457
Of $BaTiO_3$ single-domain crystals, electromechanical behavior, M. E. Caspari and W. J. Merz—1082
Cohesive energy of metallic lithium, R. A. Silverman and W. Kohn—912(L)
Currents induced in zincblende by electron bombardment, Merril F. Distad—879
Deformation potentials and mobilities in non-polar crystals, J. Bardeen and W. Shockley—72
Emission and trapping ZnS:Cu phosphors, Richard H. Bube—764(L)
Ferromagnetic resonance in nickel ferrite, W. A. Yager, J. K. Galt, F. R. Merritt, and E. A. Wood—744
Ge conductivity changes induced by α-particles, W. H. Brattain and G. L. Pearson—846
Impurity band conduction in semiconductors, Cavid Erginsoy—1104(L)
Of lead sulfide films, J. A. James, C. J. Milner, and B. N. Watts—298(L)

Crystalline state (continued)
Luminescence and trapping in zinc sulfide phosphors, Richard H. Bube—655
Luminescent decay of KBr and LiF, A. H. Morrish and A. J. Dekker—1030
Magnetic moments and eddy currents in superconducting Sn, James J. Fritz, Oscar D. Gonzalez, and Herrick L. Johnston—894
Nuclear resonance shift in Li, W. Kohn and N. Bloembergen—913(L)
Piezoelectric constants of alpha- and beta-quartz, Richard K. Cook and Pearl G. Weissler—712
Screening of electronic interactions in metals, David Bohm and David Pines—903(L)
Single crystals of Cu, internal friction, Arthur S. Nowick—249

Diamagnetism (see **Magnetic properties**)
Dielectric constants (see **Dielectrics and dielectric properties**)
Dielectrics and dielectric properties
Of liquid helium, C. J. Grebenkemper and John P. Hagen—89(L)
Diffraction of radiation
Bragg's law by use of microwaves, Roland A. Allen—927(A)
Diffusion
Activation energy for diffusion, G. J. Dienes—123(A)
Dye diffusion in a gel system, R. B. Pontius—927(A)
Au into Cu, A. B. Martin and Frank Asaro—123(A)
Self-diffusion coefficients in gases, Edward B. Winn—1024
Self-diffusion in cobalt, Foster C. Nix and Frank E. Jaumot, Jr.—119(L)
Self-diffusion of Co, Herman Branson and Woodfin Lewis—123(A)
Discharge of electricity in gases
Conductivity of ionized gas, Robert S. Cohen, Lyman Spitzer, Jr., and Paul McR. Routly—230
Electron removal in He afterglows, R. A. Johnson, B. T. McClure, and R. B. Holt—376
Flashing discharge, Carl Kenty—96(L)
Floating double probe measurements, E. O. Johnson and L. Malter—58
High temperature plasma, W. Finkelnburg and S. M. Segal—258
Ion-neutralized electron beam, E. G. Linder—99(L)
Metastable ($^3P_2$) Hg atoms in low current discharges, Carl Kenty—95(L)
Noise temperature of a d.c. plasma, Shoji Kojima and Kazuo Takayama—907(L)
Temperature effect in counters, Motoharu Kimura—761(L)
Discharge of electricity in high vacua (see also **Thermionic emission**)
Electric field at thermionic cathode, Paul L. Copeland and Delbert N. Eggenberger—298(L)
Initiation of arcs, F. E. Haworth—223
Space charge and pulsed electron beams, Surindra N. Kalra and William J. Fry—128(A)
Disintegration and excitation of nucleus (see also **Radioactivity; Photo-disintegration**)
Of Al^{27} by deuterons, levels in Mg^{25}, A. D. Schelberg, M. B. Sampson, and R. G. Cochran—574
Angular correlation, Stuart P. Lloyd—118(L)
Angular correlation in $F^{19}(p,\alpha)O^{16*}(\gamma)O^{16}$, Wayne R. Arnold—34
Angular distributions from (d,p) and (d,n), S. T. Butler—1095(L)
Angular distributions of α-particles and γ-rays from $F + p$ reaction, C. Y. Chao—1035
Angular distributions of protons from $O^{16}(d,p)O^{17}$, Hannah B. Burrows, W. M. Gibson, and J. Rotblat—1095(L)
$A^{36}(d,p)A^{37}$ reaction, A. Zucker and W. W. Watson—966
Of B by deuteron, proton spectrum, William O. Bateson—982
Of B^{10} by slow neutrons, G. C. Hanna—530
Of carbon by deuterons, long-range protons, G. C. Phillips—164
$C^{13}(d,n)N^{14}$, excitation curve, J. E. Richardson—850
$C^{13}(p,n)N^{13}$ reaction, yield, R. E. Adamson, Jr., W. W. Buechner, W. M. Preston, Clark Goodman, and D. M. Van Patter—985
Of C^{14} by deuteron, Emmett L. Hudspeth, Charles P. Swann, and N. P. Heydenburg—643
Compound nucleus, Zn^{64}, from α-Ni^{60} and p-Cu^{63} reactions, S. N. Ghoshal—939
Conversion coefficient of gamma-ray of Te^{125}, G. Friedlander, M. L. Perlman, and G. Scharff-Goldhaber—1103(L)
Of enriched Si by deuterons, proton groups, H. T. Motz and R. F. Humphreys—595
Excitation function of $C^{12}(\gamma,p)B^{11}$, A. K. Mann and J. Halpern—470(L)
Excitation function for spallation reactions, F. O. Bartell, A. C. Helmholz, S. D. Softky, and D. B. Stewart—1006
Excited state of C^{14} from $C^{13}(d,p)C^{14*}$, A. Sperduto, S. S. Holland, Jr., D. M. Van Patter, and W. W. Buechner—769(L)
By 42 Mev neutrons, cross sections, Roger H. Hildebrand and Cecil E. Leith—842
γ-ray spectrum from meson capture, Wolfgang K. H. Panofsky, Lee Aamodt, James Hadley, and Robert Phillips—94(L)
Gamma-rays from A^{38}, angular correlation, Rolf M. Steffen—115(L)
Gamma-rays from F, angular distribution, R. B. Day, C. Y. Chao, W. A. Fowler, and J. E. Perry, Jr.—131(A)
Gamma-rays from proton bombardment of P, G. Richard Grove, John N. Cooper, and J. C. Harris—131(A)
Gamma-resonances in Mg, John N. Cooper, Warren E. Taylor, J. C. Harris, and G. Richard Grove—131(A)
Of He^3 by fast neutrons, J. H. Coon—488(L)
Of Li_2O and C by α-particles and deuterons, Isadore B. Berlman—775
$Li^6(d,p)Li^7$, angular yield, R. W. Krone, S. S. Hanna, and D. R. Inglis—603
Meson absorption and emission mechanisms in nuclei, P. Cüer—906(L)
Multipole order of gamma-ray from C^{12}, R. G. Thomas—138(A)
Neutron capture gamma-ray, Bernard Hamermesh—131(A)
Neutron capture γ-rays from Cd, Cl, and C, Richard Wilson—90(L)
(n,p), (n,d) reactions, James Hadley and Herbert York—345
Neutron yield from $Be^9(\gamma,n)Be^8$, G. J. Hine and F. E. Senftle—904(L)
$N^{14}(d,p)N^{15}$ and $N^{15}(d,p)N^{16}$ reactions, proton spectra, Robert Malm and W. W. Buechner—771
Of N^{14} by fast neutrons, C. H. Johnson and H. H. Barschall—818
$N^{14}(p,\gamma)O^{15}$ reaction, D. B. Duncan and J. E. Perry, Jr.—136(A)
Polarization correlation of mixed multipoles, Irving Zinnes—386
Positively charged particles appearing near beta-ray emitters, Gerhart Groetzinger and David Kahn—108(L)
Production of high energy deuterons by energetic nucleons, theory, J. Heidmann—171
Proton bombardment of Be, neutron energy, David Bodansky—481(L)
Proton-neutron thresholds, H. T. Richards, R. V. Smith, and C. P. Browne—524
Resonances in $P^{31}(p,\gamma)S^{32}$, G. R. Grove, John N. Cooper, and J. C. Harris—107(L)
Successive nuclear radiations, directional correlation, J. A. Spiers—491(L)

Stars induced by 350–400 Mev protons, G. Bernardini, E. T. Booth, and S. J. Lindenbaum—905(L)
Stars initiated by gamma-rays, Seishi Kikuchi—492(L)
Of Ti^{45}, M. Ter-Pogossian, C. S. Cook, F. T. Porter, K. H. Morganstern, and J. Hudis—360
Transmutation of N^{15} by protons, A. W. Schardt, W. A. Fowler, and C. C. Lauritsen—136(A)

Dynamics
Gyroscopic stabilization of a free body, J. K. Tyson—129(A)

Elasticity
Forces exerted on dislocations, stress fields produced, M. Peach and J. S. Koehler—436
Influence of plastic flow on conductivity, Frederick Seitz—239

Electrical conductivity and resistance
Of Sb films, Hall coefficient, W. F. Leverton and A. J. Dekker—732
Of Ge, changes induced by α-particles, W. H. Brattain and G. L. Pearson—846
Of Ge, pressure dependence, Julius H. Taylor—919(L)
Of halide crystals, influence of plastic flow, Frederick Seitz—239
Impurity band conduction in semiconductors, Cavid Erginsoy—1104(L)
Magnetoresistance of Be, C. W. Heaps—892
On non-polar crystals, J. Bardeen and W. Shockley—72
P-N junctions, impurity diffusion, R. N. Hall and W. C. Dunlap—467(L)
Superconducting electrons, wave functions, John Bardeen—567
Superconducting transition temperature of Hg, B. Serin, C. A. Reynolds, and L. B. Nesbitt—761(L)
Superconductivity of Cb, D. B. Cook, M. W. Zemansky, and H. A. Boorse—737
Superconductivity, theory, L. Tisza—717; J. M. Luttinger—727
Superconductors, J. G. Daunt—911(L)
Transverse magnetic field on thin metallic films, E. H. Sondheimer—401

Electrodynamics (see **Electromagnetic theory**)

Electromagnetic theory (see also **Quantum electrodynamics**)
Advanced and retarded potentials, Alfred Landé—283(L)
Čerenkov radiation, spread of, Yin-Yuan Li—104(L)
Circularly polarized waves in sunspot, R. Q. Twiss—767(L)
Generation of coherent radiation, Lloyd T. Devore, Surindra N. Kalra, and William J. Fry—128(A)
Gravitational, electromagnetic, and pair fields, Marcos Moshinsky—514
Motion of electron in linear accelerator, David Caplan and Edward Akeley—125(A); Thomas Keenan and Edward Akeley—125(A)
Motion of charges in magnetic fields, A. Romero Juárez—138(A)
Sommerfeld's surface wave, C. J. Bouwkamp—294(L)

Electron diffraction
Standard substance for precise measurements, F. W. C. Boswell—91(L)

Electronic tubes
Space charge and noise reduction in electron beams, C. C. Cutler and C. F. Quate—875

Electrons, secondary
Atomic structure, E. J. Sternglass—925(L)

Electrostatics
Charging of aircraft glass, E. Stickley, M. M. Newman, and J. D. Robb—128(A)

Elements
Origin of the lighter elements, William Band—813

Errata
Ferroelectric Curie point in $KTaO_3$, J. K. Hulm, B. T. Matthias, and E. A. Long—490(L)
Nuclear isomerism and shell structure, R. D. Hill—906(L)
On the primary cosmic-ray spectrum, J. A. Van Allen and S. F. Singer—116(L)
Scattering of positrons and electrons by nuclei, H. J. Lipkin and M. G. White—770(L)

Ferroelectric phenomena
Domain structure of WO_3, R. Ueda and T. Ichinokawa—1106(L)
Ferroelectric Curie point in $KTaO_3$, erratum, J. K. Hulm, B. T. Matthias, and E. A. Long—490(L)

Ferromagnetism (see **Magnetic properties**)

Field theory (see also **Quantum electrodynamics**)
Geometrical model for unified theory, J. I. Horváth—901(L)
Gravitational, electromagnetic, and pair fields, Marcos Moshinsky—514
Gravitational self-energy of light, S. B. Nilsson and K. V. Laurikainen—291(L)
Non-local fields, D. R. Yennie—1053
Non-local fields, quantum theory, Hideki Yukawa—1047
Photon self-energy, George Snow and Hartland S. Snyder—987
Polarization of vacuum by meson fields, Juan de Oyarzábal—138(A)

Fission of nucleus (see also **Disintegration and excitation of nucleus**)
Asymmetric and symmetric fission, T. Yasaki and O. Miyatake—754(L)
Asymmetric fission, energy barrier, J. Jungerman—285(L)
Ionization defects of fission fragments, J. K. Knipp, R. B. Leachman, and R. C. Ling—478(L)
Long-range charged particles from heavy nuclei, K. W. Allen and J. T. Dewan—181
Of U^{238}, Xe and Kr in pitchblende, J. Macnamara and H. G. Thode—471(L)
Yield curve of Th^{232}, J. Niday and A. Turkevich—136(A)

Friction
In single crystals of Cu, variation with frequency and temperature, Arthur S. Nowick—249

Gases (see also **Kinetic theory**)
Transport of Al atoms by a gas, Michel Ter-Pogossian, Fred T. Porter, and C. Sharp Cook—294(L)

Gravitation
Birkhoff's gravitational field, electromagnetic and pair fields, M. Moshinsky—139(A)
Potentials in Birkhoff's theory of gravitation, Fernando Alba—127(A)

Hall effect
Coefficient of Sb films, W. F. Leverton and A. J. Dekker—732
In ferromagnetics, Emerson M. Pugh, N. Rostoker, and A. Schindler—688
Transverse magnetic field on thin metallic films, E. H. Sondheimer—401

Heat conduction (see **Thermal conductivity**)

Heat of formation
Of chemical compounds and alloys, soft x-ray spectra, K. Das Gupta—281(L)

Helium, liquid
Dielectric constant, C. J. Grebenkemper and John P. Hagen—89(L)
Second sound in He^3-He^4 mixtures, Ernest A. Lynton and Henry A. Fairbank—1043
Superflow, pressure, R. Bowers, B. S. Chandrasekhar, and K. Mendelssohn—856
Thermodynamic properties, B. M. Abraham, D. W. Osborne, and B. Weinstock—366
Two fluid theory, S. Nakajima and M. Shimizu—923(L)

Hydrodynamics
Viscous compressible fluids, Bernard Etkin and Victor G. Szebehely—767(L)
Hyperfine structure (see also **Nuclear moments and spin**)
Angular dependence for copper ion, E. F. Carr and C. Kikuchi—1107(L)
Of Zeeman levels in NO, Allan F. Henry—549

Ionization
Auto-ionization in light atoms, Ta-You Wu and L. Ourom—129(A)
By charged particles in photographic emulsions, relativistic increase, E. Pickup and L. Voyvodic—89(L)
Circularly polarized waves in sunspot, R. Q. Twiss—767(L)
Ionization defects of fission fragments, J. K. Knipp, R. B. Leachman, and R. C. Ling—478(L)
By recoil particles, Rufus C. Ling and Julian K. Knipp—106(L)
Ionization potentials
Molecular fragments of organic compounds, Anthony Donfor, Webster Kendrick, and Herman Branson—129(A)
Ions, mobility
Of He, Ne, and A, John A. Hornbeck—297(L)
Isomers, nuclear (see also **Nuclear structure; Radioactivity**)
Of Cd^{113}, β-decay, W. L. Carss, Jane R. Gum, and M. L. Pool—1028
Of Cd^{115}, E. Brock Dale and J. D. Kurbatov—126(A); P. S. Gill, C. E. Mandeville, and E. Shapiro—284(L)
Of $_{63}Eu^{153}$, 3×10^{-9} sec. state, F. K. McGowan—482(L)
Nuclear isomerism and shell structure, erratum, R. D. Hill—906(L)
And shell structure, Peter Axel—104(L)
Short-lived, W. J. MacIntyre—1018
Of Ta^{181}, W. C. Barber—332
Of Tc^{95}, Heinrich A. Medicus and Peter Preiswerk—1101(L)
Of Xe^{131}, Ingmar Bergstrom—114(L)
Of Xe^{133}, B. H. Ketelle, A. R. Brosi, and H. Zeldes—485(L)
Isotopes
Of A^{36} and A^{38}, concentration, A. Zucker and W. W. Watson—966
Berkelium (atomic number 97), radioactivity, S. G. Thompson, A. Ghiorso, and G. T. Seaborg—781
Californium (atomic number 98), radioactivity, S. G. Thompson, K. Street, Jr., A. Ghiorso, and G. T. Seaborg—790
Cm^{243} and Cm^{244}, identification of, F. L. Reynolds, E. K. Hulet, and K. Street, Jr.—467(L)
Mass of S^{32}, A. S. Penfold—116(L)
Of Pu, S. G. Thompson, K. Street, Jr., A. Ghiorso, and F. L. Reynolds—1108(L)
In rare-earth region, alpha-active, J. O. Rasmussen, F. L. Reynolds, S. G. Thompson, and A. Ghiorso—475(L)
Separation in the atmosphere, John H. McQueen—100(L)
Of Si, atomic masses, H. T. Motz and R. F. Humphreys—595
Of Tm, C. R. Lagergren and M. E. Kettner—102(L)
Of Xe and Kr, in pitchblende, J. Macnamara and H. G. Thode—471(L)

Kinetic theory
Self diffusion coefficients, Edward B. Winn—1024

Low temperature phenomena (see also **Helium, liquid**)
Heat flow in superconductors, K. Mendelssohn and J. L. Olsen—859
Magnetic moments and eddy currents in superconducting Sn, James J. Fritz, Oscar D. Gonzalez, and Herrick L. Johnston—894
Luminescence
Absorption and emission spectra of KCl:Tl phosphor, Ferd E. Williams—306(L)
Non-crystalline scintillation phosphors, Marvin G. Schorr and Franklin L. Torney—474(L)
Of KBr and LiF, A. H. Morrish and A. J. Dekker—1030
In zinc sulfide phosphors, Richard H. Bube—655

Magnetic properties (see also **Crystal structure; Magnetic resonance absorption; Nuclear moments and spin**)
Of Alnico V, theory of anisotropy, J. E. Goldman and R. Smoluchowski—302(L)
Anomalous diamagnetism of graphite, S. Mrozowski—123(A)
Antiferromagnetism, Yin-Yuan Li—457
Diamagnetic field for atoms, W. C. Dickinson—563
Domain boundaries, inertia and damping constant, C. Kittel—918(L)
Domain boundary, propagation velocity, H. J. Williams, W. Shockley, and C. Kittel—1090
Domain fringe fields, L. Marton, J. A. Simpson, and A. Van Bronkhorst—122(A)
Heisenberg's model of ferromagnetism, H. Ekstein—122(A)
Of indium single crystals, J. Verhaeghe, G. Vandermeerssche, and G. Le Compte—758(L)
Magnetization in Alnico V, E. A. Nesbitt and H. J. Williams—112(L)
Magnetostriction in Fe-Co, J. E. Goldman—301(L)
Moments and eddy currents in superconducting Sn, James J. Fritz, Oscar D. Gonzalez, and Herrick L. Johnston—894
Paramagnetic absorption on small samples, R. P. Lacroix, Ch. E. Ryter, and C. R. Extermann—763(L)
Permanent magnet alloys, K. Hoselitz and M. McCaig—757(L)
At very high frequencies. Dispersion in a ferrite, G. T. Rado, R. W. Wright, and W. H. Emerson—273
Weiss theory of ferromagnetism, P. W. Anderson—922(L)
Magnetic resonance absorption (see also **Nuclear moments and spin**)
Chemical shifts in F^{19}, H. S. Gutowsky and C. J. Hoffman—110(L)
Ferromagnetic resonance in nickel ferrite, W. A. Yager, J. K. Galt, F. R. Merritt, and E. A. Wood—744
Integration of weak signals, G. Suryan—119(L)
In NO_2, J. G. Castle, Jr. and Robert Beringer—114(L)
For K^{39}, T. L. Collins—103(L)
Spin echoes, E. L. Hahn—580
Magnetostriction (see **Magnetic properties**)
Mechanics (see **Dynamics**)
Mechanics, quantum—atomic structure and spectra
Diamagnetic field, Hartree computation, W. C. Dickinson—563
Mechanics, quantum—general
Asymptotic expansion of irregular Coulomb function, G. Breit and M. H. Hull, Jr.—392, 561
Elementary particles, theory, B. T. Darling—460
Evaluation of collision matrix, G. C. Wick—268
Radial wave functions, tables of Coulomb functions, I. Bloch, M. H. Hull, Jr., A. A. Broyles, W. G. Bouricius, B. E. Freeman, and G. Breit—553
Scattering theory of Dirac equation, George Parzen—261
Selection rules for closed loop processes, C. B. van Wyk—487(L)
Singular potentials, K. M. Case—797
Variational principle for time-dependent problems, Marcello Cini and Luigi A. Radicati—300(L)
Virial theorem and variation principle, Irvin Isenberg—917(L)
Mechanics, quantum-nuclear
Singular potentials, K. M. Case—797
Mechanics, quantum—of solid bodies'
Classical spin-wave theory of Heller and Kramers, Martin J. Klein and Robert S. Smith—1111(L)

Superconducting electrons, wave functions, John Bardeen —567
Superconductivity, theory, L. Tisza—717; J. M. Luttinger —727
Mesons (see also **Cosmic radiation**)
Absorption and emission mechanisms, P. Cüer—906(L)
Absorption in deuterium, S. Tamor and R. E. Marshak——766(L)
Absorption in hydrogen, R. E. Marshak, S. Tamor, and A. S. Wightman—765(L)
Collimated and wide-angle groups in a star, Maurice M. Shapiro and Herman Yagoda—283(L)
Complex particles?, M. el Nadi—754(L)
As composite particle, H. M. Moseley and Nathan Rosen—177
γ-ray spectrum from capture in hydrogen, Wolfgang K. H. Panofsky, Lee Aamodt, James Hadley, and Robert Phillips—94(L); In deuterium, Lee Aamodt, James Hadley, and Wolfgang Panofsky—282(L)
Interaction of π^--mesons, G. Bernardini, E. T. Booth, L. Lederman, and J. Tinlot—924(L)
Large angle scattering, H. Bradner and B. Rankin—916(L)
μ-meson decay, G. G. Harris and T. J. B. Shanley—474(L)
Multiple production, J. J. Lord, Joseph Fainberg, and Marcel Schein—970
New unstable elementary neutral particle, V. D. Hopper and S. Biswas—1099(L)
Photo-mesons from carbon, J. M. Peterson, R. S. White, and W. S. Gilbert—135(A)
Photo-mesons from hydrogen, A. S. Bishop, J. Steinberger, and Leslie J. Cook—136(A)
Of π^+ by photons on hydrogen, A. S. Bishop, J. Steinberger, and Leslie J. Cook—291(L)
π^+-mesons by x-rays, function of atomic number, R. F. Mozley—493(L)
Polarization of vacuum by meson fields, Juan de Oyarzábal 138(A)
Positive mesons by protons in liquid hydrogen, Vincent Z. Peterson—136(A)
Production of a π^+-meson beam, C. Richman, M. Skinner, J. Merritt, and B. Youtz—900(L)
Range spectrum, Lawrence Germain—616
S-matrix in meson theory, Ning Hu—1109(L)
Scattering by nuclear particles, Vachaspati—973
Self-energy, Fernando Prieto—138(A)
Spectrum and meteorological variations, D. C. Rose—106(L)
Spinless mesons in electromagnetic field, P. T. Matthews 292(L)
Metals (see **Crystalline state**)
Meteorology
Surface ozone in Arctic regions, W. S. Wilson—135(A)
Methods and instruments
Acceleration of stripped C^{12} and C^{13} nuclei, J. F. Miller, J. G. Hamilton, T. M. Putnam, H. R. Haymond, and G. B. Rossi—486(L)
α-particle range-energy curve for Ilford E-1 emulsions, Isadore B. Berlman—96(L)
Bragg's law by use of microwaves, Roland A. Allen—927(A)
CdS crystals as detector of x-radiation, John E. Jacobs—124(A)
Crystal structure analysis, automatic, Ray Pepinsky—124(A)
Deuterium-zirconium targets, J. J. Moore and R. N. Little —137(A)
Difference equation in cosmic-ray shower theory, W. T. Scott—611
Differential equations of second order, asymptotic solutions, Isao Imai—1112(L)
Double development of emulsions, Č. Jech—759(L)
Electrostatic transformer, Jose Mireles Malpica—124(A)
Faraday, new method for determining, D. Norman Craig and James I. Hoffman—487(L)
Fluorescent decay of scintillation crystals, S. H. Liebson, M. E. Bishop, and J. O. Elliot—907(L)
Gamma-ray energies with crystals of NaI(Tl), R. Hofstadter and J. A. McIntyre—131(A), 631
Gyroscopic stabilization of a free body, J. K. Tyson—129(A)
Ignitrons and servo mechanisms, F. M. Bailey—927(A)
Integration of weak nuclear magnetic resonance signals, G. Suryan—119(L)
Latent image fading, Arthur Beiser—112(L)
Low temperature x-ray diffraction goniometer, B. C. Frazer and Ray Pepinsky—124(A)
Magnetic moment of proton, direct determination, F. Bloch and C. D. Jeffries—305(L)
Motion of electrons in a linear accelerator, David Caplan and Edward Akeley—125(A); Thomas Keenan and Edward Akeley—125(A)
Mounting for an echelette diffraction grating, W. F. C. Ferguson and J. H. Greig—130(A)
NbN bolometer, microwave frequencies, Max Bodmer, Jean V. Lebacqz, and D. H. Andrews—122(A)
Non-crystalline scintillation phosphors, Marvin G. Schorr and Franklin L. Torney—474(L)
Paramagnetic absorption on small samples, R. P. Lacroix, Ch. E. Ryter, and C. R. Extermann—763(L)
Photography of atoms, generalized microscope, (author unknown)—123(A)
Photo-sensitive counter, beta-induced scintillations, C. E. Mandeville and H. O. Albrecht—117(L), 299(L), 300 (L)
Pulses in argon counters, Laura Colli, Ugo Facchini, and Emilio Gatti—92(L)
Scintillation counter, resolving time, R. F. Post and L. I. Schiff—1113(L)
Scintillation decay times, Arne Lundby—477(L)
Scintillation properties of solutions, G. T. Reynolds and F. B. Harrison—129(A)
Soft x-rays with a scintillation counter, Lyman A. Webb, Ronald S. Paul, and Francis E. Dart—129(A)
Space charge in a d.c. cut-off magnetron, D. Reverdin and L. Marton—129(A)
Stability and focusing in linear accelerators, Edwin M. McMillan—493(L)
Synchrotron-oscillation resonance, Nelson M. Blachman—125(A)
Temperature effect in counters, Motoharu Kimura—761(L)
Temperature variations in alcohol-argon G-M counters, Om Parkash—303(L)
Transport of Al atoms by a gas, Michel Ter-Pogossian, Fred T. Porter, and C. Sharp Cook—294(L)
Un cero de una cierta función de las funciónes de bessel, F. T. Rogers, Jr. and H. L. Morrison—128(A)
Variational methods in collision problems, Tosio Kato—475(L)
Variational principle for time-dependent problems, Marcello Cini and Luigi A. Radicati—300(L)
Vector boundary value problem, J. Adem and M. Moshinsky—128(A)
Voltage stabilizers, theory, J. J. Gilvarry and D. F. Rutland —129(A)
Mobility of ions (see **Ions, mobility**)
Molecular structure and constants (see also **Spectra, molecular; Raman spectra**)
Of CH_3Cl, CH_3Br, CH_3I, BrCN, and ICN, James W. Simmons and Wallace E. Anderson—338
Magnetic shielding in H_2, G. F. Newell—476(L)
Of methyl bromide, James W. Simmons and William O Swan—289(L)

Moments, of molecules (see also **Nuclear moments and spin**)
Of D_2, H. G. Kolsky, T. E. Phipps, Jr., N. F. Ramsey, and H. B. Silsbee—483(L)
Quadrupole moment of N_2, M. H. Johnson—101(L)

Neutrons
Capture in deuterium, B. B. Kinsey and G. A. Bartholomew—918(L)
In cosmic rays, energy and density distribution, William O. Davis—150
Depression of density by detecting foil, C. W. Tittle—756(L)
Diffusion in paraffin, C. W. Tittle—756(L)
Double transmission and depolarization, M. Burgy, D. J. Hughes, J. R. Wallace, R. B. Heller, and W. E. Woolf—953
γ-rays from Cd, Cl, and C, neutron capture, Richard Wilson—90(L)
Production below (p,n) threshold, B. Jennings, K. H. Sun, and H. A. Leiter—109(L)
Refraction in ferromagnets, Melvin Lax—299(L)
Resonance capture by U^{238}, Herbert L. Anderson—499
Slowing down of Sb^{124}-Be photo-neutrons in graphite, L. D. Roberts, J. E. Hill, and G. McCammon—6
Slowing down through medium and heavy nuclei, H. A. Bethe, L. Tonks, and H. Hurwitz, Jr.—11
From $V^{51}(p,n)Cr^{51}$, P. H. Stelson, W. M. Preston, and Clark Goodman—287(L)
Yield from $Be^9(\gamma,n)Be^8$, G. J. Hine and F. E. Sentfle—904(L)

Nuclear moments and spin (see also **Hyperfine structure**)
Of $_{83}Bi^{209}$, F. M. Kelly, R. Richmond, and M. F. Crawford—295(L)
Deviations from Schmidt limits, L. L. Foldy and F. J. Milford—751(L)
Diamagnetic correction for protons, H. A. Thomas—901(L)
Discrepancies in gallium and indium, H. M. Foley—288(L)
Excited states of thorium D, H. E. Petch and M. W. Johns—478(L)
Intermediate coupling in molecular beams, William A. Nierenberg—1102(L)
Magnetic moment of proton, direct determination, F. Bloch and C. D. Jeffries—305(L)
Nuclear resonance shift in Li, W. Kohn and N. Bloembergen—913(L)
Of odd nuclei, magnetic, A. de-Shalit—103(L)
Of K^{39}, magnetic resonance, T. L. Collins—103(L)
Of proton and neutron, Roald K. Wangsness—769(L)
Quadrupole moment of Li^7, sign, R. D. Present—43
Quadrupole moments, R. Sternheimer—102(L)
Ratio of deuteron to proton magnetic moment, B. Smaller, E. Yasaitis, and H. L. Anderson—137(A)
Space exchange magnetic moments, Larry Spruch—372
Of S^{33}, magnetic, J. R. Eshbach, R. E. Hillger, and C. K. Jen—1106(L)
Of $_{43}Tc^{99}$, Karl G. Kessler and William F. Meggers—905(L)
Values of μ_p, F, and M_p/m_e use of the omegatron, H. Sommer, H. A. Thomas, and J. A. Hipple—487(L)

Nuclear spectra (see also **Disintegration and excitation of nucleus**)
Of Ba^{131}, γ-rays, E. B. Dale, E. D. Richert, T. A. Redfield, and J. D. Kurbatov—763(L)
β-ray spectrum of C^{15}, Emmett L. Hudspeth, Charles P. Swann, and N. P. Heydenburg—643
Of Ca^{45}, β-rays, B. H. Ketelle—758(L)
Of Cl^{34}, Lawrence Ruby and J. Reginald Richardson—760(L)
γ-ray spectra, R. Hofstadter and J. A. McIntyre—631
γ-ray spectra, neutron capture, Bernard Hamermesh—415
γ-rays from $Be^9(\alpha,n)$, James Terrell—1076
Of Au, γ-rays, R. W. Pringle and S. Standil—762(L)
Of In^{115}, E. A. Martell and W. F. Libby—977
Of Mo^{99} and Tc^{99m}, β- and γ-rays, Merle E. Bunker and Robert Canada—961
Of S^{35}, beta-spectrum, Leonard Gross and Donald R. Hamilton—484(L)

Nuclear structure (see also **Disintegration and excitation of nucleus; Radioactivity; Nuclear spectra**)
Of Be^7, excited states, George R. Keepin, Jr.—768(L)
Boundary conditions for nuclear reactions, M. Moshinsky—137(A)
Of C^{12}, Be^8, and Ne^{20}, excited states, Luis W. Alvarez—519
Closed shells from nuclear masses, W. Low and C. H. Townes—608
Energy level of N^{14}, R. E. Adamson, Jr., W. W. Buechner, W. M. Preston, Clark Goodman, and D. M. Van Patter—985
Energy levels from bombardment of Li_2O and C by alpha-particles and deuterons, Isadore B. Berlman—775
Energy levels of A^{37}, A. Zucker and W. W. Watson—966
Energy levels of Be, B, O, and F, C. K. Bockelman—1011
Equality of n-n and p-p forces, G. Breit—1110(L)
Of Er^{166}, isomer, F. K. McGowan—923(L)
Excited state of Be^7, C. H. Johnson and H. H. Barschall—818
Interactions in (jj) coupling shell model, Dieter Kurath—98(L)
Levels of nuclei, H. A. Wilson—137(A)
Of Li^7, energy levels, G. C. Hanna—530
Of Mg^{25}, energy levels, A. D. Schelberg, M. B. Sampson, and R. G. Cochran—574
Magic numbers, third-order difference, Frank A. Valente—1110(L)
Of N^{13} and C^{13}, R. G. Thomas—136(A)
Of N^{15}, levels, Emmett L. Hudspeth, Charles P. Swann, and N. P. Heydenburg—643
Non-linear meson theory, L. I. Schiff—137(A)
Normal modes of vibration, I. Bloch—138(A)
P-P interaction from scattering experiments, Carl-Erik Fröberg—105(L)
Scattering of γ-rays by nucleons, R. G. Sachs and L. L. Foldy—824
Short-lived isomers, W. J. MacIntyre—1018

Optical constants and properties
Dichroism from adsorbed dyes, D. R. Morey and E. V. Martin—927(A)

Pair production
Distribution of recoil nucleus, R. Jost, J. M. Luttinger, and M. Slotnick—189

Photo-Disintegration
Of Be and D, photo-neutron thresholds, R. C. Mobley and R. A. Laubenstein—309
Of deuterium and beryllium, Arthur H. Snell, E. C. Barker, and R. L. Sternberg—637
Of deuteron, J. A. Phillips, J. S. Lawson, Jr., and P. Gerald Kruger—326; P. V. C. Hough—1069
Of deuteron at low energies, cross section, G. R. Bishop, C. H. Collie, H. Halban, A. Hedgran, K. Siegbahn, S. du Toit, and R. Wilson—211
Neutron yields from Li, B. D. McDaniel, R. L. Walker, and M. B. Stearns—807
Of O^{16}, Melvin A. Preston—307(L)
Of Ag and Al, B. C. Diven and G. M. Almy—407
Stars initiated by gamma-rays, Seishi Kikuchi—492(L)

Photoelectric effect and properties; cells
Changes in SrO and BaO by uv irradiation, J. E. Dickey and E. A. Taft—308(L)
Surface effect, M. J. Buckingham—704

Photography (see also **Methods and instruments**)
Influence of plastic flow on photographic properties, Frederick Seitz—239

Latent image fading, Arthur Beiser—112(L)
Photography of atoms in Crystals, M. J. Buerger—123(A)
Photons
Scattering of γ-rays by nucleons, R. G. Sachs and L. L Foldy—824
Piezoelectric effect
In $BaTiO_3$ single-domain crystals, M. E. Caspari and W. J. Merz—1082
Constants of alpha- and beta-quartz, Richard K. Cook and Pearl G. Weissler—712
Proceedings of the American Physical Society
Meeting at Mexico City, June 21–23, 1950—120
Meeting of the New York State Section, Potsdam, New York, September 29–30, 1940—927

Quantum electrodynamics (see also **Field theory**)
Charged particles without spin, F. Rohlich—666
Interaction of electrons with high frequency fields, J. C. Ward—119(L)
Longitudinal electromagnetic field, S. T. Ma—729
Mathematical formulation of theory, R. P. Feynman—440
Non-linear interactions between fields, Robert Karplus and Maurice Neuman—380
Scattering of mesons by nuclear particles, Vachaspati—973
Spinless mesons and nucleons in electromagnetic field, P. T. Matthews—292(L)
Spinless mesons in electromagnetic field, P. T. Matthews—292(L)

Radiation
Polarization correlation of mixed multipoles, Irving Zinnes—386
Radio (see also **Radiation**)
Precipitation static conditions, E. Stickley, M. M. Newman, and J. D. Robb—128(A)
Solar atmosphere and radiofrequency radiation, S. A. Korff and Y. Beers—489(L)
Radioactivity (see also **Disintegration and excitation of nucleus; Nuclear spectra**)
Of Ac^{227}, half-life, J. M. Hollander and R. F. Leininger—915(L)
Alpha-active in rare-earth region, J. O. Rasmussen, F. L. Reynolds, S. G. Thompson, and A. Ghiorso—475(L)
Alpha-emitters of low mass, Luis W. Alvarez—519
Of Am^{242}, G. D. O'Kelley, G. W. Barton, Jr., W. W. T. Crane, and I. Perlman—293(L)
Of Sb^{124}, beta-spectrum, L. M. Langer, R. D. Moffat, and H. C. Price, Jr.—126(A)
Of A^{39}, A. Zucker and W. W. Watson—966
Of Ba^{131}, γ-rays, E. B. Dale, E. D. Richert, T. A. Redfield, and J. D. Kurbatov—763(L); E. L. Zimmerman, E. B. Dale, D. G. Thomas, and J. D. Kurbatov—908(L)
Of berkelium (atomic number 97), S. G. Thompson, A. Ghiorso, and G. T. Seaborg—781
Cd^{107} from Ag, excitation function, D. N. Kundu and M. L. Pool—126(A)
Of Cd^{113} isomer, β-decay, W. L. Carss, Jane R. Gum, and M. L. Pool—1028
Of Cs^{137}, internal conversion, M. A. Waggoner—489(L)
Of californium (atomic number 98), S. G. Thompson, K. Street, Jr., A. Ghiorso, and G. T. Seaborg—790
Of Ca^{45}, β-rays, B. H. Ketelle—758(L)
Of C^{14}, shapes of β-spectrum, S. D. Warshaw—111(L)
Of C^{15}, β-ray spectrum, Emmett L. Hudspeth, Charles P. Swann, and N. P. Heydenburg—643
Of Cl^{34}, internal conversion, Lawrence Ruby and J. Reginald Richardson—760(L)
Of Cl^{39}, decay scheme, R. N. H. Haslam, L. Katz, H. J. Moody, and H. M. Skarsgard—318
Of Co^{58m}, preparation by (γ,n) reaction, Darleane Christian and Don S. Martin, Jr.—1110(L)
Of Co^{60}, Cs^{134}, Zn^{65}, internal conversion, M. A. Waggoner, M. L. Moon, and A. Roberts—420
Of Cu^{64}, half-life, A. G. W. Cameron and L. Katz—904(L)
Los espectros continuous de los β-rayos, Marguerite M. Rogers and F. T. Rogers, Jr.—126(A)
Of F^{17}, V. Perez-Mendez and P. Lindenfeld—1097(L)
Of Ga^{66}, Lawrence M. Langer and R. Douglas Moffat—651
Gamma-ray energies using single crystals of NaI(Tl), R. Hofstadter and J. A. McIntyre—631
Of Au, γ-rays, R. W. Pringle and S. Standil—762(L)
Of Hf^{181}, William W. Pratt—289(L)
Of In^{115}, E. A. Martell and W. F. Libby—977
Internal conversion in the L_I-shell, H. Gellman, B. A. Griffith, and J. P. Stanley—866
Of Fe^{55} and Co^{60}, half-life, G. L. Brownell and C. J. Maletskos—1102(L)
Isomer of Cd^{115} gamma-ray spectrum, E. Brock Dale and J. D. Kurbatov—126(A)
Of Mo^{99} and Tc^{99m}, decay scheme, Merle E. Bunker and Robert Canada—961
Natural alpha-radioactivity, theory, Bernard L. Cohen—105(L)
Neutron deficient europium activities, Geoffrey Wilkinson and Harry G. Hicks—491(L)
New unstable elementary neutral particle, V. D. Hopper and S. Biswas—1099(L)
Of Ni^{57}, K capture, G. Friedlander, M. L. Perlman, D. Alburger, and A. W. Sunyar—30
Nuclei in cosmic-ray stars, E. Pickup and L. Voyvodic—1100(L)
Of Os^{182} and Os^{183}, Betsy Jones Stover—99(L)
Of Os^{185}, Os^{191}, and Os^{193}, Merle E. Bunker, Robert Canada, and Allan C. G. Mitchell—126(A)
Penetration and diffusion of Co^{60} gamma-rays in water, Gladys R. White—154
Of P^{32}, beta-spectrum, S. D. Warshaw, Joses J. L. Chen, and G. L. Appleton—288(L)
Of Pu isotopes, S. G. Thompson, K. Street, Jr., A. Ghiorso, and F. L. Reynolds—1108(L)
Of K, M. Ceccarelli, G. Quareni, and A. Rostagni—909(L)
K capture decay of At^{211}, Lawrence S. Germain—937
Of K^{40}, branching ratio, Mark G. Inghram, Harrison Brown, Clair Patterson, and David C. Hess—916(L)
Of Pr^{142}, Erling N. Jensen, L. Jackson Laslett, and D. J. Zaffarano—862
Preparation of Th^{235} and Pa^{235}, B. G. Harvey and B. I. Parsons—1098(L)
Of Re^{182} and Re^{183}, H. Talman Dybvig and M. L. Pool—126(A)
Of Rh^{106}, C. E. Mandeville and E. Shapiro—125(A)
Of Rb isotopes, D. G. Karraker and D. H. Templeton—646
Of Rb^{84}, Walter C. Beckham and M. L. Pool—125(A)
Of Rb^{86}, low energy beta-spectrum, Herbert R. Muether and Stuart L. Ridgway—750(L)
Of Sm^{147}, mass assignment, Boyd Weaver—301(L)
Of Ag and Cd isotopes, Jane R. Gum and M. L. Pool—315
Of Ag^{110}, gamma-rays, J. M. Cork, W. C. Rutledge, C. E. Branyan, A. E. Stoddard, W. J. Childs, and J. M. LeBlanc—286(L)
Of Na^{24}, A^{38}, Br^{82}, Tc^{96}, half-lives, James W. Cobble and R. W. Atteberry—917(L)
Of Ta and W isotopes, Geoffrey Wilkinson—495
Of Tc^{95}, isomeric transition, Heinrich A. Medicus and Peter Preiswerk—1101(L)
Of Th^{232}, M. E. Bunker, L. M. Langer, and R. J. D. Moffat—468(L)
Of tritium, G. H. Jenks, F. H. Sweeton, and J. A. Ghormley—990
Of Y^{87} and Sr^{87m}, L. G. Mann and Peter Axel—759(L)
Raman spectra
Of tetramethyl diborane, Bernard Rice, J. M. Gonzalez-Berredo, and T. F. Young—129(A)

Range of particles
α-particle range-energy curve for Ilford E-1 emulsions, Isadore B. Berlman—96(L)
Of α-particles, Isadore B. Berlman—775
Electrons in gases, range-momentum measurements, G. F. O'Neill and W. T. Scott—473(L)
Energy loss of electrons in matter, S. D. Warshaw and Joses J. L. Chen—97(L)
Of stripped C^{12} and C^{13} nuclei, J. F. Miller, J. G. Hamilton, T. M. Putnam, H. R. Haymond, and G. B. Rossi—486(L)
Relativity
General motion of matter, cosmological scale, Antonio Gião—755(L)
Geometrical model for unified theory, J. I. Horváth—901(L)
Hamiltonian of general theory with electromagnetic field, Peter G. Bergmann, Robert Penfield, Ralph Schiller, and Henry Zatzkis—81
Symmetrical universe in flat space-time, Carlos Graef Fernández—127(A)

Scattering of electrons, mesons, neutrons, protons, ions, and deuterons (see also **Electron diffraction; Cross section, measurements, theory**)
Of α-particles and deuterons by Li_2O and C, Isadore B. Berlman—775
Anisotropic and inelastic scattering of neutrons, Alexander Langsdorf, Jr.—132(A)
Effect of electric field on scattering of electrons, J. Bardeen and W. Shockley—69
Of electrons from heavy nucleus, George Parzen—355
Energy loss of electrons in matter, S. D. Warshaw and Joses J. L. Chen—97(L)
Equality of *n-n* and *p-p* forces, G. Breit—1110(L)
Of fast electrons in nuclear emulsions, Dale R. Corson—303(L)
Large angle scattering of π^--mesons, H. Bradner and B. Rankin—916(L)
Of mesons by nucleons, Alejandro Medina—138(A)
Neutron scattering at high energies, Simon Pasternack and Hartland S. Snyder—921(L)
Neutron scattering by Au, J. Tittman, C. Sheer, J. Rainwater, and W. W. Havens, Jr.—903(L)
Neutrons by deuteron, Jumpei Sanada and Shotaro Yamabe—750(L)
Of neutrons by deuterons, D. G. Hurst and N. Z. Alcock—117(L)
Of neutrons by deuterons, impulse approximation, Geoffrey F. Chew—196
Of neutrons by Na^{23}, spin dependence, W. Selove—290(L)
Of neutrons in iron single crystal, polarization, D. J. Hughes, M. T. Burgy, and W. E. Woolf—481(L)
Of neutrons in noble gases, Sigmund P. Harris—20
Nucleon-nucleon scattering, spin-orbit interactions, K. M. Case and A. Pais—138(A), 203
Polarization of scattered neutrons, W. E. Meyerhof, D. B. Nicodemus, and Felix Bloch—132(A)
Of positrons and electrons by nuclei, erratum, H. J. Lipkin and M. G. White—770(L)
p-d scattering, M. M. Gordon—1111(L)
Proton-proton at 100 Mev, R. W. Birge—490(L)
P-P interaction from scattering experiments, Carl-Erik Fröberg—105(L)
Proton-proton scattering, 18.8 to 31.8 Mev, Bruce Cork—321
Scattering of mesons by nuclear particles, Vachaspati—973
Scattering theory of Dirac equation, George Parzen—261
Of slow neutrons by solid and liquid helium, theory, L. Goldstein and D. W. Sweeney—141
Thermal neutrons, H. H. A. Krueger, D. Meneghetti, G. R. Ringo, and L. Winsberg—507
Of 3.1-Mev neutrons by protons, angular distribution, Yukiyasu Oda, Jumpei Sanada, and Shotaro Yamabe—469(L)
Of 280-Mev neutrons, R. Fox, C. Leith, L. Wouters, and K. R. MacKenzie—23
Of 270-Mev neutrons, James DeJuren—27
Scattering of radiation (see also **Raman spectra**)
Compton scattering, conservation of energy and momentum, William G. Cross and Norman F. Ramsey—929
Scattering of γ-rays by nucleons, R. G. Sachs and L. L. Foldy—824
Semiconductors (see **Electrical conductivity and resistance**)
Shock waves
Magneto-hydrodynamic shocks, F. de Hoffmann and E. Teller—692
Solid state (see **Crystalline state**)
Spallation (see **Disintegration and excitation of nucleus**)
Spectra, absorption (see also **Absorption of radiation**)
Of H_2, induced by foreign gases, M. F. Crawford, H. L. Welsh, J. C. F. MacDonald, and J. L. Locke—469(L)
Spectra, atomic
Of V I and Cr II, deep configurations, Abraham A. Schweizer—1080
Isotope shift in carbon, Clyde R. Burnett—494(L)
Isotope shift in C^{14}, John R. Holmes—130(A)
U-spark spectrum, J. C. van den Bosch—100(L)
Spectra, general
Absorption and emission spectra of KCl:Tl phosphor, Ferd E. Williams—306(L)
Radiofrequency spectrum of D_2, H. G. Kolsky, T. E. Phipps, Jr., N. F. Ramsey, and H. B. Silsbee—483(L)
Spin-spin interaction within paramagnetic ions, M. H. L. Pryce—1107(L)
Spectra, microwave
Determination of constants of CH_3Cl, CH_3Br, CH_3I, BrCN, and ICN, James W. Simmons and Wallace E. Anderson—338
Internal rotation in methyl silane, David R. Lide and Donald K. Coles—911(L)
Resonance absorption of $NiOFe_2O_3$, Tosihiko Okamura, Yosiharu Torizuka, and Yūzō Kojima—910(L)
Structure of methyl bromide, James W. Simmons and William O. Swan—289(L)
Of SCSe, Børge Bak, Raymond Sloan, and Dudley Williams—101(L)
Spectra, molecular (see also **Molecular structure and constants**)
Of BS, P. B. Zeeman—902(L)
Of $(He^3)_2$, G. H. Dieke and Eugene Sant Robinson—1
Of P_2, E. J. Marais and H. Verleger—429
Of P_2, perturbations in ultraviolet, S. M. Naudé and H. Verleger—432

Thermal conductivity
Vector boundary value problems, J. Adem and M. Moshinsky—128(A)
Thermionic emission; emitting surfaces
Schottky effect for Ta, periodic deviations, R. J. Munick, W. B. LaBerge, and E. A. Coomes—887

X-rays, absorption, diffraction, scattering, reflection, refraction, and polarization
Cascade showers in Pb, synchrotron x-rays, Kenneth M. Crowe and Evans Hayward—40
X-rays, tubes, apparatus
Detection by scintillation counter, Lyman A. Webb, Ronald S. Paul, and Francis E. Dart—129(A)

Zeeman effect
In NO, hyperfine structure, Allan F. Henry—549
Of O_2, Allan F. Henry—396